Title

Nuclear Chemistry Division Annual Report, 1968

Authors

Edelstein, Norman
Hendry, David
Michel, Maynard

Publication Date

1969

UCRL-18667
c.2

NUCLEAR CHEMISTRY
Annual Report 1968

Lawrence Radiation Laboratory
University of California - Berkeley

UCRL-18667
c.2

DISCLAIMER

UCRL-18667
UC-4 Chemistry
TID 4500 (53rd Ed.)

UNIVERSITY OF CALIFORNIA
Lawrence Radiation Laboratory
Berkeley, California

AEC Contract No. W-7405-eng-48

NUCLEAR CHEMISTRY DIVISION ANNUAL REPORT, 1968

January 1969

I. Perlman, Director, Nuclear Chemistry Division
Editors: Norman Edelstein, David Hendry, and Maynard Michel

Work done under the auspices of the U. S. Atomic Energy Commission

Printed in the United States of America
Available from
Clearinghouse for Federal Scientific and Technical Information
National Bureau of Standards, U. S. Department of Commerce
Springfield, Virginia 22151
Price: Printed Copy $3.00; Microfiche $0.65

NUCLEAR CHEMISTRY DIVISION ANNUAL REPORT, 1968*

Contents

I. NUCLEAR STRUCTURE AND NUCLEAR PROPERTIES

NUCLEAR SPECTROSCOPY AND RADIOACTIVITY

Nuclear Spectroscopy Studies on ^{237}Np (E. Browne and F. Asaro) 1
Alpha Decay of ^{238}Pu (C. M. Lederer, F. Asaro, and I. Perlman) 3
Table of Isotopes (J. M. Hollander and C. M. Lederer) 9
Study of Levels in ^{92}Mo and ^{94}Ru by In-Beam γ-Ray Spectroscopy (J. M. Jaklevic, C. M. Lederer, and J. M. Hollander) 12
Systematics of Even-Even Mo and Ru Nuclei (J. M. Jaklevic, C. M. Lederer, and J. M. Hollander) 15
Low-Lying 2- State in ^{236}U (C. M. Lederer, J. M. Jaklevic, and S. G. Prussin) 18
Level Scheme of ^{176}Hf--A Study of the Decays of ^{176}Ta and ^{176m}Lu (F. M. Bernthal, J. M. Hollander, and J. O. Rasmussen) 22
Thick-Target Method for Nuclear Recoil Studies (M. K. Go and S. S. Markowitz) 29
Recoil Studies of ^{46}Ti(α, 2n)^{48}Cr (M. K. Go and S. S. Markowitz) 31
Excitation Functions for ^{47}Ti + ^{3}He Reactions (M. K. Go and S. S. Markowitz) 32
^{3}He Activation of Mg, Si, Ca, Ti, Ni, Ge, and Ta: Excitation Functions and Thick-Target Yields (J. F. Lamb, D. M. Lee, and S. S. Markowitz) . . . 34
Single-Particle Level Systematics in Odd-Mass Nuclei With 123 Neutrons (K. Valli and E. K. Hyde) 39
Isomerism in Odd-Odd Nuclei With 127 Neutrons (K. Valli and E. K. Hyde) 40
Levels of ^{208}Po from Radioactive Decay and Nuclear Reaction γ-Ray Spectroscopy (W. J. Treytl, E. K. Hyde, and T. Yamazaki) 42
Observation of the New Isotope ^{17}C Using a Combined Time-of-Flight Particle-Identification Technique (A. M. Poskanzer, G. W. Butler, E. K. Hyde, J. Cerny, D. A. Landis, and F. S. Goulding) 44
Lifetimes of Rotational States From Heavy-Ion Reactions (R. M. Diamond, F. S. Stephens, W. H. Kelly and D. Ward) 47
Gamma-Ray De-Excitation of Compound-Nucleus-Reaction Products (F. S. Stephens, R. M. Diamond, W. H. Kelly, J. O. Newton, and D. Ward) 51
Isomeric Levels in Nuclei With N = 74 (David Ward, F. S. Stephens, and R. M. Diamond) 54
Beta Decay Half-Lives for the New Isotopes ^{166,164,162}Lu, ^{160,158}Tm, and ^{160,158}Yb (Martin Neiman and David Ward) 59
Search for a 0.3-sec Spontaneous Fission Activity in Element 104 (Albert Ghiorso, Matti Nurmia, and James Harris) 61
Studies of Isotopes of Element 104 (Albert Ghiorso, Matti Nurmia, James Harris, Kari Eskola, and Pirkko Eskola) 62
New Nuclide ^{258}No (Matti Nurmia, Kari Eskola, Pirkko Eskola, and Albert Ghiorso) 63
Study of Dy(^{40}Ar, xn)Po Reactions (T. Sikkeland, R. J. Silva, M. Nurmia, and A. Ghiorso) 64

NUCLEAR REACTIONS AND SCATTERING

High-Isospin Nuclei and Multiplets in the Light Elements (Joseph Cerny) 65
Microscopic Analysis of the of the ^{3}He, t and ^{3}He, ^{3}He' Reactions on 1p Shell Nuclei (Gordon C. Ball and Joseph Cerny) 65
Carbon-10 and Mass Measurements for Light Nuclei (H. Brunnader, J. C. Hardy, and Joseph Cerny) 69
Isobaric Analog States and Coulomb Displacement Energies in the $1d_{5/2}$ Shell (J. C. Hardy, H. Brunnader, Joseph Cerny, and J. Jänecke) 72

*Preceding Annual Reports: UCRL-17989, UCRL-17299.

Location and Isospin-Forbidden Alpha Decay of the Lowest T = 2 State in ^{28}Si (Robert L. McGrath, J. C. Hardy, and Joseph Cerny). 77
The ^{31}P(t, p)^{33}P Reaction and the Usefulness of Double Stripping in Distinguishing Between Shell-Model Calculations (W. G. Davies, J. C. Hardy, and W. Darcey) 80
^{91}Y and the Failure of the Closed Shell at ^{88}Sr (J. C. Hardy) 84
Elastic α-α Scattering and the ^{7}Li(p, α)α Reaction (H. E. Conzett and R. J. Slobodrian). 87
Proton-Proton Elastic Scattering Between 6 and 10 MeV (R. J. Slobodrian, H. E. Conzett, E. Shield, and W. F. Tivol). 89
Determination of the $^{1}S_0$ Neutron-Neutron Effective-Range Parameters (R. J. Slobodrian, H. E. Conzett, H. Meiner, A. D. Bacher, J. Ernst, and F. G. Resmini). 94
Neutron-Neutron Scattering Length from Comparison of the ^{2}H(p, n)2p and ^{2}H(n, p)2n Reactions (R. J. Slobodrian, H. E. Conzett, and F. G. Resmini) 96
Proton Polarization in p-^{3}He Scattering Between 10 and 20 MeV (W. F. Tivol, D. J. Clark, H. E. Conzett, J. S. C. McKee, and R. J. Slobodrian) . . . 100
The ^{3}He(^{3}He, t)3p Reaction at 44 MeV (T. A. Tombrello and R. J. Slobodrian). 102
^{3}He-^{3}He Elastic Scattering from 18 to 80 MeV (A. D. Bacher, T. A. Tombrello, E. A. McClatchie, and F. Resmini) 104
Elastic Scattering of Polarized Protons on ^{40}Ca at 20 MeV (R. J. Slobodrian, R. de Swiniarski, W. F. Tivol, A. D. Bacher, A. Luccio, F. G. Resmini, and J. Ernst). 107
Proton-Neutron Residual Interaction in States of Configuration $(1d_{5/2})^{2}_{5+,0}$ and $(1g_{9/2})^{2}_{9+,0}$ (C. C. Lu, M. S. Zisman, and B. G. Harvey) 109
Production of the 3+ Unnatural-Parity State in ^{24}Mg by Inelastic α Scattering (M. F. Reed, D. L. Hendrie, B. G. Harvey, and N. K. Glendenning) 113
Excitation of Single Neutron-Hole States in ^{207}Pb by Inelastic Proton Scattering at 20.2 MeV (C. Glashausser, B. G. Harvey, D. L. Hendrie, J. Mahoney, E. A. McClatchie, and J. Saudinos). 118
Study of the Proton Particle-Hole States in ^{208}Pb (E. A. McClatchie, C. Glashausser, and D. L. Hendrie) 121
Energy Levels in ^{205}Tl (C. Glashausser, D. L. Hendrie, and E. A. McClatchie) 125
Excitation Functions and Angular Distributions of α Particles Scattered from ^{24}Mg (J. R. Meriwether, C. Glashausser, D. L. Hendrie, J. Mahoney, E. A. McClatchie, and J. Sherman) 128
Spin-Flip Probabilities on ^{54}Fe and ^{56}Fe (C. Glashausser, D. L. Hendrie, J. Moss, and J. Thirion). 129

NUCLEAR THEORY

Role of Inelastic Processes in (p, t) Reactions on Vibrational-Like Nuclei (R. J. Ascuitto and Norman K. Glendenning) 133
Inelastic Scattering from Strongly Deformed Nuclei (Norman K. Glendening and Raymond S. Mackintosh). 135
Calculations of the Asymmetry in the Inelastic Scattering of 20.3-MeV Protons (C. Glashausser and R. de Swiniarski) 137
Realistic Nuclear Single-Particle Hamiltonians and the Proton Shell 114 (Heiner Meldner). 140
Shell and Pairing Effects in the Fission Probability (L. G. Moretto, R. C. Gatti, S. G. Thompson, and J. T. Routti) 143
Nuclear Structure and Stability of Heavy and Superheavy Nuclei (S. G. Nilsson) 148
Stability of Superheavy Nuclei and Their Possible Occurrence in Nature (S. G. Nilsson, S. G. Thompson, and C. F. Tsang) 150
S-Wave Shape-Dependent Scattering Parameters of the Proton-Proton Interaction (R. J. Slobodrian) 151
Collective States in a Pairing-Plus-Quadrupole Model Using Wood-Saxon Representation. I. Derivation of the Quadrupole Force from a Wood-Saxon Potential (B. Sørensen and K. Kumar) 153
Boson Description of Fermion Systems: Numerical Calculations (Bent Sørensen) 155

Neutron Pairing States in Doubly Even Nuclei (Bent Sørensen) 159
Comment on the $^{10}B(t,p)$ Reaction to the ^{12}B Ground State (Bent Sørensen) . . . 163
Energy Spectrum of ^{20}Ne Using Hartree-Fock and Tamm-Dancoff Wave Functions (S. N. Tewari) 165

FISSION
Angular Distribution of Prompt γ Rays Emitted in ^{252}Cf Spontaneous Fission (E. Cheifetz, H. R. Bowman, and S. G. Thompson) 168
K x-Ray Measurements on Short-Lived Fission Products (J. B. Wilhelmy, S. G. Thompson, and J. O. Rasmussen) 170
Electron- and Bremsstrahlung-Induced Fission of Heavy and Medium-Heavy Nuclei (L. G. Moretto, R. C. Gatti, S. G. Thompson, J. T. Routti, J. H. Heisenberg, L. M. Middleman, M. R. Yearian, and R. Hofstadter) 174
Pairing Effects at the Fission Saddle Point of ^{210}Po and ^{211}Po (L. G. Moretto, R. C. Gatti, S. G. Thompson, J. R. Huizenga, and J. O. Rasmussen) 178

II. CHEMICAL AND ATOMIC PHYSICS

ATOMIC AND MOLECULAR SPECTROSCOPY
Atomic Beam Measurement of Isotope Shifts in the D_1 Line of ^{127}Cs, ^{129}Cs, ^{133}Cs, ^{134m}Cs, ^{134}Cs, and ^{137}Cs (Richard Marrus, Edmond C. Wang, and Joseph Yellin) 183
Atomic Beam Study of the $^{85-87}Rb$ Isotope Shift (Tuan H. Duong, Richard Marrus, and Joseph Yellin) 189
Electric Polarizabilities of the 4^2P Level of Potassium (Richard Marrus and Joseph Yellin) 190
Atomic Energy Levels in Berkelium II and Einsteinium II (John G. Conway and Earl F. Worden) 193
Term Analysis of DyI and DyII (John G. Conway and Earl F. Worden) 193
Zeeman Effect on Phosphorescent Lifetime of Matrix-Isolated SO_2 (John G. Conway, B. Meyer, J. J. Smith, and L. J. Williamson) 193
Energy Level Calculations for Nd^{+++} in $LaCl_3$ (Rolf Mehlhorn) 194
Electron Paramagnetic Resonance of Pu^{3+} in Cubic Symmetry Sites in CaF_2, SrF_2, and BaF_2 (N. Edelstein, H. F. Mollet, W. C. Easley, and R. J. Mehlhorn) 195
Solution Absorption Spectrum of Es^{3+} (D. K. Fujita, B. B. Cunningham, T. C. Parsons, and J. R. Peterson) 198
Radio-Frequency Stark Spectra and Dipole Moment of BaS (C. A. Melendres, A. J. Hebert, and K. Street, Jr.) 200
Dipole Moments of the Alkali Halides (A. J. Hebert, T. L. Story, Jr., and K. Street, Jr.) 201
Nuclear Quadrupole Ratio of Bromine Isotopes in Molecular LiBr (A. J. Hebert and K. Street, Jr.) 203
Experimental Study of Strontium and Lanthanum on Tungsten (F. L. Reynolds) 204
Metastable Ions in the Mass Spectra of N_2 and NO (Amos S. Newton and A. F. Sciamanna) 207
Metastable Species Produced by Electron Excitation of N_2, H_2, N_2O, and CO_2 (R. Clampitt and Amos S. Newton) 214

HYPERFINE INTERACTIONS
Spatial Asymmetry of Internal Bremsstrahlung Photons from Polarized ^{119}Sb (W. D. Brewer and D. A. Shirley) 218
Magnetic Resonance in Oriented ^{125}Sb (J. A. Barclay, W. D. Brewer, E. Matthias, and D. A. Shirley) 221
Low-Temperature Departures from the Korringa Approximation (W. D. Brewer, D. A. Shirley, and J. E. Templeton) 224
Nuclear Orientation of ^{241}Am, ^{253}Es, and ^{255}Fm in Neodymium Ethylsulfate (A. J. Soinski, N. J. Stone, and D. A. Shirley) 227
Nuclear Orientation Studies in the Region $140 < A < 150$ (D. A. Shirley, P. H. Barrett, J. Blok, and Morton Kaplan) 231

Temperature-Dependent Magnetic Hyperfine Interaction of Rhodium Nuclei in Paramagnetic Nickel (S. S. Rosenblum and D. A. Shirley) 233
Localized Moments on Rhodium in Rh-Pd Alloys (G. N. Rao, E. Matthias, and D. A. Shirley) 237
Mössbauer Resonance Study of Gold Compounds (M. O. Faltens and D. A. Shirley) 241
Theory of the Influence of the Environment on the Angular Distribution of Nuclear Radiation (Helmut Gabriel) 245

PHOTOELECTRON SPECTROSCOPY
Transition Metal Studies Using x-Ray Photoelectron Spectroscopy (C. S. Fadley and D. A. Shirley) 247
Spectroscopy of Inner Atomic Levels: Electric-Field Splitting of Core $p_{3/2}$ Levels in Heavy Atoms (T. Novakov and J. M. Hollander) 249
Photoelectron Spectroscopy of Nitrogen Compounds (D. N. Hendrickson, J. M. Hollander, and W. L. Jolly) 251
Photoelectron Spectroscopy of Phosphorus Compounds (D. N. Hendrickson, J. M. Hollander, W. L. Jolly, and M. L. Pelavin) 253

III. PHYSICAL, INORGANIC, AND ANALYTICAL CHEMISTRY

X-RAY CRYSTALLOGRAPHY
Crystal Structures and Lattice Parameters of Einsteinium Trichloride and Einsteinium Oxychloride (D. K. Fujita, B. B. Cunningham, and T. C. Parsons) 255
Crystal Structure of $[Xe_2F_3]^+ [AsF_6]^-$ (Neil Bartlett, F. O. Sladky, B. G. DeBoer, and Allan Zalkin) 256
Crystal and Molecular Structure of Phosphorus Trifluoride–Tris(difluoroboryl)-borane, $B_4F_6PF_3$ (Barry G. DeBoer, Allan Zalkin, and David H. Templeton) 258
Crystal Structure of a Brominated Carborane–Metal Sandwich Compound, $N(CH_3)_4 [(B_9C_2H_8Br_3)_2Co]$ (Barry G. DeBoer, Allan Zalkin, and David H. Templeton) 260
Crystal Structure of $[Ni_2Cl_3(C_7H_6N_2)_8] Cl \cdot 4(CH_3)_2CO$ (Michael G. B. Drew, David H. Templeton, and Allan Zalkin) 262
Crystal and Molecular Structure of Hexaaquoaluminum Hexachlororuthenate Tetrahydrate (Ted E. Hopkins, Allan Zalkin, David H. Templeton, and Martyn G. Adamson) 265
Crystal and Molecular Structure of Tetra-n-butylammonium Tribromo-(quinoline)nickelate(II), $[(n\text{-}C_4H_9)_4N] [Ni(C_9H_7N)Br_3]$ (William DeW. Horrocks, Jr., David H. Templeton, and Allan Zalkin) 267
Crystal and Molecular Structure of Tetraphenylarsonium Triiodo(triphenlyphosphine)nickelate(II), $[(C_6H_5)_4As] [Ni(C_6H_5)_3PI_3]$ (Ronald P. Taylor, David H. Templeton, Allan Zalkin, and William DeW. Horrocks, Jr.) 269
Crystal Structure of Trimethyl Platinum Hydroxide (Thomas G. Spiro, David H. Templeton, and Allan Zalkin) 273
Crystal Structure of a Hexanuclear Basic Lead(II) Perchlorate Hydrate, $Pb_6O(OH)_6(ClO_4)_4 \cdot H_2O$ (Thomas G. Spiro, David H. Templeton, and Allan Zalkin) 275

PHYSICAL AND INORGANIC CHEMISTRY
Search for Element 110 (S. G. Thompson, R. C. Gatti, L. G. Moretto, H. R. Bowman, and M. C. Michel) 277
Search for Element 114 (S. G. Thompson, W. J. Swiatecki, R. C. Gatti, H. R. Bowman, L. G. Moretto, R. C. Jared, and R. M. Latimer) 283
Amalgamation Behavior of Heavy Elements. 4. The Tracer Chemistry of Divalent Mendelevium (Jaromír Malý) 284
Nobelium: Tracer Chemistry of the Divalent and Trivalent Ions (Jaromír Malý, Torbjorn Sikkeland, Robert Silva, and Albert Ghiorso) 295
Determination of the No(II)–No(III) Potential from Tracer Experiments (R. J. Silva, T. Sikkeland, M. Nurmia, A. Ghiorso, and E. K. Hulet) . . . 297
Tracer Chemistry of Lawrencium (Robert Silva, Matti Nurmia, Torbjorn Sikkeland, and Albert Ghiorso) 299

Preparation and Crystal Structures of Dicesium Berkelium Hexachloride and Dicesium Sodium Berkelium Hexachloride (L. R. Morss and J. Fuger) 300
Preparation and Crystal Structures of Some Cubic Chlorocomplex Compounds of Trivalent Metals (L. R. Morss, N. Edelstein, and M. Siegal) 302
Oxidation States of U in CaF_2 (R. McLaughlin, N. Edelstein, U. Abed, and E. Huffman) 305
Extraction of $HReO_4$ by Trioctyl Phosphine Oxide in Nitrobenzene and in 1,2-Dichloroethane (J. J. Bucher, T. J. Conocchioli, and R. M. Diamond) 307
Extraction of HBr and HCl by Dilute Solutions of Trioctyl Phosphine Oxide in Nitrobenzene and in 1,2-Dichloroethane and Hydration of Br^- and Cl^- in These Diluents (J. J. Bucher, E. R. Held, J. A. Labinger, B. A. Sudbury, and R. M. Diamond) 310

RADIATION CHEMISTRY
Radiation Chemistry of the α-Amino Acids: γ Radiolysis of Solid Cysteine (Donald B. Peterson, John Holian, and Warren M. Garrison) 313
On the Radiation-Induced Reduction of Amide and Peptide Functions in Aquo-Organic Systems (John Holian and Warren M. Garrison) 316
Ionization and Excitation in Peptide Radiolysis (Warren M. Garrison, Michael E. Jayko, Michael A. J. Rogers, Harvey A. Sokol, and Winifred Bennett-Corniea) 318

CHEMICAL ENGINEERING
Liquid Mixing in Rectangular Vessels (Thomas D. Coughlen and Theodore Vermeulen) 322
Oscillating-Jet Measurement of Dynamic Liquid-Liquid Interfacial Tension (Sugihiko Tada and Theodore Vermeulen) 323
Development of a Jet-Mixed Extraction Column (Daniel R. Kahn and Theodore Vermeulen) 325
Improved Methods for Contacting Fluid Phases in Separation Processes (Edward J. Palkot, Jr., and C. Judson King) 326
Growth of Streptococcus faecalus in Dense Culture (L. D. Sortland and C. R. Wilke) 327

IV. INSTRUMENTATION AND SYSTEMS DEVELOPMENT

ELECTRONIC INSTRUMENTATION AND SEMICONDUCTOR DEVICES
Hypercryogenic Detector--FET Unit--Core of High-Resolution Spectrometer (Emanuel Elad and Michiyuki Nakamura) 331
Development of a Germanium Counter System for Charged-Particle Nuclear Spectroscopy (E. A. McClatchie, M. S. Zisman, A. D. Bacher, C. Glashausser, R. H. Pehl, E. Rivet, and F. S. Goulding) 332
Germanium Detector System Development (R. H. Pehl, F. S. Goulding, W. L. Hansen, E. Rivet, J. T. Walton, D. F. Malone, R. C. Cordi, R. C. Davis, and G. I. Saucedo) 335
Method for Copper-Staining Germanium Crystals (Ernest J. Rivet) 335
Computer Control System for the Field-Free Spectrometer (Ron Zane, R. L. LaPierre, and Joseph E. Katz) 337
Control Unit for Linking Pulse-Height Analyzers to a PDP-9 Computer (Richard L. LaPierre) 338
Special-Purpose Computer for Linking Pulse-Height Analyzers With a Digital Incremental Plotter (Richard L. LaPierre and Michiyuki Nakamura) 339
On-Line PDP-9 Computer for Fission Research (Craig A. Denison, James B. Hunter, Richard C. Jared, Richard L. LaPierre, Michiyuki Nakamura, and Elizabeth Quigg) 340
Pulse-Height Compensation System for Ge(Li) Timing (J. M. Jaklevic, F. M. Bernthal, J. O. Radeloff, and D. A. Landis) 341

GENERAL INSTRUMENTATION AND DEVELOPMENT
Waist-to-Waist Transport in Thin-Lens Optics (A. U. Luccio) 343
88-Inch Cyclotron Development (D. J. Clark, J. Ernst, A. U. Luccio, and F. Resmini) 345

Polarized Ion Source for the 88-Inch Cyclotron (A. U. Luccio and D. J. Clark) . . . 352
New Beam-Analysis System Installed at the 88-Inch Cyclotron (B. G. Harvey, E. A. McClatchie, F. G. Resmini, W. S. Flood, R. E. Hintz, and F. B. Selph) . . . 355
Cascade Isotope Separator (M. C. Michel and F. L. Reynolds) . . . 359
Particle Identification of the Elements up to Argon Produced by the Interaction of 5-GeV Protons with Uranium (A. M. Poskanzer, E. K. Hyde, and G. W. Butler) . . . 362
Slit Scattering Effects With 50-MeV α Particles and 20-MeV Protons (F. Resmini, A. D. Bacher, D. J. Clark, E. A. McClatchie, and R. De Swiniarski) . . . 363
Radioisotope Source-Target Assembly for x-Ray Spectrometry (Robert D. Giauque) . . . 366
Uniquely Determined Metastable Ions by Ion Accelerator Decoupling (C. W. Koch) . . . 369
Differentially Pumped Vacuum Probe Using Cryogenic and Ion Pumping (R. H. Escobales, C. E. Miner, R. M. Reimers, and M. C. Michel) . . . 372
Simple Method for Determining Waist-to-Waist Transfer Properties of Quadrupole Doublets and Triplets (F. Resmini) . . . 376
Rotating Vacuum Seal and Anode (Herman P. Robinson) . . . 379

V. THESIS ABSTRACTS . . . 381

VI. 1968 PUBLICATIONS . . . 389

VII. AUTHOR INDEX . . . 415

I. Nuclear Structure and Nuclear Properties

NUCLEAR STRUCTURE AND NUCLEAR PROPERTIES

NUCLEAR SPECTROSCOPY STUDIES ON ^{237}Np

E. Browne and F. Asaro

The conversion electrons accompanying the alpha decay of ^{237}Np were studied by alpha-electron coincidence experiments with solid-state detectors. The conversion electrons were measured in coincidence with all the α particles, with ($\alpha_{238} + \alpha_{212}$), and with ($\alpha_{86} + \alpha_{104}$). In the last two experiments the source was mounted on the inside surface of an Al cylinder with the alpha and electron detectors facing the base of the cylinder. This experimental arrangement enabled both α particles and electrons to strike their respective detectors with reasonably high efficiency without passing through a backing plate. The full width at half maximum (FWHM) for the 200-keV electrons was 1.8 keV, and the alpha resolution was 22 keV (FWHM).

We evaluated the conversion coefficients of most of the transitions, using the electron intensities obtained from these experiments and the γ-ray intensities from our previous α-γ coincidence and γ-ray singles experiments.[1] The transition multipolarities of most of the γ rays were obtained by comparing our experimental conversion coefficients with those calculated by Sliv and Band.[2] The decay scheme of ^{233}Pa based on our experimental results is shown in Fig. 1.

We had previously made the single-particle Nilsson state[3] assignments, Ω + (N, n_z, Λ), of 3/2 + (651) and 5/2 + (642) to the rotational bands whose lowest energy states were at 86 and 238 keV respectively.[1] We now believe the state at 212 keV is probably the 5/2 member of the 1/2 + (400) Nilsson state mixed with the 1/2 + (660) state through a $\Delta N = 2$ coupling.[3] This type of interaction would be significant only in that limited region of the Nilsson diagram where the states are close together in energy. This is the case in ^{233}Pa, for which the orbits effectively cross each other at a deformation of $\delta = 0.22$. The states at 201.8 and 279 keV are probably the 3/2 and 7/2 members of the same rotational band. The low hindrance factors of the alpha groups that populate the members of the 3/2 + (651) rotational band, as well as the 5/2 and 7/2 members of the 1/2 + (400) "mixed" band, could be explained by a Coriolis coupling of these bands with the favored band. The Coriolis coupling of the 1/2 + (400) "mixed" band with the favored band is due to the admixture of the 1/2 + (660) state in the 1/2 + (400) level. This coupling introduces large admixtures of the favored rotational band in the wave functions of the states mentioned above, leading to relatively strong alpha transitions populating these levels.

We performed calculations which included both Coriolis and $\Delta N = 2$ interactions in order to obtain the energies as well as the admixtures of the perturbed states. The secular equations for each spin were solved by using a computer program written by Thomas P. Clements of this Laboratory. This program solved the secular determinants for all the I values involved, simultaneously adjusting all the parameters until a least-squares fit to the experimental levels was made. We used 10 parameters in our calculations, including the matrix element of the $\Delta N = 2$ interaction. The best least-squares fit was obtained with a value of -37 keV for the $\Delta N = 2$ interaction matrix element. This value is of the same order of magnitude as that calculated for A = 160 by Andersen.[4] The following admixtures of the 5/2 + (642) band were obtained in the members of the 3/2 + (651) and 1/2 + (400) bands:

State energy (keV)	I	K	$a^2_{K=5/2}$ (%)
86.6	5/2	3/2	26
103.7	7/2	3/2	39
107.8	9/2	3/2	29
212.3	5/2	1/2	36
279	7/2	1/2	3

Because of the large number of parameters in our calculations, the excellent agreement between calculated and experimental energies could have been fortuitous. As a check on the quality of our final wave functions we evaluated the γ-ray transition probability ratios expected from these values. As seen in Table I, the ratios for unmixed Nilsson wave functions (column 4) differ considerably from the experimental values, in some cases about an order of magnitude. With our final "mixed" wave functions, the theoretical results were consistent with the experimental values.

References

1. E. Browne and F. Asaro, in Nuclear Chemistry Annual Report, 1967, UCRL-17989, Jan. 1968, p. 1.
2. L. A. Sliv and I. M. Band, Tables of Conversion Coefficients are given in the book, Alpha, Beta and Gamma-Ray Spectroscopy, Vol. 2, Ed. by Kai Siegbahn (North-Holland Publishing Co., Amsterdam, 1965), p. 1939.
3. S. G. Nilsson, Kgl. Danske Videnskab. Selskab, Mat.-Fys. Medd 29, No. 16 (1955).
4. B. L. Andersen, Nucl. Phys. A112, 443 (1968).

Table I. Reduced M1 Gamma Transition Probability Ratios in the Alpha Decay of Np^{237}.

	$K_i \to K_f$	$I_i \to I_f, I_f'$	$\frac{\lvert\langle\rangle\rvert^2}{\lvert\langle\rangle\rvert^2}$	Theoretical[a] value	Experimental value
$\frac{B_{143.3}}{B_{151.4}}$	$\frac{5}{2} \to \frac{3}{2}$	$\frac{5}{2} \to \frac{3}{2}, \frac{5}{2}$	2.33	2.8	2.8 ± 0.4
$\frac{B_{143.3}}{B_{134.3}}$	$\frac{5}{2} \to \frac{3}{2}$	$\frac{5}{2} \to \frac{3}{2}, \frac{7}{2}$	14.0	6.5	5 ± 2
$\frac{B_{117.6}}{B_{125.5}}$	$\frac{1}{2} \to \frac{3}{2}$	$\frac{5}{2} \to \frac{3}{2}, \frac{5}{2}$	0.15	32	$\geq \sim 30$
$\frac{B_{117.6}}{B_{108}}$	$\frac{1}{2} \to \frac{3}{2}$	$\frac{5}{2} \to \frac{3}{2}, \frac{7}{2}$	0.14	1.1	~ 1.3
$\frac{B_{214.0}}{B_{197}}$	$\frac{5}{2} \to \frac{3}{2}$	$\frac{7}{2} \to \frac{5}{2}, \frac{7}{2}$	1.4	1.8	1.9 ± 0.6
$\frac{B_{214.0}}{B_{193.0}}$	$\frac{5}{2} \to \frac{3}{2}$	$\frac{7}{2} \to \frac{5}{2}, \frac{9}{2}$	6.43	3.4	
$\frac{B_{197}}{B_{193.0}}$	$\frac{5}{2} \to \frac{3}{2}$	$\frac{7}{2} \to \frac{7}{2}, \frac{9}{2}$	4.57	1.9	1.7 ± 0.4[b]

[a] This value was obtained by taking into account the mixing of the rotational bands.

[b] $B_{193.0}$ used in this column was obtained from the theoretical ratio $(B_{214.0})/(B_{193.0}) = 3.4$ and the experimental value of $B_{214.0}$.

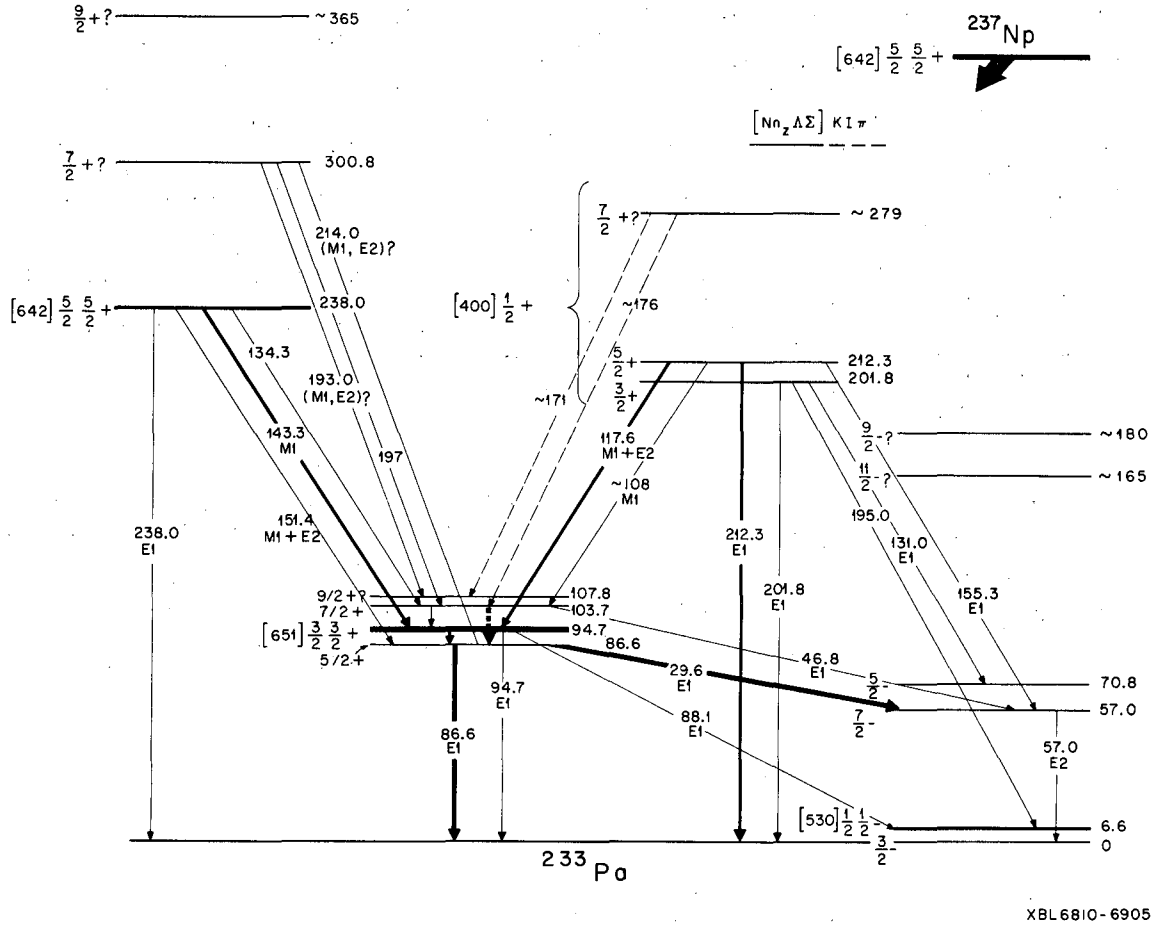

Fig. 1. Alpha decay scheme of ^{237}Np.

ALPHA DECAY OF ^{238}Pu

C. M. Lederer, F. Asaro, and I. Perlman

Alpha branches as weak as 10^{-6}% can be measured by coincidence techniques.[1,2] Due to the strong energy dependence of the α-decay process, even this high sensitivity is sufficient to observe only the lowest and least hindered intrinsic states in even-even nuclei. Simple γ-spectral measurements on strong sources are potentially more sensitive, but are subject to many difficulties: samples must be exceedingly clean, nuclear reactions of the α particles on the source and surrounding materials can give rise to spurious γ rays,[1] and spontaneous fission gives rise to complex γ spectra which place the ultimate limit on sensitivity for many isotopes. We have used a simple new technique in an attempt to solve the first two of these difficulties, and thereby succeeded in the observation of α branches from ^{238}Pu to members of five excited bands in ^{234}U.

Gamma spectra of two ^{238}Pu sources, of different origins and with different environments, were studied with a Ge(Li) spectrometer. Source I consisted of 300 mg of ^{238}Pu as the oxide in a stainless steel bottle, loaned to us from Oak Ridge. Source II was prepared from material (2.8 mg) available in this Laboratory. After chemical purification by anion exchange, it was evaporated from solution in a quartz tube attached to a stopcock and sealed under helium. This excludes atmospheric nitrogen, which would otherwise result in production of an 871-keV γ ray from the reaction ^{14}N(α, p)^{17}O*.[1]

In Table I we compare the spectra of the two sources. The intensities of low-energy transitions from source I were corrected for self-absorption by using the source II intensities for a few strong lines whose assignments are certain.

Gamma rays present in only one source, or whose intensities in the two sources are different, can be assigned to "impurities." Of the remaining γ rays, only those at 208, 238, and 305 keV do not fit between known levels or inferred rotational states of the very well-known ^{234}U level spectrum.[3-5] We believe these three lines are also due to impurities, but cannot exclude their assignment to ^{238}Pu α decay.

Table II summarizes the data obtained from both sources. The energies are recalibrated with the use of internal standards in separate measurements. Absolute intensities are obtained by normalizing to the 100- and 153-keV γ rays, whose intensities were determined by absolute α and γ counting. Considerable information can be derived from the α- and γ-branching intensities; these are discussed in a forthcoming paper.[6]

References

1. S. Bjørnholm, C. M. Lederer, F. Asaro, and I. Perlman, Phys. Rev. 130, 2000 (1963).
2. C. Michael Lederer, The Structure of Heavy Nuclei: A Study of Very Weak Alpha Branching (Ph. D. Thesis), UCRL-11028, Sept. 1963.
3. S. Bjørnholm, J. Dubois, and B. Elbek, Nucl. Phys. A118, 241 (1968).
4. S. Bjørnholm, J. Borggreen, and D. Davies, Nucl. Phys. A118, 261 (1968).
5. A. Wapstra, Nucl. Phys. A97, 641 (1967).
6. C. M. Lederer, F. Asaro, and I. Perlman, The Alpha Decay of ^{238}Pu and ^{236}Pu (in preparation).

Table I. Gamma rays from the two ^{238}Pu sources.

Source I (300 mg)		Source II (2.8 mg)	
Energy (keV)	Intensity	Energy (KeV)	Intensity
not measured		U $K\alpha_1$	315 ± 30
99.8	$[2.80 \times 10^4]$*	99.8	$(2.80 \pm 0.18) \times 10^4$
not measured		U $K_{\beta_1'}$	238 ± 55
not measured		U $K_{\beta_2'}$	74 ± 48
152.33	[3865]*	152.23	3865 ± 250
---		194.54	3 ± 1
---		196.95	22 ± 4
199.41	4.3 ± 1.0	199.62	28(grows)
200.80	[15]*	200.88	15 ± 3
---		203.80	0.7 ± 0.2
207.99	0.8 ± 0.3	207.89	0.8 ± 0.2
209.68	1.2 ± 0.3	---	
---		210.75	0.87 ± 0.15
211.65?	0.15 ± 0.10	---	
---		214.37?	0.19 ± 0.08
228.10	3.3 ± 0.3	---	
235.87	0.04 ± 0.02	236.0	0.04 ± 0.03
238.60	0.42 ± 0.05	238.50	0.61 ± 0.15
---		247.52?	0.45 ± 0.20
252.52	3.0 ± 0.2	252.55	20(grows)
258.25	0.34 ± 0.04	258.27	0.38 ± 0.10
---		263.66?	0.13 ± 0.06
277.68	4.4 ± 0.3	---	
279.90?	0.12 ± 0.07	---	
285.54	0.25 ± 0.03	---	
---		295.41	0.33 ± 0.10
299.27	0.19 ± 0.04	299.23	0.26 ± 0.10
305.54	0.45 ± 0.05	305.44	0.61 ± 0.10
312.01	0.25 ± 0.03	---	
315.97?	0.10 ± 0.06	---	
332.71	0.11 ± 0.03	---	
335.04	0.21 ± 0.03	---	
---		338.03	0.09 ± 0.05
---		344.62	0.10 ± 0.05
350.87	6.0 ± 0.4	350.72	4.9 ± 0.3
368.47?	0.08 ± 0.04	---	
375.36?	0.10 ± 0.05	---	
393.16??	0.03 ± 0.03	---	
413.63??	0.05 ± 0.03	---	

Table I. (continued)

Source I (300 mg)		Source II (2.8 mg)	
Energy (keV)	Intensity	Energy (keV)	Intensity
---		439.86	0.26 ±0.07
511 (γ±)	0.30 ±0.05	511 (γ±)	1.3 ±0.1
---		513.78	0.21 ±0.10
583.21	0.44 ±0.06	583.03	9.5 ±0.4
---		586.45?	0.26 ±0.16
589.47?	0.07 ±0.04	---	
---		609.30	0.86 ±0.10
---		669.62	0.45 ±0.09
---		672.23	0.20 ±0.08
692.12?	0.10 ±0.04	692.51	0.48 ±0.12
693.69?	0.08 ±0.04	---	
---		694.33	0.38 ±0.10
---		696.82	0.39 ±0.10
706.10	0.42 ±0.07	706.15	0.42 ±0.07
708.46	1.20 ±0.07	708.42	1.09 ±0.08
---		718.24	0.78 ±0.08
742.82	23.1 ±0.4	742.72	23.3 ±0.5
766.40	100	766.38	100
---		770.35	1.9 ±0.5
786.30	14.4 ±0.3	786.27	14.5 ±0.3
805.81	0.58 ±0.05	805.72	0.54 ±0.05
808.25	3.41 ±0.08	808.20	3.39 ±0.10
819.41	0.08 ±0.03	---	
831.36	0.06 ±0.03	---	
846.86	0.51 ±0.04	---	
851.79	5.83 ±0.17	851.70	5.70 ±0.20
865.0	0.63 ±0.15	---	
867.6	0.77 ±0.20	---	
870.76	31.2 ±1.5	870.68	1.40 ±0.08
874.82?	0.45 ±0.25	---	
880.56	0.85 ±0.08	880.52	0.58 ±0.08
883.31	3.68 ±0.10	883.24	3.37 ±0.12
---		890.60	3.34 ±0.15
904.52	0.29 ±0.03	904.33	0.32 ±0.06
---		911.18	0.60 ±0.06
911.75	0.06 ±0.03	---	
914.2?	0.02 ±0.02	---	
918.67	0.13 ±0.03	---	
924.27	0.37 ±0.04	---	

Table I. (continued)

Source I (300 mg)		Source II (2.8 mg)	
Energy (keV)	Intensity	Energy (keV)	Intensity
926.87	2.57 ± 0.06	926.72	2.45 ± 0.09
942.09	2.14 ± 0.06	941.96	2.03 ± 0.10
946.17	0.38 ± 0.05	946.00	0.46 ± 0.08
960.67	0.04 ± 0.02	---	
963.20	0.07 ± 0.02	---	
969.12	0.11 ± 0.02	969.01	0.34 ± 0.07
974.58	0.04 ± 0.02	---	
980.73	0.14 ± 0.02	---	
984.62	3.26 ± 0.10	---	
1001.21	4.39 ± 0.11	1000.92	4.40 ± 0.20
1026.11	1.18 ± 0.06	---	
1028.79	2.33 ± 0.08	---	
1042.02	0.87 ± 0.04	1041.92	0.75 ± 0.08
1085.60	0.34 ± 0.04	1085.31	0.33 ± 0.06
1115.93	0.11 ± 0.02	---	
1121.1	0.05 ± 0.02	1120.4	0.37 ± 0.06
---		1145.2	2.42 ± 0.24
---		1146.2	1.13 ± 0.15
---		1151.1	0.22 ± 0.06
---		1155.1	0.21 ± 0.07
---		1209.8	1.03 ± 0.10
---		1212.1	0.12 ± 0.06
---		1236.0	1.52 ± 0.11
---		1270.1	0.13 ± 0.07
---		1274.7	11.2 ± 0.4
1313.5	0.05 ± 0.02	---	

*The intensities of these γ rays from Source II were used to correct for self-absorption in Source I.

Table II. Best energies and intensities for γ rays assigned to ^{238}Pu α decay.

Energy (keV)	Relative intensity	$\gamma/\alpha \times 10^7$	Placement
43.50 ± 0.04[a]		3800[a]	02+ → 00+
U $K\alpha_2$	315 ± 30	10.4 ± 1.5	
99.84 ± 0.04	28000 ± 2000	920 ± 60	04+ → 02+
U $K_{\beta_1'}$	238 ± 55	7.8 ± 2.0	
U $K_{\beta_2'}$	74 ± 48	2.4 ± 1.6	
152.71 ± 0.05	3865 ± 250	127 ± 9	06+ → 04+
200.9 ± 0.2	15 ± 3	0.5 ± 0.1	08+ → 06+
235.9 ± 0.3?	0.04 ± 0.02	0.001 ± 0.0005	02+'' → 03-
258.3 ± 0.2	0.35 ± 0.05	0.011 ± 0.002	00+'' → 01-
299.2 ± 0.2	0.20 ± 0.05	0.007 ± 0.002	02+'' → 01-
706.1 ± 0.3	0.42 ± 0.06	0.014 ± 0.002	03- → 04+
708.42 ± 0.20	1.15 ± 0.09	0.038 ± 0.004	02+' → 04+
742.77 ± 0.10	23.2 ± 0.4	0.76 ± 0.07	01- → 02+
766.39 ± 0.10	100	3.3 ± 0.3	00+' → 02+
786.30 ± 0.10	14.5 ± 0.3	0.48 ± 0.04	01- → 00+
805.8 ± 0.3	0.56 ± 0.06	0.018 ± 0.002	03- → 02+
808.25 ± 0.15	3.40 ± 0.08	0.11 ± 0.01	02+' → 02+
851.70 ± 0.10	5.79 ± 0.20	0.19 ± 0.02	02+' → 00+
880.5 ± 0.3	0.7 ± 0.2	0.023 ± 0.003	23- → 04+(?)
883.23 ± 0.10	3.43 ± 0.15[b]	0.11 ± 0.01	22+ → 02+
904.37 ± 0.15	0.30 ± 0.04	0.010 ± 0.002	04+' → 02+
926.72 ± 0.15	2.53 ± 0.10	0.083 ± 0.008	22+ → 00+
941.9 ± 0.2	2.06 ± 0.09[b]	0.067 ± 0.007	02+'' → 04+
946.0 ± 0.3	0.40 ± 0.06	0.013 ± 0.002	22- → 02+
1001.03 ± 0.15	4.39 ± 0.14	0.14 ± 0.02	00+'' → 02+
1041.8 ± 0.3	0.84 ± 0.07	0.028 ± 0.003	02+'' → 02+
1085.4 ± 0.3	0.34 ± 0.04	0.011 ± 0.002	02+'' → 00+

a. The energy and intensity of this transition are taken from the literature.

b. The intensities of these lines from source I were corrected for small contributions from ^{238}Np γ rays.

TABLE OF ISOTOPES

J. M. Hollander and C. M. Lederer

The sixth edition of the Table of Isotopes, a compilation of radiation and level-scheme information on radioisotopes, was published in 1967. Planning has recently begun for the seventh edition of the Table, and we summarize here some of the new aspects of this compilation effort.

The major problem encountered today in the nuclear data compilation field is a result of the so-called "data explosion"; data are being produced at a rate that challenges our ability to assimilate them. We are making an effort to come to grips with this problem as it relates to nuclear data compilation.

The sixth edition of the Table, as the preceding ones, was produced in the "traditional" way, that is, all operations--including the abstracting of data, drawing of level schemes, and preparing of master data sheets--were done by hand. A disproportionate amount of time was consumed by this type of hand work, and it was additionally wasteful because of the multiple proofreading operations that necessarily had to accompany the copying and recopying of information. A major goal in producing further editions of the Table is to eliminate such wasteful expenditures of compilers' time on mechanical operations, so that the time can be better spent where it is vitally needed, on the analysis of data.

We are developing a new mechanics of compiling that centers around digital data files (magnetic tapes) containing all references, data, and level schemes, and involving also associated computer methods for creating, editing and updating these files. Future editions of the Table of Isotopes will be produced directly from these files, thereby eliminating most of the repetitious and time-consuming hand operations that have been unavoidable in the past. Benefits of this new approach will include (a) dramatic reduction of the time between literature cutoff and publication dates, (b) the production of new editions more frequently, and (c) the possibility of producing a variety of secondary compilations (i. e., a table of γ rays in order of energy from neutron-capture-induced activities) with little additional effort.

We emphasize our intent to computerize the mechanical aspects of compiling and not the intellectual aspects. On the contrary, by minimizing wasted effort in mechanical operations by the compiler, the use of computers can enhance his ability to serve his primary goal of accurate and speedy data recording and analysis. Computerization will in fact promote better and more efficient use of both scientific manpower and support effort.

The first step in computerizing a nuclear data compilation is to develop appropriate input and editing systems, which do not now exist. We regard the use of abstract symbolisms in input operations (presently required in key-punch devices) as antithetical to the goal of accuracy, so we have developed an expanded character input device (shown in Fig. 1) which will accommodate on its keyboard all the symbols of nuclear physics, plus provisions for variations in language, font, etc. Although this device is now operational as a card punch, we are working toward conversion to a direct input-to-tape device with simultaneous CRT display, for ease in proofreading, editing, and updating. Examples of how textual proofreading material from the Table will appear on the CRT display (or photorepro therefrom) are shown in Fig. 2. Level schemes, too, can be generated graphically by computer and displayed on CRT, or plotted, for proof checking: Fig. 3 is an example of a computer-plotted level scheme.

For final output and publication, much finer-resolution devices, such as photocomposers, will be used. Work is in progress on the development of programs for outputting textual and graphical material on these devices.

Further details of the Table of Isotopes program, including flow diagrams and descriptions of the compiling process, are given in UCRL-18530, from which this report was abstracted.

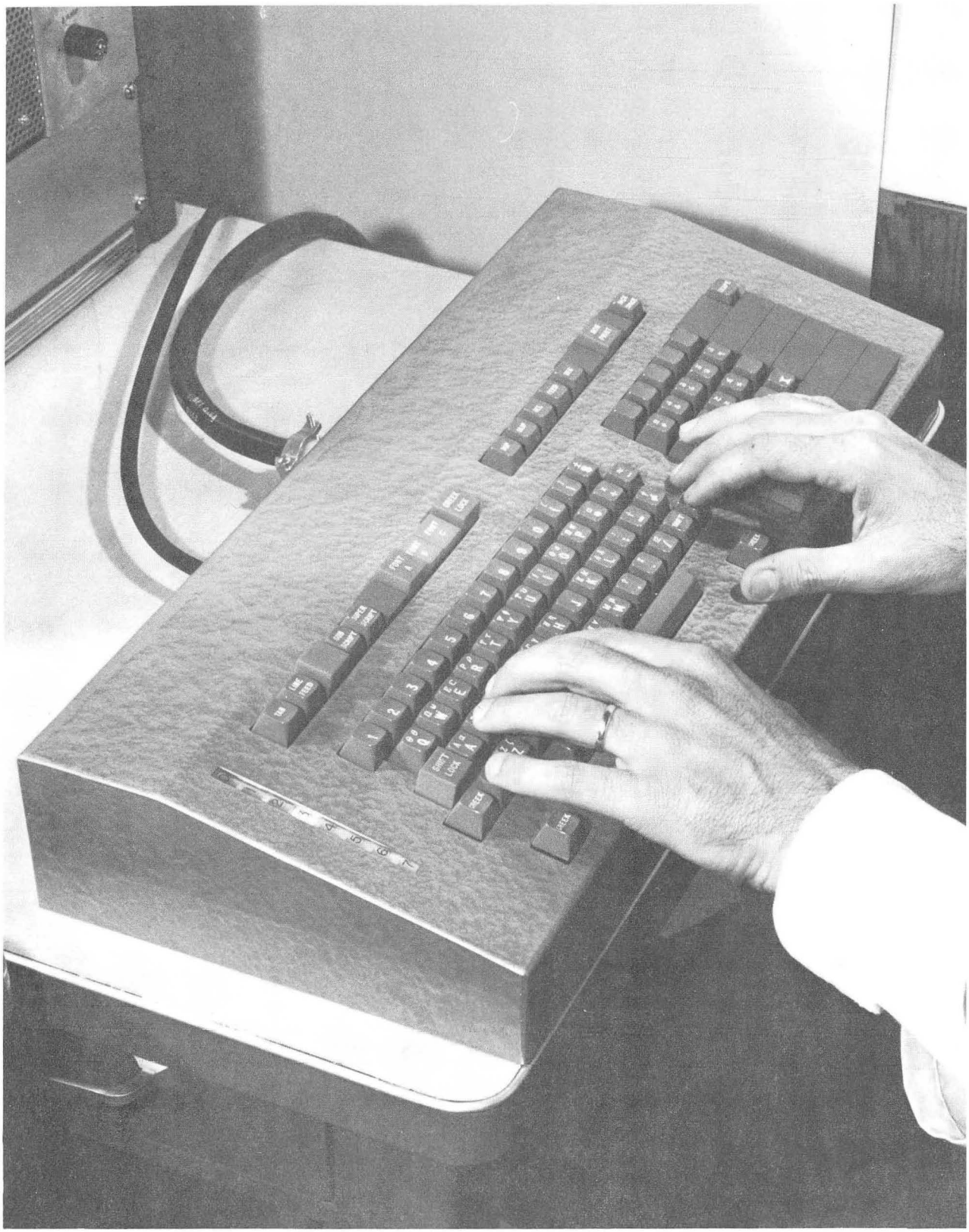

Fig. 1. The expanded character keyboard for inputting data into Table of Isotopes files.

XBB 6810-6032

EC 43%, β^- 38%, β^+ 19%
(NDS)
$(\beta^+ + EC)/\beta^-$ 1.6
(ReynJH50)
Δ −65.428 (MTW)

% 30.9 (BrowHS47)
Δ −67.27 (MTW)
σ_e 2.3 (GoldmDT64)

β^- (AmaE35)
Δ −66.26 (MTW)
σ_e 130 (GoldmDT64)

β^- (GoeR49)
Δ −67.29 (MTW)

β^- (FlaA53a)
Δ −65.4 (MTW)

[EC,β^+] (LindnL55a)

β^+, [EC] (CumJ55, LindnL55a, CumJ59),
Δ −56.6 (MTW)

XBL 6811-6177

Re^{186} (90 h):
I: 1, μ: +**1.728** atomic beam (ArmL65)
β^-: **1.071** (†77), **0.933** (†23) mag spect, $\beta\gamma$ coinc (PortF56)
others (MalyL64, JohnM56, StefR51, MetF51, CranP49a, LangeL49, BeacL49a, BashE63a)
γ with β^-: γ_2 **0.13716** cryst spect (MarkI63)
γ_2 **0.1372** ($\dagger_\gamma$100, e_K/γ 0.44, $K/L_{I+II}/L_{III}$ 91/100/58), γ_3 **0.632**($\dagger_\gamma$0.37), γ_4 **0.768** ($\dagger_\gamma$0.41) mag spect, mag spect conv, scint spect (MalyL64)
γ_2 (L_I/L_{III} 1.24) mag spect conv (SwanJ53,SwanJ53b)
γ with EC: γ_1 **0.1227** ($\dagger_\gamma/\dagger_\gamma(\gamma_2)$ 0.073, e_K/γ 0.53, $K/L_{I+II}/L_{III}$ 91/100/76) mag spect, mag spect conv, scint spect (MalyL64)
others (RiceM55, PortF56, JohnM56, NielK58, ENesM63a, StefR51, MetF51, AjzF56, AntoN53, ThosB64)
$\gamma\gamma(0)$: (LindqT57d, KinW59, BodE61a, LerjC61, VervJ63)
$\beta\gamma(0)$: (DulH63, NoveT56)
$\beta\gamma$ polariz(0): (DelM61, DeuJ60)
Isomeric level of Re^{186}: $t_{\frac{1}{2}}$ 7.0×10^{-5} s delay coinc (BranK64)

prod: $Re^{187}(\gamma,n)$ γ: K X-rays ($\dagger_\gamma$80), **0.10** ($\dagger_\gamma$1), **0.13** ($\dagger_\gamma$1) scint spect (BranK64)

XBL 6811-6178

Fig. 2. Computer-generated CRT displays of sections from the 6th edition of the Table of Isotopes.

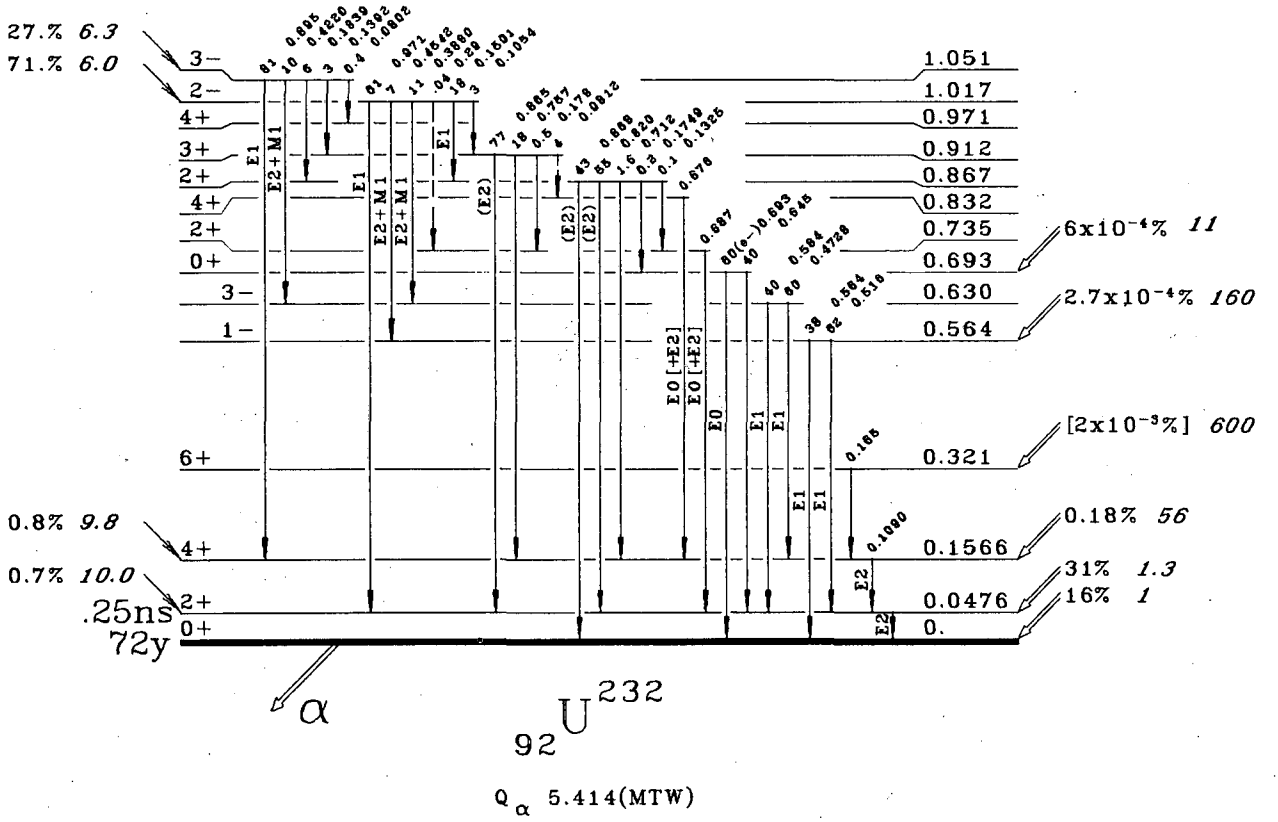

Fig. 3. Computer-drawn level scheme as would be used for proofreading and editing purposes.

STUDY OF LEVELS IN ^{92}Mo AND ^{94}Ru BY IN-BEAM γ-RAY SPECTROSCOPY†

J. M. Jaklevic, C. M. Lederer, and J. M. Hollander

The excited states of ^{92}Mo and ^{94}Ru populated in $(\alpha, 2n)$ reactions have been studied by in-beam γ-ray spectroscopic techniques. The study was performed by using Ge(Li) detectors to observe the γ rays emitted from isotopically enriched targets of ^{90}Zr and ^{92}Mo bombarded with 30-MeV α particles at the Berkeley 88-inch sector-focused cyclotron. Preliminary measurements consisted of in-beam single γ-ray spectra and two-parameter data of γ-ray energy vs time. In these latter measurements the time distributions of γ rays relative to the preceding beam pulse are observed in order to measure the lifetimes of isomeric states.[1] For 30-MeV α particles at this cyclotron, natural beam bunching produces pulses of ≈ 4 nsec width at intervals of 163 nsec. These parameters plus the instrumental time resolution of the Ge(Li) detectors impose a practical limit upon the range of half-life measurements by this technique of 2 nsec $\leq \tau_{1/2} \leq$ 500 nsec.

Figure 1 shows the level schemes for ^{92}Mo and ^{94}Ru based on the results of this work. The ordering of the levels in the decay chain is based on considerations of intensity balance. Additional data obtained with two Ge(Li) detectors in coincidence unambiguously support the level assignments for both isotopes.

The spin assignments are based on angular distributions of the γ rays relative to the beam direction.[2] Measurements of these distributions together with additional information concerning the presence or absence of cross-over transitions support the spin and multipolarity assignment indicated.[3]

The half-life of the 8^+ to 6^+ in ^{92}Mo transition and the energies of levels through the 2761-keV state are in agreement with previous results.[4] The positive-parity states can be described as simple $(g_{9/2})^2$ excitations. The spin 5 state has been tentatively assigned negative parity by comparison with a similar sequence in ^{90}Zr.

This investigation discloses the existence of new levels, which appear from their simple pattern of deexcitation to constitute a "band" of related states, based on the 5- level. The probable $(p_{1/2})_\pi (g_{9/2})_\pi$ configuration of this state and the spin 11 of the highest member suggest the four-proton configuration $(p_{1/2})(g_{9/2})^3$. The transition probability of the 11- → 9- E2 γ ray, 1.5 single-particle units, lends support to the interpretation of these levels as arising from the same configuration.

In ^{94}Ru we fail to find an isomer analogous to the 4487-keV 11- state of ^{92}Mo. The 3655- and 4346-keV levels are probably of similar structure to the 7- and 9- levels of ^{92}Mo. Angular distribution measurements are consistent with these assignments although the large observed asymmetries for the 691- and 1033-keV transitions allow other possible assignments. However, the transitions which follow them are prompt ($t_{1/2} < 2$ nsec), and we do not observe any strong transitions feeding the 4346-keV level. This may be related to the appearance of a second 9- level below the 11- level, or the greater spacing between the 11- and 9- levels in the calculated level scheme.[5]

In the positive parity band of ^{94}Ru we note that the transitions are greatly retarded relative to ^{92}Mo. This trend is to be expected as one adds more particles to the $g_{9/2}$ level. The half-life of 74 ± 7 nsec for the 6^+ state, measured by delayed γ-γ coincidence and confirmed by analysis of the complex decay curve of the 311-keV γ ray with respect to the beam pulses, is in reasonable agreement with the calculated value of 29 nsec.[5] However, the apparent half-life of the 8^+ state, 71 ± 5 μsec, is larger than predicted by a factor of ~20. This is especially surprising, since the half-lives of the 8^+ and 6^+ levels should be simply related by a common effective quadrupole moment for the $g_{9/2}$ proton. This half-life is measured by studying the decay curves of the 145- and 311-keV transitions in the microsecond pulsed beam at the heavy-ion linear accelerator. We have considered the possibility that a 71-μsec isomeric transition precedes the $8^+ \rightarrow 6^+$ transition, but there is no evidence for such a transition.

The closed 50-neutron shell and the assumed simple proton structure of the observed states, involving only two orbitals, provide a simple model for theoretical calculations. Figure 2 shows a comparison of the observed level scheme with the relevant theoretical states as calculated by assuming the above-mentioned orbital configuration.[5] In addition to the obvious agreement between the observed levels and the calculated states, the order of the calculated level also explains the failure to observe even-spin members of the $(p_{1/2})(g_{9/2})^3$ configuration.

Footnote and References

†Condensed from UCRL-18274, Dec. 1968; submitted to Physics Letters.

1. T. Yamazaki and G. T. Ewan, Nucl. Instr. Methods 62, 101 (1968).
2. J. O. Newton, F. S. Stephens, R. M. Diamond, R. Kotajima, and E. Matthias, Nucl. Phys. A95, 357 (1967).
3. T. Yamazaki, Nuclear Data A3, 1 (1967).
4. C. M. Lederer, J. M. Hollander, and I. Perlman, Table of Isotopes (John Wiley and Sons, New York, 1967).
5. J. B. Ball, J. B. McGrory, R. L. Auble, and K. H. Bhatt, Calculated Energy Levels for ^{92}Mo and ^{94}Ru, Phys. Letters (to be published).

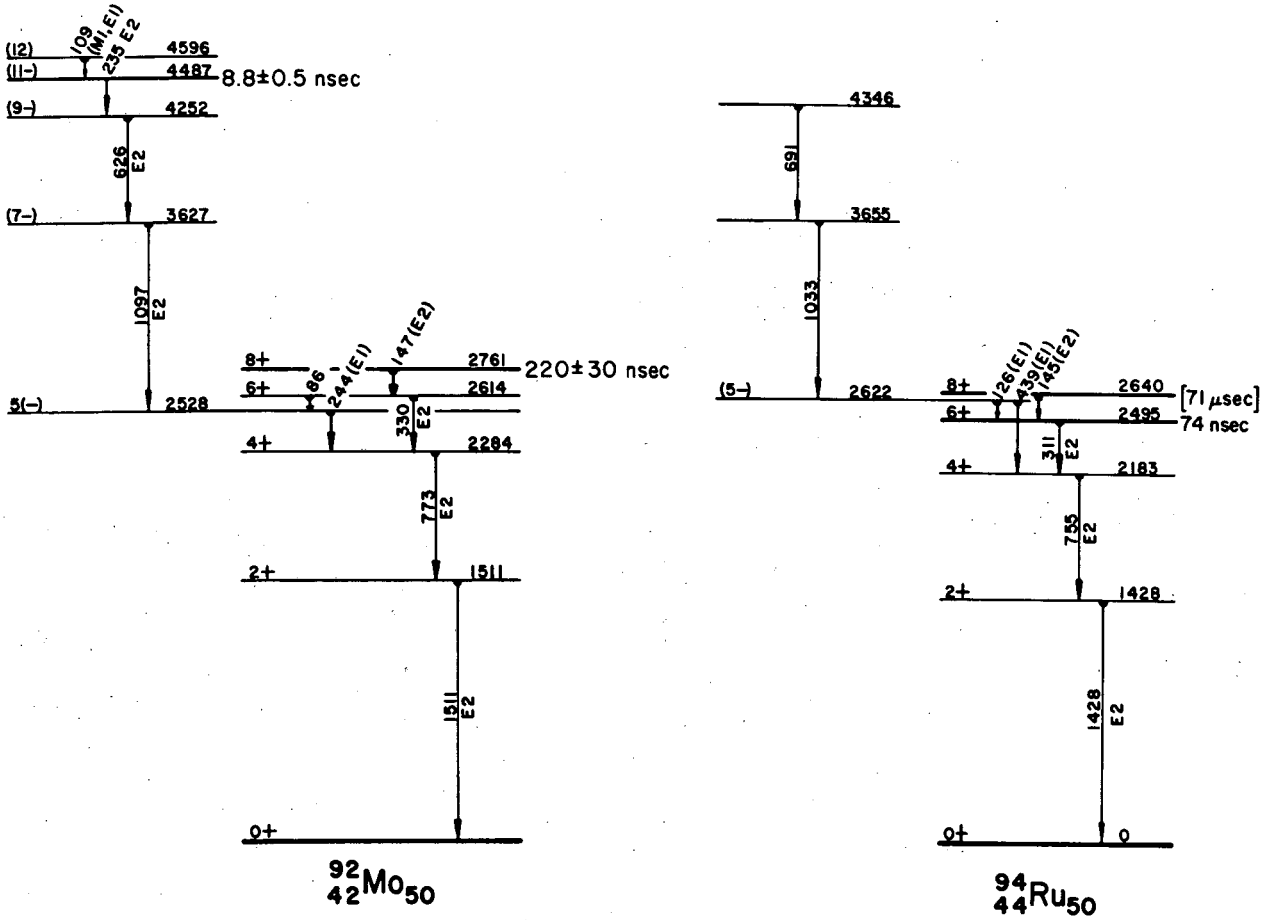

Fig. 1. Level schemes of ^{92}Mo and ^{94}Ru.

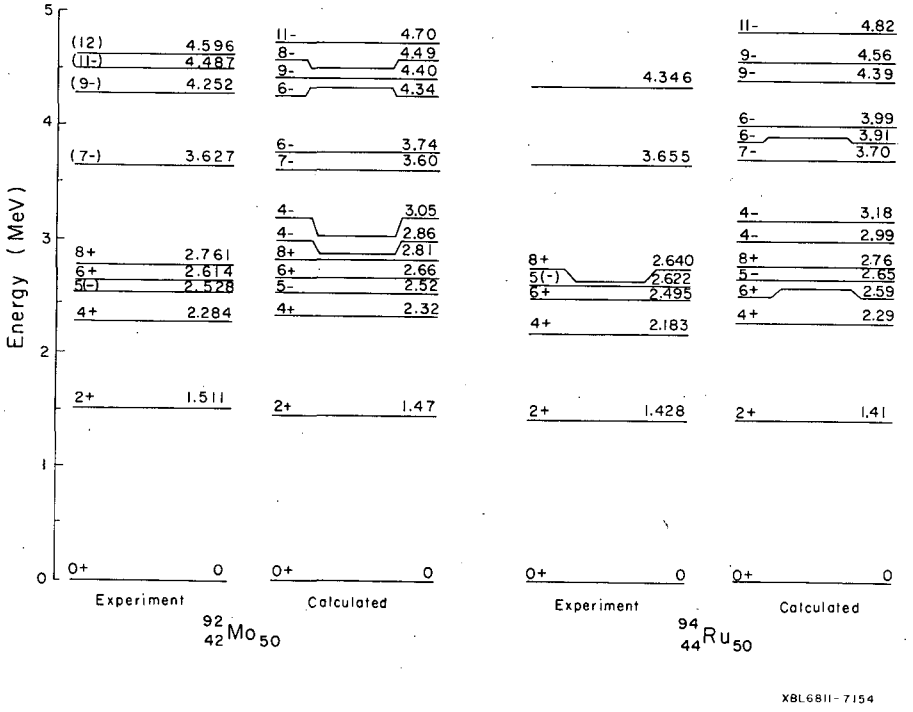

Fig. 2. Comparison of observed levels with those calculated in Ref. 5.

SYSTEMATICS OF EVEN-EVEN Mo AND Ru NUCLEI

J. M. Jaklevic, C. M. Lederer, and J. M. Hollander

As part of the program of in-beam γ-ray spectroscopy at the 88-inch cyclotron, a study is being made of the excited states of even-even Mo and Ru istopes. A detailed study of the N = 50 closed-shell nuclei ^{92}Mo and ^{94}Ru has been completed, and is described in the preceding paper. Techniques similar to those discussed therein have been applied to the heavier Mo and Ru isotopes in an attempt to establish the systematic trends of energy levels and possible isomers as one increases the neutron number beyond N = 50.

The even-even isotopes ^{92,94,96,98}Mo and ^{94,96,98,100,102}Ru were studied by using the $(\alpha, 2n)$ reaction on the appropriate Zr and Mo targets. The only evidence for isomerism ($\tau_{1/2} > 2$ nsec) attributed to these isotopes is a state of 100-nsec half-life in ^{94}Mo. We have established the location of this isomer in the level scheme, although further data will be necessary before the detailed character of this state can be determined.

In each of the isotopes studied it has been possible to tentatively assign energy levels up to and including $I\pi = 8+$. These data are summarized in Fig. 1. States indicated by heavy lines refer to previously established levels.[1,2] The levels of ^{104}Ru have not been studied in this work, but are included because of their relevance to the discussion. With the exception of ^{96}Mo, ^{98}Mo, and ^{102}Ru, the cascade relationships have been verified by γ-γ coincidence measurements. Since angular distribution measurements have been performed only on ^{92}Mo and ^{94}Ru, the spin and parity assignments for the remainder are based principally upon systematics and a knowledge of the manner in which these levels are populated in $(\alpha, 2n)$ reactions. Angular distribution measurements will be carried out in the near future in an attempt to verify these tentative assignments.

It is evident from the energy-level systematics that these nuclei become more collective as the neutron number is increased. As was pointed out in the preceding paper, the levels of ^{92}Mo and ^{94}Ru can be adequately described in terms of shell-model configurations arising from the

coupling of protons in the $2p_{1/2}$ and $1g_{9/2}$ shells. ^{96}Mo and ^{98}Ru exhibit a structure closely resembling that of the simple phonon excitations in the vibrational model. As still more neutrons are added, the levels show a trend toward a quasi-rotational structure, as evidenced in ^{102}Ru and ^{104}Ru. Figure 2 is an attempt to attain a more quantitative description of this trend. It is a plot of the ratio of the energies of the lowest-lying 8+ level to the 2+ level as a function of the ratio of 4+ to 2+ level energies for even-even nuclei. Included in the plot are data representative of other regions not covered by the isotopes studied.[1,3] The points marked "rotational" and "vibrational" represent those values calculated from the respective models. The point labeled "shell model" refers to the case in which the 0+ to 2+ level separation is much greater than the spacings between other levels.

This type of plot has been previously shown for 6+ level energies,[4] and has recently been applied to a discussion of the transition from rotational to vibrational nuclei.[5] The isotopes studied in the work reported here are seen to span a portion of the plot centered about the vibrational region, consistent with the previous discussion concerning their level structures. It is interesting to note that a correlation can be made between the order of the points along the abscissa [E(4+)/E(2+)] and the total number of particles or holes outside the nearest neutron and proton shells. Deviation from this ordering occur principally where minor closed shells (e.g., N = 40) are neglected.

This correlation parallels the smooth behavior of the B(E2) values.[6] Although its theoretical significance is not clear, it is remarkable that the correlation can be used to predict the positions of higher-spin levels of positive parity in any nucleus given only the energies of the first 2+ and 4+ levels.

References

1. C. M. Lederer, J. M. Hollander, and I. Perlman, Table of Isotopes (John Wiley and Sons, New York, 1967).
2. F. K. McCowan, R. L. Robinson, P. H. Stelson, and W. T. Milner, Nucl. Phys. A113, 529 (1968).
3. David Ward, R. M. Diamond, and F. S. Stephens, Collective Levels in Light Even Cerium Isotopes, UCRL-17945, May 1968.
4. C. A. Mallman, Phys. Rev. Letters 2, 507 (1959).
5. F. S. Stephens, David Ward, and J. O. Newton, in Proceedings of the International Conference on Nuclear Structure, Tokyo, 1967.
6. P. H. Stelson and L. Grodzins, Nucl. Data 1, 21 (1965).

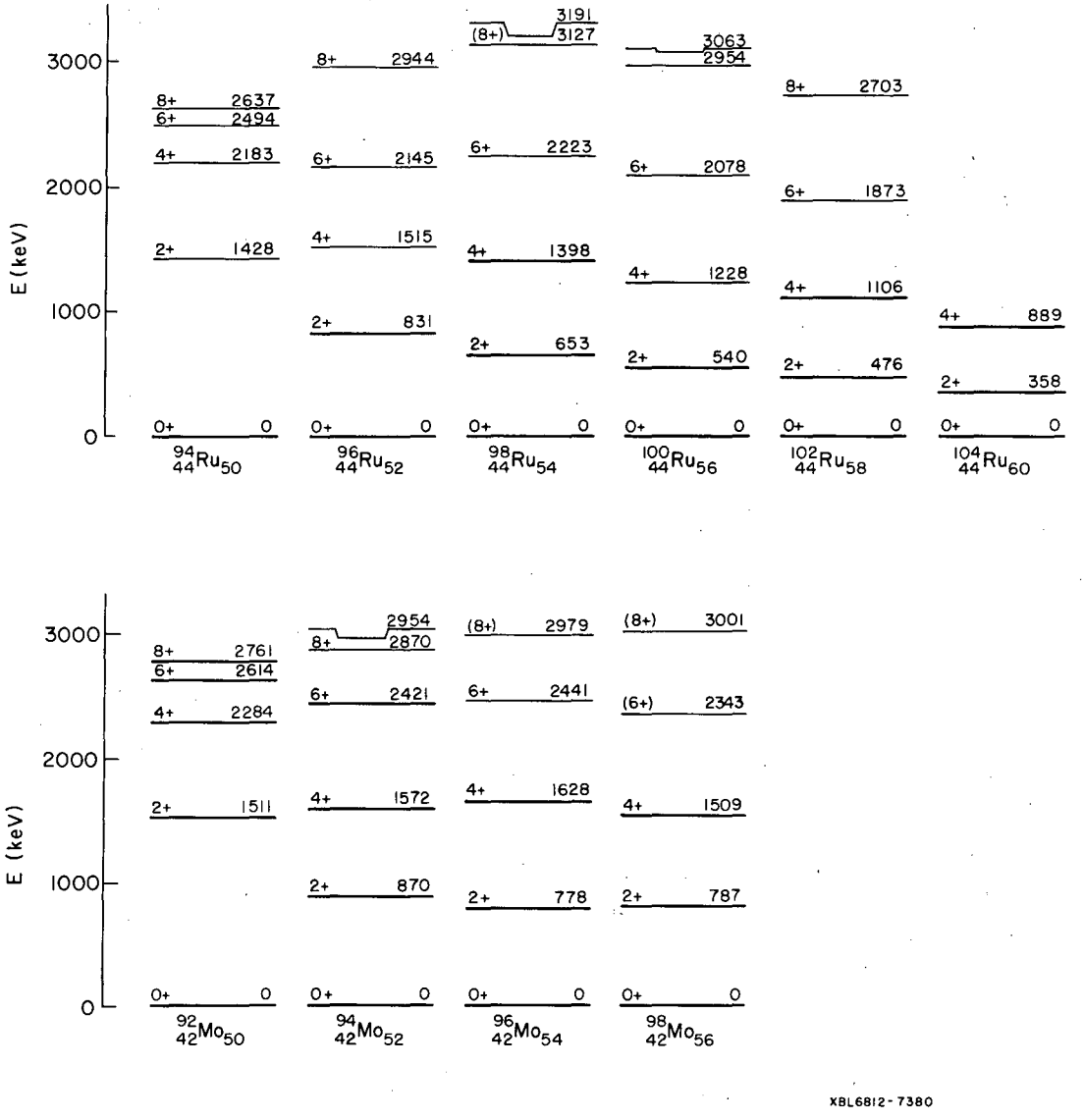

Fig. 1. Level schemes of even-even Mo and Ru isotopes.

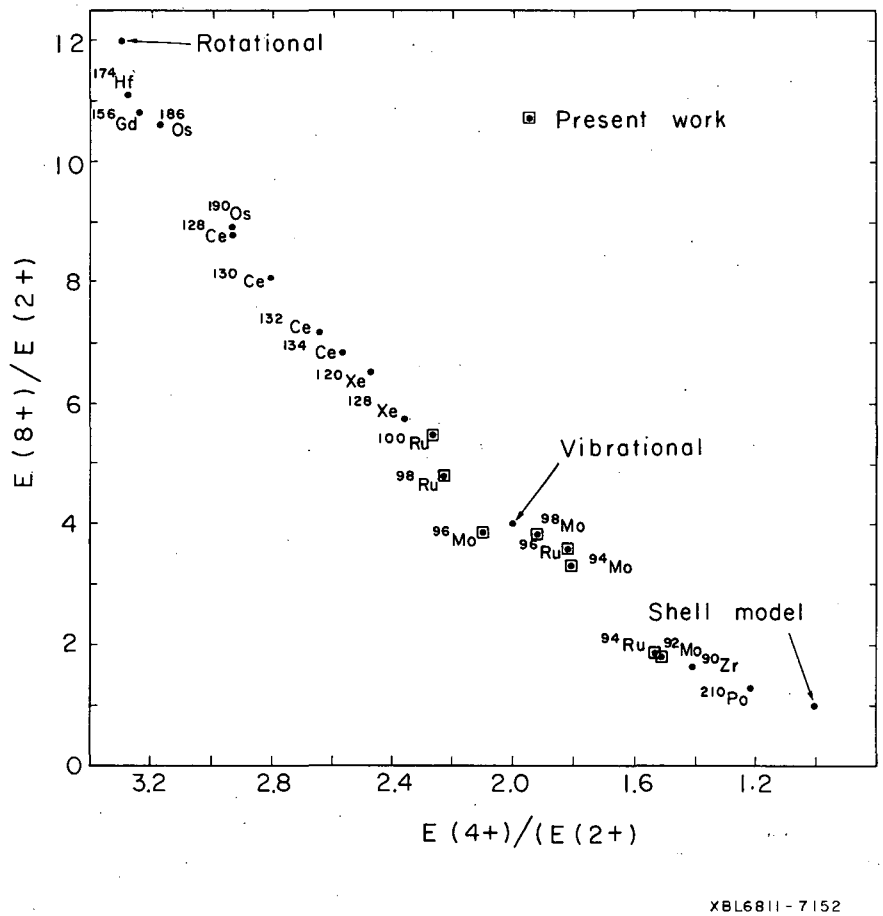

Fig. 2. Plot of E(8+)/E(2+) vs E(4+)/E(2+).

LOW-LYING 2- STATE IN ^{236}U †

C. M. Lederer, J. M. Jaklevic, and S. G. Prussin

In 1959 Gallagher and Thomas reported the existence of a level of ^{236}U at 688 keV.[1] In 1963, during an investigation of very weak α branching, Lederer observed the same state in the decay of ^{240}Pu and characterized it tentatively as a 2- state.[2] Conversion coefficients of the deexciting transitions, on which the spin assignment was based, also showed the surprising fact that the state decays by M2 transitions which compete favorably with an E1. However, the poor electron and γ-ray resolution in these experiments shed some doubt on the conversion measurements. Added to this difficulty is the impossibility of populating a 2- state directly, necessitating an assumption that the 688-keV level was fed via an α transition to a somewhat higher-lying level, although there is no direct evidence to support this assumption. It also seemed surprising to observe a 2- state at such a low energy.

In order to confirm the spin assignment and more fully characterize the 688-keV level, we have studied the decay of ^{236}Np. The results are reported in detail in a paper to be submitted to Nucl. Phys., and we summarize them briefly here.

The spectra of γ rays and K x rays were studied with a Ge(Li) spectrometer, and conversion electrons and β^- particles with a Si(Li) spectrometer. Sources were prepared by 11-MeV deuteron bombardment of ^{235}U in the 88-inch cyclotron; due to the low cross section for the ^{235}U(d, n)

reaction and much higher ones for $^{238}U[(d, n) + (d, p)^{239}U(\beta^-)]$ and $^{238}U(d, 2n)$ reactions, it was necessary to use uranium of very high enrichment (99.7%) in order to reduce the amount of ^{238}Np and ^{239}Np produced.

Tables I and II summarize the data on the electromagnetic transitions. In addition to the two transitions noted above, a new γ ray (538 keV) is observed. The 688-keV level decays to spin 0, 2, and 4 members of the ^{236}U ground-state band, which strongly supports the assignment of spin 2.

In the conversion spectrum (Fig. 1) it was possible to resolve partially the L-subshell lines of the 642- and 688-keV transitions. The conversion data (Table II) define M2 multipolarities for the 538- and 688-keV transitions and an M2 + E1 admixture for the 642-keV transition. We also observe some L lines of the transitions 45.3 keV (U) and 44.6 keV (Pu), and a β^- continuum with an end point of 537 ± 8 keV.

From the relative intensities of the β^- continuum, conversion lines, γ rays, and K x rays, we derive primary electron-capture and β^- branchings which are given on the decay scheme, Fig. 2. By measuring delayed K x ray—642-keV γ-ray coincidences (Fig 3), we determine the half-life of the 688-keV state as 4.4 ± 0.6 nsec.

The 2- state is characterized by a remarkably low energy, by fast M2 transitions, (0.1 single particle unit), and by highly hindered E1 transitions (3×10^{-8} single particle unit). As discussed in the full paper, these properties suggest that the state is very pure in K-quantum number and is quite collective, and that it may be necessary to assume coherent contributions from a number of two-quasi-particle states in order to account for the strength of the M2 transitions.

Footnote and References

†Condensed from a paper to be submitted to Nucl. Phys.

1. C. J. Gallagher, Jr., and T. D. Thomas, Nucl. Phys. 14, 1 (1959).
2. C. Michael Lederer, The Structure of Heavy Nuclei: A Study of Very Weak Alpha Branching (Ph. D. Thesis), UCRL-11028, Sept. 1963.
3. R. S. Hager and E. C. Seltzer, Nucl. Data 4, Nos. 1 and 2 (1968).

Table I. Gamma rays of ^{236}Np.

E_γ (keV)	Relative intensity	Half-life (hours)
UK_{α_2}	1047 ± 50	22.5 ± 0.4
UK_{α_1}	1712 ± 85	
$UK_{\beta_1'}$	599 ± 50	
$UK_{\beta_2'}$	not well resolved	
538.25 ± 0.20	1.11 ± 0.12	23 ± 6
642.42 ± 0.10	100	22.4 ± 0.6
687.71 ± 0.10	26.5 ± 0.5	22 ± 2

Table II. Conversion coefficients of ^{236}Np γ rays.

Coefficient and transition		Experimental value	Theoretical value[a]				
			E1	E2	E3	M1	M2
e_K/γ	642	0.112 ±0.010	0.00950	0.0186	0.0451	0.109	0.251
	688	0.22 ±0.02	0.00598	0.0165	0.0394	0.0908	0.207
$e_{L_{I+II}}/\gamma$	538	0.086 ±0.027	0.00156	0.00975	0.0532	0.0330	0.101
K/L	642	3.59 ±0.11	5.73	2.79	1.48	5.29	4.19
	688	3.27 ±0.16	5.75	2.99	1.66	5.26	4.26
L_I/L_{II}	642	11 ±4	6.2	1.24	0.61	8.1	6.3
	688	7 ±3	6.5	1.40	0.69	8.2	6.3
L_{I+II}/L_{III}	642	36^{+10}_{-7}	13.9	9.4	10.3	254	43
	688	46^{+40}_{-20}	14.5	10.5	11.4	256	48

a. Interpolated from the tables of Hager and Seltzer (Ref. 4).

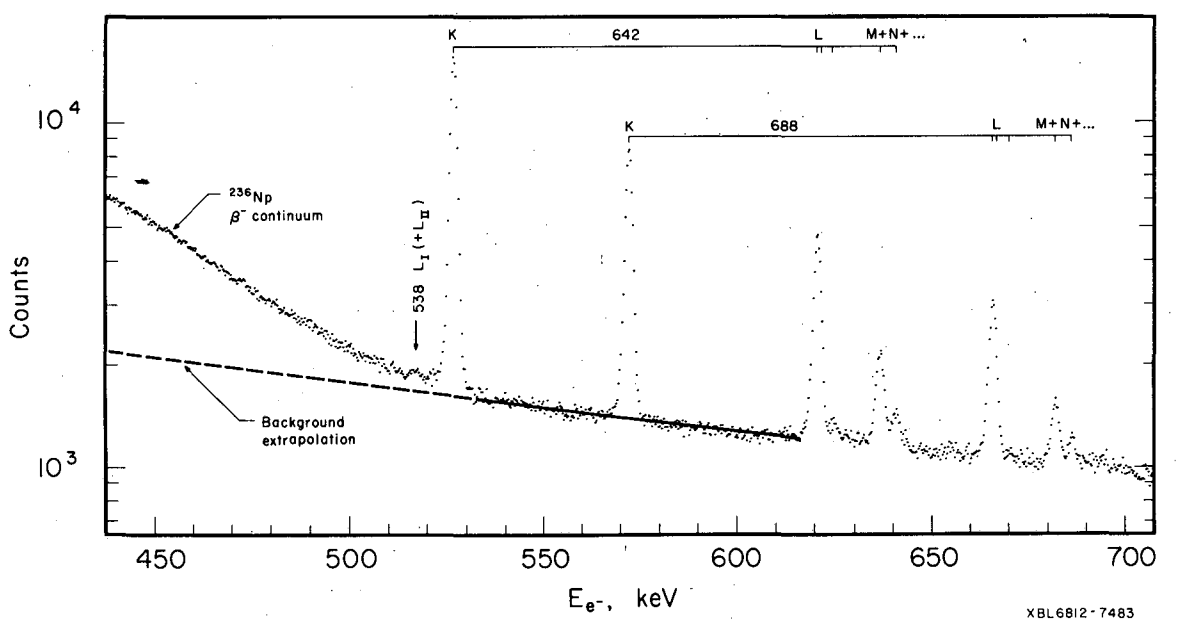

Fig. 1. A portion of the electron spectrum of ^{236}Np.

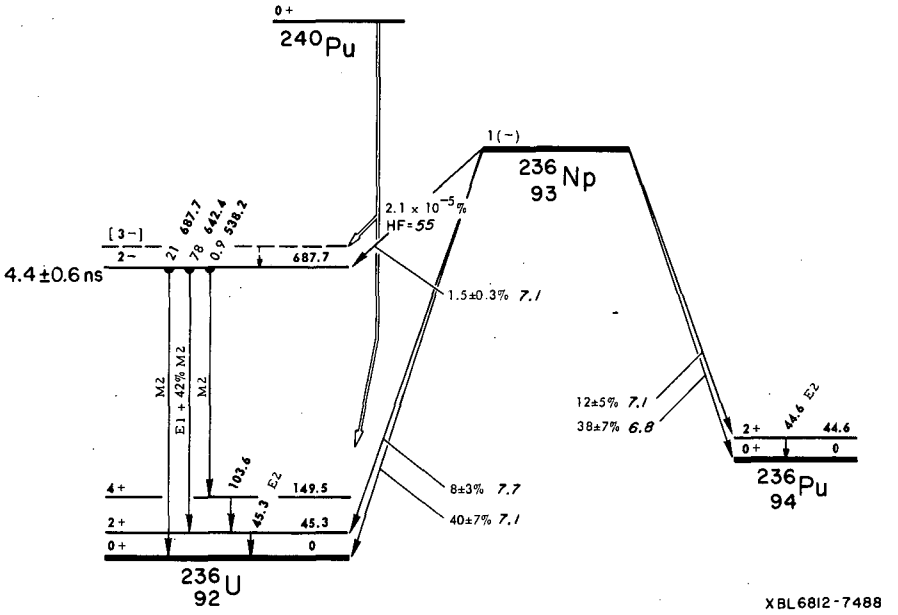

Fig. 2. The decay scheme of ^{236}Np. The assumed mode of α feeding of the 2- state in ^{236}U is also indicated.

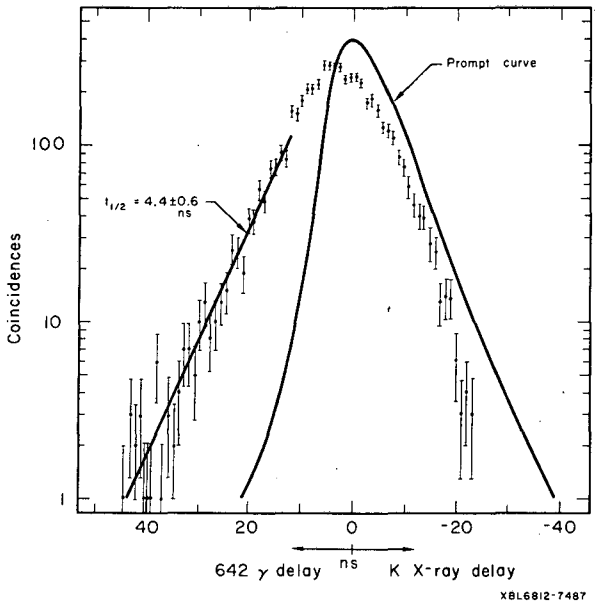

Fig. 3. Delay curve for K x-ray–642-keV γ-ray coincidences.

LEVEL SCHEME OF ^{176}Hf--A STUDY OF THE DECAYS OF ^{176}Ta AND Lu^{176m}†

F. M. Bernthal,* J. M. Hollander, and J. O. Rasmussen*

Because of the extreme complexity of the EC-β^+ decay of 8-hr ^{176}Ta to levels in ^{176}Hf, a detailed investigation this decay has until recently been an impractical if not impossible proposition. But the marriage of the computer and the semiconductor detector now permits such studies to be made with relative ease and unprecedented speed.

The ^{176}Ta activity for this study was produced via the ^{175}Lu (α, 3n)^{176}Ta reaction by irradiating 99.94% enriched $^{175}Lu_2O_3$ with 43-MeV α particles at the Berkeley 88-inch cyclotron. A 6-mil Al foil covered the $^{175}Lu_2O_3$ powder, so that the α-particle energy incident on the target material was about 40 MeV. The Ta activity was separated from other reaction products by extraction from 6N HCl solution by using 2, 4-dimethyl-3-pentanone (diisopropyl ketone), a procedure described in Ref. 1. Small amounts of ^{175}Ta, ^{177}Ta, and ^{178}Ta contamination were noted in the γ-ray spectra.

A variety of detection systems has been used to measure (a) the singles γ-ray spectrum, (b) the conversion-electron spectrum, (c) the γ-ray "pair" spectrum, and (d) the entire γ-γ coincidence spectrum of ^{176}Ta. These measurements were carried out, respectively, with the following detection systems:

(a) A 7-cm^3 planar Ge(Li) detector(resolution 2.3 keV at 1.33 MeV) in conjunction with the Compton-suppression system at LRL–Livermore; a 1-cm^3 "thin-window" Ge(Li) diode with resolution 0.85 keV at 122 keV.

(b) A 3-mm by 3-cm^2 Si(Li) diode with resolution 2.6 keV for the 1.06-MeV ^{207}Bi K-conversion line (operating temperature, about 110°K).

(c) A five-crystal pair spectrometer consisting of a NaI(Tl) annulus split into four optically isolated sections encircling a Ge(Li) planar detector 10 cm^3 in volume with resolution 2.2 keV at 1.33 MeV.

(d) A 35-cm^3 "five-sided" coaxial-drift Ge(Li) detector (resolution 3.4 keV at 1.33 MeV) and a 10-cm^3 planar detector (resolution 2.5 keV at 1.33 MeV) in conjunction with the PDP-7 multiparameter data-acquisition system.[2] In Fig. 1 we show a portion of the Compton-suppressed γ-ray singles spectrum of ^{176}Ta. In all, some 350 transitions attributed to ^{176}Ta decay have been observed at energies up to 3.0 MeV. Figure 2 shows the region of the Si(Li) conversion electron spectrum from ≈ 800 to 1300 keV. The K-conversion lines labeled 1149.9 and 1293.2 keV represent E0 transitions leading from the low-lying K = 0+ excitations at those energies. In Fig. 3 we show the 88- and 202-keV coincidence spectra as examples of the 80 coincidence spectra obtained by using the multiparameter system. Complete data on ^{176}Ta decay may be found in the full paper.

In Fig. 4 is shown the proposed level scheme of ^{176}Hf, constructed on the basis of this study of the decay of ^{176}Ta. The transitions and levels shown have all been assigned on the basis of supporting coincidence data. Additional transitions that could be placed by considering energy sums and differences alone are not included, but are displayed in a similar level scheme in the full paper. The electron-positron branching has been deduced from intensity balance and by combining our electron data with the data of Fominikh et al.[3]

Of particular interest in the ^{176}Hf level scheme are the two K = 0+ states at 1149.9 and 1293.2 keV. One of these states presumably represents the β vibration of ^{176}Hf. However, recent theoretical studies of such low-lying K = 0+ states suggest that they may possess significant pairing-vibrational character in certain cases,[4] and also that their characteristics may be substantially influenced by spin-quadrupole interactions in addition to the usual quadrupole-quadrupole interactions.[5]

Preliminary comparisons between the ^{176}Hf data and the predictions of Ref. 5 indicate that the nucleus ^{176}Hf may provide tentative confirmation of the influence of spin-quadrupole interactions on low-lying 0+ states in deformed nuclei. We observe in ^{176}Hf a second 0+ excited state, at or below the two-quasi-particle energy, with E2/E0 branching markedly different from the first 0+ excited state. Although we have no direct measurement of the E2 lifetime, the unusually small E2/E0 branching ratio for the 1293-keV 0+ state could result from a retardation of the E2 transition moment. Such a retardation would be expected to identify the low-lying 0+ excitation strongly influenced by spin-quadrupole coupling.[5]

The 2+ member of the lower K = 0+ band is found at 1226.6 keV, and the higher (K = 0, 2+) state may be at 1379.4 keV. E2 branching from excited K = 0, 2+ states to members of the ground rotational band in such nuclei is a topic of considerable current interest because of the apparent enhancement of the $\Delta I = 0$ E2 transitions of this type, an enhancement that has been proposed to arise from M1 admixture.[6]

In Table I we summarize the data of interest pertaining to the K = 0+ excited states in ^{176}Hf. The parameter X is that proposed in Ref. 7 to provide a comparison between E0 and E2 transition strengths from β-vibrational states:

$$X \left[\frac{B(E0;\ 0'+ \longrightarrow 0+)}{B(E2;\ 0'+ \longrightarrow 2+)}\right] = \frac{e^2 R_0^4 \rho^2}{B(E2)} .$$

The 1379.4-keV state is tentatively assigned as $(K = 0_3 2+)$. If this assignment is correct, the $2+0_3 \rightarrow 2+0_1$ transition would in this case be very strongly enhanced over the 1379.3- and 1089.1-keV (E2) transitions. Further investigation of the two K = 0+ bands in ^{176}Hf is clearly warranted.

Preliminary results from a reinvestigation of ^{176m}Lu (3.7 hr) decay indicate very weak feeding to the 1150-, 1227-, 1248-, and 1293-keV states, in ^{176}Hf and are in agreement with the conclusions earlier obtained from the ^{176}Ta decay data.

Footnotes and References

†Condensation from Frederick M. Bernthal, I. The $|\Delta K|$ Electric Dipole Transitions in Odd-Mass Deformed Nuclei. II. The Decay of ^{176}Ta to Levels in ^{176}Hf (Ph. D. Thesis), UCRL-18651, Feb. 1969.

*Present address: Department of Chemistry, Yale University, New Haven, Connecticut.

1. F. F. Felber, Jr., Nuclear Decay Schemes of Some of the Isotopes of Tantalum (M. S. Thesis), UCRL-3618, Jan. 1957.

2. L. B. Robinson and John D. Meng, On-Line Real-Time Operations of a PDP-7 Data-Taking System, UCRL-17220, March 1967; L. B. Robinson, F. Gin, and F. S. Goulding, Nucl. Instr. Methods 62, 237 (1968).

3. W. I. Fominikh, J. Molnar, N. Nenoff, B. Styczen, and J. Zvolsky, in Proceedings of the International Symposium on Nuclear Structure, Dubna, 1968, p. 46.

4. O. Mikoshiba, R. K. Sheline, and T. Udagawa, Nucl. Phys. A101, 202 (1967).

5. K. M. Zheleznova, N. I. Pyatov, and M. I. Chernei, Izv. Akad. Nauk SSSR, Ser. Fiz. 31, 546 (1967); N. I. Pyatov, Arkiv. Fysik 36, 667 (1967).

6. B. R. Mottelson, in Proceedings of the International Conference on Nuclear Structure, Tokyo, 1967, p 87.

7. J. O. Rasmussen, Nucl. Phys. 19, 85 (1960).

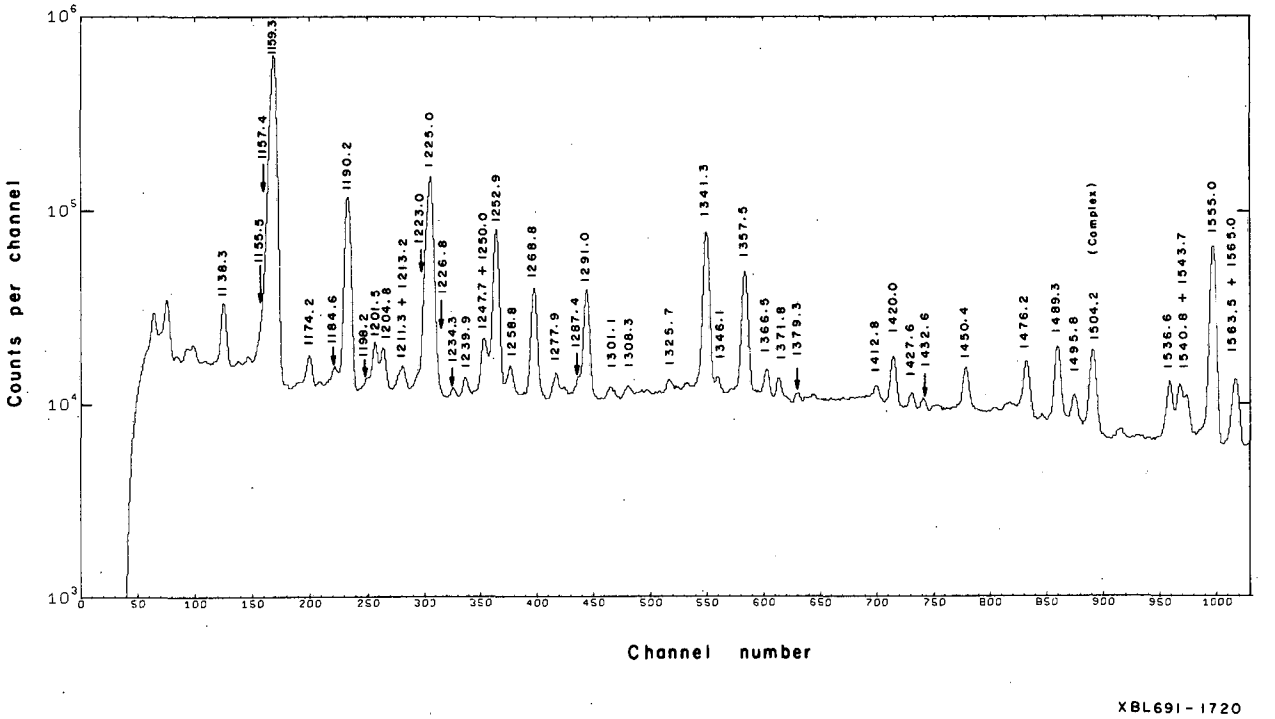

Fig. 1. The Compton-suppressed γ-ray singles spectrum of ^{176}Ta in the region 1.1 to 1.6 MeV.

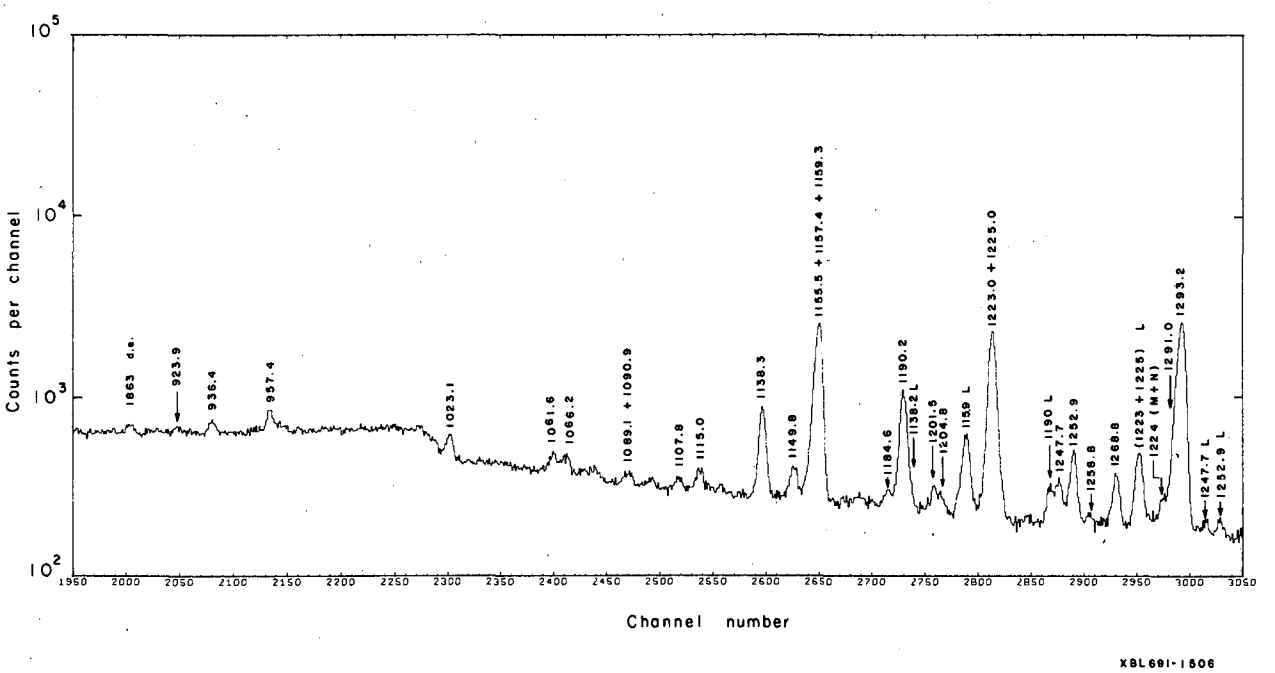

Fig. 2. The conversion-electron spectrum from ^{176}Ta decay in the region 850 to 1300 keV. Unless otherwise indicated, energy labels represent K-conversion lines according to transition energy.

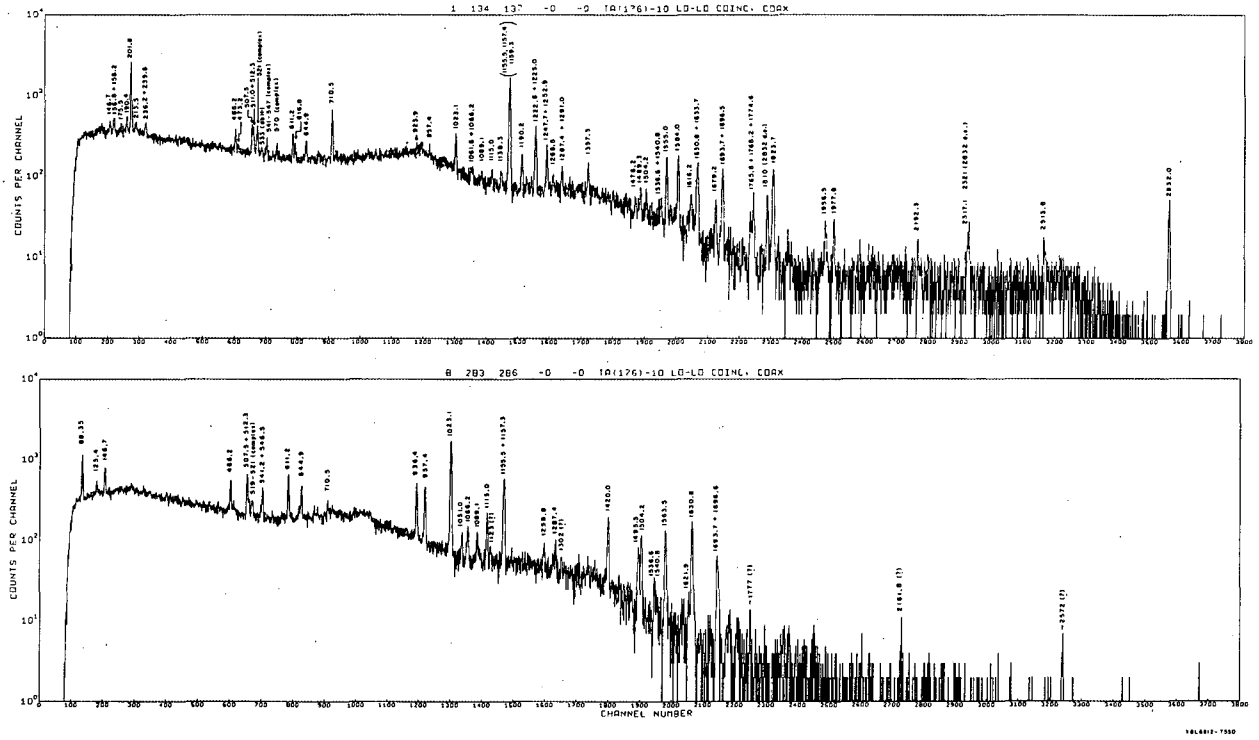

Fig. 3. The 88-keV γ-γ coincidence spectrum from ^{176}Ta decay. Taken with a 35-cm^3 coaxial detector.

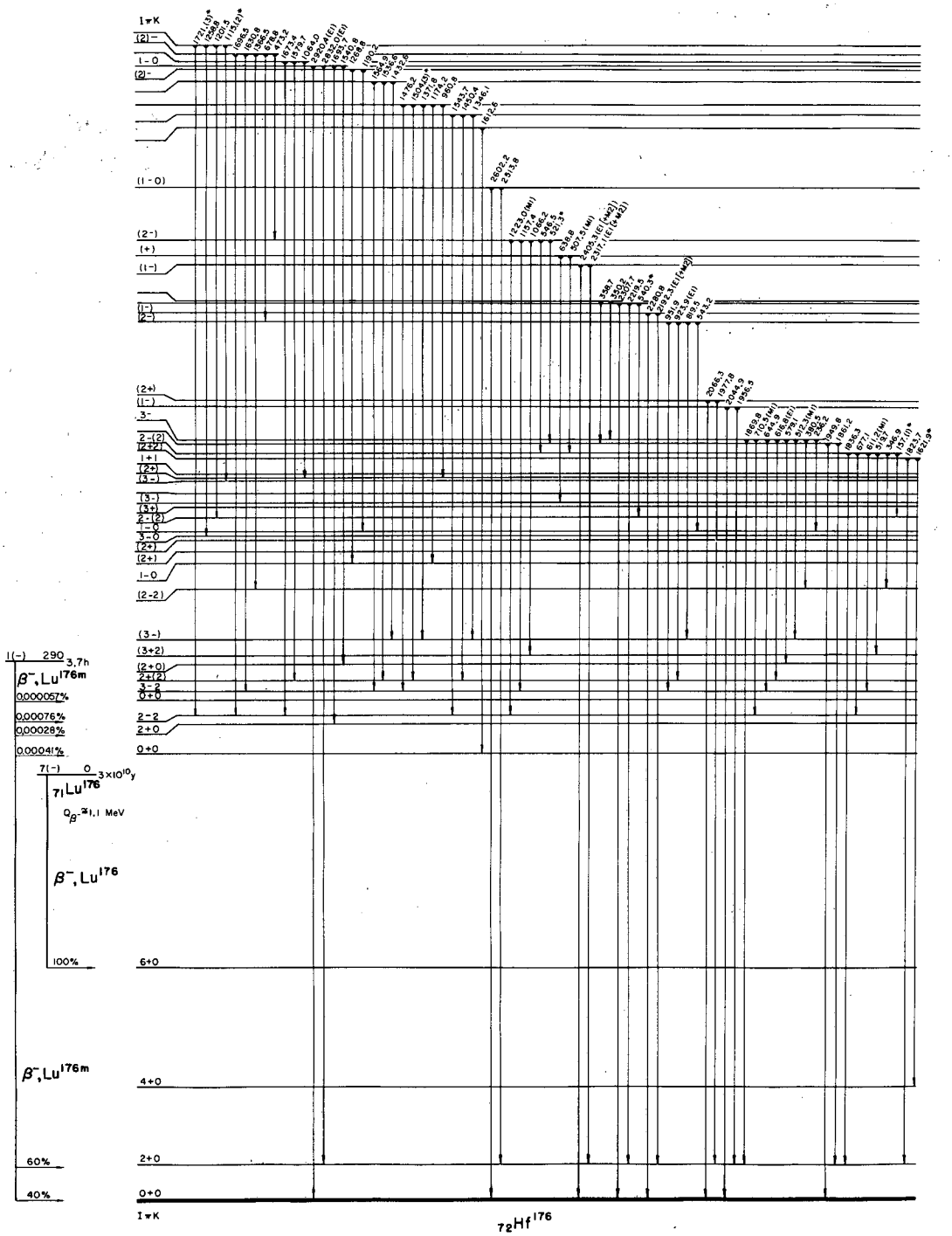

XBL 691-1642-A

Fig. 4. The decay of ^{176}Ta, ^{176}Lu,

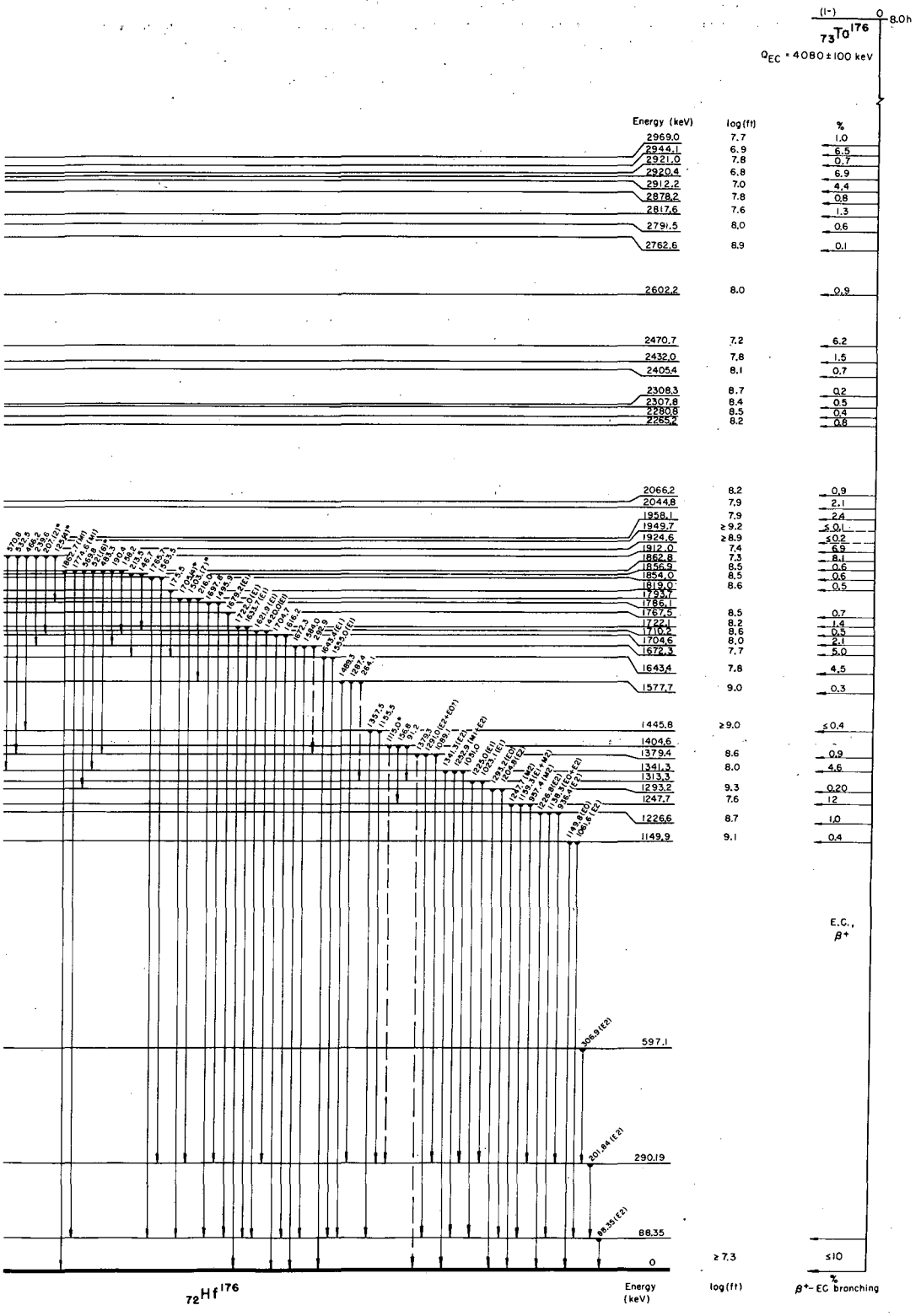

XBL 691-1642-B

and ^{176m}Lu to levels in ^{176}Hf.

Table I. Branching from K = 0+ excited states in ^{176}Hf.

Transition	Energy (keV)	Relative intensity	$\times[\frac{B(E0)}{B(E2)}]$
$0_2^+ \rightarrow 0_1^+$	1150	0.091(14)	0.16(3)
$0_2^+ \rightarrow 2_1^+$	1062	10.0(9)	
$0_3^+ \rightarrow 0_1^+$	1293	1.58(24)	7.3(1.2)
$0_3^+ \rightarrow 2_1^+$	1205	6.1(5)	

$\frac{I\pi K_n \xrightarrow{\gamma_1} I_1\pi K_1}{I\pi K_n \xrightarrow{\gamma_1} I_1'\pi K_1}$	$\frac{E\gamma_1(keV)}{E\gamma_2(keV)}$	$\frac{In+\gamma_1}{In+\gamma_2}$	$\frac{B(E2)\ I_2\rightarrow I_1}{B(E2)\ I_2\rightarrow I_1'}$
$\frac{2+\ 0_2 \rightarrow 4+\ 0_1}{2+\ 0_2 \rightarrow 2+\ 0_1}$	$\frac{936}{1138}$	$\frac{10.4(8)}{12.6(1.0)}$	2.2(2)
$\frac{2+\ 0_2 \rightarrow 0+\ 0_1}{2+\ 0_2 \rightarrow 2+\ 0_1}$	$\frac{1227}{1138}$	$\frac{5.5(1.0)}{12.6(1.0)}$	0.30(6)
$\frac{2+\ 0_2 \rightarrow 4+\ 0_1}{2+\ 0_2 \rightarrow 0+\ 0_1}$	$\frac{936}{1227}$	$\frac{10.4(8)}{5.5(1.0)}$	7.3(1.6)

THICK-TARGET METHOD FOR NUCLEAR RECOIL STUDIES

M. K. Go and S. S. Markowitz

In the recoil studies of nuclear reaction mechanism, two techniques are generally employed--thin-target and thick-target methods. In the thick-target method, the target thickness is large compared with the range of the recoiling nuclei, so only nuclei sufficiently close to the surface of the target can escape out of the target. It can be shown[1] that the fraction of recoiling nuclei (F) is related to the target thickness (W) and the projected range (R_p) as

$$F = R_p / W. \quad (1)$$

Usually F is the only quantity measured during a thick-target recoil experiment, and the projected range is inferred from Eq. (1).

In a thin-target (~10 $\mu g/cm^2$) experiment, the distribution of the recoil nuclei in a stopping medium is measured and the range is obtained directly from the distribution curve. Generally the thin-target experiment yields more information about the nature of the nuclear reaction in question. However, it is quite difficult to prepare very thin and uniform targets, and sometimes the low product yields render the subsequent detection of radioactivity impossible. It is therefore desirable to determine the range distribution by using a thick target.

The distribution of the ranges about the mean range R_0 for a thin-target experiment is[1]

$$Y(R) = (2\pi)^{-1/2}(\rho R_0)^{-1} \exp[-(R_0-R)^2/2\rho^2 R_0^2], \quad (2)$$

with ρ, the straggling parameter, given by[2] $\rho^2 = 2M_1M_2/3(M_1+M_2),$[2] where M_1 and M_2 are the masses of the recoiling and stopping nuclei respectively.

A computer program was used to simulate the recoiling nuclei from a 1-$\mu g/cm^2$ target into a few 160-$\mu g/cm^2$ stopping foils. The fractions of recoiling nuclei passing through each foil are calculated for the distribution of Eq. (2). The result is shown in Fig. 1. The straight line in this probability plot is indicative of a Gaussian distribution, and the point at 50% corresponds to R_0.

A thick target can be thought of as a stack of thin targets, and the distribution of the recoiling nuclei can be taken as the sum of the contributions from each of the thin targets in the stack. If we choose a stopping material having approximately the same stopping power as the target material, and use the recoil distribution of Eq. (2) for each of the thin targets, a curve similar to Fig. 1 can be constructed. Figure 2 represents such a calculation for a 1-mg/cm^2 target as the sum of 1000 1-$\mu g/cm^2$ targets. Since many of the recoil nuclei have been stopped in the target, the 50% point no longer corresponds to the R_0.

To test the feasibility of such a "thick target" method, recoil distribution of ^{48}Cr in Al were measured, with a 1-mg/cm^2 TiO_2 target. The target is prepared by sedimentation of TiO_2 in alcohol onto 5-mil Al foils. The TiO_2 used is enriched in ^{46}Ti, with the average mass per atom ($\bar{A}$) 26.2, and the average atomic charge ($\bar{Z}$) 12.7. The stopping power of the target material is taken as equal to that of aluminum (A = 27, Z = 13). A stack of six aluminum foils (160 $\mu g/cm^2$ each) is used as catchers. The target is bombarded at the 88-inch cyclotron with 40-MeV α particles at the rate of 1 μA. The actual alpha energy impinging on the ^{46}Ti nuclei is estimated from the range-energy curve for Al calculated by the computer program RANGES.[3] After the bombardment, the target and the catcher foils are counted with a Ge(Li) counter. The activity of ^{48}Cr is determined from the 0.116-MeV (100%) γ ray.[4] The result is plotted in Fig. 2. R_0 is estimated to be 390 $\mu g/cm^2$ Al. The implication of the experimental result to the mechanism of the ^{46}Ti $(\alpha, 2n)^{48}Cr$ reaction is described elsewhere.[5]

References

1. B. G. Harvey, Ann. Rev. Nucl. Sci. 10, 235 (1960).
2. R. B. Leachman and H. Atterling, Arkiv Fysik 13, 101 (1958).
3. Hans Bichsel, A Fortran Program for the Calculation of the Energy Loss of Heavy Charged Particles, UCRL-17538, May 1967.

4. R. K. Sheline and J. R. Wilkinson, Phys. Rev. 99, 165 (1955).
5. M. K. Go and S. S. Markowitz, following report, Recoil Studies of $^{46}Ti(^{3}He, 2n)^{48}Cr$.

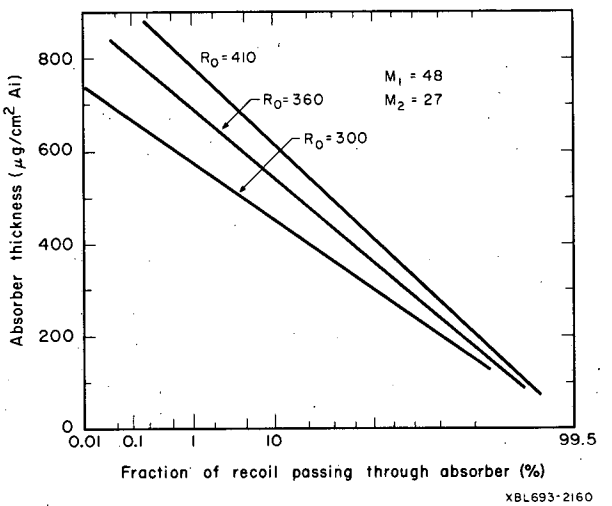

Fig. 1. Calculated probability plot for a 1-μg/cm^2 TiO_2 target with 160 μg/cm^2 Al catcher foils. Notice that R_0 corresponds to where the straight line passes through the 50% fraction. The recoil nuclei are ^{48}Cr.

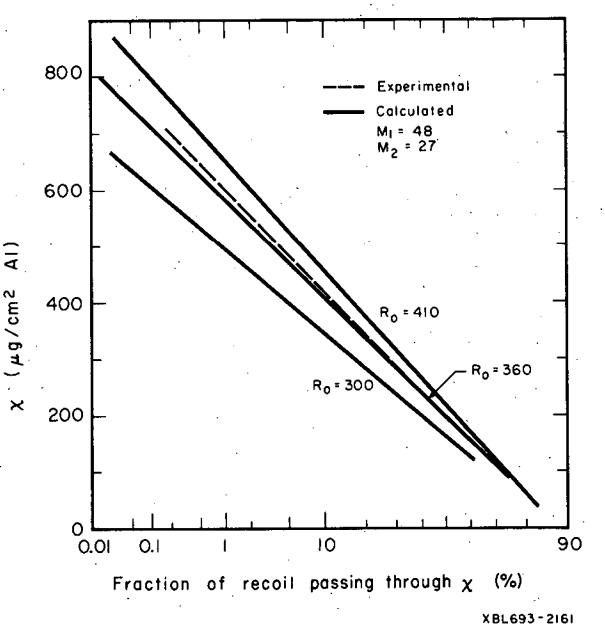

Fig. 2. Calculated plot for a 1-mg/cm^2 TiO_2 target also with 160-μg/cm^2 Al catchers. The broken line contains experimental values for the recoils of the ^{46}Ti $(\alpha, 2n)^{48}Cr$ reaction. The R_0 for the experimental data is estimated to be 390 μg/cm^2 Al.

RECOIL STUDIES OF $^{46}Ti\ (\alpha, 2n)^{48}Cr$

M. K. Go and S. S. Markowitz

The usefulness of recoil studies as applied to the compound-nucleus reaction mechanism has been pointed out by several authors.[1,2] When a projectile particle fuses with the target nucleus to form the so-called compound nucleus, the momentum transfer from the incoming particle to the compound nucleus is complete. If the subsequent deexcitation of this compound nucleus is assumed to be isotropic emission of particles, the recoil energy of the residual nucleus is given by[3]

$$E_r = \frac{A_p A_r}{(A_p + A_t)^2} E_p, \qquad (1)$$

where E = energy and A = mass number, and t, p, and r refer to target, projectile, and recoil nucleus respectively. Theoretical treatment of ion-matter interaction has been advanced by Lindhard, Scharff, and Schiøtt (LSS).[4] They obtained the range-energy relations for ions in a stopping medium. A series of universal range-energy curves for different values of the electronic stopping parameter k is plotted in the dimensionless range and dimensionless energy space. Their plot can be converted to the more conventional range-energy curves. A plot for ^{48}Cr recoiling into aluminum is calculated, and is presented in Fig. 1.

An experiment with α particles on ^{46}Ti has been performed, using the "thick target" method described previously.[5] The actual alpha energy is 31.6 MeV. According to Eq. (1), the recoiling ^{48}Cr nucleus has a recoil energy of 2.4 MeV. The experimental average range of ^{48}Cr recoil is 390 $\mu g/cm^2$-Al, as seen from Fig. 2 of the preceding report. This value is consistent with the value 400 $\mu g/cm^2$-Al from Fig. 1. From a simple forward fraction measurement[5] the range is 396 $\mu g/cm^2$ in TiO_2.

The Gaussian distribution of the recoil can be inferred from the straight line of Fig. 2 of the preceding report. This Gaussian distribution and the good agreement between the experimental and theoretical average ranges strongly indicate that the $^{46}Ti\ (\alpha, 2n)^{48}Cr$ reaction proceeds predominantly via a compound-nucleus route, and the subsequent neutron decay is isotropic.[6]

References

1. V. Subrahmanyam and M. Kaplan, Phys. Rev. 142, 174 (1966).
2. J. Alexander and G. Simonoff, Phys. Rev. 162, 952 (1967).
3. Charles F. Smith, Jr., Decay of the $^{64*}Zn$ Compound Nucleus Formed by Nuclear Reactions of p, ^3He, ^4He, and ^{12}C With ^{63}Cu, ^{61}Ni, ^{60}Ni, and ^{52}Cr, Respectively (Ph. D. Thesis), UCRL-11862, Jan. 1965.
4. J. Lindhard, M. Scharff, and H. Schiøtt, Danske Videnskab Selskab Mat.- Fys. Medd. 33, No. 14 (1963).
5. M. Go and S. Markowitz, Thick-Target Method for Nuclear Recoil Studies, preceding report.
6. The same conclusion can be reached by assuming that the neutrons are emitted symmetrically about an axis perpendicular to the beam direction.

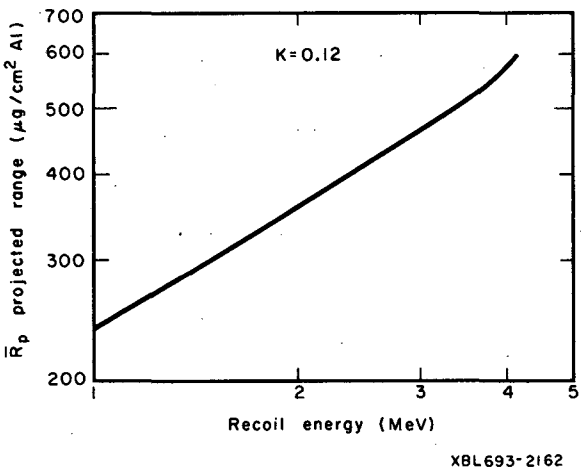

Fig. 1. Conventional range-energy curve for ^{48}Cr nuclei from ^{46}Ti (α, 2n)^{48}Cr reaction recoil into aluminum stopper. Calculated from the theoretical curves in LSS (Ref. 4).

EXCITATION FUNCTIONS FOR ^{47}Ti + ^{3}He REACTIONS

M. K. Go and S. S. Markowitz

Nuclear reactions for medium-weight nuclei ($45 < A < 100$) at energies up to 10 MeV per incident nucleon have been successfully described by the statistical theory.[1] The main feature of this theory is that a compound nucleus is formed during a nuclear reaction and the subsequent decay of this compound nucleus can be treated statistically. Schematically the reaction of the incident particle a with the target nucleus A to yield the residual nucleus B and outgoing particle b can be represented as

$$a + A \rightarrow C \rightarrow b + B, \tag{1}$$

where C is the compound nucleus. The reaction cross section for such a reaction is

$$\sigma(a, b) = \sigma_c(\epsilon_a)\, W_b'(U) / \sum_j W_j(U), \tag{2}$$

where $\sigma_c(\epsilon_a)$ is the cross section for the formation of the compound nucleus with ϵ_a as the kinetic energy of a, $W_b'(U)$ is the probability per unit time that only b is emitted from the compound nucleus with excitation energy U, and the summation includes all particles that can be evaporated.

Weisskopf[2] has shown that the probability per unit time for evaporating a particle j with kinetic energy between ϵ and $\epsilon + d\epsilon$ is

$$P_j(\epsilon)d\epsilon = \frac{g_j m_j}{\pi \hbar^3}\, \sigma(\epsilon)\, \frac{\rho_f}{\rho_i}\, \epsilon d\epsilon, \tag{3}$$

where g_j is the statistical weight of particle j, m_j is the reduced mass of the system, $\sigma(\epsilon)$ is the inverse cross section for the evaporation process, and ρ_i, ρ_f are the level densities of the initial and final nuclei. The level density is usually taken as[3]

$$\rho(U) = C \exp\{2[a^{1/2}(U-\delta)^{1/2}]\}, \tag{4}$$

where C is a constant and a is proportional to A within a small range of A; δ is a pairing energy correction.

The cross section of the reaction given by (1) can then be expressed explicitly as[4]

$$\sigma(a,b) = \sigma_c(\epsilon_a) g_b m_b \left[\int_A^{U-S_b-\delta_b} \sigma(\epsilon_b) \exp\left\{ 2[a(U-S_b-\delta_b-\epsilon_b)]^{1/2} \right\} \epsilon_b d\epsilon_b \right.$$
$$\left. + \int_{U-S_b-\delta_b}^{U-S_b} \sigma(\epsilon_b)\epsilon_b d\epsilon_b \right] \Big/ \sum_j g_j m_j \left[\int_0^{U-S_j-\delta_j} \sigma(\epsilon_j) \exp\left\{ 2[a(U-S_j-\delta_j-\epsilon_j)]^{1/2} \right\} \epsilon_j d\epsilon_j \right.$$
$$\left. + \int_{U-S_j-\delta_j}^{U-S_j} \sigma(\epsilon_j)\epsilon_j d\epsilon_j \right], \qquad (5)$$

where $A = U-S_b-S_2$ (if $U-S_b-S_2 < 0$, $A = 0$), and S_b is the separation energy of b from the compound nucleus. S_2 is the separation energy of the most loosely bound particle after the evaporation of b. For a simple calculation the summation is taken over neutron, proton, and α particle only. In this work, the empirical formula for the inverse cross section is taken from Dostrovsky et al.[3] The separation energies are taken directly from a calculation by Seeger.[5]

Equation (5) was programmed for computation on the CDC 6600 computer. The program was also able to calculate the evaporation of two neutrons. The result is presented in Fig. 1.

The experimental points were obtained by a stacked-foil method. Targets were made by sedimentation of TiO_2 (enriched in ^{47}Ti) in alcohol onto aluminum foils. A 30-MeV ^3He beam from the 88-inch cyclotron was used for bombardment. The 0.116-MeV γ ray (100%) from the ^{48}Cr decay was counted with a Ge(Li) detector. The ^3He energy at each target was estimated with the computer program RANGES.[6]

The determination of $^{47}Ti(^3He,n)^{49}Cr$ cross section has been unsuccessful, since the target contains $^{48}Ti(16.5\%)$, and the $^{48}Ti(^3He, 2n)^{49}Cr$ reaction cross section is expected to be much greater than that of $^{47}Ti(^3He, n)^{49}Cr$.

References

1. D. Bodansky, Ann. Rev. Nucl. Sci. 12, 79 (1962).
2. V. Weisskopf, Phys. Rev. 52, 295 (1937).
3. I. Dostrovsky, Z. Fraenkel, and G. Friedlander, Phys. Rev. 116, 683 (1959).
4. K. Chen and J. Miller, Phys. Rev. 134, B-1269 (1964).
5. P. Seeger, Nucl. Phys. 25, 1 (1961).
6. H. Bichsel, A Fortran Program for the Calculation of the Energy Loss of Heavy Charged Particles, UCRL-17538, May 1967.

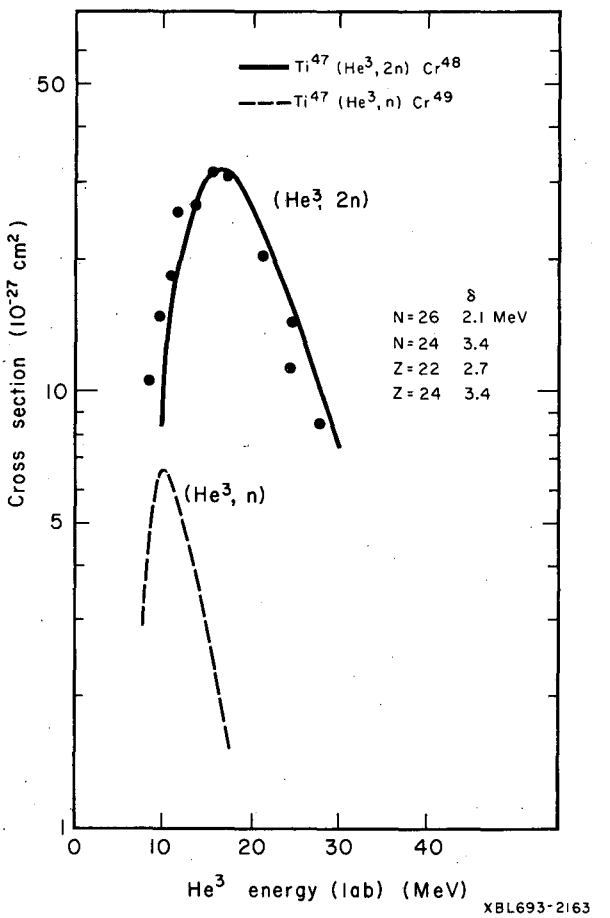

Fig. 1. Excitation functions for $^{47}Ti(^{3}He, n)^{49}Cr$ and $^{47}Ti(^{3}He, 2n)^{48}Cr$ reactions. The δ values are taken from Chen and Miller (Ref. 4). The level density parameter "a" is taken to be 2. The dots are experimental values. Solid line and dashed line are calculation results.

^{3}He ACTIVATION OF Mg, Si, Ca, Ti, Ni, Ge, AND Ta: EXCITATION FUNCTIONS AND THICK-TARGET YIELDS

J. F. Lamb, D. M. Lee, and S. S. Markowitz

Nuclear reactions induced in Mg, Si, Ca, Ti, Ni, Ge, and Ta by 0- to 30-MeV ^{3}He ions have been studied in order to investigate the application of ^{3}He activation analysis both for estimation of these elements and for determining other elements in their presence.

The ^{3}He ion bombardments were performed at the Berkeley Hilac at beam currents ranging from 0.05 to 0.5 μA. Cross-section data were obtained by using both stacked-foil techniques and individual foil irradiations with the ^{3}He ion beam energy adjusted from its initial 31.2 MeV by aluminum degrader foils. Range-energy data were taken from Ref. 1. Product activities were obtained nondestructively by γ-ray spectroscopy using both NaI(Tl) scintillation detectors and Ge(Li) detectors coupled to multichannel analyzers.

Figures 1 through 7 show the reaction cross sections measured. Since naturally occurring materials were used throughout these experiments, absolute excitation functions were determined only in the cases in which production of a particular nuclide was either unambiguous or in which contributing reactions could be assumed negligible. Among the former case are $^{26}Mg(^{3}He, p)^{28}Al$ and $^{26}Mg(^{3}He, 2p)^{27}Mg$; the latter includes $^{40}Ca(^{3}He, p)^{42m}Sc$, $^{181}Ta(^{3}He, 4n)^{180}Re$, and $^{181}Ta(^{3}He, 3n)^{181}Re$. In calculating the cross sections for the Ta reactions, however, 100% relative intensity was assumed for the γ-ray line measured because the decay schemes of the Re

isotopes are incomplete in the literature.[2] All other cross-section data are represented as total production cross sections; i. e., no corrections for target isotopic abundances were made.

The excitation functions in Figs 1 through 7 were used to calculate thick-target reaction yields, which roughly measure the obtainable analytical sensitivities for these elements. Each curve was graphically integrated, with 20-MeV ^{3}He energy used as the upper limit. The lower integration limit was chosen as the beam energy corresponding to a cross section equal to 1% of the maximum σ below 20 MeV. The average cross section over the energy range thus determined was used to calculate the yield by

$$\text{yield} = \frac{\text{dpm}}{\mu\text{g}} = n\sigma_{avg} I(1-e^{-\lambda\tau}),$$

where $\frac{\text{dpm}}{\mu\text{g}}$ = end-of-bombardment activity resulting from irradiation of 1 μg of the element sought,
n = number of nuclei per cm^2 per μg of the element sought in the target,
I = 1.873×10^{14} ^{3}He/min (1 μA of beam),
$(1-e^{-\lambda\tau})$ = 0.5 (λ is the decay constant of the product activity and τ the bombardment length, here set equal the half-life).

The target is assumed to be such that the beam, in passing through, is degraded in energy by an amount equal to the integration interval and that the 1 μg/cm^2 of the element sought is uniformly distributed over this thickness. The thick-target yields are shown in Table I. The interferences listed in the last column of the table refer only to reactions of other elements which, if present, might lead to the same final product. The excitation functions of only a few of these reactions have been obtained. These are ^{3}He + Al,[3,4] ^{3}He + Na,[5] and ^{3}He + Cu.[6] In order to obtain an analytical sensitivity from the yield data, corrections for detection efficiency of the equipment used to measure activities must be made, and the target matrix specified. For example, 1 μg/cm^2 of Ti distributed over 81 mg/cm^2 of Zr would result, under the above bombardment conditions, in production of about 1.5×10^5 dpm of ^{49}Cr. Using a typical solid-state detector, this activity may be detected with an overall detection coefficient ($= \frac{\text{cpm}}{\text{dpm}}$) of about 4.5×10^{-3}, resulting in an initial count rate of about 680 cpm. The composition of such a sample is about 24 ppm Ti. A convenient counting interval for this 42m half-life activity might be about 20 min, so that a statistically significant analysis might be performed down to fractional ppm.

References

1. C. Williamson, J. P. Boujot, and J. Picard, Tables of Range and Stopping Power of Chemical Elements for Charged Particles of Energy 0.05 to 500 MeV, Centre D'Etudes Nucléaires de Saclay, Report CEA-R 3042, 1966.
2. C. M. Lederer, J. M. Hollander, and I. Perlman, Table of Isotopes, Sixth Edition (John Wiley and Sons, Inc., New York, 1967).
3. O. D. Brill, J. Nucl. Phys. (USSR) 1, 55 (1965).
4. D. Cochran and J. Knight, Phys. Rev. 128, 1281 (1963).
5. R. L. Hahn and E. Ricci, Nucl. Phys. A101, 353 (1967).
6. E. A. Bryant, D. R. F. Cochran, and J. D. Knight, Phys. Rev. 130, 1512 (1963).

Table I. Thick-target yields from nuclear reactions induced by 20-MeV ^{3}He ions. T = target element (natural composition); P = reaction product; $T_{1/2}$ = half-life of product activity; dpm/μg = yield as defined in text.

T	P	$T_{1/2}$	Reactions	dpm/μg	Interferences
Mg	^{28}Al	2.3m	^{26}Mg(^{3}He, p)^{28}Al	8.9×10^3	^{27}Al(^{3}He, 2p)^{28}Al
	^{27}Mg	9.5m	^{26}Mg(^{3}He, 2p)^{27}Mg	1.1×10^4	^{27}Al(^{3}He, 3p)^{27}Mg
	^{24}Na	15h	^{26}Mg(^{3}He, αp)^{24}Na ^{24}Mg(^{3}He, 3p)^{24}Na	1.6×10^4	^{23}Na(^{3}He, 2p)^{24}Na
Si	^{30}P	2.5m	^{28}Si(^{3}He, p)^{30}P ^{28}Si(^{3}He, n)^{30}S→^{30}P ^{29}Si(^{3}He, d)^{30}P ^{30}Si(^{3}He, t)^{30}P	1.3×10^5	^{31}P(^{3}He, α)^{30}P ^{32}S(^{3}He, αp)^{30}P ^{32}S(^{3}He, αn)^{30}S→^{30}P
Ca	^{42m}Sc	61s	^{40}Ca(^{3}He, p)^{42m}Sc	1.3×10^4	^{41}K(^{3}He, 2n)^{42m}Sc
Ti	^{49}Cr	42m	^{47}Ti(^{3}He, n)^{49}Cr ^{48}Ti(^{3}He, 2n)^{49}Cr ^{49}Ti(^{3}He, 3n)^{49}Cr	1.5×10^5	^{50}Cr(^{3}He, α)^{49}Cr
	^{48}Cr	23h	^{46}Ti(^{3}He, n)^{48}Cr ^{47}Ti(^{3}He, 2n)^{48}Cr ^{48}Ti(^{3}He, 3n)^{48}Cr	1.5×10^{2a}	^{50}Cr(^{3}He, αn)^{48}Cr
	^{48}V	16d	^{46}Ti(^{3}He, p)^{48}V ^{47}Ti(^{3}He, d)^{48}V ^{49}Ti(^{3}He, t)^{48}V	3.2	^{50}Cr(^{3}He, αp)^{48}V
Ni	^{59}Cu	82s	^{58}Ni(^{3}He, d)^{59}Cu	1.7×10^5	^{59}Co(^{3}He, 3n)^{59}Cu
	^{60}Cu	24m	^{58}Ni(^{3}He, p)^{60}Cu ^{58}Ni(^{3}He, n)^{60}Zn→^{60}Cu ^{60}Ni(^{3}He, t)^{60}Cu	2.8×10^4	^{59}Co(^{3}He, 2n)^{60}Cu
	^{61}Cu	3.3h	^{60}Ni(^{3}He, d)^{61}Cu ^{60}Ni(^{3}He, 2n)^{61}Zn→^{61}Cu ^{61}Ni(^{3}He, t)^{61}Cu	4.0×10^5	^{59}Co(^{3}He, n)^{61}Cu ^{63}Cu(^{3}He, αn)^{61}Cu
Ni	^{62}Zn	9.3h	^{60}Ni(^{3}He, n)^{62}Zn ^{61}Ni(^{3}He, 2n)^{62}Zn ^{62}Ni(^{3}He, 3n)^{62}Zn	2.1×10^{3a}	^{64}Zn(^{3}He, αn)^{62}Zn
	^{57}Ni	36h	^{58}Ni(^{3}He, α)^{57}Ni	5.3×10^{2a}	^{56}Fe(^{3}He, 2n)^{57}Ni
	^{56}Ni	6.1d	^{58}Ni(^{3}He, αn)^{56}Ni	4.3×10^{2a}	^{56}Fe(^{3}He, 3n)^{56}Ni ^{54}Fe(^{3}He, n)^{56}Ni
Ge	^{71}As	62h	^{70}Ge(^{3}He, d)^{71}As ^{70}Ge(^{3}He, 2n)^{71}Se→^{71}As	2.2×10^{3a}	^{69}Ga(^{3}He, n)^{71}As
	^{74}As	18d	^{72}Ge(^{3}He, p)^{74}As ^{73}Ge(^{3}He, d)^{74}As ^{74}Ge(^{3}He, t)^{74}As	8.0^a	^{75}As(^{3}He, α)^{74}As
	^{75}Se	120d	^{73}Ge(^{3}He, n)^{75}Se ^{74}Ge(^{3}He, 2n)^{75}Se	3.4×10^{1a}	^{74}Se(^{3}He, 2p)^{75}Se ^{76}Se(^{3}He, α)^{75}Se ^{75}As(^{3}He, t)^{75}Se

Table I. (continued)

T	P	$T_{1/2}$	Reactions	dpm/μg	Interferences
Ta	^{180}Re	2.4m	^{181}Ta(^{3}He, 4n)^{180}Re	1.2×10^{4}[b]	^{180}W(^{3}He,t)^{180}Re
	^{181}Re	18h	^{181}Ta(^{3}He,3n)^{181}Re	5.9×10^{3}[a]	^{182}W(^{3}He,4n)^{181}Os→^{181}Re
					^{180}W(^{3}He,d)^{181}Re

a. The yields for products whose half-lives are longer than 4 hours are based on an irradiation time of 1 hour.
b. The yield of ^{180}Re is based on an entrance beam energy of 30 MeV.

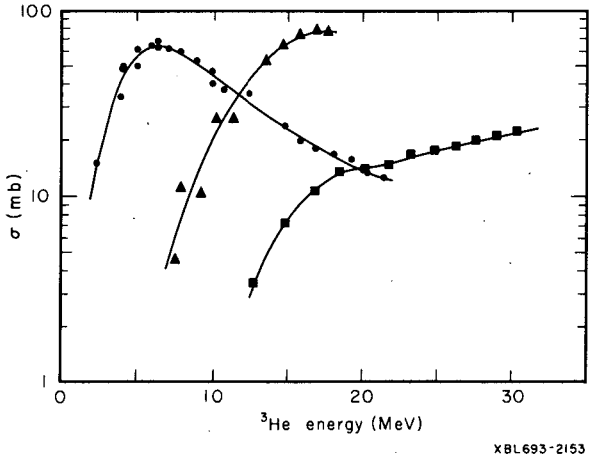

Fig. 1. Absolute excitation functions and total production cross sections for reactions ^{3}He + Mg.
● ^{26}Mg(^{3}He, p)^{28}Al
▲ ^{26}Mg(^{3}He, 2p)^{27}Mg
■ ^{3}He + Mg→ ^{24}Na

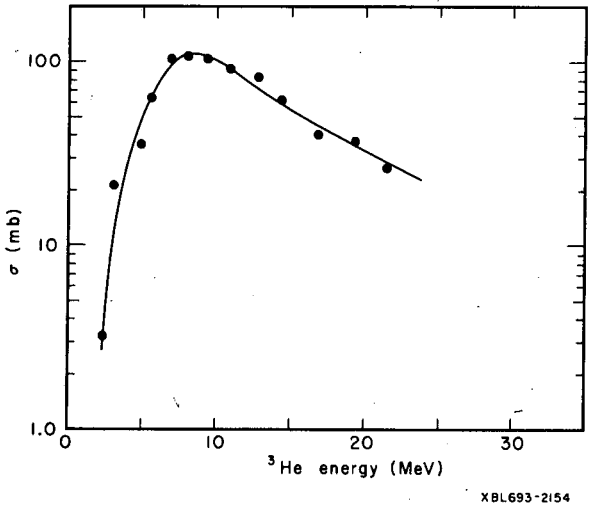

Fig. 2. Total production cross section for the reaction ^{3}He + Si → ^{30}P.

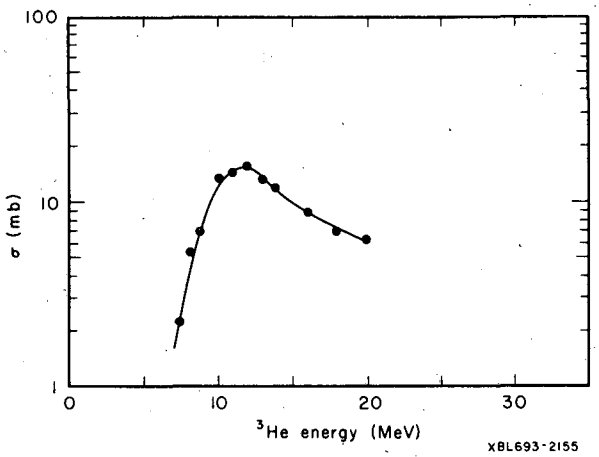

Fig. 3. Absolute excitation function for the reaction $^{40}Ca(^{3}He, p)^{42m}Sc$.

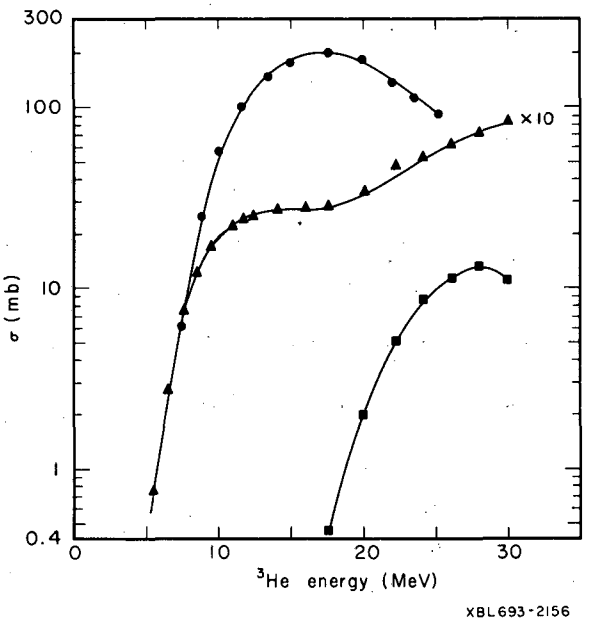

Fig. 4. Total production cross sections for reactions ^{3}He + Ti.

▲ $^{3}He + Ti \rightarrow {}^{48}Cr$

● $^{3}He + Ti \rightarrow {}^{49}Cr$

■ $^{3}He + Ti \rightarrow {}^{48}V$

Fig. 5. Total production cross sections for reactions ^{3}He + Ni.

● $^{3}He + Ni \rightarrow {}^{61}Cu$

▼ $^{3}He + Ni \rightarrow {}^{59}Cu$

▲ $^{3}He + Ni \rightarrow {}^{56}Ni$

■ $^{3}He + Ni \rightarrow {}^{60}Cu$

○ $^{3}He + Ni \rightarrow {}^{57}Ni$

◆ $^{3}He + Ni \rightarrow {}^{62}Zn$

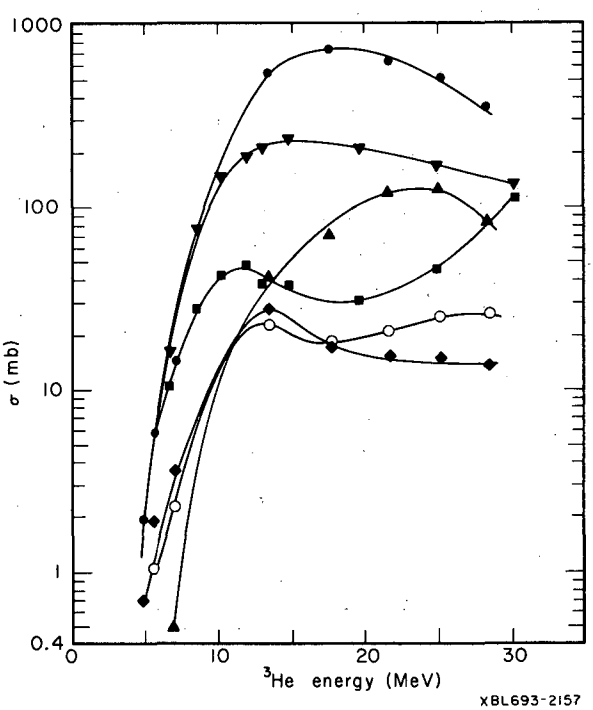

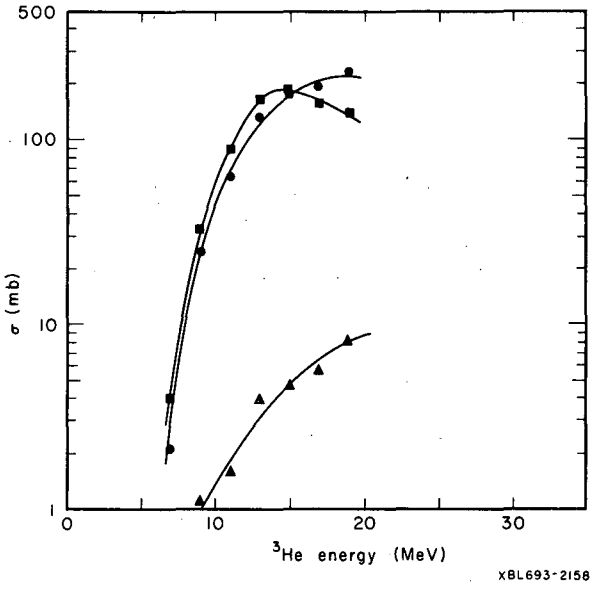

Fig. 6. Total production cross sections for reactions ^{3}He + Ge.
- ● ^{3}He + Ge → ^{71}As
- ■ ^{3}He + Ge → ^{75}Se
- ▲ ^{3}He + Ge → ^{74}As

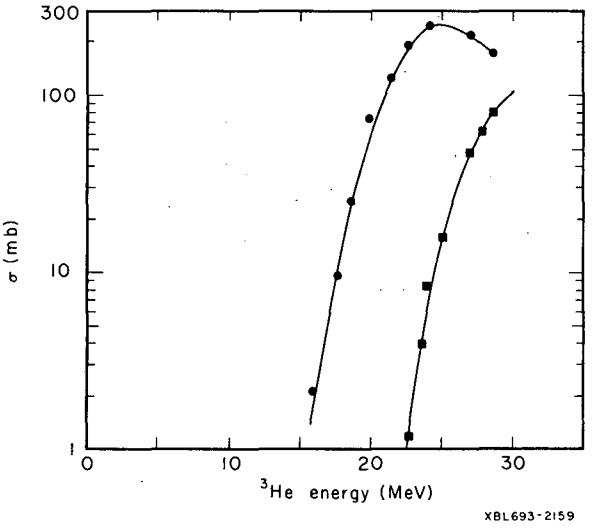

Fig. 7. Excitation functions for reactions ^{3}He + Ta.
- ● ^{181}Ta(^{3}He, 3n)^{181}Re
- ■ ^{181}Ta(^{3}He, 4n)^{180}Re

SINGLE-PARTICLE LEVEL SYSTEMATICS IN ODD-MASS NUCLEI WITH 123 NEUTRONS†

K. Valli* and E. K. Hyde

During the course of investigation of alpha-decay properties of many nuclei with neutron number 126 or less produced by reactions induced by nuclear projectiles accelerated in the heavy-ion linear accelerator, we have studied the complex alpha structure in the decay of 2.7-min ^{213}Ra and 1.2-sec ^{215}Th. If we compare the α-decay schemes of these nuclei with those of other even-Z nuclei containing 125 neutrons, some systematic trends in the levels of the daughter nuclei can be discerned. Figure 1 summarizes the data we wish to discuss. The data on ^{215}Th and ^{213}Ra come from our work;[1] those for ^{211}Rn and ^{209}Po come from the references cited by Lederer, Hollander, and Perlman.[2] In the case of the daughter nuclei, ^{205}Pb and ^{207}Po, many other excited levels are known, but we show only the lowest-lying ones, which are the ones populated by α decay. The properties of the levels of ^{205}Pb are well established and there seems little question that the 1/2-, 5/2-, and 3/2- levels can be assigned to the $p_{1/2}$, $f_{5/2}$, and $p_{3/2}$ wave functions of the independent particle shell model. The 5/2 and 1/2 levels are also well established in ^{207}Po and, in particular, the ground-state spin has been established to be 5/2 by the work of Axensten and Olsmats.[3]

The figure reveals a regular trend in the relationship of the three lowest levels, and although the alpha spectra do not establish the spins of the levels in ^{209}Rn and ^{211}Ra, it is tempting to make the assignments shown in parentheses and to regard the shifts in the level positions as a reflection of the operation of residual internucleon forces as the proton pairs are increased beyond the 82-proton shell. No one has treated this particular problem with any of the current theoretical models for the residual internucleon forces, although the shift in these levels in going from ^{207}Pb to ^{205}Pb has been treated by several authors.

Assuming that this identification of the levels shown in the figure is correct, we can make the predictions of the levels of ^{213}Th and the α-decay pattern of ^{217}U shown in the figure.

Footnotes and References

†Excerpted from Phys. Rev. 176, 1377 (1968).
*Present address: Department of Physics, University of Helsinki, Finland.

1. Full article [Phys. Rev. 176, 1377 (1968)] and K. Valli, W. Treytl, and E. K. Hyde, Phys. Rev. 161, 1284 (1967).
2. C. M. Lederer, J. M. Hollander, and I. Perlman, Table of Isotopes, sixth edition (John Wiley and Sons, Inc., New York, 1967).
3. S. Axenten and C. M. Olsmats, Ark. Fys. 19, 461 (1961).

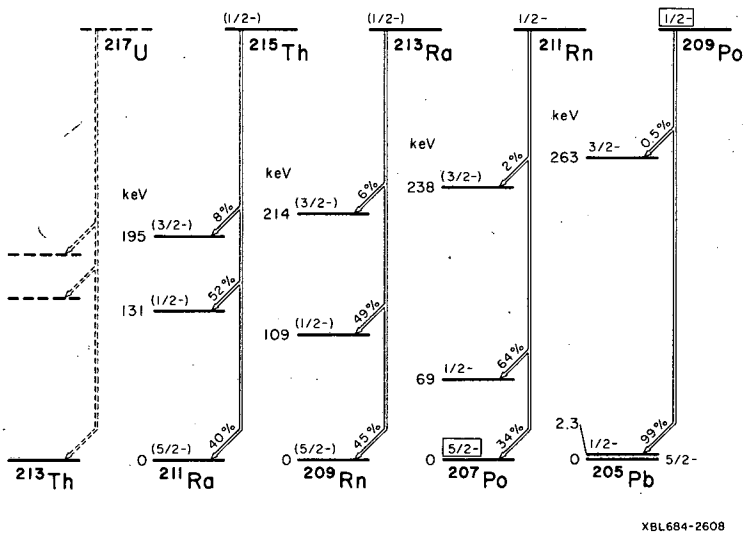

Fig. 1. Alpha-decay schemes of the 125-neutron isotopes of the even elements polonium, radon, radium, and thorium. The framed values have been measured directly, those shown without parentheses have been derived from extensive data, and those given in parentheses are suggested assignments. The predicted decay scheme of ^{217}U is indicated by broken lines.

ISOMERISM IN ODD-ODD NUCLEI WITH 127 NEUTRONS†

K. Valli* and E. K. Hyde

As a result of the work of Jones[1] on ^{212}At, of Torgerson, Gough, and Macfarlane[2] on ^{214}Fr, of ourselves[3] on ^{214}Fr, and of the authors cited in The Table of Isotopes[4] on ^{210}Bi, we now have proof of the systematic occurrence of isomerism in nuclides of odd elements above lead containing 127 neutrons. The cases are summarized in Fig. 1.

The isomerism can be explained by the high spins of the odd neutron and proton. The shell model predicts $g_{9/2}$ for an odd proton lying just above the 82-proton shell and $h_{9/2}$ for an odd neutron just above the 126-neutron shell, so that close-lying levels of 0- and 9- are possible. The case of ^{210}Bi is particularly interesting from the standpoint of theory,[5] because it provides an opportunity to test the np interaction for a single neutron and single proton of high spin beyond a double-closed-shell core. The residual interaction between these two particles gives rise to a multiplet

of 10 negative-parity levels with spins from 0 to 9. The correct ordering of these levels seems to occur only if a short-range tensor force is added to a central force of the type successfully used to explain the nn interaction in such nuclei as ^{206}Pb. A particularly interesting feature in ^{210}Bi is that the ground state is 1- rather than 0-. The 0- level occurs at 47 keV and then a wide spin gap occurs; the next state is 9- at 250 keV. Theoretical calculations on ^{212}At, ^{214}Fr, and ^{216}Ac would be more complex because of the extra pairs of protons beyond the closed shell; but the experimental results prove that a wide gap in spin is preserved in the ground-state multiplet, at least for the first two. The data also suggest strongly that 1- rather than 0- is preserved as the ground state in ^{212}At and ^{214}Fr. This conclusion comes from the fact that the pair of alpha groups from the isomer have the same energy separation as the pair from the ground state, indicating that the ground and first excited states are being populated in both instances. But this could not be the case if the ground state of ^{212}At or ^{214}Fr were 0-, because the selection rules of alpha decay would forbid a 0- to 4+ transition, and it is highly likely that the ground state and first excited state of the daughter nuclei are 5+ and 4+, respectively, resulting from the coupling of $p_{1/2}$ neutron and $h_{9/2}$ proton.

For ^{216}Ac the systematic trends would suggest the occurrence of isomerism. In our work,[3] we have observed four α groups and a tentative indication of isomerism, but more measurements are required.

Footnotes and References

†Excerpted from Phys. Rev. 176, 1377 (1968).

*Present address: Department of Physics, University of Helsinki, Finland.

1. W. B. Jones, Phys. Rev. 130, 2042 (1963).
2. D. F. Torgerson, R. A. Gough, and R. D. Macfarlane, Phys. Rev. 174, 1494 (1968).
3. K. Valli and E. K. Hyde, Phys. Rev. 176, 1377 (1968).
4. C. M. Lederer, J. M. Hollander, and I. Perlman, Table of Isotopes, sixth edition (John Wiley and Sons, Inc., New York, 1967).
5. Y. E. Kim and J. O. Rasmussen, Nucl. Phys. 47, 184 (1963).

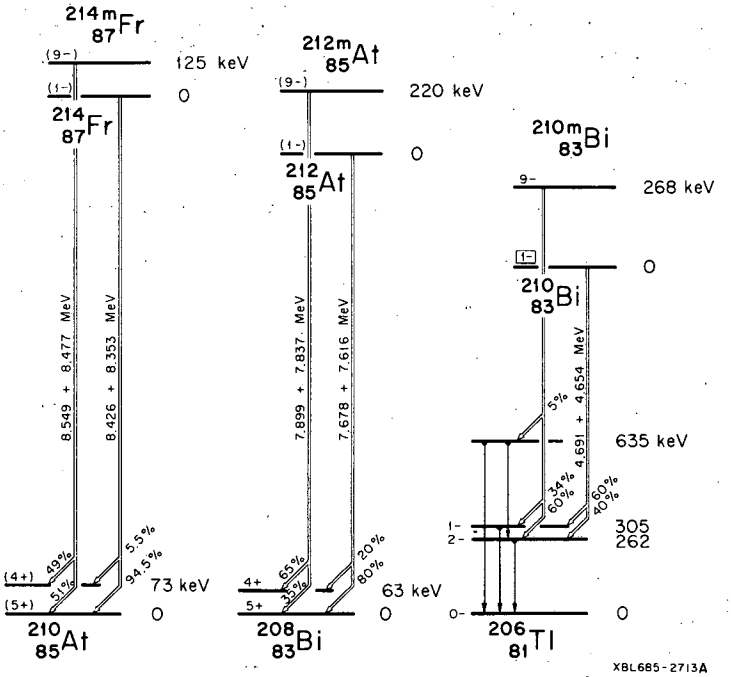

Fig. 1. Alpha-decay schemes of the 127-neutron isotopes of the odd elements bismuth, astatine, and francium. The framed spin value has been measured directly, those shown without parentheses have been derived indirectly, and those given in parentheses are probable values based on shell-model predictions and similarities between the schemes.

LEVELS OF ^{208}Po FROM RADIOACTIVE DECAY AND NUCLEAR REACTION γ-RAY SPECTROSCOPY†

W. J. Treytl, E. K. Hyde, and T. Yamazaki*

A detailed study was made of the radiations emitted by 1.7-hr ^{208}At in its electron-capture decay to ^{208}Po. Additional information was obtained by on-line measurements of ^{208}Po radiations emitted during the course of ^{209}Bi(p, 2n)^{208}Po and ^{206}Pb(α, 2n)^{208}Po reactions carried out at the 88-inch cyclotron. The purpose of the work was to determine the level scheme of ^{208}Po, a nucleus which is only two protons and two neutrons away from doubly magic ^{208}Pb and hence of considerable theoretical interest.

Pure samples of ^{208}At were prepared by first isolating its 20-min parent, ^{212}Fr, which was made at the heavy-ion linear accelerator by the nuclear reaction ^{205}Tl(^{12}C, 5n)^{212}Fr. The ^{212}Fr parent was prepared in radioactivity--pure form and, after a suitable decay period, the ^{208}At daughter was isolated by chemical procedures specific for astatine. The ^{208}At γ radiations were studied with Ge(Li) detectors by singles and coincidence techniques. Electrons were measured by silicon semiconductors. Delayed transitions were studied by the technique of delayed coincidence.

In the in-beam measurements at the cyclotron, both prompt and delayed coincidences were measured, and angular distributions were measured for the prominent γ cascade.

The results of the measurement are summarized in Fig. 1. Many of the lower-lying levels of ^{208}Po can be interpreted by examining the level schemes of ^{210}Po and ^{206}Pb and by assuming

weak coupling for the interaction of the two neutron hole states with two proton states beyond a closed shell. Such a comparison is shown in Fig. 2. The most prominent feature is a group of levels associated with the $(h_{9/2})^2$ proton configuration, and the most interesting member of the group is the 8+ level, which has a half-life of 380 nsec. The energy of the E2 transition connecting the 8+ and 6+ levels is 10 keV or less, and because of experimental difficulties the radiations (electrons) corresponding to this transition were not observed.

Footnotes

†Condensed from Nucl. Phys. A117, 481 (1968).
*Present address: Department of Physics, University of Tokyo, Japan.

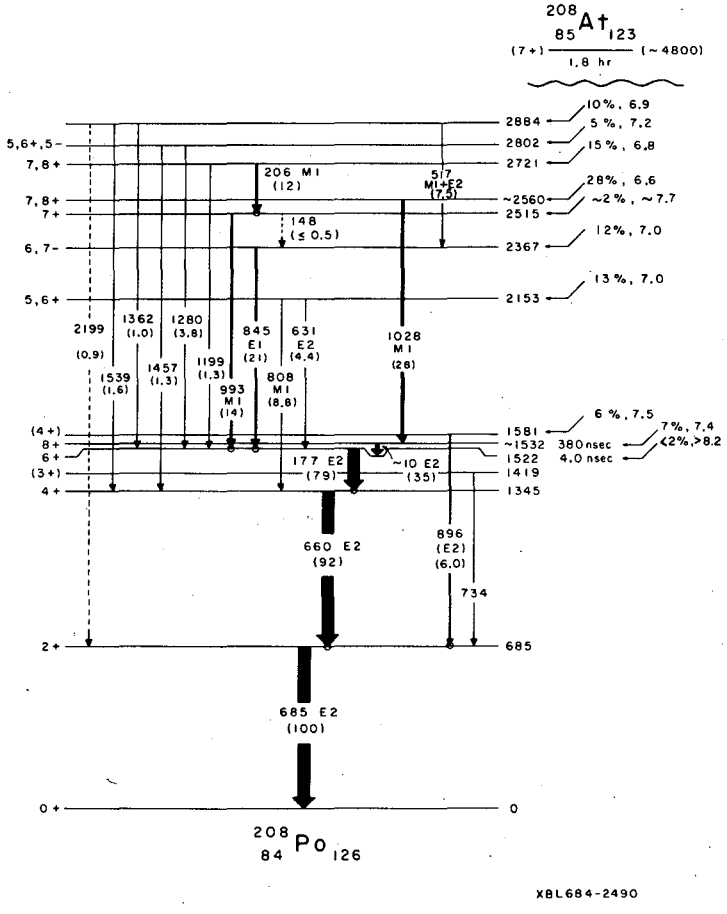

Fig. 1. Decay scheme of ^{208}At, showing ^{208}Po levels and transitions. Numbers in parentheses are percent transition intensities. Coincidence relationships established by experiment are indicated by circles at arrowheads.

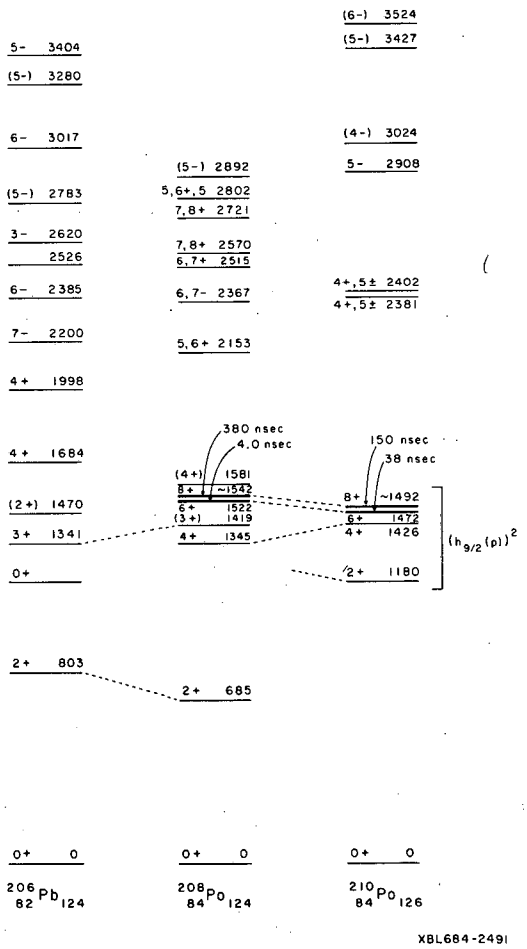

Fig. 2. Comparison of the levels of ^{206}Pb, ^{208}Po, and ^{210}Po. Levels of similar character are connected by dotted lines.

OBSERVATION OF THE NEW ISOTOPE ^{17}C USING A COMBINED TIME-OF-FLIGHT PARTICLE-IDENTIFICATION TECHNIQUE†

A. M. Poskanzer, G. W. Butler, E. K. Hyde, J. Cerny, D. A. Landis, and F. S. Goulding

Addition of time of flight to the particle-identification technique used previously for the study of light nuclei ejected from uranium by 5.5-GeV protons has established the existence of ^{17}C and the particle instability of ^{13}Be.

The interaction of GeV protons with a high-Z target leads to the production of all isotopes of the light elements, therefore a systematic search for previously unreported particle-stable isotopes can be carried out. In a previous publication[1] we demonstrated the utility of the technique by proving the existence of ^{11}Li, ^{14}B, and ^{15}B, the particle instability of ^{10}Li, and the probable particle instability of ^{13}Be. We report here new results which depend upon an extension of the earlier technique to include mass identification by a time-of-flight measurement in addition to particle identification by energy-loss measurements.

The experiment was performed by using the Bevatron's 5.5-GeV external proton beam to bombard a uranium metal target of 27 mg/cm^2 thickness. Beam pulses 0.6 sec long and containing about 3×10^{11} protons occurred every 6 sec. In a preliminary experiment not involving time of flight a telescope of phosphorus-diffused silicon counters, collimated to 4×6 mm^2, was located 22 cm from the target at an angle of 30 deg to the beam. Details of the circuitry employed with the

detectors to effect the particle identification can be found elsewhere.[2] Figure 1 shows the particle spectrum covering the region of the Be, B, C, and N isotopes that resulted from 35 hr of data collection. The isotopes ^{14}B and ^{15}B are better resolved in Fig. 1 than in our previous work, and it is now quite clear that ^{13}Be does not exist.[3] However, in an attempt to determine the existence of other isotopes a difficulty arose in that the particle-identifier signals corresponding to the heaviest isotopes of one element overlapped those for the lightest isotopes of the next element. There appears to be evidence for a ^{17}C peak in this figure, but in order to verify this and to resolve some of the other ambiguities we decided to change our apparatus to permit measurement of an additional parameter, the time of flight of the fragments, and from this and their energy to obtain an independent determination of fragment mass.

The telescope used for the combined time-of-flight particle-identification measurements consisted of five detectors at an angle of 45 deg to the beam. The time resolution varied from 0.3 nsec for ^{15}N up to 0.5 nsec for ^{7}Be. The time-of-flight signal t, and E_T, the total energy deposited in the E detector and the two ΔE detectors, were sent to a circuit which performed the analog calculation $E_T \times t^2$ and thus produced a signal proportional to the mass of the fragment. The particle spectrum obtained during 5 days of data collection showed clear evidence for a ^{17}C peak. Mass spectra were then summed for the ten indicated regions in the particle spectrum, and these are plotted in Fig. 2. Almost all the events that fell in the ^{17}C region of the particle spectrum also fell in the mass 17 region of the mass spectrum, thus clearly proving the existence of ^{17}C.

We thank R. P. Lothrop and M. D. Roach for making the detectors.

Footnotes and References

†Condensed from Phys. Letters 27B, 414 (1968).

1. A. M. Poskanzer, S. W. Cosper, E. K. Hyde, and J. Cerny, Phys. Rev. Letters 17, 1271 (1966).

2. G. W. Butler, J. Cerny, S. W. Cosper, and R. L. McGrath, Phys. Rev. 166, 1096 (1968), and references therein.

3. We also have another spectrum in which the yield ratio ^{12}Be/^{13}Be is greater than 100, whereas if ^{13}Be exists this ratio should be similar to the ^{10}Be/^{11}Be and ^{13}B/^{14}B ratios, which are about 10.

4. G. T. Garvey and I. Kelson, Phys. Rev. Letters 16, 197 (1966).

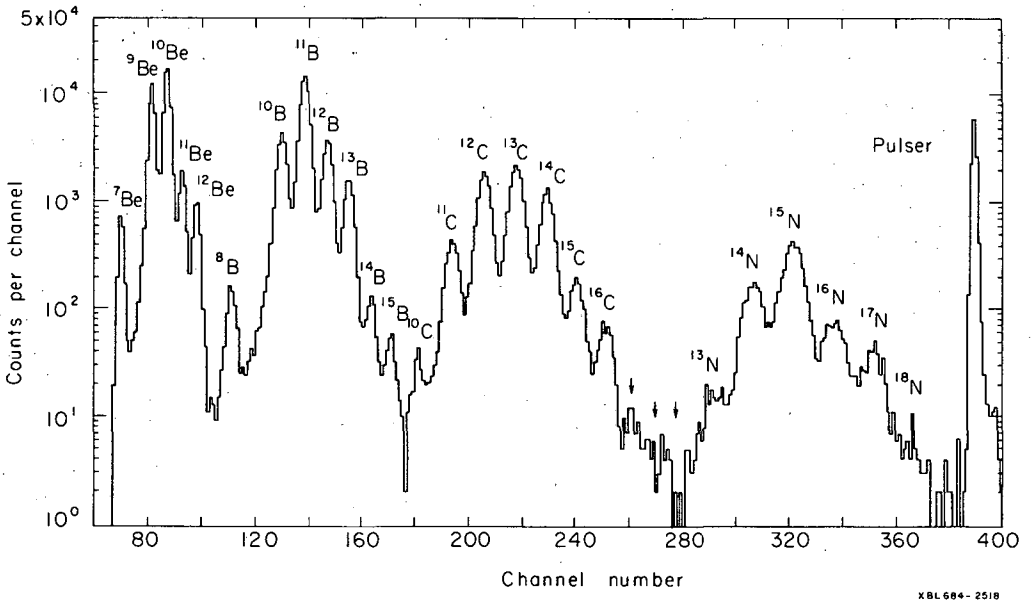

Fig. 1. Particle spectrum derived from energy loss measurements in semiconductor detectors. The fragments were produced by the bombardment of uranium by 5.5-GeV protons. The three arrows indicate in order the positions that would be expected for ^{17}C, ^{18}C, and ^{12}N. (Peak areas do not accurately reflect relative yields because of the narrow and different ranges of total energy accepted for each isotope.)

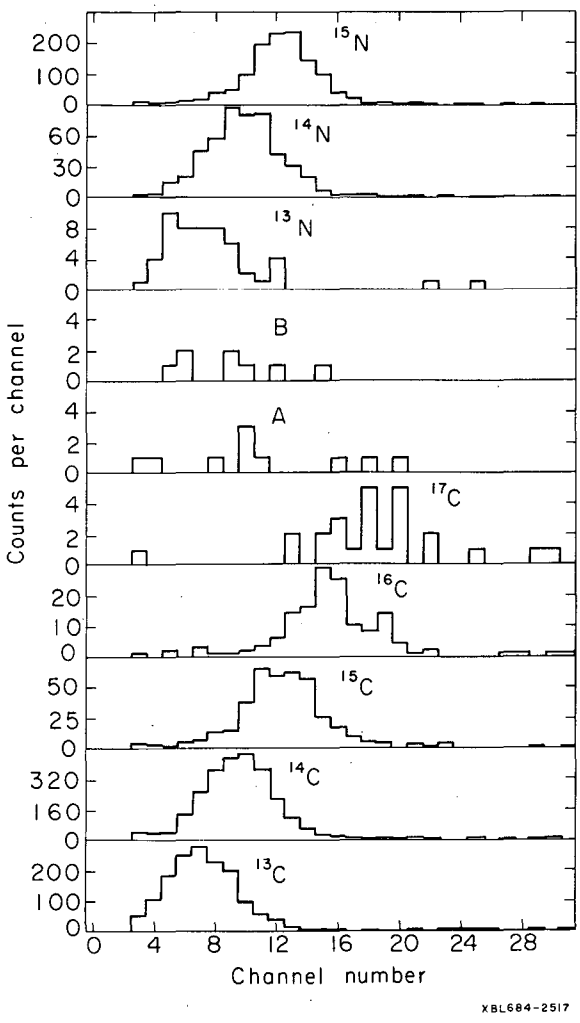

Fig. 2. Mass spectra derived from time-of-flight and energy measurements. Each mass spectrum corresponds to the region in the particle spectrum for the indicated isotope. The expected position of ^{18}C is in region A and of ^{12}N in regions A and B.

LIFETIMES OF ROTATIONAL STATES FROM HEAVY-ION REACTIONS†

R. M. Diamond, F. S. Stephens, W. H. Kelly,* and D. Ward‡

The measurement of transition moments is an important method of testing nuclear models. In particular, the E2 moments of the $2 \rightarrow 0$ transitions in the ground-state collective bands of even-even nuclei have yielded much information on the nature of these bands. In this work we have measured the $2 \rightarrow 0$ and several higher ground-band E2 moments (lifetimes) in each of three even-even Er nuclei, using the recoil-distance Doppler-shift method. These nuclei were produced in the reactions ^{120,122,124}Sn(Ar, 4n)^{156,158,160}Er.

The recoil-distance Doppler-shift method[1] is well suited to measure half-lives in the range 10^{-9} to 10^{-12} sec.[2-5] Basically this method consists of stopping part of the excited nuclei recoiling from a thin target with a movable plunger placed closely behind the target. The fraction of the nuclei that live long enough to reach the plunger before emitting their radiation will yield a normal γ-ray line, whereas the rest will decay in flight and yield a Doppler-shifted line. By varying the distance of the plunger from the target, the fraction of unshifted transitions can be changed, and one can obtain the half-life of the transition if the velocity of the recoiling nucleus is also known.

The (^{40}Ar, 4n) reaction produces a tightly collimated beam of product nuclei recoiling along the beam direction. Using a Ge(Li) detector at 0 deg to the beam direction, we were able to completely resolve the shifted and unshifted lines for all transitions over ≈ 100 keV. The average recoil velocity could be obtained directly from the fractional energy difference of the shifted and unshifted lines, after a correction was made for the finite solid angle of the detector (the effective angle is different from 0 deg for large solid angles). Some typical spectra for ^{160}Er are shown in Fig. 1. We have integrated the areas under the shifted and unshifted peaks, and calculated the fraction of each line that is unshifted at each distance. The analysis of these data is rather complex, as account must be taken of the earlier rotational transitions, and also of the 10 to 20 unobserved lines that precede entry into the ground band. We have used a computer program which considers three consecutive transitions at a time, e.g., $8 \rightarrow 6 \rightarrow 4 \rightarrow 2$. The program makes a least-squares fit to the first set of data ($8 \rightarrow 6$ above) using three arbitrary transitions and an origin displacement to mock up the cascade preceding this transition. Simultaneous least-square fits to the following two sets of data ($6 \rightarrow 4$ and $4 \rightarrow 2$ above) are made with their lifetimes as the only two additional variables.

A number of corrections had to be considered. An important one was due to attenuation of the angular distribution of the γ radiation by the large hyperfine field (40 MG) acting at the nucleus when the highly stripped target ion recoils into vacuum.[6,7] This caused a maximum correction of 6% for half-lives of the order of 3×10^{-11} sec. The most significant error for the fast transitions is in the peak area integrations. The spectra are not particularly clean, and a small extraneous peak could cause a systematic error in the integration of a particular line. The uncertainty introduced by the integrations is estimated to be $\pm 0.6 \times 10^{-12}$ sec for ^{160,158}Er and $\pm 1.0 \times 10^{-12}$ sec for ^{156}Er, which has somewhat poorer spectra. An error of ±5% has been set for the best transitions to account for other systematic errors and for the fact that a number of corrections ranging up to a few percent in magnitude had to be made to the raw data.

Figure 2 shows a comparison of the experimental points and the computer-calculated curves for ^{160}Er. The lowest points of the fastest transitions tend systematically to be high, which probably indicates small amounts of somewhat slower feeding. The half-life values obtained are shown in Table I together with the energies of the transitions and the ratio of v/c for the recoils. Also listed are the experimental B(E2) values, and these are compared with three theoretical B(E2) values.

Several qualitative conclusions can be drawn from the B(E2) values in Table I. Within our limits of error all these values are nearly consistent with the rigid-rotor limit; however, those for ^{160}Er probably fall below this limit for high spin values, whereas those for the other two nuclei probably go above this limit. In fact, the B(E2) values for ^{156}Er are perhaps more consistent with the vibrator limit, as might be expected from the energy-level spacings in this nucleus. Since the more vibrational nuclei start with smaller B(E2; $2 \rightarrow 0$) values than the rotors, but increase more rapidly with increasing spin, there is a tendency for the B(E2) values to become the same at higher spins. Thus for the three nuclei studied here the spread between the B(E2; $2 \rightarrow 0$) values is a factor of 2.5, but between the B(E2; $6 \rightarrow 4$) values is only a factor of 1.3. This type of behavior has already been noted for the transition energies of even-even nuclei at high spin,[8] and suggests that the differences between the rotational- and vibrational-type nuclei near the ground state are disappearing with increasing angular momentum.

It is also of interest to compare the B(E2) values with the predictions of the centrifugal stretching model,[9] which gives a good empirical fit to the energy levels of the ground-state band.[8] The last column in Table I makes this comparison for ^{158}Er and ^{160}Er, using the calculations of Davydov and Ovcharenko.[10] For ^{160}Er the B(E2) values do not increase so much as predicted. Thus we would conclude that centrifugal stretching is not the only change taking place in this nucleus with increasing angular momentum. This conclusion has previously been reached in other similar cases based on (a) the mixing of the ground- and β-bands,[11,12] (b) the Mössbauer isomer-shift work,[13-17] (c) the μ-mesic x-ray studies,[18] and (d) theoretical calculations.[19,20] It is generally supposed that the other important change occurring with increasing angular momentum is a reduction of the pairing correlations due to the Coriolis force. It is not clear how this reduction would affect the B(E2) values. For ^{158}Er, however, this model fits very well, and it will be of interest to see if such nuclei between rotors and vibrators do indeed stretch.

The decay curves, such as those in Fig. 2, also indicate the mean time interval between the reaction (d = 0) and the population of the ground band (1/e point on the curves for the fastest rotational transitions). These mean feeding times are $(6 \pm 3) \times 10^{-12}$, $(1.1 \pm 0.3) \times 10^{-11}$, and $(1.6 \pm 0.3) \times 10^{-11}$ sec, respectively, for ^{160}Er, ^{158}Er, and ^{156}Er. Considering that 10 to 20 transitions must be emitted in this time interval, these feeding times seem surprisingly short,

especially for the rotor, ^{160}Er. The trend between ^{160}Er and ^{156}Er is rather striking, and it will be of interest to see if this reflects a general difference between rotors and vibrators, or is just something peculiar to these three cases.

Footnotes and References

†Condensed from Phys. Rev. Letters (to be published Mar. 17, 1969).

*Permanent address: Department of Physics, Michigan State University, East Lansing, Michigan 48823.

‡Present address: Nuclear Physics Division, Chalk River Nuclear Laboratories, Chalk River, Ontario, Canada.

1. S. Devons, G. Manning, and St. P. Bunbury, Proc. Phys. Soc. (London) A68, 18 (1955).
2. I. F. Wright, Bull. Am. Phys. Soc. 6, 285 (1961).
3. T. K. Alexander and K. W. Allen, Can. J. Phys. 43, 1563 (1965).
4. T. K. Alexander, K. W. Allen, and D. C. Healey, Phys. Letters 20, 402 (1965); K. W. Allen, T. K. Alexander, and D. C. Healey, Phys. Letters 22, 193 (1966).
5. P. G. Bizzetti, A. M. Bizzetti-Sona, S. Kalbitzer, and B. Povh, Z. Physik 201, 295 (1967).
6. D. Ashery, N. Bahcall, G. Goldring, A. Sprinzak, and Y. Wolfson, Nucl. Physics A101, 51 (1967).
7. I. Ben Zvi, P. Gilad, M. Goldberg, G. Goldring, A. Schwarzschild, A. Sprinzak, and Z. Vager, Nucl. Phys. A121, 592 (1968).
8. F. S. Stephens, N. Lark, and R. M. Diamond, Phys. Rev. Letters 12, 225 (1964); R. M. Diamond, F. S. Stephens, and W. J. Swiatecki, Phys. Letters 11, 315 (1964).
9. A. S. Davydov and A. A. Chaban, Nucl. Phys. 20, 499 (1960).
10. A. S. Davydov and V. I. Ovcharenko, Soviet J. Nucl. Physics 3, 740 (1966).
11. Y. Yoshizawa, B. Elbek, B. Herskind, and M. C. Olesen, Nucl. Phys. 73, 273 (1965).
12. G. G. Seaman, J. G. Greenberg, D. A. Bromley, and F. K. McGowan, Phys. Rev. 149, 925 (1966).
13. J. Fink and P. Kienle, Phys. Letters 17, 326 (1965).
14. D. Yeboah-Amankwah, L. Grodzins, and R. B. Frankel, Phys. Rev. Letters 18, 791 (1967).
15. P. Steiner, E. Gerdau, P. Kienle, and H. J. Körner, Phys. Letters 24, B515 (1967).
16. U. Atzmony, E. R. Bauminger, J. Hess, A. Mustachi, and S. Ofer, Phys. Rev. Letters 18, 1061 (1967).
17. P. Kienle, W. Henning, G. Kaindl, H. J. Körner, H. Schaller, and F. Wagner, in Proceedings of the International Conference on Nuclear Structure, Tokyo, 1967, Ed. by J. Sanada; J. Phys. Soc. Japan 24, 207 (1968).
18. S. Bernow, S. Devons, I. Duerdoth, D. Hitlin, J. W. Kast, E. R. Macagno, J. Rainwater, K. Runge, and C. S. Wu, Phys. Rev. Letters 18, 787 (1967).
19. T. Udagawa and R. K. Sheline, Phys. Rev. Letters 16, 325 (1966).
20. E. R. Marshalek, Phys. Rev. Letters 20, 214 (1968).

Table I. Lifetimes of collective transitions in $^{160, 158, 156}Er$.

Nucleus	Transition	Energy (keV)	Recoil v/c(%)	$T_{1/2}$ (psec)	$\alpha_T \times 10^2$ $(\alpha_K + 1.3\alpha_L)$	B(E2;I→I-2) $(e^2 \times 10^{-48} cm^4)$	$B(E2)_{rot}$	$B(E2)_{vib}$	$B(E2)_{c.s.}$
^{160}Er	2 → 0	126.2	1.96	919±46	1.30	.83 ± .04	(0.83)	(0.83)	(0.83)
	4 → 2	264.3	1.80	34.5 ±1.7	0.089	1.16 ± .06	1.19	1.66	1.25
	6 → 4	376.3	1.80	5.39 ±.49	0.037	1.34 ± .12	1.31	2.49	1.48
	8 → 6	464.6	1.80	2.16 ±.48	0.020	1.18 ± .27	1.37	3.32	1.70
	10 → 8	532.1	1.80	1.24 ±.47	0.014	1.05 ± .40	1.40	4.15	1.91
^{158}Er	2 → 0	192.7	1.96	300±15	0.283	0.55 ± .03	(0.55)	(0.55)	(0.55)
	4 → 2	335.7	1.87	14.4 ±.72	0.050	0.87 ± .04	.79	1.10	0.87
	6 → 4	443.8	1.87	2.80 ±.46	0.026	1.14 ± .18	.87	1.65	1.11
	8 → 6	523.8	1.87	1.21 ±.47	0.015	1.16 ± .45	.91	2.20	1.35
^{156}Er	2 → 0	344.4	2.20	33.2 ±1.7	0.047	0.33 ± .02	(0.33)	(0.33)	
	4 → 2	452.9	2.20	5.42 ±.65	0.022	0.53 ± .06	0.47	0.66	
	6 → 4	543.2	2.20	1.14 ±.66	0.013	1.03 ± .60	0.52	0.99	

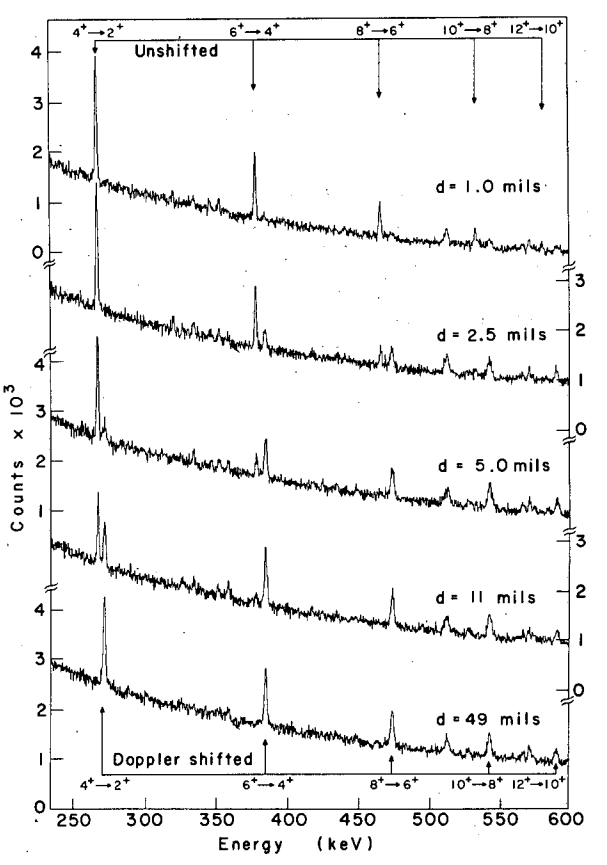

Fig. 1. Spectra from $^{124}Sn(^{40}Ar, 4n)^{160}Er$ taken with the plunger set at the indicated distances from the target. The positions of the unshifted lines are given at the top of the figure, the shifted at the bottom.

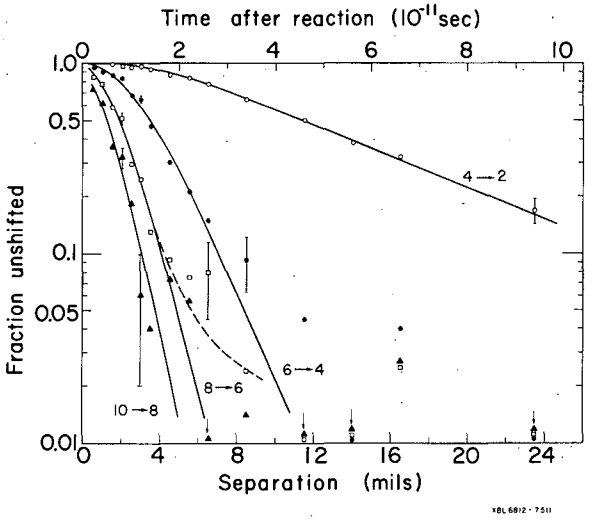

Fig. 2. The fraction of each transition which is unshifted in energy vs the separation distance of the target and plunger. The symbols represent experimental points for the ground-band transitions in ^{160}Er. The solid lines are the computer-calculated curves, and the dashed line for the 8→6 transition shows the effect of using the program that allows two components to feed the ground-state band.

GAMMA-RAY DEEXCITATION OF COMPOUND-NUCLEUS-REACTION PRODUCTS†

F. S. Stephens, R. M. Diamond, W. H. Kelly,* J. O. Newton,‡ and D. Ward††

A number of studies have been made of the γ rays emitted in the deexcitation of the product nuclei following compound-nucleus reactions. It is now well known that when this product nucleus is doubly even, the strongest discrete lines in the gamma-ray spectrum are the transitions between members of the ground-state collective band (gsb). This has been found to be true for projectiles ranging all the way from protons to ^{40}Ar. We feel that the data now available on the population of the gsb following such reactions are sufficient to provide considerable insight into the entire γ-ray deexcitation process, particularly if the initial angular momentum is large.

The following four points have been established.

(1) The maximum spin observable in the gsb (states populated to the extent of $\gtrsim$ 10% of the 2+ state) ranges from 14 to 18 for rotors to around 6 for vibrators. This maximum is the same for a given product nucleus whether it be made by a (He, 4n) reaction ($\ell_{max} \approx 16$) or an (^{40}Ar, 4n) reaction ($\ell_{max} \approx 40$).

(2) For reactions initiated by lighter ions the gsb receives independent feeding to all the band members. For ^{11}B this feeding is ≈ 10 to 20% to each band member. On the other hand, with ^{40}Ar projectiles essentially all the independent feeding is to the highest observed two or three members of the band.

(3) The alignment of the angular momentum introduced by the reaction is typically almost completely preserved throughout the deexcitation process.

(4) The mean time interval between the reaction and the population of the gsb in three ^{40}Ar-induced reactions[1] was found to be $\approx 10^{-11}$ sec. Although in some cases there appeared to be components with somewhat different feeding times, less than 5% of the feeding was appreciably slower than this. If these three cases ($^{156, 158, 160}$Er) are representative, the feeding time for rotors like ^{160}Er ($\approx 6\times10^{-12}$ sec) is appreciably less than that for vibrators like ^{156}Er ($\approx 1.6\times10^{-11}$ sec).

We believe these features of the gsb population follow rather naturally from a general description of the deexcitation process recently given by Grover and co-workers.[2] We will first outline this description of the deexcitation process, and then examine in somewhat greater detail certain critical aspects of it. The general scheme is shown in Fig. 1, which is a plot of excitation energy in the final product nucleus (having mass ≈ 160) versus angular momentum. The line is an estimate of the lowest-energy non-gsb states existing in this nucleus for each angular momentum. Grover calls the lowest level for each spin the yrast level. It is clear that the gsb members are the yrast levels for the lowest angular momentum values, and the dots and dashes indicate gsb energies for a vibrator like ^{190}Hg and a rotor like ^{160}Er, respectively. The short heavy lines in

Fig. 1 indicate the initial angular-momentum ranges and average excitation energies in this nucleus following (^{4}He, 4n) and (^{40}Ar, 4n) reactions. The average excitation energies are taken to be about one neutron-binding energy above the yrast levels.

In the de-excitation process Grover proposes that high-energy photons, probably mostly dipole, will first be emitted down to the vicinity of the yrast levels. In the (^{4}He, 4n) reaction producing a rotational product nucleus, we believe that this population goes more or less directly into the various gsb members, as these members comprise the yrast levels over most of the populated angular-momentum range. This results in independent feeding to all these gsb members. For the (^{40}Ar, 4n) reaction, however, the population collects in the vicinity of the yrast line and then trickles down near this line, entering the gsb at that point where its members become the yrast levels. If several levels for each spin are involved along the non-gsb yrast line (to spread the population and thereby avoid generating discrete γ-ray lines), this simple picture accounts very nicely for points (1) and (2) above. It also offers an explanation for the fact that β- and γ-vibrational bands are not appreciably populated in reactions with medium or heavy ions (fed via an yrast cascade), but are populated in proton and α-particle-induced reactions (fed more or less directly from above). Regarding point (3), Rasmussen and Sugihara have shown[3] that if the initial angular momentum is rather large, and the band is fed at a reasonably high spin value, then the alignment will be preserved for almost any intervening cascade. In fact, the observed alignments are in accord with those expected. We now need to examine the non-gsb yrast region in more detail to see if feeding times as short as 10^{-11} sec are plausible and whether several levels are likely to be involved at each spin value.

One can easily estimate that the yrast cascade following an (^{40}Ar, 4n) reaction must carry off $\approx 20\,\hbar$ of angular momentum and ≈ 10 MeV of energy. Thus the cascade could involve about ten E2 transitions of average energy ≈ 1 MeV whose average lifetime would have to be $\approx 10^{-12}$ sec in order to account for the observed feeding times. Such transitions would be about 10 times as fast as the Weisskopf single-particle estimate for E2 transitions (10 spu). Similarly it could involve around twenty M1 or E1 transitions, which would have to be about 0.1 or 10^{-3} spu, respectively. None of these average lifetimes seems implausible, and the yrast cascade probably involves them all to some extent; however, the systematic absence of traps in the Er nuclei (states with lifetimes greater than 10^{-11} sec) preceding the gsb population suggests to us that the levels in the yrast region have considerable regularity. We propose that the presence of collective bands is the most likely origin of this regularity, and at the same time such bands provide a natural explanation for E2 transitions of about the required lifetime.

In Fig. 2 we show schematically the yrast region for spins I, I+1, and I+2, where $I \approx 30\,\hbar$. A few of the hundreds of possible transitions among these levels are indicated. The energy separations between the three yrast levels correspond to that given by a rigid moment of inertia. Considering the nature of these levels, we believe the following three properties are likely: (1) the pairing correlations are absent, having been destroyed by the large angular momentum or the large number of quasi-particles (or both); (2) the states consist partly, perhaps mostly, of collective states based on lower-spin states in the yrast region, rather than of just quasi-particle states as considered by Grover; and (3) the states of a given spin are heavily admixed into each other over regions of at least a few hundred keV (the Coriolis force becomes extremely large and should normally be able to ensure this). If the levels have these properties, then it seems to us that the observed features of the cascade can be understood. The mixing can prevent traps (ranging out to and beyond the millisecond region) which might otherwise arise due to structural differences between various bands--differences in K value between rotational bands being the most obvious example. The collective-band character of the levels can provide both the very regular energy spacings and the enhanced E2 transitions necessary for the observed short feeding times. It is clear, however, that E1 transitions must frequently compete with these collective ones, since traps that might correspond to the termination of negative parity bands were not observed with these Er nuclei. The pairing correlations must be absent, it seems to us, since otherwise there would be an energy gap and hence an energetically favored band that would be heavily populated, giving rise to intense lines (which are not observed). In fact, in this picture it is just the onset of pairing, as the spin decreases, that favors the ground band energetically and causes it to be heavily populated.

A final point has to do with the energy region above the yrast levels over which population occurs. We can estimate a minimum width for this energy region. If the levels were completely mixed so that the only differentiation among them would be the energy dependence of the E2 transition probabilities (M1 or E1 transitions would be similar for these purposes), then the insert in Fig. 2 shows the relative population of a level versus its energy above the yrast level. One

sees that the population would be spread over 200 or 300 keV. A lack of complete mixing of the levels would probably increase this somewhat. This range seems about right for our purposes, as (a) it is large enough to imply a number of levels for each spin (Grover would estimate two or three levels in this energy range, but the inclusion of collective levels would raise this number considerably), thereby preventing the occurrence of intense individual γ-ray lines; and (b) it is small enough, and the differential population is large enough, to dump the population quickly into the ground band once an appreciable energy separation develops.

Footnotes and References

†Condensed from UCRL-18358, Dec. 1968.

*Permanent address: Department of Physics, Michigan State University, East Lansing, Michigan 48823.

‡Permanent address: Department of Physics, University of Manchester, Manchester 13, England.

††Present address: Nuclear Physics Branch, Chalk River Nuclear Laboratories, Chalk River, Ontario, Canada.

1. R. M. Diamond, F. S. Stephens, W. H. Kelly, and D. Ward, Phys. Rev. Letters (to be published March 17, 1969.

2. J. R. Grover and J. Gilat, Phys. Rev. 157, 802 (1967); ibid. 814; ibid. 823; J. R. Grover, Phys. Rev. 157, 832 (1967).

3. J. O. Rasmussen and T. T. Sugihara, Phys. Rev. 151, 992 (1966).

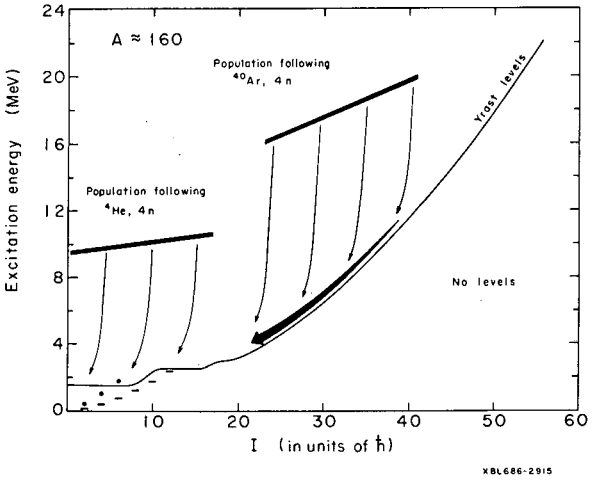

Fig. 1. Schematic figure showing the energy levels in a nucleus of mass ≈ 160 vs angular momentum. Indicated on the figure are (a) the lowest non-gsb energy levels of a given spin (yrast levels), (b) the region of populated states following (He, 4n) and (Ar, 4n) reactions, and (c) the gsb levels of a typical vibrator (dots) and rotor (dashes).

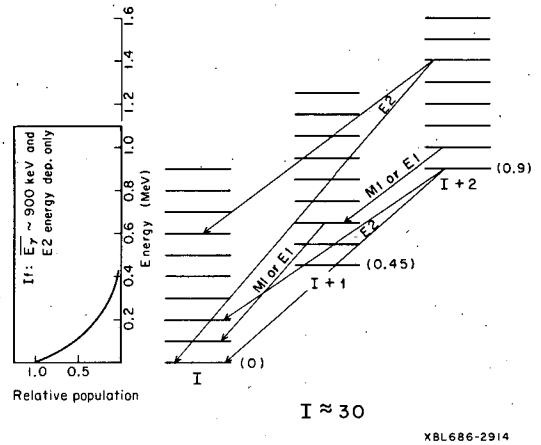

Fig. 2. Schematic illustration of the lowest energy levels having spin ≈ 30 in a nucleus. The insert shows relative populations of these levels if the only differentiation among them is the E2 energy dependence.

ISOMERIC LEVELS IN NUCLEI WITH N = 74

David Ward, F. S. Stephens, and R. M. Diamond

In the course of experiments on neutron-deficient isotopes of Ce, an isomer of 13 ± 1 msec was observed in ^{132}Ce (N = 74).[1] Since no isomeric activity was detected in any of the other cerium isotopes, it was suggested that the isomeric level was a two-quasi-particle level associated with the configuration of 74 neutrons. A systematic study of the N = 74 isotones ^{126}Te, ^{128}Xe, ^{130}Ba, ^{132}Ce, and ^{134}Nd has been performed to test this suggestion. These nuclei were produced by a variety of (H.I, xn) reactions, as shown in Table I. The gamma spectra were recorded both during and between the beam bursts of the Hilac (beam bursts of 5 msec duration at a repetition rate of 40 per sec) using a Ge(Li) counter.

Isomeric activity was detected in ^{130}Ba and ^{134}Nd; however, for ^{126}Te and ^{128}Xe there appeared to be no activity. The results from the γ-ray experiments for the ground bands are shown in Table II. For all these nuclei, with the exception of ^{134}Nd, some levels of the ground-state bands have been previously identified.[1-5] Typical γ spectra are shown in Fig. 1. A complete table of the γ rays associated with the isomer for ^{130}Ba is shown in Table III. Decay curves for prominent transitions in ^{130}Ba and ^{132}Ce were measured by electronic techniques applied between the beam bursts,[6] and found to be 13.5 ± 1 and 13 ± 1 msec respectively. For ^{134}Nd it was necessary to subdivide the beam burst by "chopping" the beam after the injector stage to bursts of 0.1 msec. The half-life for the isomer in ^{134}Nd was found to be 0.5 ± 0.1 msec. The main features of the level schemes for these nuclei established in the present experiments are shown in Fig. 2.

Further work on ^{130}Ba was performed by using a solenoid β-ray spectrometer to study the spectrum of conversion electrons emitted between the beam bursts, as shown in Fig. 3. By comparing the spectrum with the corresponding gamma spectrum (Fig. 1), the conversion coefficients for the 462.7- and 883.0-keV transitions are determined as $\alpha_K = 0.028 \pm 0.003$ and 0.0052 ± 0.0005 respectively. Both these transitions must therefore be of a predominantly E3 multipolarity (a small admixture of M2 cannot be ruled out). It is possible to construct a level scheme for ^{130}Ba from these data, as shown in Fig. 4. We may also infer the total conversion coefficient for the 80.3-keV transition from the intensities of the 80.3- and 803-keV γ rays; in this way we find $\alpha_T = 0.37 \pm 0.08$, which is consistent only with E1 multipolarity. These multipolarity assignments in ^{130}Ba imply a spin and parity of 8^- or 9^- for the isomeric level; $J^\pi = 9^-$ appears more likely to be the case in view of the E3 nature of the 883.0-keV transition. The systematic occurrence of the isomeric level in ^{130}Ba, ^{132}Ce, and ^{134}Nd strongly suggests that it is a two-quasi-particle level formed by breaking a pair of neutrons.

The weak side branch in ^{130}Ba is suggested by the energy sums and intensity balance. There is a similar side branch in ^{132}Ce, and possibly in ^{134}Nd as well, though the data become

progressively poorer for these cases. In attempting to understand these isomers and level structures we have considered both spherical and nonspherical equilibrium shapes. Discussion of these analyses will appear elsewhere;[7] however, a clear choice for the shape of these nuclei does not seem to be indicated.

References

1. David Ward, R. M. Diamond, and F. S. Stephens, Nucl. Phys. A117, 309 (1968).
2. P. J. Stelson and F. K. McGowan, Phys. Rev. 110, 489 (1958).
3. I. Bergstrom, C. J. Herrlander, A. Kerek, and A. Luukko, in Proceedings of the International Conference on Nuclear Structure, Tokyo, Sept. 1967, p. 659.
4. H. Morinaga and N. L. Lark, Nucl. Phys. 67, 315 (1965).
5. G. Gerschel, M. Pantrat, R. A. Ricci, J. Teillac, and J. van Horenbeeck, Nuovo Cimento 37, 1756 (1965).
6. J. Burde, R. M. Diamond, and F. S. Stephens, Nucl. Phys. 85, 481 (1966).
7. D. Ward, R. M. Diamond, and F. S. Stephens, in preparation.

Table I. Bombarding conditions for production of the N = 74 nuclei.

Nucleus	Target	Reaction	Bombarding energy (MeV)
^{126}Te	^{124}Sn	(^{4}He, 2n)	27
^{128}Xe	^{126}Te	(^{4}He, 2n)	27
^{130}Ba	^{124}Sn	(^{12}C, 6n)	90
	^{122}Sn	(^{12}C, 4n)	62
^{132}Ce	^{120}Sn	(^{16}O, 4n)	78
	^{116}Cd	(^{20}Ne, 4n)	85
^{134}Nd	^{122}Te	(^{16}O, 4n)	88
	^{118}Sn	(^{20}Ne, 4n)	92

Table II. Relative γ-ray yields (R. Y.) observed both in (R. Y. in) and out (R. Y. out) of the beam bursts. The yields apply to a beam burst of 5 msec at 40 pulses/sec.

Transition		2 → 0	4 → 2	6 → 4	8 → 6
E(keV)		666.0			
R. Y. (IN)	^{126}Te	100			
R. Y. (OUT)		< 0.3			
E(keV)		442.8	589.8	704.3	
R. Y. (IN)	^{128}Xe	100	65 ± 7	40 ± 5	
R. Y. (OUT)		< 0.6			
E(keV)		357.2	544.5	691.1	803.6
R. Y. (IN)	^{130}Ba	100	79 ± 8	89 ± 10	51 ± 6
R. Y. (OUT)	$\tau_{1/2}$ = 13.5 msec	31 ± 3	26 ± 3	22 ± 3	3.8±.5
E(keV)		325.4	533.1	684.2	788
R. Y. (IN)	^{132}Ce	100	87 ± 10	74 ± 10	30 ± 6
R. Y. (OUT)	$\tau_{1/2}$ = 13 msec	21 ± 3	17 ± 3	15 ± 3	---
E(keV)		294.0	494.6	631.0	726.5
R. Y. (IN)	^{134}Nd	100	86 ± 10	64 ± 10	46 ± 10
R. Y. (OUT)	$\tau_{1/2}$ = 0.5 msec	5.8 ± 1	4±2	6±2	

Table III. Gamma rays associated with the isomeric decay in ^{130}Ba. The transitions were assigned from consideration of their decay curves.

Transition	Relative yield	Assignment
80.3 ± .2	6.7 ± 0.7	$9^- \rightarrow 8^+$
357.2 ± .3	100	$2^+ \rightarrow 0^+$
420.3 ± .5	3 ± 1	
452.5 ± .5	3 ± 1	
463.1 ± .4	13 ± 2	
544.5 ± .5	85 ± 10	$4^+ \rightarrow 2^+$
652.5 ± .5	7 ± 1	
691.1 ± .5	76 ± 10	$6^+ \rightarrow 4^+$
802.9 ± .5	9 ± 1	$8^+ \rightarrow 6^+$
883.0 ± .5	66 ± 8	$8^-, 9^- \rightarrow 6^+$
1004 ± .8	5 ± 2	
1111 ± 1	2.5 ± 1	

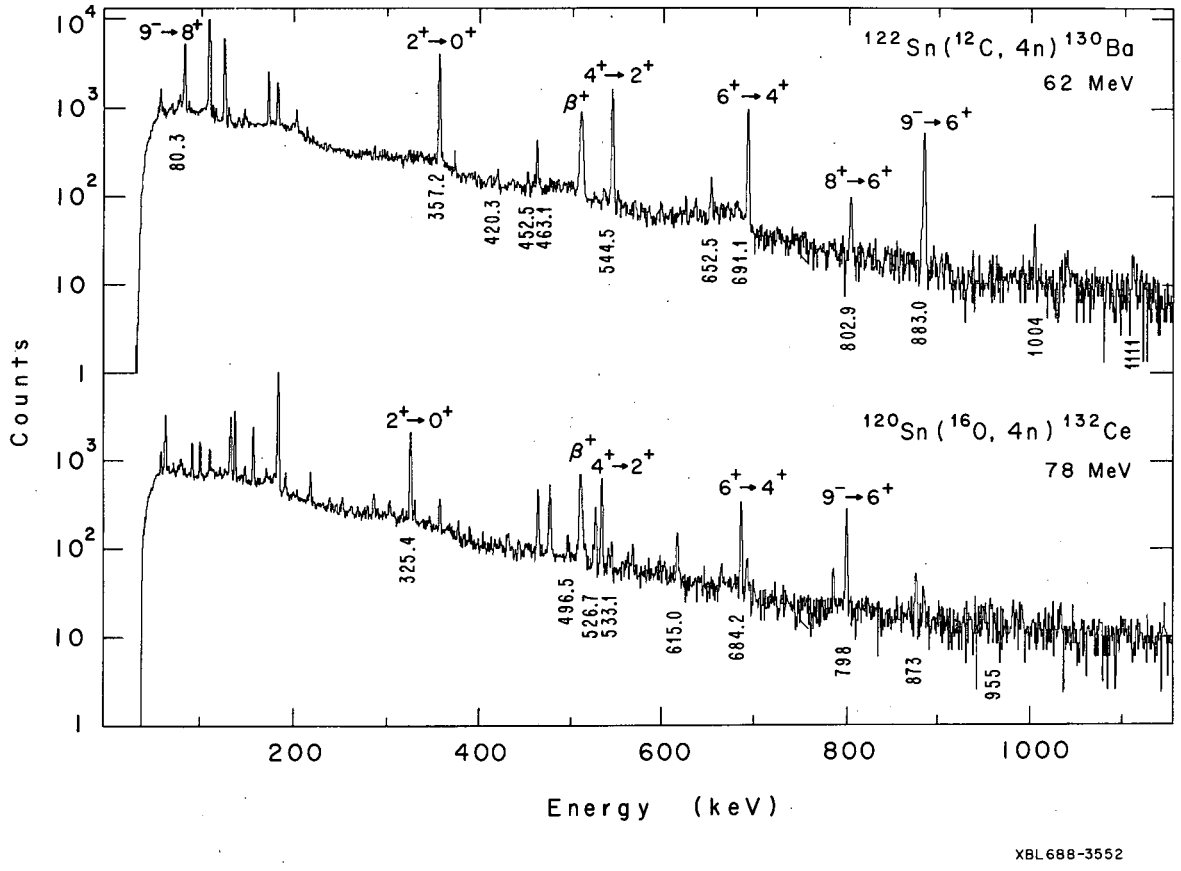

Fig. 1. Spectra of γ rays emitted between the beam bursts following the reactions ^{122}Sn(^{12}C, 4n)^{130}Ba at 62 MeV and ^{120}Sn(^{16}O, 4n)^{132}Ce at 78 MeV.

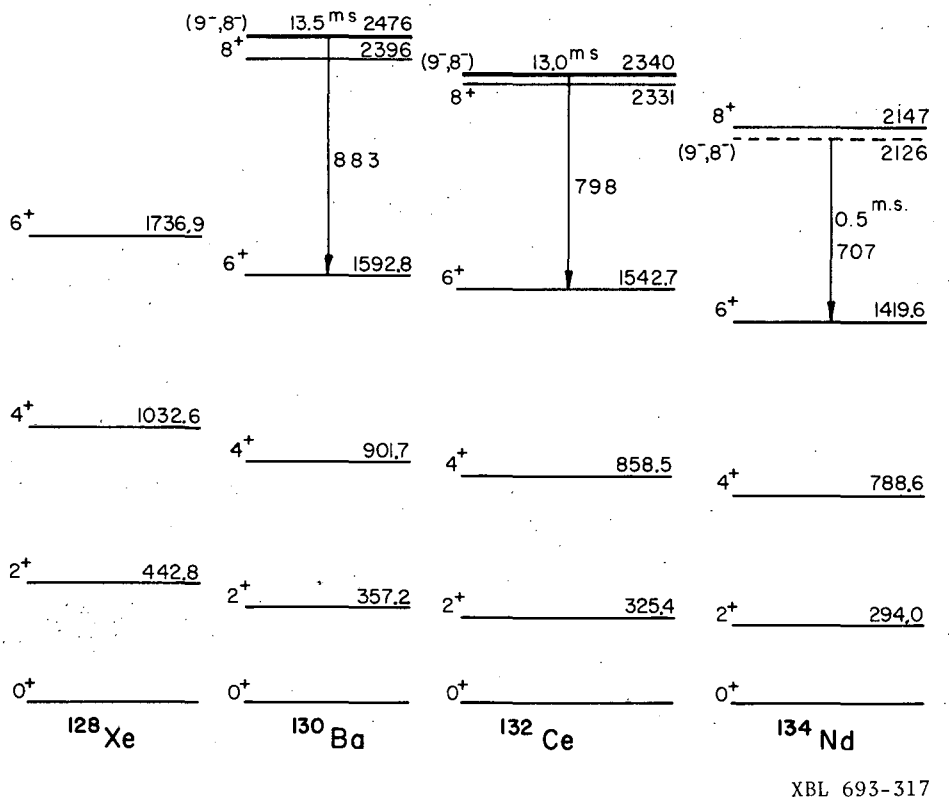

Fig. 2. The ground-state bands and the isomeric level in the N = 74 isotopes established in these experiments.

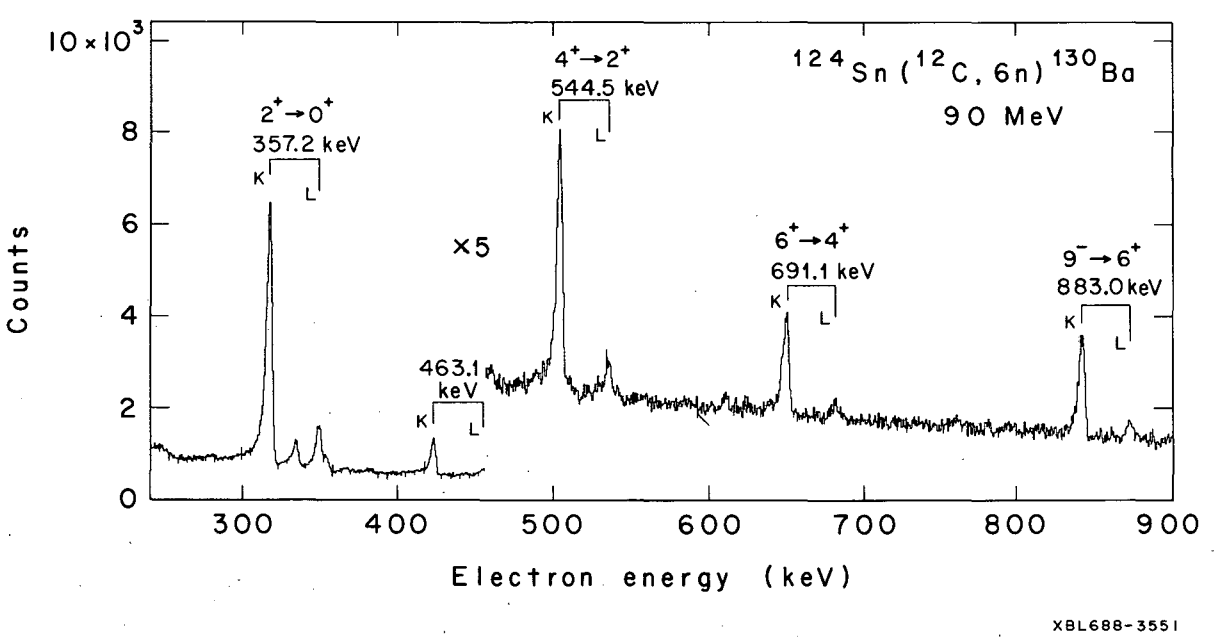

Fig. 3. Spectrum of conversion electrons observed between the beam bursts following the reaction $^{124}Sn(^{12}C, 6n)^{130}Ba$ at 90 MeV. The detector was a cooled Si(Li) counter operating at 3.0 keV resolution.

Fig. 4. Proposed decay scheme for the isomer in ^{130}Ba. Spin assignments in parentheses are tentative. The side branch was deduced from the energy sums and intensity balance.

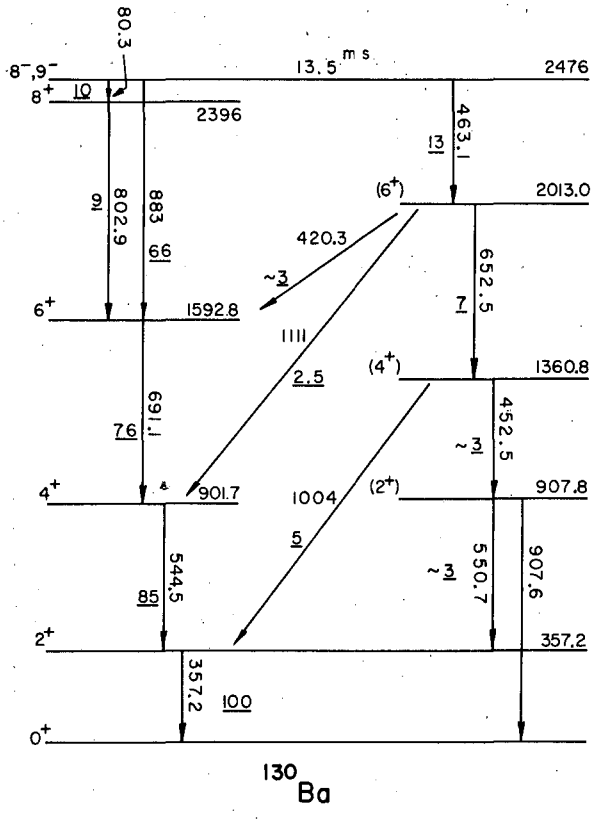

XBL 693-316

BETA DECAY HALF-LIVES FOR THE NEW ISOTOPES ^{166,164,162}Lu, ^{160,158}Tm, AND ^{160,158}Yb

Martin Neiman and David Ward

For some time, in-beam γ-ray studies have been made of the final products in (H.I., Xn) reactions.[1] Considerably less attention has been given to the study of the β decay of the products. The (H.I., xn) reaction generally produces nuclei which are very neutron-deficient, so that the half-life of the parent is typically only a few minutes; furthermore, a sequence of several β decays may be needed to reach stability.

In experiments reported here we have used the Berkeley Hilac to produce isotopes of Lu, Tm, and Yb by the reactions

$$^{152,150,148}\mathrm{Sm}(^{19}\mathrm{F}, 5n)^{166,164,162}\mathrm{Lu},$$
$$^{150,148}\mathrm{Sm}(^{14}\mathrm{N}, 4n)^{160,158}\mathrm{Tm},$$
and
$$^{124,122}\mathrm{Te}(^{40}\mathrm{Ar}, 4n)^{160,158}\mathrm{Yb}.$$

The gamma spectra observed between beam bursts were detected in a Ge(Li) counter. After several minutes of irradiation the beam was turned off, and the decay of the activity was studied. Typical gamma spectra are shown in Fig. 1, and decay curves in Figs. 2 and 3. The isotopes were assigned from the known gamma transitions in the daughter nuclei for the Lu and Tm isotopes (Yb and Er isotopes), and from the known granddaughters for the Yb isotopes (Er isotopes).[2]

The results for the half-lives are conveniently summarized in Fig. 4. In this work we have confined ourselves entirely to transitions in the ground-state quasi rotational bands in the even nuclei. It is evident from the large number of transitions at higher energies, not shown in Fig. 1, that many other levels are populated by the β decay. Further work is continuing in an effort to build up more complete decay schemes. Until this work is completed it is not possible to discuss the details of the β decays, such as ft values, for example.

References

1. A fairly comprehensive bibliography of previous (H.I., xn) work may be found in F. S. Stephens et al., Gamma-Ray De-Excitation of Compound-Nucleus Reaction Products, UCRL-18358, Dec. 1968.

2. D. Ward, F. S. Stephens, and J. O. Newton, Phys. Rev. Letters 19, 1247 (1967).

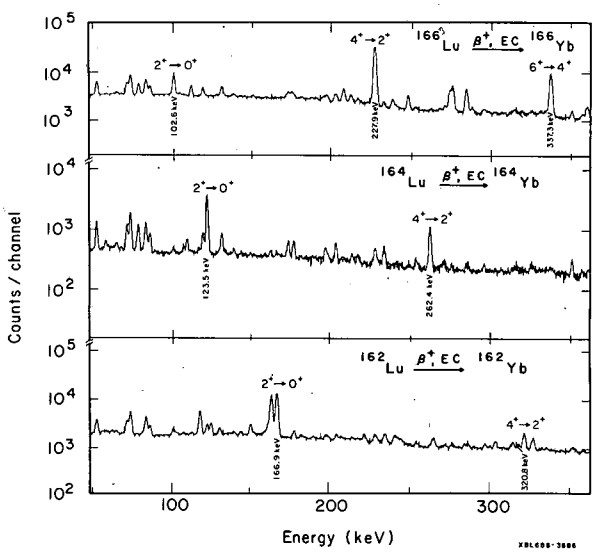

Fig. 1. Gamma spectra recorded between beam bursts following the reactions ^{152,150,148}Sm(^{19}F, 5n)^{166,164,162}Lu at 95 MeV. The transitions indicated are in the ground-state bands of the daughter nuclei (Yb isotopes) (established in Ref. 2).

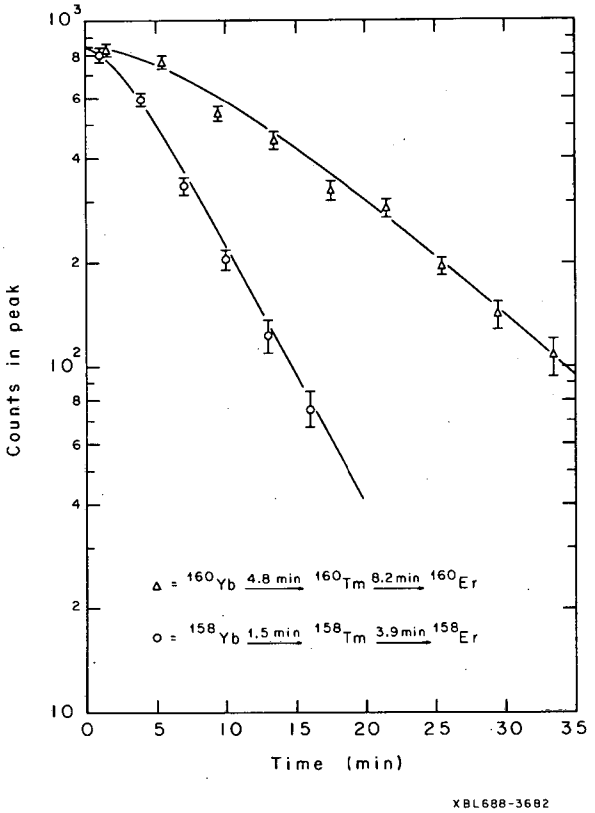

Fig. 2. Decay curves for ^{160}Yb and ^{158}Yb into the granddaughters ^{160}Er and ^{158}Er. The half-lives for ^{160}Tm and ^{158}Tm were established in earlier experiments. The curves represent the best fit to the data by varying the half-life for the decay Yb → Tm.

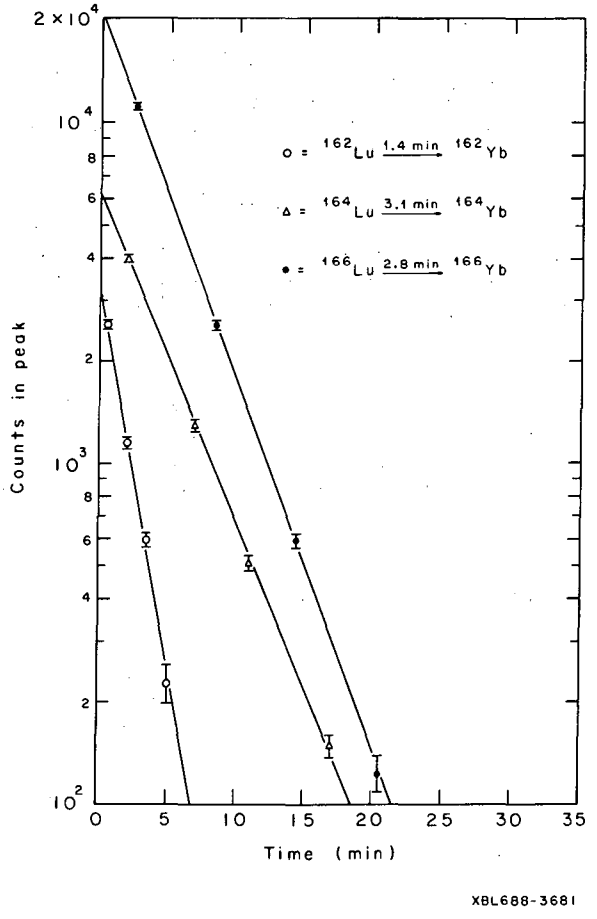

Fig. 3. Decay curves for the Lu isotopes. The gamma transitions in the daughter nuclei were the $2^+ \rightarrow 0^+$ for ^{164}Yb and ^{162}Yb and the $4^+ \rightarrow 2^+$ for ^{166}Yb.

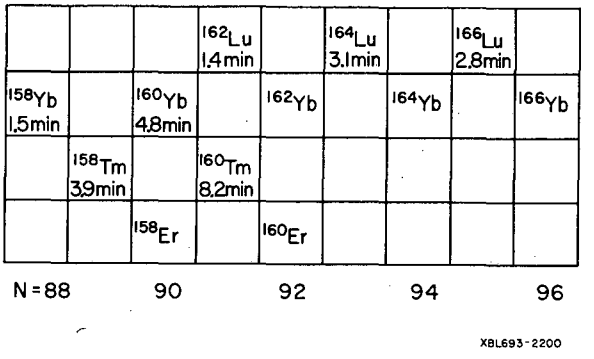

Fig. 4. Summary of the half-lives measured in these experiments. It should be noted that the levels observed here may not necessarily be the ground states.

SEARCH FOR A 0.3-sec SPONTANEOUS FISSION ACTIVITY IN ELEMENT 104†

Albert Ghiorso, Matti Nurmia, and James Harris

In 1964 Flerov et al.[1] reported the observation of a 0.3-sec spontaneous fission activity produced by irradiating ^{242}Pu with ^{22}Ne. The activity was assigned to an isotope of element 104 with mass 260. The experiments were reported to rule out the assignment of this activity to other isotopes of element 104 or to other elements.

In an attempt to verify these results we have bombarded targets of einsteinium (containing 1.2 and 3.8 μg of ^{253}Es and minor amounts of ^{254}Es and ^{255}Es) with ^{10}B and ^{11}B ions from the Berkeley Hilac. The activities produced in the bombardments were deposited by a helium gas jet onto a standard 6.3-mm magnetic tape that was pulled at a constant speed past a series of mica fission detectors. After etching, the mica foils were scanned with an optical microscope and the position of each fission track was recorded with a two-parameter analyzer coupled to two linear potentiometers attached to the microscope stage.

No spontaneous fission activity with a half-life between 0.2 and 1 sec was detected in experiments involving a total of several hundred μA-hr of ^{11}B beam. Due to a background caused by the fission of ^{256}Fm and the rare fission branching of ^{256}No, the limit of detectability corresponded to a production cross section of about 8 nanobarns. The expected cross section for the reaction $^{253}Es(^{11}B, 4n)^{260}104$ is 17 nanobarns (Ref. 2) at a bombarding energy of 60.7 MeV, which was used in most experiments. We are thus unable to confirm the assignment of the 0.3-sec fission activity to $^{260}104$.

Independent objections against this assignment have been raised on the basis of the production cross section of the 0.3-sec activity reported by the Soviet investigators.[1] Sikkeland et al.[3] point out that the observed cross section would be in better agreement with predictions if the 0.3-sec activity were in fact $^{261}104$. The systematics of the spontaneous-fission half-lives of even-even nuclides[4] are also in conflict with the assignment of the 0.3-sec activity to $^{260}104$, which is expected to have a fission half-life of the order of a microsecond or less. This disagreement, too, is removed if the 0.3-sec activity is assumed to be $^{261}104$.

In our experiments we should have seen the 0.3-sec activity even if it were due to $^{261}104$, assuming that its production cross section is not substantially less than the calculated value of 16 nb. However, although we feel that the assignment of the 0.3-sec activity to $^{260}104$ (Ref. 1) is likely to be in error, we cannot at present exclude the possibility that this activity could be reassigned to $^{261}104$.

Footnote and References

†Condensed from UCRL-18714, Jan. 1969.

1. G. N. Flerov, Yu. Ts. Oganesyan, Yu. V. Lobanov, V. I. Kuznetsov, V. A. Druin, V. P. Perelygin, K. A. Gabrulov, C. P. Tret'yakova, and B. M. Plotko, At. Energ. (USSR) 17, 310 (1964) [Engl. Transl.: Soviet J. At. Energy 17, 1046 (1964)]; Phys. Letters 13, 73 (1964).
2. T. Sikkeland and D. Lebeck (Lawrence Radiation Laboratory), unpublished data.
3. T. Sikkeland et al., Phys. Rev. 172, 1232 (1968).
4. M. Nurmia, K. Eskola, P. Eskola, and A. Ghiorso, New Nuclide ^{258}No, UCRL-18712, Jan. 1969.

STUDIES OF ISOTOPES OF ELEMENT 104†

Albert Ghiorso, Matti Nurmia, James Harris, Kari Eskola,* and Pirkko Eskola‡

We have investigated the activities formed when ^{249}Cf is bombarded with ^{12}C, ^{13}C, ^{14}N, ^{15}N, and ^{16}O ions. The nuclear spectroscopy was done with an improved helium jet system that deposits the products of the nuclear reactions onto the periphery of a vertically mounted light plastic wheel. The wheel is periodically turned to move the activity past a series of solid-state detectors, and the data are collected in various configurations of time subgroups from each detector with the help of a PDP-9 computer.

In bombardments of the ^{249}Cf target with ^{12}C we have observed a prominent alpha activity with a half-life of about 4 sec. Its spectrum is complex, but it is characterized by a double or triple alpha peak between 8.94 and 9.01 MeV, with possible additional peaks in the region of 8.57 to 8.86 MeV. Its production cross section and the variation of the cross section with the energy of the bombarding ^{12}C ions are consistent with the expected yield of $^{257}104$ from the reaction $^{249}Cf(^{12}C, 4n)^{257}104$. This assignment is further supported by results of cross bombardments and by alpha energy and half-life systematics.

By bombarding ^{249}Cf with ^{13}C we have produced a less well-defined alpha activity whose spectrum largely overlaps that of $^{257}104$. The data on its production conform with the expected behavior of $^{259}104$ from the reaction $^{249}Cf(^{13}C, 3n)^{259}104$. Milking experiments have confirmed the genetic relationship between $^{257}104$ and $^{259}104$ and their daughter isotopes, ^{253}No and ^{255}No.

We have also studied the spontaneous fission activities formed from ^{249}Cf in bombardment with ^{12}C and ^{13}C in a rotating-drum system equipped with mica detectors. We have observed an

11-msec fission activity that is formed with both ^{12}C and ^{13}C in the manner expected for $^{258}104$ from the reactions $^{249}Cf(^{12}C, 3n)^{258}104$ and $^{249}Cf(^{13}C, 4n)^{258}104$. This activity was not produced in a bombardment of ^{249}Cf with ^{14}N or ^{11}B, or in bombardments of ^{246}Cm or ^{248}Cm with ^{13}C or ^{13}C. These observations suggest that it may be tentatively assigned to 104.

Footnotes

†Summary of UCRL-18711, Jan. 1969.
*On leave of absence from Department of Nuclear Physics, University of Helsinki, Finland.
‡Guest scientist supported by the Finnish National Research Council for Sciences.

NEW NUCLIDE ^{258}No†

Matti Nurmia, Kari Eskola,* Pirkko Eskola,‡ and Albert Ghiorso

From the trend of the alpha decay energies of known nobelium isotopes and other neighboring nuclides we estimate the alpha decay energy of ^{258}No to be about 8.4 MeV, which would correspond to an alpha half-life of approximately 10 sec. In the 1966-67 Berkeley survey of the No isotopes[1] this expected alpha activity was not observed, and it was concluded that ^{258}No must decay by spontaneous fission. Further experiments failed to reveal any such fission activity down to the limit of detection of the rotating-drum device then in use, or about 10 msec.

With the help of an improved rotating-drum system we have now observed a 1.2-msec fission activity that may be tentatively assigned to ^{258}No. This activity was produced by bombarding a target of ^{248}Cm with ^{13}C ions, but it was not formed when the same target was bombarded with ^{12}C or ^{11}B, or when ^{246}Cm was bombarded with ^{13}C. Because no other activities, either alpha emission or spontaneous fission, assignable to the ground state of ^{258}No have been observed in an extensive series of experiments, the above results suggest that the 1.2-msec activity is due to ^{258g}No and not to an isomeric state of this or some other nuclide.

The systematics of the spontaneous-fission half-lives of the heaviest elements, in the light of our present results and of our recent tentative observation of $^{258}104$ as a 11-msec spontaneous fission activity,[2] is shown in Fig. 1. Our results are obviously in disagreement with the claim of Flerov et al.[3] to have discovered element 104 on the basis of having observed $^{260}104$ as a 0.3-sec spontaneous fission activity.

Footnotes and References

†Summary of UCRL-18712, Jan. 1969.
*On leave of absence from Department of Nuclear Physics, University of Helsinki, Finland.
‡Guest scientist supported by Finnish National Research Council for Sciences.

1. A. Ghiorso, T. Sikkeland, and M. J. Nurmia, Phys. Rev. Letters 18, 401 (1967).
2. A. Ghiorso, M. Nurmia, J. Harris, K. Eskola and P. Eskola, Studies of Isotopes of Element 104, UCRL-18711, Jan. 1969.
3. G. N. Flerov, Yu. Ts. Oganesyan, Yu. V. Lobanov, V. I. Kuznesov, V. A. Druin, V. P. Perelygin, K. A. Gabrulov, C. P. Tret'yakova, and B. M. Plotko, Phys. Letters 13, 73 (1964).

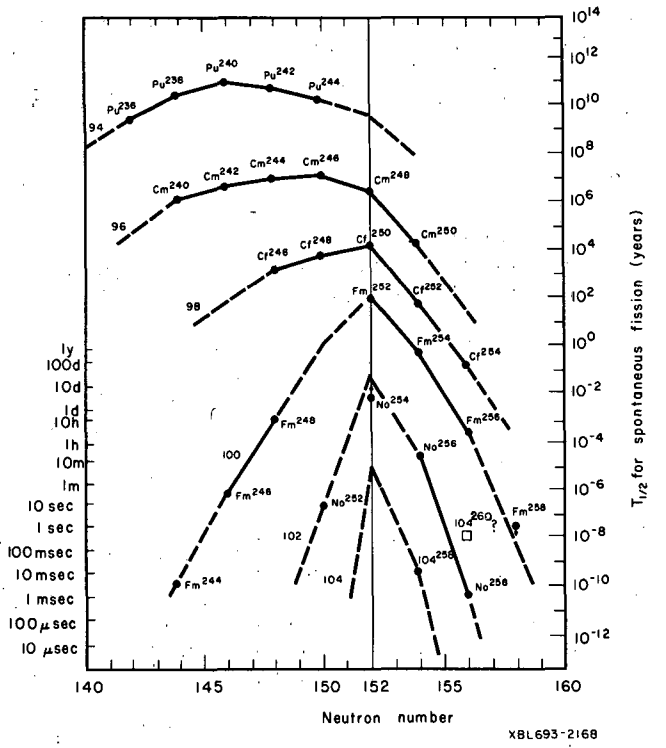

Fig. 1. Spontaneous-fission half-life systematics of the even-even isotopes of the heaviest elements.

STUDY OF Dy(^{40}Ar, xn)Po REACTIONS†

T. Sikkeland,* R. J. Silva,‡ M. Nurmia, and A. Ghiorso

Cross sections for the production of Po nuclides with mass numbers from 194 to 200 in bombardments of a 92.7% ^{164}Dy target with ^{40}Ar ions have been measured in the ion energy range 160 to 280 MeV. The maximum cross sections in millibarns were 0.5, 2.5, 10, 28, 60, 65, and 20 for the production of mass numbers 194, 195, 196, 197, 198, 199, and 200, respectively. Isomer ratios for the odd-A nuclides were obtained. A good fit is obtained between the shapes of calculated and experimental excitation function curves. The fit involved (a) calculation of the compound nucleus cross section by the use of the parabolic approximation to the real part of the optical-model potential with parameters $V_0 = -70$ MeV, $r_0 = 1.26$ F, and $d = 0.44$ F; (b) modification of Jackson's formula for the probability for neutron emission to include angular momentum effects using T = 1.2 MeV and $\mathfrak{I}/\mathfrak{I}^0 = 1.8$, and (c) assumption of an energy independence for the average partial level width for neutron emission. In the fitting process experimental values for the latter quantity are obtained to which a semi-empirical formula is fitted.

Footnotes

†Abstract of UCRL-18674, Jan. 1969 (to be submitted to Phys. Rev.).

*Present address: Norsk Hydro's Institute for Cancer Research, Oslo, Norway.

‡Present address: Special Training Division, Oak Ridge Associated Universities, Oak Ridge, Tennessee 37830.

NUCLEAR REACTIONS AND SCATTERING

HIGH-ISOSPIN NUCLEI AND MULTIPLETS IN THE LIGHT ELEMENTS†

Joseph Cerny

This article presents a review of the progress made in establishing the limits of stability toward the emission of nucleons in the light elements, as well as an assessment of the data on high isospin states ($T \geq 3/2$) and the resulting isobaric multiplets in the mass region $5 \leq A \leq 40$. Data on $T = 3/2$ states in $T_z = \pm 1/2$ nuclei and on $T = 2$ states in $T_z = 0, 1$ nuclei obtained from both direct reaction experiments and isospin-forbidden resonance reactions are evaluated and tabulated. The isobaric multiplet mass equation is discussed and tested by using the available data on complete isobaric quartets; it is then used to predict masses of unknown neutron-deficient nuclei of mass number 40 and below.

Footnote

†Condensed from Ann. Rev. Nucl. Sci. 18, 27 (1968).

MICROSCOPIC ANALYSIS OF THE ^{3}He, t AND ^{3}He, ^{3}He' REACTIONS ON 1p SHELL NUCLEI†

Gordon C. Ball* and Joseph Cerny

There has been growing interest recently in the applications of a microscopic description to the inelastic and charge-exchange scattering of various projectiles by nuclei.[1-9] Utilizing the available experimental data from the (p, n) and (p, p') reactions, several attempts have been made to determine an effective nucleon-nucleon interaction in terms of a simple local potential with an arbitrary spin-isospin exchange mixture.[2-7] In particular, the population of ground and excited isobaric analog states in the (p, n) reaction provides a direct measurement of the isospin $V_{ST} = V_{01}$ and spin-isospin V_{11} terms in the effective two-body interaction, whereas the levels that are strongly populated in inelastic scattering are generally sensitive to the spin-independent terms.

One of the main purposes of this investigation was to employ the microscopic description in an analysis of the (^{3}He, t) and (^{3}He, ^{3}He') reactions on several 1p shell nuclei--specifically, ^{9}Be, ^{12}C, ^{13}C, ^{14}C, ^{14}N, and ^{15}N. These experiments were carried out at ^{3}He energies of 40 to 50 MeV, and therefore the population of well-known levels up to an excitation energy of 15 to 20 MeV could be investigated. The (^{3}He, t) and (^{3}He, ^{3}He') reactions were studied simultaneously by using two (dE/dx)-E counter telescopes which fed Goulding-Landis particle identifiers.[10] Typical energy spectra for the ^{13}C(^{3}He, t)^{13}N and ^{13}C(^{3}He, ^{3}He')^{13}C reactions are shown in Fig. 1.

The DWBA calculations were performed by using the microscopic description of inelastic and charge-exchange scattering developed by Madsen.[1] Spectroscopic factors were calculated by use of the intermediate-coupling wave functions of Cohen and Kurath[11] for p-shell states, while simple j-j configurations were assumed for the levels formed by promoting a $p_{1/2}$ nucleon to the $s_{1/2}$ or $d_{5/2}$ shell. A Yukawa interaction with a range of $\alpha^{-1} = 1.2$ F was found to give the best overall agreement for all transitions.

Theoretical angular distributions for (^{3}He, t), L = 0 and (^{3}He, ^{3}He'), L = 3 transitions are compared with experiment in Figs. 2 and 3. The fits are representative of the best obtained in this analysis. The average strengths V_{ST} obtained for all single-particle transitions and L transfers are summarized in Table I, and also compared with the results obtained in previous

analyses of the (p, p'),[2-5] (p, n),[3, 5-7] and (^{3}He, t)[8, 9] reactions. In all cases, the values obtained for the effective projectile-nucleon interaction at α^{-1} = 1.2 F have been converted to an effective nucleon-nucleon interaction at α^{-1} = 1.0 F by using the relationships given previously by Wesolowski et al.[9] and Johnson et al.[2]

Several interesting results were obtained from this analysis. First, the average values computed for V_{01}[20.6 MeV] and V_{11}[16.5 MeV] from the (^{3}He, t) $p_{3/2}$, $p_{1/2} \rightarrow p_{1/2}$, dominant L = 0 transition were in excellent agreement with those obtained previously in analyses of (p, n) L = 0 transitions.[3, 5-7] In addition, the strengths required to fit the (^{3}He, t) $p_{1/2} \rightarrow s_{1/2}$, L = 1 transitions agreed well with these L = 0 strengths. Second, the strengths required to fit the (^{3}He, t) $p_{3/2} \rightarrow p_{1/2}$, L = 2 and $p_{1/2} \rightarrow d_{5/2}$, L = 1, 3 transitions were enhanced, whereas the experimental angular distributions for these transitions had less structure than those predicted by the theory. This suggests that core polarization effects[3, 4] or particle exchange could be contributing to the cross sections for these transitions. A similar effect has been observed for L = 2 transitions in the (p. n) reaction.[6, 7]

As expected, it was found that the transitions that were strongly populated in the (^{3}He, ^{3}He') reaction were generally insensitive to the spin- and isospin-dependent terms in the effective interaction. However, the absolute strengths obtained herein for V_{00} were much smaller than those required to fit the inelastic transitions observed in the (p, p') reaction on several heavier nuclei.[3] As a result, it can be concluded that core polarization effects are much less important for 1p shell nuclei, though, as noted above, they may still be contributing. Unfortunately, an accurate determination of the spin-dependent V_{10} term could not be obtained from these data. In particular, those (^{3}He, ^{3}He') transitions which were restricted to be pure S = 1 were also populated in the (α, α') reaction with approximately the same relative intensity, indicating that other mechanisms such as multiple excitation also contribute significantly to the cross sections for these transitions.

Finally, it can be shown that the effective interaction obtained in this analysis is very similar to those used in simple shell-model calculations and those required to fit low-energy nucleon-nucleon scattering data.

Footnotes and References

†Condensed from Phys. Rev. Jan. 20, 1969.

*Present address: Chalk River Nuclear Laboratories, Chalk River, Ontario, Canada.

1. V. A. Madsen, Nucl. Phys. 80, 177 (1966).
2. M. B. Johnson, L. W. Owen, and G. R. Satchler, Phys. Rev. 142, 748 (1966).
3. G. R. Satchler, Nucl. Phys. A95, 1 (1967).
4. W. G. Love and G. R. Satchler, Nucl. Phys. A101, 424 (1967).
5. P. J. Locard, S. M. Austin, and W. Benenson, Phys. Rev. Letters 19, 1141 (1967).
6. C. Wong, J. D. Anderson, J. McClure, B. Pohl, V. A. Madsen, and F. Schmittroth, Phys. Rev. 160, 769 (1967).
7. S. D. Bloom, J. D. Anderson, W. F. Hornyak, and C. Wong, Phys. Rev. Letters 15, 264 (1965); C. Wong, J. D. Anderson, S. D. Bloom, V. A. Madsen, and F. Schmittroth, UCRL-70451, 1967.
8. L. F. Hansen, M. L. Stelts, J. G. Vidal, and J. J. Wesolowski, UCRL-70454, 1967; L. F. Hansen, M. L. Stelts, J. G. Vidal, J. J. Wesolowski, and V. A. Madsen, Phys. Rev. 174 [4], 1155 (1968).
9. J. J. Wesolowski, E. H. Schwarcz, P. G. Roos, and C. A. Ludemann, Phys. Rev. 169, 878 (1968).
10. F. S. Goulding, D. A. Landis, J. Cerny, and R. H. Pehl, Nucl. Instr. Methods 31, 1 (1964).
11. S. Cohen and D. Kurath, Nucl. Phys. 73, 1 (1965).

Table I. Average strengths for the effective nucleon-nucleon interaction at α^{-1} = 1.0 F obtained from (^{3}He, ^{3}He') and (^{3}He, t) transitions.

	(^{3}He, t) present work				Previous work	
	$p_{1/2}$, $p_{3/2} \rightarrow p_{1/2}$	$p_{3/2} \rightarrow p_{1/2}$	$p_{1/2} \rightarrow d_{5/2}$	$p_{1/2} \rightarrow s_{1/2}$		
	(L=0)	(L=2)	(L=1, 3)	(L=1)	(p, n)[a]	(^{3}He, t)[b]
V_{ST}	(CK)	(CK)	(jj)	(jj)	L=0	L=0
V_{01}	20.6 ± 0.4	42.4 ± 5	32.8 ± 12	19.4 ± 3	19-26	31 ± 6
V_{11}	16.5 ± 1.1	42.4 ± 5	30.7 ± 11	17.3 ± 5	$\frac{V_{11}}{V_{01}} \approx 0.6\text{-}1.0$	20 ± 4

		(^{3}He, ^{3}He') present work			(p, p') previous work		
		$p_{3/2} \rightarrow p_{1/2}$	$p_{1/2} \rightarrow d_{5/2}$	$p_{1/2} \rightarrow s_{1/2}$			
		(L=2)	(L=3)	(L=1)			
V_{ST}	Exchange mixture	(CK)	(jj)	(jj)	Target	Without core polarization[c]	With core polarization[d]
V_{00}	Wigner	60.3 ± 6	76.0 ± 10	53.9 ± 9	^{7}Li	90	-
V_{00}	Serber	60.2 ± 10	67.3 ± 13	47.2 ± 6	^{12}C	86.9	-
					^{18}O, ^{90}, ^{92}Zr, ^{208}Pb	≈ 200	≈ 80
		(L=0)	(L=1)				
V_{10}	Serber	≈ 27	≈ 22		^{89}Y, ^{90}Zr, ^{208}Pb	≈ 40[d]	

[a] See Ref. 3, 5-7. [b] See Ref. 8, 9. [c] See Ref. 3, 5. [d] See Ref. 4.

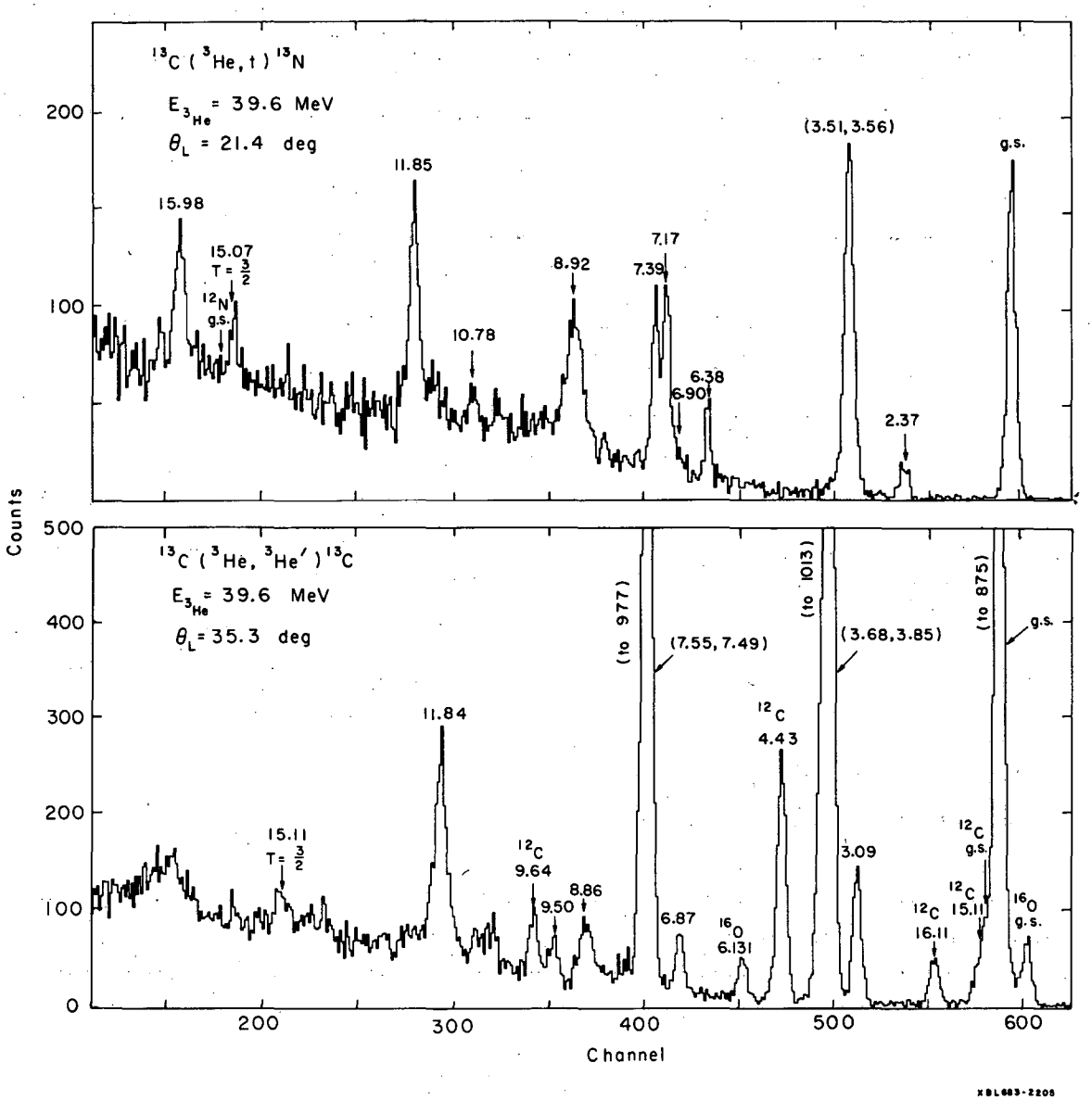

Fig. 1. Energy spectra of the $^{13}C(^{3}He, t)^{13}N$ and $^{13}C(^{3}He, ^{3}He')^{13}C$ reactions at a ^{3}He energy of 39.6 MeV. The spectra were recorded on separate analyzers with different gains. The peaks corresponding to the 15.11- and 16.11-MeV levels of ^{12}C represent an α contamination in the ^{3}He spectrum.

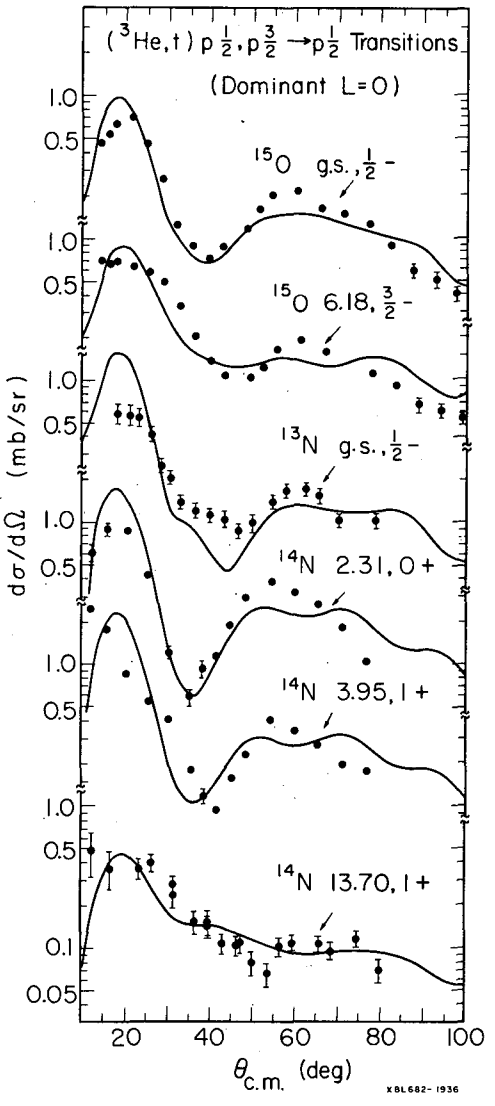

Fig. 2. Angular distribution for (^{3}He, t) $p_{1/2}$, $p_{3/2} \rightarrow p_{1/2}$ (dominant L = 0) transitions. The solid curves are DWBA predictions obtained by using the wave functions of Cohen and Kurath.

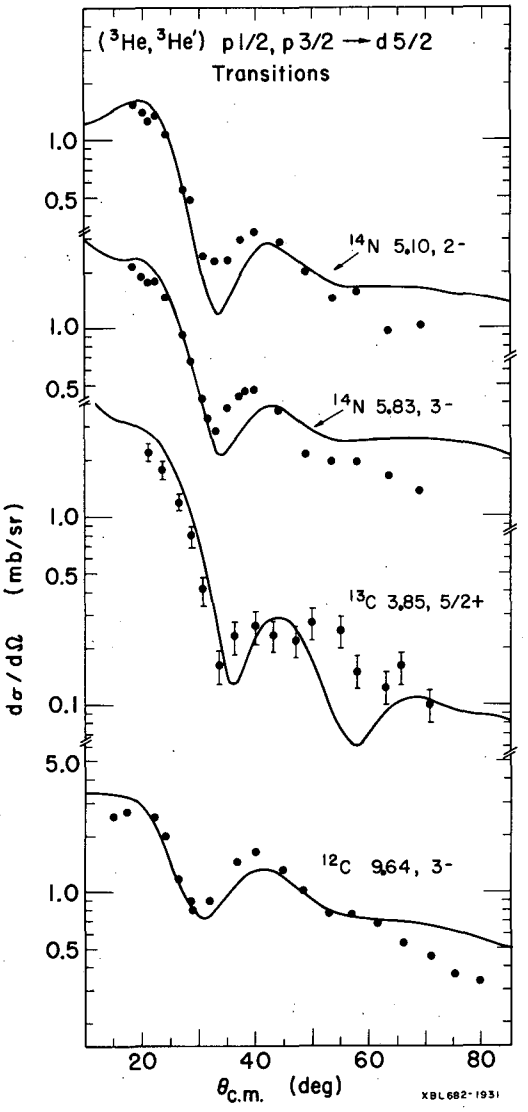

Fig. 3. Angular distribution for (^{3}He, ^{3}He') $p_{1/2}$, $p_{3/2} \rightarrow d_{5/2}$ (L = 3) transitions. The solid curves are DWBA predictions obtained by using j-j wave functions and a Serber exchange mixture.

CARBON-10 AND MASS MEASUREMENTS FOR LIGHT NUCLEI†

H. Brunnader,* J. C. Hardy, and Joseph Cerny

A recent investigation of analog states throughout the $1d_{5/2}$ shell[1] included a remeasurement of the (p, t) and (p, ^{3}He) reactions on ^{22}Ne and ^{26}Mg targets to which carbon impurities had been added to provide an energy calibration. The ground and first excited states of ^{10}C, produced in the reaction ^{12}C(p, t)^{10}C, result in triton peaks whose energies bracket that of the T = 2 states in ^{20}Ne and ^{24}Mg. Since the ground-state mass of ^{10}C taken from the current mass table[2] was 15.658 MeV with a quoted error of ± 13 keV, it was surprising to observe a discrepancy of ≈ 45 keV between this and the accepted[3] energies (± 5 keV) of the T = 2 states. This discrepancy has led to the present reevaluation of the mass of ^{10}C and the energy of its first excited state.

There have been three previous measurements[4-6] of the mass of ^{10}C, and these are summarized in Table I. Only the first two results are included in the average value quoted in Ref. 2. Although the error bar on the third measurement is significantly smaller than the others, the fact that it differed from them by ≈ 45 keV, while using a similar experimental method, made it desirable to perform an independent measurement of a different type. For this purpose, the reaction $^{10}B(^3He, t)^{10}C$ was chosen.

The experiment was carried out by using a 30-MeV ^3He beam from the 88-inch cyclotron. A diagram and general description of the experimental layout have been given elsewhere.[7] Reaction products were detected in two independent counter telescopes on opposite sides of the beam. Each consisted of a 150-μ phosphorus-diffused silicon ΔE transmission counter and a 3.0-mm lithium-drifted silicon E counter operated in coincidence, followed by a 500-μ lithium-drifted silicon E-reject counter operated in anticoincidence to eliminate long-range particles. The signals from these telescopes were fed to Goulding-Landis particle identifiers, and the data were stored according to particle type in four 1024-channel groups of a 4096-channel analyzer. In addition to the telescopes, two single 1-mm "monitor" counters were mounted at $\theta_{lab} = +27.5$ deg and -18.0 deg. The angular resolution of the telescopes and monitors was about 0.25 deg.

Figure 1 shows the energy spectrum of tritons observed from the $(^3He, t)$ reaction on a 280-$\mu g/cm^2$ boron target, 92% enriched in ^{10}B; the lab angle was +22.7 deg. Kinematic calculations show a change in the energy of ^{10}C peaks relative to those from ^{11}C of about 10 keV per degree, and thus, if the Q values for the production of states in ^{10}C are to be determined by comparison with known states in ^{11}C, a precise knowledge of the lab angle must be maintained. Consequently, during this and all other runs, elastically scattered ^3He particles were recorded in the fixed monitor counters and observed frequently throughout a run. Although this permitted a continuous sensitive determination (to about 0.1 deg) of variations in the beam angle, no beam-angle excursions were detected during any of the experiments.

As a further precaution, in two runs spectra were recorded with counter telescope 1 set at the same nominal angle on opposite sides of the beam, while telescope 2 remained fixed at $\theta_{lab} = -60.1$ deg to detect any significant beam energy change. Additional spectra using the enriched boron target were also taken at $\theta_{lab} = +18.3$ and -55.2 deg, and for comparison, a 500-$\mu g/cm^2$ natural boron target was bombarded at the same energy.

The data were analyzed by using the computer program LORNA.[8] This program establishes an energy scale by finding a least-squares fit to peaks whose Q values are known, after correcting all incoming and outgoing particles for kinematic effects and absorber losses. The states taken as known were the ground and first three excited states[9] of ^{11}C. Our final result for the mass excess of ^{10}C is (15.700±0.010) MeV. Comparison with Table I shows this value to be consistent with that obtained in Ref. 6 and inconsistent with the other two. Thus we confirm the mass excess of ^{10}C to be (15.7025 ± .0018) MeV.

There have been three previous measurements[10-12] relating to the first excited state of ^{10}C: two have determined its mass excess, and the other, its excitation energy. By use of the correct ground-state mass excess, good agreement is obtained among these measurements and the value we obtain. A summary of all experimental data on this state is given in Table II, together with the averaged result; this corresponds to an excitation energy of (3.344 ± .008) MeV.

Our results also confirm the previously reported[10] existence of states in ^{10}C at 5.28 and 6.58 MeV, but indicate that the tentative assignment of states at 5.03 and 5.60 MeV should be dropped.

The earlier values for the masses of the ground and first excited states of ^{10}C were used in determining the energies of analog states and certain mass excesses for a number of light nuclei. Thus, the results of these measurements must be changed to take account of the revised ^{10}C masses. Table III lists references,[7,13] previous values, and the revised excitation energies for those earlier measurements which were sufficiently precise to warrant adjustment.

Footnote and References

†Condensed from Phys. Rev. 174, 1247 (1968).

*Present address: Chemistry Department, McMaster University, Hamilton, Ontario, Canada.

1. J. C. Hardy, H. Brunnader, and J. Cerny, Bull. Am. Phys. Soc. 13, 561 (1968); H. Brunnader, J. C. Hardy, J. Cerny, and J. Jänecke, Isobaric Analog States and Coulomb Displacement Energies in the $1d_{5/2}$ Shell, submitted to Phys. Rev.

2. J. H. E. Mattauch, W. Thiele, and A. H. Wapstra, Nucl. Phys. 67, 1 (1965); C. C. Maples, G. W. Goth, and J. Cerny, Nuclear Data 2A, 429 (1966).
3. J. Cerny, Ann. Rev. Nucl. Sci. 18, 27 (1968).
4. S. Takayanagi, N. H. Gale, J. B. Garg, and J. M. Calvert, Nucl. Phys. 28, 494 (1961).
5. F. J. Bartis, Phys. Rev. 132, 1763 (1963).
6. J. M. Freeman, J. G. Jenkins, and G. Murray, Phys. Letters 22, 177 (1966).
7. G. W. Butler, J. Cerny, S. W. Cosper, and R. L. McGrath, Phys. Rev. 166, 1096 (1968).
8. LORNA is a program written by C. C. Maples, whom we thank for making it available.
9. F. Ajzenberg-Selove and T. Lauritzen, Energy Levels of Light Nuclei (VII) Nucl. Phys. A114, 1 (1968).
10. N. Mangelson, F. Ajzenberg-Selove, M. Reed, and C. C. Lu, Nucl. Phys. 88, 137 (1966).
11. L. G. Earwaker, J. G. Jenkins, and E. W. Titterton, Nucl. Phys. 42, 521 (1963).
12. R. E. Segal, P. P. Singh, S. S. Hanna, and M. A. Grace, Phys. Rev. 145, 736 (1966).
13. R. L. McGrath, J. Cerny, and E. Norbeck, Phys. Rev. Letters 19, 1442 (1967).

Table I. Previous measurements of the mass of the mass of ^{10}C.

Experiment	Ref.	Mass excess (MeV)
(p, n) threshold	4	15.663 ± 0.025
β^+ end point	5	15.656 ± 0.015
(p, n) threshold	6	15.7025 ± 0.0018

Table II. Summary of experimental data on the first excited state of ^{10}C.

Experiment	Ref.	Mass excess (MeV)
$^{10}B(^3He, t)^{10}C$	10	19.028 ± 0.030
(p, n) threshold	11	19.039 ± 0.020
γ decay	12	(19.053 ± 0.010)[a]
$^{10}B(^3He, t)^{10}C$	this work	19.042 ± 0.015
Average		19.047 ± 0.008

a. This measurement was of the excitation energy rather than the mass excess; it has been converted by using the best balue for the ground-state mass excess of ^{10}C(15.703 MeV).

Table III. Original and revised experimental values which depend for calibration upon the ground and first excited states of ^{10}C.

Reaction	Ref.	Measured	Previous value (MeV)	New value (MeV)
$^{24}Mg(^3He, ^6He)^{21}Mg$ g. s.	7	Mass excess	+10.62±0.12	+10.66±0.12
$^{40}Ca(^3He, ^6He)^{37}Ca$ g. s.	7	Mass excess	-13.24±0.05	-13.23±0.05
$^9Be(p, t)^7Be^*(T = 3/2)$	13	excitation	10.97±0.04	11.01±0.04
$^{10}B(p, t)^8B^*$(2nd excited)	13	excitation	2.33±0.04	2.34±0.04
$^{23}Na(p, t)^{21}Na^*(T = 3/2)$	7	excitation	8.92±0.03	8.97±0.03
$^{39}K(p, t)^{37}K^*(T = 3/2)$	7	excitation	5.035±0.025	5.046±0.025

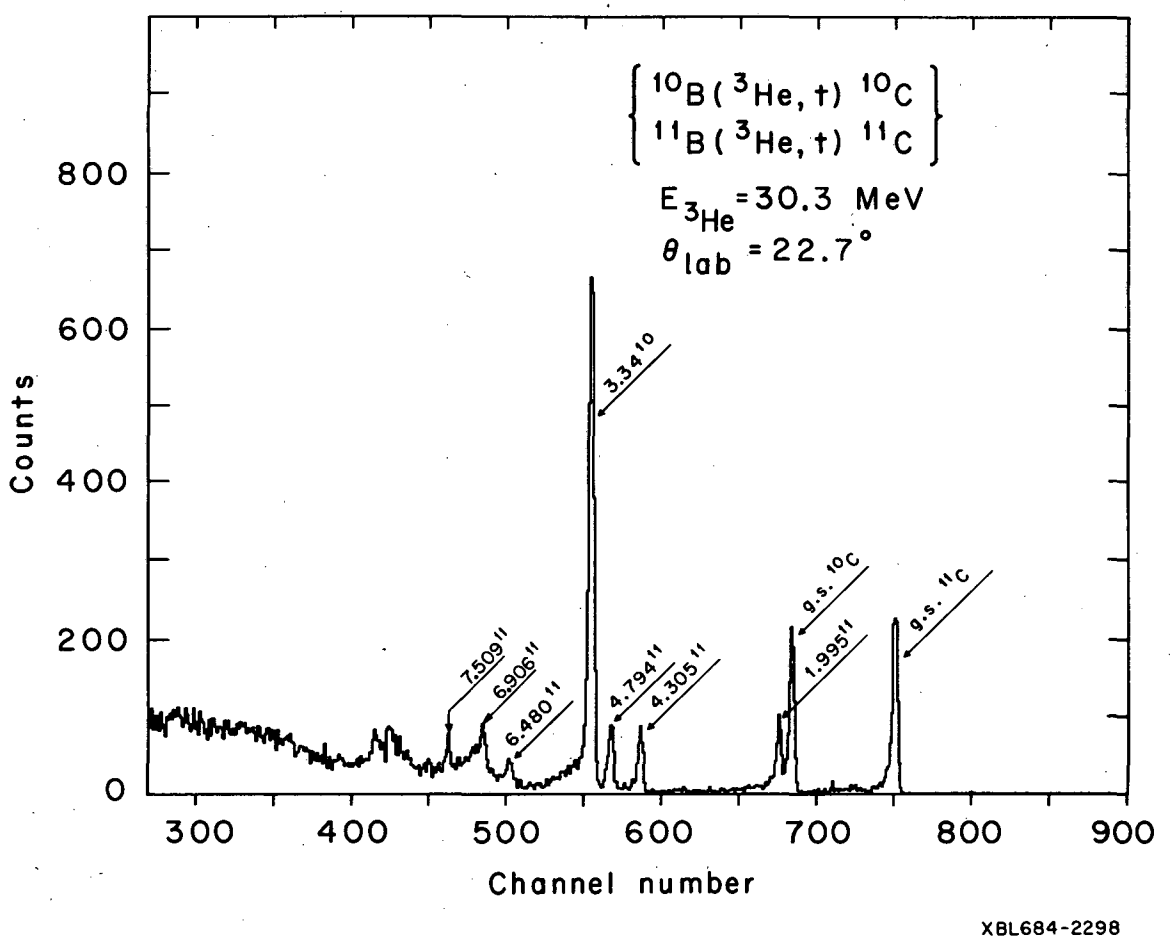

Fig. 1. A triton energy spectrum obtained at θ_{lab} = 22.7 deg, from a boron target 92% enriched in ^{10}B.

ISOBARIC ANALOG STATES AND COULOMB DISPLACEMENT ENERGIES IN THE $1d_{5/2}$ SHELL†

J. C. Hardy, H. Brunnader,‡ Joseph Cerny, and J. Jänecke*

The success of the isobaric-multiplet mass equation in relating the masses of states within a multiplet has been remarkable.[1] It is now clear that in order to examine the effects of non-Coulomb charge-dependent forces the most valuable data will concern the variation of the coefficients in the mass formula as functions of mass number (A) and isospin (T). So as to minimize the number of extraneous effects, we chose to investigate Coulomb displacement energies within a single shell, the $1d_{5/2}$. For this shell, including the six measurements reported here, displacement energies are known within multiplets over the full range of possible A's for all values of $T \leq 2$ with a single exception—the T = 2 multiplet in mass 22.

We have located three previously unobserved T = 3/2 analog levels in ^{19}F, ^{19}Ne, and ^{23}Mg, in addition to significantly improving the precision on the energy of the T = 3/2 state in ^{23}Na and the T = 2 states in ^{20}F and ^{24}Na. All measurements involved (p, t) and (p, ^{3}He) reactions and were made by using the external 45-MeV proton beam from the 88-inch cyclotron. Both solid and gas targets were used, the reaction products being detected in two independent counter telescopes located on opposite sides of the scattering chamber. The energy signals from the counters were

fed to Goulding-Landis particle identifiers, and the total-energy signals were routed according to particle type into 1024-channel groups of a 4096-channel analyzer.

If a target nucleus has isospin T_i, then the ratio of the differential cross sections for (p, t) and (p, ^{3}He) reactions leading to analog final states with isospin $T_f = T_i + 1$ is $(k_t/k_{^3He}) \times 2/(2T_f - 1)$. The angular distributions should be identical in shape. The analog states having thus been identified, their excitation energies were determined by analyzing the data with the computer program LORNA.[2] This program establishes an energy scale by finding a least-squares fit to peaks whose Q values are known, after correcting all incoming and outgoing particles for kinematic effects and absorber losses. The principal source of calibration[3,4] was from the reactions ^{12}C(p, t)^{10}C and ^{12}C(p, ^{3}He)^{10}B.

The results are summarized in Table I and a sample spectrum appears in Fig. 1.

The 28 known displacement energies in the $1d_{5/2}$ shell were fitted by parameterizing generalizations of the Coulomb energy formulae of Hecht.[5] Two limiting coupling schemes were considered, the jj-coupling low-seniority scheme and the Wigner supermultiplet scheme. In both schemes, the formulae have the same form, and it might be expected that they should apply in any intermediate coupling scheme as well. The original equations[5] were expressed in terms of three parameters which related to Coulomb energy matrix elements; the present generalization introduces two additional parameters–one which takes account of additional non-Coulomb charge-dependent effects, and another which accounts for the variation of the average Coulomb interaction radius with mass number.

A sample of the fitted displacement energies calculated for both coupling schemes and compared with experiment is shown in Table II. The only states considered are those for which, in the simplest model, all active nucleons can be considered to be in the $1d_{5/2}$ shell. Anomalies were apparent for the T = 1, A = 18 and T = 1/2, A = 19 displacement energies, but when these were excluded from the fitting procedure an acceptable χ^2 was obtained. (The reason for these anomalies is presumably the large 2s-shell admixtures known to occur[6] for the states considered in these nuclei.) The final parameter values obtained agree reasonably well with calculations based on harmonic oscillator wave functions, and correspond to an increase of $\approx 9\%$ in the interaction radius from the beginning to the end of the shell.

Using the "best-fit" parameters it is, of course, possible to calculate any Coulomb displacement energy within the $1d_{5/2}$ shell. Thus, if the mass of any member of a multiplet is known, the masses of all other members can be readily predicted. We have calculated in this manner the masses, as yet unmeasured, of six neutron-deficient nuclei. The results for both schemes are shown in Table III,[7] where the quoted errors include only the experimental error in the masses upon which the predictions depend. Only ^{19}Na is predicted to be unstable (by 360 keV).

Footnotes and References

†Condensed from UCRL-18566, Jan. 1969.

‡Present address: Chemistry Department, McMaster University, Hamilton, Ontario, Canada.
*Physics Department, University of Michigan, Ann Arbor, Michigan.

1. J. Cerny, Ann. Rev. Nucl. Sci. 18, 27 (1968).
2. LORNA is a program written by C. C. Maples, whom we thank for making it available.
3. H. Brunnader, J. C. Hardy, and Joseph Cerny, Phys. Rev. 174, 1247 (1968).
4. F. Ajzenberg-Selove and T. Lauritzen, Nucl. Phys. A114, 1 (1968).
5. K. T. Hecht, Nucl. Phys. A102, 11 (1967); A114, 280 (1968).
6. J. P. Elliot and B. H. Flowers, Proc. Roy. Soc. (London) A229, 536 (1955).
7. I. Kelson and G. T. Garvey, Phys. Letters 23, 689 (1966).

Table I. Summary of experimental results.

Nucleus	Analog state J^π, T	Excitation energy: This work (MeV±keV)	Excitation energy: Previous work (MeV±keV)	Average value (MeV±keV)
^{24}Mg	0^+, 2	15.426±30	15.436±5	15.436±5
^{24}Na	0^+, 2	5.978±35	5.98 ±48	5.979±28
^{23}Mg	$5/2^+$, 3/2	7.788±25	not reported	7.788±25
^{23}Na	$5/2^+$, 3/2	7.910±30	7.890±30	7.900±21
^{20}Ne	0^+, 2	16.722±25	16.732±2.4	16.732±2.4
^{20}F	0^+, 2	6.523±35	6.43 ±100	6.513±33
^{19}Ne	$3/2^+$, $3/2^a$	7.620±25	not reported	7.620±25
^{19}F	$3/2^+$, $3/2^a$	7.660±35	not reported	7.660±35

a. These levels are not the lowest-energy T = 3/2 levels in mass 19, but are analogs to the first excited state (0.095 MeV) of ^{19}O.

Table II. A sample of the experimental and calculated Coulomb displacement energies in the $1d_{5/2}$ shell.

A	T	T_z	J^π	Experimental $\Delta E_c(A, T, T_z-1\|T_z)$ (keV)	Seniority ΔE_c (keV)	Calculations ΔE_c(calc) $-\Delta E_c$(exp) (keV)	Supermultiplet ΔE_c (keV)	Calculations ΔE_c (calc) $-\Delta E_c$ (exp) (keV)
17	1/2	+1/2	5/2+	3542.0± 1.0	3542.2	0.2	3542.8	0.6
21	1/2	+1/2	5/2+	4315.3± 8.3	4316.6	1.3	4314.8	-0.5
25	1/2	+1/2	5/2+	5062.5± 1.1	5062.6	0.1	5062.2	-0.3
18	1	+1	0+	3478.9± 1.0	3549.4	70.5	3510.4	31.5
22	1	+1	0+	4282.1± 2.8	4279.0	-3.1	4280.0	-2.1
26	1	+1	0+	5014.8± 4.2	5021.1	6.3	5025.0	10.2
22	1	0	0+	4931.6±20.2	4901.2	-30.4	4897.0	-34.6
26	1	0	0+	5623.2±11.6	5592.8	-30.4	5632.1	8.9
19	3/2	+3/2	3/2+	3528.3±35.9	3524.6	-3.7	3501.8	-26.5
23	3/2	+3/2	5/2+	4302.7±21.3	4268.8	-33.9	4268.4	-34.3
19	3/2	+1/2	3/2+	3980.4±43.0	3997.3	16.9	3989.0	8.6
23	3/2	+1/2	5/2+	4726.0±32.7	4739.3	13.3	4747.7	21.7
20	2	+2	0+	3484.4±33.9	3516.0	31.6	3481.7	-2.7
24	2	+2	0+	4292.4±29.7	4259.9	-33.1	4245.5	-46.9
20	2	+1	0+	3971.4±33.0	3986.4	15.00	3966.8	-4.6
24	2	+1	0+	4724.4±28.4	4721.0	-3.4	4722.8	-1.6

Table III. Mass predictions for neutron-deficient nuclei within the $d_{5/2}$ shell.

Nucleus	Mass excess calculated by use of:		Garvey-Kelson prediction (Ref. 7) (MeV)
	Seniority scheme (MeV±keV)	Supermultiplet scheme (MeV±keV)	
^{19}Na	12.965±25[a]	12.968±25[a]	12.87
^{20}Mg	17.509±2	17.510±2	17.40
^{21}Mg	10.916±7	10.910±7	10.79
^{23}Al	6.743±25	6.758±25	6.71
^{24}Si	10.765±5	10.813±5	10.72
^{25}Si	3.828±8	3.804±8	3.77

a. The ground-state mass excess is calculated with the assumption that the lowest 5/2+ state in ^{19}Na is at 0.095 MeV, as in its mirror ^{19}O.

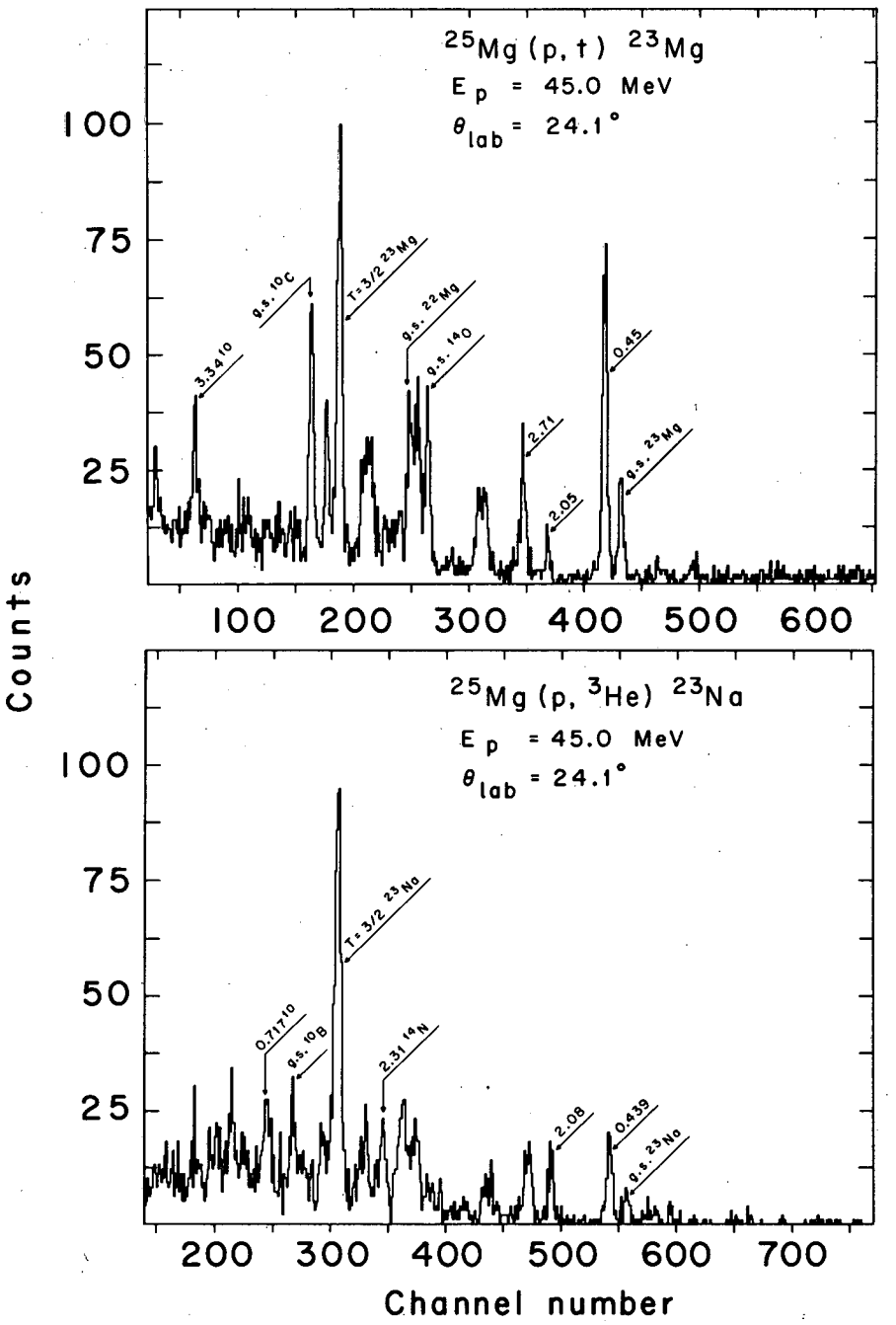

Fig. 1. Energy spectra of the reactions ^{25}Mg(p, t)^{23}Mg and ^{25}Mg(p, ^{3}He)^{23}Na taken at θ_{lab} = 24.1 deg for 970 μ Coulombs. The target was 91.5% enriched in ^{25}Mg. All peaks whose energies are marked were used to establish calibrations.

LOCATION AND ISOSPIN-FORBIDDEN ALPHA DECAY OF THE LOWEST T = 2 STATE IN ^{28}Si †

Robert L. McGrath, * J. C. Hardy, and Joseph Cerny

In the past several years the lowest T = 2 isobaric analog states in a number of T_z = 0 or 1 light nuclides have been located. [1] These states were first observed by using two-nucleon transfer reactions [2, 3] and, later, in several instances, [4, 5] as isospin-forbidden compound-nucleus resonances. Since the states have no available isospin-allowed particle decay modes, their widths are expected to be relatively small; all available data are consistent with this expectation, the widths being less than the experimental resolution in the transfer reaction studies (upper limits about 20 to 80 keV) and less than 2.5 keV for the states in ^{20}Ne, [4] ^{24}Mg, and ^{32}S, [5] which were observed by use of resonance techniques. In general, the T = 2 states of T_z = 0 nuclides lie at least 3.5 MeV above proton or α-particle (isospin-forbidden) decay thresholds; these narrow widths imply that charge-dependent interactions only slightly perturb the T = 2 wave functions. Studies of the partial widths for both particle and gamma decay provide information about the components of wave functions admixed by these interactions either into the T = 2 states or the residual states formed by the decay process. The results can reflect directly upon the character of the charge-dependent forces themselves.

We have measured the excitations of the lowest T = 2 states in ^{28}Si and ^{28}Al, utilizing the ^{30}Si(p, t)^{28}Si and ^{30}Si(p, ^{3}He)^{28}Al reactions. These states have spin-parity 0^+ and are analogs of the ^{28}Mg ground state. In addition, by examination of coincidences between tritons forming the ^{28}Si T = 2 state, and protons or α particles from its decay, the decay branching ratios to ^{27}Al(ΔT=1 or 2) and ^{24}Mg (ΔT = 2) states have been determined. A previously reported [6] attempt to populate this ^{28}Si state via proton scattering on ^{27}Al was unsuccessful, although tentative evidence for its observation at 15.13±0.020 MeV via the ^{26}Mg(^{3}He, n)^{28}Si reaction has been reported. [7]

Triton and ^{3}He energy spectra at angles from 14 to 36 deg (lab) were obtained with the 46-MeV proton beam of the 88-inch cyclotron bombarding a 420 μg/cm^2 evaporated silicon foil enriched to 89% ^{30}Si. Standard techniques were followed in these measurements. [2] The coincidence data were collected with three telescopes--a triton telescope and two "decay" telescopes. Each telescope consisted of ΔE, E, and E-reject silicon detectors (the last being used to reject particles that passed through the E counter) and fed electronics built around Goulding-Landis [8] particle-identifier systems. The triton telescope, subtending 9.2×10^{-4} sr, was positioned at +22 deg, the second maximum in the L = 0 angular distribution to the analog state. Fast-slow coincidences were required between tritons in this telescope and either identified protons or particles stopping in the ΔE counters (50 μ thick) of either decay telescope. The latter telescopes were positioned at -90 and -125 deg and subtended about 1.3×10^{-2} sr. Energy signals from all free triton events together with coincident events and their associated logic signals were fed to a multiplexer analog-to-digital converter and, subsequently, into an on-line computer.

The triton energy spectrum shown at the top of Fig. 1 was accumulated during the coincidence experiment, but is representative of the region of higher excitation in the spectra obtained during the earlier angular distribution measurements. The prominent peak located at 15.206±0.025 MeV in ^{28}Si is identified as the lowest 0^+, T = 2 state; the ^{3}He data [9] yield the ^{28}Al analog excitation as 5.983±0.025 MeV.

The coincidence data, displayed as two-dimensional energy spectra, exhibited events distributed along bands determined by the three-particle final-state kinematics. Final states including both the ^{27}Al ground state and (0.84+1.01)-MeV states (the latter two being unresolved) were evident in the triton-proton arrays. Coincident events with more than 2 MeV energy loss in the ΔE decay counters could unambiguously be identified as α particles. These α-particle events fell along bands in the triton-ΔE arrays which corresponded to the ^{24}Mg ground state and 1.37-MeV state.

Events lying along different kinematic bands were "projected" onto the triton energy axis, and the summed projections from both decay telescopes are shown in the lower portion of Fig. 1. Branching ratios were found by comparing the net coincidence events in the various projections to the number predicted from the triton singles counts, decay telescope geometries, and the Jacobian relating the laboratory and ^{28}Si recoil coordinates. The sum of branching ratios to the three lowest ^{27}Al states and the lowest two states of ^{24}Mg was 89.1±15.7%. Figure 2 summarizes these results. The summed branching ratios have been renormalized to 100% for clarity;

it is not implied that gamma decays or unobserved particle decays could not make small contributions to the total width. Clearly, alpha emission to the ^{24}Mg ground state dominates the decay strength.

In self-conjugate nuclei, $\Delta T = 2$ isospin impurities (necessary to explain alpha emission) can arise only from the isotensor component of charge-dependent interactions. The contrast with the $T = 2$ state in ^{24}Mg, which decays principally by proton emission,[10] is striking, and an attempt to understand the decay properties in terms of admixtures of specific two-particle, two-hole states in these nuclei is being undertaken.

Footnotes and References

†Condensed from Phys. Letters 27B, 443 (1968).

*Present address: Department of Physics, State University of New York, Stonybrook, Long Island, N. Y.

1. For summaries: J. Cerny and G. T. Garvey, in Isobaric Spin in Nuclear Physics, edited by J. D. Fox and D. Robson (Academic Press, Inc., New York, 1966), p. 514 and 517; J. Cerny, Ann. Rev. Nucl. Sci. 18, 27 (1968).

2. G. T. Garvey, J. Cerny, and R. H. Pehl, Phys. Rev. Letters 12, 726 (1964); J. Cerny, R. H. Pehl, and G. T. Garvey, Phys. Letters 12, 234 (1964).

3. E. Adelberger and A. B. McDonald, Phys. Letters 24B, 270 (1967), and Erratum, Phys. Letters 24B, 618 (1967).

4. R. Bloch, R. E. Pixley, and P. Truöl, Phys. Letters 25B, 215 (1967); H. M. Kuan, D. W. Heikkinen, K. A. Snover, F. Riess, and S. S. Hanna, Phys. Letters 25B, 217 (1967).

5. F. Riess, W. J. O'Connell, D. W. Heikkinen, H. M. Kuan, and S. S. Hanna, Phys. Rev. Letters 19, 367 (1967); D. W. Heikkinen, H. M. Kuan, K. A. Snover, F. Riess, and S. S. Hanna, Bull. Am. Phys. Soc. 13, 884 (1968).

6. H. M. Kuan, F. Riess, K. A. Snover, D. W. Heikkinen, D. C. Healey, and S. S. Hanna, Bull. Am. Phys. Soc. 13, 884 (1968).

7. G. H. Lenz and D. Bernard, Bull. Am. Phys. Soc. 13, 673 (1968); and private communication.

8. F. S. Goulding, D. A. Landis, J. Cerny, and R. H. Pehl, Nucl. Instr. Methods 31, 1 (1964).

9. These data will be included in a paper by H. Brunnader, J. C. Hardy, and J. Cerny, $T = 2$ and $T = 3$ Analog States, $28 \leq A \leq 40$, to be submitted to Phys. Rev.

10. R. L. McGrath, S. W. Cosper, and J. Cerny, Phys. Rev. Letters 18, 243 (1967); R. L. McGrath, G. W. Goth, and J. Cerny, Bull. Am. Phys. Soc. 12, 1144 (1967).

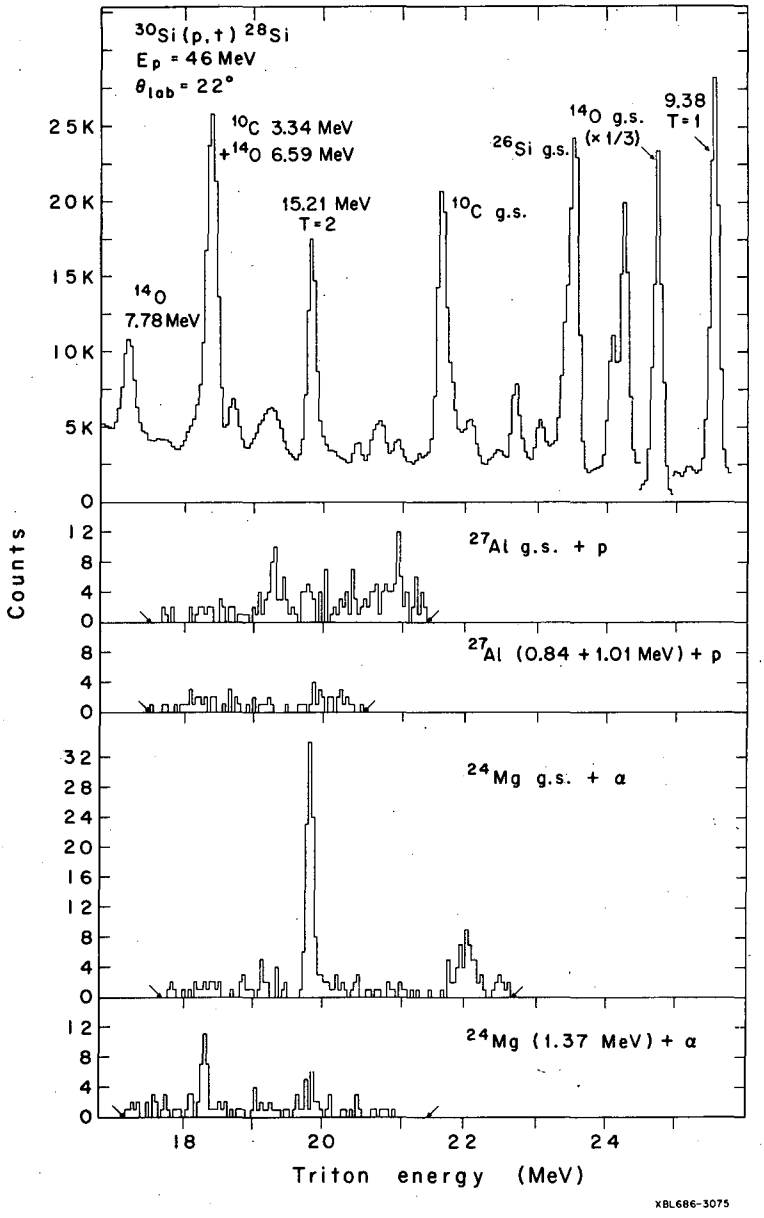

Fig. 1. The top spectrum presents the triton singles data containing a peak corresponding to the lowest ^{28}Si T = 2 state at 15.206 ± 0.25 MeV. The lower spectra are summed projections, from both decay telescopes, of events lying along kinematic bands in the coincidence data onto the triton energy axis; the arrows in these spectra mark the energy cutoffs determined by kinematics and detector thicknesses.

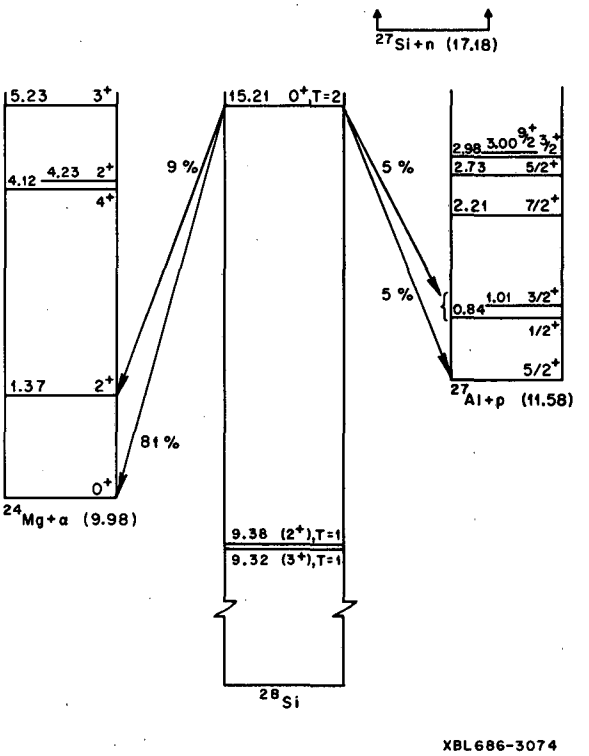

Fig. 2. Energy-level diagram showing the the ^{28}Si T = 2 state and the various available proton or α-particle isospin-forbidden decay modes. The observed transitions are indicated by arrows; the numbers are fractional branching ratios normalized to 100% as discussed in the text.

THE ^{31}P(t, p)^{33}P REACTION AND THE USEFULNESS OF DOUBLE STRIPPING INDISTINGUISHING AMONG SHELL-MODEL CALCULATIONS†

W. G. Davies,* J. C. Hardy, and W. Darcey‡

The (t, p) reaction has previously been used[1] in the ($2s_{1/2}$, $1d_{3/2}$) shell to investigate some of the consequences of existing shell-model calculations.[2-4] A particularly simple case was chosen, the target being the "core" nucleus ^{28}Si, in order to single out the effects of particular two-body matrix elements. It is now of interest to investigate the same reaction on nuclei whose wave functions depend not just on the choice of a few two-body matrix elements, but on that of all 15 matrix elements (and two single-particle binding energies) necessary to specify the entire shell. There have been a number of determinations of these matrix elements using various criteria,[1-4] all of which lead to similar fits to experimental energy levels. It is then particularly valuable to have an additional sensitive test of the merits of these calculations.

The experiment chosen for this purpose was ^{31}P(t, p)^{33}P. The nuclei involved have enough active particles that their wave functions depend upon all matrix elements, and there is the additional advantage that none of the levels in ^{33}P were used in the original determination of the matrix-element values, thus providing an independent assessment.

The experiment was performed with 12.1-MeV incident tritons from the A. W. R. E. (Aldermaston) tandem Van de Graaff. The emitted protons were recorded on nuclear emulsions placed in the focal planes of the 24-gap magnetic spectrograph. Figure 1 shows the energy spectrum recorded at 27.5 deg for a 3000-μC exposure, where the energy range covered includes all levels in ^{33}P up to 5.8 MeV excitation. Angular distributions of those proton groups which corresponded to levels below 5 MeV and appeared to be predominantly stripping in character are displayed in Fig. 2. The curves in the figure were computed by using the "point triton"[5] (PT) and "zero-range interaction"[6] (ZI) approximations. The optical-model parameters for tritons were

interpolated from the elastic scattering results[7] for 12-MeV tritons on ^{27}Al and ^{35}Cl, while those for protons were taken[8] from 17.6-MeV data on ^{27}Al.

The energies of the observed levels along with the L-values giving best fit to the data are listed in Table I together with previous results.[9-11]

In comparing the experimental results with shell-model calculations, five sets of matrix elements were considered. Set I: empirically determined matrix elements taken from Ref. 3: Set II: the same set modified according to Ref. 1; Sets III and IV: empirically determined matrix elements taken from Ref. 4 (Set I and V in that reference); Set V: matrix elements calculated assuming a surface-delta interaction, three parameters being determined empirically.[4] All matrix-element sets were determined by fitting energy-level data in nuclei between ^{28}Si and ^{40}Ca. Each set produces acceptable agreement with the level spacings in ^{33}P. In Table II we have compared the experimentally observed relative peak intensities with those obtained with DWBA computations using the PT approximation. (Calculations using the ZI approximation yielded the same results.) Here an additional ambiguity arises. The relative sign of the s and d single-particle radial wave functions is undefined in effective-interaction shell-model calculations of the type considered here (Sets I-IV). The calculations denoted by "a" assumed that all single-particle wave functions were positive asymptotically, while those denoted by "b" made the opposite choice for the relative signs. The ambiguity does not occur for the surface-delta calculations.

It can be readily seen from the Table II that dramatically different results are predicted by using the various sets of two-body matrix elements and sign conventions; the best overall agreement is produced by Sets IVb and V. Both sets also predict that no positive-parity states above the third excited state should be strongly excited, and this is confirmed by the data in Table I.

That this reaction proved to be such a sensitive probe of the details of the calculations seemed especially interesting when compared with calculations involving other, more common, spectroscopic tools--single-nucleon transfer reactions and β decay. Spectroscopic factors and log ft values were calculated and compared with results from the ^{34}S(d, ^{3}He)^{33}P reaction[9] and the β^+ decay[12] of ^{33}Ar to $T_{3/2}$ states in ^{33}Cl, since both involve the same wave functions. Neither calculation shows comparable sensitivity to the matrix-element set used.

The excellent agreement between the (t, p) experiment and the calculations with Sets IV and V is noteworthy, particularly considering that there is good evidence from the (d, ^{3}He) reaction that at least the 1.845-MeV level contains significant admixtures of configurations which include holes in the $1d_{5/2}$ shell. Apparently the calculations, all of which considered that shell to be closed, do account reasonably well for those parts of the wave functions which include active nucleons only in the $2s_{1/2}$ and $1d_{3/2}$ shells.

Footnotes and References

†Condensed from UCRL-18686, Jan. 1969; submitted to Nucl. Phys.

*Nuclear Physics Laboratory, Oxford, England, and Nuclear Research Center, The University of Alberta, Edmonton, Alberta, Canada.

‡Nuclear Physics Laboratory, Oxford, England.

1. J. C. Hardy and I. S. Towner, Phys. Letters 25B, 577 (1967).
2. P. W. M. Glaudemans, G. Wiechers, and P. J. Brussaard, Nucl. Phys. 56, 529 (1964).
3. P. W. M. Glaudemans, G. Wiechers, and P. J. Brussaard, Nucl. Phys. 56, 548 (1964).
4. P. W. M. Glaudemans, B. H. Wildenthal, and J. B. McGrory, Phys. Letters 21, 427 (1966).
5. J. R. Rook and D. Mitra, Nucl. Phys. 51, 96 (1964).
6. N. K. Glendenning, Phys. Rev. 137, B102 (1965).
7. R. N. Glover and A. D. W. Jones, Nucl. Phys. 81, 268 (1966).
8. P. E. Hodgson, The Optical Model of Elastic Scattering (Oxford University Press, London, 1963).
9. R. C. Bearse, D. H. Youngblood, and J. L. Yntema, Phys. Rev. 167, 1043 (1968).
10. W. M. Currie and J. E. Evans, Phys. Letters 24B, 399 (1967).
11. C. E. Moss, R. V. Poore, N. R. Roberson, and D. R. Tilley, Phys. Rev. 174, 1333 (1968).
12. J. C. Hardy and R. I. Verrall, Can. J. Phys. 43, 418 (1965), and A. M. Poszkanzer, R. McPherson, R. A. Esterlund, and P. L. Reeder, Phys. Rev. 152, 995 (1966).

Table I. Experimental results.

This experiment					Previous results [a]
Level	Energy (keV)	L	J^{π}	Relative peak intensities	Energy (keV)
g. s.	0	0	$1/2^+$	1.000	0
1	1427±15	2	$3/2^+$	0.005	1435± 3
2	1845±15	2	$5/2^+$	0.030	1850± 3
3	2530±15	2	$3/2^+$	0.027	2543± 4
4	3272±15	(2)	$(3/2^+, 5/2^+)$	0.002	
5	3488±15			~0.001	3500± 8
6	3623±15			~0.001	3638±10
7	4044±15			~0.001	
8	4218±15	3	$7/2^-$	0.040	
9	4847±20				
10	5039±20				
11	5177±20				
12	5368±20				
13	5438±20				
14	5485±20				
15	5535±20				
16	5619±20				
17	5650±20	0	$1/2^+$	0.170	
18	5783±20				

a. See Refs. 9-11.

Table II. Comparison of experimental relative peak cross sections for $^{31}P(t, p)^{33}P$ with those calculated by using various sets of two-body matrix elements. The distorted-wave calculations assumed the PT approximation.

Level energy (MeV)	J^{π}	Experiment	Calculations using matrix element set								
			Ia	Ib	IIa	IIb	IIIa	IIIb	IVa	IVb	V
0	$1/2^+$	1.000	1.000	1.000	1.000	1.000	1.000	1.000	1.000	1.000	1.000
1.427	$3/2^+$	0.005	0.035	0.301	0.007	0.0007	0.008	0.0005	0.011	0.002	0.005
1.845	$5/2^+$	0.030	2.559	0.315	0.003	0.068	0.013	0.067	0.019	0.062	0.065
2.530	$3/2^+$	0.027	2.087	0.122	0.0006	0.070	0.0008	0.065	0.003	0.053	0.061

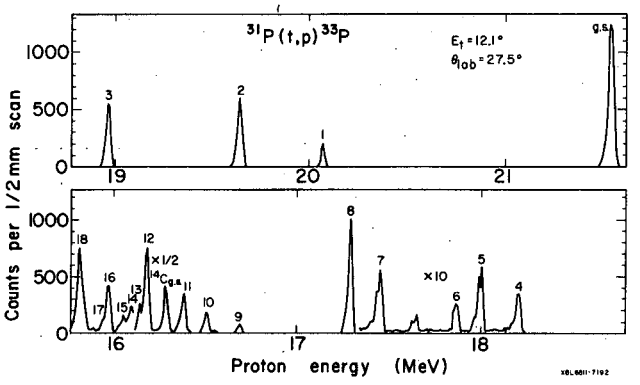

Fig. 1. Energy spectrum for the reaction $^{31}P(t, p)^{33}P$ recorded at a lab angle of 27.5 deg.

Fig. 2. Angular distributions of selected proton groups from the reaction $^{31}P(t, p)^{33}P$. The results of DWBA calculations for the indicated L values are also shown: the solid curve corresponds to the PT approximation; the dashed curve, to the ZI approximation.

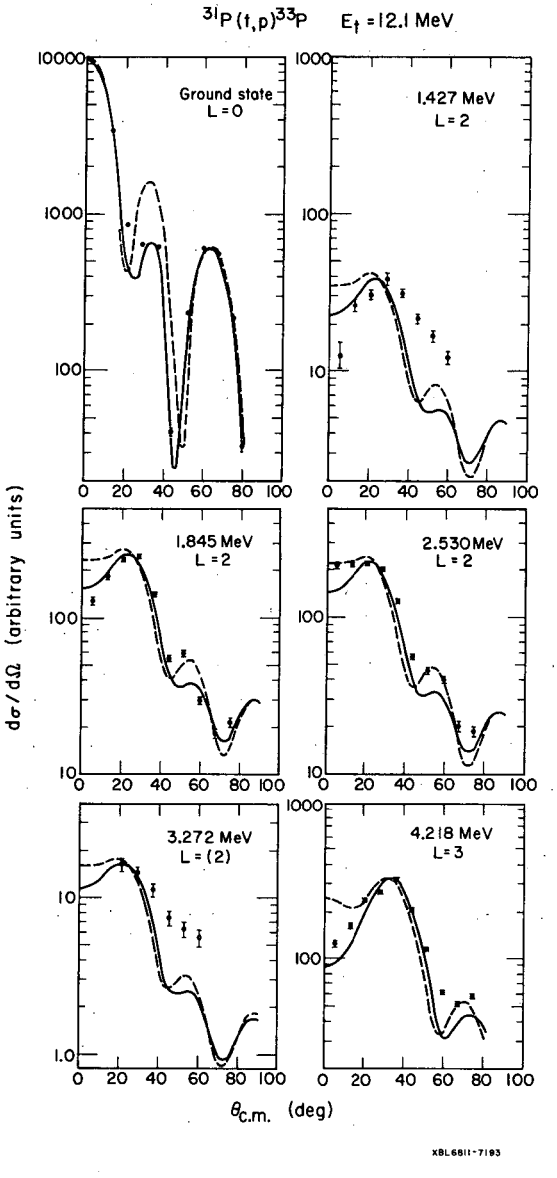

^{91}Y AND THE FAILURE OF THE CLOSED SHELL AT ^{88}Sr†

J. C. Hardy, W. G. Davies,* and W. Darcey‡

Recently, there have been several shell-model calculations which investigated the structure of nuclei in the mass A = 90 region.[1-4] Talmi and Unna[1] and Auerbach and Talmi[3] consider the $1f_{5/2}$ proton shell and the $1g_{9/2}$ neutron shell to be closed (at ^{88}Sr), and all active nucleons to occupy the $2p_{1/2}$ and $1g_{9/2}$ proton shells and the $2d_{5/2}$ neutron shell. In calculations restricted to the isotopes of Nb, Mo, and Tc, Bhatt and Ball[3] assume that the $2p_{1/2}$ proton shell is also closed (at ^{90}Zr), and allow only two active shells. Vervier[4] follows both approaches, considering ^{88}Sr as a core for calculations of isotopes of Y, Zr, and Nb while ^{90}Zr is taken as a core for isotopes of Nb, Mo, and Tc. All authors conclude from comparison with rather meager experimental evidence that the assumed shell closures were justified.

The reactions ^{92}Zr(t, α)^{91}Y and ^{89}Y(t, p)^{91}Y were initiated with 12.1-MeV tritons from the A. W. R. E. (Aldermaston) tandem Van de Graaff. The emitted particles were recorded on nuclear emulsions placed in the focal planes of the 24-gap magnetic spectrograph. Figure 1 shows the alpha spectrum from ^{92}Zr(t, α)^{91}Y recorded at 27.5 deg for a 2801-μC exposure and the proton spectrum from ^{89}Y(t, p)^{91}Y recorded at 27.5 deg for a 2636-μC exposure. In both spectra, the energy range covered includes levels in ^{91}Y up to 3 MeV excitation.

The energies of levels in ^{91}Y observed in the (t, α) and (t, p) reactions are given in columns two and four, respectively, of Table I. The average excitation energies appear in column six. Since the ground states of ^{92}Zr and ^{89}Y have spin-parities of 0^+ and $1/2^-$ respectively, it is possible to make a unique assignment of the spin and parity of every level in ^{91}Y for which an unambiguous determination of the transferred angular momenta can be obtained in both the (t, α) and (t, p) experiments. The transferred ℓ(L) values obtained from DWBA calculations also appear in Table I together with the deduced spin-parities. The energy-level diagram showing the results of this experiment is given in Fig. 2, and compared with the earlier work of Ames et al.[5] The levels observed by these authors at 1.30 and 1.58 MeV do not appear in either of our experiments.

Shell-model calculations in which ^{88}Sr is assumed to be a closed core[4] predict that only four levels at low excitation should be produced in the ^{92}Zr(t, α)^{91}Y reaction (two of them, very weakly), and five in the ^{89}Y(t, p)^{91}Y reaction, the ground state being the only one expected to be common to both. In fact, eleven states below 3 MeV excitation are produced in both reactions, nine of them with significant intensity. A further comparison shows, for example, that instead of a single low-lying $3/2^-$ level in ^{91}Y, with the configuration $(\pi p_{1/2})(\nu d_{5/2})^2_2$, three are observed below 3 MeV in both the (t, p) and (t, α) reactions, and the same is true for $5/2^-$ levels. The fact that these levels are produced strongly in the (t, α) reaction provides conclusive evidence of large admixtures of $(\pi p_{3/2})^{-1}$ and $(\pi f_{5/2})^{-1}$ hole configurations in these states. Thus, if any meaningful calculations are to be made for this nucleus, it is clear that ^{88}Sr cannot be considered a closed core, and that particle-hole excitations from at least the $2p_{3/2}$ and $1f_{5/2}$ shells must be included.

It is interesting to note that for the first four excited states, the calculated energies agree quite well with the experimentally observed levels despite the fact that the wave functions are considerably in error.

Footnotes and References

†Condensation from Nucl. Phys. 121, 103 (1968).

*Nuclear Physics Laboratory, Oxford, England, and Nuclear Research Center, The University of Alberta, Edmonton, Alberta, Canada.

‡Nuclear Physics Laboratory, Oxford, England.

1. I. Talmi and I. Unna, Nucl. Phys. 19, 225 (1960).
2. K. H. Bhatt and J. B. Ball, Nucl. Phys. 63, 286 (1965).
3. N. Auerbach and I. Talmi, Nucl. Phys. 64, 458 (1965).
4. J. Vervier, Nucl. Phys. 75, 17 (1966).
5. D. P. Ames, M. E. Bunker, L. M. Langer, and B. M. Sorenson, Phys. Rev. 91, 68 (1953).

Table I. Comparison of data from the $^{92}Zr(t,\alpha)^{91}Y$ and $^{89}Y(t,p)^{91}Y$ reactions, as well as average level energies and deduced spin-parities.

Level	$^{92}Zr(t,\alpha)^{91}Y$		$^{89}Y(t,p)^{91}Y$		FINAL RESULTS	
	Energy (keV)	ℓ-value	Energy (keV)	L-value	Energy (keV)	J^{π}
0	0	1	0	0	0	$1/2^-$
1	550 ± 10	4	--		550 ± 10	$9/2^+$
2	653 ± 10	1	654 ± 10	2	654 ± 7	$3/2^-$
3	922 ± 10	3	926 ± 10	2	924 ± 7	$5/2^-$
4	--	--	1186 ± 10	4	1186 ± 10	$(7/2, 9/2)^-$
5	1481 ± 10	1	1472 ± 10	2	1476 ± 7	$3/2^-$
6	1552 ± 10	3	1547 ± 10	--	1550 ± 7	$(5/2, 7/2)^-$
7	1974 ± 10	3	1968 ± 10	2	1971 ± 7	$5/2^-$
8	2058 ± 25	--	2065 ± 10	--	2064 ± 9	--
9	2159 ± 25	--	2158 ± 15	2	2158 ± 13	$(3/2, 5/2)^-$
10	2205 ± 25	3	2198 ± 10	2	2199 ± 9	$5/2^-$
11	2475 ± 25	1	2470 ± 15	2	2472 ± 11	$3/2^-$
12	2569 ± 15	1	2566 ± 15	0	2568 ± 11	$1/2^-$
13			2822 ± 15	(2)	2822 ± 15	$(3/2, 5/2)^-$

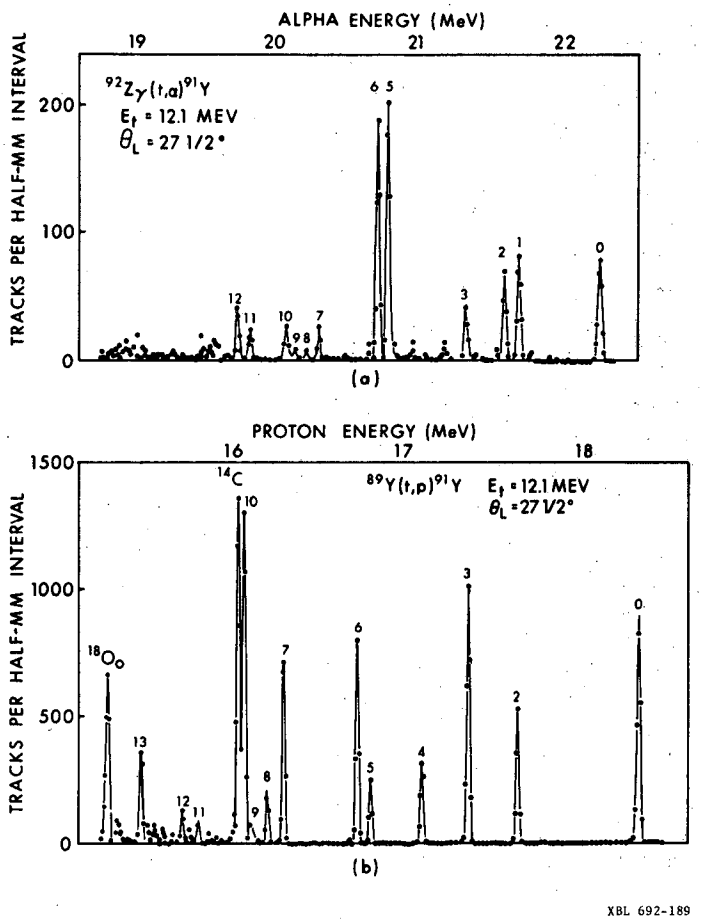

Fig. 1. Energy spectrum for the reaction (a) $^{92}Zr(t,\alpha)^{91}Y$ and (b) $^{89}Y(t,p)^{91}Y$ recorded at a lab angle of 27.5 deg. (From Nucl. Phys. 121, 103 (1968).

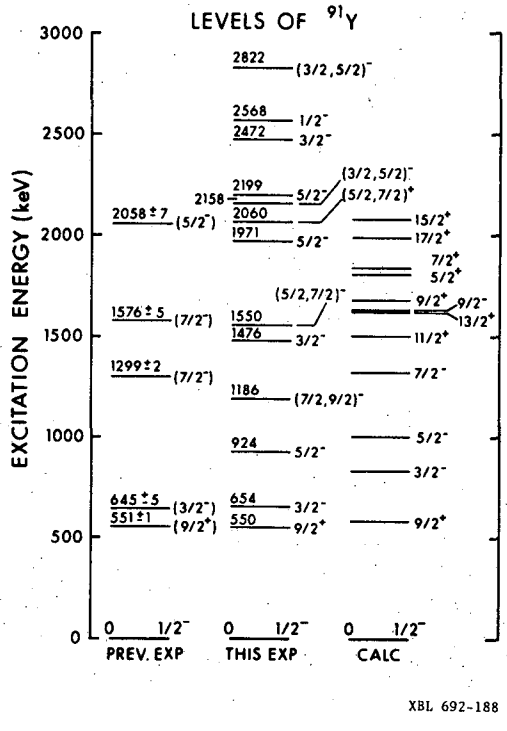

Fig. 2. Experimental energy-level diagrams deduced from this work and from that of Ref. 5, as well as a calculated spectrum taken from Ref. 4. (From Nucl. Phys. 121, 103 (1968)).

ELASTIC α-α SCATTERING AND THE ^{7}Li(p, α)α REACTION

H. E. Conzett and R. J. Slobodrian*

The ^{7}Li(p, α)α reaction was first observed 36 years ago by Cockcroft and Walton[1] at proton energies up to 500 keV. Fifteen years later Heydenberg et al.[2] made the first observation of resonance behavior in the excitation function near E_p = 3 MeV, but it is interesting to note that there still has not been a completely satisfactory theoretical description of that resonance behavior. The most recent attempt by Freeman and Mani[3] to fit the data between 1 and 6.5 MeV assumed two 2^+ resonances, one each at 3 and 5.5 MeV proton energy. Their fit to the integrated cross section as a function of energy was very satisfactory, but they could not fit the angular distributions, and concluded that another level had to be assumed.

Resonances of even spin and parity alone can decay into the 2α channel, and this selectivity is extremely useful in identifying states of ^{8}Be that lie above the ^{7}Li + p threshold. For example (Fig. 1), there are six or seven states of ^{8}Be in some 5 MeV above the proton threshold, but only two peaks appear in the (p, α) reaction excitation function. The technique of resonance elastic proton scattering on ^{7}Li might seem to be useful here, but those four or five other states, which do not communicate with the α-channel but do so with the proton channel, complicate the analysis enormously. However, elastic α-α scattering has just the advantage of resonance elastic scattering without the accompanying disadvantage of exciting those unwanted states.

Phase-shift results from our elastic α-α scattering data[4] show clear evidence for resonances in both the $\ell = 2$ and $\ell = 4$ partial waves near 20 MeV cm, as shown in Figs. 2 and 3. Since the channel-spin is zero, this provides the immediate assignment of spin and parity 4^+ and 2^+ to ^{8}Be levels near 19.5 and 19.9 MeV, respectively.

Barker's[5] intermediate-coupling shell-model calculation, which predicts a 4^+, T = 0 state at 21.5-MeV excitation of ^{8}Be, prompted Kermode[6] to reexamine the phase shifts from Igo's optical-model analysis[7] of older α-α scattering data in this energy region. By adding 180 deg to the $\ell = 4$ phase shift above 19.7 MeV cm, he assigned a 4^+ resonance near 19.5 MeV with a width of 360 keV. This calculation, assuming an elasticity, Γ_α/Γ, of 0.95, gave a narrower width than would have resulted from a smaller Γ_α/Γ. Our result, Fig. 3, provides $\Gamma_\alpha/\Gamma \approx 3/4$ or 1/4 and a consequent larger width, $\Gamma \approx 750$ keV.

This additional 4^+ resonance, which clearly communicates with the proton channel, should make it possible to finally provide a satisfactory fit to the ^{7}Li(p, α)α data.

Footnote and References

*Present address: Université Laval, Quebec 10^e, Canada.

1. J. D. Cockcroft and E. T. S. Walton, Proc. Roy. Soc. (London) A137, 229 (1932).
2. N. P. Heydenburg, C. M. Hudson, D. R. Inglis, and W. D. Whitehead, Phys. Rev. 73, 241 (1947); 74, 405 (1948).
3. R. M. Freeman and G. S. Mani, Proc. Phys. Soc. (London) 85, 267 (1965).
4. H. E. Conzett, E. Shield, R. J. Slobodrian, and S. Yamabe, Bull. Am. Phys. Soc. 9, 704 (1964).
5. F. C. Barker, Nucl. Phys. 83, 418 (1966).
6. M. W. Kermode, Phys. Letters 25B, 183 (1967).
7. G. Igo, Phys. Rev. 117, 1075 (1960).

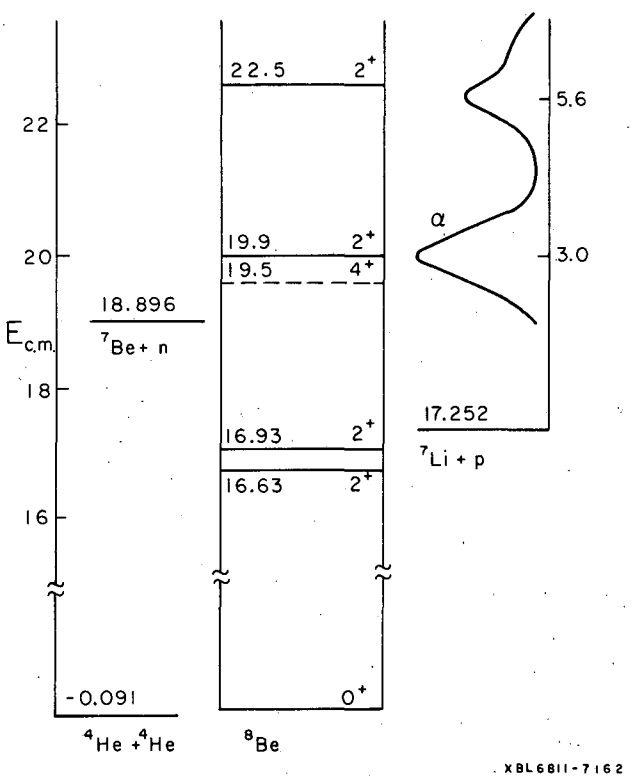

Fig. 1. Even spin and parity levels of ^{8}Be between 16 and 23 MeV excitation. The 4^+ level near 19.5 MeV is assigned from analysis of our α-α scattering data.

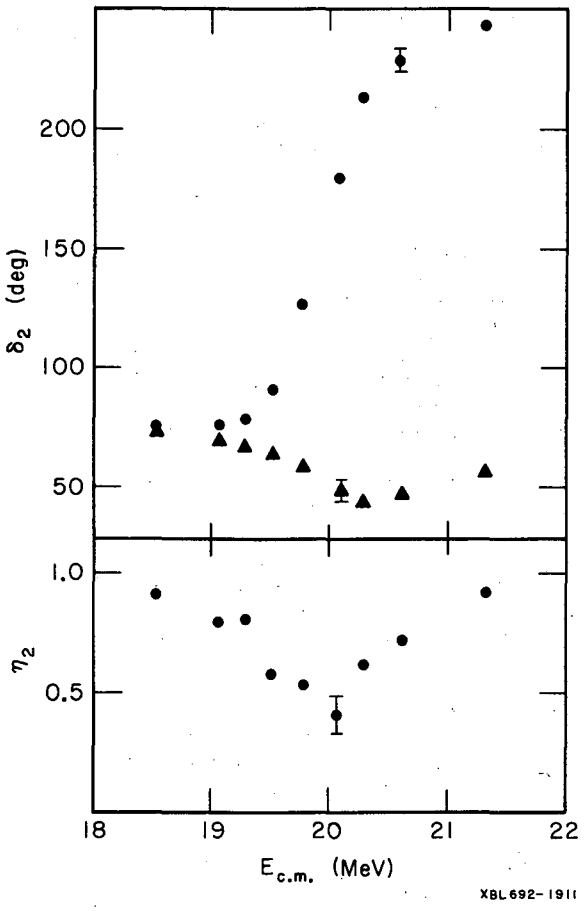

Fig. 2. Nuclear phase shift, δ_2, and elasticity parameter, η_2, for the $\ell = 2$ partial wave. The S-matrix element is $S_2 = \eta_2 \exp(2i\delta_2)$. The dots correspond to a resonance with $\Gamma_\alpha/\Gamma > 1/2$; triangles, $< 1/2$.

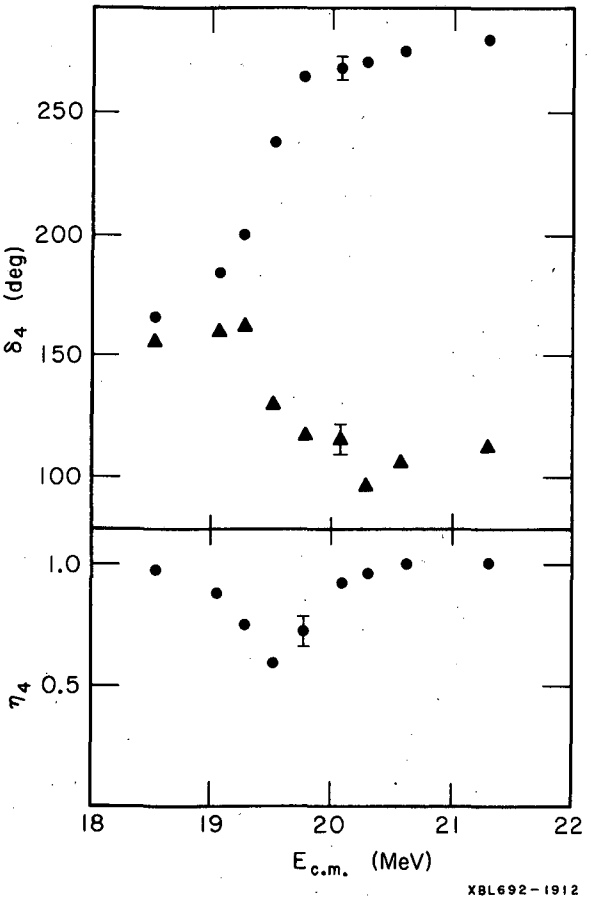

Fig. 3. Resonance behavior of δ_4 and η_4. The dots correspond to $\Gamma_\alpha/\Gamma > 1/2$; triangles, $< 1/2$.

PROTON-PROTON ELASTIC SCATTERING BETWEEN 6 AND 10 MeV†

R. J. Slobodrian,* H. E. Conzett, E. Shield,‡ and W. F. Tivol

Low energy proton-proton scattering has been the object of very accurate experimental investigation,[1,2] and, except for electromagnetic complications,[2] it is the most suitable source of information concerning the nuclear interaction of two nucleons in the S wave. The research carried out at Wisconsin was particularly fruitful; two different experimental groups[3,4] covered the range between 1.397 and 4.203 MeV (laboratory-system energies). Between 4.203 and 10 MeV there have been several other experiments,[5-10] but significant disagreement among these data has indicated the need for more accurate differential cross sections in this energy range.

A comprehensive analysis of the experimental information below 40 MeV was done first by MacGregor,[11] using a selection of data in this energy range. The WMF data[3] were the first to show a definite "anomaly" with respect to pure S-wave scattering, and thus indicated the necessity of P waves in the analysis of low energy p-p cross-section data.[12] Early analyses were performed in terms of the S-wave phase shift K_0 and an "effective" P-wave K_1. MacGregor[11] stressed the insufficiency of cross-section data alone, and his analysis resulted in a fourfold ambiguity among

phase-shift solutions using S, split P, and D waves. These solutions predicted different, though small, polarizations, and later measurements[13-15] showed these to be, indeed, small. Thus, large P-wave splittings should be excluded.

One of the interesting aspects of low energy p-p scattering is the possibility of the determination of shape-dependent effects on the S-wave phase shift. This is not yet feasible for n-p scattering, for which only total cross sections are presently available; and thus even the effective-range parameter is rather inaccurately known.

The ideal region for such a determination is between zero and 10 MeV. An important experiment has been performed in this connection, consisting of the precise determination of the energy of the interference minimum in p-p scattering.[16] This was found to be 0.38243 ±0.00020 MeV, and from this a very accurate value for the $^1S_0$ phase shift was derived.[17] This phase shift, in conjunction with the data of Ref. 4, was used by several authors to attempt a determination of shape-dependent parameters in the expression $C^2k \cot \delta_0 + 1/R\, h(\eta) = -1/a_p + 1/2\, r_e k^2 - P r_e^3 k^4 + Q r_e^5 k^6 - \cdots$, where the symbols have the usual meaning.[18] Reference 18 contains a summary of the situation concerning this point. There are uncertainties if the analysis is restricted to the interference minimum datum and to the KMBND[4] data set. The inclusion of the WMF data in the analysis reduces such uncertainties,[18] but, nevertheless, the shape-dependent scattering parameters are not determined unambiguously. Heller[2] has recently added the phase shift at 9.69 MeV, obtained from the data of Johnston and Young,[10] to the interference minimum datum and to the KMBND data set. The analysis was carried out by using the effective-range expansion up to and including a cubic term in the energy. The shape-dependent coefficients P and Q were obtained with large errors. It is also well known that the point at 9.69 MeV is too close to the radius of convergence of the series to warrant a fit with a small number of terms in the expansion. This was recognized by Heller himself.

Another approach was made recently by Noyes and Lipinski[19] in analyzing the 9.69-MeV data[10] and incorporating in the analysis a ratio of spin-orbit to tensor effects; they calculated higher partial waves in terms of a model. They neglected vacuum polarization and electromagnetic structure effects in the S wave. They concluded that the $^1S_0$ phase shift determined in the analysis was in modest agreement with the predicted OPE shape correction.

The measurement of precise angular distributions between 4.203 and 10 MeV to better than 1% absolute accuracy seemed to be another promising angle of attack to solve the problem of shape dependence.[20] Another paper[21] will describe the determination of the shape-dependent parameters P and Q from the interference minimum phase shift, the WMF data, the KMBND data, and the results reported here.

Spectra were measured between 6 and 50 deg lab, and we have consistently recorded the energy spectra at all measured angles. For consistency with the "discriminator methods" used in the experiments mentioned above we have evaluated the peak counts by means of the simulation of a discriminator setting (from now on called D data). However, if a "background" line is extrapolated from the spectrum shape at energies below the peak, the cross section values are reduced between 0.5 and 1%. Therefore, we have also determined cross sections, using a background subtraction method (from now on called BGS data). Figure 1 shows our angular distributions of D data, together with data obtained at neighboring energies by other groups.

A phase-shift analysis was performed by use of a program developed by Knecht[22] and written by Jenkins. It was adapted for use with a CDC 6600 computer. This program includes S, P, and D waves. The conclusions reached by Noyes and Lipinski[19] at 9.69 MeV concerning the negligible contribution of F waves are also applicable at 9.918 MeV, and, a fortiore, they hold at lower energies. Also, the results of recent phenomenological phase-parameter fits by the Yale group[23] show negligible F-wave contributions at 10 MeV. Consequently, we have considered that an analysis limited to S, P, and D waves is valid and meaningful for experiments of the order of 0.5 to 1% accuracy. Vacuum polarization corrections for $\ell = 1$ were carried out by use of formulae derived by Durand.[24] The S-wave vacuum polarization correction was not performed, as it is easily done using the procedure of Foldy and Eriksen[25] in the effective range expansion.

Noyes and Lipinski[19] have concluded that the $^3P_{0,1,2}$ phase shifts $\delta_{1,J}$ should have the + - + OPE signature at 9.69 MeV and that Δ_{LS}/Δ_T should be in the range 0.07 to 0.15, where

$$\Delta_{LS} = (-2\,\delta_{1,0} - 3\,\delta_{1,1} + 5\,\delta_{1,2})/12$$

and

$$\Delta_T = 5(2\,\delta_{1,0} - 3\,\delta_{1,1} + \delta_{1,2})/72.$$

Nevertheless, following a more phenomenological approach, we have chosen in our analysis to retain the possibility of two different signatures of the split-P-wave phase shifts. One is consistent with a tensor interaction producing negative polarizations, while the other (+ + - signature) produces a positive polarization at small angles and corresponds to a dominant spin-orbit interaction. In both cases the strength of the splitting was kept small, consistent with the existing experimental values of polarization.[13, 14]

A sample result of our analysis is given in Table I. The listed errors are based on the criterion of an increase of 1 in χ^2, and, alternatively, in the parameter $\Phi = \chi^2/N$ (where N is the number of data points). The program adjusts the S-wave, the central force part of the P-wave, and the D-wave phase shifts in successive steps.

Figure 2 contains a plot of the $^1S_0$ shifts obtained from our D data and from other sources.

Our cross sections at 9.918 MeV disagree with the extrapolated values obtained from the Minnesota experiment at 9.69 MeV, assuming a 1/E dependence of the cross section, by more than one standard deviation, and the plot of phase shifts in Fig. 2 bears this out. However, the cross sections measured at Minnesota are on the order of 1 to 2% higher than the values obtained at the Rutherford high energy laboratory[26] at the energies where they overlap. MacGregor et al.[27] assign a probable normalization of 1.015 to the final search in fitting the data; this means that the data should be scaled by 0.985 for consistency with their phase-shift solution. Figure 3 shows the polarizations calculated from our phase shifts with the two different P-wave splittings.

Figure 2 shows that the information reported in this paper maps the region of the maximum of the p-p $^1S_0$ phase shift. It indicates that there is some need for measurements in smaller energy steps both below 10 MeV and between 10 and 20 MeV.

Another aspect still requiring attention and more thorough investigation is that of bremsstrahlung effects. They probably originate in transitions involving mainly the P wave, and therefore, although such effects are small, they may be relevant to a more exact formulation of the scattering amplitude, assumed to be purely elastic below the meson production threshold. Precise measurements have been repeatedly advocated, as they may provide a means for distinguishing between nucleon-nucleon potentials fitted to elastic scattering data.[28]

Footnotes and References

†Condensed from Phys. Rev. 174, 1122 (1968).

*Present address: Universite Laval, Quebec 10e, Canada.

‡Deceased.

1. A summary of work prior to 1950 is contained in J. D. Jackson and J. M. Blatt, Rev. Mod. Phys. 22, 77 (1950).

2. L. Heller, Rev. Mod. Phys. 39, 584 (1967), and references therein.

3. H. R. Worthington, J. N. McGruer, and E. D. Findley, Phys. Rev. 90, 899 (1953), referred to as WMF.

4. D. J. Knecht, S. Messelt, E. D. Berners, and L. C. Northcliffe, Phys. Rev. 114, 550 (1959); D. J. Knecht, P. F. Dahl, and S. Messelt, Phys. Rev. 148, 1031 (1966), referred to as KMBND.

5. James Rouvina, Phys. Rev. 81, 593 (1951).

6. K. B. Mather, Phys. Rev. 82, 133 (1951).

7. J. C. Allred, A. H. Armstrong, R. O. Bondelid, and L. Rosen, Phys. Rev. 88, 433 (1952).

8. E. J. Zimmermann, R. O. Kerman, S. Singer, P. Geral Kruger, and W. Jentschke, Phys. Rev. 96, 1322 (1954).

9. B. Cork and W. Hartsough, Phys. Rev. 94, 1300 (1954).

10. L. H. Johnston and D. E. Young, Phys. Rev. 116, 989 (1959).

11. M. H. MacGregor, Phys. Rev. 113, 1559 (1959).

12. H. H. Hall and J. L. Powell, Phys. Rev. 90, 912 (1953).

13. J. Alexeff and W. Haeberli, Nucl. Phys. 15, 609 (1960).

14. R. J. Slobodrian, J. S. C. McKee, H. Bichsel, and W. F. Tivol, Phys. Rev. Letters 19, 704 (1967), and reference therein.

15. P. Catillon, J. Sura, and A. Tarrats, Phys. Rev. Letters 20, 602 (1968).
16. J. E. Brolley, Jr., J. D. Seagrave, and J. G. Berry, Phys. Rev. 135, B1119 (1964).
17. M. L. Gursky and L. Heller, Phys. Rev. 136, B1693 (1964).
18. R. J. Slobodrian, Nucl. Phys. 85, 33 (1966), and references therein.
19. H. Pierre Noyes and L. Lipinski, Phys. Rev. 162, 884 (1967).
20. R. J. Slobodrian, H. E. Conzett, E. Shield, and W. F. Tivol, in Proceedings of the International Nuclear Physics Conference at Gatlinburg, 1966 (Academic Press, New York).
21. R. J. Slobodrian, Phys. Rev. Letters 21, 438 (1968).
22. D. J. Knecht, Technical Documentary Report No. WLTDR-64-78, 1964.
23. R. E. Seamon, K. A. Friedman, G. Breit, R. D. Haracz, J. M. Holt, and A. Prakash, Phys. Rev. 165, 1579 (1968).
24. L. Durand III, Phys. Rev. 108, 1597 (1957).
25. L. L. Foldy and E. Eriksen, Phys. Rev. 98, 775 (1955); M. de Wit and L. Durand, Phys. Rev. 111, 1597 (1958).
26. C. J. Batty, R. S. Gilmore, and G. H. Stafford, Nucl. Phys. 41, 388 (1963); C. J. Batty, G. H. Stafford, and R. S. Gilmore, loc. cit. 51, 255 (1964).
27. M. H. MacGregor, R. A. Arndt, and R. M. Wright, Phys. Rev. 169, 1128 (1968).
28. V. B. Brown, Phys. Letters 25, 506 (1967), and references therein.
29. S. Kikuchi, J. Sanada, S. Suwa, I. Hayashi, K. Kisimura, and K. Fukunaga, J. Phys. Soc. Japan 15, 9 (1960).
30. S. I. Bile'kaya, Yu. M. Kazarinov, F. Lehar, and Z. Janout, Yadern. Fiz. 4, 892 (1966) [translation: Soviet J. Nucl. Phys. 4, 635 (1967)].
31. C. J. Batty and J. K. Perring, Phys. Letters 16, 301 (1965).

Table I. Results of the phase-shift analysis of D data assuming a P-wave splitting consistent with OPE. Columns labeled σ correspond to an increase of 1 in χ^2, and τ to an increase of 1 in ϕ.

E_{lab} (MeV)	χ^2	Phase shift [degrees]											
		$^1S_0$	σ_s ±	τ_s ±	$^3P_0$	$^3P_1$	$^3P_2$	σ_P ±	τ_P ±	$^1D_2$	σ_D ±	τ_D ±
6.141	5.56	55.67	0.025	0.109	2.317	-1.283	0.157	0.038	0.168	0.075	0.130	0.576
8.097	13.68	55.91	0.021	0.114	3.135	-1.665	0.255	0.050	0.271	0.067	0.126	0.686
9.918	9.37	55.09	0.031	0.159	3.826	-2.174	0.226	0.106	0.532	0.009	0.230	1.154

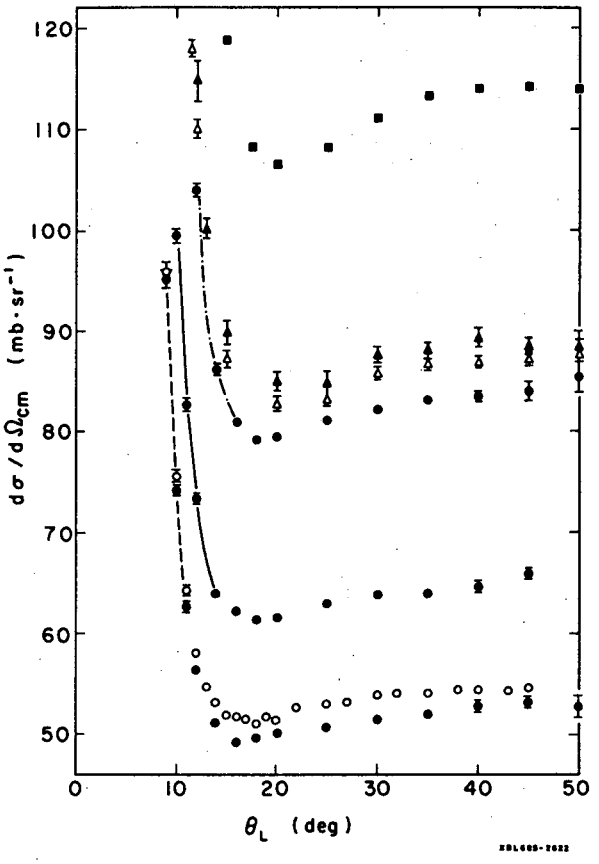

Fig. 1. Angular distributions in p-p scattering. The solid circles were measured in this set of experiments. The squares were taken from Ref. 3. The triangles (open and solid) were taken from Ref. 8. The open circles were measured by Johnston and Young, Ref. 10.

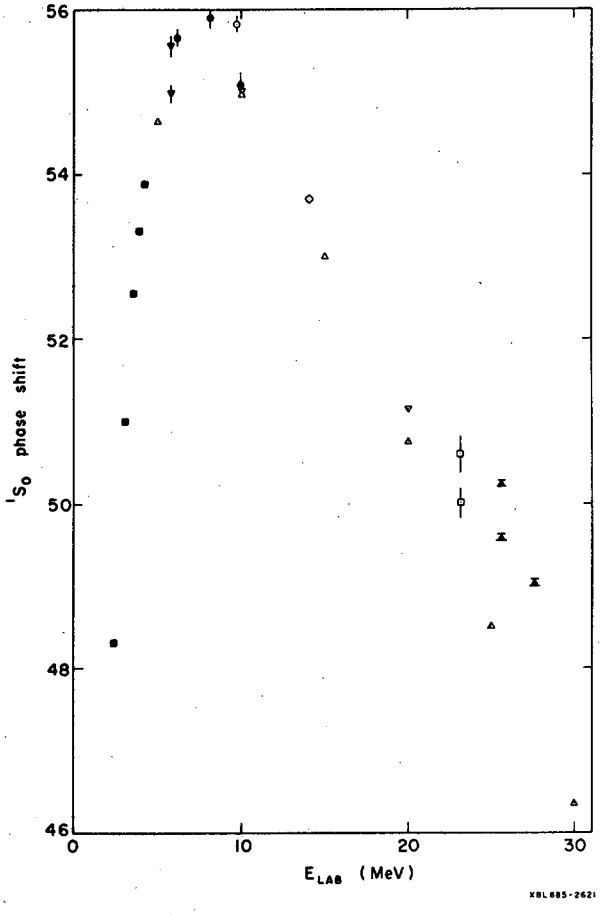

Fig. 2. $^1S_0$ phase shifts. Solid squares were obtained with the data of Refs. 3 and 4. Inverted solid triangles are from Ref. 8. The open upright triangles are the solution from Ref. 27; the inverted open triangles are from Ref. 23; the solid dots were obtained with D data and OPE P-wave splitting in our experiments; the open circle is obtained from the data of Ref. 10; the open diamond comes from Ref. 29; the open squares are two values obtained by Ref. 30; and the solid triangles were obtained by Ref. 31.

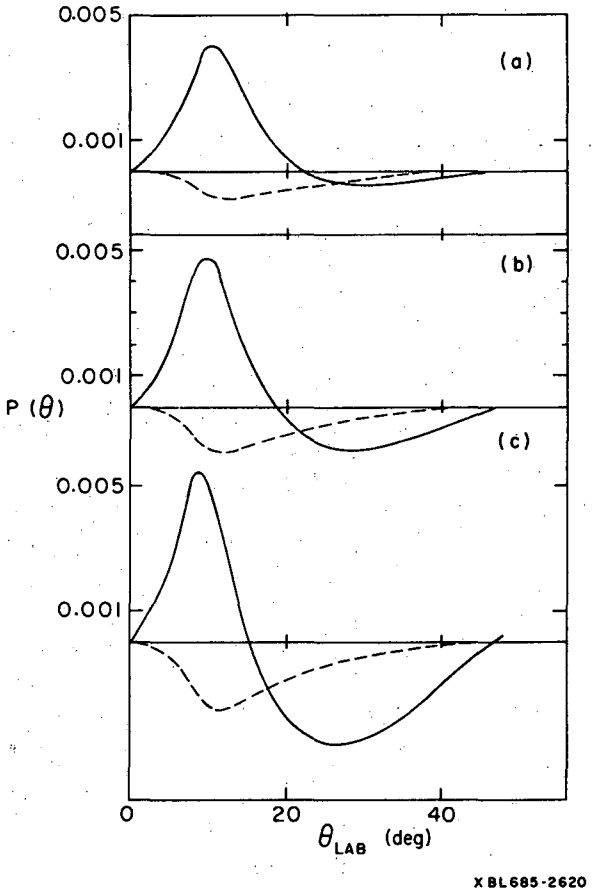

Fig. 3. Angular distributions of polarizations obtained with the P-wave spin orbit splitting (solid line) and the OPE splitting (dashed line).
(a) 6.141 MeV; (b) 8.097 MeV; (c) 9.918 MeV.

DETERMINATION OF THE $^1S_0$ NEUTRON-NEUTRON EFFECTIVE-RANGE PARAMETERS

R. J. Slobodrian,† H. E. Conzett, H. Meiner*, A. D. Bacher, J. Ernst,‡ and F. G. Resmini

The $^1S_0$ neutron-neutron effective-range parameters are still not very accurately determined, although several experiments have been done in recent years to determine the scattering length, a_{nn}.[1-3] In this experiment we have studied the 2n final-state interaction in the T(d, ^{3}He) 2n reaction with good statistics and determined both the scattering length, a_{nn}, and the effective range, r_{nn}.

We have measured ^{3}He spectra from the T(d, ^{3}He)2n reaction near 30 MeV, using the deuteron beam of the Berkeley 88-inch cyclotron. The experimental techniques were basically the same as described elsewhere.[2] The analysis employed a procedure[4] by which the simple Watson-Migdal (WM) final-state interaction theory[5] was modified for effects not included originally. Spectra[6] from the ^{3}He(d, t)2p reaction at the same final-state c.m. energy were used to determine the ratio between the experimental triton spectrum and the WM calculation for the known values of the $^1S_0$ p-p effective-range parameters[7] (a_{pp} = - 7.72 F, r_{pp} = 2.65 F). This ratio, $\overline{|g(\theta, E)|^2} = d^2\sigma/d\Omega\, dE / (d^2\sigma/d\Omega\, dE)_{WM}$, under the assumption of charge symmetry of nuclear forces, was then used to correct the measured ^{3}He spectrum from the mirror reaction T(d, ^{3}He)2n. A WM fit to the corrected spectrum (Fig. 1) then determined both a_{nn} and r_{nn}. The best fit for the high-energy end of the spectrum, corresponding to relative n-n energies E_{nn} = 0 to 3.7 MeV, yields a_{nn} = -16.4 F; r_{nn} = 3.1 F.

The errors in the a_{nn} - r_{nn} plane are shown in Fig. 2 for different ranges of E_{nn} included in the analysis. Comparison with other experiments is also shown. Within the errors, our values agree with those determined theoretically from the p-p effective-range parameters,[8] and our errors are considerably smaller than those of the previous experiments.

Footnotes and References

†Present address: Université Laval, Quebec 10[e], Canada.
*Visitor from University of Basel, Switzerland.
‡Visitor from University of Bonn, Germany.

1. R. P. Haddock, R. M. Salter, M. Zeller, T. B. Czirr, and D. R. Nygren, Phys. Rev. Letters 14, 318 (1965).
2. E. Baumgartner, H. E. Conzett, E. Shield, and R. J. Slobodrian, Phys. Rev. Letters 16, 105 (1966).
3. T. P. Nicholson, P. G. Butler, N. Cohen, and A. N. James, Phys. Letters 27B, 452 (1968); Phys. Rev. Letters 21, 470 (1968), and references therein.
4. R. J. Slobodrian, H. E. Conzett, and F. G. Resmini, Phys. Letters 27B, 405 (1968).
5. K. M. Watson, Phys. Rev. 88, 1162 (1952); A. B. Migdal, Soviet Phys. JETP 1, 2 (1955).
6. These spectra were obtained by R. J. Slobodrian, H. Bichsel, J. S. C. McKee, A. U. Luccio, and W. F. Tivol (Lawrence Radiation Laboratory), private communication.
7. R. J. Slobodrian, Nuovo Cimento 40, 443 (1965).
8. E. M. Henley, Charge Independence and Charge Symmetry of Nuclear Forces, in Isospin in Nuclear Physics (to be published).

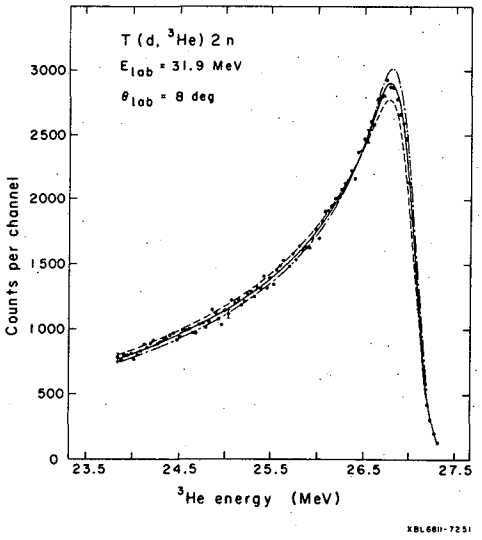

Fig. 1. ^{3}He spectrum at 8 deg lab from the reaction T(d, ^{3}He)2n at 31.9 MeV. The dots are experimental points. The solid line is the best fit for a_{nn} = -16.4 F; the dashed line is obtained with a_{nn} = -14.2 F and the dash-dot line with a_{nn} = -18.6 F. In all three cases r_{nn} = 3.1 F.

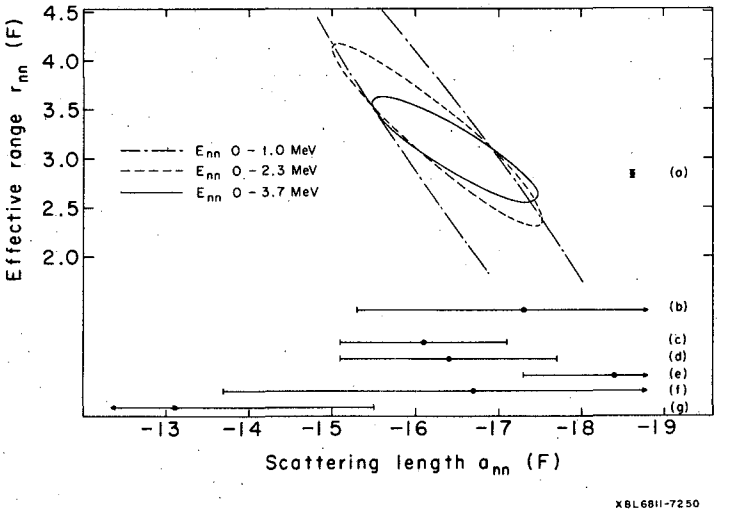

Fig. 2. Probable error fields for different ranges of the spectrum included in the analysis. The dash-dot line gives the boundary of the probable error for an analysis which included the range E_{nn} = 0 to 1.0 MeV, the dashed line for E_{nn} = 0 to 2.3 MeV, and the solid line for E_{nn} = 0 to 3.7 MeV. Our results are compared with previous works and with theoretical values assuming charge symmetry of nuclear forces. (a) and (b) are calculated values for r_{nn} and a_{nn} assuming charge symmetry (Ref. 8); (c) is the result from Ref. 2, (d) from Ref. 1, (e) from a new analysis, Ref. 8 of (d), (f) from Ref. 4, and (g) from Ref. 3. All previous analyses, (c) through (g), of experimental data assumed fixed values for r_{nn}.

NEUTRON-NEUTRON SCATTERING LENGTH FROM COMPARISON OF THE ^{2}H(p, n)2p AND ^{2}H(n, p)2n REACTIONS†

R. J. Slobodrian,* H. E. Conzett, and F. G. Resmini

Studies of the differential energy spectra of the reaction ^{2}H(n, p)2n near 14 MeV (lab) have yielded values for the $^1S_0$ neutron-neutron scattering length which display a considerable spread,

$$a_n = -21.7 \pm 1 \text{ F},^1 \quad -23.6^{+2.0}_{-1.6} \text{ F},^2 \quad \text{and} \quad -14 \pm 3 \text{ F},^3$$

where the assigned error in Ref. 1 was due only to statistics. References 1 and 3 used similar analyses appropriate to a long-range process that results from the large spatial extension of the deuteron.[4] Thus, the disagreement between those two results is unexplained, and its clarification is important to the validity of the assumption of charge symmetry in the nucleon-nucleon interaction.[5] Voitovetskii et al.[2] used a formalism based on Feynman diagrams. The result near the high energy end of the proton spectrum is similar to that of the Watson-Migdal[6,7] treatment, which is, however, more appropriate for a short-range process. It has been pointed out that an analysis based either on the long-range assumption[4] or on a more rigorous three-body theory[8] would give a smaller value of a_n. Figure 1a shows that the three sets of data are self-consistent within the experimental errors, statistical uncertainties, and differences in resolution. Thus, the different values obtained for a_n result from differences among the analyses employed. An experimental test of the theoretical formulations is clearly desirable.

In contrast, a study[9] of the reaction ^{3}H(d, ^{3}He)2n near 32 and 40 MeV has provided a value $a_n = -16.1 \pm 1.0$ F. The validity of the Watson-Migdal theory employed in this work was verified through analysis of data from the mirror reaction ^{3}He(d, t)2p. The deduced proton-proton scattering length agreed with the value known from low-energy p-p scattering.

Similarly, study of the reaction ^{2}H(p, n)2p can provide a test of the theory used in the analysis of data from the reaction ^{2}H(n, p)2n. Spectra at 30 and 50 MeV[10] from ^{2}H(p, n)2p obtained with 1.4 and 2.0 MeV resolution respectively have been fitted quite well with the impulse approximation of Phillips,[4] although the relatively poor resolution reduced the sensitivity of the fits to variations of the scattering length. Data have also been obtained at 14.1 MeV[11] and at 8.9 MeV,[12] and they are in qualitative agreement with the impulse approximation prediction.

We have studied the ^{2}H(p, n)2p reaction near 20 MeV lab, using protons from the Berkeley 88-inch variable-energy cyclotron. The target was gaseous deuterium, 99.9% pure, at 1 atmos. pressure, enclosed in a cell with 13 mg/cm^2 aluminum entrance and exit windows. Neutrons were detected with a proton-recoil spectrometer.[13] The overall resolution of the system, as determined empirically with the reaction ^{14}N(p, n)^{14}O, was 600 keV in the relevant high energy region of the spectrum. Spectra were measured between 5 and 12 deg lab. They showed a small anisotropy of the neutron peak, in agreement with other experiments.[14] Figure 2a, b shows the high energy region of the spectra obtained at 5 and 8 deg lab.

The differential energy spectrum can be written as

$$\frac{d^2\sigma}{dE d\Omega} = \frac{2\pi}{\hbar} \frac{1}{v_i} \sum_{\text{spins}} \left| T_{if} \right|^2 \rho, \qquad (1)$$

where T_{if} is the transition matrix element, ρ is the density of final states, and v_i is the velocity of the projectile.

In general, $T_{if} = \int \psi_f^+ V \psi_i \, d\tau$, where V is the interaction causing the transition. In a reaction of the form A + B → X + 2N the final-state interaction of the two-nucleon pair (2N) in a ^{1}S state of low relative energy results in a peak at the high energy end of the spectrum of particle X. Restricting our discussion to that region of the spectrum, and assuming that there the effect of the interaction between X and N is negligible, we can factor the wave function $\psi_f = \psi_{2N} \phi_R \psi_X$, where ϕ_R describes the relative motion between X and the 2N system. For $r \geq b$, where b is the radius at which the internal and external wave functions are matched,

$$\psi_{2n} = e^{i\delta} \sin(kr + \delta)/kr$$

and

$$\psi_{2p} = e^{i\delta}[F_0(kr)\cos\delta + G_0(kr)\sin\delta]/kr,$$

where k is the relative N-N momentum in units of $\hbar$, δ is the $^1S_0$ phase shift, and $F_0(kr)$ and $G_0(kr)$ are the regular and irregular Coulomb S-wave functions. Thus, we have

$$T_{if} = \frac{e^{-i\delta}\sin\delta}{k}\int (f_n\phi_R\psi_X)^+ V\psi_i d\tau = \frac{e^{-i}\sin\delta}{k} g_n(\theta,k) \quad \text{for nn,} \tag{2a}$$

$$T_{if} = \frac{e^{-i\delta}\sin\delta}{kC}\int (f_p\phi_R\psi_X)^+ V\psi_i d\tau = \frac{e^{-i\delta}\sin\delta}{kC} g_p(\theta,k) \quad \text{for pp,} \tag{2b}$$

with

$$f_n(k,r) = (\sin kr\cot\delta + \cos kr)/r, \quad \text{for } r \geq b,$$
$$= f_n^0(k,r), \quad \text{for } r \leq b,$$

$$f_p(k,r) = C[F_0(kr)\cot\delta + G_0(kr)]/r, \quad \text{for } r \geq b,$$
$$= f_p^0(k,r), \quad \text{for } r \leq b,$$

where $C^2 = 2\pi\eta/(\exp 2\pi\eta - 1)$, $\eta = e^2/(\hbar v)$, v is the p-p relative velocity, and θ is the c.m. angle of particle X. Equations (2) reduce to the Watson-Migdal short-range approximation and to the long-range impulse approximation under the appropriate assumptions.

For $r \leq b$ and for the small values of k which are important here, f_n^0 and f_p^0 are equal to within a few percent [15] and, in any case, contribute little to g_n and g_p because of the small overlap with the deuteron wave function contained in the initial state, ψ_i. Also, it can be seen [16] that f_n and f_p have a remarkably similar energy dependence in the important range of values of kr. Consequently, for mirror reactions at equivalent c.m. energies, we assume that

$$g_n(\theta,k) = \text{Const. } g_p(\theta,k). \tag{3}$$

An experimental determination of $|g_p|^2$ thus provides a $|g_n|^2$ which can be used in the analysis of nn final-state spectra. The important point is that this obviates the need for a direct calculation of g_n via (2a). Therefore, the necessary approximations and uncertainties of such a calculation are eliminated. As an example, Fig. 1c shows a verification of (3) in the context of the calculation by Phillips. [4]

We have compared our $^2H(p,n)2p$ spectra with those calculated from (1) and (2b), using the ^1S effective-range expansion for δ, with the known scattering length, $a_p = -7.7$ F, and effective range, $r_e = 2.63$ F. [17] This provides an experimental determination of $|g_p|^2$. With $|g_n|^2$ given by (3), [18] a comparable analysis was made of the statistically best nn final-state data. [2] Figure 1b shows the resulting best-fit calculation, with

$$a_n = -16.7^{+2.6}_{-3.0}\ \text{F, for which } \chi^2 \text{ min/N} = 0.3 \text{ (where N = number of degrees of freedom).}$$

The probable errors were determined from a χ^2 criterion with a fixed (optimum) value for the spectrum end-point energy.

The value of a_n deduced in our analysis of these $^2H(p,n)2p$ and $^2H(n,p)2n$ data is consistent with the values $a_n = -16.4 \pm 1.3$ F and $a_n = -16.1 \pm 1$ F determined respectively from the $^2H(\pi^-, 2n)\gamma$ [19] and $^3H(d, ^3He)2n$ [9] reactions.

Footnotes and References

†Condensed from Phys. Letters 27B, 405 (1968).

*Present address: Université Laval, Quebec 10^e, Canada.

1. M. Cerineo, K. Ilakovac, I. Šlaus, P. Tomaš, and V. Valković, Phys. Rev. 133, B948 (1964); I. Šlaus, Rev. Mod. Phys. 39, 575 (1967); W. T. H. van Oers and I. Šlaus, Phys. Rev. 160, 853 (1967).

2. V. K. Voitovetskii, I. L. Korsunskii, and Yu. F. Pazhin, Phys. Letters 10, 109 (1964) and Nucl. Phys. 69, 513 (1965).

3. E. Bar-Avraham, R. Fox, Y. Porath, G. Adam, and G. Frieder, Nucl. Phys. B1, 49 (1967). A ^{2}H(n, 2n)^{1}H neutron-coincidence spectrum, which yields a value $a_n = -18.8^{+5.5}_{-11.9}$ F, has been reported by R. Honecker and H Grässler, Nucl. Phys. A107, 81 (1968).

4. R. J. N. Phillips, Nucl. Phys. 53, 650 (1964).

5. L. Heller, P. Signell, and N. R. Yoder, Phys. Rev. Letters 13, 577 (1964); E. M. Henley, in Proceedings of the Conference on Isobaric Spin in Nuclear Physics, Ed. by J. D. Fox and D. Robson (Academic Press, New York, 1966), p. 3.

6. K. M. Watson, Phys. Rev. 88, 1162 (1952).

7. A. B. Migdal, Zh. Eksperim. i Teor. Fiz 28, 3 (1955) [Translation: Soviet Phys. -JETP 1, 2 (1955)].

8. R. Aaron and R. D. Amado, Phys. Rev. 150, 857 (1966).

9. E. Baumgartner, H. E. Conzett, E. Shield, and R. J. Slobodrian, Phys. Rev. Letters 16, 105 (1966).

10. C. J. Batty, R. S. Gilmore, and G. H. Stafford, Phys. Letters 16, 137 (1965).

11. J. D. Anderson, C. Wong, J. W. McClure, and B. A. Pohl, Phys. Rev. Letters 15, 66 (1965).

12. M. P. Nakada, J. D. Anderson, C. C. Gardner, J. McClure, and C. Wong, Phys. Rev. 110, 594 (1958).

13. R. J. Slobodrian, H. Bichsel, J. S. C. McKee, and W. F. Tivol, Phys. Rev. Letters 19, 595 (1967).

14. V. K. Voitovetskii, I. L. Korsunskii, and Yu. F. Pazhin, Nucl. Phys. 69, 531 (1965); K. Debertin, K. Hoffmann, and E. Rössle, Nucl. Phys. 81, 220 (1960).

15. H. A. Bethe, Phys. Rev. 76, 38 (1949).

16. This point will be demonstrated in more detail in a later paper; but, for example, as $k \to 0$, $f_n = -(a_n)^{-1} + r^{-1}$ and $f_p = -(a_p)^{-1} + r^{-1}$ for $\geq b$.

17. R. J. Slobodrian, Nuovo Cimento 40, 443 (1965). These values do not contain the vacuum polarization correction, and therefore represent the experimental data more directly.

18. Since our data were taken at 20 MeV, we have determined from the ^{2}H(p, n)2p data of Ref. 11 at 14 MeV that $|g_p|^2$ has the same dependence on k at these two incident proton energies.

19. R. P. Haddock, R. M. Salter, Jr., M. Zeller, J. B. Czirr, and D. R. Nygren, Phys. Rev. Letters 14, 318 (1965).

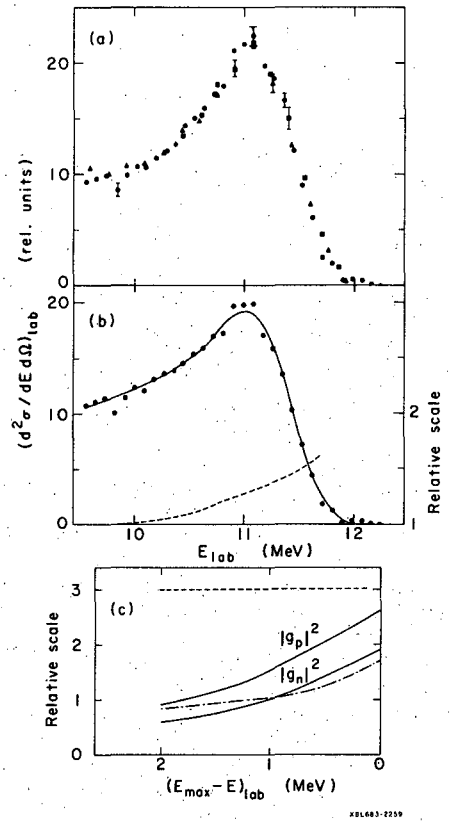

Fig. 1. (a) Experimental spectra near 0 deg of the reaction ^{2}H(n, p)2n near 14 MeV. Triangles correspond to Ref. 1, circles to Ref. 2, and squares to Ref. 3. The data of Refs. 1 and 3 were energy shifted to superimpose them properly on the data of Ref. 2, for comparison purposes.
(b) The dots are the ^{2}H(n, p)2n data of Ref. 2 corrected with the form factor $|g_n(\theta,k)|^2$ obtained from the mirror reaction ^{2}H(p, n)2p. The solid line is a plot of the best fit with $a_n = -16.7$ F. The dashed line is a plot of the form factor $|g_n(\theta, k)|^2$ as a function of the energy of the third particle (proton).
(c) Form factors from the calculation of Ref. 4 are indicated with solid lines; the dashed line is the ratio $|g_p|^2/|g_n|^2$. The dash-dot line is the phenomenological form factor deduded from the ^{2}H(p, n)2p reaction.

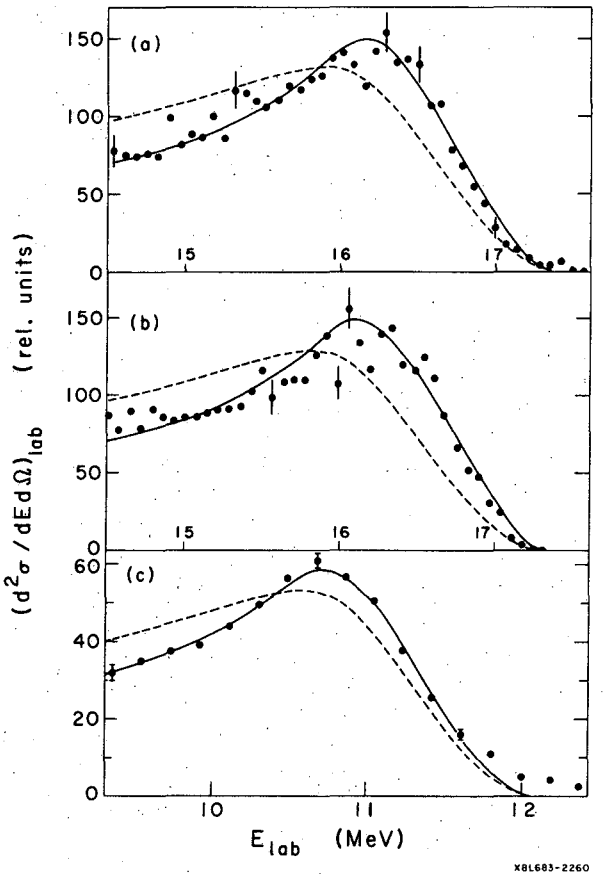

Fig. 2. Data from the reaction ^{2}H(p, n)2p at 19.7 MeV obtained in this experiment, and at 14.1 MeV taken from Ref. 11. Dashed lines are Watson-Migdal curves calculated with $a_p = -7.7$ F. Solid lines are Watson-Migdal curves with $a_p = -13.3$ F which show that the data can be simulated with a large value of a_p. Curves are normalized to the same area
(a) Data at 19.7 MeV and 5 deg lab.
(b) Data at 19.7 MeV and 8 deg lab.
(c) Data at 14.1 MeV from Ref. 11, at 3 deg lab. The resolution at the high energy region of the spectrum is approximately 1 MeV.

PROTON POLARIZATION IN p-^{3}He SCATTERING BETWEEN 10 AND 20 MeV

W. F. Tivol, D. J. Clark, H. E. Conzett, J. S. C. McKee,* and R. J. Slobodrian**

Using the polarized-beam facility of the 88-inch cyclotron, we have investigated the proton polarization in p-^{3}He elastic scattering. Angular distributions of the polarization, consisting of approximately twenty points, were obtained for each of five energies in the range from 10 to 20 MeV.

Tombrello[1] has summarized the data obtained in p-^{3}He scattering prior to 1965. That summary and the references contained in it include all the experimental and important theoretical work done on the p-^{3}He system to that time. It can been seen that very few measurements of the polarization were available, especially in the region between 10 and 20 MeV where the inelastic processes first become important. The energy range of this experiment was chosen so that the lower end would allow comparison with previous data. The range was made broad enough so that inelastic effects would more than likely be observed.

The proton-^{3}He system is a spin 1/2–spin 1/2 system, but, unlike the extensively studied nucleon-nucleon system, it has no simplifying symmetries. With the exception of the S wave--which has only one triplet phase shift, one singlet phase shift, and no spin mixing--and the P wave–which is not coupled to a lower ℓ value--each ℓ value consists of four coupled phase shifts. Thus there are four S-wave parameters, nine P-wave parameters, and ten parameters for each $\ell \geq 2$, giving 10 ℓ_{max} + 3 parameters needed to describe the system.

Tombrello et al.[2] define eight scattering amplitudes from which the values of the various experimental quantities can be calculated. The only change in the approach used in this experiment was to allow for complex phase shifts by inserting the inelastic parameters, η, in the expressions containing the phase shifts.

Given data and errors, a set of trial phase shifts was chosen, which yielded calculated values for the data points. The χ^2 function was formed:

$$\chi^2(\vec{x}) = \sum_{1}^{\text{No. of data}} \left(\frac{\text{datum - calculated value}}{\text{error}} \right)^2 .$$

This function was then minimized to give phase-shift solutions.

Phase-shift fits were found for the lowest four energies. In order to fit the polarization data, it was necessary to have cross-section data also. Cross-section data are available for 11.48 and 19.4 MeV, and the 11.7- and 19.7-MeV polarization data were fitted along with those data. Since the cross section varies more with energy than the polarization, the energy used in the fit was the energy of the cross-section data. For 13.6 and 16.2 MeV, cross-section data had to be interpolated. For the 13.6-MeV data, interpolations between the data at 11.48 and 14.5 MeV were used; for the 16.2-MeV data interpolations between the data at 14.5 and 19.4 MeV were used.

The interpolation procedure is somewhat uncertain; however, it was one way to get a sufficient amount of data to attempt a fit. Since there were no cross-section data to go with the 21.3-MeV data, no fits were attempted at that energy.

Classically, we expect $\ell_{max} = k r$, where k is the proton momentum and is the distance of closest approach, which would be the sum of the radii of the proton and the ^{3}He. Using $r = 1.4 A^{1/3}$F, we get r = 3.4F. So for the energies 11.7, 13.6, 16.2, and 19.7 MeV we get ℓ_{max} of 2.2, 2.4, 2.6, and 2.9, respectively. Searches were made at the three lowest energies using both $\ell_{max} = 2$ and $\ell_{max} = 3$. At the lower two energies, the value of ϕ (χ^2 per free parameter) for the $\ell_{max} = 2$ fit was lower than that for the $\ell_{max} = 3$ fit, and at the third energy the ϕ value for the $\ell_{max} = 3$ fit was lower than that for the $\ell_{max} = 2$ fit, which indicates that the classical expectations are fulfilled. However, the $\ell = 3$ phase shifts in the $\ell_{max} = 3$ solutions are not necessarily small. At 11.5 MeV the largest $\ell = 3$ phase shift is nearly 13 deg, and one inelastic parameter is less than 0.8. Both these conditions lead to rather large $\ell = 3$ amplitudes, which indicates that the program is fitting not only the trend of the data, but the statistical fluctuations of the individual data points as well. If there were, for example, exactly 33 data points, so that there would be the same

number of parameters as points for $\ell_{max} = 3$, one would expect to be able to find an exact solution which would give χ^2 equal to zero. Clearly, such a solution would have more arithmetic than physics contained in it.

Figure 1 shows a sample plot of the data and the calculated fits from the phase-shift analysis. The energy dependence of the phase shifts indicates, however, that the data are insufficient to determine them uniquely.

Generally the p-^{3}He polarization curves are similar in shape to those in the p-^{4}He system. This is an indication that the spin-orbit effects are quite large. In the p-^{4}He case at comparable energies, however, the maximum at the back angles is nearly 100% polarization, whereas in for p-^{3}He it is roughly 60 to 70%.

Footnotes and References

*University of Birmingham, England.
**Present address: Université Laval, Quebec 10^e, Canada.

1. T. A. Tombrello, Phys. Rev. 138, B40 (1965).
2. T. A. Tombrello, C. M. Jones, G. C. Phillips, and J. L. Weil, Nucl. Phys. 39, 541 (1962).

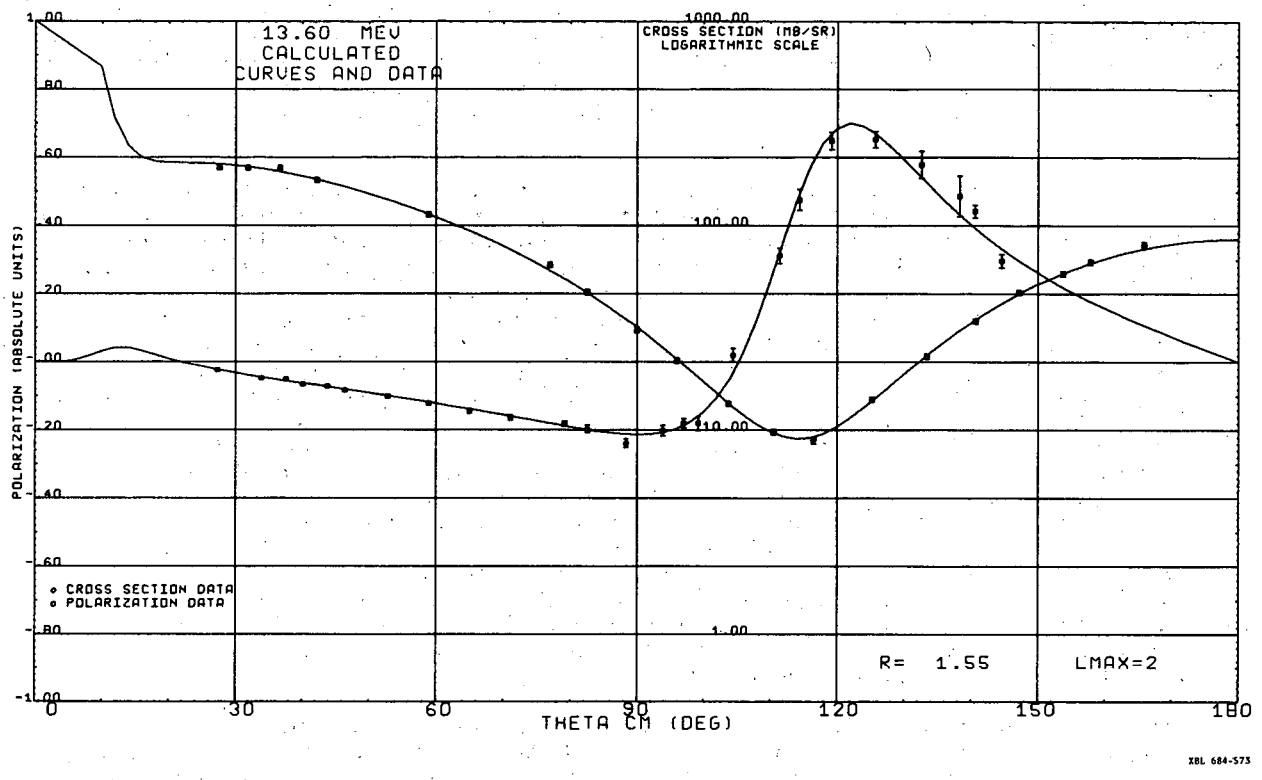

Fig. 1. Fits to cross-section and polarization data in p-^{3}He scattering at 13.6 MeV with $\ell_{max} = 2$.

THE ^{3}He(^{3}He, t)3p REACTION AT 44 MeV†*

T. A. Tombrello‡ and R. J. Slobodrian††

In the last few years considerable attention has been devoted to the study of the three-nucleon system. In particular, experiments have been concerned with the possibility of excited states of these nuclei--especially those with isospin 3/2, corresponding to trineutron or triproton states. The results obtained show remarkable disagreement.

(i) Ajdačić et al. reported the existence of a particle-stable trineutron from a study of the t(n, p)3n reaction.[1] When this work was repeated by Thornton et al., no such proton group was seen, and the upper limit on the cross section is only about one-tenth that originally observed.[2]

(ii). Measurements of ^{3}He(p, p')^{3}He* by Kim et al.[3] indicated the presence of two or three excited states of ^{3}He, the lowest of which might be the analog state of the trineutron seen by Ajdačić et al.[1] None of these levels, however, was observed in investigations of the same reaction by Cerny et al.,[4] Austin et al.,[5] and Mancusi et al.[6] Neither are they observed[7] in ^{3}He(^{3}He, ^{3}He')^{3}He*.

(iii) Two experiments that do agree on a null result are investigations of the ^{3}He(p, n)3p reaction. Both Cookson[8] and Anderson et al.[9] set upper limits on the total cross section, which is determined by the former to be less than 23 μb. This upper limit is smaller by several orders of magnitude than that obtained for the mirror reaction in the experiment of Ajdačić et al.[1]

It is certainly not obvious that anyone has actually observed excited states of the mass-three nuclei, and we must remain rather skeptical. The experiment described here also pertains to this problem, and no levels of ^{3}Li were observed. However, the absence of a sharp anomaly in the energy spectrum for a particular reaction does not necessarily preclude the existence of a strong final-state interaction but only sets limits on its width--as in reactions involving the broad first excited state of ^{5}Li or ^{5}He.

The ^{3}He beam was obtained from the 88-inch cyclotron at the Lawrence Radiation Laboratory. The beam energy was determined to be 44 MeV from range measurements, which allow a precision of 1 to 2%. Particles were detected and identified by using a two-counter telescope composed of 500-μ and 3-mm-thick Li-drifted silicon detectors together with the standard Goulding-Landis power-law particle identifier.[10] This system allowed excellent separation of tritons down to about 13 MeV--corresponding to their range in the 500-μ detector. The total angular aperture of the detector collimator was 0.25 deg, and the over-all resolution of the detection system for tritons was 350 keV. This last figure was obtained by using the ^{14}N(^{3}He, t)^{14}O* reaction at the same bombarding energy; this calibration also allowed an energy scale to be obtained for the pulse-height spectra.

Spectra for ^{3}He(^{3}He, t)3p were measured at lab angles of 6, 10, 15, 20, and 25 deg. All the spectra were similar--a smooth distribution extending out to the four-body end point of the reaction; Fig. 1 shows the spectrum taken at 6 deg. The abrupt truncation (indicated by the label ΔE cutoff) marks the range of tritons in the first detector of the telescope. If a sharp state of the three-proton system lies below an excitation energy of 12 MeV (as measured from the point of zero relative energy), then limits can be placed on its cross section depending on the width of the level. If its width were less than or equal to our experimental resolution, then at this angle the cross section would be less than 60 μb/sr. If the level had a c.m. width of 1 MeV, then the corresponding limit would be 160 μb/sr. (If such a state lay below an excitation energy of 3 MeV, these limits would be 30 μb/sr and 100 μb/sr, respectively.)

The solid curve shown in Fig. 1 is the four-body phase-space prediction. It has about the right shape but peaks at too low an energy. As in beta decay, however, one would expect that the Coulomb forces between the outgoing particles should strongly shift the energy spectrum. The dashed curve was obtained by combining with the phase-space distribution a Gamow penetration factor for the interaction of the triton with the protons. This provides the proper shift of the peak but overestimates the extent of such penetration effects, thereby making the calculated distribution too sharp.

When this same reaction was studied at lower energies (18 to 20 MeV), it was found that the triton spectra had an end point well below the four-body end point, and all data are consistent with a sequential decay involving the formation of the 20-MeV level of ^{4}He and its subsequent decay into a proton and a triton.[11] The data at 44 MeV do not show such an effect, as evidenced by the

arrows showing the maximum triton energy available from this sequential decay process.

To summarize, we see no evidence for narrow excited states of the three-proton system, and find that the triton spectra are qualitatively consistent with a statistical distribution if the Coulomb forces between the particles are considered.

Footnotes and References

†Condensed from Nucl. Phys. A111, 236 (1968).
*This work was supported in part by the Office of Naval Research [Nonr-220(47)].
‡California Institute of Technology, Pasadena, California.
††Present address: Université Laval, Quebec 10e, Canada.

1. V. Ajdačić, M. Cerineo, B. Lalović, G. Paić, I. Šlaus, and P. Tomaš, Phys. Rev. Letters 14, 444 (1965).
2. S. T. Thornton, J. K. Blair, C. M. Jones, and H. B. Willard, Phys. Rev. Letters 17, 701 (1966).
3. C. C. Kim, S. M. Bunch, D. W. Devins, and H. H. Forster, Phys. Letters 22, 314 (1966).
4. J. Cerny, C. Detraz, H. Pugh, and I. Šlaus, unpublished.
5. S. M. Austin, W. Benenson, and R. A. Paddock, Bull. Am. Phys. Soc. 12, 16 (1967).
6. M. D. Mancusi, C. M. Jones, and J. B. Ball, Phys. Rev. Letters 19, 1449 (1967).
7. R. J. Slobodrian, J. S. C. McKee, D. J. Clark, W. F. Tivol, and T. A. Tombrello, Nucl. Phys. A101, 109 (1967).
8. J. A. Cookson, Phys. Letters 22, 612 (1966).
9. J. D. Anderson, C. Wong, J. W. McClure, and B. A. Pohl, Phys. Rev. Letters 15, 66 (1965).
10. F. S. Goulding, D. A. Landis, J. Cerny, and R. H. Pehl, Nucl. Instr. 31, 1 (1964).
11. A. D. Bacher and T. A. Tombrello, Bull. Ann. Phys. Soc. 10, 693 (1965).

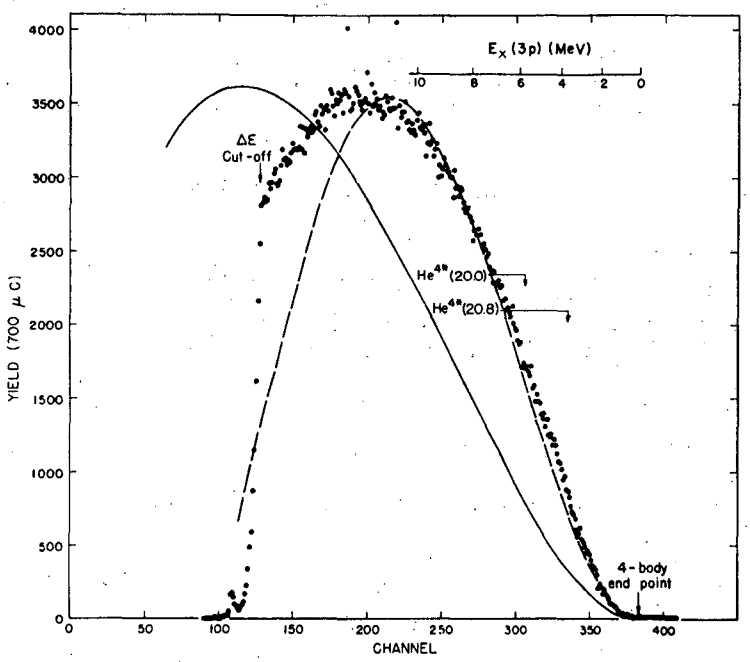

XBL 692-181

Fig. 1. The triton spectrum from ^{3}He(^{3}He, t)3p at a lab angle of 6 deg and a bombarding energy of 44 MeV. The arrow labeled by "four-body end point" indicates the maximum energy available to the tritons from this reaction. The abrupt truncation of the spectrum indicated by "ΔE cutoff" corresponds to the range of 13-MeV tritons in the 500-μ detector of the telescope; any fine structure observed in this region is probably due to slight nonuniformities in the thickness of this detector. The two additional arrows refer to the maximum energy available to the tritons if the reaction had proceeded sequentially through a sharp state of ^{4}He at 20.0 or 20.8 MeV. The solid curve is the triton spectrum predicted by a four-body phase-space distribution; the dashed curve is a modification of this distribution by including a Gamow factor to represent the Coulomb interaction of the triton and the three protons. [From Nucl. Phys. A111, 236 (1968).]

^{3}He-^{3}He ELASTIC SCATTERING FROM 18 TO 80 MeV†

A. D. Bacher, T. A. Tombrello,* E. A. McClatchie, and F. Resmini

The resonating group structure method, originally proposed by Wheeler, [1] has been successfully applied to a number of scattering reactions involving very light nuclei. In this approximation the scattering phase shifts are determined from a variational calculation using a totally antisymmeterized cluster wave function (in the one-channel limit the individual clusters are the scattered particles) and a nucleon-nucleon interaction which correctly describes the low energy two-nucleon scattering data. At high bombarding energies, where an independent phase-shift analysis of scattering measurements is complicated by the presence of broad overlapping levels and many open reaction channels, the resonating group calculations provide a useful starting point for an investigation of the level structure in these light nuclear systems.

Recent theoretical work on the $^3He + ^3He$ system by Thompson and Tang[2] is in good agreement with low energy ^3He-^3He elastic scattering measurements.[3,4] In addition to correctly predicting a broad $\ell = 3$ resonce in ^6Be near 24 MeV excitation, these calculations also predict very broad resonance structure in the $\ell = 4$, $\ell = 5$, and $\ell = 6$ partial waves. The work presented here, which covers a region of excitation in ^6Be between 20 and 50 MeV, was undertaken to investigate the validity of this prediction of higher levels in ^6Be. Angular distributions have been measured at 34 energies between 18 and 80 MeV by use of a ^3He beam from the 88-inch cyclotron magnetically analyzed to 0.03% in energy.

Figure 1 shows excitation functions at c.m. angles of 70 deg (a zero of P_4) and 90 deg (a zero of $P_{odd\ \ell}$). The results of this work (solid dots) are in good agreement with previous measurements at lower energy (crosses and open circles). The curves represent the results of the resonating group calculations by Thompson and Tang. At 70 deg the broad $\ell = 3$ resonance is quite pronounced and appears to be slightly narrower and lower in energy than the theoretical prediction. At 90 deg the slight bump at the position of the $\ell = 3$ resonance indicates that the spin-flip contribution to the scattering is not appreciable. This probably indicates that the splitting of the three angular momentum states associated with $\ell = 3$ is small. The broad bump in the calculation is due to the predicted resonance structure in the $\ell = 4$ partial wave. This behavior is clearly not seen in the experimental results.

Figure 2 shows excitation functions at center-of-mass angles of 31 deg (a zero of P_4) and 55 deg (a zero of P_2). In these cases and in Fig. 3, which shows the excitation function at 40 deg (where the effect of the $\ell = 3$ resonance is minimized), the disagreement with the theoretical predictions is rather striking, particularly at the higher bombarding energies.

In order to investigate the causes of this discrepancy, a rather crude phase-shift analysis was performed in which the Thompson and Tang phase shifts were used as starting values at each energy. As in the resonating group calculation, the triplet, odd-ℓ partial waves were considered unsplit. Complex phase shifts from $\ell = 0$ through $\ell = 6$ were allowed to vary in searching for a stable (though not necessarily unique) solution close to the predicted values. In this preliminary analysis both the $\ell = 4$ and $\ell = 6$ phase shifts were found to be negative, in contradiction with the theoretical prediction of broad resonance structure in the $\ell = 4$, 5, and 6 partial waves.

Part of the problem with the resonating-group calculation can be traced to neglecting the reaction channels which become significant for energies above 18 MeV. In addition, however, there appears to be a systematic difference between the resonating-group predictions and the experimental results in which the odd-parity partial waves are well-described and the higher even-parity partial waves disagree. The nature of this discrepancy is being investigated further.

Footnotes and References

†Condensed from Bull. Am. Phys. Soc. 13, 1366 (1968).
*Summer visitor from California Institute of Technology.
1. J. A. Wheeler, Phys. Rev. 52, 1083 (1937).
2. D. R. Thompson and Y. C. Tang, Phys. Rev. 159, 806 (1967).
3. T. A. Tombrello and A. D. Bacher, Phys. Rev. 130, 1108 (1963).
4. A. D. Bacher, R. J. Spiger, and T. A. Tombrello, Nucl. Phys. A119, 481(1968).

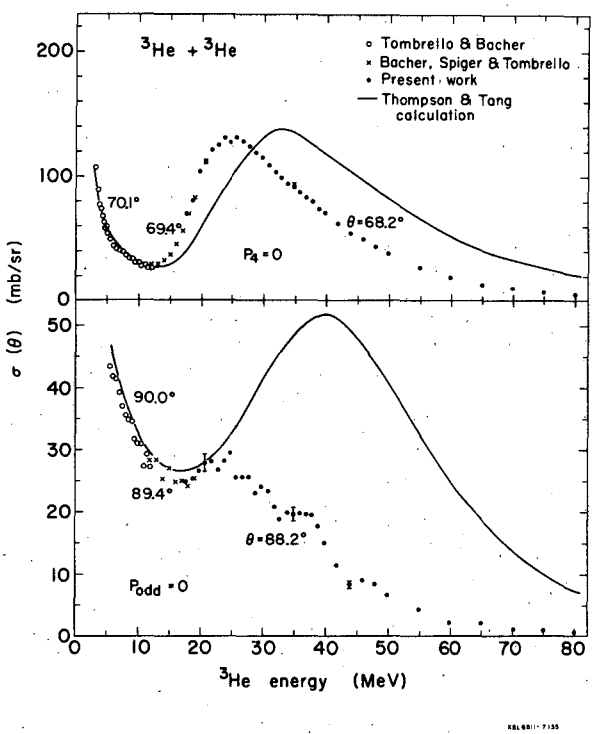

Fig. 1. Excitation functions for the ^{3}He-^{3}He elastic scattering at c.m. angles of 70 deg ($P_4 = 0$) and 90 deg ($P_{odd} = 0$). The results of this work (solid circles) are shown along with previous measurements at lower energy by Tombrello and Bacher (open circles, Ref. 3) and Bacher, Spiger, and Tombrello (crosses, Ref. 4). The solid curve shows the resonating-group prediction of Thompson and Tang (Ref. 2 and private communication).

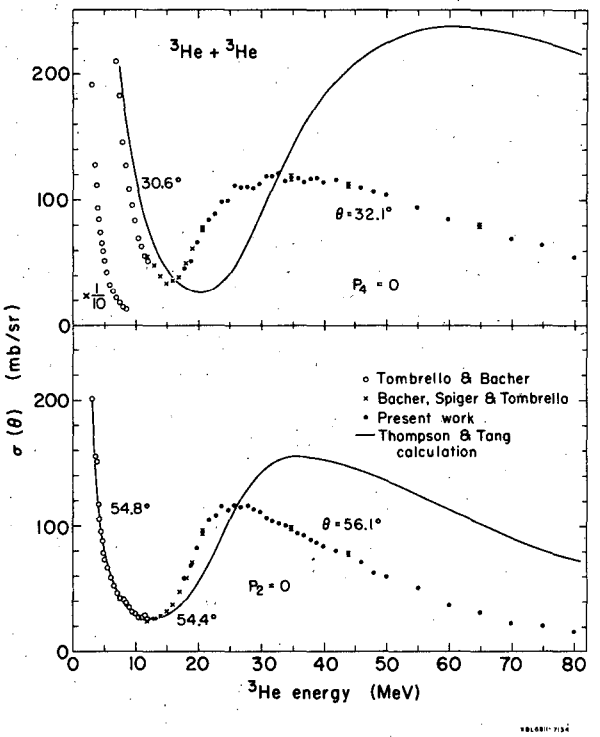

Fig. 2. Excitation functions for the ^{3}He-^{3}He elastic scattering at c.m. angles of 31 deg ($P_4 = 0$) and 55 deg ($P_2 = 0$). (See caption for Fig. 1.)

Fig. 3. Excitation function for the ^{3}He-^{3}He elastic scattering at a c.m. angle of 40 deg ($P_3 = 0$). (See caption for Fig. 1.)

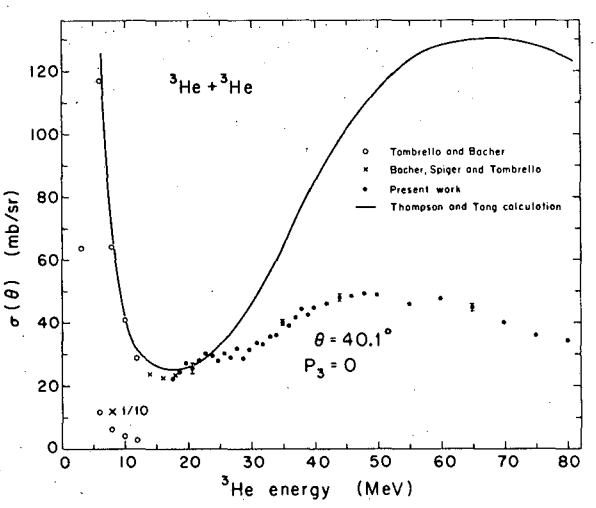

ELASTIC SCATTERING OF POLARIZED PROTONS ON ^{40}Ca AT 20 MeV

R. J. Slobodrian,† R. de Swiniarski,* W. F. Tivol, A. D. Bacher, A. Luccio
F. G. Resmini, and J. Ernst

Previous measurements[1] of the elastic scattering of polarized protons on ^{40}Ca have been interpreted as requiring an imaginary spin-orbit term (W_{so} = 1.5 to 2 MeV) in the optical potential in order to explain the polarization between 15 and 20 MeV. In addition, measurements of the inelastic scattering of 18.6-MeV polarized protons on nuclei in the $f_{7/2}$ region[2] have shown that the large asymmetries obtained after the excitation of the first 2^+ state in ^{54}Fe and ^{52}Cr could be reproduced by introducing an imaginary spin-orbit term in the optical potential (W_{so} = - 2 MeV). Although an imaginary spin-orbit term is usually not required at these low energies, ^{40}Ca in particular has for some time been recognized as "a bête noire" as far as optical model calculations are concerned.

In this work, the elastic scattering of polarized protons on ^{40}Ca has been measured at 20 MeV by using the polarized beam facility of the Berkeley 88-Inch Cyclotron. The experimental setup has been described previously.[3] The energy resolution of the polarized beam was 1.2 MeV, the ^{40}Ca target was 7 mg/cm^2 thick, and the angular acceptance of the detector was ±3 deg.

Figure 1 shows the polarization obtained at 20 MeV along with some measurements at 20.3 MeV from Saclay.[4] The agreement between the two sets of data is good.

Optical model calculations have been performed by use of the code MERCY, which is a modified version of the code SEEK,[5] and the parameter search was made by using both the cross section and polarization measurements. Perey's standard set of optical-model parameters[6, 1] was used as a starting point, and the search was done on the strengths V, W_D, and V_{so} and on r_{so}, the radius of the spin-orbit potential. Figure 2 shows the results with W_{so}, the imaginary spin-orbit strength equal to zero. The fit is quite good for angles greater than 70 deg but less good at forward angles, although the general shape of the polarization is well reproduced.

When W_{so} is introduced in the optical potential and included in the parameter search the resulting fit is very similar (Fig. 3); however, its final value is close to zero (W_{so} = - 0.18 MeV). Figure 4 shows the results when W_{so} is kept constant at a value of 2 MeV. The fit is now considerably worse and the shape of the theoretical curve is substantially changed.

The fit to the forward-angle measurements could be improved by introducing a_{so}, the spin-orbit diffuseness, in the search; however, the final value of a_{so} was too small to be acceptable (a_{so} = 0.24 F). Quite different sets of parameters have been used; all lead to the same conclusion as above. It seems quite clear from these measurements that it is not necessary to include an imaginary spin-orbit term in the optical potential in order to explain the polarization for ^{40}Ca at 20 MeV. Measurements at 18 MeV indicate that the shape of the polarization is changing rapidly in this energy region. Additional measurements are planned as soon as the new polarized ion source is available.

Footnotes and References

†Present address: Department of Physics, Laval University, Quebec 10^e, Canada.
*NATO-Fulbright Fellow; permanent address: Institut des Sciences Nucléaires de Grenoble, France.

1. D. G. Bough, J. C. Dore, G. W. Greenlees, J. Lowe, and S. Roman, Phys. Letters 13, 63 (1964), and R. M. Craig et al., Nucl. Phys. 58, 515 (1964).
2. C. Glashausser, R. de Swiniarski, A. D. Hill, and J. Thirion, Phys. Rev. 164, 1437 (1967).
3. William F. Tivol, Proton-^{3}He Polarization in the Range from 10 to 20 MeV, (Thesis) UCRL-18137, April 1968.
4. A. G. Blair, unpublished results.
5. M. A. Melkanoff, J. Raynal, and T. Sawada, UCLA-66-10.
6. F. G. Perey, Phys. Rev. 131, 745 (1963).

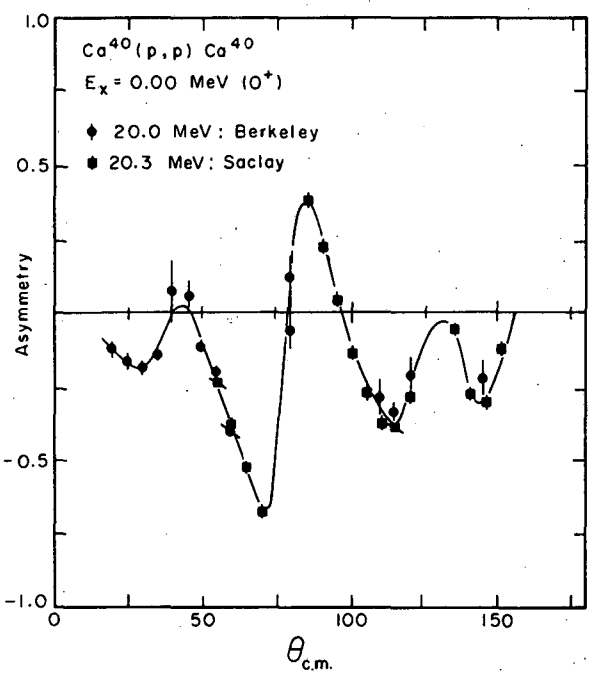

Fig. 1. The experimental polarization for 20.0-MeV polarized protons on ^{40}Ca along with the 20.3-MeV measurements from Saclay. The solid line serves only as a visual guide.

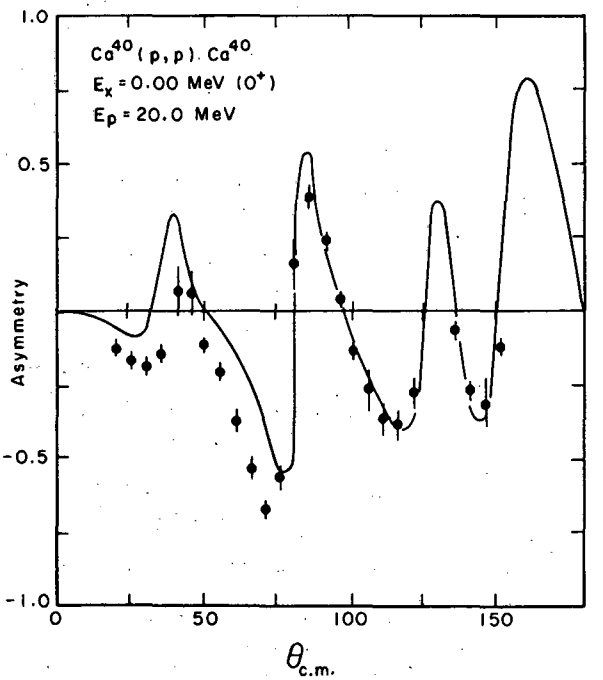

Fig. 2. Optical-model fit using Perey's standard set of parameters,

$r_0 = r_I = 1.25$ F, $a_0 = a_I = a_{so} = 0.47$ F.

The search was made on V, W_D, V_{so}, and r_{so} with W_{so} set equal to zero. The final search values obtained are V = 47.3 MeV, W_D = 7.5 MeV, V_{so} = 2.4 MeV, r_{so} = 1.14 F.

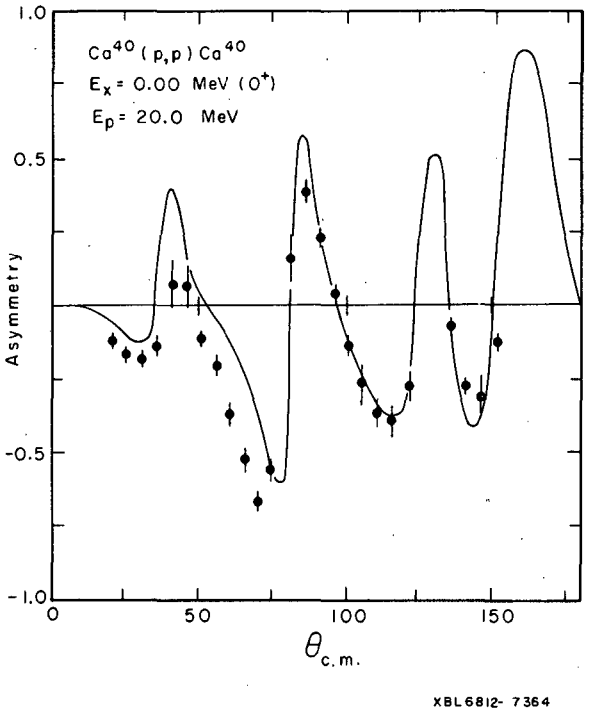

Fig. 3. Optical-model fit using the same geometry as above and search on V, W_D, V_{so}, W_{so}, and r_{so}; the final values obtained for these terms are V = 47.1 MeV, W_D = 6.95 MeV, V_{so} = 2.55 MeV, r_{so} = 1.12 F, W_{so} = -0.18 MeV.

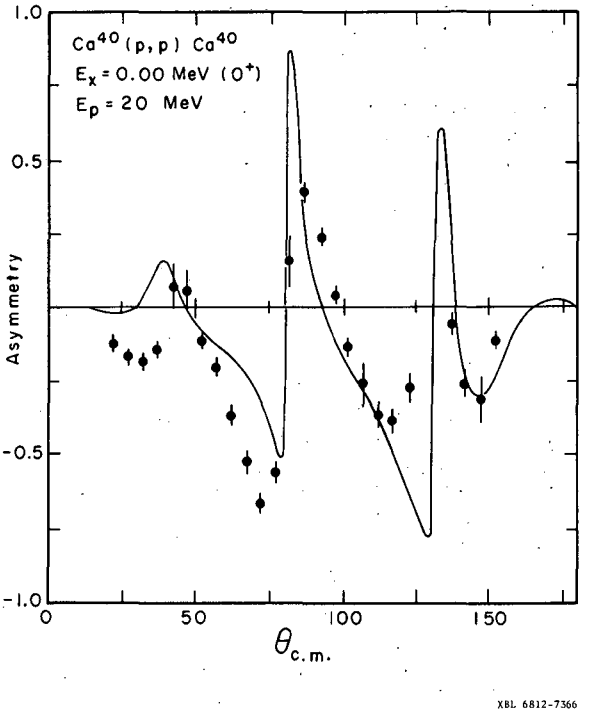

Fig. 4. Optical-model fit using the same parameters as in Fig. 2 with W_{so} fixed at 2 MeV.

PROTON-NEUTRON RESIDUAL INTERACTION IN STATES OF CONFIGURATION $(1d_{5/2})^2_{5^+,0}$ AND $(1g_{9/2})^2_{9^+,0}$

C. C. Lu, M. S. Zisman, and B. G. Harvey

Spectroscopic studies of the (α, d) reaction on light and medium-mass targets by use of 40- to 50-MeV α-particle beams from the Berkeley 88-Inch Cyclotron[1,2] have indicated that the most strongly populated states are those in which the captured proton and neutron enter the same shell-model state and couple to the maximum angular momentum with zero isobaric spin. States with configuration $[(\text{core})\ (1d_{5/2})^2_{5^+,0}]$, $[(\text{core})\ (1f_{7/2})^2_{5^+,0}]$, and $[(\text{core})\ (1g_{9/2})^2_{9^+,0}]$ were suggested,[1,2] where the square bracket indicates vector coupling.

The residual interaction energy between the proton and neutron in the configurations $(1d_{5/2})^2_{5^+,0}$ and $(1g_{9/2})^2_{9^+,0}$ was derived from the excitation energies determined in Refs. 1 and 2 and excitation energy data from neighboring nuclei. These interaction energies are about -3.9 MeV and -2.2 MeV, respectively, for the two configurations. The results are listed in the last columns of Tables I and II.

Conventional shell-model calculations of the $(1d_{5/2})^2_{5^+,0}$ and $(1g_{9/2})^2_{9^+,0}$ residual interactions have been performed using harmonic oscillator wave functions and a potential given by True,[3]

$$V_{TE} = -52 \exp(-0.2922\ r^2)\ (\text{MeV}).$$

In carrying out the calculations two different methods for obtaining the oscillator parameter, ν, were tried. The first set, referred to as ν_1 in Tables I and II, was obtained from the formula $\nu_1 = (2n + \ell - 1/2)/\langle r^2 \rangle$, where n and ℓ are the radial and angular momentum quantum numbers of the shell-model state and $\langle r^2 \rangle$ is associated with its rms radius. For the $(1d_{5/2})^2_{5^+_0}$ configuration the radius used was the equivalent uniform radius of the A = 17 nuclei, and for the $(1g_{9/2})^2_{9^+_0}$ configuration the radius of ^{73}Ge (the first $1g_{9/2}$ neutron) was used. In order to account for the change in nuclear size the oscillator parameter was assumed proportional to $A^{-1/3}$, and this factor was used in correcting the value of ν_1 for the different nuclei.[4]

The second set of oscillator parameters, ν_2 of Tables I and II, was chosen to reproduce the experimental interaction energy of each configuration in one of the nuclei. (^{18}F and ^{66}Ga were used for the $(1d_{5/2})^2_{5^+_0}$ and $(1g_{9/2})^2_{9^+_0}$ interactions, respectively.) The other ν_2 values were obtained from these two by again assuming a proportionality to $A^{-1/3}$. The results of calculations based on the two choices of oscillator parameter, listed as E_1 and E_2 in Tables I and II, can be seen to satisfactorily reproduce the experimental values.

Assuming that the proton-neutron residual interaction in the configuration $(1d_{5/2})^2_{5^+_0}$ is about -3.9 MeV, one can calculate the excitation energy of states having this configuration in other nuclei, either by using level information from neighboring nuclides or from $(1g_{1/2}, 1d_{5/2})_{J,T}$ matrix elements obtained by Talmi and Unna.[5] The results of such calculations for the nuclei ^{15}N, ^{16}N, ^{16}O, and ^{17}O are shown in Figs. 1 and 2. In general it was found that the former method, using information only from neighboring nuclides, gives better agreement with the experimental results.

Footnotes and References

1. E. Rivet, R. H. Pehl, J. Cerny, and B. G. Harvey, Phys. Rev. 141, 1021 (1966).
2. C. C. Lu, M. S. Zisman, and B. G. Harvey, Phys. Letters 27B, 217 (1968).
3. W. W. True, Phys. Rev. 130, 1530 (1963).
4. Clearly this is not consistent with the formula used for calculating ν_1, which would indicate a dependence on $A^{-2/3}$. However, the $A^{-1/3}$ dependence gives much better agreement with the experimental interaction energies. The latter approach corresponds to assuming that the energy of the level is approximately equal to the well depth, which yields a dependence on $A^{-1/3}$. [See J. M. Ferguson, Nucl. Phys. 59, 97 (1964).]
5. I. Talmi and I. Unna, Ann. Rev. Nucl. Sci. 10, 353 (1960).

Table I. Comparison between theoretical and experimental proton-neutron residual interaction energies of $(1d_{5/2})^2_5$+ configuration.

Nucleus	Shell-model calculation[a]				Experimental
	ν_1(in F^{-2})	E_1	ν_2(in F^{-2})	E_2	$E(1d_{5/2})^2_{5,0^+}$
^{14}N	0.326	-4.601	0.306	-4.291	-4.05
^{15}N	0.318	-4.481	0.299	-4.177	-3.57
^{16}N	0.311	-4.365	0.292	-4.068	-3.82
^{16}O	0.311	-4.365	0.292	-4.068	-3.52
^{17}O	0.304	-4.258	0.285	-3.968	-3.69
^{18}F	0.298	-4.165	0.280	-3.880	-3.88
^{22}Na	0.278	-3.847	0.261	-3.582	-3.47
^{26}Al	0.262	-3.601	0.246	-3.349	-4.04

a. The choices of two sets of ν's are discussed in the text. All the energies are in units of MeV.

Table II. Comparison between theoretical and experimental proton-neutron residual interaction energies of $(1g_{9/2})^2_{9,0}^+$ configuration.

Nucleus	Shell-model calculation[a]				Experimental
	ν_1(in F^{-2})	E_1	ν_2(in F^{-2})	E_2	$E(1g_{9/2})^2_{9,0}^+$
^{54}Mn	0.226	-2.198	0.244	-2.400	-(2.49)
^{56}Co	0.224	-2.167	0.241	-2.366	-(2.54)
^{60}Cu	0.219	-2.111	0.236	-2.303	-2.42
^{62}Cu	0.216	-2.083	0.233	-2.275	-2.32
^{64}Cu	0.214	-2.059	0.231	-2.247	-(1.93)
^{66}Ga	0.212	-2.033	0.228	-2.221	-(2.22)
^{68}Ga	0.209	-2.008	0.226	-2.195	-(2.07)

a. The choices of two sets of ν's are discussed in the text. All the energies are in units of MeV.

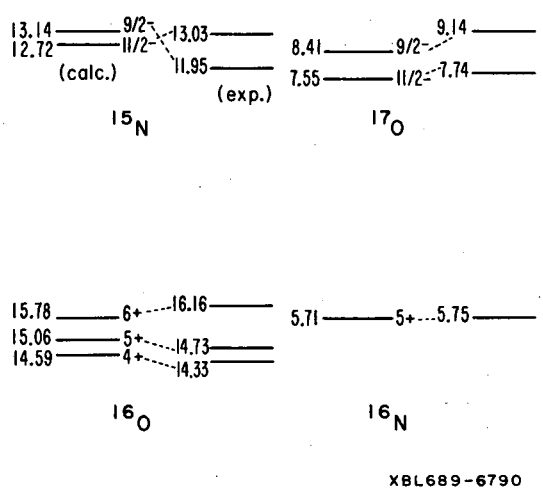

Fig. 1. Comparison between the experimental excitation energies of the $(1d_{5/2})^2_{5}^+$ levels and the theoretical values using level information only from neighboring nuclides.

shape is defined by

$$R = R_0\left(1 + \sum_{\lambda k} \alpha_{\lambda k} Y_{\lambda k}\right).$$

In this calculation the first three excited states (0^+, 2^+, 4^+) of ^{24}Mg were assumed to be members of a K = 0 ground-state rotational band, the next three states (2^+, 3^+, 4^+) were assumed to be members of a K = 2 band. In the calculations, complex coupling of all orders with even angular momentum transfers up to L = 8 and K transfer of 0 and 2 were allowed between these six states. Other results from using a similar program indicate that inclusion of higher members would not significantly change the results of the calculations. The optical and deformation parameters (Table I) were chosen for consistency at the four incident energies, the only parameters that were changed were W and r_i.

The coupled-channel results, shown in Figs. 1 through 4, indicate that this calculation yields quite good agreement over the entire range of data. Specifically, the unique behavior of the 3+ cross section is reproduced, even to magnitude of cross section. It was found necessary to enhance the direct excitation component to the second 4+ by $\alpha_{42} = 0.085$. Although a much smaller amount of α_{40} might be suggested to improve the fit to the first 4+ state at small angles, especially for the 50-MeV data, this was not included in this calculation.

Footnote and References

*Present address: Centre College, Danville, Kentucky.

1. W. W. Eidson and J. G. Cramer, Phys. Rev. Letters 9, 497 (1962).
2. W. J. Braithwaite, J. G. Cramer, and R. A. Hinrichs, University of Washington Nuclear Physics Laboratory Annual Report, 1966, p. 18.
3. J. Kokama, K. Fukunaga, N. Inoue, and H. Nakamura, Phys. Letters 8, 342 (1964).
4. J. S. Blair, N. Cue, and D. Shreve, University of Washington Nuclear Physics Laboratory Annual Report, 1965, p. 3.
5. F. W. Bingham, Phys. Rev. 145, 901 (1966).
6. B. G. Harvey, E. J-M. Rivet, A. Springer, J. R. Meriwether, W. B. Jones, J. H. Elliott, and P. Darriulat, Nucl. Phys. 52, 465 (1964).
7. J. S. Vincent, E. T. Boschitz, and J. R. Priest, Bull. Am. Phys. Soc. 11, 333 (1966).
8. J. S. Vincent, E. T. Boschitz, and J. R. Priest, Phys. Letters 25B, 81 (1967).
9. T. Tamura, Nucl. Phys. 73, 241 (1965).
10. R. E. Malmin, P. P. Singh, D. W. Devins, J. G. Wills, C. R. Bingham, and M. L. Halbert, Bull. Am. Phys. Soc. 13, 117 (1968).
11. W. R. Smith, The Hauser-Feshbach Nuclear Scattering Computer Code LIANA, Oak Ridge National Laboratory Report ORNL-TM-1234, 1965.
12. G. Chenevert, I. Halpern, B. G. Harvey, and D. L. Hendrie, The Evaporation of α Particles from Heavy Nuclei, Nucl. Phys. (to be published).
13. N. K. Glendenning, Inelastic Scattering and Nuclear Structure, Lectures for International School of Physics "Enrico Fermi," UCRL-17503, Aug. 1967.

Table I. List of optical and deformation parameters for fits to the ^{24}Mg (α, α) data.

E (MeV)	V (MeV)	W (MeV)	(F.)	(F.)	(F.)	(F.)	α_{20}	α_{22}	α_{40}	α_{42}
50	100	16	1.38	1.45	0.69	0.58	0.335	0.071	0	0.085
65.7	100	18	1.38	1.45	0.69	0.58	0.335	0.071	0	0.085
81	100	17	1.38	1.6	0.69	0.58	0.335	0.071	0	0.085
119.7	100	23	1.38	1.6	0.69	0.58	0.335	0.071	0	0.085

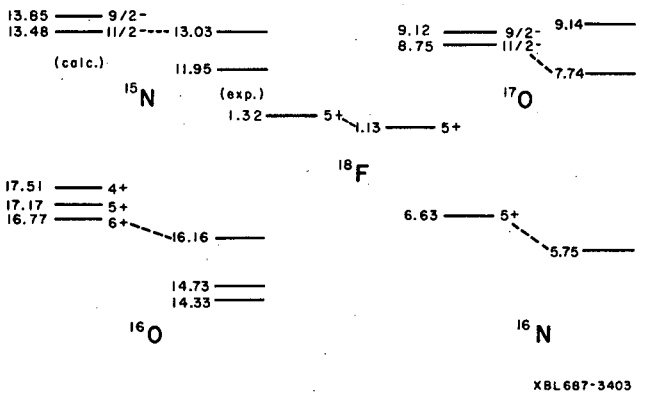

Fig. 2. Comparison between the experimental excitation energies of the $(1d_{5/2})^2_{5,0}$ levels and the theoretical values using Talmi's method of shell-model calculation.

PRODUCTION OF THE 3+ UNNATURAL-PARITY STATE IN ^{24}Mg BY INELASTIC α SCATTERING

M. F. Reed,* D. L. Hendrie, B. G. Harvey, and N. K. Glendenning

In the past few years the nuclear reaction mechanism leading to the production of unnatural-parity states ($\pi \neq (-1)^J$) in even-even nuclei by inelastic α scattering has been the subject of much research.[1-10] The interest in these energy levels stems from the fact that they cannot be excited in this reaction by simple direct mechanisms.[1] However, these states are often excited with relatively large cross sections. Thus, they afford a unique opportunity to study more complicated nuclear interactions between spinless projectiles and targets.

A study of the excitation of the ^{24}Mg 3+ level at higher bombarding energies was undertaken at the 88-inch variable-energy cyclotron to investigate the mechanism of the reaction. In this series of experiments, α particles of 50, 65.7, 81, and 119.7 MeV were scattered from isotopically enriched (99.96%) self-supporting ^{24}Mg targets. Energy spectra of the scattered α particles were measured with lithium-drifted silicon detectors and stored in 1024-channel groups of a 4096-channel pulse-height analyzer. In these spectra the 3+ level was well separated from the other ^{24}Mg levels. However, ^{16}O and ^{12}C impurities masked some of the ^{24}Mg levels at a few forward angles.

The angular distributions obtained from these spectra for the natural-parity states show the usual diffraction oscillations which correspond reasonably well with a "universal" plot as a function of QR, where Q is the momentum transferred to the nucleus, and R is an effective interaction radius. The 3+ state, however, shows two very broad and strong peaks which do not at all correlate with a QR plot.

Calculations for the compound nucleus and multiple excitation mechanisms have been carried out. A Hauser-Feshbach computer code[11] was used to generate angular distributions on the assumption the compound nucleus mechanism was a major contributor. The large difference between these calculated angular distributions and the measured ones and the very small cross sections expected from the compound mechanism at high energies[12] allow us to conclude that this mechanism does not play a significant role in the excitations at the studied energies.

The multiple excitation mechanism was investigated by a coupled-channels code.[13] In this model, the α particle interacts with a permanently asymmetrically deformed optical potential whose

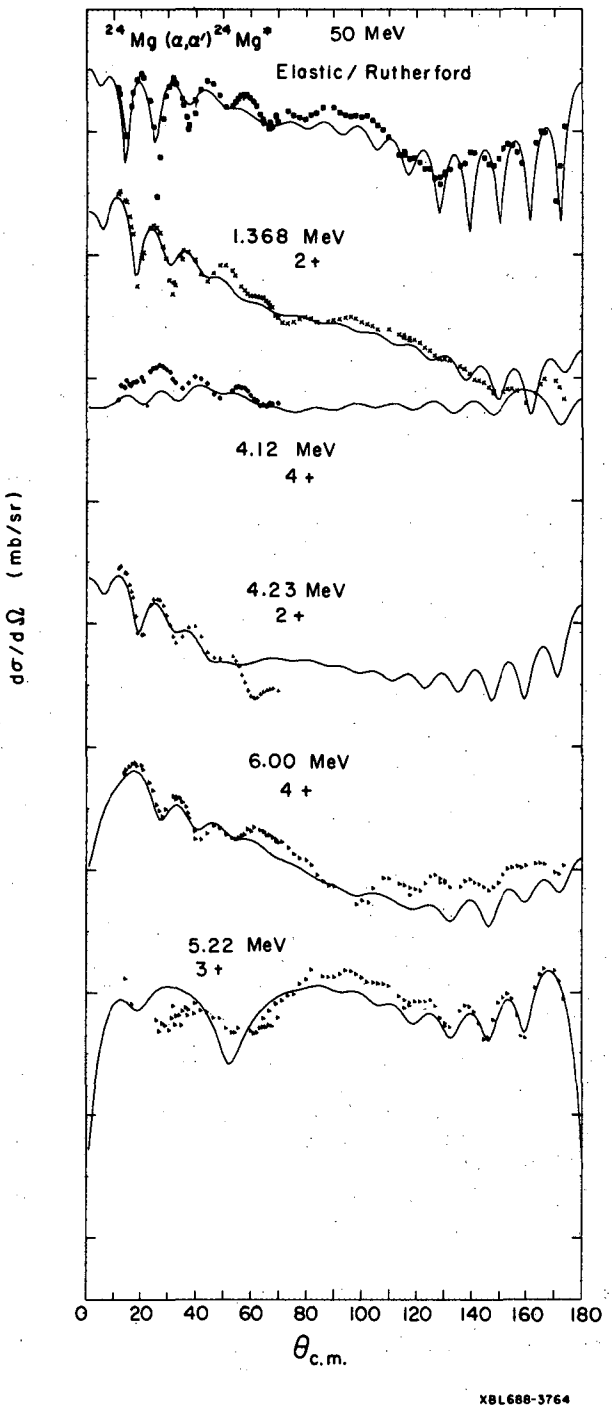

Fig. 1. Experimental data and coupled-channel fits for the ^{24}Mg(α, α')^{24}Mg reaction at 50 MeV.

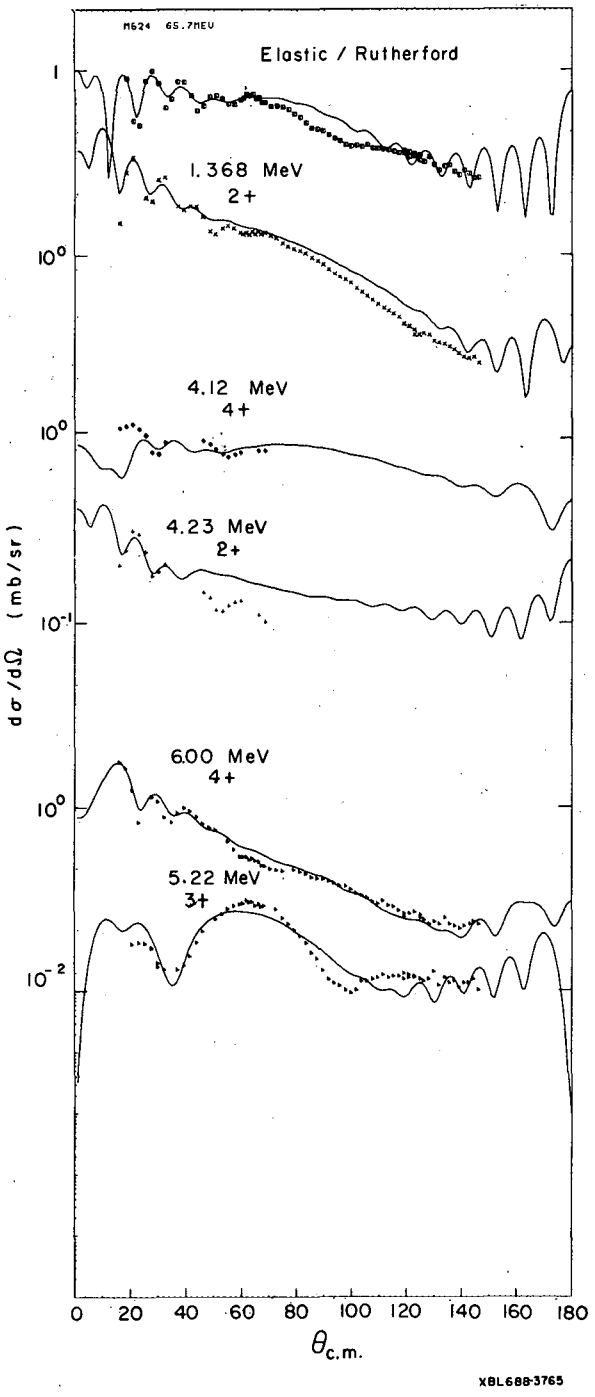

Fig. 2. Experimental data and coupled-channel fits for the $^{24}Mg(\alpha,\alpha')^{24}Mg$ reaction at 65.7 MeV.

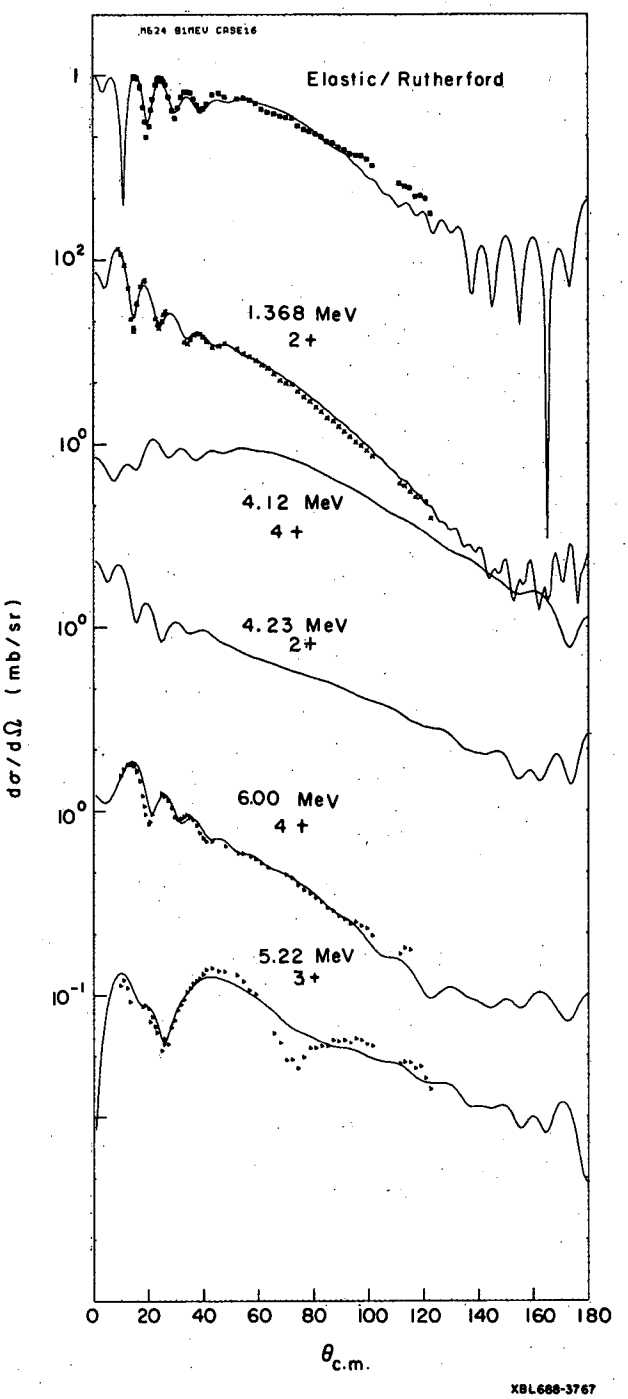

Fig. 3. Experimental data and coupled-channel fits for the $^{24}Mg(\alpha,\alpha')^{24}Mg$ reaction at 81 MeV.

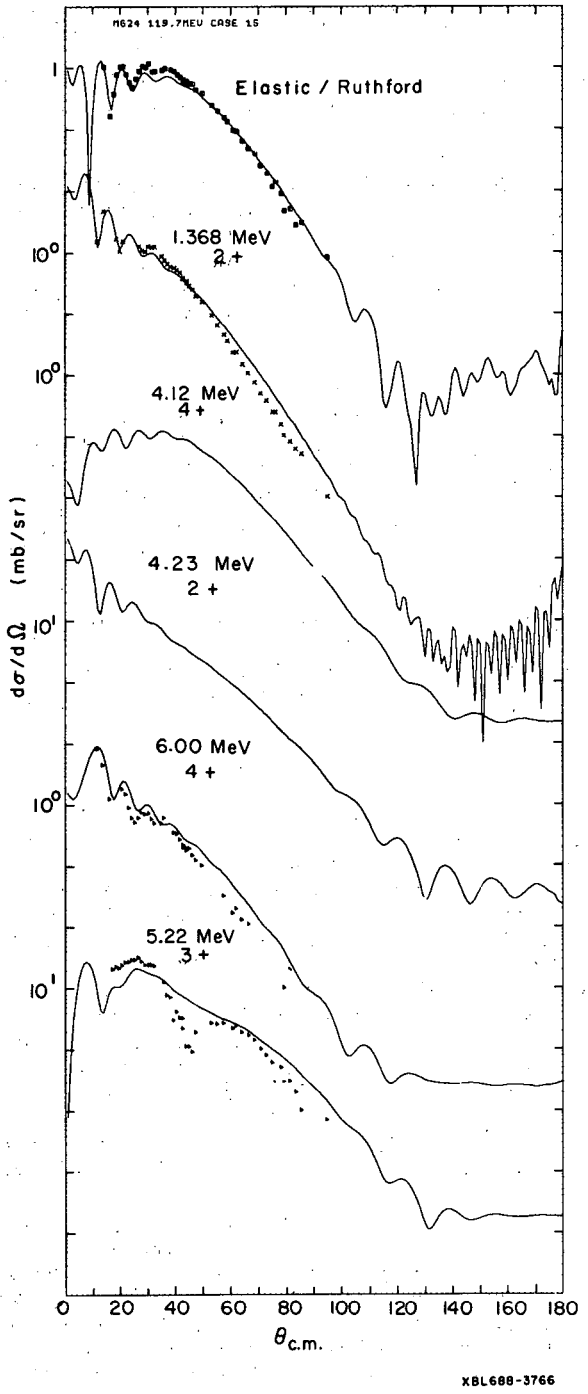

Fig. 4. Experimental data and coupled-channel fits for the $^{24}Mg(\alpha,\alpha')^{24}Mg$ reaction at 119.7 MeV.

EXCITATION OF SINGLE NEUTRON HOLE STATES IN ^{207}Pb BY INELASTIC PROTON SCATTERING AT 20.2 MeV†

C. Glashausser, B. G. Harvey, D. L. Hendrie, J. Mahoney
E. A. McClatchie, and J. Saudinos*

Differential cross sections for the excitation of single-particle or single-hole states provide a direct test of the microscopic model[1,2] of inelastic proton scattering. Few experimental data[3] exist, however, since the cross sections are generally much smaller than the cross sections for the excitation of collective states. Angular distributions have been measured here for five such transitions in ^{207}Pb at an incident proton energy of 20.2 MeV. The analysis of these data in terms of the microscopic model indicates that a large part of the observed cross section is due to excitation of the ^{208}Pb core.

The first five states in ^{207}Pb, at 0.0, 0.570, 0.894, 1.633, and 2.33 MeV, are considered to be single $3p_{1/2}$, $2f_{5/2}$, $3p_{3/2}$, $1i_{13/2}$ and $2f_{7/2}$ neutron holes, respectively, in a ^{208}Pb core. The $9/2^+$ state at 2.74 MeV has been identified as the $[2g_{9/2}, \ ^{206}\mathrm{Pb}\ \mathrm{gs}]_{9/2^+}$ state in (d, p) reactions[4] on ^{206}Pb; recent analysis[5] of reactions which proceed via the analog of this state indicates a 6% admixture of the $[2g_{9/2}, \ ^{206}\mathrm{Pb}\ 2^+]_{9/2^+}$ configuration. The data from single-nucleon transfer reactions indicate that the hole states are reasonably pure configurations.[6] However, the effective charge deduced from the measured values of B(E2) in ^{207}Pb and ^{209}Bi is about one for neutrons and two or larger for protons.[7,8]

Inelastic scattering data were taken with the 20.2-MeV proton beam of the 88-inch cyclotron; the energy resolution was about 30 keV. The differential cross sections are shown in Fig. 1, together with theoretical curves described below. These microscopic-model calculations assumed a direct (D) projectile-target nucleus interaction of the standard form,

$$V_{ij}(r_{ij}) = (V_0 + V_1 \sigma_i \cdot \sigma_j)\, g(|r_{ij}|);$$

a Yukawa shape with range 1 F was chosen for $g(|r_{ij}|)$. The strength of the potential V_1, which allows transfer of spin angular momentum (S) to the target, was set to $V_0/3$. A nonlocality range of 0.85 F was assumed in the computation of bound-state wave functions; the curves shown do not include nonlocality in the distorted waves. The depth of the bound-state Woods-Saxon well was adjusted to give the correct binding energy; the radius was $1.20\ A^{1/3}$ (F) and the diffuseness was 0.7 F. Antisymmetrization of the projectile with the target nucleons was not included.

Predictions[9] of this model are shown by the dashed curves in Fig. 1. The values of V_0 obtained by normalizing these curves to give the best fit to the experimental data are listed in Table I. (This is the normalization illustrated in Fig. 1B). Note that the strengths are much larger than the free proton-neutron interaction strength although they are comparable with the values found in other similar microscopic-model analyses in even-even nuclei.[1,10] Uncertainties in the parameters of the calculation can reduce V_0(D) by no more than about 30%. However, if the knockout-exchange amplitudes are included, considerations based on the recent calculations by Atkinson and Madsen[11] indicate that the values of V_0(D) might all be reduced to about 100 MeV.

The fact that the values generally found for V_0 are so large has led Love and Satchler[12] to develop a phenomenological method of treating core polarization (CP) effects. Calculations of this type for transitions with known B(E2) are shown by the solid curves in Fig. 1A. With a V_0 of 60 MeV, the magnitudes of the cross sections predicted by the microscopic model are now in reasonable agreement with the data. With this value of V_0, (D+CP) calculations for the higher states (the solid curves of Fig. 1B) determine B(EL) for these transitions; from B(EL), values of the effective charge were deduced. These are shown in the last column of Table I.

Footnotes and References

†Condensed from 18376 Phys. Rev. Letters 21, 918 (1968).
*Present address: SPNME, CEN--Saclay, France.

1. N. K. Glendenning and M. Veneroni, Phys. Rev. 144, 839 (1966).
2. G. R. Satcher, Nucl. Phys. 77, 481 (1966); K. A. Amos, V. A. Madsen, and I. E. McCarthy, Nucl. Phys. A94, 103 (1967).

3. G. Vallois, thesis, University of Paris (1967); C. B. Fulmer, J. B. Ball, A. Scott, and M. L. Whiten, Phys. Letters 24B, 505 (1967); M. M. Stautberg, J. J. Kraushaar, and B. W. Ridley, Phys. Rev. 157, 977 (1967).
4. P. Mukherjee and B. L. Cohen, Phys. Rev. 127, 1284 (1962); W. Darcey, A. F. Jeans, and K. N. Jones, Phys. Letters 25B, 599 (1967).
5. N. Auerbach and N. Stein, Phys. Letters 27B, 122 (1968).
6. G. Muehllehner, A. S. Poltorak, W. C. Parkinson, and R. H. Bassel, Phys. Rev. 159, 1039 (1967); W. C. Parkinson, D. L. Hendrie, H. H. Duhm, J. Mahoney, J. Saudinos, and G. Satchler, Phys. Rev. (Feb. 20, 1969).
7. Cf. O. Nathan and S. G. Nilsson, Alpha-, Beta-, and Gamma-Ray Spectroscopy, ed. Kai Siegbahn (North-Holland Publishing Company, Amsterdam, 1965), p. 601.
8. S. Gustaffson, K. Johannsson, E. Karlsson, and A. G. Svensson, Phys. Letters 10, 191 (1964).
9. We are grateful to A. D. Hill and P. D. Kunz for making their computer codes available to us.
10. G. R. Satchler, Nucl. Phys. A95, 1 (1967).
11. Jay Atkinson and V. A. Madsen, Phys. Letters 21, 295 (1968), and V. A. Madsen, private communication.
12. W. G. Love and G. R. Satchler, Nucl. Phys. A101, 424 (1967).

Table I. Strength parameters. The values $V_0(D)$ were derived without core polarization. The parameters $V_0(D+CP)$, $\langle r^L \rangle$, and e_{eff} were used in the core polarization calculations. The parameter R_c is $1.2\ A^{1/3}$ (F).

State	L	S	J	$V_0(D)$ (MeV)	$V_0(D+CP)$ (MeV)	$\frac{\langle r^L \rangle}{R_c^L}$	e_{eff}
5/2 -	2	0	2	160	60	0.62	1.0 e
	2	1	2				
3/2 -	2	0	2	110	60	0.71	1.0
	0	1	1				
13/2 +	7	0	7	285	60	0.84	0.73
	5	1	6				
7/2 -	4	0	4	170	60	0.75	1.0
9/2 +	5	0	5	175	60	1.10	0.75

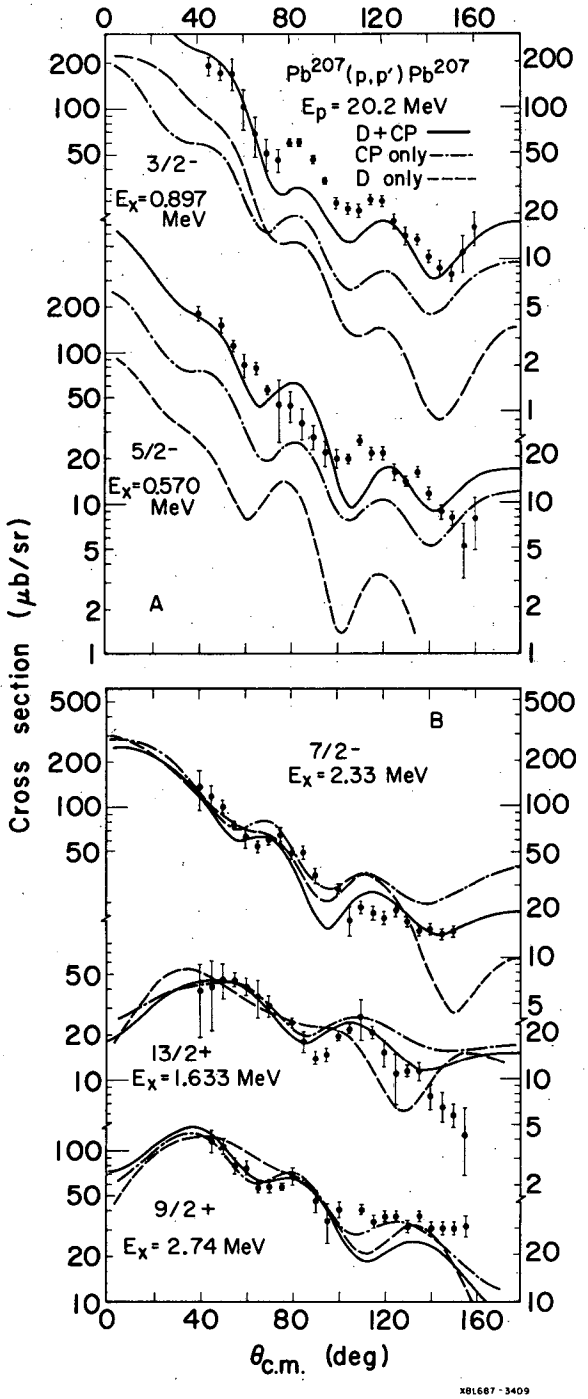

Fig. 1. (A). Measured cross sections and predictions of the microscopic model. The label D refers to the direct or single particle cross section alone; the label CP refers to the core polarization cross section alone. The (D+CP) calculations include the coherent contributions of each. The normalization of all curves assumes the (D+CP) values of Table II. (B). The solid curves are normalized as in Fig. 1A. The normalizations of the D and CP curves are adjusted to give the best fit to the data.

STUDY OF THE PROTON PARTICLE-HOLE STATES IN ^{208}Pb

E. A. McClatchie, C. Glashausser, and D. L. Hendrie

In the past few years the neutron particle-hole states of ^{208}Pb have been extensively studied;[1-3] however, the proton configurations have by comparison received scant attention. With the availability of detailed shell-model calculation in the lead region of nuclei[4] it is of great interest to subject the predicted wave functions to exhaustive experimental test.

A convenient way of reaching the proton particle-hole configurations in ^{208}Pb is to use the (d, ^{3}He) reaction on ^{209}Bi. Assuming the ^{209}Bi ground state to be well described as an $h_{9/2}$ proton coupled to a closed-shell ^{208}Pb core, a proton pickup reaction should populate states of the form $h_{9/2}(nlj)^{-1}$, where $(nlj)^{-1}$ specifies the proton hole state in ^{207}Tl. The (d, ^{3}He) reaction on ^{208}Pb[5] populates almost exclusively four low-lying states in ^{207}Tl, which have been identified as $(3s_{1/2})^{-1}$, $(2d_{3/2})^{-1}$, $(1h_{11/2})^{-1}$, and $(2d_{5/2})^{-1}$; these are known to be quite pure proton hole configurations. Thus the (d, ^{3}He) reaction on ^{209}Bi should populate the four proton configurations $h_{9/2}(3s_{1/2})^{-1}$, $h_{9/2}(2d_{3/2})^{-1}$, $h_{9/2}(1h_{11/2})^{-1}$, and $h_{9/2}(2d_{5/2})^{-1}$ in ^{208}Pb, giving rise to a spectrum of states based on each hole configuration. The unperturbed energies of the above configurations are shown in Table I.

The ^{209}Bi (d, ^{3}He) reaction was studied by using the 50-MeV deuteron beam of the 88-inch cyclotron. Two ΔE-E solid-state counter telescopes combined with Goulding-Landis identifiers were used to examine the ^{3}He spectra, an example of which is shown in Fig. 1. The typical energy resolution was 60 to 75 keV FWHM, of which about 50 keV could be attributed to spread in the incident beam. ^{3}He spectra were recorded at angles from 10 to 50 deg lab in 2.5-deg or smaller steps.

In a typical spectrum, Fig. 1, 15 ^{3}He groups can be identified up to an excitation energy of 5.7 MeV. The energies shown in Fig. 1 are probably good to ±10 keV for the strong groups and ±20 keV for the weaker ones. Other peaks in Fig. 1 arise from target contaminants or α-particle leak-through to the ^{3}He spectrum. At channel 975 is the pulser peak, which was used to monitor the gain stability and dead time of the electronics.

Angular distributions of nine of the ^{3}He groups are shown in Fig. 2. This experiment was designed so as to directly utilize the results of the ^{208}Pb (d, ^{3}He) experiment. The solid curves of Fig. 2 are smooth lines drawn through the ^{208}Pb (d, ^{3}He)^{207}Tl data points and arbitrarily normalized to superimpose on the ^{209}Bi (d, ^{3}He)^{208}Pb data. Since the l-transfers in the ^{208}Pb (d, ^{3}He) data are known, we can thus identify the l-transfers in the ^{209}Bi data, without recourse to a DWBA analysis. Furthermore, the relative cross sections of the two sets of data provide a direct measure of the (d, ^{3}He) pickup strength from ^{209}Bi to a particular group in ^{208}Pb. We were able to account for almost all the $(3s_{1/2})(2d_{3/2})$, $(1h_{11/2})$, and $(2d_{5/2})$ pickup strength in the states between 2.6 and 5.7 MeV.

The fact that the angular distributions of Fig. 2 are fitted so well by a single value of l-transfer indicates that little configuration admixture is present in any of these groups, even though it is reasonable to assume that some of the groups may correspond to more than one state in ^{208}Pb.

We have used the Kuo-Brown wave functions[4] for ^{208}Pb and calculated the strengths of $h_{9/2}(nlj)^{-1}$ proton particle-hole states from them. Figure 3 shows the comparison of the theoretical strengths vs the experimental ones determined from the (d, ^{3}He) data. The $h_{9/2}(1h_{11/2})^{-1}$ multiplet is not shown, since the Kuo-Brown wave functions for positive parity states with spin larger than 5^+ were not available. The general agreement of the spacings, widths, and positions of the three $h_{9/2}(nlj)^{-1}$ multiplets is readily apparent in Fig. 3; however, detailed level-to-level comparisons do not, in general, obtain.

Finally it is of interest to compute the predicted and observed centroids of the various multiplets and compare them. These are shown in Table I. Note that the centroids are uniformly below the unperturbed energy E_0 for every multiplet. This is in sharp contrast to the situation for proton-particle neutron-hole states in ^{208}Bi, where the multiplet centers of gravity are calculated and observed to be above the unperturbed energies.[6] With more detailed theoretical understanding of these results, we should gain additional information about the particle-hole residual interaction in the lead region.

References

1. J. Bardwick and R. S. Tickle, Phys. Rev. 161, 1217 (1967).
2. C. F. Moore, J. G. Kulleck, and P. von Brentano, Phys. Rev. 164, 1559 (1967).
3. P. Richard, W. G. Weitkamp, W. Wharton, H. Weiman, and P. von Brentano, Phys. Letters 26B, 8 (1967).
4. T. T. S. Kuo and G. E. Brown, private communication.
5. W. C. Parkinson, D. L. Hendrie, H. H. Duhm, J. Mahoney, J. Saudinos, and G. R. Satchler, Phys. Rev. (Feb. 20, 1969).
6. W. P. Alford, J. P. Schiffer, and J. J. Schwarz, Phys. Rev. Letters 21, 156 (1968).

Table I. Energies of the proton-particle-hole multiplets in ^{208}Pb.

Multiplet	E_0 [a] (MeV)	$\bar{E}_{exp}$ [b] (MeV)	$\bar{E}_{theor}$ [c] (MeV)
$h_{9/2}\,(s_{1/2})^{-1}$	4.225	3.876	4.029
$h_{9/2}\,(d_{3/2})^{-1}$	4.575	4.222	4.377
$h_{9/2}\,(h_{11/2})^{-1}$	5.565	5.157	--
$h_{9/2}\,(d_{5/2})^{-1}$	5.895	5.582	5.757

a. Unperturbed energies calculated from ^{209}Bi (d, ^{3}He)^{208}Pb and ^{208}Pb (d, ^{3}He)^{207}Tl Q values.
b. Experimentally observed multiplet centroids in this ^{209}Bi (d, ^{3}He)^{208}Pb experiment.
c. Calculated multiplet centroids from the Kuo-Brown wave functions (Ref. 5).

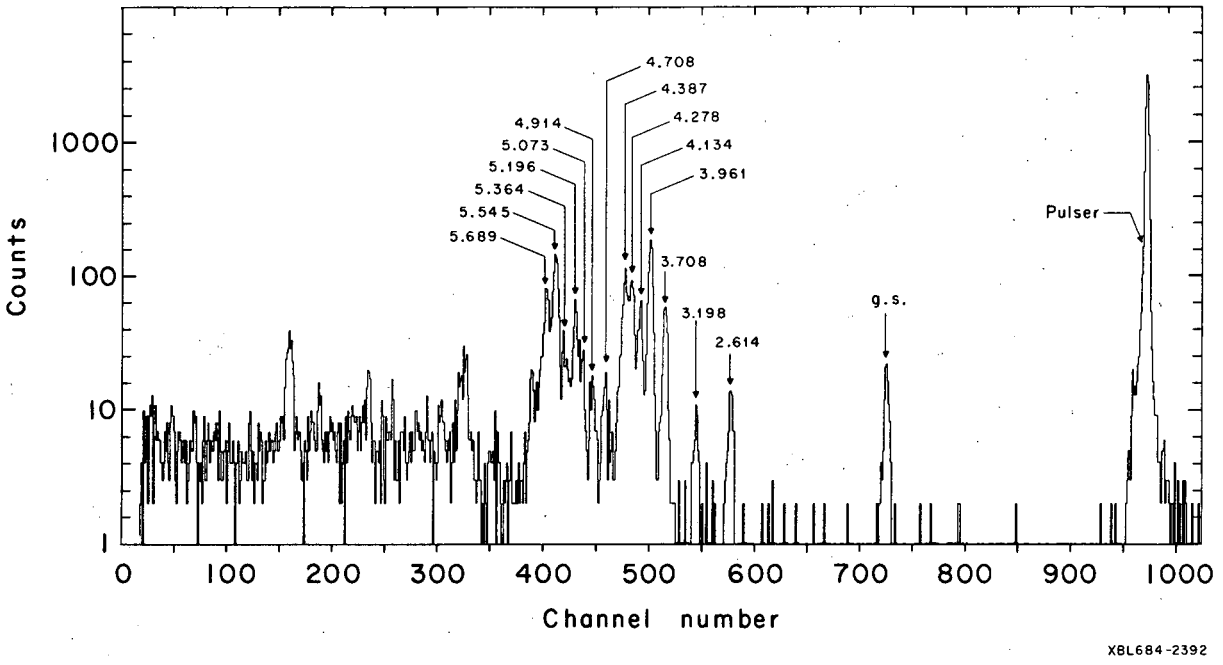

Fig. 1. Spectrum of ^{3}He particles from $^{209}Bi(d, ^{3}He)^{208}Pb$ at 27.5 deg lab (10 000 μC).

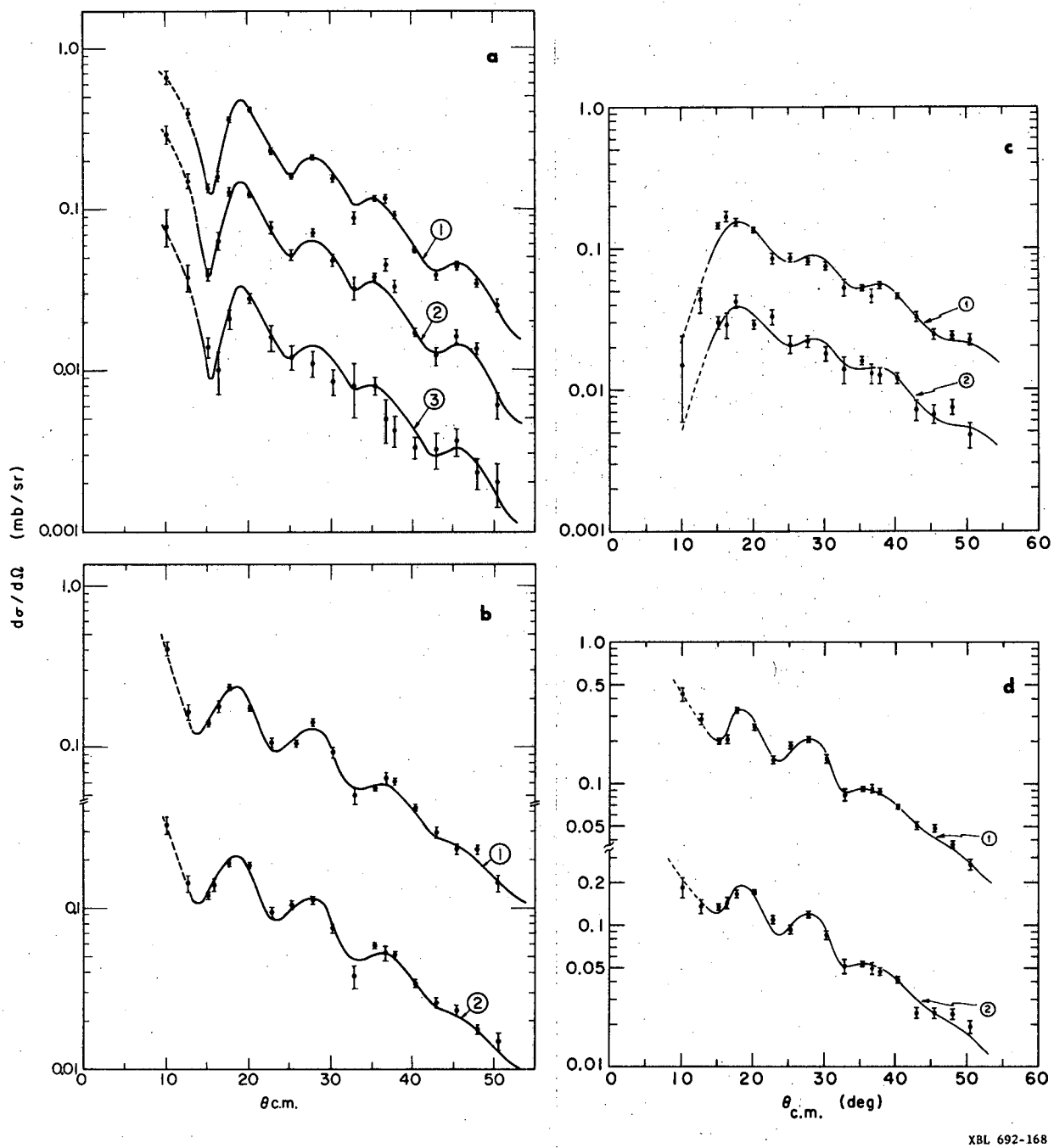

Fig. 2. Angular distributions of $^{209}Bi(d, ^{3}He)^{208}Pb$ reactions.
(a) $s_{1/2}$ transfer: ① 3.961 MeV 4^-, 5^-, ② 3.708 MeV 5^-, ③ 3.198 MeV 5^-;
(b) $d_{3/2}$ transfer: ① 4.387 MeV, ② 4.278 MeV;
(c) $h_{11/2}$ transfer: ① 5.196 MeV, ② 4.914 MeV;
(d) $d_{5/2}$ transfer: ① 5.689 MeV, ② 5.545 MeV.

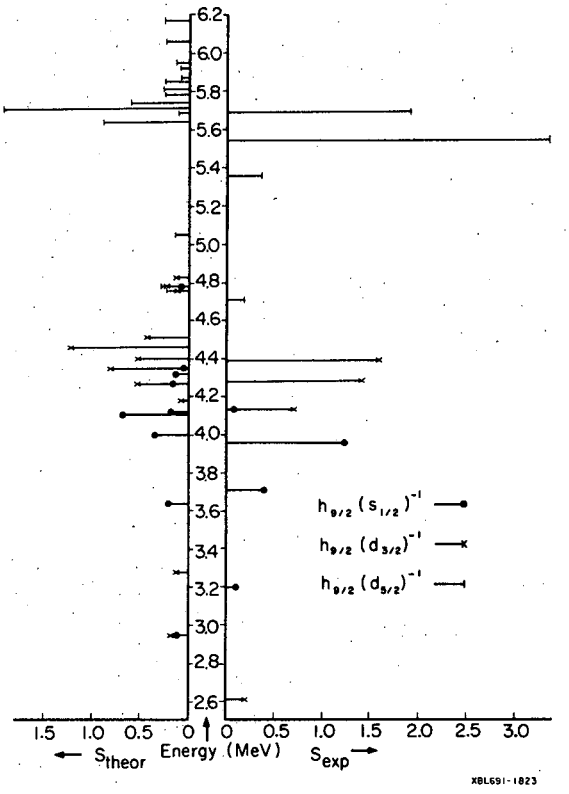

Fig. 3. Comparison of theoretical and experimental spectroscopic factors for the ^{209}Bi (d, ^{3}He)^{208}Pb reaction.

ENERGY LEVELS IN ^{205}Tl

C. Glashausser, D. L. Hendrie, J. Mahoney, and E. A. McClatchie

It is interesting to extend the study[1] of proton particle-hole states to ^{206}Pb. Since ^{207}Bi is not stable, the (d, ^{3}He) reaction cannot be used. However, Nolen[2] has found that the spectrum of the (p, α) reaction on isotopic targets of copper and zinc at 17.5 MeV incident energy closely resembles the spectrum of the (d, ^{3}He) reaction on the isotope with two fewer neutrons. If this correspondence persists in the lead region, it should be possible to investigate the proton particle-hole structure of ^{206}Pb by the (p, α) reaction on ^{209}Bi. Now the (t, α) and (d, ^{3}He) reactions on ^{208}Pb excite the same states,[3] and the ^{206}Pb(t, α)^{205}Tl reaction has been performed by Hinds et al.[4] A comparison of the latter results with the results of the ^{208}Pb(p, α)^{205}Tl reaction should thus determine the usefulness of performing the (p, α) reaction on ^{209}Bi. Since the results of Hinds et al.[4] are the only published data on the levels of ^{205}Tl above the second excited state, the ^{208}Pb(p, α)^{205}Tl data should also be interesting in themselves.

Angular distributions were taken in 1- or 2-deg steps between 11 and 30 deg at an incident energy of 35.2 MeV. A spectrum at a lab angle of 19 deg is shown in Fig. 1; the energy resolution is 35 keV. The energy calibration was performed by using the energies quoted to ±20 keV by Hinds et al.[4] They, however, did not observe the level at 0.92 MeV, but did observe three levels between 1.14 and 1.33 MeV which are not seen here. Above 2.12 MeV, there is little correspondence between the ^{206}Pb(t, α)^{205}Tl and the ^{208}Pb(p, α)^{205}Tl spectra. The situation is summarized in Table I. The energy levels seen in either of the two reactions are listed in the left. The maximum cross sections observed are listed in the next two columns. A dash in the cross section column indicates that some strength was observed at these locations, but not enough to definitely confirm the state. It is clear from this figure that the two reactions show quite different spectra.

To confirm the (t, α) results we have made a cursory investigation of the $^{206}Pb(d, ^{3}He)^{205}Tl$ reaction at four angles between 12.5 and 20 deg. The deuteron energy was 40 MeV and the energy resolution was 50 keV. The results are consistent with the (t, α) data[4] and indicate that the 1.48-MeV level is indeed an $11/2^-$ level, as suggested by Hinds et al.[4]

Finally, the $^{205}Tl(p, p')^{205}Tl$ reaction has been carried out at 20.07 MeV. Only preliminary results are presently available for the energy levels and angular distributions; a spectrum is shown in Fig. 2. The state at 0.92 MeV observed in the $^{208}Pb(p, \alpha)^{205}Tl$ spectrum is also seen here; most of the other levels seen up to 4 MeV do not correspond to states strongly excited in the (p, α) reaction. (States at 1.48, 3.52, and 3.99 MeV are obscured by contaminants in Fig. 3). The preliminary analysis indicates that the strong levels at 2.48, 2.60, and 2.72 MeV all have $\ell = 3$ angular distributions. Most of these levels observed here in (p, p') have also been observed by Diamond and Tjøm[5] in the $^{205}Tl(d, d')^{205}Tl$ reaction at 13 MeV at lab angles of 125 and 150 deg. In addition, they were able to resolve two levels at 1.43 MeV separated by 15 keV.

References

1. See preceding article.
2. J. A. Nolen, thesis, Princeton University, 1965, unpublished.
3. S. Hinds et al., Phys. Letters 17, 302 (1965); W. C. Parkinson, D. L. Hendrie, H. H. Duhm, J. Mahoney, J. Saudinos, and G. Satchler, Phys. Rev. (Feb. 20, 1969).
4. S. Hinds et al., Nucl. Phys. 83, 17 (1966).
5. Richard Diamond (Lawrence Radiation Laboratory), private communication.

Table I. Energy levels seen in the $^{208}Pb(p, \alpha)^{205}Tl$ and $^{206}Pb(t, \alpha)^{205}Tl$ reactions.

E (MeV)	$^{208}Pb(p, \alpha)^{205}Tl$ σ_{max} (relative)	$^{206}Pb(t, \alpha)^{205}Tl$ σ_{max} (relative)
0.0	1	1
0.20	1.8	1
0.62	2	0.2
0.92	1.3	not seen
1.14	not seen	0.5
1.21	not seen	0.3
1.34	not seen	0.3
1.43	1.7	0.13
1.48	2.3	1.2
1.58	weak	0.1
1.86	weak	0.3
1.92	weak, wide	not seen
1.96	---	0.5
2.04	1.7	0.5
2.12	1.3	0.2
2.18	weak	not seen
2.30	weak, wide	not seen
2.40	weak, wide	---
2.43	---	0.1
2.49	---	0.17
2.55	2	not seen
2.60	---	0.3
2.74	---	0.1
2.90	5	not seen
3.48	wide	not seen
3.66	wide	not seen

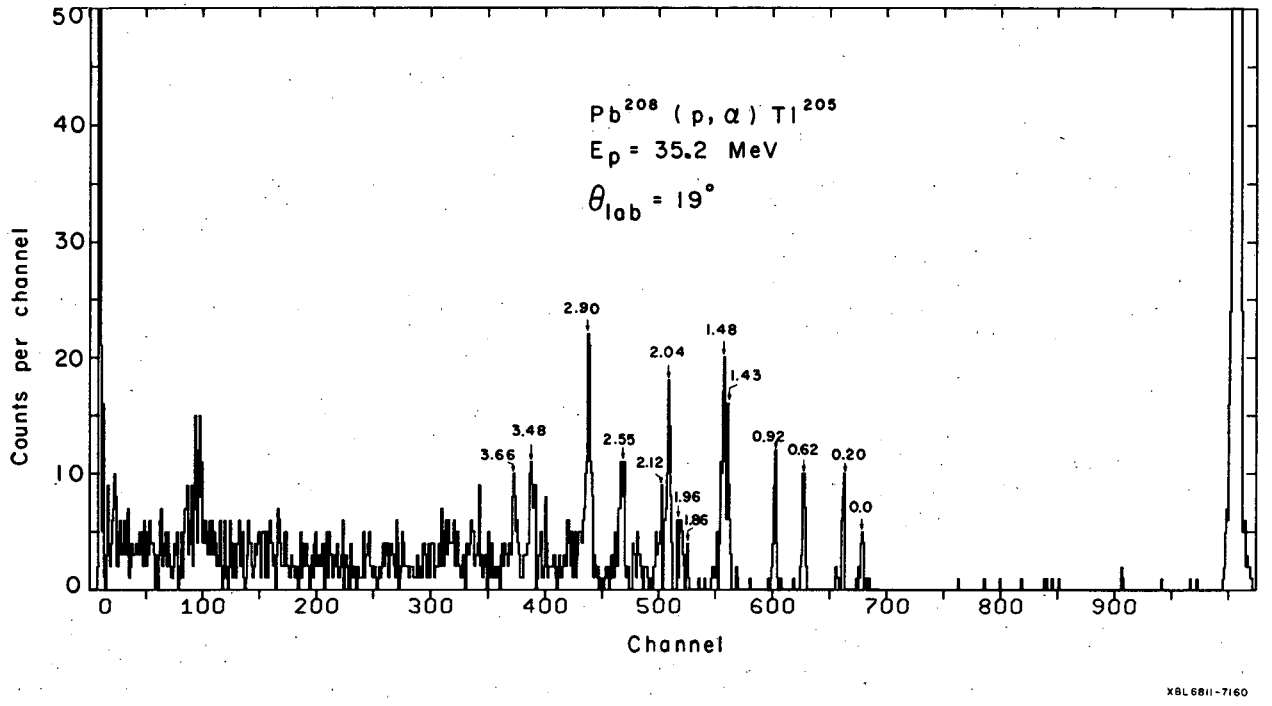

Fig. 1. Spectrum of α particles observed following proton bombardment of ^{208}Pb at 35.2 MeV; θ_{lab} = 19 deg.

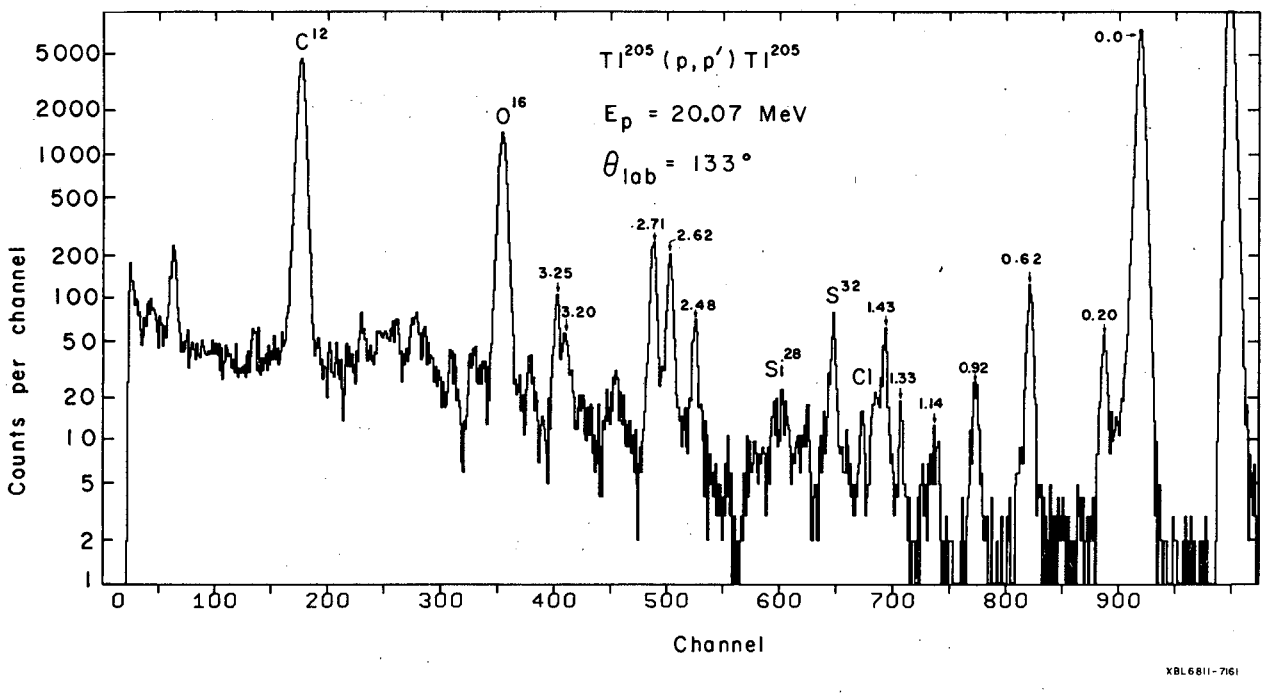

Fig. 2. Spectrum of protons scattered from ^{205}Tl at an incident proton energy of 20.07 MeV.

EXCITATION FUNCTIONS AND ANGULAR DISTRIBUTIONS OF α PARTICLES SCATTERED FROM ^{24}Mg

J. R. Meriwether,* C. Glashausser, D. L. Hendrie, J. Mahoney, E. A. McClatchie, and J. Sherman

The measurements of the differential cross section for the elastic and inelastic scattering of α particles from ^{24}Mg as a function of angle and incident energy begun in 1967[1] have been continued. The emphasis of the later experiments has been to extend the previous measurements to backward angles.

Twelve lithium-drifted-silicon detectors were arranged at 6-deg intervals from 107 to 173 deg. In addition, four counters were arranged at equal intervals from 56 to 92 deg to provide an overlap with the previously taken forward angle data. The output of each detector was individually amplified and routed into a 256-channel group of a ND-160 4096-channel pulse height analyzer. After a sufficient number of events were accumulated in each of the sixteen spectra, the data were transferred to a PDP-5 computer where the appropriate alpha groups were integrated and the cross section determined. At each incident energy between 24.25 and 40.0 MeV, after spectra were obtained from the counters, the entire counter assembly was rotated 3 deg and the counting procedure repeated. The incident energy was then changed by 250 keV and a new set of data taken. The incident energy was set to a precision of about 20 keV by using a 110-deg beam-analyzing magnet.

The total data now taken in these experiments now consist of the following: Differential cross sections of the $^{24}Mg(\alpha,\alpha)^{24}Mg$ g.s. and $^{24}Mg(\alpha,\alpha')^{24}Mg$ 1.368 MeV 2+ reactions have been measured at 3 deg angular intervals from 20 to 176 deg, at energies between 24.25 and 40.0 MeV in 0.25-MeV steps. These data thus define two surfaces in the $d\sigma/d\Omega$, $\theta_{c.m.}$, E space noted above, each surface being defined by 3392 points. Figure 1 is an isometric representation of part of the data, showing the elastic alpha differential cross section; only the earlier forward angle data are presented. Typical of the new data is the excitation function shown in Fig. 2. The large variations in the differential cross section become more pronounced as the angle increases. Work is now under way to understand these cross-section resonances in terms of highly excited states of the compound nucleus ^{28}Si.

Footnote and Reference

*Permanent address: University of Southwestern Louisiana, Lafayette, La.

1. J. R. Meriwether et al., in Nuclear Chemistry Annual Report, 1967, UCRL-17989, Jan. 1968, p. 52.

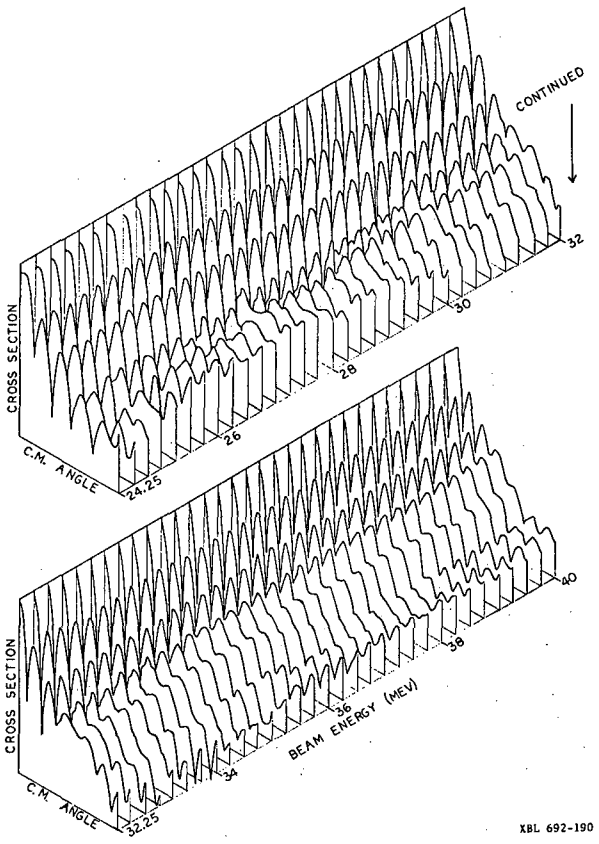

Fig. 1. An isometric representation of the differential cross section for $^{24}Mg(\alpha,\alpha)$ as a function of excitation energy. The angular range is from 20 to 113 deg.

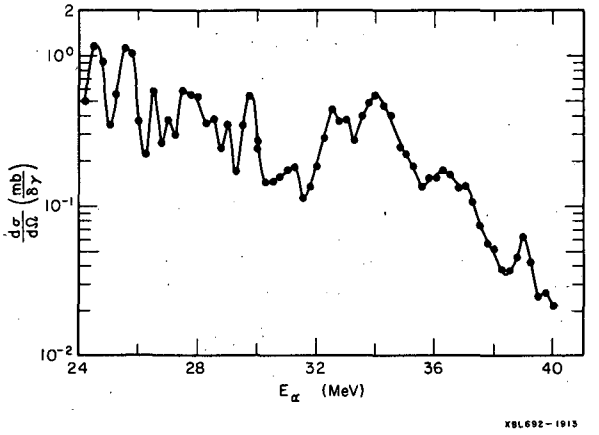

Fig. 2. Excitation function for elastic scattering from ^{24}Mg at 151.4 deg c.m. from 24- to 40-MeV incident α particles.

SPIN-FLIP PROBABILITIES ON ^{54}Fe AND ^{56}Fe

C. Glashausser, D. L. Hendrie, J. Moss, and J. Thirion†

Recent measurements[1] using the polarized proton beam of the Saclay cyclotron have provided an interesting problem in nuclear structure and scattering. The scattering asymmetries measured for the first 2^+ states of nuclei in which the neutron shell is closed at 28 (such as ^{54}Fe) differ greatly from the asymmetries for the first 2^+ states of neighboring nuclei (such as ^{56}Fe). In order to further understand this difference, we have performed a spin-flip measurement on the first 2^+ states of ^{54}Fe and ^{56}Fe. The resulting spin-flip probabilities (SFP) should provide, in general, more detailed information about the spin-dependent nucleon-nucleon interaction, as well as details of the wave functions of the two target nuclei.

The experiment reported here utilized the p, p'γ correlation method first explored by Schmidt et al.,[2] in which coincidences between protons and deexcitation γ rays perpendicular to the reaction plane are measured. A beam of 39.2-MeV H_2^+ (19.6-MeV protons) was provided by the 88-inch cyclotron. Two individually movable Si(Li) counters cooled to -40°C were used to detect the protons. Gamma rays were detected by a 40-cm^3 coaxial Ge(Li) counter. The electronics consisted of a high-rate amplifier and pile-up rejection system[3] for each counter. The energy outputs, gated by a fast-slow coincidence system, were fed into a multiplexed 4096 ADC and subsequently to an on-line PDP-5 computer. Coincidences created by feeding pulses through each system were

used to monitor the dead time.

The SFP can be obtained from the following expression for perpendicular geometry:

$$S(\theta) = (5/8\pi)\, \epsilon_\gamma\, \Omega_\gamma\, (R/N),$$

where $\epsilon_\gamma \Omega_\gamma$ is the efficiency–solid angle product for the γ detector, R the number of real coincidences, and N the number of singles counts detected by the proton counter; $S(\theta)$, except for small corrections due to finite geometry, is the SFP.

Figures 1 through 3 show the SFP for the first 2+ states of ^{54}Fe and ^{56}Fe; also shown are the asymmetries and cross sections for these states along with collective-model predictions which will be discussed shortly. It is obvious that the large differences between the asymmetries for the two states are not reflected in the SFP's.

In previous collective-model analyses of asymmetry data[1,4] it was found necessary to include the deformation of the spin-orbit potential as well as that of the real and imaginary parts of the optical potential. Sherif and Blair[5] have presented the most complete treatment of the deformed spin orbit (DSO) interaction in which the full Thomas (FT) term is calculated; earlier models used a simplified DSO term in which only the radial derivative of the potential was included. We have included both these models in this analysis.

Figures 1 through 3 show the predicted inelastic quantities using the FT term, simplified DSO, and no DSO. There is little to choose from among the calculations for the cross sections and SFP's; however, the FT term significantly improves the fit to the asymmetries. As a whole, however, the fits to the ^{54}Fe asymmetry and SFP are quite poor; in addition there is no indication of the experimentally observed differences between the ^{54}Fe and ^{56}Fe asymmetries and cross sections. Finally, the SFP's show structure, particularly near 70 deg, which is not suggested by the collective-model treatment. The predictions are not improved by reasonable variations in the optical parameters. However, preliminary results using a microscopic description of the nuclear states indicate that the SFP data may be explained in this way, although this model does not seem to be able to account for the differences in asymmetry.

Footnote and References

†Permanent address: CEN Saclay, Gif-sur-Yvette, S.-et-O., France.

1. C. Glashausser, R. de Swiniarski, J. Thirion, and A. D. Hill, Phys. Rev. 164, 1437 (1967).
2. F. H. Schmidt, R. E. Brown, J. B. Gerhart, and W. A. Kolasinski, Nucl. Phys. 52, 353 (1964).
3. F. S. Goulding, D. A. Landis, and R. H. Pehl, The Design and Performance of a High-Resolution High-Rate Amplifier System for Nuclear Spectrometry, UCRL-17560, May 1967.
4. M. D. Fricke, E. E. Gross, and A. Zucker, Phys. Rev. 163, 1153 (1967).
5. H. Sherif and J. S. Blair, Phys. Letters 26B, 489 (1968).

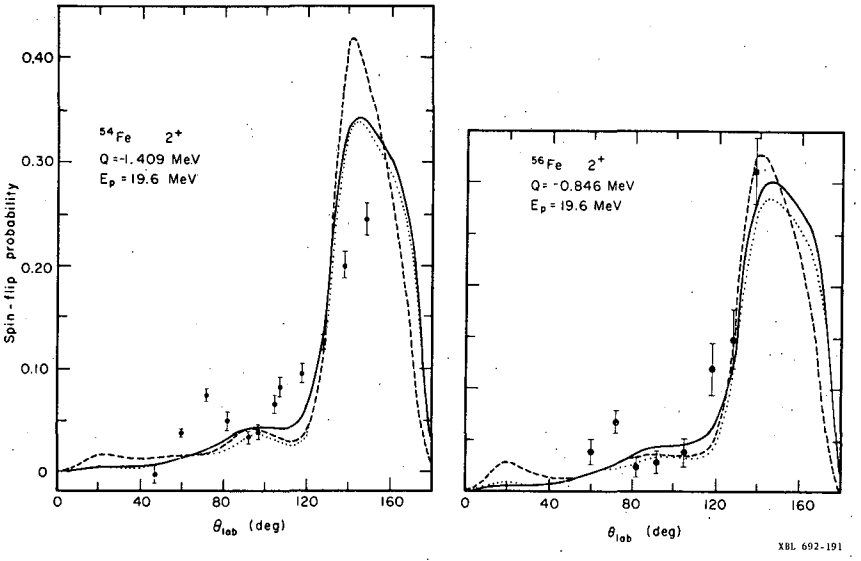

Fig. 1. Spin-flip probability for the first 2+ states of (left) ^{54}Fe and (right) ^{56}Fe. Curves are DWBA predictions using the FT term (——), simplified DSO (· · · · ·), and no DSO (- - - - -).

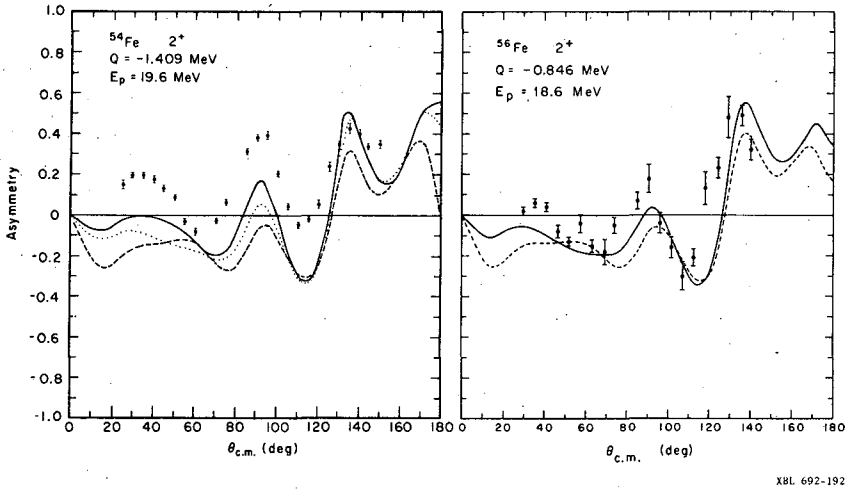

Fig. 2. Asymmetry for the first 2+ states of (left) ^{54}Fe and (right) ^{56}Fe. Curves are DWBA predictions using the FT term (——), simplified DSO (· · · · · ·), and no DSO (- - - - -).

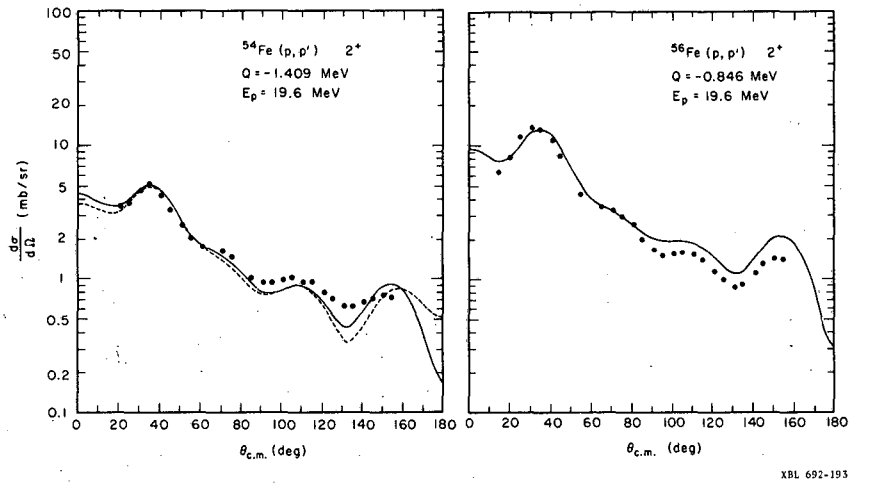

Fig. 3. Differential cross section for the first 2+ states of (left) ^{54}Fe and (right) ^{56}Fe. Curves are DWBA predictions using the FT term (———), and no DSO (-----).

NUCLEAR THEORY

THE ROLE OF INELASTIC PROCESSES IN (p, t) REACTIONS ON VIBRATIONAL-LIKE NUCLEI

R. J. Ascuitto and Norman K. Glendenning

The existent treatments of the two-nucleon transfer reaction all neglect the effect of inelastic processes. There are two circumstances under which this neglect is not justified. The first concerns a question of parentage. If in the reaction $p + (A+2) \rightarrow t + A$ the configuration of the group of A nucleons is the same in the target ground state as in the residual state of interest, then the usual treatment may be valid. However, if the state of motion of any of the core nucleons is different, then a description of the inelastic processes that produced this difference becomes essential, if in fact the state is excited in the reaction. Clearly most nuclear states, especially at higher excitation, fall into the second category; in the low-energy spectrum there will be some states with significant components belonging to both and some dominantly to the first. The two categories of states are illustrated schematically in Fig. 1. The second circumstance under which inelastic processes are crucial for a correct description arises when some inelastic transitions in either the target or residual system, or both, are so strong as to produce significant de-excitation back into the elastic channel (compound elastic scattering). In this circumstance the usual one-channel optical potential does not provide a good description of the relative motion in the vicinity of the nucleus.

We have reported elsewhere a method whereby the effects of the inelastic processes on transfer reactions can be incorporated conveniently.[1] The transfer reaction itself is treated, as usual, as weak, but the inelastic processes are calculated to all orders among the retained channels. Here we describe the first results of our investigation.

We have chosen the reaction ^{62}Ni(p, t) as a model on which to investigate the two effects described above. We adopt, for a description of some of the nuclear levels, the two-quasi-particle calculation of Arvieu and Veneroni.[2] To these we add a triplet of "two-phonon" states constructed from the coherent operator that produces the collective 2_1^+ state. The two quasi-particle states, including the collective one, belong to the first category of states that can be produced directly in a simple single-step transfer. The two-phonon states belong to the second category, which can be produced only if accompanied by an inelastic process either before or after the transfer. Possible routes for exciting two-phonon states are illustrated in Fig. 2.

The calculated cross sections for the (p, t) reaction in which all possible inelastic processes are taken into account are shown by the solid lines in Fig. 3. The most important inelastic transition is between the ground and 2_1^+ state, and its strength was adjusted to fit the experimental strengths in both proton and triton channels.[3] The p, t transition to the ground state and the collective 2_1^+ are the strongest ones. Concerning the remaining states the significant feature is that the transitions to the two-phonon states, which can be excited only indirectly, are as strong as those to the other noncoherent states, which can be excited directly. The significance of this result is, that to the extent that a state possesses two-phonon character, the inelastic processes cannot be neglected in calculating its two-nucleon transfer cross section.

Finally, for the states that can be excited by the direct transfer process, we calculated their cross sections in the usual way, where inelastic effects are neglected. To make this calculation conform to what is done in practice we adopted the elastic cross section, computed with the effects of inelastic scattering included, as the "experimental data," since of course any observed elastic cross section automatically contains these effects. Then we searched for the optical-model parameters that reproduce this cross section in the usual one-channel optical model (see Table I). This was done for both protons and tritons. These parameters we used in the DWBA calculations of the (p, t) reaction shown by dashed lines in Fig. 3.

The remarkable observation here is that the DWBA fails by as much as a factor of 10 and typically by a factor of 5 in this model nucleus in which the degree of collectivity is rather modest.

We have not yet investigated how weak the inelastic coupling must be before it may be neglected without significant error in a calculation of the (p, t) reaction, but we can say that in a typical vibrational-like nucleus the coupling is already too strong to be neglected.

References

1. N. K. Glendenning, Two-Nucleon Transfer Reactions, UCRL-18225, June 1968; R. J. Ascuitto and N. K. Glendenning, Inelastic Processes in Particle Transfer Reactions, UCRL-18529, Oct. 1968.
2. R. Arvieu and M. Veneroni, Compt. Rend. 250, 992 (1960); 250, 2155 (1960); 252, 670 (1960); R. Arvieu, Ann. Phys. (Paris) 8, 407 (1963).
3. We are indebted to E. Flynn for transmitting the Los Alamos data on (t, t') inelastic scattering before publication.

Table I. Proton and triton optical-model parameters. Those labeled "coupled" were used in a coupled-channel calculation. The strength of coupling to the collective 2^+ state was, for both projectiles, fixed by the experimental cross sections. The parameters labeled "uncoupled" reproduce the same elastic cross section as above in the usual one-channel optical model.

	V	W	W_D	r_V	r_W	a_V	a_W	V_{SO}	r_{SO}	a_{SO}
Proton										
Coupled	55.8	2.86	5.58	1.099	1.286	0.772	0.688	5.74	1.022	0.688
Uncoupled	56.157	3.992	5.832	1.105	1.280	0.774	0.655	5.74	1.022	0.688
Triton										
Coupled	154	24.3	0	1.24	1.36	0.674	0.912	1.91	1.24	0.674
Uncoupled	137.021	35.529	2.935	1.342	1.123	0.595	1.066	1.91	1.342	0.595

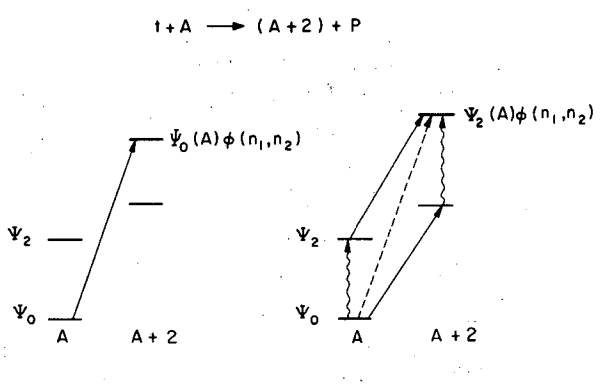

Fig. 1. In the left-hand figure, the state of interest in (A+2), as its wave function indicates, has the core nucleons A in the same state ψ_0 as in the target, and so can be produced directly as illustrated by the solid arrow. In the right-hand figure, the core is excited ψ_2 and so the direct transition shown with a dotted arrow is forbidden. Instead this state can be produced only if the core is excited by an inelastic collision with the triton before, or the proton after, the transfer reaction takes place.

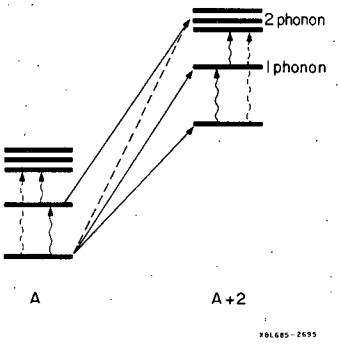

Fig. 2. In an ideal vibrational nucleus the inelastic transitions (shown by wiggly arrows) and transfer reactions (straight arrows) that are dashed are forbidden; the solid ones are enhanced over typical transitions to states of a nonphonon character. The two-phonon states are therefore examples of states that can be produced only through intermediate inelastic events.

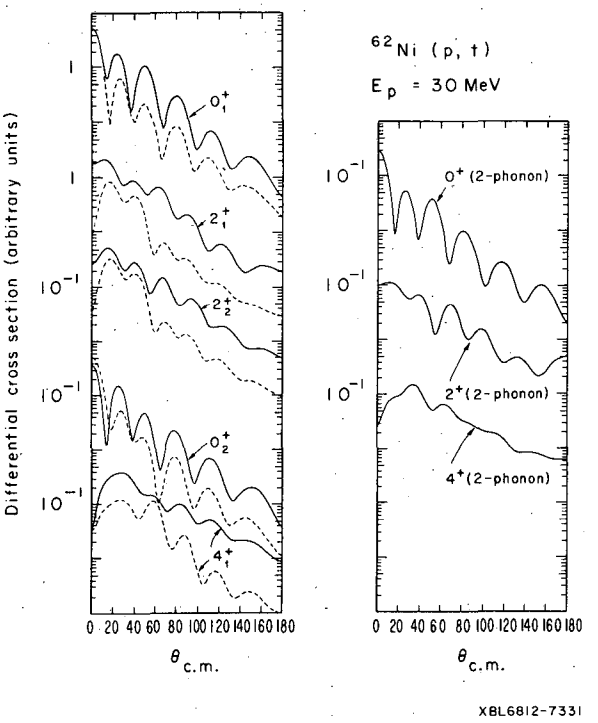

XBL6812-7331

Fig. 3. Cross sections for the ^{62}Ni(p, t) reactions at 30 MeV. Solid lines are calculated by solving the coupled equations, which include inelastic effects to all orders, whereas the reaction itself is treated in first order. The dashed curves show the result of neglecting the inelastic effects while nonetheless using optical-model parameters which do reproduce the elastic cross sections of the coupled systems, corresponding to the procedure adopted in practical applications.

INELASTIC SCATTERING FROM STRONGLY DEFORMED NUCLEI

Norman K. Glendenning and Raymond S. Mackintosh

To determine the importance of departures from strict rigidity of the shape of strongly deformed nuclei on previous determinations[1] of nuclear deformation parameters, we have carried out calculations of inelastic α-particle scattering in which some representation of the nonrigidity is included. We have used the collective wave functions of Faessler and Greiner[2] in which the ground band is mixed by the vibration-rotation interaction with the β and γ vibrational bands, as well as various bands of higher excitation, which we have ignored.

The scattering cross sections were calculated by the coupled-channel method[3] by use of an optical-model coupling with the nuclear surface expanded about the nonspherical equilibrium shape to second order in the vibrational coordinates; the second-order terms have an appreciable effect in some cases.

The nonrigidity would be expected to be most prominent at each end of the strongly deformed region: ^{152}Sm is "soft" to β vibration (the stretching mode) and ^{192}Os can be represented in a model calculation as a slightly deformed nucleus, very soft to γ vibrations. Accordingly, the

cross sections for the ground-state band of ^{152}Sm are shown in Fig. 1, where the cross section of the 6^+ level is increased by as much as 30% over the rigid rotor cross section. The Faessler-Greiner wave functions and elastic constants used give a reasonable fit to the ^{152}Sm energies. As the results depend on the elastic constants (the β vibrations are sometimes of doubtful collectivity) and on the optical-model coupling (some of our calculations suggest a reduction in coupling to levels less collective than rotational levels), the effect shown should be regarded as an upper bound.

We find that, as suggested by Diamond et al.,[4] the Faessler-Greiner values of $\langle \beta_2 \rangle$ for the 4^+ and 6^+ levels closely correspond to the stretching required to give the same fit to the spectra, supposing a constant inertial parameter. However, simply modifying the rigid rotor program to stretch the nucleus in the 6^+ state induces a smaller increase in the 6^+ cross section than that quoted above. The inclusion, among the coupled channels, of β-band levels results in a small increase in the 6^+ cross section.

From our series of calculations it is evident that in most cases the values determined for the multipole moments are not affected by nuclear nonrigidity, except for certain nuclei such as ^{152}Sm and ^{154}Gd, where there is considerable mixing of ground and β bands. In these cases B2 and B4 may need to be changed in order to fit the 6^+. We note that introducing a Y_6 deformation affects the forward angle 6^+ cross section, whereas stretching increases the cross section more uniformly.

We have also attempted to fit existing data[5] for the 2^+ and 4^+ γ band levels in ^{166}Er. We are able to fit the 2^+ level within the framework of quadrupole vibrations, with parameters that fitted the energy levels provided the complex optical-model coupling was reduced by a factor of 0.7. It was not possible to fit the 4^+ level by any manipulation (ad hoc band mixing, static Y_4 deformations, etc.) of a quadrupole vibration model; the existence of a degenerate β-band 0^+ level at this energy would give a reasonable fit but is most unlikely on theoretical grounds. The slope and the anomalously large magnitude of the 4^+ cross section suggests a direct excitation, and we believe that the $k\pi = 2^+$ band possesses some Y_4 vibrational character, which is supported by the work of Tjøm and Elbek.[6] We note the good I(I+1) nature of the band.

A typical fit to the γ band of ^{166}Er, without using any Y_4 excitations of the γ band, is shown in Fig. 2. The Davydov picture gives somewhat similar results to that shown in the figure provided that an asymmetry is used which is twice as large as that needed to fit the energy-level spacing.

References

1. Hendrie et al., Phys. Letters 26B, 127 (1968).
2. A. Faessler, W. Greiner, and R. K. Sheline, Nucl. Phys. 70, 33 (1965).
3. See, for example, N. K. Glendenning, Lectures, Varenna 1967, UCRL-17503, Aug. 1967.
4. R. M. Diamond, F. S. Stephens, and W. J. Swiatecki, Phys. Letters 11, 315 (1964) (they actually mention the Davydov-Chaban model, which has much in common with the Faessler-Greiner model).
5. B. G. Harvey et al. (Lawrence Radiation Laboratory), unpublished data.
6. P. O. Tjøm and B. Elbek, Nucl. Phys. A107, 385 (1968).

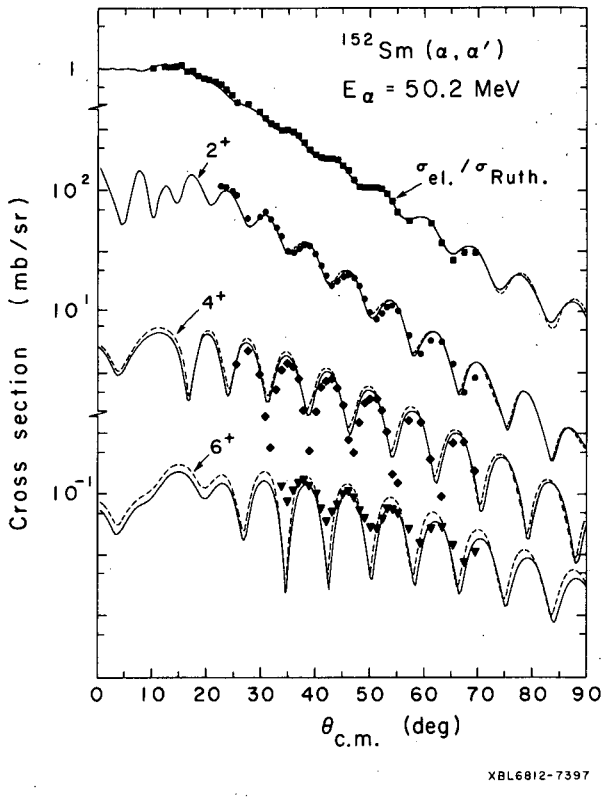

Fig. 1. Angular distributions for the ground band of ^{152}Sm, comparing the excitation of a rigid rotor and a rotor coupled to various vibrational modes. The data, shown for the 6^+, contain the unresolved 0^+ β bandhead. The solid curve shows the scattering when ^{152}Sm is treated as a rigid rotor; the dashed curve shows the effect of introducing vibrational degrees of freedom.

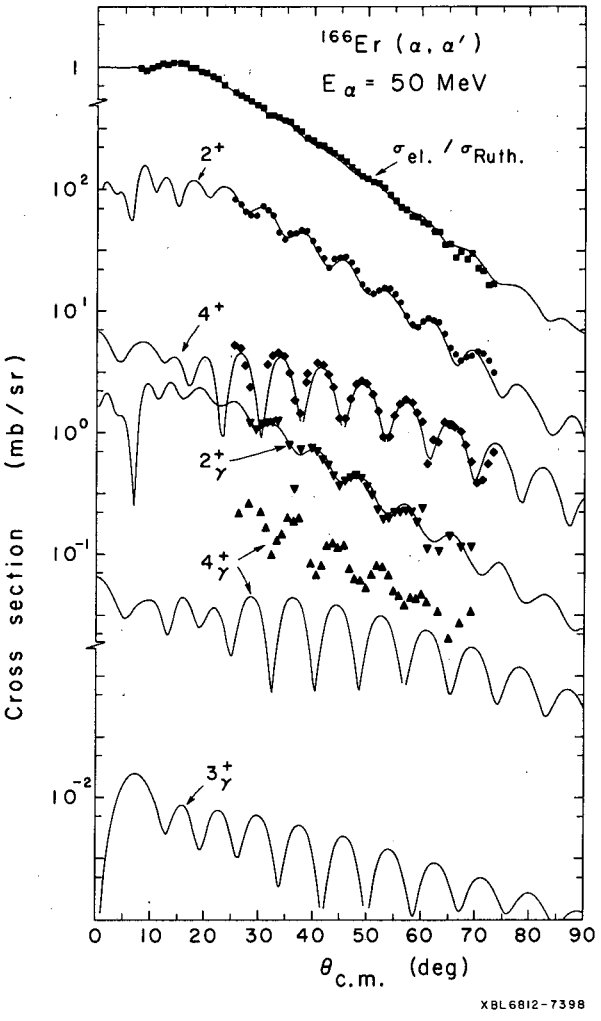

Fig. 2. Typical angular distribution to the ground band and γ band of ^{166}Er. There are no data for the 3^+ level.

CALCULATIONS OF THE ASYMMETRY IN THE INELASTIC SCATTERING OF 20.3-MeV PROTONS

C. Glashausser and R. de Swiniarski†

The asymmetry in the inelastic scattering of 20.3-MeV polarized protons has recently been measured at Saclay for a number of light and medium-weight nuclei.[1] Coupled-channels and DWBA calculations have been carried out here for several representative targets, including ^{24}Mg, ^{28}Si, ^{40}Ca, ^{90}Zr, and ^{92}Zr. Optical-model parameters have been obtained by searching on both elastic cross sections and polarizations with the code MERCY, a modified version of SEEK.[2] Very good fits to the elastic data were obtained for the heavier nuclei; the fits for the lighter nuclei were only fair, probably because the strong coupling between the ground state and the excited states was neglected.

Figures 1 and 2 show coupled-channel calculations for the 2^+ and 3^- states in ^{90}Zr and ^{92}Zr. The Oxford coupled-channels program[3] was used with only the real central term of the optical

potential deformed (REAL), with both real and imaginary central terms deformed (COMPLEX), and with the entire optical potential deformed (COMPLEX + DSO). Coulomb excitation was included in all the calculations. The addition of the imaginary and spin-orbit distortions improves the fit for both 2^+ and 3^- states. The COMPLEX + DSO predictions are still in poor agreement with the 2^+ data, however; the 3^- fits are considerably better, but a problem remains at forward angles. Both predictions are considerably improved by including a spin-orbit term of the full Thomas form;[4] these calculations are also shown in Figs. 1 and 2. The effect is particularly clear for the 2^+ data when the increase in magnitude is almost sufficient to match the first maximum for ^{92}Zr. (The effect of the full Thomas term is, however, slightly exaggerated, since the deformation parameter for the spin-orbit term β_{so} was set to 1.5 β.)

Microscopic model predictions for the 2^+ states in ^{90}Zr are no more successful; they are shown in Fig. 3. A simple proton transition of the type $[g_{9/2}]^2_{0^+} - [g_{9/2}]^2_{2^+}$ was assumed for the direct term; a Yukawa interaction of range 1.0 F was assumed. Core polarization (CP) was added according to the model of Love and Satchler[5] with an effective charge of 2.4 e. The predictions with the direct term only (D) are unable to account for the data. The addition of core polarization does not improve the fit, and even makes it considerably worse if the deformation of the spin-orbit term is neglected.

Macroscopic model calculations for ^{24}Mg are shown in Fig. 4. The first three states of this nucleus are usually described as members of a K = 0 rotational band; the deformation parameter β_2 is about 0.50. The fits to the elastic data are considerably modified when this coupling is included but the spherical parameters have been used for the predictions shown. For the 2^+ state the introduction of the full Thomas term again produces a considerable improvement in the quality of the fit, but the agreement is still only fair. On the other hand, the fits to the 4^+ data are very poor; they are not improved by the inclusion of the full Thomas term.

Footnotes and References

†NATO–Fulbright Fellow. Permanent address: Institut des Sciences Nucléaire de Grenoble (France).

1. A. G. Blair, C. Glashausser, J. Goudergues, R. M. Lombard, R. de Swiniarski, J. Thirion, and P. Vaganov, in Proceedings of the International Conference on Nuclear Physics, Tokyo, 1967.

2. M. A. Melkanoff, J. Raynal, and T. Sawada, UCLA report 66-10, Jan. 1966.

3. We are grateful to A. D. Hill for making this program available to us.

4. H. Sherif and J. S. Blair, Phys. Letters 26B, 489 (1968); H. Sherif and R. de Swiniarski, Phys. Letters 28B, 96 (1968).

5. W. G. Love and G. R. Satchler, Nucl. Phys. A101, 424 (1967).

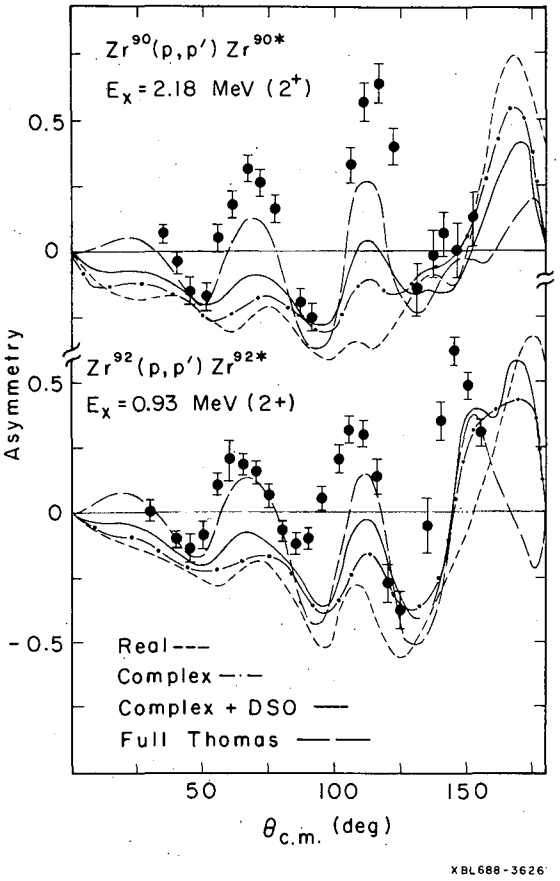

Fig. 1. Macroscopic model predictions for the asymmetry of the 2^+ states in ^{90}Zr and ^{92}Zr. In the calculations with the full Thomas term, β_{so} was set to 1.5 β.

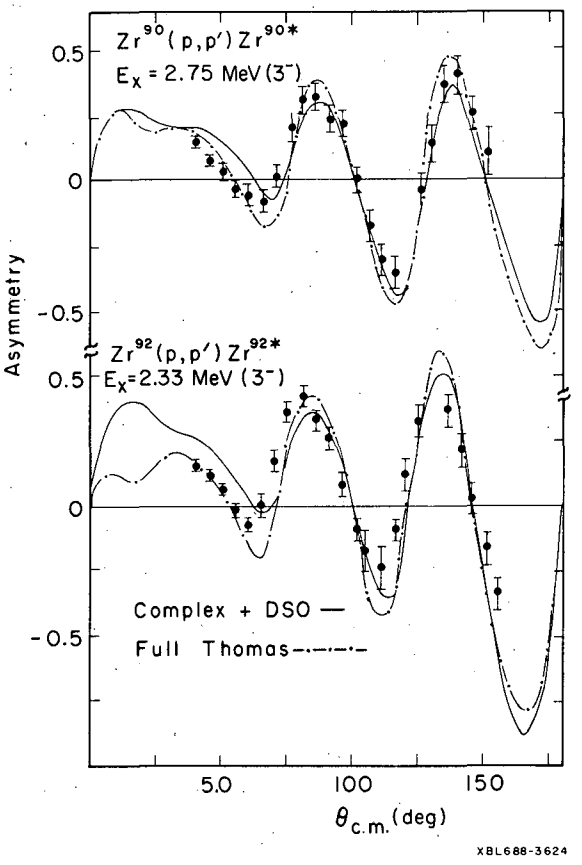

Fig. 2. Macroscopic model predictions for the asymmetry of the 3^- states in ^{90}Zr and ^{92}Zr. In the calculations with the full Thomas term β_{so} was set to 1.5 β.

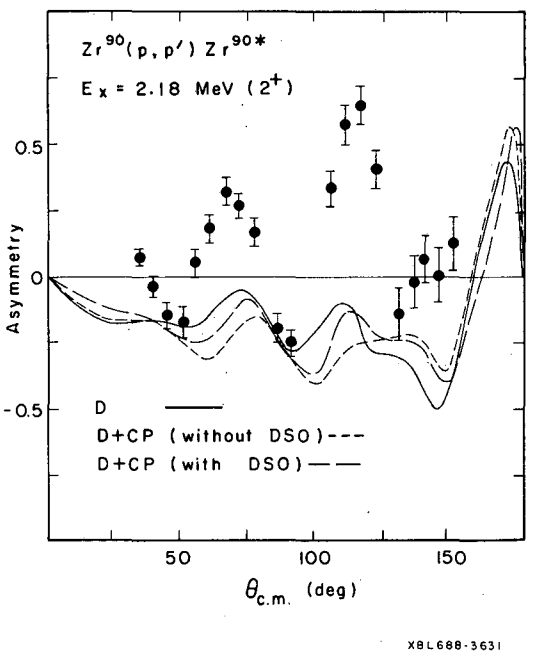

Fig. 3. Microscopic model predictions for the asymmetry of the 2.18-MeV state in ^{90}Zr.

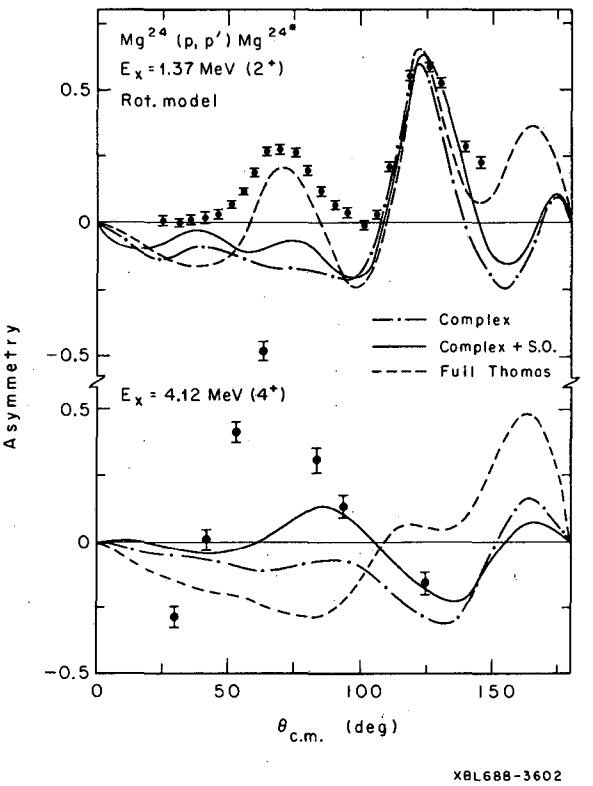

Fig. 4. Rotational model calculations for the asymmetry of the first 2^+ and 4^+ states in ^{24}Mg.

REALISTIC NUCLEAR SINGLE-PARTICLE HAMILTONIANS AND THE PROTON SHELL 114†

Heiner Meldner*

A simple self-consistent single-particle equation was investigated. The proposed model is designed to be particularly suitable for the calculation of (adiabatic) fission processes. The kernel of this integro-differential equation has a structure that allowed satisfactory reproduction of nuclear gross and shell structure data throughout the periodic table[1] with one constant set of five physical parameters. Hence, it seems that all future work in this direction has to confirm quantitatively the essential features determined here; in particular the nonlocality and rearrangement effects. Rearrangement energies appear explicitly, since the model discussed here, like self-consistent fields of appropriate many-body formalisms, yields different eigenvalue spectra and mass defects for different occupation functions.

The constant set of five parameters which was used in all calculations gave, e.g., a good fit to all difference data in the Ca region. One typical example is the first neutron hole state for ^{47}Ca: The observed mass difference to the ground state of about 2.6 MeV is reproduced by the present single-particle Hamiltonian that gives at least 6 MeV for the corresponding level spacing; i.e., more than 3.4 MeV result from orbital rearrangement (cf. Ref. 2).

The agreement with the mass data is also excellent for the $^{40}Ca \pm$(one nucleon) differences (see Ref. 1). For this example another type of rearrangement effect is revealed in Fig. 1. Conventionally, the eigenvalues were fitted to the experimental total binding energy differences; i.e., rearrangement was totally neglected. Of course, one could not do better in calculations that had

no chance to get the right order of magnitude for the total binding--as in local potential model fits. Here, in Fig. 1, the observed binding energy differences are reproduced within 0.2 MeV (cf. Ref. 1). However, due to rearrangement, they differ up to 6 MeV from the corresponding eigenvalues.

It might be argued that for some reason this model strongly overestimates rearrangement effects. But the magnitude of this model's rearrangement response can be checked to some extent by a comparison with the calculated isomer shifts due to single-particle excitations. Their order of magnitude seems to be confirmed by some relevant data. This confirmation corroborates the present results on rearrangement energies because of the well-known radial and eigenvalue shift correlation for single-particle potential models.

The magnitude of the rearrangement also casts doubts on shell-model calculations that use the observed total binding energy differences (of A±1 nucleon systems) as the eigenvalues for one constant single-particle Hamiltonian: Rearrangement destroys the orthogonality of the wave functions for single-particle states of nuclei with different excitations or nucleon numbers.

Figure 2 shows density distributions of protons and neutrons (lower and upper solid lines) for the five fixed parameters used here. One point of recent interest is the "neutron skin" of heavy nuclei,[3-6] the Johnson-Teller effect.[7] In ^{208}Pb, for example, the results of pionic scattering and isobaric analog-state analyses seem to disagree significantly with mu- or K-mesic experiments. There is a 2% rms radius difference between neutron and proton densities deduced from the former type of data,[3,6] whereas a difference of more than 10% is reported from μ^- atoms and K^- capture as well as from some optical and shell-model analyses.[4] The present self-consistent model gives rms(n) - rms(p) = 0.07 F, in excellent agreement with the value 0.07 ± 0.03 F due to an analysis of the isobaric analog state,[5] which is consistent with recent $\pi^\pm$-Pb scattering data.[6] In addition, the absolute magnitude of the ^{208}Pb rms charge radius given in Ref. 1 agrees perfectly with elastic electron scattering experiments yielding the value 5.42 ± 0.03 F.[8] One should notice the neutron skin or halo of ^{208}Pb shown in Fig. 2, which looks surprisingly large in view of the small rms radius difference. In ^{40}Ca, the effect is reversed. According to the present calculation, the rms radius of neutrons is 0.04 F smaller than that of the protons, in qualitative agreement with a recent optical-model analysis.[9]

The partial derivative $\partial E/\partial Z$ of the total binding energy (mass) changed considerably at the proton number Z = 114 when the present Hamiltonian was used for superheavy nuclei (cf. Ref. 1). This confirmed an earlier suggestion made 4 years ago by this author on the basis of a gap in the proton eigenvalue spectrum at Z = 114. The present calculations checked the real shell effect in the nuclear masses. For N = 172 and 186 they showed a significant decrease of the shell effect for isotopes far from the extrapolated beta stability line. At N = 172 and Z = 114, the lack of neutron excess seems to smooth out the step in the mass function to an insignificant wiggle (cf. Ref. 1). For 186 neutrons the shell effect has the magnitude observed at established magic numbers. Therefore, experiments on Z = 114 should aim for compound nuclei with mass numbers around 290 or higher.

Recent experiments seem to indicate the existence of nuclei with Z = 110 in the charge spectrum of cosmic ray nuclei.[10] An increasing amount of other effort is now being spent to produce such superheavy nuclei.[11]

Footnotes and References

†Condensed from UCRL-17801 Rev., Phys. Rev., to be published.

*Present address: Freie Universität Berlin, West Berlin.

1. For tables and further data see the shortened version of the original UCRL-17801 in the 1967 annual report. This year's abstract contains mainly additional information given in UCRL-17801 Rev., Oct. 1968.

2. H. Meldner, Nuovo Cimento 53B, 195 (1968).

3. D. H. Wilkinson, in 1968 International Symposium on Nuclear Structure, Dubna, USSR and Comments on Nuclear and Particle Physics I, 80 (1967).

4. L. R. B. Elton, Phys. Letters 26B, 689 (1968); G. W. Greenless, G. S. Pyle, and Y. C. Tang, Phys. Rev. Letters 17, 33 (1968); B. Holmquist and T. Wiedling, Phys. Letters 27B, 411 (1968); H. A. Bethe and P. J. Siemens, Phys. Letters 27B, 549 (1968).

5. S. A. Nolen, Jr., J. P. Schiffer, and N. Williams, Phys. Letters 27B, 1 (1968).

6. E. H. Auerbach, H. M. Querski, and M. M. Sternheim, Phys. Rev. Letters 21, 162 (1968).

7. cf. M. H. Johnson and E. Teller, Phys. Rev. 93, 357 (1954).
8. J. Bellicard and K. J. van Oostrum, Phys. Rev. Letters 19, 242 (1967).
9. N. Berovic, P. M. Rudolph, and S. M. Scarott, Phys. Letters 27B, 477 (1968).
10. P. H. Fowler, University of Bristol, Wills Physics Laboratory preprint. I am grateful to Professor N. Flerov for drawing my attention to this work.
11. G. T. Seaborg, Elements Beyond 100, Present Status and Future Prospects, to be published in Ann. Rev. Nucl. Sci. (1968); S. G. Thompson (Lawrence Radiation Laboratory), private communication; N. Flerov, in 1968 International Symposium on Nuclear Structure, Dubna, USSR; A. M. Weinberg, Phys. Today 20 [6], 23 (1967).

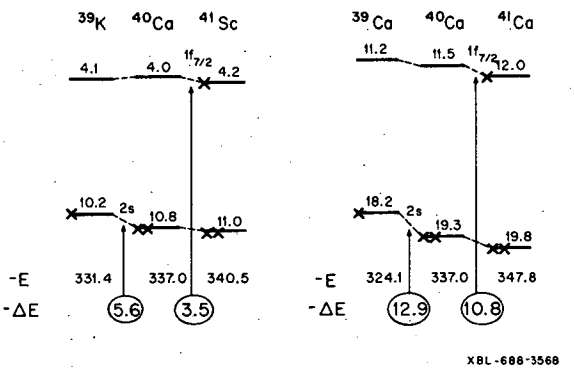

Fig. 1. Example of rearrangement effects: N = Z = 20 shell±(one nucleon). Compare the eigenvalues/MeV (arrows) with the circled total binding energy differences, ΔE/MeV. An excellent fit to the data results (cf. Ref. 1) when a pairing correction of 2.4 MeV is added for ^{40}Ca. Conventionally, the eigenvalues are identified with total binding-energy differences.

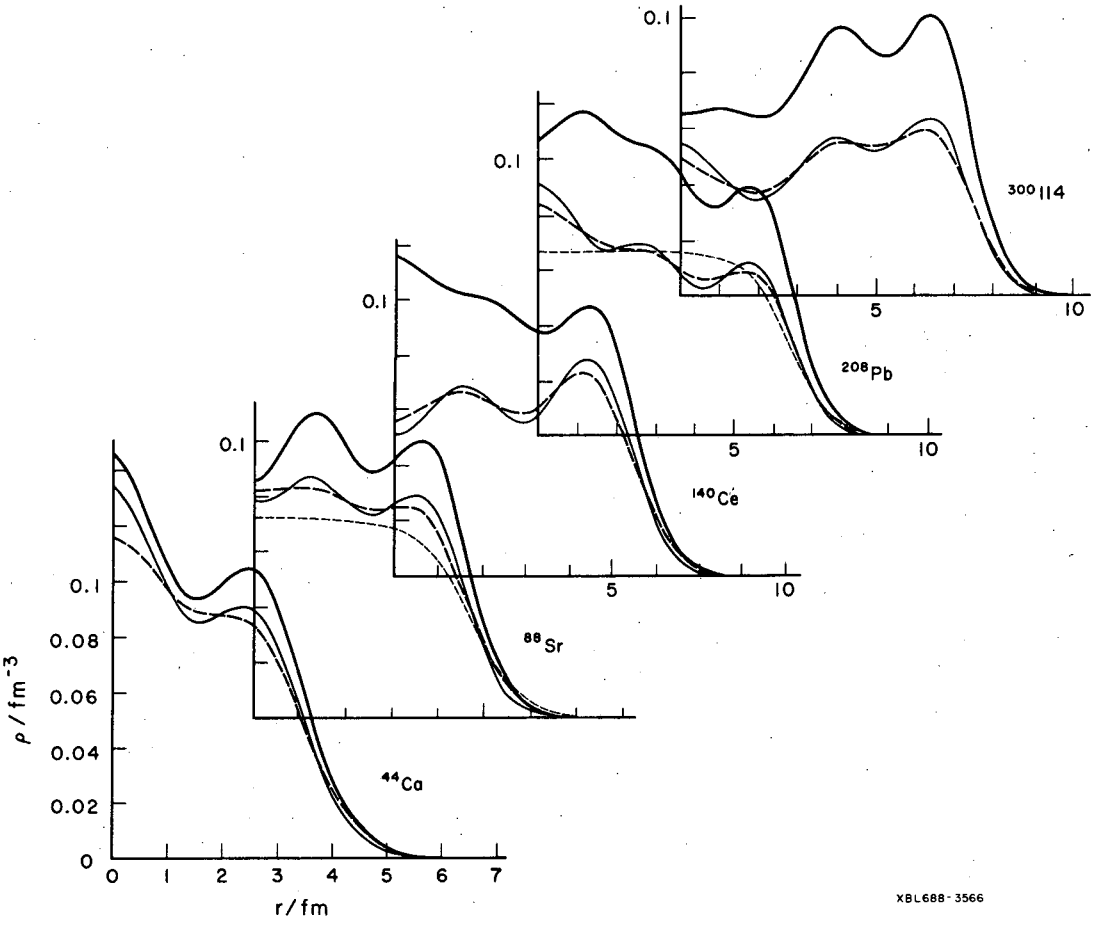

Fig. 2. Upper and lower solid curves give the density distributions of protons and neutrons for some nuclei on the beta stability line. The dashed curves are the nuclear charge densities calculated from the corresponding (bare) proton densities. Examples of Fermi function fits to electron scattering data are shown as dotted curves.

SHELL AND PAIRING EFFECTS IN THE FISSION PROBABILITY

L. G. Moretto, † R. C. Gatti, S. G. Thompson, and J. T. Routti*

Over the past few years a large amount of experimental data has been obtained on the fission cross sections for nuclei below radium. [1] There have been difficulties in the complete interpretation of these data.

If the total compound nucleus cross section can be either measured or calculated, then the ratio σ_f/σ_R can be used to evaluate the ratio between the fission width and the total decay width Γ_f/Γ_T. Since the charged-particle evaporation is highly hindered in heavy nuclei, the relation $\Gamma_f/\Gamma_T = \Gamma_f/\Gamma_f + \Gamma_n$ holds, where Γ_n is the neutron decay width. The theoretical analysis of the experimental data is therefore reduced to the evaluation of Γ_f/Γ_n.

From statistical considerations the following expressions for Γ_f and Γ_n are obtained: [2]

$$\Gamma_f = \frac{1}{2\pi\rho(E)} \int_0^{E-B_f} \rho_s(x)\,dx, \quad \Gamma_n = \frac{2}{2\pi\rho(E)} \int_0^{E-B_n} (E-B_n-x)\rho_n(x)\,dx, \qquad (1)$$

where $\rho(E)$ is the compound nucleus level density, $\rho_s(x)$ is the level density at the fission saddle point, $\rho_n(x)$ is the level density of the nucleus after neutron emission, and B_f, B_n are the fission barrier and the neutron binding energy respectively.

The quantities that contain nuclear information are (a) the level densities at the fission saddle point and for the residual nucleus after neutron emission, (b) the fission barrier height, and (c) the neutron binding energy.

When one uses the level density expressions obtained for a Fermi gas (a set of fermions, non-interacting, and distributed on equally spaced single-particle levels), it is difficult to fit the experimental ratio Γ_f/Γ_T over a large range of excitation energies. An example of this difficulty is shown in Fig. 1. The experimental values of Γ_f/Γ_T are shown for the reaction ^{197}Au(^{4}He, fission), together with the values of Γ_f/Γ_T fitted to the lowest 15 MeV above the fission barrier. When the function is extended at higher excitation energies, it overshoots the experimental data. Such a discrepancy is even larger, since σ_f/σ_R is bigger than the true Γ_f/Γ_T because of the multiple-chance fission, which becomes very relevant at high excitation energies.

It is reasonable to think that such a failure is due not to inadequacy of the expressions (1) but most likely to the Fermi gas expressions for the level densities, which may not be sufficiently realistic.

The main deviations of a nucleus from the Fermi gas model are two:
(a) the presence of shells generated by the bunching and the degeneracy of the single-particle levels;
(b) the pairing interaction that generates a correlation similar to superconductivity in metals.

The first effect may be of great importance in the evaluation of Γ_n for nuclei near closed shells, whereas it is expected to be negligible as far as Γ_f is concerned, since for the large saddle-point deformations the single-particle levels should be almost completely debunched.

The second effect is rather small for normal nuclei at sufficiently high excitation energies, and therefore not very important in the evaluation of Γ_n. However, at the fission saddle point large pairing effects seem to be present, and therefore it may be dangerous to exclude them in the evaluation of Γ_f.

On this basis, we introduce the shell effects in the evaluation of Γ_n, making a very simple correction for the pairing, and we introduce the pairing effect in the expression for Γ_f in detail without making any shell correction.

Level Density Including Shell Effects

The shell effects are included in the level density obtained by using the relations developed by Gilbert.[3] The model assumes an originally uniform single-particle level spectrum which is periodically bunched. In this way energy gaps corresponding to the shell's gaps in real nuclei are generated. The bunching parameter b and the period d define the magnitude of the energy gap, $\delta = bd$. The parameter b ranges in value from 0 (no bunching) to 1 (complete bunching). The density of single-particle states is represented as in Fig. 2.

The single-particle level density within each bunch is $G' = G1/(1-b)$, where G is the single-particle level density of the unbunched spectrum.

The position of the neutron and proton Fermi levels with respect to the shells is defined by the parameters Φ_N and Φ_Z, expressed by the relations

$$\Phi_N = \frac{|N-N_0|}{\Delta N}, \qquad \Phi_Z = \frac{|Z-Z_0|}{\Delta Z},$$

where ΔN and ΔZ are the number of neutrons and protons in a shell, and $|N-N_0|$ and $|Z-Z_0|$

represent the number of particles or holes separating a nucleus from a closed shell. Examples of level densities are shown in Fig. 3.

Level Density Including Pairing Effects

The model here is represented by a system of uniformly spaced doubly degenerate single-particle levels (uniform model) populated by fermions which interact through a residual interaction as described by Bardeen et al.[4] Because of this residual (pairing) interaction the nucleons are correlated pairwise, and the energy necessary to break a pair of nucleons is $2\Delta_0$, where Δ_0 is given by[4]

$$\frac{2}{gG} = \int_{-w}^{+w} \frac{d\epsilon}{\sqrt{\epsilon^2 + \Delta_0^2}},$$

where g is the density of the doubly degenerate single-particle levels, G is the pairing strength, ϵ is the energy in the single-particle spectrum, and $\pm w$ is the energy range over which the pairing correlation extends.

When pairs are broken by introducing excitation energy, the unpaired particles occupy single-particle levels that become unavailable for the pairing correlation, which therefore decreases. It is possible to account statistically for such an effect by making Δ temperature-dependent, according to

$$\frac{2}{gG} = \int_{-w}^{+w} \frac{\operatorname{tgh}\left[\frac{1}{2}\beta\sqrt{\epsilon^2 + \Delta^2(\beta)}\right]}{\sqrt{\epsilon^2 + \Delta^2(\beta)}}\, d\epsilon, \qquad (2)$$

where $\beta = 1/t$, t being the nuclear temperature.

The dependence of Δ on t can be seen in Fig. 4. We can observe that Δ decreases with increasing t until it vanishes with a vertical tangent at a critical temperature, t_c. Beyond such a value the system reverts back to the uncorrelated Fermi gas conditions.

By using expression (2) it is possible to evaluate the equations of state of the system, such as energy, entropy, specific heat, and also level density as a function of temperature.

All of these quantities revert back to those of an uncorrelated Fermi gas beyond the critical temperature.

So far we have implicitly assumed we are dealing with an even-even nucleus. When the odd-A or odd-odd nuclei are to be considered, one takes into account the effect of the one or two initially unpaired particles by adding to the corresponding even-even nucleus excitation energy the quantity Δ or 2Δ.

Calculations

Both the saddle-point and ground-state level densities are evaluated as a function of the nuclear temperature together with the respective excitation energies. Such tables of level density and excitation energy as a function of temperature can be interpolated and the quantities Γ_f and Γ_n can be evaluated. The expression $\Gamma_f/(\Gamma_n + \Gamma_f)$ is then calculated and compared with experimentally determined values by means of a minimization procedure. An example of a preliminary attempt to fit the experimental data for ${}^{206}_{82}\mathrm{Pb} + {}^{4}_{2}\mathrm{He} \rightarrow {}^{210}_{84}\mathrm{Po}$ is shown in Fig. 5.

Footnotes and References

†Present address: Laboratorio di Radiochimica, Università di Pavia, Pavia, Italy.
*Health Physics Group, Lawrence Radiation Laboratory, Berkeley.

1. S. G. Thompson, Arkiv Fysik 36, 267 (1967).
2. J. R. Huizenga, R. Chaudhry, and R. Vandenbosch, Phys. Rev. 126, 210 (1962).
3. Arnold Gilbert, UCRL-18095, Feb. 1968.
4. G. Bardeen, L. N. Cooper, and J. R. Schrieffer, Phys. Rev. 108, 1175 (1957).

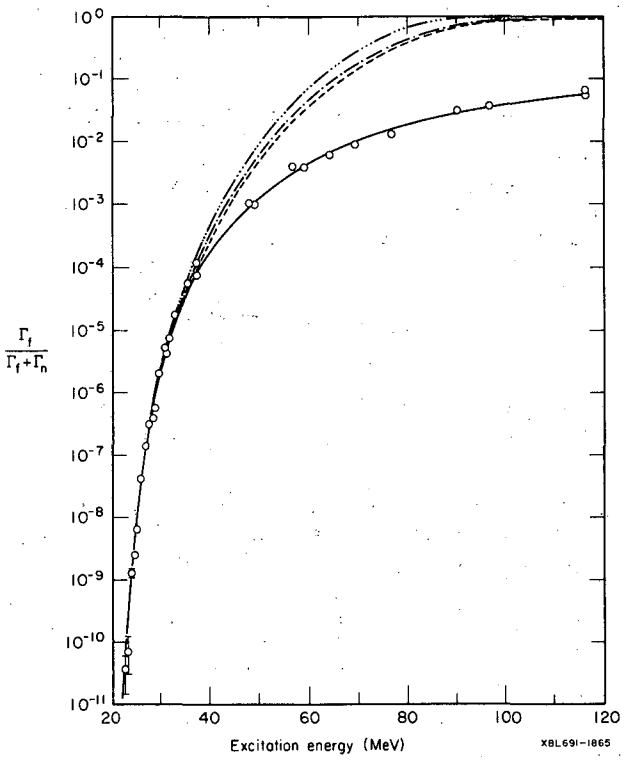

Fig. 1. Ratio $\Gamma_f/\Gamma_f + \Gamma_N$ in ^{4}He-induced fission of ^{197}Au

——— Experimental data
— — — No correction
—·—·— Angular momentum correction ($_2B_n$ = 20 MeV)
—···—··· Angular momentum and higher-order fission corrections ($_2B_n = {}_3B_n = \cdots = {}_{10}B_n$ = 8.270 MeV)

The high energy data for each of the last three curves were calculated by using parameters derived from fitting low energy (up to 40 MeV) data. The value of the parameters were as follows:

B_f = 22.1 MeV
a_f = 17.8 (MeV)$^{-1}$
a_n = 13.2 (MeV)$^{-1}$
$_1B_n$ = 8.270 MeV
$\hbar\omega$ = 0 MeV

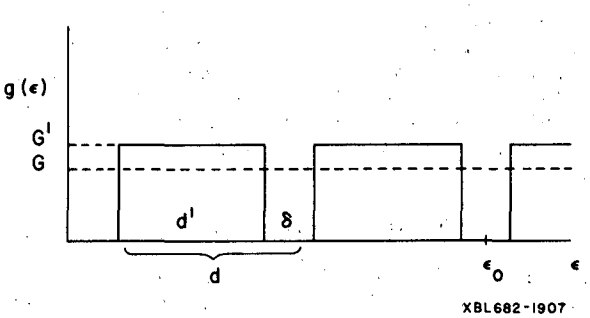

Fig. 2. Periodic spectrum for the bunching model. The density of single particles is G' between two shell gaps; its average value is G; d is the period, δ the size of the shell gap, and ϵ_0 the center of a gap.

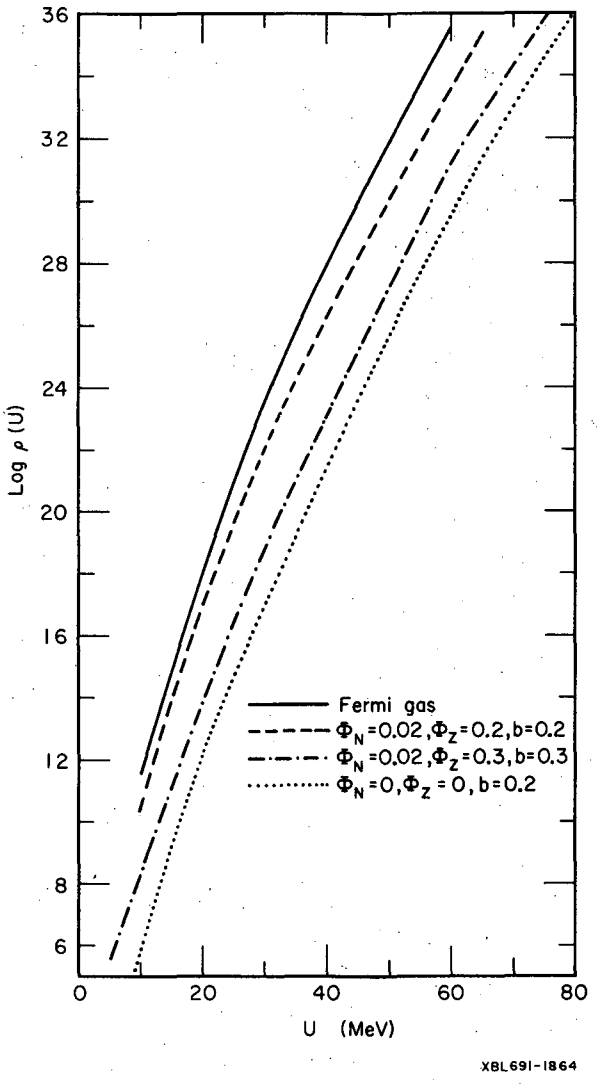

Fig. 3. Level densities for nuclei of $A \approx 210$. The case $\Phi_N = \Phi_Z = 0$ corresponds to a doubly magic nucleus like ^{208}Pb. One neutron particle or hole away from a closed shell contributes 0.02 to Φ_N, and one proton particle or hole contributes 0.03 to Φ_Z. The level density evaluated for an unbunched Fermi gas is shown for comparison.

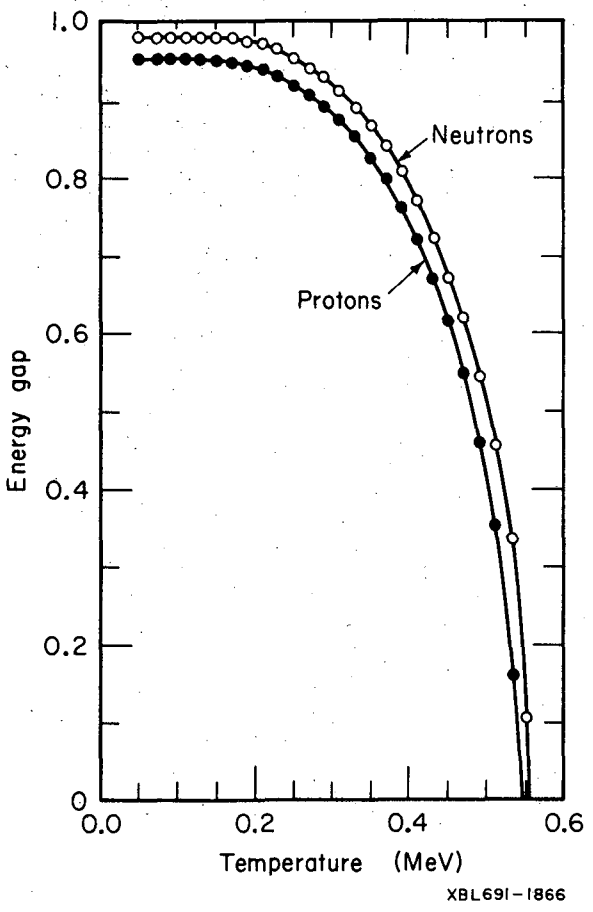

Fig. 4. Temperature dependence of the gap parameter.

Fig. 5. Plot of Γ_f/Γ_n versus excitation energy in MeV for $^{206}Pb + ^{4}He \rightarrow {}^{210}_{84}P_0 \rightarrow$ fission. Experimental points are indicated by triangles; the calculated curve is indicated by squares. The calculated curve takes into account the effect of pairing at the fission saddle point and the influence of shell structure in Γ_n using Gilbert's relations (Ref. 3). $a_f = 17.97\ MeV^{-1}$, $a_n = 16.42\ MeV^{-1}$, $B_f = 20.9$ MeV, d = 8.9 MeV, b = 0.1, $\Delta_n = 1.0$ MeV, $\Delta p = 0.95$ MeV.

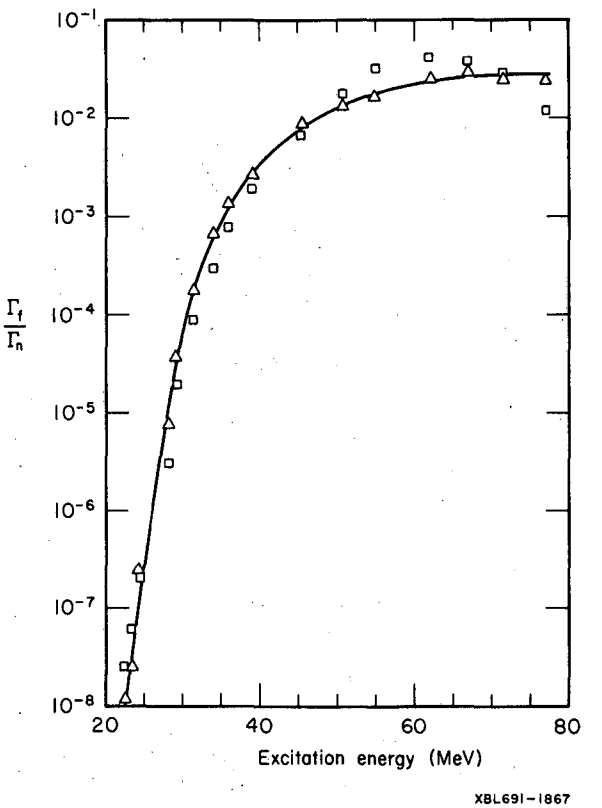

NUCLEAR STRUCTURE AND STABILITY OF HEAVY AND SUPERHEAVY NUCLEI

S. G. Nilsson† and C. F. Tsang*

Potential energy surfaces as a function of quadrupole and hexadecapole distortions have been worked out on a deformed shell model for heavy and superheavy nuclei, $150 < A < 310$. These surfaces have been normalized to the average trend given by the liquid-drop model by means of a generalized Strutinsky prescription.[1] By this means we hope to obtain both the spectroscopic (level schemes) and macroscopic (total binding energy) properties correctly.

For the known region our level schemes compare well with experiments. We find a proton magic number at Z = 114 and neutron magic number at N = 184, confirming previous studies by various authors. From the lowest minima in the energy surfaces we obtain the ground-state masses and deformations, which can be compared directly with experiments (Figs. 1 and 2).

The occurrence of a secondary stable (isomeric) state at some distortions away from the ground state is seen in a large number of nuclei near A = 240 ($Z \approx 94$). These correspond to the so-called shape (fission) isomers which have recently stimulated intensive experimental interests.

Spontaneous fission half lives[2] and alpha and beta stabilities have been studied. These turn out to be in fair agreement with experiments for the actinides. For the superheavy nuclei,[3] one finds an island of stability centering around Z = 114 and N = 184. From the total half-lives, several candidates can be suggested that may perhaps live long enough to be found in nature, if not in earthly matter, then possibly in the cosmic radiation.

Footnotes and References

†Present address: Department of Mathematical Physics, Lund Institute of Technology, Lund, Sweden.

*Theoretical Physics Group, LRL-Berkeley.

1. S. G. Nilsson, Nuclear Structure and Superheavy Elements, UCRL-18355, Sept. 1968.
2. S. G. Nilsson, J. R. Nix, A. Sobiczewski, Z. Szymanski, S. Wycech, C. Gustafson, and P. Moller, Nucl. Phys. A115, 145 (1968).
3. S. G. Nilsson, S. G. Thompson, and C. F. Tsang, Phys. Letters 28B, 458 (1969).

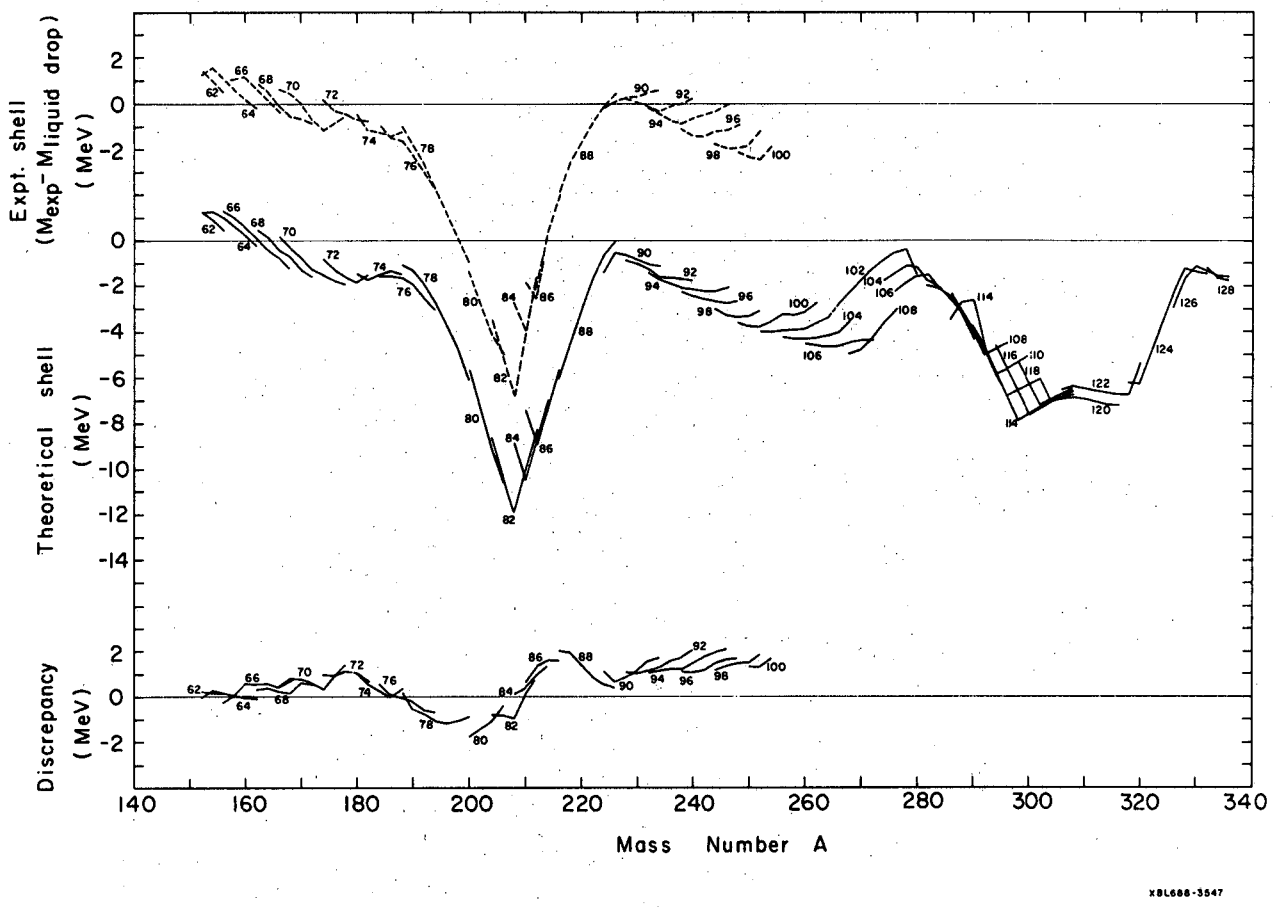

Fig. 1. Experimental and theoretical mass values for $150 < A < 310$ relative to the spherical liquid-drop values.

Fig. 2. Empirical hexadecapole (β_4) distortions of the rare earth nuclei as compared with our calculated values.

—•— Present theoretical (polarization, pairing, and Coulomb effects included)

Experimental, Hendrie et al.

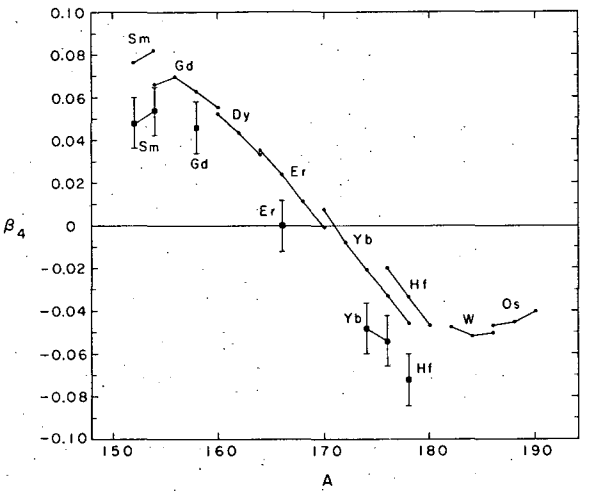

STABILITY OF SUPERHEAVY NUCLEI AND THEIR POSSIBLE OCCURRENCE IN NATURE†

S. G. Nilsson,* S. G. Thompson, and C. F. Tsang‡

Ground-state masses and potential energies of superheavy nuclei--i.e., nuclei around Z = 114 and N = 184--as a function of deformations have recently been calculated.[1] From this we have been able to estimate the alpha and spontaneous fission half-lives and to test for beta stability of these nuclei. The results are summarized in Fig. 1.

There are great uncertainties in this figure, as discussed in the full paper, but the main features should be reliable. The longest spontaneous fission half-lives center around the doubly magic nucleus $^{298}114$, and the half-lives decrease rapidly as one goes away from this nucleus. The alpha half-lives increase as one goes to lighter elements. The beta-stable nuclei lie approximately along the extrapolated beta stability line given by Green. The total lifetime appears to be longest around $^{294}110$, which may perhaps survive somewhere in nature.

The element 110 has chemical properties similar to those of platinum. A preliminary search for it in a platinum ore has not been fruitful. The experiments indicate an upper limit on the presence of the element as 1 part in 10^{10} of platinum. On the other hand, the experiments are unable to detect it if the half-life is less than $\approx 2 \times 10^8$ years. The primary cosmic radiation is estimated to have a lifetime of 10^4 to 10^{10} years, so that possibly it is more hopeful to look in the cosmic rays, where one may perhaps see a few more superheavy nuclei around $^{294}110$. Recently P. H. Fowler, P. B. Price, and R. M. Walker have conducted a balloon experiment to look for very heavy nuclei in the cosmic rays. Their data are still under analysis.

Footnotes and References

†Resumé of paper Physics Letters, 28B, 458 (1969).

*Present address: Department of Mathematical Physics, Lund Institute of Technology, Lund, Sweden.

‡Theoretical Physics Group, Lawrence Radiation Laboratory, Berkeley.

1. S. G. Nilsson, C. F. Tsang, A. Sobiczewski, Z. Szymanski, S. Wycech, P. Möller, and C. Gustafson, to be published in Nucl. Phys.

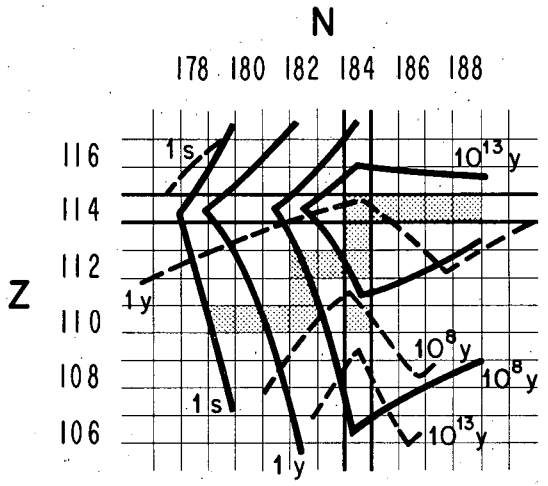

Fig. 1. Contours of theoretical half lives in the vicinity of Z = 114 and N = 184. The thick dark lines are contours of spontaneous fission half lives. The broken lines are contours of alpha half lives. Beta stable nuclei are shaded.

S-WAVE SHAPE-DEPENDENT SCATTERING PARAMETERS OF THE PROTON-PROTON INTERACTION†

R. J. Slobodrian*

The s-wave nucleon-nucleon interaction between 0 and 10 MeV can be parameterized by a convergent power series, [1] and thus can be approximated by a polynomial

$$K = \sum_{0}^{n} A_n E^n, \tag{1}$$

where E is the energy, usually expressed in MeV. The relation of (1) with the $^1S_0$ p-p phase shifts and more currently used scattering parameters is obtained through the equation K = RFG:

$$G = C^2 k \cot \delta_0 + \frac{1}{R} h(\eta) = -\frac{1}{a_p} + \frac{1}{2} r_e k^2 - P r_e^3 k^4 + Q r_e^5 k^6 - \cdots \tag{2}$$

where $C^2 = \frac{2\pi\eta - 1}{e^{2\pi\eta} - 1}$, $R = \frac{\hbar^2}{M_p \epsilon^2}$, $h(\eta) = \mathrm{Re}\,\frac{\Gamma'(-i\eta)}{\Gamma(-i\eta)} - \ell n(\eta)$,

k is the relative momentum in units of $\hbar$, $\eta = \epsilon^2/\hbar v$ (Coulomb parameter), ϵ is the proton charge, v is the relative velocity, a is the proton-proton scattering length, r_e is the effective range, and P, Q ··· are known as shape-dependent parameters, i.e., their values and sign depend on the detailed shape of the potential well in a Hamiltonian formulation or on model characteristics in general. Conversely, an empirical determination of such parameters would prescribe a shape for the potential of interaction or determine a model.

Calculations of the parameters P and Q for different well shapes or models are available in the literature. [2-4] Noyes [3] attempted first a determination of the shape parameter P for the ^1S proton-proton interaction. This work was based on five accurate phase shifts at 0.38243, [5] 1.397, 1.855, 2.425, and 3.037 MeV. [6] A summary of difficulties associated with a determination based on these five phase shifts may be found in Ref. 7. However, the ambiguity is reduced [7] if the effective-range expansion analysis includes the higher-energy data of Worthington, McGruer, and Findley. [8] Heller [9] has recently added the phase shift from data at 9.69 MeV [10] to the low-energy phase shifts of Refs. 5 and 6, and performed fits up to and including the parameter Q. Heller recognized that the radius of convergence of (1) or (2) is approximately 10 MeV, and

therefore the number of terms necessary may extend beyond the assumed polynomial. The errors of the parameters P and Q turn out to be large. From a practical point of view, the energy gap between 3.037 and 9.69 MeV is very large, and conclusions drawn from such a set of data should be viewed warily. Noyes and Lipinski[11] have recently reanalyzed the data at 9.69 MeV, extrapolating the recent information on spin-correlation parameters.[12] They conclude that at 9.69 MeV there is modest evidence for shape dependence consistent with OPE. However, the cross section measured at 9.69 MeV may be systematically high, as noted by several authors,[11, 13, 14] and thus conclusions drawn from these data at a single energy may be subject to revision. Noyes and Lipinski[11] nevertheless also conclude that the shape correction is established beyond reasonable doubt if the results below 3 MeV and near 27 MeV are added to the result at 9.69 MeV. In the opinion of this author the evidence drawn from data between 0 and 3 MeV is questionable, as explained in Ref. 7, and therefore another attack on the problem is very desirable. The advent of new cross-section results at 6.141, 8.097, and 9.918 MeV accurate to less than 1%,[14] and their phase shifts, has made possible determination of the shape-dependent parameters P and Q, with reanalysis of the existing experimental cross sections of Refs. 5, 6, 8, and 10.

The reanalysis of previous experimental data was advisable in order to avoid possible systematic differences in the central values of the phase shifts, related to criteria employed in the analysis, values of fundamental constants, approximations employed for relativistic effects, etc. A program due to Knecht[15] was used for the phase-shift analysis. Another program was written for the effective-range expansion analysis. Both programs were used with CDC 6600 machines of the LRL computing center. The aim of this work has been to obtain the shape-dependent coefficients P and Q of the effective range expansion on a basis as empirical as possible, and ascertain their stability. The reanalysis of experimental differential cross sections was carried out consistently, as described in Ref. 14. Two different p-wave splittings were employed, one consistent with the OPE signature (+ - +), the other appropriate to spin-orbit effects producing positive polarizations at small angles (+ + -). The strength was extrapolated from 10 MeV down, as prescribed by the low-energy limit of phase shifts, valid when $\sin\delta_\ell \approx \delta_\ell$, and by the possible absolute value of polarizations.[16] The value for the phase shift at 0.38243 MeV was taken in common for both sets of phase shifts, as determined by Noyes.[3] The justification for this is that both sets of phase shifts converge to the same low-energy limit. The analysis in terms of expansions (1) and (2) was carried out up to and including a term in k^8 (shape parameter R). Vacuum polarization effects in the s-wave phase shifts were corrected following Foldy and Eriksen.[16] Effects due to the electromagnetic structure of nucleons were explored in terms of the approach of Ref. 15. The preferred values of proton-proton scattering parameters are

$$a = -7.7856 \pm 0.0078 \text{ F}, \quad r = 2.8398 \pm 0.009 \text{ F}, \quad P = 0.072 \pm 0.005, \quad Q = 0.034 \pm 0.004.$$

They correspond to a calculation correcting for electromagnetic effects as appropriate in the absence of a core (or when it is velocity-dependent and negligible at low energies). However, there are uncertainties in the electromagnetic form factors, and thus, these corrections may have produced a minimum in χ^2 fortuitously. Figure 1 shows a plot of the preferred fit.

The values obtained from phase shifts, assuming a splitting of p waves giving a positive polarization at small angles, are

$$a = -7.7870 \pm 0.0063 \text{ F}, \quad r = 2.8462 \pm 0.011 \text{ F}, \quad P = 0.080 \pm 0.003, \quad Q = 0.062 \pm 0.007.$$

The shape dependence in the range from 0 to 10 MeV is established in the s wave independently from the accuracy of the VPC, because the exclusion of the points at 0.38243 and 1.397 MeV does not affect the sign of the parameters P and Q. It is also established independently of the assumed splitting of p waves as long as polarization effects are kept small, in agreement with experiment.

The central values of P and Q differ from estimates made in the past on assumption of a Yukawa potential, but are not really inconsistent with it. The parameters P and Q are strongly correlated, and if Q is assumed at the value calculated in Ref. 2 (Q = 0.019), P also falls very close to the value calculated there (P = 0.055).

Summarizing, the shape dependence is established in the range from 0 to 10 MeV from the context of a large amount of experimental data, and quite independently from effects attributable to corrections or assumptions made in their analysis.

It is hoped that nuclear calculations based on the detailed proton-proton interactions will abandon the use of potential shapes (or models) inconsistent with the results reported here.

Footnotes and References

†Condensed from Phys. Rev. Letters 21, 438 (1968).
*Present address: Université Laval, Québec 10e, Canada.

1. J. S. Schwinger, Hectographed notes on nuclear physics, Harvard, 1947, Phys. Rev. 72, 742A (1947).
2. J. D. Jackson and J. M. Blatt, Rev. Mod. Phys. 22, 77 (1950).
3. H. Pierre Noyes, Phys. Rev. Letters 12, 171 (1964).
4. V. V. Babikov, J. Nucl. Phys. (USSR) 1, 793 (1965); Sov. J. Nucl. Phys. 1, 567 (1965).
5. G. E. Brolley, Jr., J. D. Seagrave, and J. G. Beery, Phys. Rev. 135, B1119 (1964).
6. D. J. Knecht, P. F. Dahl, and S. Messelt, Phys. Rev. 148, 1031 (1966).
7. R. J. Slobodrian, Nuovo Cimento 40, 443 (1965); Nucl. Phys. 85, 33 (1966) and references therein.
8. H. R. Worthington, J. M. McGruer, and D. E. Findley, Phys. Rev. 90, 899 (1953).
9. L. Heller, Rev. Mod. Phys. 39, 584 (1967).
10. L. H. Johnston and D. E. Young, Phys. Rev. 116, 989 (1959).
11. H. Pierre Noyes and L. Lipinski, Phys. Rev. 162, 884 (1967).
12. P. Catillon, D. Garreta, and M. Chapellier, Nucl. Phys. B2, 93 (1967).
13. M. H. Mac Gregor, R. A. Arndt, and R. M. Wright, Phys. Rev. 169, 1128 (1968).
14. R. J. Slobodrian, H. E. Conzett, E. Shield, and W. F. Tivol, Proton-Proton Elastic Scattering Between 6 and 10 MeV, Phys. Rev. 174, 1122 (1968).
15. R. J. Slobodrian, Phys. Rev. 145, 766 (1966), the calculations described in this paper were extended to 10 MeV.
16. L. L. Foldy and E. Eriksen, Phys. Rev. 98, 775 (1955).
17. A more extensive table is available upon request.

Fig. 1. Plot of the nonlinear part of the function K; $\Delta K = K - (A_0 + A_1 E)$. The solid line corresponds to a four-parameter fit to 14 experimental points. The dashed line is obtained with the interference minimum datum and the KMBND results. The circles correspond to Refs. 5, 6, and 8. The squares correspond to Ref. 14.

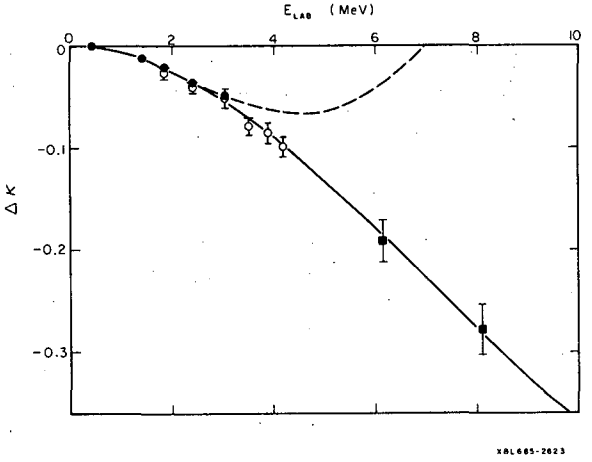

COLLECTIVE STATES IN A PAIRING-PLUS-QUADRUPOLE MODEL USING WOOD-SAXON REPRESENTATION I. DERIVATION OF THE QUADRUPOLE FORCE FROM A WOOD-SAXON POTENTIAL†

B. Sørensen and K. Kumar*

The radial dependence P(r) of a quadrupole force

$$V(\underline{r}_1, \underline{r}_2) = -\chi P(r_1)\, P(r_2) \sum_{\mu} Y^*_{2\mu}(\hat{\underline{r}}_1)\, Y_{2\mu}(\hat{\underline{r}}_2)$$

can be determined by a self-consistency argument from the average potential generated by this interaction.[1]

This leads to $P(r) = r\partial U_0(r)/\partial r$, where U_0 is the spherical part of the average potential generated by the force. In addition one obtains the self-consistent coupling strength

$$\chi = c\left[\int P(r)^2 r^2 dr\right]^{-1},$$

where

$$c = \frac{4\pi}{A}\int U_0(r) r^2 dr.$$

The formulae above can be generalized to include two kinds of particles and spin-dependent interaction.

We have considered an average potential U_0 of Wood-Saxon type with a Coulomb term and a spin-orbit part. This may lead to a quadrupole force which has a more realistic radial shape than the usual r^2, which corresponds to U_0 equal to a harmonic oscillator well. We have calculated reduced matrix elements of the quadrupole operator for use in calculations of nuclear deformations and energy levels by the Kumar-Baranger method,[2] noting, however, a surprising similarity to the r^2 matrix elements. On the other hand, the A dependence (or rather N, Z dependence) of the self-consistent χ which is shown in Fig. 1 is quite different, and in agreement with former criticism[2] of the usual quadrupole force.

Footnotes and References

†Condensed from UCRL-18593, Nov. 1968.
*Present address: The Niels Bohr Institute, Copenhagen, Denmark.

1. A. Bohr and B. Mottelsen, Nuclear Structure, monograph (to be published).
2. K. Kumar and M. Baranger, Nucl. Phys. A110, 510 (1968).

Fig. 1. Self-consistent quadrupole strength for usual quadrupole force (χ_1) and for modified quadrupole force using Wood-Saxon potential with (χ_3) and without (χ_2) Coulomb part.

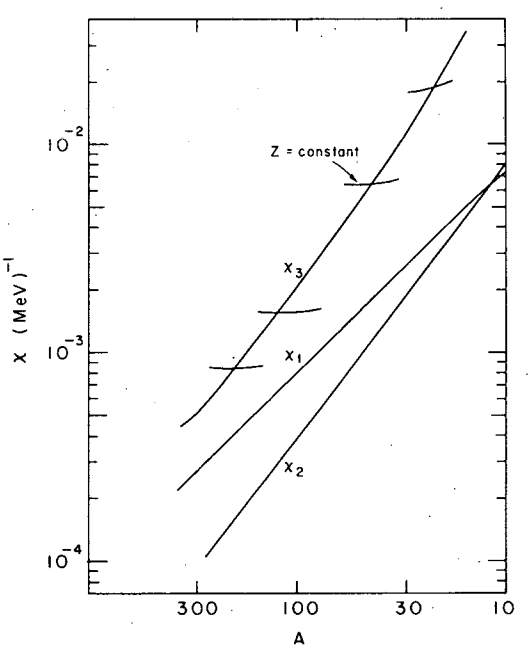

BOSON DESCRIPTION OF FERMION SYSTEMS: Numerical Calculations

Bent Sørensen

The boson method developed for the description of collective excitations in nuclei[1] has only tentatively been used for calculation of quadrupole vibrations.[2] We here present examples of numerical calculations using expansions carried to fourth order. All details of the theory and the method of calculation has been given in Ref. 3, so we will just mention that the method is supposed to give at least a qualitative description of the phase transition between spherical and deformed shapes and to describe rather accurately the anharmonicity of nearly harmonic vibrations.

The interaction is chosen as pairing plus modified quadrupole force, the latter being described in the contribution by Sørensen and Kumar to this report. Figure 1 shows calculated and experimental quadrupole states in Sm isotopes. The essential characteristics of the deformation genesis--lowering of the first excited states and grouping in rotational bands, increase in $B(E2, 2+ \rightarrow 0+)_{gr.}$, and in the static electric quadrupole moment--all these features are reproduced by the model, although numerical agreement gets poorer for larger deformation, due to the decreased validity of the fourth-order truncation of the anharmonic Hamiltonian. It must be kept in mind that the expansion is in terms of a spherical quadrupole boson c^+, so that high powers become important when the system is strongly deformed.

Another way to look at the phase transition in the boson model is from the boson expansions of the mass quadrupole moment Q and the conjugate momentum P to express the boson operators (c^+, c) in terms of the hermitean (iP, Q) and introduce these in the boson Hamiltonian $H = H(c^+, c) = V(Q) + T(Q, P)$. In Figs. 2 and 3 we show the calculated potential energy functions $V(\underline{Q})$ for the three Sm isotopes as functions of Q and γ, defined by transforming the quadrupole tensor $\underline{Q}_{2M}$ to the intrinsic system defined by the principal directions of the tensor itself, $Q'_{20} = Q \cos\gamma$; $Q'_{22} = Q'_{2-2} = 2^{-1/2} Q \sin\gamma$. In Fig. 2 the $\gamma = 0$ contour is given, and in Fig. 3 the equipotential surfaces $V(Q, \gamma) = \text{constant}$. In addition to the Q scale (the quadrupole operator is given in units of the oscillator parameter $b^2 \approx A^{1/3}$) another scale gives the more conventional deformation parameter β, which is related approximately to Q by

$$Q \approx \frac{15}{16\pi} \left(\frac{3}{2}\right)^{1/3} A^{4/3} \beta.$$

We now turn to the region around $Z_0 = 50$, where Figs. 4 and 5 show two sets of nuclei, each with the same neutron numbers, and proton numbers Z_0-2 and Z_0+2, respectively. These cases are chosen because of characteristic behaviors of energies and transition rates, and these quantities seem indeed reproduced by the boson calculations to the extent one can expect when simplified forces are employed. Potential energy surfaces are given in Figs. 6-8. There remains, however, one completely unresolved puzzle, that of the static quadrupole moments of the first 2+ states, which are reported to have the same magnitudes and signs in ^{114}Cd and ^{122}Te,[4] namely -10 ± 4 (again in units of b^2). The neutron contribution to Q(2+) cannot be very different from that in the corresponding Sn isotopes, i.e., small and presumably positive. As for the proton contribution, it is negative in ^{114}Cd because of the importance of the configuration $(g_{9/2})^{-2}$ and positive in ^{122}Te for any low-lying configuration. This simple argument predicts a small negative quadrupole moment in ^{114}Cd and a larger positive one in ^{122}Te, results which are confirmed by the boson calculations for a wide range of parameters (single-particle energies and force strengths). The disagreement with experiment can thus not be a matter of merely improving the calculation by inclusion of higher-order terms etc., but rather presents a basic error in the description, or in the experiment. Recently, some doubt has been cast on the ^{114}Cd experiment,[5] actually revising the Q(2+) to the value we predict. However, the crucial quantity to expose to further experimentation is rather the ^{122}Te quadrupole moment, which is not subjected to cancellations between proton and neutron contributions, which depends critically on details of the nuclear interaction.

The numerical calculations were performed at the Niels Bohr Institute and NEUCC, Copenhagen, Denmark.

References

1. B. Sørensen, Nucl. Phys. A97, 1 (1967).
2. B. Sørensen, Phys. Letters 24B, 328 (1967).
3. B. Sørensen, Progr. Theoret. Phys. (Kyoto) 39, 1468 (1968).
4. J. deBoer and J. Eichler, Adv. Nucl. Phys. 1, 1 (1968).
5. J. Simpson et al., Phys. Letters 27B, 633 (1968).

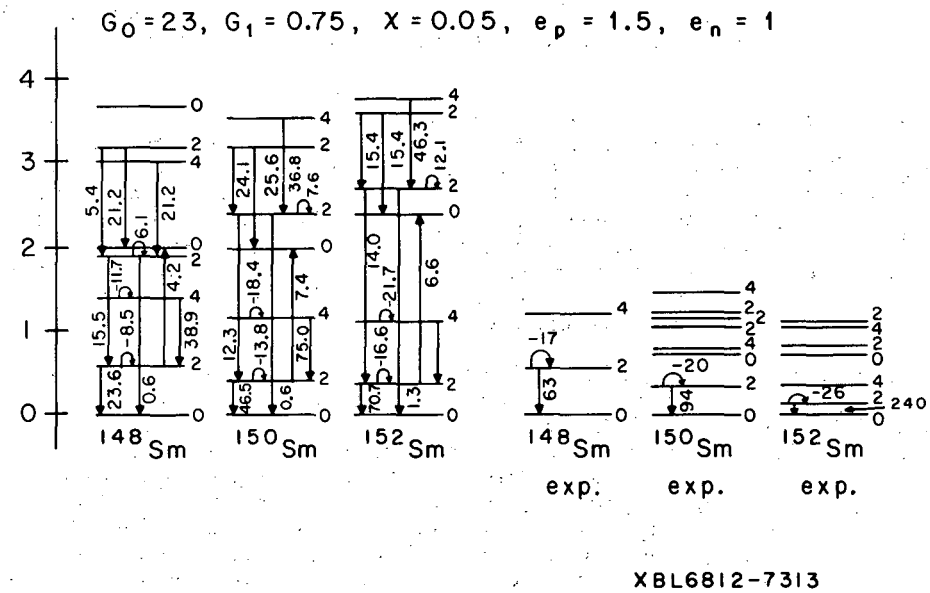

Fig. 1. Experimental and theoretical energies and quadrupole transition strengths for some Sm isotopes. States are labeled by J, and the numbers attached to arrows between states are BE2 values in units of b^4. Arrows ending in starting states indicate static quadrupole moments in units of b^2. Indicated are effective charges, pairing strength (isoscalar and isovector parts G_0 and G_1), and quadrupole strength χ. Unless otherwise indicated y^0 is zero.

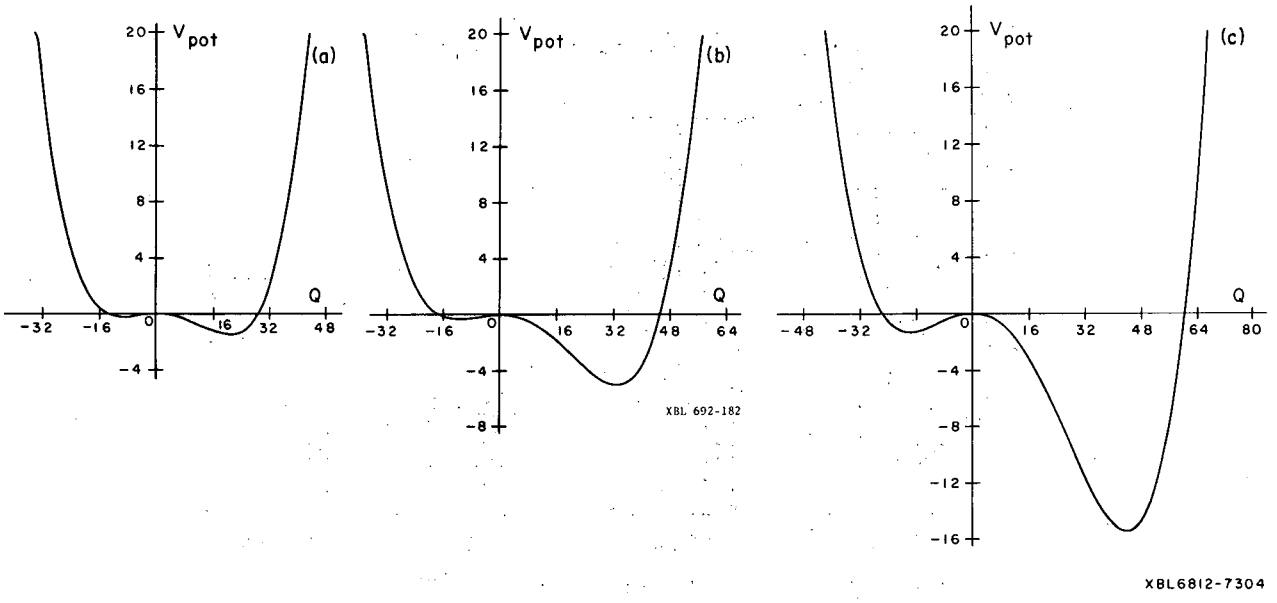

Fig. 2. $\gamma = 0$ potential energy contour for (a) ^{148}Sm, (b) ^{150}Sm, and (c) ^{152}Sm.

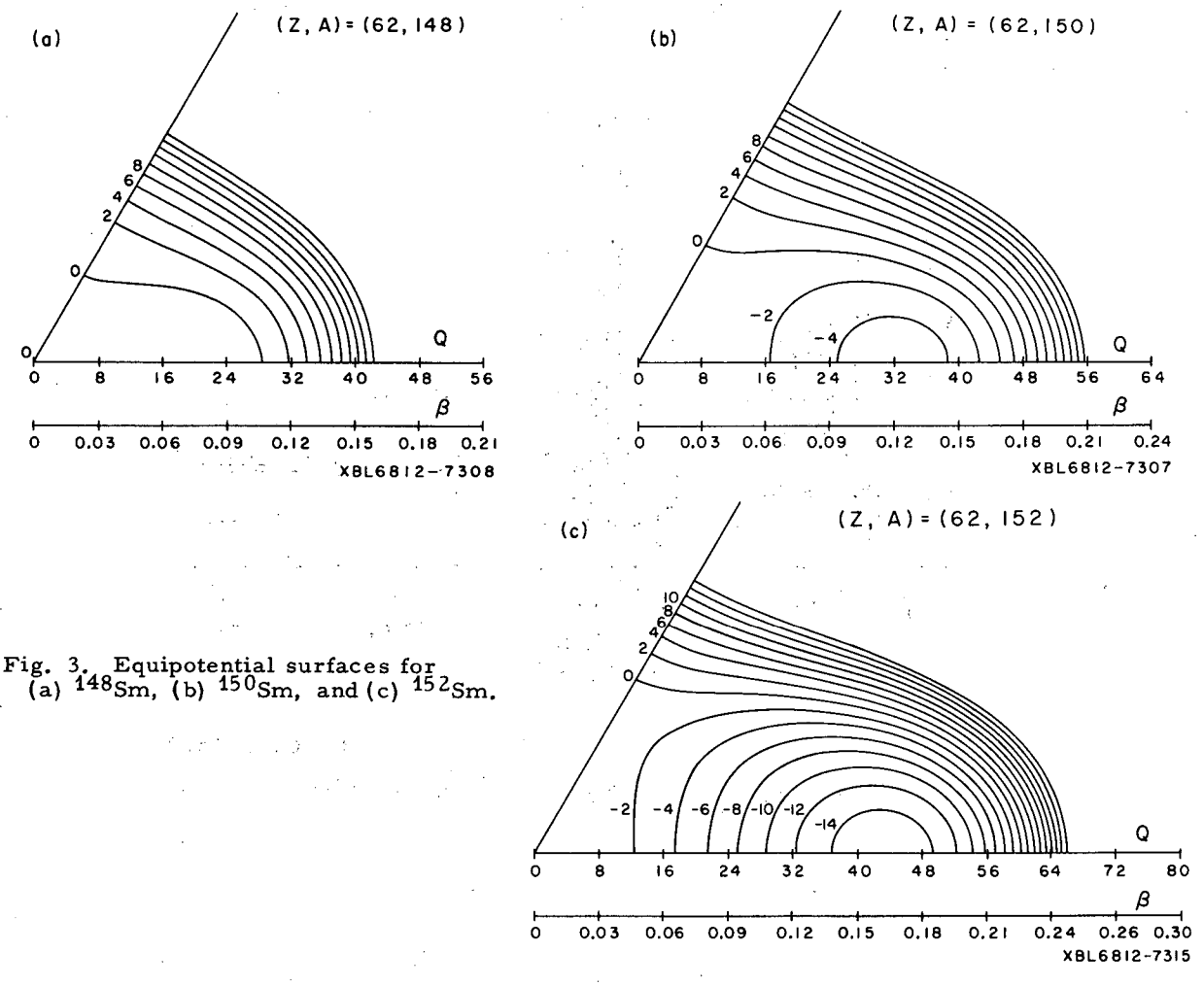

Fig. 3. Equipotential surfaces for (a) ^{148}Sm, (b) ^{150}Sm, and (c) ^{152}Sm.

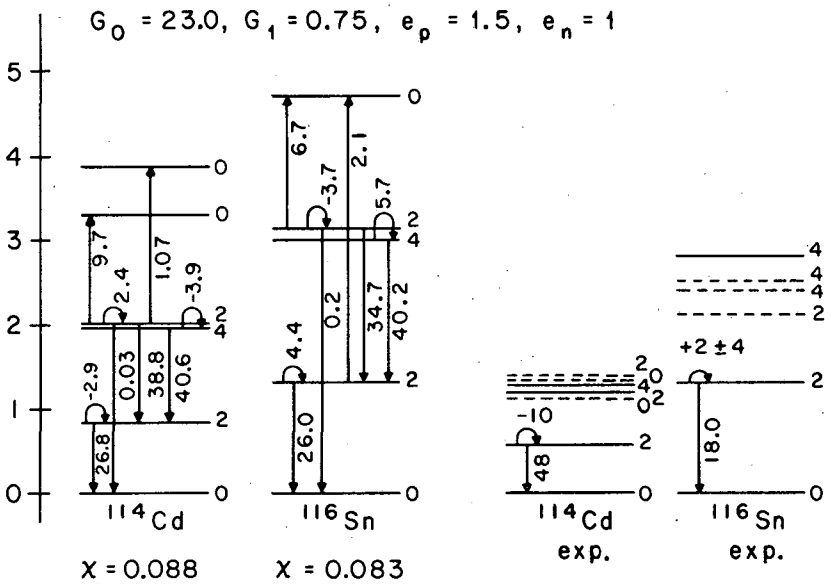

Fig. 4. Same as Fig. 1 for ^{114}Cd and ^{116}Sn.

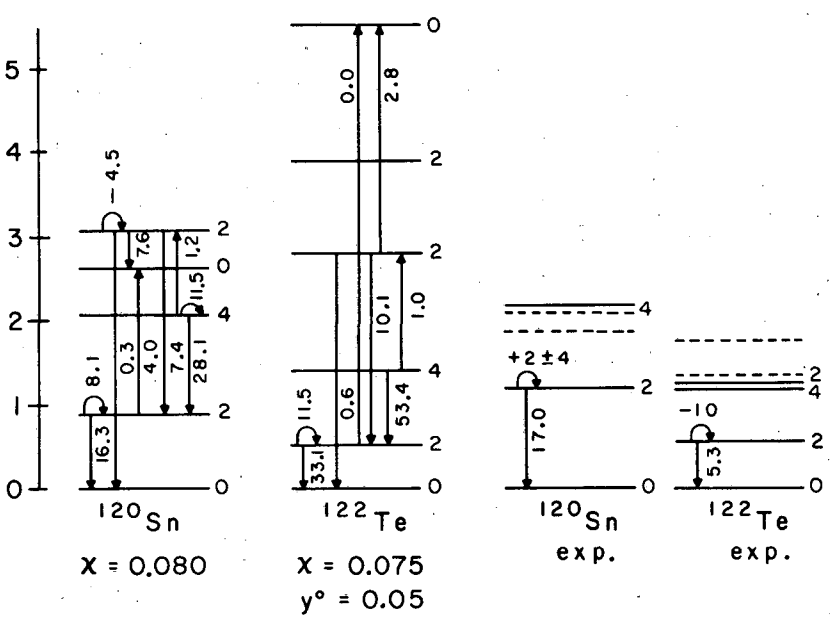

Fig. 5. Same as Fig. 1 for ^{120}Sn and ^{122}Te.

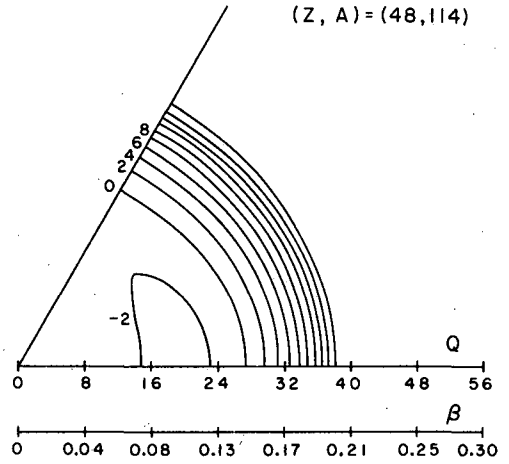

Fig. 6. Equipotential surfaces for ^{114}Cd.

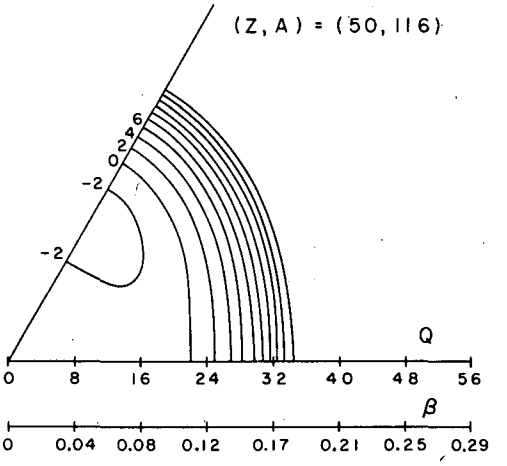

Fig. 7. Equipotential surfaces for ^{116}Sn

Fig. 8. Equipotential surfaces for ^{122}Te.

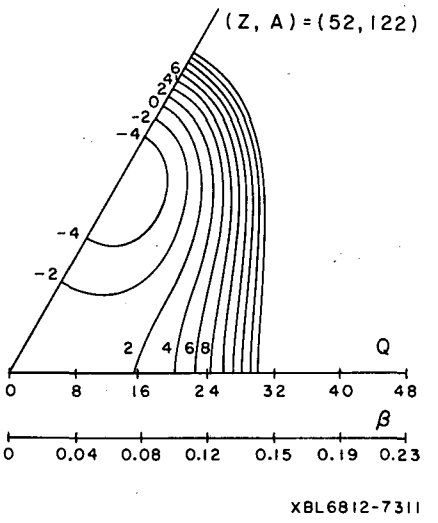

NEUTRON PAIRING STATES IN DOUBLY EVEN NUCLEI

Bent Sørensen

The boson theory for collective excitations put forward in Ref. 1 has proven especially applicable for the description of pair vibrations.[2] The method for calculating this type of state, which is described in Sec. 7 of Ref. 1, is here extended to a simultaneous description of collective and noncollective states, all of the restricted seniority-zero type, where an even number of particles are pairwise coupled to angular momentum zero. Only neutrons are considered, since the most complete experimental data concerning this type of state come from (tp) and (pt) reactions. The aim of the present investigation is to establish the merits and limitations of the assumption that the neutron seniority zero states arising from a pairing residual interaction are approximately uncoupled from other degrees of freedom. In addition we consider whether the pure pairing

interaction can account for the ground-state energy systematics, implying that the only interaction energy which changes in going from a nucleus N to N ± 2 is the pairing energy. This is certainly violated by the Coulomb energy, which we then systematically have subtracted from the experimental masses, assuming it to be of the form

$$\mathcal{E}_c = \frac{3}{5}\frac{Z^2e^2}{R_c}\left[1 - 5\left(\frac{3}{16\pi Z}\right)^{2/3}\right],$$

where $R_c = r_c A^{1/3}$, with fixed r_c. Calculations start from a closed-shell configuration or closed-subshell configuration, and the boson method allows one to then increase and decrease N in steps of two, until the truncation point of the Hamiltonian (in our case four-boson operators) becomes insufficient. We have performed calculations for around 25 such shell closures, obtaining in most regions a remarkably good agreement for ground-state energies as well as some excited states, both of collective and noncollective nature. The experimental spectra often contain additional 0+ levels, which is natural, since proton degrees of freedom have been left out, and similarly quadrupole degrees of freedom. These, of course, have no basic (tp) or (pt) strength, but when they mix with the neutron pairing states, one observes a distribution of strength over several levels. Indications of such isospin and pairing-quadrupole couplings are present in most regions of the periodic table, but only in specific regions do they destroy the main structure predicted by the pairing model. Figures 1 through 4 give a few examples of the situation in various regions, starting from the closed shells of ^{26}Mg, ^{32}S, ^{48}Ca, and ^{208}Pb. Heavily drawn levels belong to the collective coupling scheme, lightly drawn ones are noncollective. Numbers quoted for each level are tp or pt strength relative to the corresponding ground-state transition, according to the direction of the arrow (tp: arrow points right). Finally, relative ground-state cross sections are quoted below the ground state.

References

1. B. Sørensen, Nucl. Phys. A97, 1 (1967).
2. R. Broglia and B. Sørensen, Nucl. Phys. A110, 241 (1968).

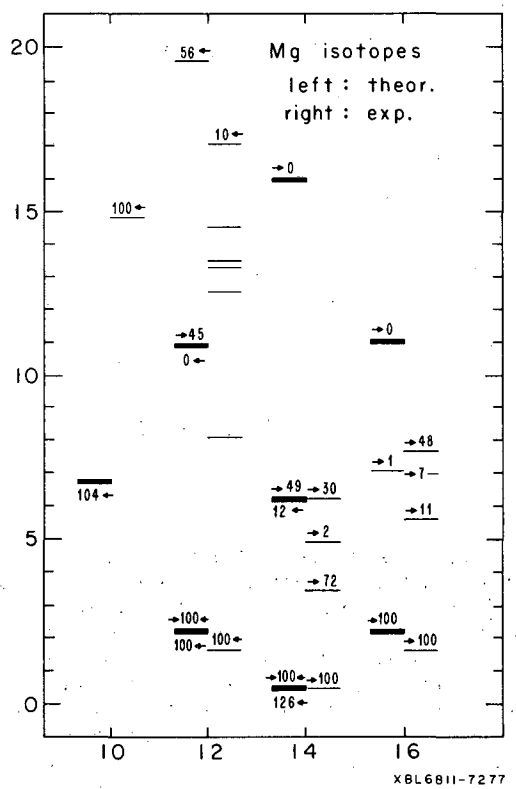

Fig. 1. Energies (in MeV) are plotted versus neutron number (N). For explanation of indicated (tp) and (pt) strengths see text.

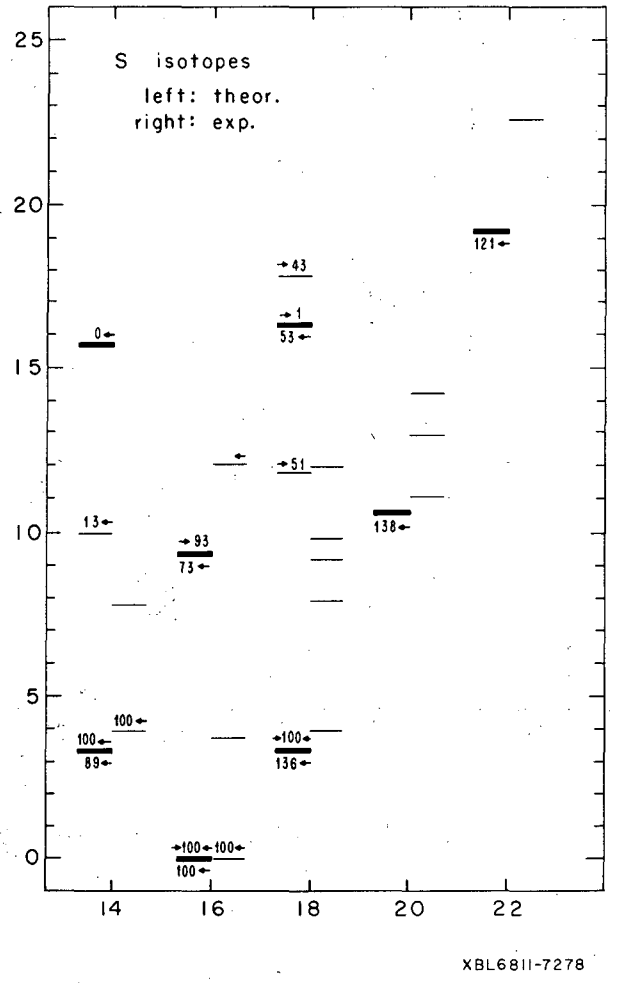

Fig. 2. Energies (in MeV) are plotted versus neutron number (N). For explanation of indicated (tp) and (pt) strengths see text.

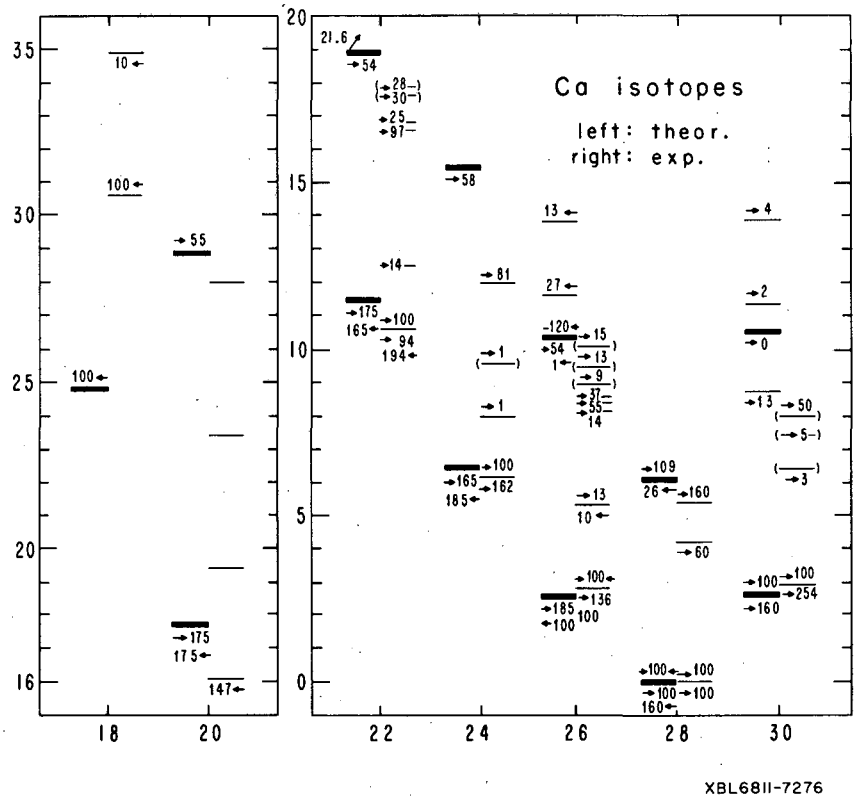

Fig. 3. Energies (in MeV) are plotted versus neutron number (N). For explanation of indicated (tp) and (pt) strengths see text.

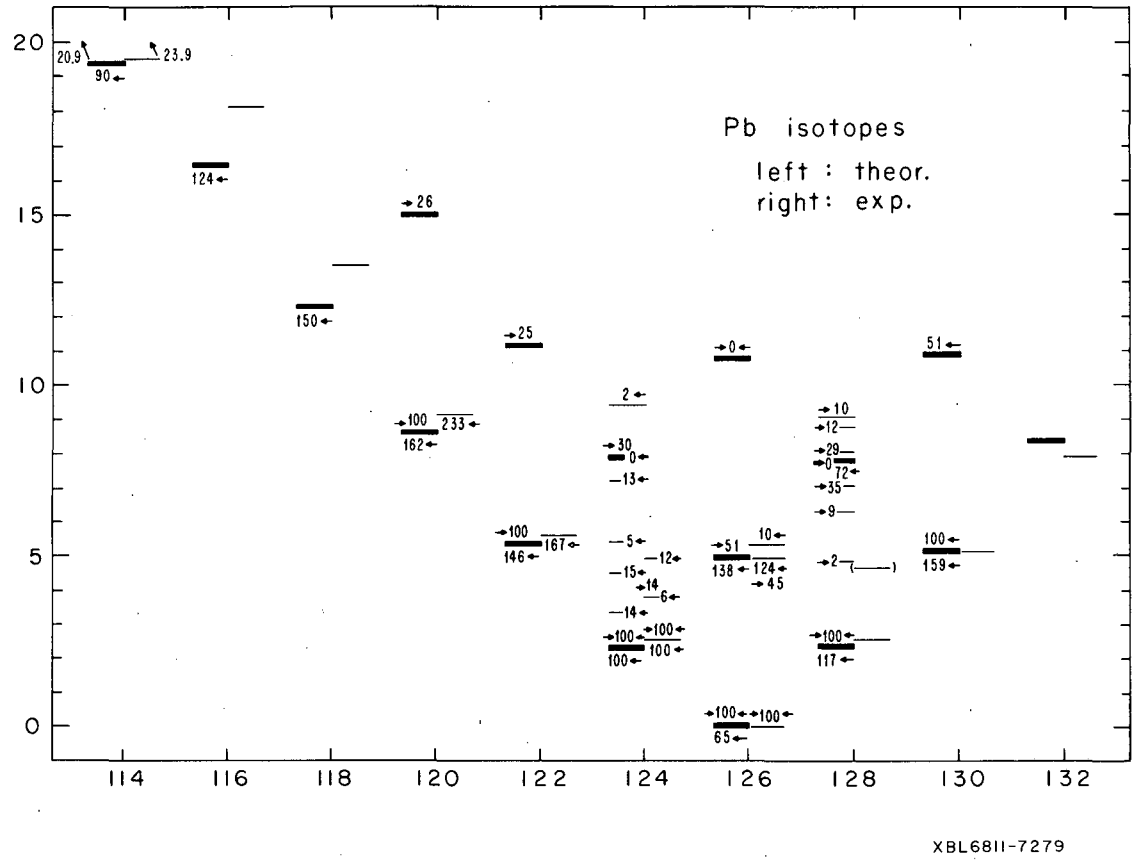

Fig. 4. Energies (in MeV) are plotted versus neutron number (N). For explanation of indicated (tp) and (pt) strengths see text.

A COMMENT ON THE ^{10}B(t, p) REACTION TO THE ^{12}B GROUND STATE†

Bent Sørensen

A priori there is hardly any reason to believe that a two-nucleon transfer reaction should proceed in one step by simultaneous transfer of the two particles involved, as in Fig. 1(a). However, this model has been able to provide a fair to good description of most experiments performed during the last decade, with the exception of reactions with very low incident energy and with the possible exception of light nuclei. Examples of two-step mechanisms for the transfer reactions are indicated in Fig. 1(b) (two subsequent single-neutron transfers) and Fig. 1(c) (inelastic scattering followed by transfer). The remarks made above imply that the effects of the competing mechanisms in Fig. 1(b),(c) have to be searched for in small anomalies of angular distributions or in magnitudes of cross sections. As no theory at present seems refined enough to describe such details, some effort has been made in looking for peculiar reactions, in which the two-step mechanisms are sufficiently important to influence the cross sections in a decisive way.

Bang et al.[1] argue that the process shown in Fig. 1(b) will be important if the binding energies of the two neutrons are very different, and they quote the ^{10}B(t, p) reactions as one of the most favorable cases to look at. This experiment was done at E_t = 10 MeV (well above the known anomalies occurring for reactions at E_t about 1 MeV) by Middleton and Pullen,[2] and indeed they concluded, after comparison with a plane-wave stripping theory, that the ground-state transition, which must have ℓ = 2, has an angular distribution (decreasing from θ = 0 deg) which is incompatible with the expected ℓ = 2 distribution (which increases from θ = 0 deg up to a maximum

around θ = 60 deg). By calculating the Fig. 1(b) process, again using plane waves, Bang et al. could, by adjusting the weights of the direct and two-step processes phenomenologically, obtain a reasonable fit to the experimental distribution.

In order to test the validity of the proof for existence of the two-step process, we decided to perform a DWBA analysis of the Fig. 1(a) process and see whether reasonable variation in optical-model parameters or nuclear-structure factors could reproduce the experimental distribution, in which case the argument for a mechanism like Fig. 1(b) would be weakened, although of course not excluded.

We used the two-nucleon transfer theory of Glendenning,[3] concentrating the nuclear structure information in coefficients G_N, of which only $G_0 \neq 0$ as long as the two neutrons are in the p shell. Only if both are in the sd shell can we have $G_1 \neq 0$. This, however, can hardly be expected to have a large amplitude for the ground state of ^{12}B, so we varied G_1/G_0 from zero to 0.17, for all sets of optical-model parameters. Using a DWBA code written by Glendenning, we obtained the best fit, shown in Fig. 2, for the proton and triton parameters listed in Table I (only triton parameters have been extensively varied). The curve shown in Fig. 2 corresponds to $G_1/G_0 = 0.17$, and by increasing this ratio a better reproduction of the first minimum can be obtained.

This, however, we would not consider physically acceptable, and although the DWBA in this case is completely different from the earlier plane-wave results, and actually does provide a fair fit, there still remains some anomaly in the distribution, which may stimulate an investigation of the two-step processes in Fig. 1(b) and 1(c) [which should not be less significant than 1(b)].

Footnotes and References

†Condensed from UCRL-18663, Jan. 1969.

1. J. Bang et al., J. Nucl. Phys. (U.S.S.R.) 4, 962 (1966).
2. R. Middleton and D. Pullen, Nucl. Phys. 51, 50 (1963).
3. N. Glendenning, Phys. Rev. 137, B102 (1965).

Table I. Optical-model parameters.

	V	W	W_D	r_V	r_W	r_C	a_V	a_W
Proton	49.2	0	11.5	1.25	1.25	1.25	0.65	0.67
Triton	138.0	40	0	0.85	1.5	1.4	0.7	1.1

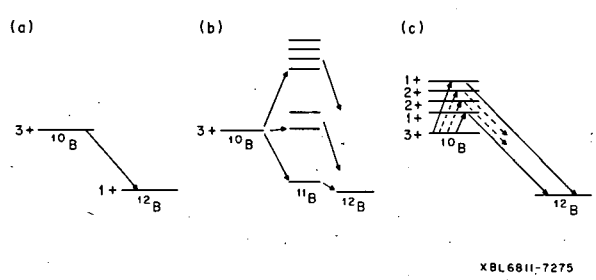

Fig. 1(a-c). Various mechanisms for the $^{10}N(tp)^{12}B$ ground-state reaction.

Fig. 2. Experimental and DWBA angular distributions for $^{10}B(tp)^{12}B$ ground state.

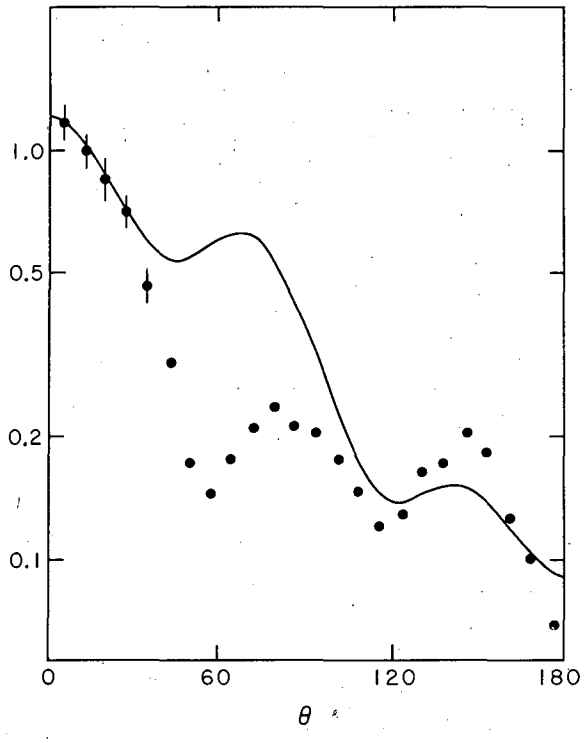

XBL6811-7274

ENERGY SPECTRUM OF ^{20}Ne USING HARTREE-FOCK AND TAMM-DANCOFF WAVE FUNCTIONS

S. N. Tewari

The static Hartree-Fock (HF) theory together with the angular-momentum projection technique has been successfully applied to explain the energy spectrum of the ground 0^+ band in ^{20}Ne.[1,2] The accuracy of the projected HF wave functions of ^{20}Ne and many other nuclei in the 2S, 1d shell has been studied in several recent publications,[3-6] and it is clear from these works that the projected wave functions are, to a very good approximation, the eigenstates of the nucleus.

Attempts have been made to explain the first excited 0^+ band and its energy spectrum in the framework of HF theory.[7,8] The energy spectrum of the excited 0^+ band, unlike the ground-state band, does not show very much of the rotational character. A natural approach in the framework of the HF theory for explaining the excited 0^+ band may consist of describing it by a superposition of configurations composed of hole-particle excitations out of the HF state describing the ground band. The time-dependent HF formalism is the approximate form of HF theory for treating such hole-particle excited states. This approach has been utilized by Bassichis et al.[7] to derive the excited-state bands of ^{20}Ne and ^{24}Mg. The energies of the different states in a given band were calculated by then using the energy formula of the rotational model with some empirical value for the moment of inertia $\mathfrak{z}$. Since the excited bands are not purely rotational, there was some latitude in the choice of $\mathfrak{z}$ for them, and by choosing a suitable value they obtained a fair agreement with the experiment. However, a very interesting and significant aspect of the work of Bassichis et al.[7] is that they find that the effect of correlations in the ground state giving rise to the so-called backward-going graph is negligible except for the spurious solutions. The result implies that one can safely use the Tamm-Dancoff approximation (TDA) instead of TDHF for ^{20}Ne and ^{24}Mg. The starting point of the work presented here, therefore, is to assume that the TDA provides a satisfactory scheme for deriving the intrinsic state of the first excited 0^+ band.

The calculation was performed by using the interaction Hamiltonian of Ref. 9. First the intrinsic state of the ground band was derived by a HF calculation. [1] Next the Tamm-Dancoff approximation was applied, to construct the intrinsic state of the excited 0^+ band. [For a discussion on the method of the Tamm-Dancoff approximation the reader is referred to Refs. 7 and 8.] Physical states of the two bands were constructed by using the method of the Hill-Wheeler integral to project out good angular momentum states. [10] Energies of the physical states were then calculated by the techniques discussed in Refs. 1, 11, and 12. The effect of the admixture of the projected HF states and the projected TDA states on the energy spectrum was also calculated. The comparison of the predicted energy spectrum with experiment is shown through Table I and Fig. 1. For a detailed discussion of the results and other aspects of this calculation the reader is referred to Ref. 9.

References

1. G. Ripka, Lectures in Theoretical Physics (University of Colorado Press, Boulder, Colorado, 1966).
2. A. P. Stamp and M. B. Spencer, Nucl. Phys. A111, 353 (1968).
3. M. K. Banerjee and G. Stephen, Rotation and the Hartree-Fock Theory, submitted to Phys. Rev.
4. S. N. Tewari and M. K. Banerjee, Nucl. Phys. 82, 337 (1966).
5. M. R. Gurge, Phys. Letters 27B, 136 (1968).
6. L. Satpathy and S. C. K. Nair, Phys. Letters 26B, 257 (1968).
7. W. H. Bassichis, C. A. Levinson, and I. Kelson, Phys. Rev. 136B, 380 (1966).
8. J. Bar-Touv, Phys. Rev. 166, 1241 (1967).
9. S. N. Tewari, Energy Spectrum of ^{20}Ne Using Hartree-Fock and Tamm-Dancoff Wave Functions, UCRL-18628, Nov. 1968.
10. D. L. Hill and J. A. Wheeler, Phys. Rev. 89, 1106 (1953).
11. S. N. Tewari and D. Grillot, Projected Spectrum of ^{28}Si Including the Effects of Pairing and Shape-Mixing, Phys. Rev. (to be published).
12. S. N. Tewari, Construction of Eigenstates in Terms of Hartree-Fock Solutions (in preparation).

Table I. Comparison between the experimental and the predicted spectrum (all values in MeV). Theory (a) and theory (b) correspond to results without and with admixture of projected states.

J	Experiment	Theory (a)	Theory (b)
0^+	0.0	0.0	0.0
2^+	1.63	1.25	1.22
4^+	4.25	4.01	3.92
0^+	6.72	6.17	6.38
2^+	7.84	7.95	7.99
6^+	8.79	7.81	7.82
4^+	11.07	10.46	10.79

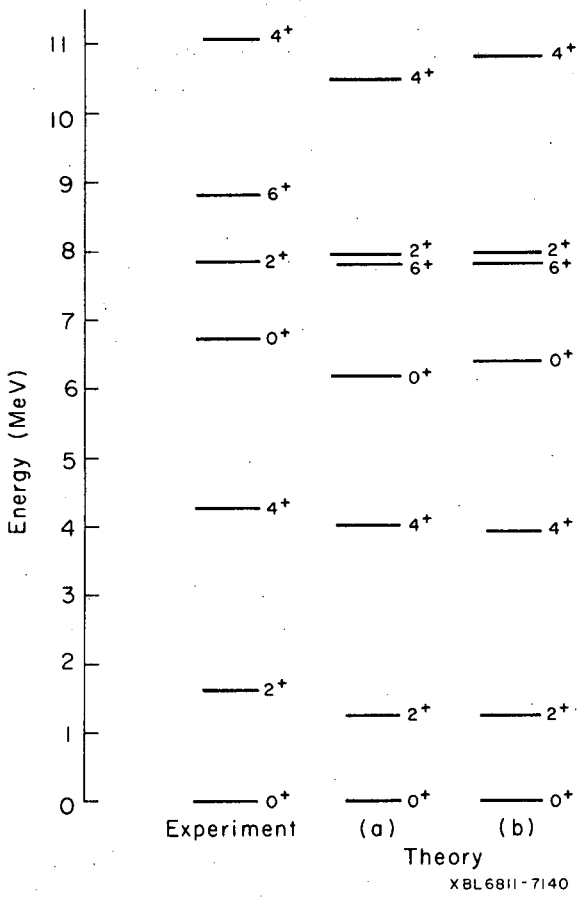

Fig. 1. Comparison between the experimental and theoretical spectrum of the ground-state 0^+ and first excited 0^+ band in ^{20}Ne. Theory (a) and theory (b) imply the same as in Table I. For facility of comparison only the relevant experimental energies are shown.

FISSION

ANGULAR DISTRIBUTION OF PROMPT γ RAYS EMITTED IN ^{252}Cf SPONTANEOUS FISSION

E. Cheifetz,† H. R. Bowman, and S. G. Thompson

Anisotropy of the broad spectrum of prompt γ rays emitted in spontaneous fission of ^{252}Cf and in thermal neutron-induced fission of ^{233}U, ^{235}U, and ^{239}Pu has been observed by several investigators.[1] The observed anisotropies, defined as the ratio 0 deg/90 deg in numbers of γ rays with respect to the fission direction, range from 1.10 to 1.15. This information, taken together with data on the relatively high yields of fission products having isomeric transitions and the high yield of prompt x rays in fission, suggests on the basis of statistical considerations that the fragments at scission have average angular momenta of more than 6 units $\hbar$ pointed normal to the fission direction and also that many of the transitions have an E2 multipolarity.

Recent high-resolution studies in this Laboratory of prompt gamma radiation from ^{252}Cf reveal many well-defined peaks in the 50- to 350-keV region. More than 20 peaks can be seen even without sorting the fragments into mass groups. Our experimental arrangement consists of a point ^{252}Cf source electroplated on platinum foil, a 6-cm^3 germanium detector (resolution: 1.4 keV FWHM at 280 keV) placed 7 cm behind the source holder, and three 300-mm^2-area fission detectors at a distance 4 cm from the source which define the 0-, 45-, and 90-deg directions. By plating the fission source on a platinum backing thick enough to stop the fragments, some of the difficulties in the interpretation of the anisotropy of the broad gamma spectrum are avoided. The difficulties arise from (a) the effect of the Doppler shift in the energy and intensity of the γ rays emitted by the moving fragments and (b) the energy dependence of the efficiency of the detector. Furthermore, there is a disorientation of angular momentum direction produced by the magnetic field resulting from the effect of missing electrons in the highly charged fragments. The latter effect should be largest when the fragments are moving in a vacuum.

The pulses corresponding to fragment and gamma energies of coincident-fragment–γ-ray events are fed into a PDP-9 on-line computer which regulates the stability of the detectors, displays the single-parameter spectra, and records the multiparameter events on magnetic tapes. The tapes are scanned by the computer at the end of the experimental run and sorted into six 4096-channel γ-ray spectra corresponding to the light and heavy fragment groups at each of the three angles. The spectra are stored in a rotating disk allowing rapid data access, and the data are plotted out for permanent copies of the results.

The energy of a gamma transition from a fragment appears Doppler-shifted when it is emitted from a moving fragment and unshifted when emitted from a fragment which is stopped in the backing if the transition lifetime exceeds $\approx 5 \times 10^{-13}$ sec. An example from some preliminary results is shown in Fig. 1. At the left of the figure the two peaks close together at energies of 241.3 keV and 242.3 keV are shown when the γ rays are emitted from fragments that are stopped in the platinum foil. The three cases correspond to gammas emitted at the angles 0, 45, and 90 deg with respect to the original fragment direction. On the right side the corresponding peaks (indicated by arrows) are shown when the γ rays are emitted at the angles 90, 135, and 180 deg from the fragments moving in a vacuum.

The greater width of the peaks at the angle 90 deg with respect to the moving fragments is due to Doppler broadening. The area under the peaks is found by a computer program that depends on assuming a predetermined peak shape. The anisotropy of the 241.3-keV line peak is 1.6 ± 0.2 (the correction for finite solid angle would increase this value of the anisotropy). The mass of the fragment from which the γ ray is emitted is assigned by comparing our results with the Doppler-shifted spectra of γ rays measured in coincidence with the two fragment energies and sorted into mass groups.[2] The 241.3-keV line is emitted by fragments having masses in the range 109 to 111 amu, and its multipolarity has been determined as E2 by Watson from measurements of the K/L conversion ratio.[3]

The sharp peaks in the γ-ray spectrum are assumed to be transitions from low-lying states of some of the more abundant prompt fission products, fed by a multiplicity of γ rays emitted from the fragments excited initially to an average energy of 4 to 5 MeV. For some transitions, such as the 241.3-keV line described above, the fragments retain a significant amount of their original angular momentum orientation, in a way similar to the prompt γ rays emitted from products of α-particle- and heavy-ion-induced reactions.[4]

Footnotes and References

†On leave from Weizmann Institute of Science, Rehovoth, Israel.

1. S. A. E. Johansson and P. Kleinheinz, in Alpha, Beta and Gamma Ray Spectroscopy, edited by K. Siegbahn (North-Holland Publishing Co., Amsterdam, 1965), Vol. 1, p. 805.

2. H. R. Bowman and R. C. Jared (Lawrence Radiation Laboratory), private communication.

3. R. L. Watson, A Study of the Internal Conversion Electrons Emitted Within 3 nsec After the Spontaneous Fission of ^{252}Cf, (Ph. D. Thesis), UCRL-16798, July 1966.

4. J. O. Newton, F. S. Stephens, R. M. Diamond, K. Kotajima, and E. Matthias, Nucl. Phys. A95, 357 (1967).

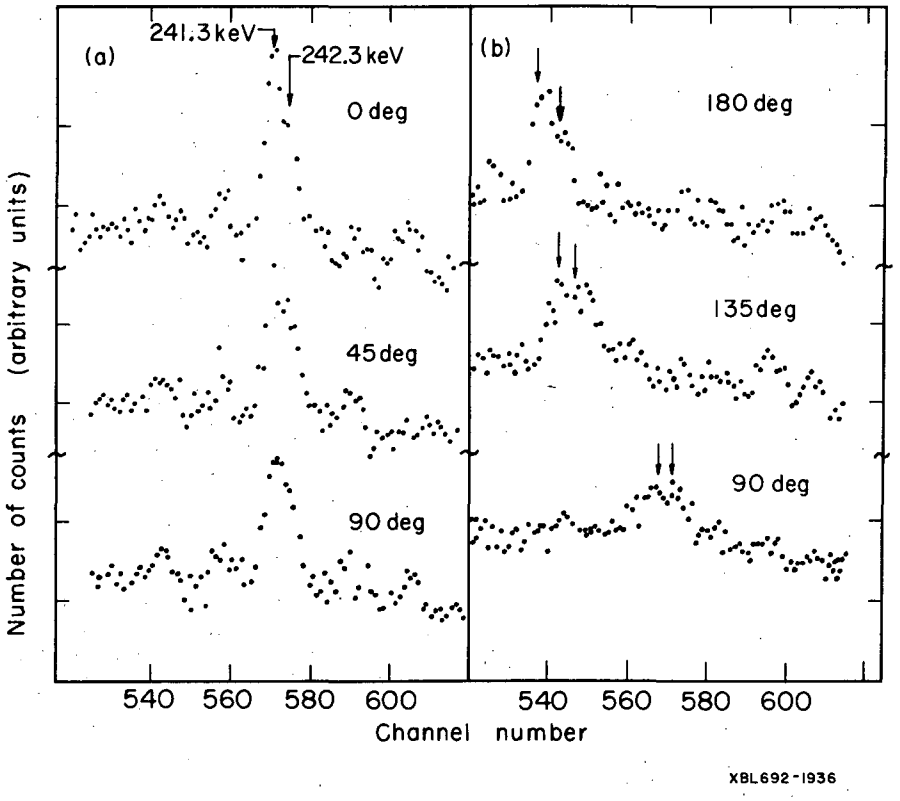

Fig. 1. Spectra of γ rays emitted (a) when the light fragment stopped in the platinum backing at 0, 45, and 90 deg to the fragment, (b) at 90, 135, and 180 deg by the moving light fragment.

K x-RAY MEASUREMENTS ON SHORT-LIVED FISSION PRODUCTS

J. B. Wilhelmy, S. G. Thompson, and J. O. Rasmussen†

Measurements to determine the yields of the K x rays have been performed on the short-lived isotopes produced from the spontaneous fission of ^{252}Cf. Due to the continued improvement in resolution of the solid-state spectrometers it has become possible to resolve the K x-ray groups from adjacent elements. This allows the determination of x-ray yields of specific elements as opposed to overall, average properties for groups of elements.

To study the short-lived fission products a belt transport system was designed to perform measurements on products with half-lives as short as 0.25 sec.[1] An approximately 10-μg source of ^{252}Cf ($\approx 3.7 \times 10^8$ f/min) was electroplated on a platinum plate. The source was placed in the center of a 2-ft^3 Lucite shield over a continuously moving belt of magnetic tape. Due to their high kinetic energy the fission fragments became embedded in the tape. They were then transported past a detector placed approximately 50 cm from the source. A variable gear system coupling a synchronous motor and the capstan tape drive allowed the transit time from the source to the detector to be varied. The detector used was a 0.25-cm^2 by 3-mm lithium-drifted silicon diode. By use of a preamplifier such as that described by Jared and Kilian,[2] resolution of 450 eV (FWHM) at 15 keV was obtained.

Forty-one x-ray spectra were recorded with transit times from source to detector ranging from 0.29 sec to 4.8 hours. Figure 1 is a composite of spectra taken at three different transit times. The x-ray resolution obtained for these spectra demonstrated the feasibility of obtaining information on K x-ray yield for the individual elements. To process the data and obtain these yields a computer code was developed by Rugge using a peak-fitting method patterned after that of Routti and Prussin.[3] In this code the peaks are treated as Gaussian with a linear exponential tail on the low-energy side. To treat the data adequately it was necessary to consider the elemental K x rays to be composed of four subgroup peaks; the $K\alpha_1$, $K\alpha_2$, $K\beta_1'$, and $K\beta_2'$. The parameters necessary for fitting the experimental data were obtained from our x-ray fluorescence measurements of stable elements which are in the fission product region. Figure 2 shows the x-ray spectra obtained by fluorescing Mo, In, and Nd. By using these as standards it was possible to fix the mean values, shape parameters, and relative intensities of the four subgroup peaks. This left only one parameter free for each element, the value which was to be measured, namely the intensity of the K x rays emitted. Figure 3 shows the spectra and computer fits for the shortest and longest transit times measured in the experiment.

K x-ray intensities obtained by computer fit were then used for determination of the average K x-ray yields for each element following beta decay. Using the formalism developed by Wahl[4] in which the prompt fission yield for each mass chain is assumed to have a Gaussian distribution about a most probable charge, Watson[5] calculated the expected yield for all prompt isotopes produced from the spontaneous fission of ^{252}Cf. The fission products, being β^- emitters, decay along a mass chain, increasing the atomic number with each decay. The amount of any isotope produced from beta decay in a mass chain is then equal to the sum of all the independent yields of isotopes with a lower value of Z in this mass chain. This summation is performed over the short-lived isotopes. Those which are long-lived or stable terminate the beta decay process, stopping the increase in yield for the higher-Z members of the chain. To obtain the total beta-decay yield for any one element the chain yields of that element are summed over all the mass chains. Isotopes with half-lives short compared with the longest experimentally measured time (4.8 hours) have totally decayed, thus giving a beta-decay yield equal to their total yield. Isotopes with half-lives comparable to, or longer than, 4.8 hours give beta-decay yields which are equal to their total yields multiplied by the fraction that has decayed in 4.8 hours. Therefore a value is obtained for the total number of β decays that occur for each element in 4.8 hours. The experimentally measured K x-rays at each of the 41 points were corrected for an effective counting time to give a true counting rate. These values were then integrated by numerical methods over the experimental range of times. These integrated yields were then divided by the total calculated beta-decay yields to obtain the number of K x rays per decay for each element. These results are plotted in Fig. 4. The errors shown are for the propagation of the statistical errors obtained in performing the peak integration, and should be regarded as indicating the relative accuracy of the yields between elements. To obtain an absolute yield it was necessary to normalize to K x-ray yields, which were calculated for relatively long-lived isotopes by use of data reported in the literature.[6] The mean calculated from these literature values was chosen as the normalization factor, but the standard deviation of these values was 26%. Therefore the absolute accuracy must have an uncertainty reflecting this discrepancy.

The general features of the K x-ray yield are in agreement with expectations. There are oscillations from element to element, emphasizing the fact that the conversion-electron yields are consequences of the properties of the specific levels populated in the decay scheme of an isotope. The most apparent feature of the yields is the marked increase for the heaviest elements. This is in accord with the assumption that this is a region of stable deformation which has a higher density of low-lying states, thus giving a higher x-ray yield. Interest has also been centered on the region containing elements 44 through 48, where another region of stable deformation is predicted. The low x-ray yields in this region do not rule out the possibility of this deformation, but suggest that if it occurs there is not a high density of low-lying states. Though the calculated deformation for these isotopes is fairly large[7] ($\beta \approx 0.23$), the mass is much lower than for the rare earth region, therefore giving a lower moment of inertia. By use of empirical data presented by Hyde[8] for $\Im/\Im_{rigid}$, the calculated value for the rotational constant is found to be $\hbar^2/2\Im$ = 47 keV. With such a small moment of inertia, the spacing between the states in the rotational band would be fairly large, resulting in a low x-ray yield.

The general shape of the K x-ray yields after beta decay when compared with the yields occurring promptly with fission[9, 10] show good agreement. Both indicate some structure between elements and an increase in yield for the heaviest products. However, there is a major discrepancy in the absolute value of the yields. The prompt yields tend to be greater by approximately a factor of 3 than the x-ray yields following beta decay. A sampling of literature values for K x ray yields following beta decay for a variety of elements is in agreement with our results and supports this large discrepancy with the prompt fragments. The beta decay process and the deexcitation of the prompt fragments do not necessarily populate the same states, so a complete correlation would not be expected. The prompt fragments on the average gamma-deexcite from a higher energy and have to carry away more angular momentum than states populated in beta decay. The conversion coefficient is, however, very sensitive to the energy and multipolarity of the transitions, with only the low-energy and high-multipolarity transitions yielding substantial quantities of conversion electrons. High-energy transitions from the population of higher energy states should not contribute substantially to the x-ray yield. The removal of the initial angular momentum by a probable cascade through the ground-state rotational band also does not appear to be able to give such a high x-ray yield.

Footnotes and References

†Present address: Sterling Chemical Laboratory, Yale University, New Haven, Connecticut.

1. J. B. Wilhelmy, S. G. Thompson, and J. O. Rasmussen, in Nuclear Chemistry Division Annual Report, 1967, UCRL-17989, Jan. 1968, p 134-137.
2. R. C. Jared and G. W. Kilian, Experimental Results of Selection and Biasing of FET's for Low-Energy x-Ray and γ-Ray Spectrometers, UCRL-17528, May 1967.
3. J. T. Routti and S. G. Prussin, UCRL-17672, Dec. 1968 (unpublished).
4. A. C. Wahl, R. L. Ferguson, D. R. Nethaway, D. E. Troutner, and K. Wolfsberg, Phys. Rev. 126, 1112 (1962).
5. R. L. Watson, UCRL-18632, Dec. 1968.
6. C. M. Lederer, J. M. Hollander, and I. Perlman, Table of Isotopes (John Wiley and Sons, New York, 1967).
7. W. D. Myers and W. J. Swiatecki, Nucl. Phys. 81, 1 (1966).
8. E. K. Hyde, I. Perlman, and G. T. Seaborg, The Nuclear Properties of the Heavy Elements (Prentice-Hall Inc., Englewood Cliffs, New Jersey, 1964), Vol. I, p 109.
9. R. L. Watson, H. R. Bowman, and S. G. Thompson, Phys. Rev. 162, 1169 (1967).
10. S. S. Kapoor, H. R. Bowman, and S. G. Thompson, Phys. Rev. 140, B1310 (1965).

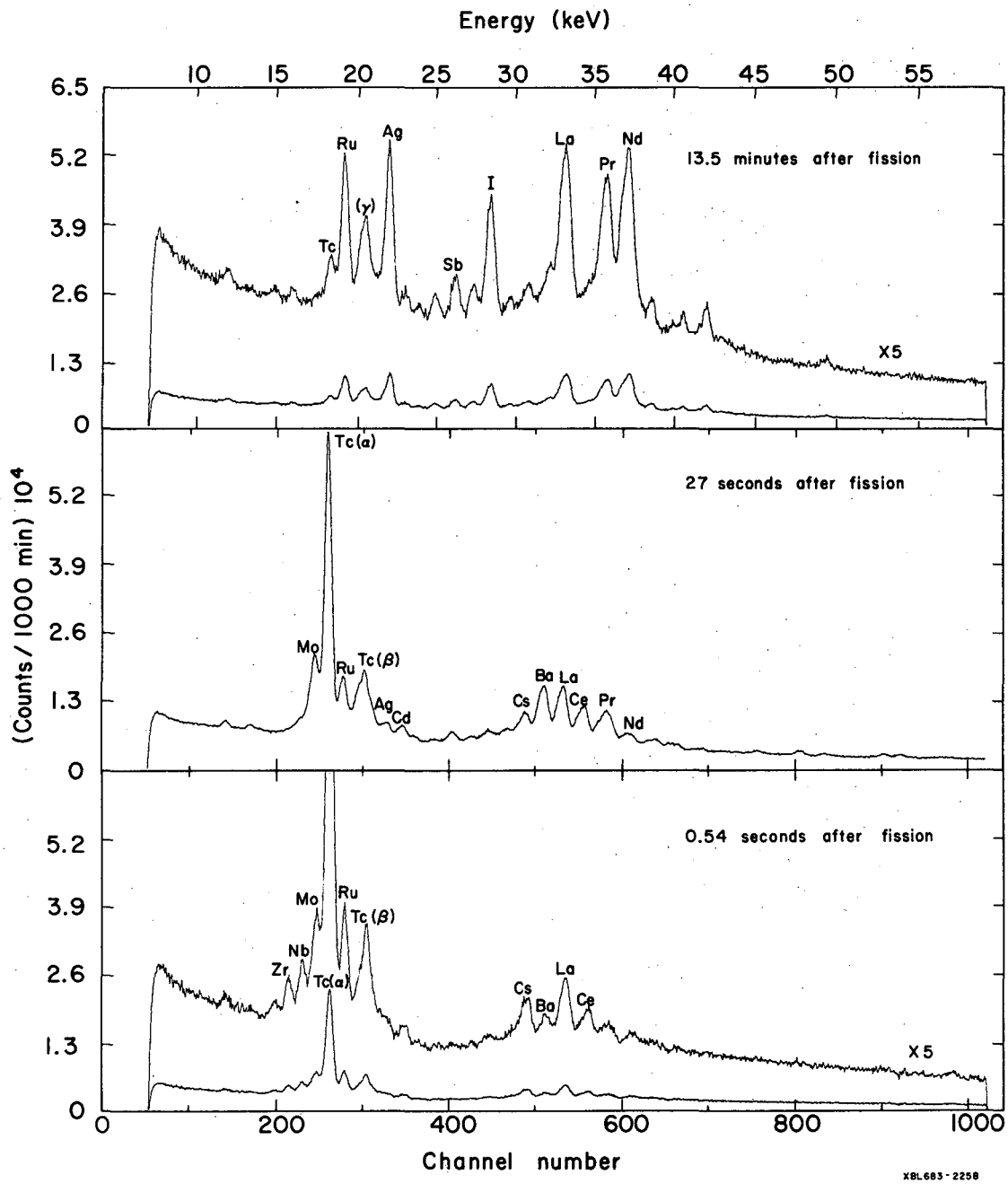

Fig. 1. X-ray spectra recorded with transit timing from source to detector of 13.5 min, 27 sec, and 0.54 sec.

Fig. 2. The x-ray fluorescence spectra for the elements Mo, In, and Nd. The dashed curves are the computer fit results for the $K\alpha_1$, $K\alpha_2$, $K\beta_1'$, and $K\beta_2'$ subgroups for each element.

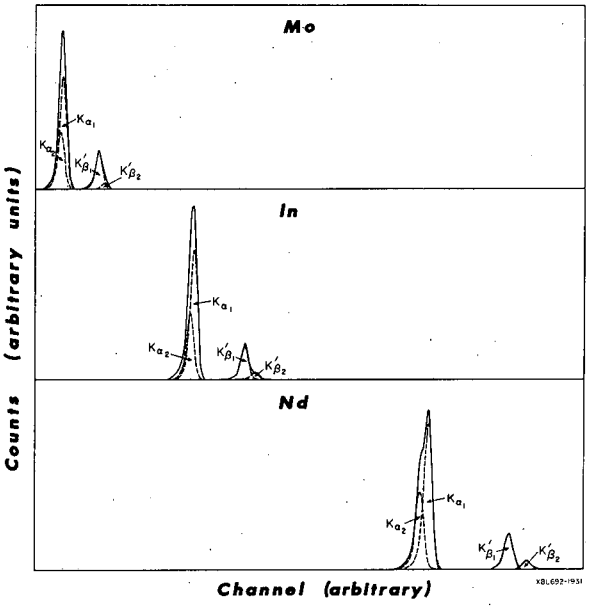

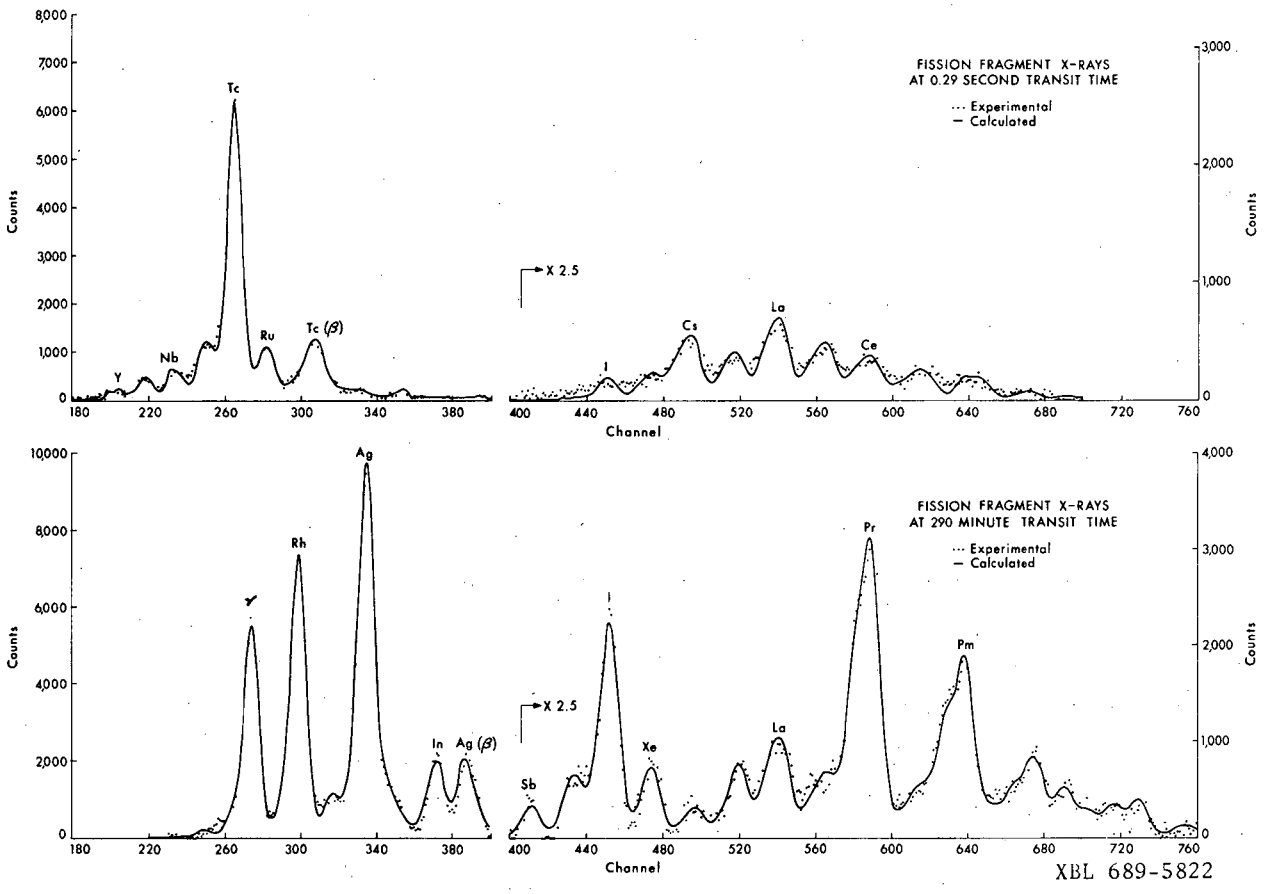

Fig. 3. Experimental and calculated values for the K x-ray distribution for transit times of 0.29 sec and 290 min.

Fig. 4. The K x-ray yield per element normalized by the calculated number of beta decays of that element occurring within 4.8 hours after the fission of ^{252}Cf.

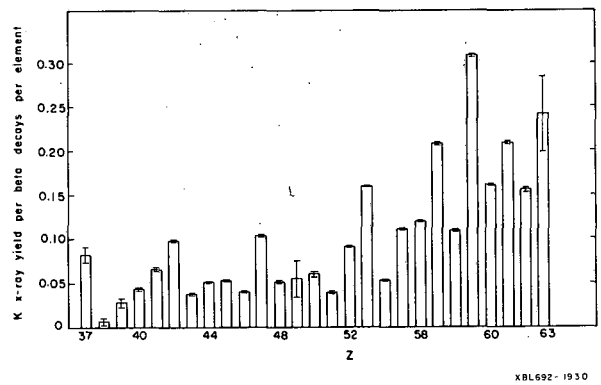

ELECTRON- AND BREMSSTRAHLUNG-INDUCED FISSION OF HEAVY AND MEDIUM-HEAVY NUCLEI†*

L. G. Moretto,‡ R. C. Gatti, S. G. Thompson, J. T. Routti, J. H. Heisenberg,†††** L. M. Middleman,†† M. R. Yearian,†† and R. Hofstadter††

The electron- and bremsstrahlung-induced fission of nuclei can be seen as a two-step process: first the excitation of the nucleus through the electromagnetic interaction and then the decay by fission.

The bremsstrahlung-induced fission cross section $\sigma_{B,f}$ is related to the photofission cross section $\sigma_{\gamma,f}$ through the bremsstrahlung spectrum $K^B(E_0, E)$ by the relation

$$\sigma_{B,f} = \int_0^{E_0} \sigma_{\gamma,f}(E)\, K^B(E_0, E)\, dE, \tag{1}$$

where E_0 and E are the electron and photon energies. Also the electron-induced fission cross section $\sigma_{e,f}$ can be related to the photofission cross section by

$$\sigma_{e,f} = \int_0^{E_0} \sigma_{\gamma,f}(E)\, K^e(E_0, E, \ell)\, dE, \tag{2}$$

where $K^e(E_0, E, \ell)$ is the distribution of virtual photons that can be associated with the electron and which are available to induce transitions of energy E and multipolarity ℓ.[1,2]

Since the theoretical expressions for $K^B(E_0, E)$ and $K^e(E_0, E, \ell)$ are known,[2,3] it is possible to check their consistency with experimental data. This could be done, for instance, by measuring $\sigma_{e,f}$ as a function of E_0, obtaining $\sigma_{\gamma,f}(E)$ by solving the integral Eq. (2), introducing such a function in Eq. (1), and comparing the result with the experimentally determined $\sigma_{B,f}$.

The electron- and bremsstrahlung-induced fission cross sections have been measured for the isotopes ^{238}U, ^{209}Bi, ^{208}Pb, ^{174}Yb, and ^{154}Sm in the energy range 60 to 1000 MeV.

The electron beam was provided by the Stanford Mark III Electron Linear Accelerator. The beam was deflected twice before entering the heavily shielded target area in order to eliminate unwanted bremsstrahlung associated with the electron beam.

The beam, after passing through the thin targets, was collected by a Faraday cup. By integrating the beam current, the total number of electrons striking the targets could be deduced. The targets were obtained by evaporating thin layers of the metals (Bi, Pb, Yb, Sm) or of the fluoride (U) on 1.8-mg/cm^2 Al foils.

The fission fragments were collected on mica strips covering the angular range from 45 to 205 deg with respect to the beam. Chemical etching of the mica with 48% hydrofluoric acid made the fission tracks in mica visible (and countable) under an optical microscope.

Radiators of different thickness could be put in front of the target to produce bremsstrahlung.

The electron-induced fission cross sections are presented in Fig. 1. The electron- plus bremsstrahlung-induced fission cross sections are presented in Fig. 2.

In order to check the consistency of the theoretical expressions for the bremsstrahlung spectrum and the electron virtual photon spectrum with the experimental data, the photofission cross sections have been obtained from the electron-induced fission cross sections by using the theoretical expressions for $K^{e}(E_0, E, \ell)$ in Eq. (2).

The photofission cross sections were integrated over the theoretical expression for $K^{B}(E_0, E)$ and the bremsstrahlung data were then compared with the calculated values.

In Fig. 3 one example of such a comparison is shown. The experimental points indicate the relative increase in fission cross section as a function of radiator thickness or bremsstrahlung intensity. The solid lines are the predictions on the basis of electron-induced fission cross-section data. It can be seen that the agreement is good. This procedure involves the solution of the integral Eq. (2) in order to obtain the photofission cross section. One example of a complete photofission cross section curve is shown in Fig. 4 for ^{209}Bi together with the electron-induced fission cross-section data and the fit to it obtained by integrating back the photofission cross section over the virtual-photon spectrum. It appears that the photofission cross section is strongly energy-dependent in the lowest photon energy range.

Such a dependence is shown also by the other nuclei of lower Z. Such a feature was observed before[4] and usually attributed to the onset of the π-meson photoproduction, whose threshold happens to be within the region of strong energy dependence of the cross section. However, no attempt was usually made to isolate the energy dependence of the photon-interaction cross section from that of the fission probability.

In order to ascertain whether the photon-interaction cross section, or the fission probability, or both, are responsible for the photofission cross section energy dependence, we have attempted to understand the energy dependence of the fission probability. On the basis of simple statistical considerations we have found an empirical relation between total fission probability P_F and excitation energy,

$$\ln P_F \simeq a - bE_x^{-1/2}. \tag{3}$$

Such behavior is presented for ^{4}He-induced fission of some nuclei in Fig. 5.

A plot of the logarithm of the photofission cross section against $E^{-1/2}$ shows, as in the example in Fig. 6, that there is a linear behavior in the energy range 80 to 250 MeV. This suggests that the energy dependence of the photofission cross section is determined to a great extent by the fission probability.

On the other hand, Levinger has shown[5] that at high photon energies, the photon interaction with a nucleus should occur with pairs of neutrons and protons called quasi-deuterons. The photon-interaction cross section with the nucleus turns out to be proportional to the deuteron photodisintegration cross section,

$$\sigma_0 = 8 \frac{NZ}{A} \sigma_D. \tag{4}$$

An inspection of the deuteron photodisintegration cross section shows it to be essentially constant in the energy region 80 to 250 MeV, as one would have expected from the behavior of the photofission cross sections described above. If now one divides the photofission cross sections by the calculated photon-interaction cross section (4) one should obtain the corresponding fission probability. This is also shown in Fig. 5; the linear dependence of the logarithm of such a quantity with $E^{-1/2}$ indicated that it is indeed the fission probability. Also the absolute value of the fission probability obtained this way seems to be reasonable, as proven by the value obtained independently in neutron-induced fission by Goldanski et al.,[6] indicated by a square in Fig. 6.

This seems to indicate that (a) the energy dependence of the photofission cross sections is mainly due to the energy dependence of the fission probability; (b) the quasi-deuteron model seems to account for all the interaction cross section relevant to the fission decay; and (c) mechanisms like π-meson photoproduction do not seem to transfer enough energy to make the nucleus undergo fission with sizable probability in the energy range considered (up to 400 MeV).

Footnotes and References

†Condensation of UCRL-18535, to be published in Phys. Rev.
*Work partially supported by the U. S. Office of Naval Research, Contract [Nonr 225(67)].
‡Present address: Laboratorio di Radiochimica, Università di Pavia, Pavia, Italy.
††Department of Physics and High Energy Physics Laboratory, Stanford University, Stanford, California.
**Work supported in part by Bundesministerium für Wissenschaft und Forschung.

1. K. F. Weizsacker, Z. Physik 88, 612 (1934); E. J. Williams, Phys. Rev. 45, 729 (1934).
2. W. C. Barber, Phys. Rev. 111, 1642 (1958).
3. Bruno Rossi, High Energy Particles (Prentice Hall, Englewood Cliffs, New Jersey, 1956), p 48.
4. A. V. Mitrofanova, Yu. N. Ranyuk, and P. V. Sorokin, Yad. Fiz. 6, 703 (1967); Sov. Nucl. Phys. 6, 512 (1968).
5. J. S. Levinger, Nuclear Photo-Disintegration (Oxford University Press, London, 1960).
6. V. I. Goldanski, V. S. Penkina, and E. A. Tamurov, Soviet Phys. -JETP 29, 778 (1955); Soviet Phys. -JETP 2, 677 (1956).
7. S. G. Thompson, Arkiv Fysik 36, 267 (1967).
8. L. G. Moretto, R. C. Gatti, and S. G. Thompson, in Nuclear Chemistry Annual Report, 1967, UCRL-17989, Jan. 1968, p 141.

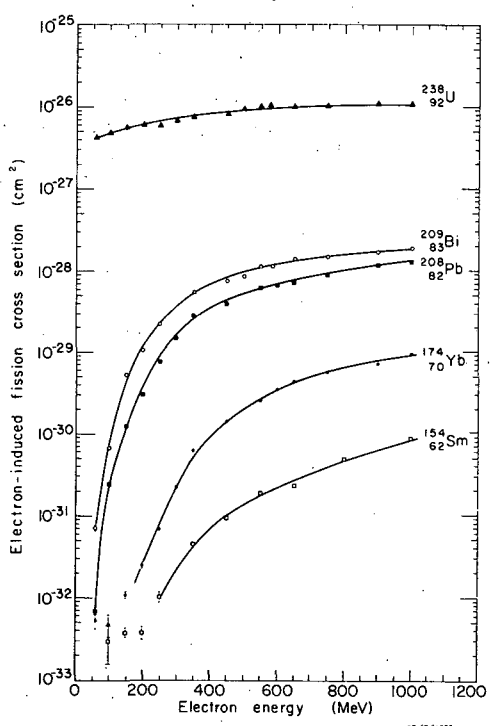

Fig. 1. Electron-induced fission cross-section data. Different symbols for the same isotope refer to different targets.

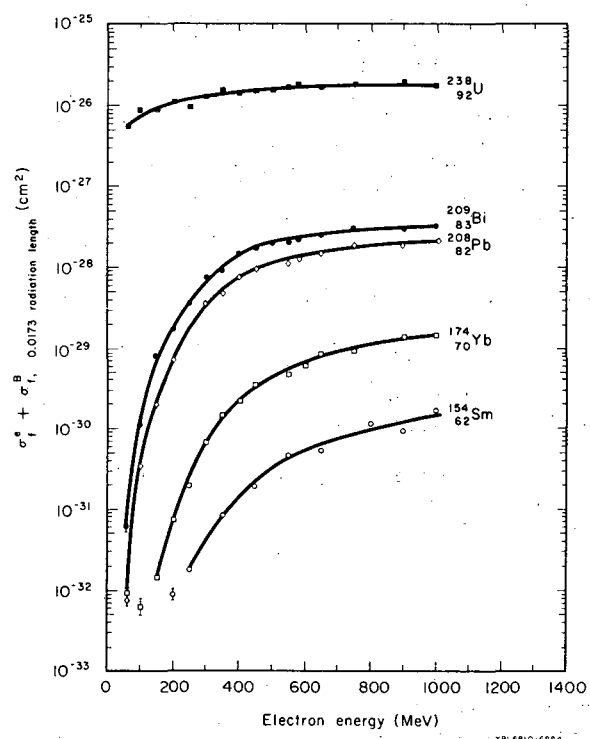

Fig. 2. Electron- plus bremsstrahlung-induced fission cross-section data. The bremsstrahlung were produced by an aluminum radiator of thickness 0.0173 radiation lengths, corresponding to 422 mg/cm^2.

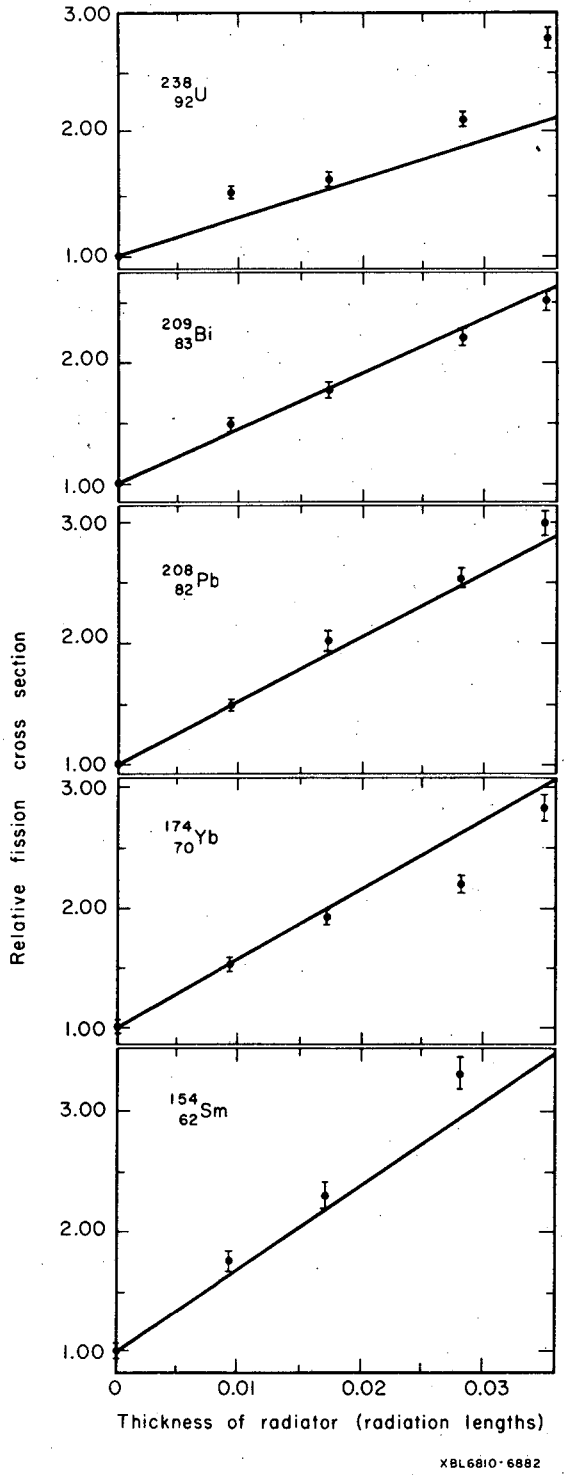

Fig. 3. Fission cross section as a function of radiator thickness. The thickness is expressed in radiation lengths. The measurements were made with 650-MeV electrons.

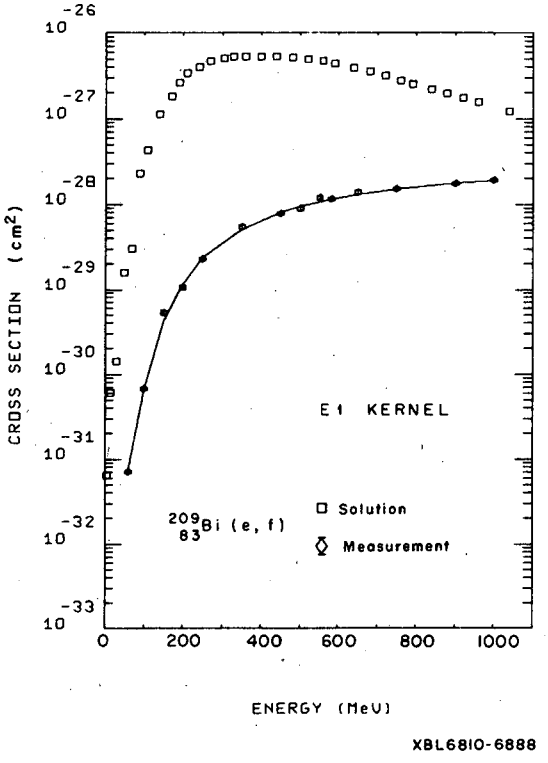

Fig. 4. Photofission cross section as a function of energy for $^{209}_{83}Bi$ (open squares), as obtained by unfolding the electron-induced fission cross section data (diamonds) with the E1 kernel. The solid line is the fit to the electron-induced fission cross sections, which is obtained by folding back the photofission cross section into the E1 kernel.

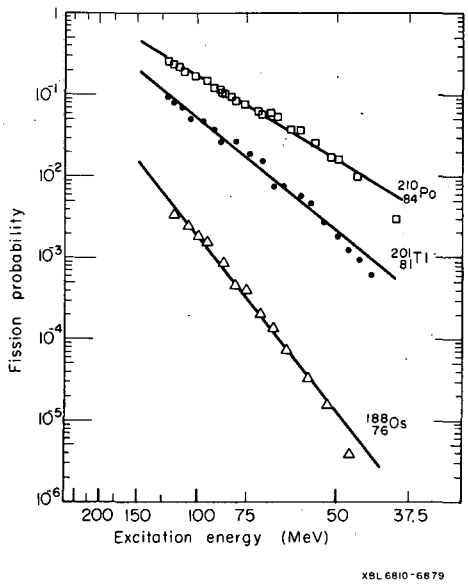

Fig. 5. Fission probability σ_f/σ_0 as a function of $E_x^{-1/2}$ for the reactions $^{206}_{82}$Pb (^{4}He, fission) (Ref. 7), $^{197}_{79}$Au (^{4}He, fission) (Ref. 7), and $^{184}_{74}$W (^{4}He, fission) (Ref. 8). For convenience the scale of the abscissa gives directly the energy in MeV.

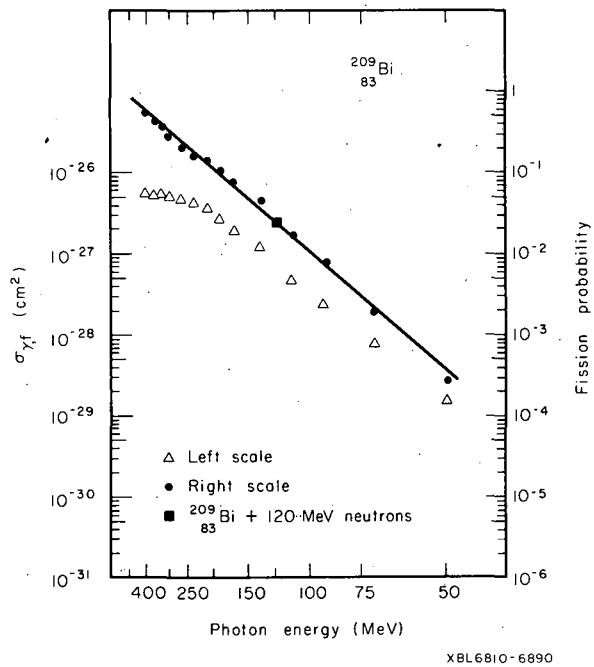

Fig. 6. Photofission cross section (△, left scale) and fission probability σ_f/σ_0 (●, right scale) as a function of $E_x^{-1/2}$ for $^{209}_{83}$Bi. The point indicated by a square is the fission probability calculated from the data of Goldanski et al. (Ref. 6).

PAIRING EFFECTS AT THE FISSION SADDLE POINT OF ^{210}Po AND ^{211}Po†

L. G. Moretto,* R. C. Gatti, S. G. Thompson,
J. R. Huizenga,‡ and J. O. Rasmussen††

Rather large pairing effects have been observed in some U and Pu isotopes at their fission saddle points.[1] The possibility that such an increase of pairing effects with respect to the ground state should be due to the increase in nuclear surface[2] has suggested extending such an investigation to nuclei like Po isotopes; in such nuclei the saddle-point deformation is larger than that of U and Pu isotopes and the increase in surface area is correspondingly larger.

The fission-fragment angular distributions were measured for ^{4}He-induced fission of ^{206}Pb and ^{207}Pb; the compound nuclei were obtained at excitation energies ranging from 3 to 20 MeV above the fission barriers. A small fission chamber was used (2.84 cm radius) (Fig. 1); a strip of mica was laid on the inner cylindrical surface to detect the fission fragments. The ^{4}He beam was provided by the 88-inch variable-frequency cyclotron in Berkeley. Such a beam, collimated to a diameter of 1.59 mm, was directed on the targets. The targets were obtained by evaporating the isotopes in metallic form on a copper block covered with ≈20 mg/cm^2 high-purity silver.

After the experiments the mica strips were developed in 48% HF and scanned under an optical microscope in the angular range from 85 to 170 deg with respect to the beam direction.

The experimental data, transformed to the center-of-mass system, were fitted by a theoretical expression relating the angular distribution of fission fragments to the distribution of the total angular momentum I and of the angular momentum projection K on the nuclear symmetry

axis at the saddle point. By a least-squares fitting procedure the variance K_0^2 of the K distribution was obtained. Two examples of angular distributions with the theoretical fit are shown in Figs. 2 and 3.

It can be shown that the quantity K_0^2 is approximately proportional to the average number of quasi particles: $K_0^2 \approx \bar{n}k^2$, where k^2 is the average contribution of one quasi particle. Since the quasi particles are obtained by breaking pairs of nucleons, K_0^2 contains information regarding the pairing effects at the saddle point.

In Figs. 4 and 5 the quantity K_0^2 is plotted against excitation energy for ^{210}Po and ^{211}Po.

In the case of the even-even nucleus ^{210}Po the K_0^2 value approaches zero at about 3 MeV above the barrier. This would indicate that the pairing gap (region where there is no quasi-particle excitation) should be at least as large as 3 MeV. In the case of the odd-A nucleus ^{211}Po, K_0^2 remains rather large even at $\approx$3 MeV above the fission barrier. This should be due to the substantial contribution to K_0^2 of the residual quasi particle.

The experimental difference in K_0^2 between the even-even and the odd-A nucleus at corresponding energies is approximately constant (about 7.5 units). This can be seen as an even-odd effect, and more precisely the difference of 7.5 units of K_0^2 can be interpreted as the average contribution to K_0^2 of a single neutron quasi particle. This checks rather well with the Nilsson model, which predicts a value of approximately 8 units for the same quantity. Some structure visible in the two curves seems also consistent with such a picture. In ^{210}Po two flattenings occur at $K_0^2 \approx 16$ and $K_0^2 \approx 29$, values which are consistent with the expected ones for two- and four-quasi-particle states. Similarly in ^{211}Po two flattenings can be seen at $K_0^2 \approx 22.5$ and $K_0^2 \approx 37.5$, again very close to the expected values for three- and five-quasi-particle states. The overall picture seems to indicate a pairing gap even larger than the 3 MeV deduced before from the low K_0^2 values in ^{210}Po at small energies above the barrier. A more consistent value for the pairing gap of ^{210}Po might be 4 MeV or possibly larger.

An analysis of the even-odd differences at the saddle point would indicate also a pairing gap of 3.62 MeV. This value is in good agreement with the value estimated above, but suffers from some uncertainties.

Attempts to predict such large pairing gaps by making the strength of the pairing interaction surface dependent seem to be moderately successful,[2] although more experimental data is needed for other nuclei. In Fig. 6 the calculated surface dependence of the gap parameter Δ is shown on the assumption of a surface-dependent pairing strength. In ^{210}Po the relative increase of the surface at the saddle point is $\approx$20%. It can be seen that the calculation presented in Fig. 6 is not able to account for the whole effect.

Footnotes and References

†Condensation of UCRL-18390, to be published in Phys. Rev.
*Present address: Laboratorio di Radiochimica, Università di Pavia, Pavia, Italy.
‡Present address: Nuclear Structure Research Laboratory, River Campus Station, The University of Rochester, Rochester, New York.
††Present address: Sterling Chemical Laboratory, Yale University, New Haven, Connecticut.
1. F. A. Rickey, Jr., and H. C. Britt, Bull. Am. Phys. Soc. 13, 36 (1968).
2. W. Stepien and Z. Szymanski, Phys. Letters 26B, 181 (1968).

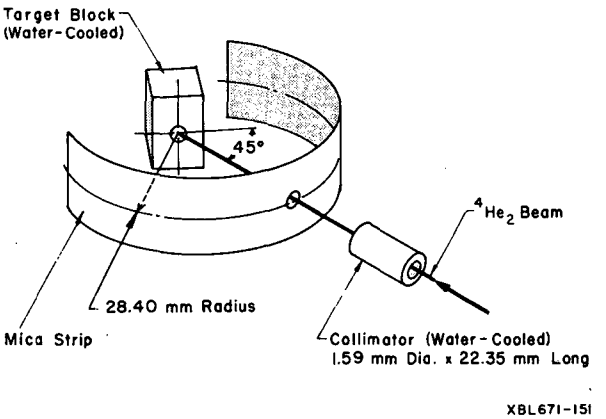

Fig. 1. Schematic drawing of the apparatus used in measuring angular distributions of fission fragments.

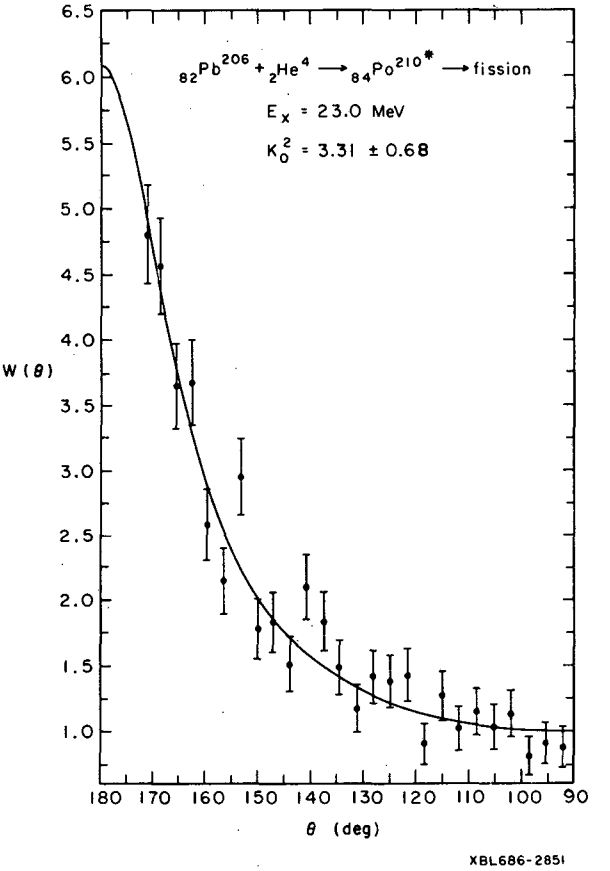

Fig. 2. Center of mass angular distribution of fission fragments in 29 MeV ^{4}He induced fission of ^{206}Pb. The continuous line is the least-squares fit to the experimental data.

Fig. 3. Center of mass angular distribution of fission fragments in 31 MeV ^{4}He induced fission of ^{207}Pb. The continuous line is the least-squares fit to the experimental data.

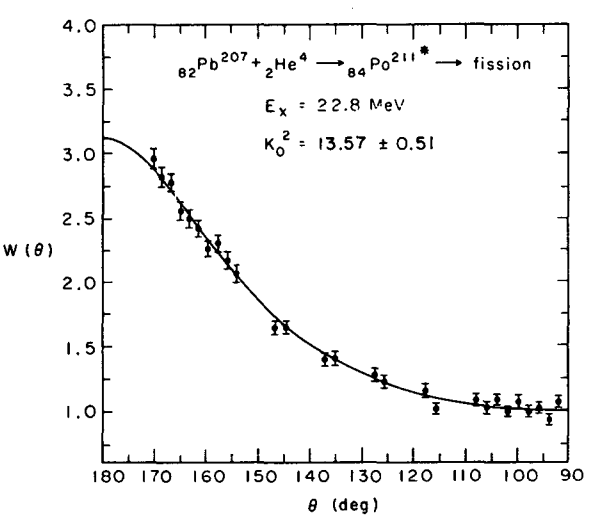

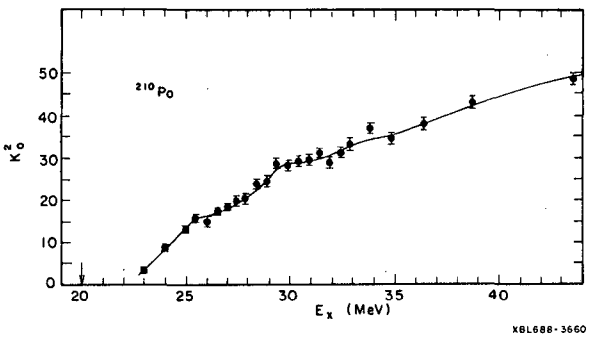

Fig. 4. K_0^2 dependence on excitation energy at the fission saddle point of ^{210}Po. The arrow indicates the position of the fission barrier.

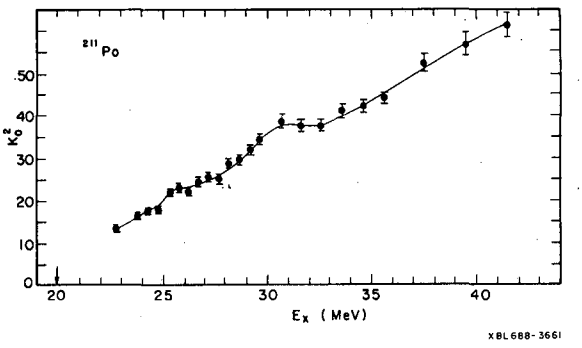

Fig. 5. K_0^2 dependence on excitation energy at the fission saddle point of ^{211}Po. The arrow indicates the position of the fission barrier.

Fig. 6. Calculated dependence of the gap parameter on the nuclear surface.

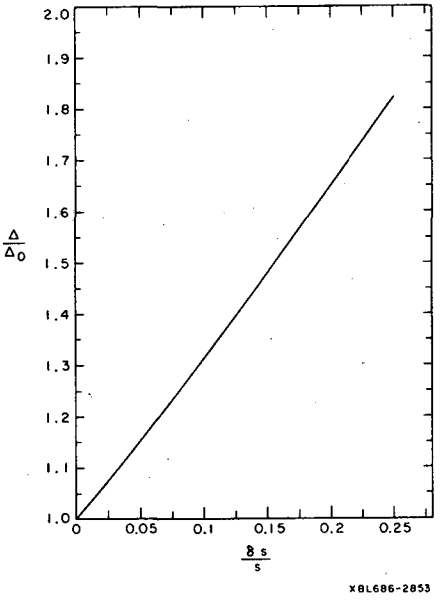

II. Chemical and Atomic Physics

ATOMIC AND MOLECULAR SPECTROSCOPY

ATOMIC BEAM MEASUREMENT OF ISOTOPE SHIFTS IN THE D_1 LINE OF ^{127}Cs, ^{129}Cs, ^{133}Cs, ^{134m}Cs, ^{134}Cs, AND ^{137}Cs †

Richard Marrus, Edmond C. Wang, and Joseph Yellin

Historically, the measurement of isotope shifts has always been done by methods in which light is detected. Conventional optical spectroscopy, optical scanning methods,[1] and laser methods[2] all have this feature in common. Associated with the light-detecting experiments are certain inherent problems which have long inhibited the study of radioactive isotopes. In particular, carrier-free samples of the radioactive isotopes under study must be employed, for otherwise the weak light from the small number of radioactive isotopes under study will be swamped by the intense light of the carrier atoms. For neutron-produced isotopes, this implies that a very expensive and time-consuming mass separation must be performed. For cyclotron-produced isotopes a chemical separation must be performed. Both of these put stringent limits on the half-lives of the isotopes that can be studied. Additionally, there is the problem of wall interaction of the isotopes with the walls of the container in which they are placed. Although there has been some progress in extending the range of radioisotopes studied,[3] it is clear that the fundamental problems still remain, particularly as regards isotopes with half-lives of a few hours or less.

Recently, a method employing the atomic-beam technique has been reported for investigating isotope shifts.[4] With the atomic beam technique as applied to radioactive isotopes, detection is directly on the radioactivity of the isotopes under study, and the basic problems besetting the light-detecting experiments are circumvented. As a result, the atomic-beam technique has enjoyed a great deal of success in the study of hyperfine structures of radioactive isotopes, to the extent that several hundred have, by now, been successfully studied.[5] Hence the atomic-beam technique would seem to offer fair hope of substantially extending the range of isotope-shift measurements in radioactive isotopes.

In this paper we report the first measurement of isotope shifts on a number of radioactive isotopes of the same element, cesium. From many points of view, cesium is an almost ideal element for a first study of this kind. From a purely experimental point of view, the experimental methods for producing and detecting a large number of cesium isotopes are already known from earlier atomic-beam hyperfine-structure studies.[6] In addition, cesium lamps producing intense D-line radiation are easy to make, and finally the Stark shifts of the D_1 line are sufficiently large[7] that the line separations between the different isotopes are easily spanned. Also, from the point of view of nuclear physics, the cesium isotopes offer interesting possibilities. The neutron-deficient cesium isotopes around ^{127}Cs are believed to be strongly deformed, while ^{137}Cs has a magic number of 82 neutrons and is well described by the shell model. Hence a study of the isotope shifts over a large change of neutron number should determine the systematics of the change in the mean value of $\langle r^2 \rangle$ in going from highly deformed nuclei to spherical nuclei.

The basic apparatus employed is a conventional atomic beam machine with flop-in magnet geometry.[8] The only new features are a pair of electric-field plates capable of sustaining fields up to nearly 10^6 V/cm and hardware associated with the cesium resonance radiation incident on the C region.

The most important requirement on our electric-field plates is that they be able to sustain an electric field sufficiently intense to Stark-shift the D line through an amount greater than the hyperfine structure of the cesium ground state. This implies fields of the order of several hundred thousand V/cm. In addition we ask for the best homogeneity possible over a region equal in height to the beam height and as long as the light irradiation length (about 0.040 by 2 in.). We have been able to achieve about 0.5% at the highest fields. A schematic of the basic design is shown in Fig. 1.

An interesting feature of the electric field plates is that because of the narrow gap and the length (about 6 in.), they act as a state selector in the atomic-beam apparatus. It can be seen in

Fig. 2 that by rotating the plates with respect to the beam axis, either the trajecotry with $m_J = +1/2$ in the A magnet or the trajectory with $m_J = -1/2$ in the A magnet can be blocked out. With reference to a Breit-Rabi diagram[9] for $J = 1/2$, it is observed that essentially all atoms with $m_J = +1/2$ in the A magnet arise from the upper hyperfine level ($F = I + 1/2$), whereas all atoms with $m_J = -1/2$ in the A magnet arise from the lower hyperfine level ($F = I - 1/2$). This feature is very useful, and has been employed extensively in our experiment.

The basic method employed results from the idea of a tuning experiment; this idea has already been used successfully in the study of the isotope shifts in the mercury isotopes.[1] In those experiments a magnetic field was used to tune the emission lines of lamp atoms with the absorption lines of the isotopes under study. However, in atoms, such as cesium, which exhibit considerable hyperfine structure (hfs), a magnetic field is not a suitable tuning mechanism. The reason is that the magnetic field will lift the Zeeman degeneracy, which gives rise to a complicated splitting pattern. In the case of ^{133}Cs, for example, with a nuclear spin of $I = 7/2$, there are 16 Zeeman sublevels in the ground state alone. Moreover, most of them are connected by optical matrix elements to six excited states and the resultant tuning signals are too complicated to be interpretable.

The D_1 transition ($6^2p_{1/2} \rightarrow 6^2s_{1/2}$) of cesium has, however, a property that makes the employment of electric fields an almost ideal tuning mechanism; namely, that both states involved in the transition have electronic angular momentum $J = 1/2$. To understand the special nature of states with $J = 1/2$, consider the second-order Stark matrix element determining the energy shift,

$$\Delta W(n^2\ell_J I F m_F) = \sum_{\psi} \frac{|\langle n^2\ell_J I F m_F | -e\bar{r}\cdot\bar{E}|\psi\rangle|^2}{\Delta E(\psi; n^2\ell_J I F m_F)} \quad , \tag{1}$$

where ΔW is the induced energy shift in the state with the indicated quantum numbers, $\bar{r}$ is the dipole operator, and $\bar{E}$ is the applied electric field. It can be shown[7] that for the case in which $J = 1/2$, the matrix element squared, $|\langle n^2\ell_J I F m_F | -e\bar{r}\cdot\bar{E}|\psi\rangle|^2$, is independent of all the angular momentum quantum numbers for the state. This means that the only mechanism by which states of different F can have a differential shift results from the fact that, in the denominator of (1), different hyperfine levels, F, belonging to the same multiplet (n, I, J, ℓ), have slightly different energies. However, this is clearly a very small effect, being of order O (hfs/optical energy separation) $\approx 10^{-5}$. If the possibility is now considered of inducing a differential shift in states of the same F, but different m_F (lifting of Zeeman degeneracy), it is seen that the expression (1) gives no mechanism for doing so. Since lifting of Zeeman degeneracy must occur in a higher order of perturbation theory, it is reasonable to expect that such an effect is even smaller than the differential shift of the hyperfine levels. Thus the largest shift is the gross Stark shift, which affects all the hyperfine states equally. Experiment values of the gross Stark shift,[7] differential hyperfine shift,[10] and lifting of the Zeeman degeneracy[11] are all in the literature. In order to understand the significance of these effects for the Stark tuning experiments reported here, the magnitude of the latter two effects needs to be compared with the line width expected in the experiment. The smallest possible line which is the natural line width of the D_1 transition, about 10 MHz. This is substantially larger than either of these effects. Hence we conclude that for purposes of a tuning experiment the only significant effect of an electric field is to shift all hyperfine states belonging to an atomic level by an equal amount, all other effects being negligible.

Unlike the Zeeman tuning experiments, in which the frequency shift induced for a given applied magnetic field is accurately calculable from the well-understood Zeeman effect, the Stark effect is not well known. Hence any experiment employing an electric field as a tuning mechanism must have a built-in mechanism for determining the Stark effect, i.e., for obtaining a calibration of frequency shift vs (applied voltage)^2. The method for doing this has been reported in Ref. 4.

The basic apparatus is shown in Fig. 3. Light from a cesium discharge lamp is passed through a filter which transmits only the D_1 line. This line consists, in the lamp, of two resolved components which are separated by the ground-state hfs. The width of each of these components is about 1500 MHz, the principle sources of this width being the hfs of the excited $6\,^2p_{1/2}$ state and the Doppler width. In order to improve the precision of the experiment, the light is now passed through a cell containing an optically dense cesium absorption beam. Such a beam will absorb the light in two lines from each of the components emitted by the lamp. The separation of the two lines is equal to the hfs of the excited $6\,^2p_{1/2}$ state. The width of the lines is characteristic of the beam collimation and is about 150 MHz. Within the lines we have been able to achieve almost

complete absorption (> 50%) for several hours. The light so filtered and structured is now allowed to fall incident between the plates of an electric field apparatus located in the C region of the atomic beam apparatus.

Consider now the behavior of a ^{133}Cs beam in the C region of the atomic beam apparatus under the irradiation of this light. At zero electric field the absorption lines (see Fig. 4) of the atoms in the atomic beam apparatus coincide with the absorption lines of cesium atoms in the absorption cell, and a minimum in the intensity curve is observed. However, as the electric field is turned on, the Stark effect decreases the frequency of the absorption lines of atoms in the beam apparatus, and the observed signal increases until the electric field is sufficient to shift the frequency by an amount equal to the hfs of the excited ($6\,^2p_{1/2}$) state, when a second intensity minimum is observed. At higher electric fields the frequency is shifted by an amount equal to the ground-state hfs, and the beam absorption line is brought into resonance with the second lamp emission line. Here, three intensity minima can be observed corresponding to the overlap positions indicated in the energy-level diagram. These three minima are equally spaced and correspond to a shift by an amount equal to the hfs of $6\,^2p_{1/2}$. The unlabeled minima correspond to structure present in the lamp line. As can be seen from the energy-level diagram, the separation between the two minimum points labeled α and δ corresponds to a Stark shift of the energy levels equal to 91.92 MHz, the hfs of the ^{133}Cs ground state. It is this that we use as a calibration.

This same method, applied to atomic beams of other isotopes, can be used to determine the isotope shifts. Consider now a ^{134m}Cs beam. Here, the hfs of both $6\,^2s_{1/2}$ and $6\,^2p_{1/2}$ is smaller than for ^{133}Cs, so that Stark tuning can bring about only one overlap of the beam-absorption lines with the lamp-emission lines. However, there are four possible overlap positions of the Stark-shifted energy levels of ^{134m}Cs beam atoms with the unshifted levels of ^{133}Cs atoms in the absorption cell. As seen in Fig. 5, these overlap positions correspond to minima in the observed intensity pattern. From the energy-level diagram, it is clear that the separations between the minima α and β and between γ and δ correspond to the hfs of the $6\,^2p_{1/2}$ state of ^{134m}Cs. These are experimentally seen to be equal. Moreover, the separations between α and γ and between β and δ should correspond to the hfs of the $6\,^2p_{1/2}$ state of ^{133}Cs. This also agrees with our observations. From the absolute positions of the four minima and a knowledge of the hfs of the ground and excited states, the isotope shift can be deduced. We find Isotope shift: $-1.4(1.5)\times10^{-3}$ cm^{-1}, where the negative sign indicates that the energy of the D_1 line in ^{134m}Cs is smaller than that in ^{133}Cs.

Similar data have been obtained for all the other isotopes reported here. Results are given in Table I.

In Table I are given the results to date on all cesium isotope shift measurements for the D_1 line. In the case of ^{131}Cs and ^{132}Cs the measurements are actually made for the D_2 line, but we infer the D_1 isotope shift from these results and the ratio of D_2 to D_1 isotope shift given by Hühnermann and Wagner[13] for ^{134}Cs. These measurements form a rather complete picture for the isotopes in the range ^{127}Cs to ^{137}Cs.

There are several striking features to the data. First we note that there seems to exist a small but finite isomer shift between ^{134m}Cs and ^{134}Cs, the size of the effect being larger than two standard deviations if one employs Hühnermann and Wagner's value for ^{134}Cs. This is very strong evidence that the observed shifts are due primarily to nuclear effects, since mass effects would not give rise to an isomer shift. Also bearing on this point are recent calculations by a nonrelativistic Hartree-Fock approximation by Bauche[14] on the specific mass effect in cesium. Bauche's result is a shift of -0.77 mK between ^{132}Cs and ^{134}Cs, where the minus sign indicates the shift is in the direction opposite to the normal (reduced) mass shift. The normal mass shift can be calculated exactly and is equal to +0.69 mK between the same two isotopes, and the two mass effects substantially cancel each other out. Although there is certainly an error to be associated with Bauche's calculation, we believe that the main conclusion that mass effects are small relative to the measured shifts is well supported by the ^{134}Cs - ^{134m}Cs isomer shift.

If it is accepted that the observed shifts are indeed nuclear effects, then there are several qualitative comments that can be made. First we note that the observed shifts are only a small fraction of the shifts predicted by the normal volume effect. The prediction of the normal nuclear effect can be calculated from the usual expressions,[15] using for $|\psi^2(0)|$ the value determined from the ^{133}Cs ground state hfs and the NMR value[16] for the nuclear moment. It is found that $\delta(\Delta E)$ = 10 mK/neutron. The observed shifts are seen to be almost an order of magnitude smaller over the entire range of measurement. A similar situation has been found to exist in the measured isotope shifts in the xenon isotopes[17] (z = 54) and in the barium isotopes[18] (z = 56).

There would appear to be at least two possible explanations for the smallness of these shifts. One possibility is that in the approach to a closed shell of neutrons the normal volume effect should be somewhat diminished. Another possible explanation is suggested by the fact that the cesium isotopes on the neutron-deficient side of ^{133}Cs seem to have increased deformations. Recent measurements[19] of the quadrupole moments of ^{131}Cs and ^{132}Cs confirm this point. Hence the deformation effect may offset the volume effect on the neutron-deficient side of ^{133}Cs.

Footnote and References

†Condensed from Phys. Rev. (Jan. 1969).

1. O. Buhl, Z. Physik 109, 180 (1938); 110, 395 (1938); F. Bitter, S. P. Davis, B. Richter, and J. Young, Phys. Rev. 96, 1531 (1954).
2. R. H. Cordover, P. A. Bonczyk, and A. Javan, Phys. Rev. Letters 18, 730 (1967).
3. See, for example, S. P. Davis, T. Aung, and H. Kleiman, Phys. Rev. 147, 861 (1966).
4. R. Marrus and D. W. McColm, Phys. Rev. Letters 15, 813 (1965); R. Marrus, E. Wang, and Y. Yellin, Phys. Rev. Letters 19, 1 (1967).
5. For measurements made by the atomic beam method, see the Tables of V. W. Cohen and G. Fuller, Nuclear Moments, May 1965. For a review of the method as applied to radioactive isotopes see W. A. Nierenberg, Ann. Rev. Nucl. Sci. 7, 349 (1957).
6. W. A. Nierenberg, H. A. Shugart, H. B. Silsbee, and R. H. Sunderland, Phys. Rev. 104, 1380 (1956); H. H. Stroke, D. S. Edwards, Jr., V. Jaccarino, and R. Weiss, Phys. Rev. 105, 590 (1957).
7. R. Marrus, D. McColm, and J. Yellin, Phys. Rev. 147, 55 (1966).
8. J. R. Zacharias, Phys. Rev. 61, 270 (1942).
9. See, for example, N. F. Ramsey, Molecular Beams (Oxford University Press, London, 1956), p 79.
10. R. D. Haun, Jr., and J. R. Zacharias, Phys. Rev. 107, 107 (1957).
11. P. G. H. Sandars and E. Lipworth, Phys. Rev. Letters 13, 716 (1964).
12. E. W. Otten and S. Ullrich (Erstes Physikalisches Institut du Universität Heidelberg), private communication, and Z. Physik (to be published).
13. H. Hühnermann and H. Wagner, Phys. Letters 21, 303 (1966); H. Hühnermann and H. Wagner, Z. Physik 199, 239 (1967).
14. J. Bauche (Laboratoire Aime-Cotton, Orday, France), private communication.
15. H. Kopfermann, Nuclear Moments (Academic Press, Inc., New York, 1958).
16. H. E. Walchli, ORNL-1775, 1954.
17. J. Koch and E. Rasmussen, Phys. Rev. 77, 722 (1950).
18. D. A. Jackson and D. H. Tuan, Proc. Roy. Soc. (London) A291, 9 (1966); 274A, 145 (1963).
19. F. Ackermann, E. W. Otten, G. Zu Putlitz, A. Schenck, and S. Ullrich, Phys. Letters 26B, 367 (1968).

Table I. Measured isotope shifts in the cesium isotopes (10^{-3} cm^{-1}).

Isotope	127	129	131	132	134	134m	135	137
This work	5.9(1.5)	2.8(1.5)			1.8(1.0)	-2.2(1.2)		-6.0(1.5)
Otten and Ullrich (Ref. 12)			-0.31(5)	1.6(5)				
Hühnermann and Wagner (Ref. 13).					1.17(5)		-1.23(7)	-4.81(6)

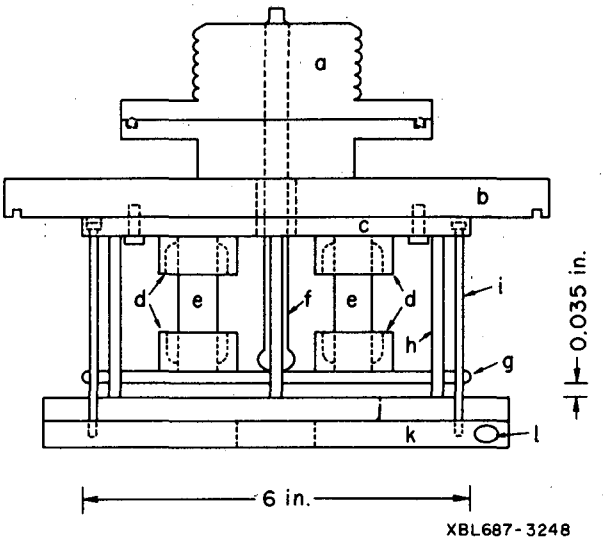

Fig. 1. Schematic diagram of the electric field plate construction.

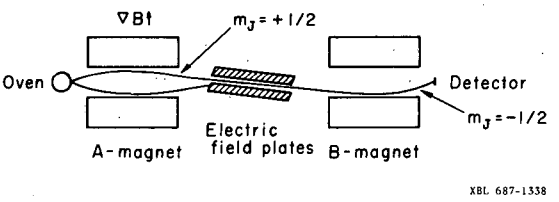

Fig. 2. Schematic diagram (exaggerated) showing how the electric field plates can select either of the two trajectories.

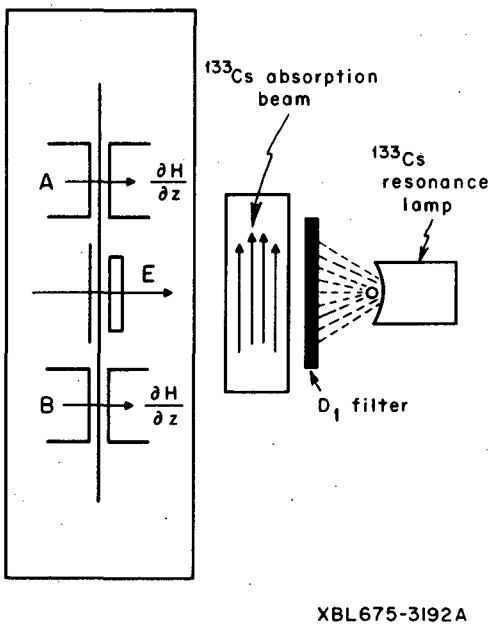

Fig. 3. Schematic diagram of the apparatus.

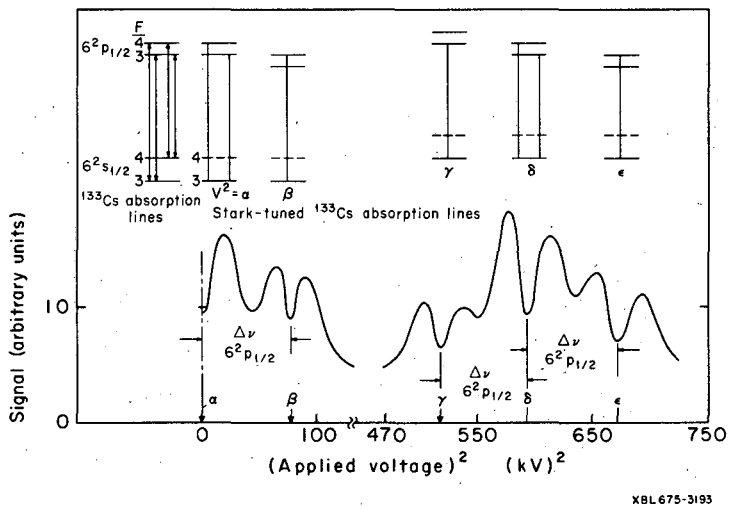

Fig. 4. Observed ^{133}Cs signal vs square of applied voltage. The position of the Stark-shifted absorption lines relative to those in the absorption cell for each of the observed minima is indicated directly above the the minima. The separation between α and δ corresponds to a shift equal to the ground-state hyperfine separation and serves as a calibration.

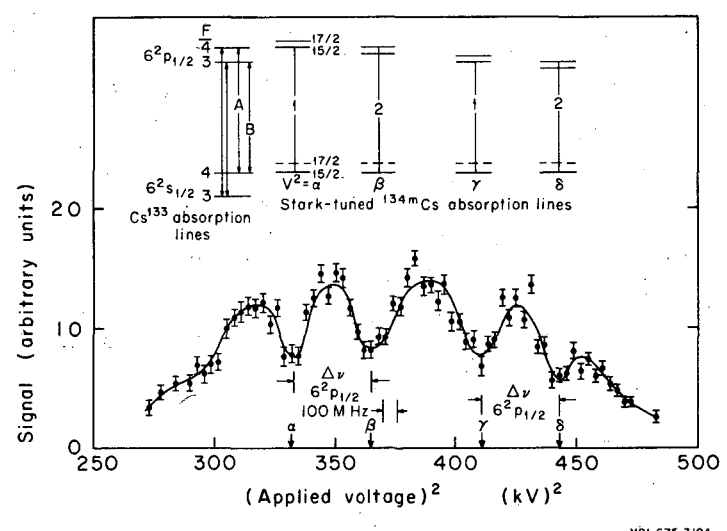

Fig. 5. Observed ^{134m}Cs signal vs square of applied voltage. The minimum α occurs when beam-absorption line 1 coincides with ^{133}Cs absorption line A; β occurs when line 2 coincides with A; γ occurs when 1 coincides with B; and δ occurs when 2 coincides with B.

ATOMIC BEAM STUDY OF THE $^{85-87}$Rb ISOTOPE SHIFT †

Tuan H. Duong, Richard Marrus, and Joseph Yellin

The most reliable estimates of the $^{85-87}$Rb isotope shift (IS) are based on early spectroscopic studies of the resonance lines of these isotopes by Kopfermann and Krüger[1] and by Hollenberg.[2] On the basis of these studies Brix and Kopfermann[3] have determined the isotope shift, IS < +3 mk (1 mK= 10^{-3} cm^{-1}). In the experiment reported here the atomic beam method has been used to obtain a more precise measurement of the IS.

An atomic beam apparatus with flop-in geometry is used. The C region consists of a pair of electric field plates with a gap of 0.035 in. ^{87}Rb atoms (99.16% enriched) from the oven of the atomic beam apparatus are state-selected by the gap so that only atoms in the $m_J = -1/2$ state pass through the C region. This means that essentially only atoms in the lower hyperfine state, F = 1, can be refocused. Light from an enriched ^{85}Rb (99.54%) resonance lamp illuminates the region between the electric field plates after filtration by a D_1 interference filter. The lamp line consists of a doublet separated by the ground-state hyperfine structure (hfs) of ^{85}Rb, the $^2P_{1/2}$ hfs not being resolved in the lamp. If an electric field is applied across the gap, the transition frequencies of the ^{87}Rb resonance line are decreased by the Stark effect and for certain values of the electric field become equal to the transition frequencies of the ^{85}Rb lines (see Fig. 1). Resonance absorption of ^{85}Rb photons by ^{87}Rb atoms then takes place and ^{87}Rb atoms are pumped into the $m_J = +1/2$ and thus F = 2 level. These atoms refocus and a signal is observed at the detector. As the electric field is increased from 0 to 380 kV/cm two resonances are observed, separated by the ground-state hfs of ^{85}Rb. A crude measurement of the relative isotope shift (RIS) can then be obtained from the voltages at which resonances occur, and the hfs of ^{85}Rb and ^{87}Rb. The Stark shift is calibrated by using the same isotopes in both the atomic beam apparatus and lamp, and measuring the voltages required to shift through the known ground-state hfs of the ^{85}Rb (or ^{87}Rb).

Precision is obtained by filtering the ^{85}Rb D_1 line by a dense beam of Rb in natural abundance. Each resonance is then resolved into two pairs of intensity minima, the separation between pairs equaling the ^{87}Rb $5^2P_{1/2}$ hfs, while the separation within a pair is the ^{85}Rb $5^2P_{1/2}$ hfs (see Ref. 5). In this experiment widths of approximately 200 MHz were achieved and the RIS could be determined to within 0.5 mK, which is three times the mean error.

An alternative though less satisfactory way to improve the precision is to have the lamp line self-reversed. Intensity minima having widths of 400 to 500 MHz are obtained in this way. Measurements were made with an absorption beam and with the line self-reversed, and the results show that the position of the resonance was not affected by the increased line width. The roles of the ^{85}Rb and ^{87}Rb were reversed and additional measurements made, with consistent results. Typical data are shown in Fig. 1. The average of 24 determinations yields for the ^{85,87}Rb RIS 3.5 ± 0.5 mK, with the ^{87}Rb isotope having the higher ($5^2P_{1/2}$ - $5^2S_{1/2}$) transition frequency. This value is not corrected for the Bohr mass effect, which contributes 1.9 mK. In addition the ^{87}Rb $^2P_{1/2}$ hfs has been determined to be 812 ± 15 MHz, in agreement with the results of Rabi and Senitzky.[6] We have used the latter's atomic beam double-resonance determination of the $5^2P_{1/2}$ hfs of the Rb isotopes in reducing our data.

Footnote and References

†Condensed from Phys. Letters 27B[9], 565 (1968).

1. H. Kopfermann and H. Krüger, Z. Physik 103, 485 (1936).
2. A. V. Hollenberg, Phys. Rev. 52, 139 (1937).
3. Brix and Kopfermann, in Landolt-Bornstein Vol. 1, Pt. 5, 23 (1952); also H. Kopfermann, Nuclear Moments (Academic Press, Inc., New York, 1958), p 166.
4. R. Marrus and D. McColm, Phys. Rev. Letters 15, 813 (1965); see also R. Marrus, D. McColm, and J. Yellin, Phys. Rev. 147, 55 (1966).
5. R. Marrus, E. Wang, and J. Yellin, Phys. Rev. Letters 19, 1 (1967).
6. B. Senitzky and I. I. Rabi, Phys. Rev. 103, 315 (1959); M. L. Perl, I. I. Rabi, and B. Senitzky, Phys. Rev. 98, 611 (1955).

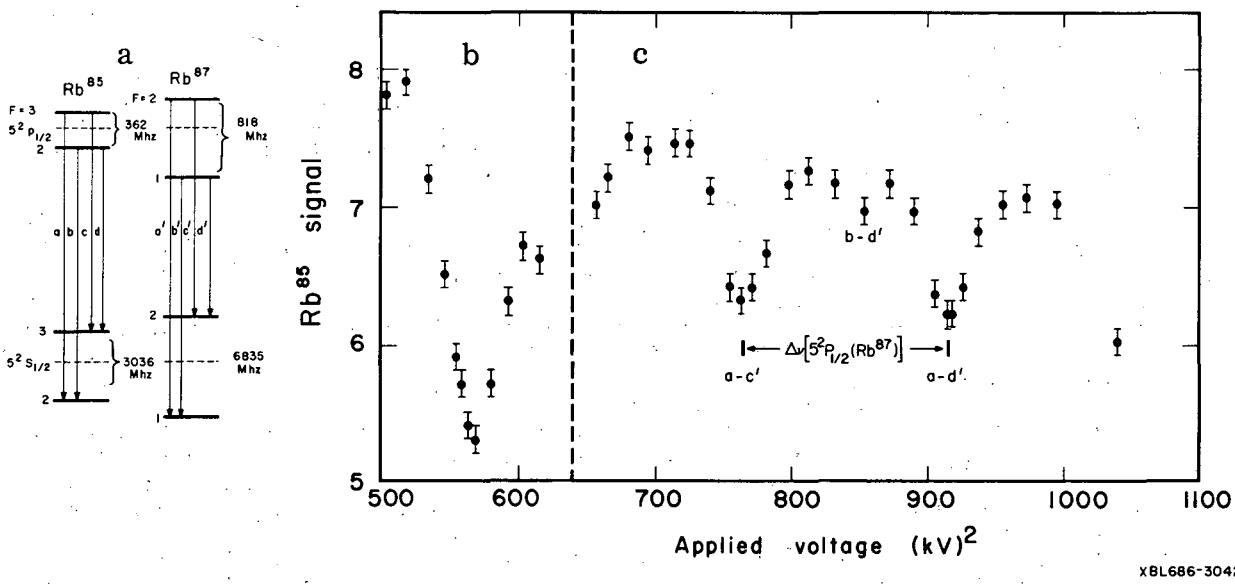

Fig. 1(a). When an electric field is applied to ^{87}Rb, atoms in the F = 1 state eight coincidences may be obtained between the lines a' and b' of ^{87}Rb and a, b, c, and d of ^{85}Rb. The Stark shifts required to produce the overlaps are calculated assuming zero RIS, and their displacement from the actual overlaps fixes the RIS.

(b). Stark-shift calibration using ^{85}Rb lamp and beam. The intensity minimum corresponds to simultaneous overlaps b-d and a-c and represents a shift of 3036 MHz.

(c). Isotope shift data using a ^{87}Rb lamp and a ^{85}Rb beam. Overlaps are indicated on the figure.

ELECTRIC POLARIZABILITIES OF THE 4^2P LEVEL OF POTASSIUM†

Richard Marrus and Joseph Yellin

The Stark shifts of an atomic level are directly determined by the oscillator strengths connecting the level under study to near-lying levels of opposite parity. Hence measurement of these shifts serves as a direct test of theoretical calculations of oscillator strengths. Recently we have begun a program for checking the applicability of the Bates and Daamgard[1] oscillator strengths to the Stark effect in the first excited p level of the alkalis. The Coulomb approximation of Bates and Daamgard is perhaps the simplest theoretical method available for calculating oscillator strengths, and yields numerical results rather easily. We report here a study of the Stark effect in the D lines ($4^2P_{1/2,\ 3/2} \rightarrow 4^2S_{1/2}$) of potassium. Previously we reported a similar study on rubidium and cesium.

The basic method employed is the atomic beam method used in the study of rubidium and cesium.[2,3] However, due to the small hyperfine structure (HFS) of ^{39}K, it is necessary to employ an absorption cell to obtain narrow absorption lines from the broad lamp emission lines.[4] The absorption cell containing potassium in natural abundance (93.1% ^{39}K, 6.88% ^{41}K) is placed between the ^{39}K lamp and the C region. The light from the ^{39}K lamp is filtered first by an interference filter which passes either the D_1 or D_2 line, and then by an optically dense beam of K in the absorption cell. The absorption beam removes a doublet from the lamp line. The components of the doublet are separated by the ground-state hfs of 462 MHz and each has a width of about 200 MHz. The hfs of the excited p states is sufficiently small that it plays no role in these experiments and may be ignored.

The Stark-effect signals may be understood with reference to Fig. 1. Consider the case in which D_1 light is passed. It is well known[2] that for $J = 1/2$, all the states of a hyperfine multiplet are shifted equally under the action of an electric field except for small hyperfine and higher-order effects. These latter effects are negligible for the purposes of this experiment. Therefore, at zero electric field, where the absorption lines of atoms in the beam overlap the absorption lines of atoms in the cell, a minimum is observed in the signal intensity. As the electric field is turned on, the Stark effect "detunes" the two absorption lines and the signal increases. Eventually, however, the Stark effect is sufficient to shift the absorption lines by an amount equal to the ground-state hfs, and a second absorption minimum is observed. In Fig. 2 is plotted the signal intensity observed as a function of the square of the applied voltage.

Under the action of an electric field the $4^2P_{3/2}$ state splits into a doublet corresponding to $m_J = \pm 3/2$ and $m_J = \pm 1/2$. Apart from the absorption minimum at zero field there are two higher-field minima corresponding to the relative positions of the energy levels indicated in Fig. 1. The observed signal is shown in Fig. 3.

The data are analyzed in the following way. If the polarizability of a level $\alpha(n^2 l_j m_j)$ with quantum numbers n, l, j, m_j is defined as usual by

$$w(n^2 l_j m_j) = -\frac{1}{2}\alpha\,(n^2 l_j m_j)\,E^2,$$

where w is the energy shift induced by the electric field E, then the position of the three nonzero field overlaps (signal minima) are described by

$$\frac{E_1^2}{2}\left[\alpha\,(4^2P_{1/2} \pm 1/2) - \alpha\,(4^2S_{1/2} \pm 1/2)\right] = 461.72\ \text{MHz},$$

$$\frac{E_2^2}{2}\left[\alpha\,(4^2P_{3/2} \pm 1/2) - \alpha\,(4^2S_{1/2} \pm 1/2)\right] = 461.72\ \text{MHz},$$

$$\frac{E_3^2}{2}\left[\alpha\,(4^2P_{3/2} \pm 3/2) - \alpha\,(4^2S_{1/2} \pm 1/2)\right] = 461.72\ \text{MHz}.$$

If our measured values are employed for E_1, E_2, and E_3 and if the result of Salop et al.[5] is used for $\alpha\,(4^2S_{1/2} \pm 1/2)$, then these equations determine the three polarizabilities characterizing the 4p level. These are tabulated in Table I along with the predictions by the Bates and Daamgard theory.

In the limit of zero spin-orbit coupling it can be shown[2] that

$$\alpha\,(4^2P_{1/2} \pm 1/2) = \frac{1}{2}\left[\alpha\,(4^2P_{3/2} \pm 3/2) \pm \alpha\,(4^2P_{3/2} \pm 1/2)\right].$$

This relationship is seen to be very well satisfied by the measurements, in contradistinction to the case of the first excited p state in cesium, which shows marked spin-orbit effects.

Footnotes and References

†Condensed from Phys. Rev. (Jan. 1968).

1. D. R. Bates and A. Daamgard, Phil. Trans. Roy. Soc. London A242, 101 (1949).
2. R. Marrus, D. McColm, and J. Yellin, Phys. Rev. 147, 55 (1966).
3. R. Marrus, and D. McColm, Phys. Rev. Letters 15, 813 (1965).
4. R. Marrus, E. Wang, and J. Yellin, Phys. Rev. Letters 19, 1 (1967).
5. A. Salop, E. Pollack, and B. Bederson, Phys. Rev. 124, 1431 (1961).

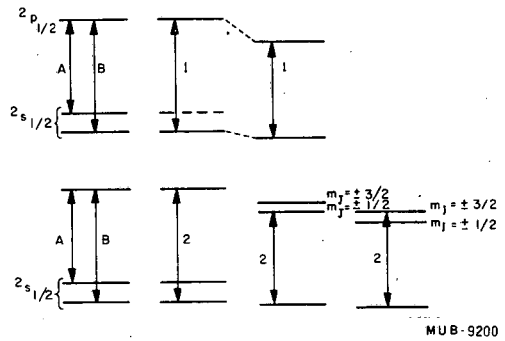

Fig. 1. Schematic diagram of energy levels. The lines A and B are almost completely resolved by the atomic beam absorption cell. At zero electric field, the absorption line B of atoms in the cell. Absorption is also maximized at electric fields such that the lines 1 and 2 are made to resonate with line A.

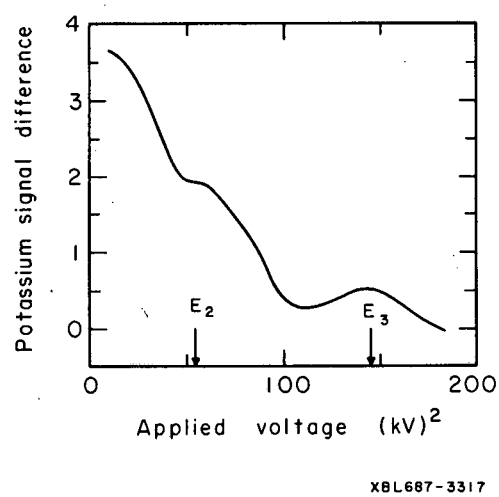

Fig. 3. Observed absorption signal with D_2 light incident. The signal with absorption has been subtracted from the signal without absorption so that the minima here appear as maxima.

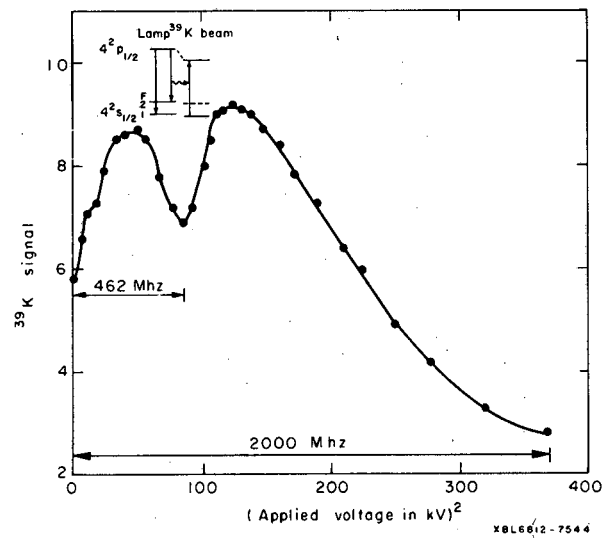

Fig. 2. Observed absorption signal with D_1 light incident.

Table I. Polarizabilities in the 4^2p level of potassium (units of 10^{-24} cm^3).

	This experiment	Bates and Daamgard
$\alpha(4^2P_{1/2} \pm 1/2)$	87(13)	93
$\alpha(4^2P_{3/2} \pm 1/2)$	114(16)	109
$\alpha(4^3P_{3/2} \pm 3/2)$	68(10)	80

ATOMIC ENERGY LEVELS IN BERKELIUM II AND EINSTEINIUM II†

John G. Conway and Earl F. Worden*

A search of limited line lists of Es and Bk for the splitting of the lowest levels has produced intervals which are real. The levels can be confirmed by rules regarding the sum of the hyperfine widths.

In Bk II a third level has been found. The known levels are for the configurations $5f^9$ 7s, and are $^7H_8 = 0$, $^5H_7 = 1487.53$, and $^5H_6 = 5598.11$ cm^{-1}.

The two levels for Es II of the configuration $5f^{11}$7s cm are $^5I_8 = 0$, and $^3I_7 = 938.7$ cm^{-1}.

A fitting of these data to their respective matrices yields values for Bk II, $G^3 = 2132.8$ and for Es II, $G^3 = 2234.7$.

Footnotes

†Abstract of paper to be submitted to J. Opt. Soc. Am.
*Lawrence Radiation Laboratory–Livermore.

TERM ANALYSIS OF Dy I AND Dy II†

John G. Conway and Earl F. Worden*

The spectrum of dysprosium has been photographed and measured from 2400 to 9200 Å. Ion classification results in assignments of about 70% of the lines as I or II. The lowest three levels of Dy I ($4f^{10}6s^2$) are $^5I_8 = 0$, $^5I_7 = 4134.24$, and $^5I_6 = 7060.61$ cm^{-1}. Several intervals of another low-lying configuration are known. The 10 lowest levels of Dy II ($4f^{10}6s$) are $^6I_{8\frac{1}{2}} = 0$, $^4I_{7\frac{1}{2}} = 828.31$, $^6I_{7\frac{1}{2}} = 4341.10$, $^4I_{6\frac{1}{2}} = 4755.66$, $^6I_{5\frac{1}{2}} = 7463.88$, $^6I_{6\frac{1}{2}} = 7485.09$, $^6I_{4\frac{1}{2}} = 9432.07$, $^4I_{5\frac{1}{2}} = 9870.99$, $^6I_{3\frac{1}{2}} = 10953.94$, and $^4I_{4\frac{1}{2}} = 11801.01$ cm^{-1}. There also appears to be a low-lying configuration with levels below 10 000 cm^{-1}.

Footnotes

†J. Opt. Soc. Am. 58, 1564 (1968).
*Lawrence Radiation Laboratory–Livermore.

ZEEMAN EFFECT ON PHOSPHORESCENT LIFETIME OF MATRIX-ISOLATED SO_2†

John G. Conway, B. Meyer,* J. J. Smith,* and L. J. Williamson*‡

The phosphorescent lifetime of SO_2 as a function of magnetic field has been studied at 4°K in sulfur hexafluoride, oxygen, and zenon at zero and 26 kgauss and at 20°K in sulfur hexafluoride between 0 and 90 kgauss. At high fields, the decay consists of two lifetime components. One is identical with the zero-field lifetime of SO_2; the second has a lifetime approximately 50% longer, depending on magnetic field.

Footnotes

†Abstract of paper submitted to J. Chem. Phys.

*Chemistry Department, University of Washington, Seattle, and Inorganic Materials Research Division, Lawrence Radiation Laboratory–Berkeley.

‡NSF Undergraduate Research Fellow.

ENERGY LEVEL CALCULATIONS FOR Nd^{+++} IN $LaCl_3$

Rolf Mehlhorn

Recent improvements in the theory of complex atoms were embodied in an energy level calculation for Nd^{+++} ions situated in a $LaCl_3$ crystal lattice. In preceding calculations [1,2] it had been found that configuration splittings due to interactions within the ion could not be calculated with the same accuracy as the crystal field splittings, so a direct energy matrix had to be augmented with arbitrary parameters to correct the "free ion" levels. Our calculation succeeded in removing this deficiency. In addition, several previously unclassified levels were identified.

Although we confined our attention to the lowest configuration $4f^3$, interactions with excited configurations, e.g. $4f^2 6p$, were treated approximately by means of effective operators acting within the $4f^3$ shell. [3,4] We also introduced relativistic corrections into the Hamiltonian. [5] These included the spin-other-orbit interaction, whose magnitude can be as large as several hundred wavenumbers.

We fit 77 observed levels with a mean error of 5 cm^{-1}, corresponding to about 0.02% of the total spread in energies. This accuracy is due, in part, to the presence of enough electrostatic parameters to determine the term positions exactly. The crystal field splitting of the $(^2H2)_{11/2}$ level agreed poorly with the calculation and was excluded from the fit. Nevertheless, our calculations of the Zeeman splitting factors confirmed Carlson's identification of the components arising from this level. [6]

McLaughlin is presently extending the observations into the ultraviolet region. When the additional terms become available for fitting, the error will probably increase to at least 15 cm^{-1}. This is evident from recent work on the free-ion spectrum of Pr^{++}. [7]

Twenty-four parameters were determined from the least-squares fit to the observed levels. They are set out, along with their statistical errors, in Table I. Not all the magnetic--i.e., spin-dependent--interaction parameters could be determined simultaneously from the fit. We used Hartree-Fock values [8] for the relativistic parameters to deduce the remaining spin-dependent interactions to first order. These were then fixed in the final least-squares calculation.

One important result of our calculation is the confirmation of Judd's suggestion that excited configurations produce magnetic interaction effects of magnitude comparable to the relativistic operators. [5] Thus there does not seem to be any point in adding relativistic corrections to the Hamiltonian unless adequate treatment of configuration interaction effects is provided.

References

1. B. R. Judd, Proc. Roy. Soc. (London) A251, 134 (1959).
2. J. C. Eisenstein, J. Chem. Phys. 39, 2134 (1963).
3. K. Rajnak and B. G. Wybourne, Phys. Rev. 132, 280 (1963).
4. K. Rajnak and B. G. Wybourne, Phys. Rev. 134, A596 (1964).
5. B. R. Judd, H. M. Crosswhite, and Hannah Crosswhite, Phys. Rev. 169, 130 (1968).
6. E. H. Carlson, J. Chem. Phys. 40, 3444 (1964).
7. Hannah Crosswhite, H. M. Crosswhite, and B. R. Judd, Phys. Rev. 174, 89 (1968).
8. M. Blume, A. J. Freeman, and R. E. Watson, Phys. Rev. 134, A320 (1964).

Table I. Parameters for Nd^{+++} in $LaCl_3$.

E^0	4627.0 ± 0.8	T^8	524 ± 26
E^1	5090.7 ± 2.6	M^0	2.44 ± 0.07
E^2	22.97 ± 0.05	M^2	1.22 ± 0.16
E^3	478.4 ± 0.7	M^4	0.91 ± 0.12
ζ_{4f}	873.8 ± 0.8	P_2	1.21
α	22.79 ± 0.11	P_4	0.36
β	-677 ± 4	P_6	0.09
T^2	487 ± 22	B_0^2	252 ± 8
T^3	38.3 ± 0.9	B_0^4	360 ± 16
T^4	62.8 ± 1.4	B_0^6	-925 ± 21
T^6	-336 ± 7	B_6^6	582 ± 18
T^7	524 ± 26		

ELECTRON PARAMAGNETIC RESONANCE OF Pu^{3+} IN CUBIC SYMMETRY SITES IN CaF_2, SrF_2, AND BaF_2

N. Edelstein, H. F. Mollet, W. C. Easley, and R. J. Mehlhorn

In a continuing investigation of actinide ions in crystals of the fluorite type,[1] we have measured the electron paramagnetic resonance (EPR) spectrum of trivalent Pu in cubic symmetry sites in CaF_2, SrF_2, and BaF_2. Two effects have to be taken into account in order to interpret the measured g values. The first is the effect of intermediate coupling caused by the large spin-orbit coupling energies of the actinide ions on the sign and magnitude of calculated operator equivalent factors, and the second is the effect of crystal-field mixing of the first excited J state with the ground state. In this paper we describe our experimental results and calculations from which the fourth-order crystal-field parameter is determined.

Single crystals of $^{239}Pu^{3+}$ in CaF_2, SrF_2, and BaF_2 were grown as described earlier.[1] The EPR measurements were made at either 1°K or 4°K with a conventional superheterodyne spectrometer operating at approximately 9.2 GHz.

A trivalent ion substituted in a host such as the alkaline earth fluorides may go into a number of different site symmetries. The Pu isotope used, ^{239}Pu ($t_{1/2}$ - 24 360 years), has a nuclear spin I = 1/2. In the crystals of Pu^{3+} in CaF_2 and SrF_2 we found that the strongest resonance was isotropic and could be fitted to a spin Hamiltonian of the type

$$H = g\beta\, \overline{H}\cdot\overline{S}' + A\,\overline{I}\cdot\overline{S}', \qquad (1)$$

where $S' = 1/2$ and $I = 1/2$. The parameters measured are given in Table I. The nonisotropic resonances were much weaker, and we have done no further work on them. However, we had trouble growing good BaF_2 crystals, and in a number of these crystals we found only trigonal resonances which were fitted to a spin Hamiltonian of the type

$$H = g_{\parallel}\beta H_z S_z + g_{\perp}\beta(H_x S_x + H_y S_y) + A_{\perp}(I_x S_x + I_y S_y) + A_{\parallel} I_z S_z\,. \qquad (2)$$

We finally obtained a crystal which, besides the trigonal resonances, also contained a weak isotropic resonance which could be fitted to the spin Hamiltonian of Eq. (1) with S' = 1/2 and I = 1/2. The results for BaF_2 are also given in Table I. In all the measurements made on Pu^{3+} in cubic sites we had to work at the lowest microwave powers available (≈ 1 μW) in order to minimize saturation effects.

The electronic configuration of Pu^{3+} outside the closed shells is $5f^5$. The optical spectrum was originally obtained and interpreted for this ion by Lämmermann and Conway[2] and refined further by Conway and Rajnak.[3] We consider first the configuration f^5. The ground term is ^6H, which, with the inclusion of spin orbit coupling, breaks up into a $^6H_{5/2}$ state lying lowest and a $^6H_{7/2}$ as the first excited state. The spin orbit interaction mixes states with different L and S but is diagonal in J, so this quantum number is used to label the intermediate coupled states. For Pu^{3+} the lowest state has J = 5/2, and the J = 7/2 first excited state is at 3190 cm^{-1}. We have used the data of Lämmermann and Conway on Pu^{3+} in $LaCl_3$ and made the assumption that the free-ion energy levels in the alkaline earth fluorides are the same as in $LaCl_3$.

The crystalline field at cubic symmetry sites in alkaline earth fluorides is cubic; eight F^- ions surround the trivalent ion. The Hamiltonian for the crystalline field is[4]

$$H_c = B_4(O_4^0 + 5\,O_4^4) + B_6(O_6^0 - 21\,O_6^4), \tag{3}$$

where B_4 and B_6 are adjustable parameters used to fit the experimental data, and the O_n^m terms are angular momentum operators of the appropriate symmetry. For a pure J = 5/2 state the sixth order term will be zero.

Let us now consider only the J = 5/2 state. In a cubic crystalline field this state will split into a doublet Γ_7 and a quartet Γ_8, and the energy-level diagram is shown in Fig. 1. The cubic field splitting of the J = 7/2 level is also shown. The fourth-degree parameter is defined as

$$b_4 = 60\,B_4 = 60\,A_4^0\langle r^4\rangle\langle\psi_J||\beta||\psi_J\rangle, \tag{4}$$

where $\langle r^4\rangle$ is the expectation value for the magnetic electrons, $\langle\psi_J||\beta||\psi_J\rangle$ is the fourth-degree operator equivalent factor, and A_4^0 may be treated as a parameter, or in the approximation of the point charge model, it is the potential at a particular point in the lattice resulting from the sum of all the charges. From the free-ion wave functions we may calculate the fourth-degree operator equivalent factor as described earlier.[1] Table II lists the second-, fourth-, and sixth-degree (where applicable) operator equivalent factors for Pu^{3+} and Sm^{3+} for the ground J = 5/2 state and next highest state, J = 7/2. The point-charge model usually gives the correct sign for the splittings in the alkaline earth fluorides, and for cubic symmetry A_4^0 is negative. From Table II we see that the sign of $\langle\psi_J||\beta||\psi_J\rangle$ is positive for Sm^{3+} but negative for Pu^{3+}. Therefore, for Sm^{3+} the Γ_8 state should be lowest, but for Pu^{3+} the Γ_7 state is lowest, as found experimentally. For Pu^{3+}, the effects of intermediate coupling are large enough to change the sign of the fourth degree operator equivalent factor and thereby reverse the crystalline-field energy levels in the ground J = 5/2 state with respect to the $4f^5$ lanthanide Sm^{3+}. This is not true for the first excited state J = 7/2. As shown in Table II these operator equivalent factors have the same sign for the f^5 configuration in the 4f and 5f series.

If we assume that the crystalline field is small compared with the splitting between the J = 5/2 and 7/2 states we can calculate the g value of the Γ_7, J = 5/2 state, and find it to be -0.700. This does not agree with our experimental value, so we have to consider the crystalline field mixing of these states. The correct way of calculating this mixture would be to simultaneously diagonalize the electrostatic, spin orbit, and crystalline field matrix elements for the f^5 configuration. This would require diagonalization of a very large matrix, which is not feasible, so we have instead done two calculations. In one in which we calculate matrix elements, using the complete free-ion set of states for the lowest J = 5/2 and J = 7/2 levels, but include only the fourth-order crystalline field mixing between these two states. The second calculation is to simultaneously diagonalize the electrostatic, spin orbit, and crystalline field matrix elements for a truncated basis set consisting of only the ^6H and ^6F terms. The second calculation gives us the wrong spin-orbit splitting between the lowest two states but allows us to estimate the error in ignoring high-J states and the sixth-degree term in the first crystalline field calculation.

The results of the first calculation are shown in Fig. 2. We have plotted the g value for the ground state of Pu^{3+} vs the parameter B_4', where $B_4' = 8\,A_4^0\langle r^4\rangle$. From this figure we see there

are three possible values of $A_4^0 \langle r^4 \rangle$ that will give the experimental g. In order for the Γ_7 state to be lowest, B_4' must be negative, therefore we do not need to consider positive values of B_4'. Our data show that $|g|_{Pu^{3+}CaF_2} > |g|_{Pu^{3+}SrF_2} > |g|_{Pu^{3+}BaF_2}$, and the arrows on Fig. 2 indicate the values we believe most likely. Table III summarizes our results.

A rough estimate of the errors in our analysis were deduced from a study of the complete energy matrices of the ^6H and ^6F terms. This showed that the crystalline-field admixture of J values greater than 7/2 into the J = 5/2 ground state is negligible. The crystalline field also introduced a small fraction of the ^6F term into the ground state, but this has little effect on the g value. For our parameter values, contributions to the Γ_7 state from the preceding sources amounted to less than 2%.

A much more important source of error is our neglect to the B_6 parameter. We obtained a crude estimate of its relative importance from rare earth spectra.[5] With a ratio of B_6 to B_4 of 1/10, we found that the calculated g value changed by about 25% in the CaF_2 region. Thus we estimate the error in our determination of B_4 to be about 25%.

References

1. N. Edelstein and W. Easley, J. Chem. Phys. 48, 2110 (1968).
2. H. Lämmermann and J. G. Conway, J. Chem. Phys. 38, 259 (1963).
3. J. G. Conway and K. Rajnak, J. Chem. Phys. 44, 348 (1966).
4. K. R. Lea, M. J. Leask, and W. P. Wolf, J. Phys. Chem. Solids 23, 1381 (1962).
5. M. J. Weber and R. W. Bierig, Phys. Rev. 134, A1492 (1964).

Table I. Spin Hamiltonian parameters for Pu^{3+} in various alkaline earth fluorides obtained from EPR spectra.

Ion	Matrix	Site	$\|g\|$	$\|A\|$
Pu^{3+}	CaF_2	Cubic	1.293 ± .001	3 ± 2 gauss
Pu^{3+}	SrF_2	Cubic	1.250 ± .001	145 ± 6 gauss
Pu^{3+}	BaF_2	Cubic	1.190 ± .004	184 ± 6 gauss
Pu^{3+}	BaF_2	Trigonal	$g_\perp$ = 1.296 ± .005	$A_\perp$ = 385 ± 20 gauss
			$g_\parallel$ = .79 ± .03	$A_\parallel$ = 385 ± 20 gauss

Table II. Operator equivalent factors for Pu^{3+} and Cm^{3+}.

		$\langle \psi_J \|\| \alpha \|\| \psi_J \rangle$	$\langle \psi_J \|\| \beta \|\| \psi_J \rangle$	$\langle \psi_J \|\| \gamma \|\| \psi_J \rangle$
Pu^{3+}	J = 5/2	4.477×10^{-2}	-3.476×10^{-4}	0
	J = 7/2	1.820×10^{-2}	-4.955×10^{-4}	1.314×10^{-4}
Sm^{3+}	J = 5/2	4.151×10^{-2}	22.690×10^{-4}	0
	J = 7/2	1.671×10^{-2}	-2.402×10^{-4}	1.505×10^{-4}

Table III. Crystalline field parameters derived from measured g values.

Matrix	g	$B_4(cm^{-1})$	$B_4/B_4(CaF_2)$
CaF_2	-1.293	-9 600±25%	1
SrF_2	-1.250	-8 400±25%	0.88
BaF_2	-1.190	-7 100±25%	0.74

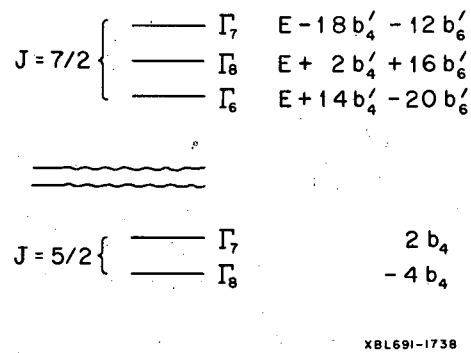

Fig. 1. Energy level diagram for a J = 5/2 ground state and a J = 7/2 excited state in a cubic crystalline field. In this diagram $E >> V_c$.

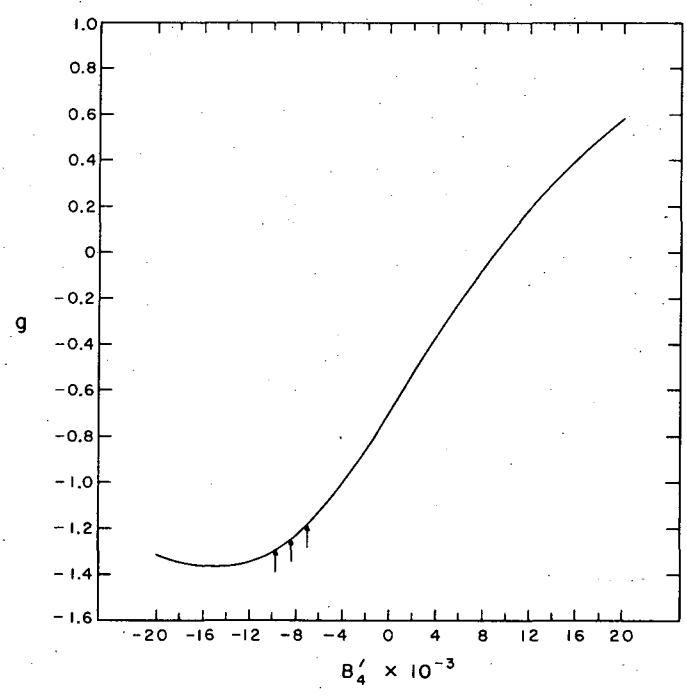

Fig. 2. Calculated g value vs crystalline field parameter B_4'.

SOLUTION ABSORPTION SPECTRUM OF Es^{3+} †

D. K. Fujita, B. B. Cunningham, T. C. Parsons, and J. R. Peterson*

Our first observations of the absorption spectrum of approximately 1 μg of ^{253}Es in hydrochloric acid solutions have been reported previously.[1] Confirmatory experiments became possible with the availability of a larger quantity of einsteinium and greatly improved spectra in the wavelength region from 3 700 to 10 600 Å were obtained.

About 7.5 μg of ^{253}Es produced in the HFIR at Oak Ridge National Laboratory was used in this work. The einsteinium was carefully purified by ion exchange, as described in our previous report.[1]

Absorption spectra were obtained in 3 to 6-M HCl solutions, with Es^{3+} concentrations ranging from ≈ 0.1 M to ≈ 5 M and solution volumes from ≈ 100 nanoliters (nl) down to ≈ 3 nl. Two sets of spectra, each composed of several wavelength scans, were obtained within 56 hr of the separation of ^{253}Es from its decay product ^{249}Bk. Absorption peak positions were measured independently by two observers and the results averaged.

The construction details and techniques of operation of the microabsorption light-pipe cell, adapted for use with the Cary Model-14 Recording Spectrophotometer, have already been described.[1,2] In our recent experiments, light transmission through the microcell was improved further by coating the entrance light pipe with chromium overlayed with silicon monoxide up to the light exit face.

Preliminary test scans with ≈ 3-M Nd^{3+} solutions yielded excellent spectra in the wavelength range 2 500 to 10 000 Å. Peaks with molar absorptivities ≥0.1 in the visible light region and >0.2 in the infrared region were readily detected. Base-line deviations due to instrumental effects were investigated by scanning the wavelength region of interest with an air gap or water droplet between the light pipes. These cell blank scans indicated the presence of minor absorption "peaks" at ≈ 7 650 Å and ≈ 9 650 Å. The Nd^{3+} and Es^{3+} spectra were corrected for these spurious effects.

Figure 1 shows the best Es^{3+} solution absorption spectrum in the wavelength region from 3 500 to 7 200 Å observed on the Cary spectrophotometer traces. The high background absorbance at the shorter wavelengths is believed to be caused by the presence of Cl_2 and H_2O_2 produced by the radioactive decay of ^{253}Es in the aqueous HCl solutions. No peaks in the region from 7 000 to 10 600 Å having molar absorptivities >0.2 were observed. All together 18 absorption bands were observed in the wavelength region from 3 700 to 10 600 Å. The molar absorptivities of the observed peaks were found to be small. Although accurate calculations could not be performed due to the variation of the Es^{3+} concentration during wavelength scans, the molar absorptivity of the most prominent peak at 4950 Å was estimated to be ≈ 5.

The observed Es^{3+} solution spectrum was compared with the three theoretically derived spectra for the $5f^{10}(Es^{3+})$ configuration calculated by Fields et al.[3] and by Conway,[1,4] using different parameters. The agreement between calculated and experimental levels is considered unsatisfactory in each case. The detection of absorption bands in the infrared region (perhaps masked in these experiments by the instrument-caused absorptions mentioned previously) would, one hopes, allow assignments of J values to the low-lying energy levels; the resulting calculated energy levels would then possibly show an improved "fit" with the observed levels.

Footnotes and References

†Condensed from Inorg. Nucl. Chem. Letters (to be published).

*Present address: Department of Chemistry, The University of Tennessee, Knoxville, Tennessee 37916.

1. B. B. Cunningham, J. R. Peterson, R. D. Baybarz, and T. C. Parsons, Inorg. Nucl. Chem. Letters 3, 519 (1967).

2. J. R. Peterson, (Ph. D. Thesis), The Solution Absorption Spectrum of Bk and the Crystallography of Berkelium Dioxide, Sesquioxide, Trichloride, Oxychloride, and Trifluoride, UCRL-17875, (Oct. 1967).

3. P. R. Fields, B. G. Wybourne, and W. T. Carnall, Argonne National Laboratory Report ANL-6911, July 1964.

4. J. G. Conway (Lawrence Radiation Laboratory), private communication, October 1968.

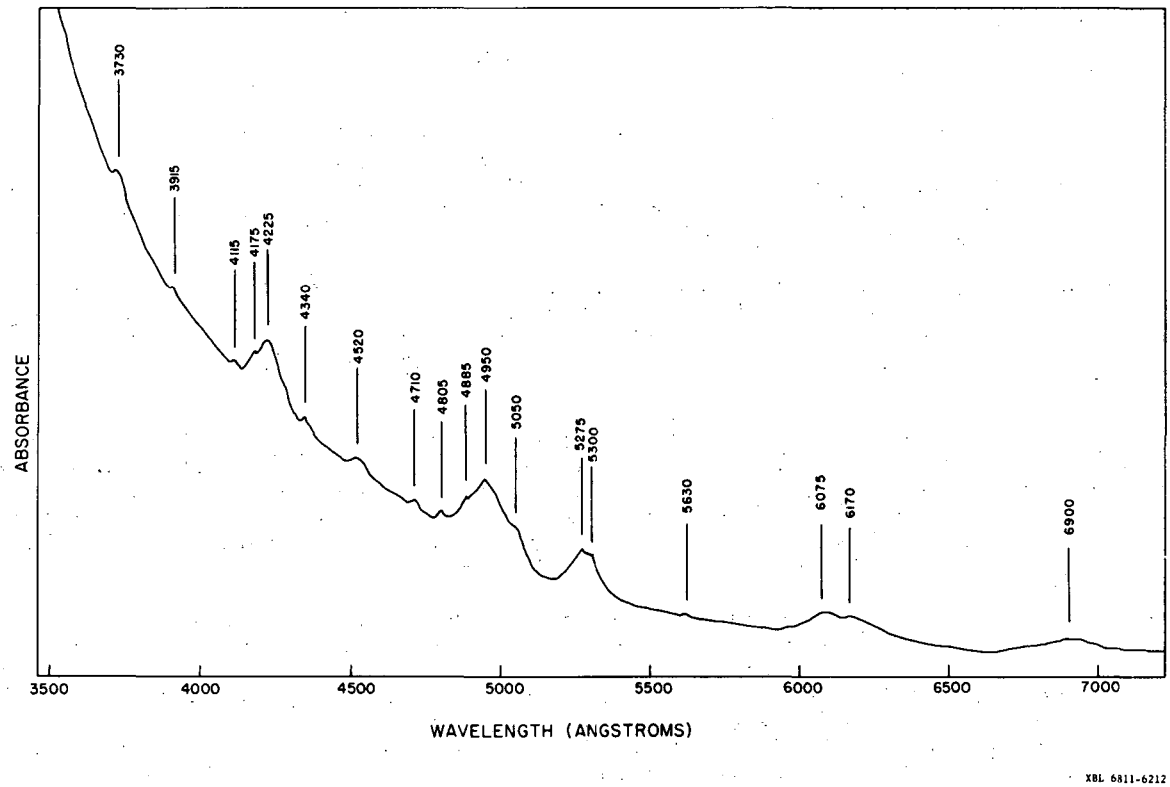

Fig. 1. The absorption spectrum of Es^{3+}.

RADIO-FREQUENCY STARK SPECTRA AND DIPOLE MOMENTS OF BaS†

C. A. Melendres,*‡ A. J. Hebert, and K. Street, Jr.

The radio-frequency Stark spectra of $^{138}Ba\ ^{32}S$ had been observed at moderate fields by use of a molecular beam spectrometer that has been described previously.[1,2] A single spectral line corresponding to the $J = 1$, $M_J = \pm 1 \rightarrow J = 1$, $M_J = 0$ transition was observed for the three lowest vibrational states. Spectral frequencies obtained at field strengths of 30, 45, 60, and 75 V/cm were fitted with the equation[3] $\nu = 3.801887 \times 10^{-2}\ \mu^2E^2/B$, where ν = transition frequency, MHz; E = field strength, V/cm; μ = dipole moment, Debye; and B = rotational constant, MHz. Correction for fourth-order Stark effect was negligible. The following ratios of μ^2 to the rotational constant, B, were obtained: v, μ^2/B (D^2/MHz); 0, 0.03816(10); 1, 0.03841(12); 2, 0.03872(18).

No rotational constants for BaS have been published in the literature; however, Clements and Barrow have recently obtained a value for B_0 for the ground vibrational state from a study of an absorption-band system of BaS.[4] By use of their value of $B_0 = 0.010308(4)\ cm^{-1}$ and our experimental value of $(\mu^2/B)_0$, the value $\mu = 10.86 \pm 0.02$ D is obtained for the dipole moment of the $v = 0$ state of BaS.

The quantity μ/er is sometimes used as a relative measure of "ionic character" in comparing chemical bonds.[5] The near equality of this quantity for BaO (0.85)[6] and BaS (0.90) indicates the close similarity of bonding in these two molecules. Further, the 6% increase in μ/er in going from BaO to BaS reflects a similar 6% increase found in going from CsF to CsCl.

The rather broad line widths of the spectral lines (from 10 to 15 kHz) and difficulties in generating a molecular beam of BaS did not permit the study of the Stark spectra at strong electric fields. Further details of this work appear elsewhere.[7]

Footnotes and References

†Condensed from UCRL-18550, Oct. 1968, to be submitted to J. Chem. Phys.

*Present address: Physics Department, Atomic Research Center, Philippine Atomic Energy Commission, Herran St., Manila, Philippines.

‡Received fellowship support from the Agency for International Development and the Philippine Atomic Energy Commission during the course of this work.

1. A. J. Hebert, F. W. Breivogel, Jr., and K. Street, Jr., J. Chem. Phys. 41, 2368 (1964).
2. F. J. Lovas, Radio-Frequency Stark Spectra of RbF, RbCl, CsF, CsCl, and NaI (Ph. D. Thesis), UCRL-17909, Nov. 1967.
3. P. Kusch and V. W. Hughes, in Handbuch der Physik (Springer Verlag, Berlin, 1939) vol. 37/1, p 139.
4. R. F. Barrow (Oxford), private communication, July 1968; R. M. Clements and R. F. Barrow, Chem. Communs. (1968) (to be published).
5. L. Pauling, The Nature of the Chemical Bond, 3rd edition (Cornell University Press, Mt. Vernon, 1960), p 78.
6. L. Wharton, M. Kaufman, and W. Klemperer, J. Chem. Phys. 37, 621 (1962).
7. C. A. Melendres, Radio-Frequency Stark Spectra of NaCl, NaBr, and BaS by the Molecular Beam Electric Resonance Method, UCRL-18344, June 1968.

DIPOLE MOMENTS OF THE ALKALI HALIDES

A. J. Hebert, T. L. Story, Jr., and K. Street, Jr.

In a recently completed set of experiments involving the electric field deflection of velocity-selected molecular beams, the dipole moments of KI, RbBr, RbI, CsBr, and CsI have been determined. Although deflection experiments are inherently less accurate than resonance experiments, the intensities obtainable with the above molecules precluded the use of the molecular beam electric resonance method. Completion of these experiments makes available dipole moments for all the alkali halide molecules. Table I gives a compilation as determined in this Laboratory (values determined elsewhere for KF and KBr are included for completeness).

Reference

1. T. L. Story, Jr., Dipole Moments of Alkali Halides by the Electric Deflection Method (Ph. D. thesis), UCRL-18484, Sept. 1968.

Table I. Dipole moments of the alkali halides.[a] Dipole moment function for vibrational state v; $\mu_v = \mu_e + \mu_I(v+1/2) + \mu_{II}(v+1/2)^2$.

Molecule	Notes	μ_e	μ_I	μ_{II}
$^{6}Li^{19}F$	b, c	6.28409(25)	0.08627(5)	0.00054(2)
$^{7}Li^{19}F$	b, c	6.2839(12)	0.08153(30)	0.00044(12)
$^{6}Li^{35}Cl$	b, c	7.0853(13)	0.0868(4)	0.00056(14)
$^{6}Li^{37}Cl$	b, c	7.0853(13)	0.0864(5)	0.00064(16)
$^{6}Li^{79}Br$	b, d	7.22624(160)	0.08318(100)	0.00057(30)
$^{6}Li^{81}Br$	b, d	7.22611(160)	0.08312(100)	0.00060(30)
$^{6}Li^{127}I$	e	7.3867(20)	0.0835(20)	
$^{23}Na^{19}F$	f	8.12349(150)	0.06436(80)	0.00037(30)
$^{23}Na^{35}Cl$	b, g	8.9721(13)	0.05963(20)	0.00017(10)
$^{23}Na^{37}Cl$	b, g	8.9721(13)	0.0593(6)	
$^{23}Na^{79}Br$	b, g	9.09177(127)	0.05308(70)	-0.0001(4)
$^{23}Na^{81}Br$	g	9.09178(130)	0.05310(70)	-0.0001(4)
$^{23}Na^{127}I$	b, h	9.2103(30)	0.0507(8)	
$^{39}K^{19}F$	i, j, k	8.5583(8)	0.06841(4)	0.000256(7)
$^{39}K^{35}Cl$	b, c	10.2384(12)	0.0611(9)	0.00055(40)
$^{39}K^{79}Br$	l	10.603(1)	0.0503(8)	0.0003(3)
$^{39}K^{81}Br$	l	10.603(1)	0.0502(8)	0.0002(3)
$^{39}K^{127}I$	m	10.82(10)		
$^{85}Rb^{19}F$	b, h	8.5131(7)	0.06650(28)	0.00026(12)
$^{87}Rb^{19}F$	h	8.5130(7)	0.0665(3)	0.00026(12)
$^{85}Rb^{35}Cl$	b, h	10.483(6)	0.054(3)	
Rb Br	m	10.86(10)		
Rb I	m	11.48(20)		
$^{133}Cs^{19}F$	b, h	7.8486(13)	0.0704(6)	0.00018(20)
$^{133}Cs^{35}Cl$	b, h	10.358(5)	0.058(1)	
^{133}Cs Br	m	10.82(10)		
$^{133}Cs^{127}I$	m	11.69(10)		

a. All values are in debyes and were calculated using $h = 6.6252 \times 10^{-27}$ erg-sec and $c = 2.997925 \times 10^{10}$ cm/sec except for KF and KBr.
b. A. J. Hebert, F. J. Lovas, C. A. Melendres, C. D. Hollowell, T. L. Story, Jr., and K. Street, Jr., J. Chem. Phys. 48, 2825 (1968).
c. A. J. Hebert, C. D. Hollowell, T. L. Story, and K. Street, Jr., UCRL-17256, March 1967.
d. A. J. Hebert, F. W. Breivogel, Jr., and K. Street, Jr., J. Chem. Phys. 41, 2368 (1964).
e. F. W. Breivogel, A. J. Hebert, and K. Street, Jr., J. Chem. Phys. 42, 1555 (1965).
f. C. D. Hollowell, A. J. Hebert, and K. Street, Jr., J. Chem. Phys. 41, 3540 (1964).
g. C. A. Melendres, A. J. Hebert, and K. Street, Jr., UCRL-17916, Nov. 1967.
h. F. J. Lovas, (Ph. D. thesis), UCRL-17909, Nov. 1967.
i. L. Grabner and V. Hughes, Phys. Rev. 79, 819 (1950). The values given are the most accurate ones from Ref. k.
j. A. J. Hebert, (Ph. D. thesis), UCRL-10482, Sept. 1962.
k. R. Van Wachem, F. H. deLeeuw, and A. Dymanus, J. Chem. Phys. 47, 2256 (1967).
l. Calculated from data in Ref. k.
m. Ref. 1.

NUCLEAR QUADRUPOLE RATIO OF BROMINE ISOTOPES IN MOLECULAR LiBr†

A. J. Hebert and K. Street, Jr.

Previous reports from this Laboratory on ^{6}LiBr molecular beam electric resonance experiments[1] led Bonczyk and Hughes to suggest[2] that a discrepancy between our previously observed nuclear quadrupole coupling constant ratio for ^{79}Br to ^{81}Br of 1.19728(8) and the value 1.1970568(15) obtained by Brown and King[3] for atomic bromine might be attributable to nuclear polarization. A more accurate determination for the molecular LiBr ratio was suggested.

Several recent experimental refinements, mentioned below, allow us more than an order-of-magnitude improvement in accuracy over our previous measurements. (Reference 1 describes apparatus previously used and treatment of the data.)

FWHM of the present lines is 2 kHz, compared with the previous 5 kHz. This reduction is mainly due to the use of lower deflecting field voltages, which allowed selective observation of a slower portion of molecules in the beam. The faster molecules, with their greater uncertainty line width, are not sufficiently deflected for detection. This results in a lower signal level; however, the incorporation of a multichannel analyzer as a memory device more than compensates for the reduction.

In the experiments described here radio-frequency transitions were induced under weak electric field conditions by sweeping a phase-locked signal generator at a 19-Hz rate across each line in synchronization with the channel advance in a modified Northern Scientific multichannel analyzer. The detected "flop-in" transitions were all $J = 1$, $m_J = \pm 1$ to $J = 1$, $m_J = 0$ for the three lowest vibrational levels of each isotope. Peak signal intensities were better than 10^4 transitions per channel above background for all observed lines with no observable base-line slope. Typical run times were from 1 to 3 hours (approximately 70 to 210 thousand sweeps) for each line, with signal-to-noise ratios of 100 or better. Line position reproducibility was better than 1 part in 10^6 of frequency for runs made on different days. This corresponds to an uncertainty of less than 15 Hz at 15 MHz, compared with the previous several hundred Hz. All observed lines occurred between 8 and 20 MHz.

Previous strong-field electric dipole moment measurements[1] were checked and found to be accurate. Measurements performed in this Laboratory by Breivogel on the ^{7}LiBr isotopes[4] allowed hyperfine corrections for the ^{6}Li quadrupole and spin-rotation interactions. Second-order quadrupole, Stark quadrupole, and magnetic dipole spin-spin interaction effects were included in treating the data. Calculations indicate that a large electron-coupled spin-spin interaction (i.e., greater than the calculated dipole spin-spin interaction of approximately 90 Hz), would have a negligible effect on the values reported here.

The results of this experiment for each of the three vibrational states measured are in agreement with our previously reported values. The bromine nuclear quadrupole moment ratios from this work are lower than those previously reported by almost three times the probable error. This discrepancy arises primarily from the manner in which the data were treated. In the previous report the quadrupole coupling constants for each isotopic species were separately extrapolated to $v = -1/2$ and the ratio then taken. The probable error was assigned on the assumption that the errors would be random. The new measurements indicate that there was a nonrandom trend in the data, which was accentuated by extrapolation to the equilibrium internuclear distance. In our opinion, this nonrandom trend was produced by a combination of decreasing signal-to-noise ratio for higher vibrational states, and a previous lack of knowledge about the magnitude of the ^{6}Li quadrupole interaction.

In looking for a nuclear polarizability effect a much better method of treating the data is to simply interpolate the ^{81}Br coupling constant for each vibrational state the very short distance in v necessary to achieve the same energy as the corresponding ^{79}Br vibrational state. This small correction is much less sensitive to uncertainties in $(eqQ)_I$ and $(eqQ)_{II}$. Treating the previous data in the same manner gives an average ^{79}Br-to-^{81}Br nuclear quadrupole ratio of 1.19712(8) for the weak field data, and an average of 1.19706(8) for the three states observed at intermediate electric field strength.

The best present ^{79}Br-to-^{81}Br nuclear quadrupole ratio of 1.197056(6) for LiBr (calculated from the v = 0 vibrational states corrected to a common energy) is in excellent agreement with the value 1.1970568(15) observed by Brown and King for atomic Br, thus indicating no observable nuclear polarizability effect.

Footnote and References

†Condensed from Phys. Rev. (to be published).

1. A. J. Hebert, F. W. Breivogel, Jr., and K. Street, Jr., J. Chem. Phys. 41, 2368 (1964), and 47, 2202 (1967).
2. P. A. Bonczyk and V. W. Hughes, Phys. Rev. 161, 15 (1967).
3. H. H. Brown and J. G. King, Phys. Rev. 142, 53 (1966).
4. F. W. Breivogel, Jr., (Ph.D. Thesis), UCRL-11665, Sept. 1964.

EXPERIMENTAL STUDY OF STRONTIUM AND LANTHANUM ON TUNGSTEN†

F. L. Reynolds

The surface ionization of Sr and La atoms, as from an atomic beam impinging on a hot single-crystal plane of tungsten, is the subject of this study. The (110) plane and the (100) plane were compared by using the above elements. The work used mass spectrometer techniques; the source was constructed so that the various W planes as ribbon filaments or as a polycrystalline filament could be placed so as to receive the atomic beams. Magnetic shutters could interrupt the beams from hitting the target filaments. The single-crystal[1] ribbon filaments were prepared by spark-erosion techniques. The effect of trace amounts of oxygen on the emission at various filament temperatures was part of this study.

An index of the experimental results on these surfaces is reflected in the work function calculated from the experimental data by use of the Saha-Langmiur (SL) equation.[2] As modified by Dobretsov,[3] this equation is

$$\alpha = \frac{n_+}{n_0} = \frac{Q_+}{Q_0} \exp\,(\phi - I)/KT, \qquad (1)$$

where

$$\frac{Q_+}{Q_0} = \frac{g_+}{g_0} + \frac{\Sigma_j g_+ \exp(-E_+^j/KT)}{\Sigma_j g_0^j \exp(-E_0^j/KT)},$$

and α is the ratio of ions to neutrals leaving the filament. The ratio Q_+/Q_0 is the statistical weight g_+/g_0 and the sum of the jth excitation level of energies E^j where the subscript + refers to the ion and 0 is the neutral atom, ϕ is the surface work function, I is the first atomic ionization potential, and e/k and T have their usual meanings.

The experimental data are obtained by measuring the slope from a plot of the logarithm of the positive ion current, which is proportional to n_+, against the filament temperature in °K. From the slope, ϕ can easily be obtained when I is known. Deviations from linear plots are a sensitive experimental index of surface conditions for elements whose ionization potential is a volt or so greater than ϕ, the surface work function.

Emission from the (110) Plane

From a previously determined value of $\phi_{(110)}$ the ionization of Sr on this surface of W should result in a SL plot having essentially no slope.[4] This value of ϕ was 5.41 ± 0.04 eV.[4] The work reported here, with closer oriented (110) filaments, gave ϕ = 5.52 ± 0.05 eV. With Sr on this

$W_{(110)}$ surface, a well-aged and clean surface gave straight SL plots at temperatures above 1650 °K. Below this temperature nonequilibrium conditions exist, and the Sr metal begins to coat the surface of the filament. See the top curve in Fig. 1.

Most interesting is the result when a very small fraction if a monolayer of oxygen is present. Figure 1, in which ^{88}Sr ion current is plotted against 1/T, shows the behavior of Sr with trace amounts of oxygen. The extrapolated line indicates the behavior under clean no-oxygen conditions. From the work of Hopkins[5] it is postulated that the concentration of oxygen present in these experiments would not increase the work function. It seems more likely that some mechanism is present in the production of the low-temperature Sr emission peak other than can be explained by the increase in work function alone. Werning[6] also came to this conclusion with studies of Ba on polycrystalline tungsten.

Additional chemical evidence of changes was noted in the presence of small amounts of oxygen. The time to reach an equilibrium ion current condition with Sr between 1600 and 2200 °K was greatly increased with oxygen present. When oxygen was removed, the response time was very rapid. (The time taken to reach half of the maximum emission was used as a measure of the response time.)

La studies on the $W_{(110)}$ plane were not carried out at temperatures below 2100 °K. La metal shows considerable residence time on this surface, making data taking tedious. At 2100 °K, the metal atoms required 18 seconds to reach half peak intensity, and a burst of La ions resulted upon suddenly flashing to the higher temperatures. The calculated work function was 5.44 ± 0.05 eV using La on $W_{(110)}$, which compares quite well with the value obtained with Sr.

Emission from the (100) Plane

Surface ionization on this plane seems to be very sensitive to emission anomalies. Long after the $W_{(110)}$ and polycrystalline surfaces gave a straight-line SL plot with Sr, the $W_{(100)}$ surface retained a plateau in the emission curve, as shown in Fig. 2.

The anomalies showed up with $W_{(100)}$ and La experiments. Initially with La, the surface work function was 4.60 ± 0.03 eV, but some 25 determinations later, this same surface seemed to have stabilized on a surface work function of 4.80 ± 0.03 eV. This same surface with Sr gave a value of 4.56 ± 0.04 eV. During the Sr run the La oven remained hot, but cut off by the shutter.

It was thought that this difference of 0.24 eV could be accounted for by assuming that the La low-lying energy states of the La ion and the La atom could contribute. Sr has no low-lying energy states below 4121 cm^{-1} wave numbers. Calculation of all the possible energy states in this energy region and summing these data over the experimental temperature range could account for a correction of only 0.01 eV. No other known explanation could account for this difference.

Efficiency Measurements

A comparison experiment was done using two different crystal planes of tungsten, and with Sr as the atomic beam. The relative efficiencies were determined at 2500 °K for both planes, and are shown in Table I.

These two planes gave work function values of $\phi_{(110)} = 5.53 \pm 0.03$ and $\phi_{(100)} = 4.62 \pm 0.04$ eV. Based on these values, and from the known ionization potential of Sr, the calculated efficiencies from the SL equation should be 32.27% for $W_{(110)}$ and 0.69% for $W_{(100)}$. Thus, their ratio equals 46.76. From the above table the average of five determinations gives a ratio of 53. This demonstrates the gain in ion emission that can be obtained from a tungsten filament having an increase in ϕ of 0.9 eV.

Polycrystalline Filaments

Surface ionization on polycrystalline ribbon filaments are shown in Table II. All data are at high temperatures between 2800 and 2400 °K. Values are the surface work function in eV. About the same difference appears between La and Sr as with the work on $W_{(100)}$ single crystal. No evidence of LaO^+ could be found at working pressures of 1×10^{-8} torr until severe out-gassing raised the source pressure to 10^{-7} torr or higher.

In summary there is reasonable agreement with the $W_{(110)}$ surface with either Sr or La. There is an approximately 0.24-eV disagreement with $W_{(100)}$ and $W_{(poly)}$ using Sr and La. Full

reason for this divergence is not known at present, but some attempts are made to point out various experimental conditions that influence the data.

The work function of the $W_{(110)}$ plane was redetermined and found to be 5.52 ± 0.05 eV. The value found for the $W_{(100)}$ plane is 4.56 ± 0.04 eV.

In a change of source pressure from 1×10^{-9} torr to 2 to 3×10^{-9} torr by addition of oxygen, the $W_{(110)}$ crystal surface shows evidence of surface change at elevated temperatures. Apparently other planes of lower ϕ are exposed, reducing ϕ permanently from 5.52 eV to 5.30 eV in these experiments. This change is not rapid, and in the absence of oxygen no change was ever noted after operation for many hours in the residual gases in the mass spectrometer within the above pressure region.

Footnotes and References

†Condensed from Surface Science (to be published).

1. F. L. Reynolds, Spark-Erosion Fabrication of Single-Crystal Tungsten Ribbon Filaments, Rev. Sci. Instr. 37, 1730 (1966).
2. I. Langmiur and K. H. Kingdon, Proc. Roy. Soc. (London) 107, 61 (1925).
3. L. N. Dobretsov, Electron and Ion Emission, NASA. Transl. TT-F-73, 1963.
4. F. L. Reynolds, J. Chem. Phys. 39, 1107 (1963).
5. B. J. Hopkins, R. R. Pendes, and S. Usami, in Fundamentals of Gas-Surface Interactions (Academic Press, New York, 1967), p 284.
6. J. R. Werning, Thermal Ionization at Hot Metal Surfaces (Ph. D. Thesis), UCRL-8455, Sept. 1958.

Table I. Relative intensity measurements in the (110) and (100) pulses.

Planes		
(110)	(100)	Ratio
15 300	325	47
14 200	230	61
15 300	360	42
15 000	282	53
13 640	212	64

Table 2. Work functions for La and Sr on the same polycrystalline W surface.

La	Sr
4.75	4.51
4.77	4.51
4.75	4.50
4.85	4.52
4.76	4.49
4.88	4.57

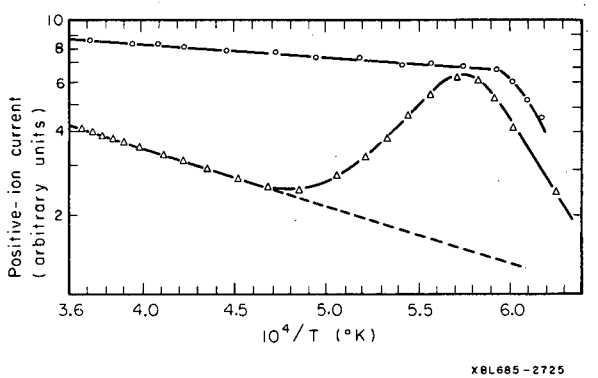

Fig. 1. Strontium on $W_{(110)}$. Circle plot shows the slope of the emission before introduction of oxygen and final adsorption of Sr at low temperatures. Triangle plot is the permanent final slope after oxygen treatment and the effect of oxygen on the emission at low temperatures. If the oxygen is removed, the permanent slope continues, as indicated by the broken line.

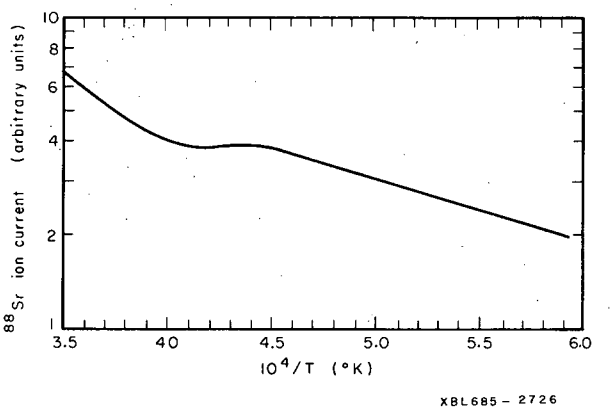

Fig. 2. Strontium on $W_{(100)}$, showing the plateau effect.

METASTABLE IONS IN THE MASS SPECTRA OF N_2 AND NO†

Amos S. Newton and A. F. Sciamanna

Metastable peaks in the mass spectra of singly charged diatomic ions have not been reported; several authors[1-3] have reported the collision-induced dissociation of N_2^+ ions. Kupriyanov[4] has reported the unimolecular dissociation of CO^{++} to occur with a half-life between 2 and 400 μsec. Dibeler and Rosenstock[5] have reported the ion HS^+ to dissociate by a unimolecular process to $S^+ + H$ with a half-life observable in the mass spectrometer.

The occurrence of metastable peaks in the mass spectra of small molecules is of considerable interest because the quasi-equilibrium theory cannot be expected to apply to such molecules, and further, the energetic characteristics of such peaks can be of aid in defining levels on the potential energy surfaces of the ionic states of such molecules. Gilmore[6] used the ionization-efficiency curves of Curran[7] and Cěrmák and Herman[8] of N_3^+ formation in N_2 to place the $\nu = 0$ level of the $^4\Sigma_u^+$ and $^4\Delta_u$ states of N_2^+ at 21.04 and 21.9 eV respectively.

The experiments were performed with a Consolidated Electrodynamics Corporation Model 21-103B mass spectrometer, which has been considerably modified to increase the vacuum and electronics capability.[9-11] The amplifier sensitivity was increased to 1×10^{-16} A per chart division. A 1.5-mm collector slit was used, which increased the sensitivity for broad metastable peaks. A total increase of sensitivity by factors of 130 for normal peaks and up to 260 for broad metastable peaks was achieved. Ionization-efficiency curves were made on an X-Y recorder. An external voltage source driven in parallel to the ionizing voltage was used to monitor the latter.

The mass spectrum of N_2 in the mass region $M/q = 6$ to $M/q = 8$ is shown in Fig. 1 at ionizing energies above and below the appearance potential (AP) of N_2^{++}, and with and without application of a retarding potential at the collector (metastable supressor voltage, V_{mss}) of 55% of the accelerating voltage V_A. The broad peak at $M/q = 7$ is clearly from the fragmentation of N_2^+ to N^+ after acceleration as N_2^+. Figure 2 shows the mass spectrum of NO in the mass range $M/q = 6$ to $M/q = 9$. Apparent metastable peaks occur near the calculated masses of 6.53 and 8.53 for the fragmentation of NO^+ into N^+ and O^+ respectively after acceleration as NO^+.

In Fig. 3 the dependence of peak sensitivity (peak intensity/pressure) on pressure in the inlet system is shown. The peak at $(M/q)^* = 6.53$ shows zero sensitivity at zero pressure, and arises entirely from a collision-induced transition,

$$NO^+(coll) \rightarrow N^+ + O; \quad (M/q)^* = 6.53. \tag{1}$$

The peaks at $(M/q)^* = 7$ and $(M/q)^* = 8.53$ in N_2 and NO respectively have nonzero intercepts and, in the pressure range studied, arise largely from unimolecular processes,

$$N_2^+ \rightarrow N^+ + N; \qquad (M/q)^* = 7.00; \tag{2}$$

$$NO^+ \rightarrow O^+ + N; \qquad (M/q)^* = 8.53. \tag{3}$$

Linearity of peak sensitivity with ionizing electron current showed secondary ion-source processes to be absent.[3] Tests for surface-induced processes[9, 10] showed such processes to be absent for the peaks at $(M/q)^* = 7.00$ and $(M/q)^* = 8.53$. [A peak at $(M/q)^* = 6.67$ in N_2 was found to be the result of a surface-induced dissociation in N_2^{++}, and is discussed later.]

Appearance potentials were determined for these peaks as well as for other peaks of interest in the mass spectra of these compounds. These are shown in Table I. The AP curve for the $(M/q)^* = 7$ peak in N_2 is shown in Fig. 4, and that of the $(M/q)^*$ peak in NO in Fig. 5. In Fig. 6 is shown the ionization-efficiency curve for the $(M/q)^* = 7.00$ peak in N_2, measured on the shoulder at $(M/q)^* = 6.85$ to eliminate the interference of N^{++} at $M/q = 7.00$. Also shown is the efficiency curve at $(M/q)^* = 6.58$, at which point the peak is almost completely collision-induced. The separate unimolecular (dashed line) and collision-induced processes at $(M/q)^* = 6.85$ were obtained from pressure-sensitivity curves at various ionizing voltages. Above electron energies of 100 eV there is an interference in these curves from a peak at $(M/q)^* = 6.67$ from the surface-induced dissociation of N_2^{++} into $N^{++} + N$ at the ion-source focus slit. This peak is shown in Fig. 7, and its variation with the potential on the inner focus slit in Fig. 8. The agreement with the calculated line[9] proves the mechanism. In Fig. 9 is shown the ionization-efficiency curve for $(M/q)^* = 8.53$ in NO separated into its unimolecular and collision-induced components. The slow falloff above 50 eV suggests the metastable level is filled by cascade processes from higher levels.

The kinetic energy release in these respective transitions was determined by the change in peak width with change in V_A and the width of the metastable supressor cutoff curve.[11] The results are consistent with T, the kinetic energy release in dissociation, being 0.55 ± 0.10 eV for the $(M/q)^* = 7.00$ in N_2 and 0.04 ± 0.02 eV for the $(M/q)^* = 8.53$ peak in NO.

No measurements of the half-lives of the transitions leading to these peaks are possible, but the fact that the peak intensities are not strong functions of V_A -- as they are in the case of the $(M/q)^* = 20.45$ peak in N_2O -- leads to the conclusion that the half-lives are each > 0.1 μsec.

Metastable unimolecular transitions in N_2 and NO as shown in Eqs. 2 and 3 have been observed. The AP of 20.2 ± 0.2 and $T = 0.04 \pm 0.02$ eV in NO shows the state of dissociate to the dissociation limit $N(^4S^0) + O^+(^4S^0)$ of NO^+ at 20.101 eV, while in N_2, the AP of 24.9 ± 0.3 and $T = 0.55 \pm 0.10$ eV shows the dissociation to be to the dissociation limit $N(^4S^0) + N^+(^3P)$ of N_2^+ at 24.30 eV. Possible mechanisms for states dissociating to these limits are as follows:

(a) Excitation to a state which radiates with a long half life (> 0.1 μsec) to a dissociative state at the proper dissociation limit. In each case discussed here, the equality of the sum of the energy of the dissociation limit and the kinetic energy with the AP of the metastable fragment shows this mechanism to be highly improbable, since the radiation would be in the far infrared.

(b) Direct excitation to a state at a point above the dissociation limit but from which dissociation is impeded by a low potential energy barrier. Radiation from this state to lower-lying states must be a long-lived process. The state may dissociate by tunneling through the barrier. Approximate calculations[12] show that for N_2 and NO half-lives of the order of 1 μsec are achievable with barrier heights of ≈ 1 eV and thickness of ≈ 0.15 Å.

(c) Excitation to an excited state, A, which has a long lifetime for radiation to lower states. If there is an inter-system crossing to a dissociative state, B, crossing may occur and dissociation immediately follow. The half-life of metastable-ion formation is determined by the rate of crossing, the rate of radiation depopulation of the state, or both in competition. Herzberg discusses[13] the selection rules and possible variations in this predissociation process.

The excitation function of N_2^{+*} which leads to $(M/q)^* = 7.00$ shows a marked resemblance to that of direct excitation to the $^4\Sigma^+$ state of N_2^+ observed by Čermák and Hermann[7] if that curve were displaced upward in energy by ≈ 3 eV. It also resembles excitation functions for excitation to allowed states such as the excitation of the $A\ ^2\Pi_g$ state of N_2^+ (Meinell band system).[14] Two possible mechanisms are:

(a) Direct excitation to a forbidden state such as $^4\Pi_g$ (if the barrier is higher than suggested by Gilmore[8]) or a $^4\Sigma$ state which has a barrier above the dissociation limit. Both these would dissociate by tunneling.

(b) Excitation to an allowed state which has a long radiative lifetime (radiation in the visible or near infrared) with an intersystem crossing to a forbidden state above the dissociation limit. Possible states are $^2\Delta_u$, $^2\Sigma_u^-$, and $^2\Pi_u$ which predissociate to a $^4\Pi_u$ or $^4\Sigma$ state.[8]

In NO one might have direct production of a $^5\Sigma^+$ state, followed, if it has a barrier to dissociation, by tunneling. Predissociation is possible by excitation to an unknown triplet state followed by an intersystem crossing to the $^5\Sigma^+$ state.

The present data do not allow a choice of these mechanisms or designation of the actual states involved.

Footnote and References

†Condensation from J. Chem. Phys. (to be published).

1. H. H. Harris and M. E. Russell, J. Chem. Phys. 47, 2270 (1967).
2. M. V. Tikhomirov, V. N. Komarov, and N. N. Tunitskii, Z. Fiz. Khim. 38, 955 (1964).
3. N. R. Daly and R. E. Powell, Proc. Phys. Soc. (London) 89, 273 (1966).
4. S. E. Kupriyanov, Soviet Physics-Technical Physics 9, 659 (1964).
5. V. H. Dibeler and H. M. Rosenstock, J. Chem. Phys. 39, 3106 (1963).
6. R. K. Curran, J. Chem. Phys. 38, 2974 (1963).
7. V. Čermák and Z. Herman, Coll. Czech. Chem. Commun. 27, 1493 (1962).
8. F. R. Gilmore, J. Quant. Spectry. & Radiative Transfer 5, 367 (1965).
9. A. S. Newton, A. F. Sciamanna, and R. Clampitt, J. Chem. Phys. 46, 1779 (1967).
10. A. S. Newton, A. F. Sciamanna, and R. Clampitt, ibid. 47, 4843 (1967).
11. A. S. Newton and A. F. Sciamanna, J. Chem. Phys. 44, 4327 (1966).
12. W. Kauzmann, Quantum Chemistry (Academic Press, Inc., New York, 1957), p 197.
13. G. Herzberg, Molecular Spectra and Molecular Structure, I. Spectra of Diatomic Molecules, 2nd Ed. (D. Van Nostrand Co., Inc., Princeton, N. J., 1950), p 387-450.
14. I. P. Zapesochnyi and V. V. Skubenich, Opt. Spectry. (USSR) 21, 86 (1967).
15. J. Cuthbert, J. Farren, and B. S. P. Rao, Proc. Phys. Soc. (London) 91, 63 (1967).
16. F. H. Dorman and J. D. Morrison, J. Chem. Phys. 35, 575 (1961).
17. F. H. Dorman and J. D. Morrison, J. Chem. Phys. 39, 1906 (1963).
18. A. C. Hurley, J. Mol. Spectry. 9, 18 (1962).

Table I. Appearance potentials of some ions in the mass spectra of N_2 and NO.

Ion	(M/q)	AP	Breaks	Std.	Value published earlier	Reference
N_2						
$(N_2^+)^*$	7.00 (uni)[a]	24.9 ± 0.3	30.6 ± 0.5	He^+		
$(N_2^+)^*$	7.00 (coll)[b]	18 ± 1	22	He^+		
N^{++}	7.00	$58.6^{+0.3}_{-2.0}$[c]	65	Ne^{++}	54.2 ± 0.5	15
					≈55	3
$(^{14}N^{15}N)^{++}$	14.5	42.7 ± 0.2	43.5 ± 0.3	Ar^{++}	43.5 ± 0.3	16
					42.7 ± 0.1	17
					44.2 ± 1	15
					42.7 calc.	18
NO						
$(NO^+)^*$	8.53 (uni)	20.2 ± 0.2	25.4 ± 0.5	He^+		
$(NO^+)^*$	8.53 (coll)	17 ± 1	---	He^+		
$(NO^+)^*$	6.53 (coll)	16 ± 1	---	He^+		
N^{++}	7.00	57.6 ± 1.0	66	Ne^{++}		
O^{++}	8.00	62.2 ± 1.0	67	Ne^{++}		
NO^{++}	15.0	38.3 ± 0.5	---	Ar^{++}	39.8 ± 0.3	16
					38.10 calc.	18

a. Unimolecular component of metastable peak.
b. Collision-induced component of metastable peak.
c. A lower state may exist to which there is a low transmission probability.

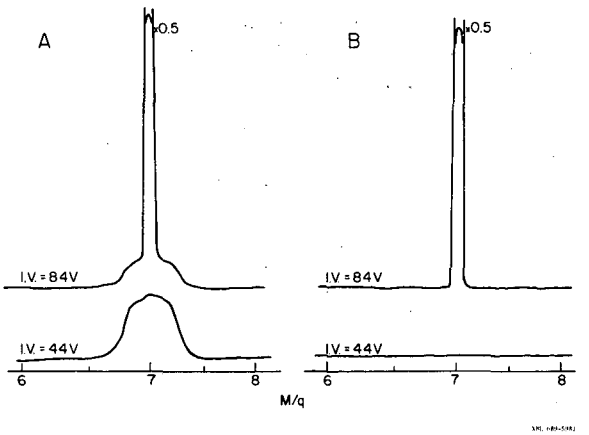

Fig. 1. Mass spectrum of N_2 in the mass range M/q = 6 to M/q = 8 with ionizing electron energies at M/q = 7 of 84 and 44 eV respectively. Inlet pressure = 100 μ; MV_A = 17 500. Focus adjusted for maximum intensity on metastable peak. A, normal operation; B, with retarding potential at collector equal to 0.55 V_A.

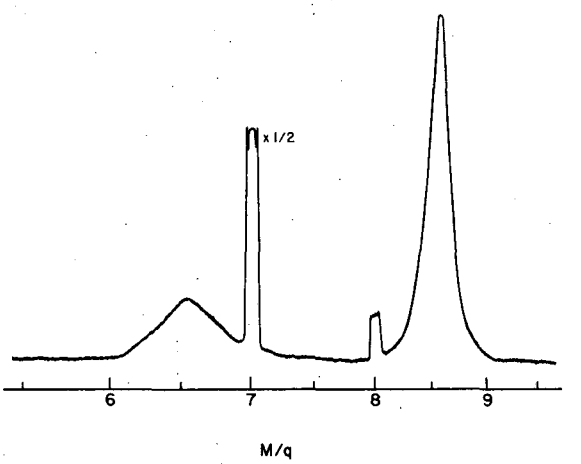

Fig. 2. Mass spectrum of NO in the mass range M/q = 6 to M/q = 9. Inlet pressure = 200 μ; MV_A = 10 000; V_e = (62 + 0.00558 V_A) eV. Focus to maximize peak at $(M/q)^*$ = 8.53.

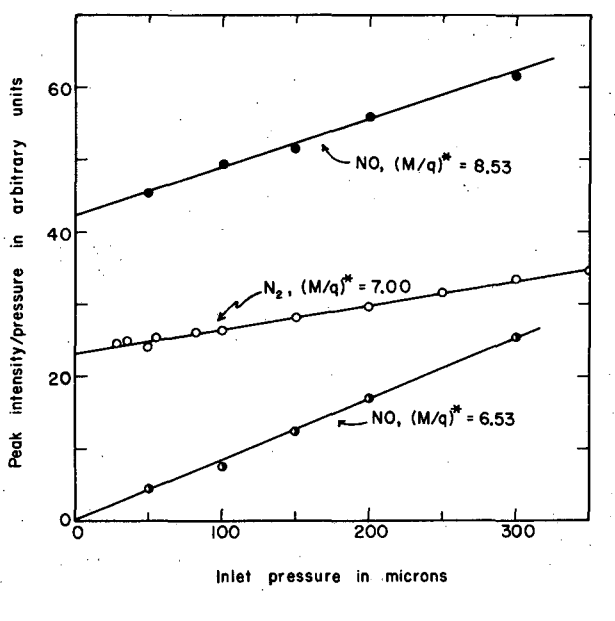

Fig. 3. Linearity of peak intensity with pressure for $(M/q)^*$ = 8.53 and $(M/q)^*$ = 6.53 in NO and $(M/q)^*$ = 7.00 in N_2.
Conditions:
N_2: V_A = 2500 V, V_e = 44 eV;
NO, $(M/q)^*$ = 6.53: V_A = 3484 V, V_e = 72.5 eV;
NO, $(M/q)^*$ = 8.53: V_A = 2670 V, V_e = 68 eV.

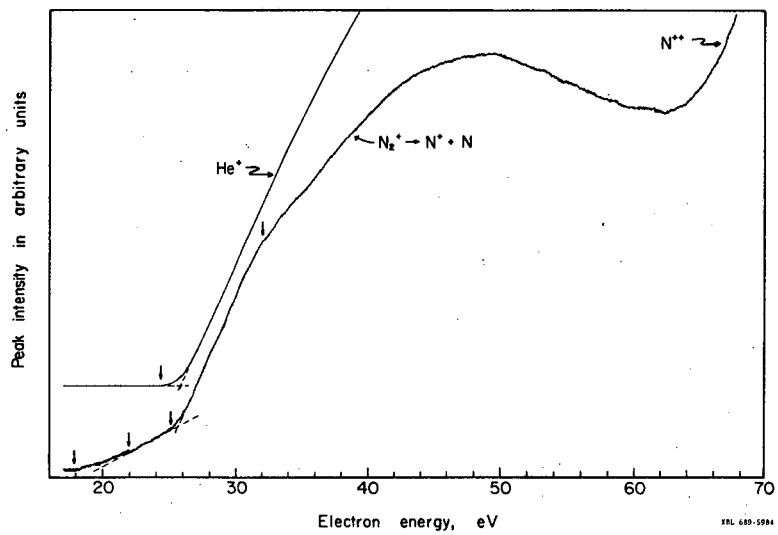

Fig. 4. Ionization-efficiency curve of $(M/q)^* = 7.00$ in N_2 with He^+ as a calibrating standard. Electron energy scale corrected to initial break in He^+ curve. Conditions: inlet pressure = 300 μ N_2; V_A = 1500 V; I_e = 37.5 μA; focus to maximize $(M/q)^* = 7$ at electron energy = 48 eV; $V_R = 0.1115\ V_A$.

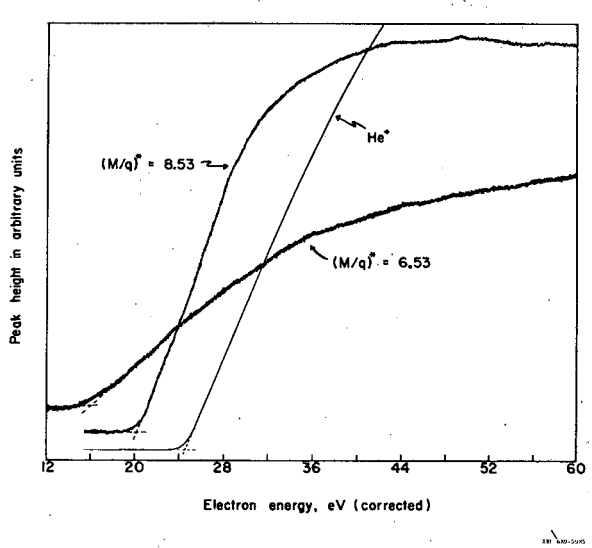

Fig. 5. Ionization-efficiency curves for $(M/q)^* = 8.53$ and $(M/q)^* = 6.53$ peaks in NO compared with He^+. Electron energy scale corrected to agree with the linear extrapolation of He^+ curve at 24.6 eV. Zeros of curves have been shifted for clarity of presentation. V_A = 1500 V; inlet pressure = 200 μ; I_e = 37.5 μA.

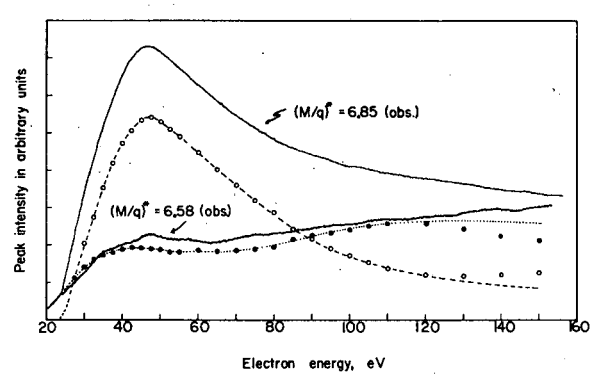

Fig. 6. Ionization-efficiency curves of broad peak at $(M/q)^* = 7$ in N_2. Solid curves are experimental at $(M/q)^* = 6.85$ and $(M/q)^* = 6.58$ respectively. Open circles are derived for the unimolecular components at $(M/q)^* = 6.85$, and dots are derived for the collision-induced component at $(M/q)^* = 6.85$. Level of the observed ion intensity at $(M/q)^* = 6.58$ peak was normalized to an approximate fit of the derived curve of the collision-induced component by adjusting the sensitivity in the recording system. Voltage scale is corrected to ±2 eV. N^{++} was shown to be completely absent at $(M/q)^* = 6.85$.

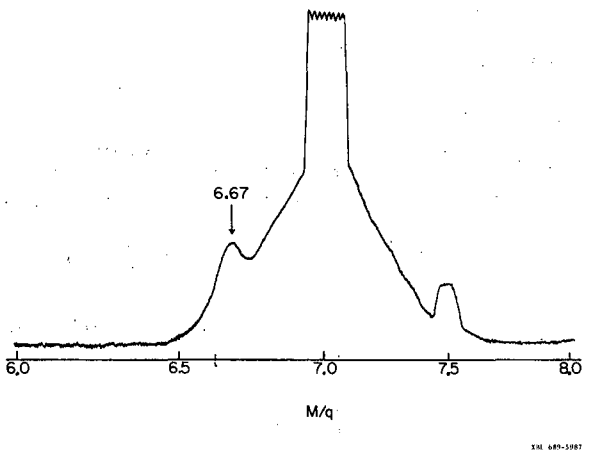

Fig. 7. Mass spectrum of N_2 in mass range 6 to 8 at an ionizing electron energy of 148.5 eV. MV_A = 10 275; inlet pressure = 200 μ; I_e = 38 μA. $(M/q)^*$ = 6.67 arises from the surface-induced transition $N_2^{++} \xrightarrow{S} N^{++} + N$ at the ion source focus slit. Peak at M/q = 7.5 is $^{15}N^{++}$.

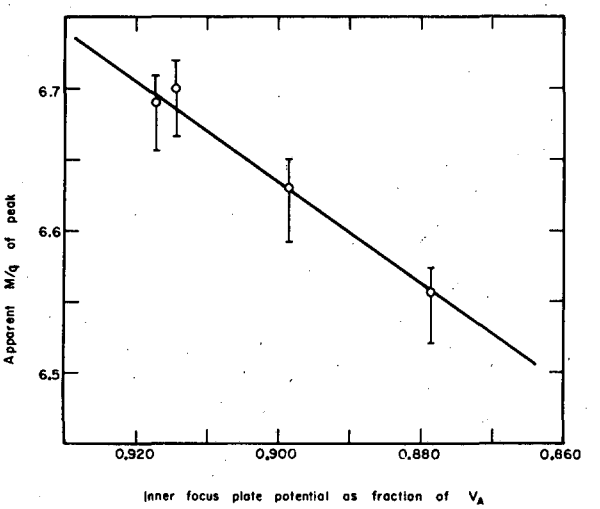

Fig. 8. Shift in apparent mass of the peak at a nominal mass 6.67 in the mass spectrum of N_2 with change in potential on the focus electrodes. Points experimental; line calculated for the surface-induced transition $N_2^{++} \xrightarrow{S} N^{++} + N$ at the inner focus electrode. V_e = 148 eV; inlet pressure = 200 μ.

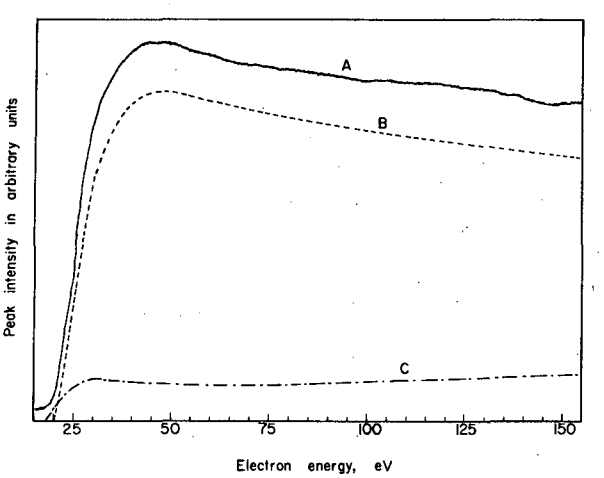

Fig. 9. Ionization-efficiency curve of $(M/q)^*$ = 8.53 in NO. Solid line, A, is the observed curve. Line B is the derived unimolecular component. Line C is the derived collision-induced component. Electron energy scale corrected to ±1 eV. Inlet pressure = 200 μ; I_e = 38 μA; V_R = 0.01115 V_A; V_A = 1500 V. Zero of curve A has been shifted upward for clarity of presentation.

METASTABLE SPECIES PRODUCED BY ELECTRON EXCITATION OF N_2, H_2, N_2O, AND CO_2 †

R. Clampitt* and Amos S. Newton

The excitation of molecules in a molecular beam by electron impact and the detection of the neutral electronically excited metastable species produced by Auger de-excitation at a metal surface has been previously described.[1-3] The apparatus used has also been previously described.[4]

The work presented here describes some results obtained mainly by time-of-flight resolution of the excited species formed in beams of H_2, CO_2, and N_2O.

The time-of-flight distribution of excited species may be described as follows. If a molecular beam, formed from a gas exhibiting a Maxwellian distribution of velocities, is excited by electrons, then the probability P of the excited molecule's having a velocity v is

$$P(v) \propto v^2 \exp(-v^2/\alpha^2) \exp(-S/v\tau), \tag{1}$$

where $\alpha = (2kT/M)^{1/2}$, k is the Boltzmann constant, T is the absolute temperature, S is the distance from excitation to the detector, and τ is the mean life of the excited state. The time-of-flight probability, P(t), is

$$P(t) \propto t^{-4} \exp(-S^2/\alpha^2 t^2) \exp(-t/\tau). \tag{2}$$

When $\tau < 20\,\bar{t}$, where $\bar{t}$ is the most probable time of flight, the P(t) distribution becomes sharper as t becomes smaller, and the measured most probable velocity is greater than the true value.

If a molecule M dissociates to form an excited fragment m, with a discrete amount of kinetic energy E_0, the P(t) distribution of m is[5,6]

$$P(t) \propto t^{-3} \exp[-A(t^{-1} - t_0^{-1})^2] \exp(-t/\tau), \tag{3}$$

where $A = S^2/\beta\alpha^2$, $\beta = m/M$, $t_0 = S(m/2E_0)^{1/2}$.

If the fragment is formed with a Maxwellian distribution of kinetic energies with a most probable kinetic energy E_0, then the P(E) distribution is[7]

$$P(E) \propto \exp\left(-\frac{E}{E_0 + \beta kT}\right). \tag{4}$$

A. Nitrogen

The nitrogen results have been described previously.[4]

B. Hydrogen

The photon yield from electron excitation of H_2 is greater than the yield of metastable H_2 ($C\,^3\Pi_u$) molecules,[8] and a P(t) distribution of photons and H_2^* shows barely discernible H_2^* when the channels for photon determination are saturated. This result is shown in Fig. 1. In Fig. 2 is shown the experimental excitation function for photon production with a theoretical curve[9] for the excitation of the $^3\Sigma_g^+$ state normalized at 15 eV. The threshold at 11.8 eV is close to the theoretical threshold of 11.72 eV.

Figure 3 shows the excitation function of H_2^* obtained by delayed-coincidence counting. The threshold is close to the theoretical value of 11.86 eV. A theoretical curve[9] for the excitation of the $C\,^3\Pi_u$ state is also shown, as are the line intensities for electron excitation of the $\nu = 0$ to

$v = 7$ vibrational levels of the state.[10] As predicted,[11] only the $v = 0$ level appears metastable.

Metastable H(2S) atoms were not observed under our experimental conditions. By use of a different apparatus[12] with more intense molecular and electron beams, two groups of H(2S) atoms were observed, a high-kinetic-energy group (4.7 eV) and a low-energy group (0.32 eV) as previously observed by Levanthal, Robiscoe, and Lea.[13] The P(t) distribution of the low-energy group is shown in Fig. 4. This distribution can be described by Eq. 4 in contrast to the results of Levanthal et al.,[13] who found the distribution to be deficient in low-velocity components.

C. Carbon Dioxide

Freund and Klemperer[3] reported an electronically excited, kinetically energetic, polar fragment from CO_2 at a threshold energy of 12 to 15 eV. The fragment is most likely CO ($a^3\Pi$). Our threshold energy is 11.0 ± 0.6 eV and the mean kinetic energy is 0.25 eV. These values lead to a dissociation limit of 10.3 eV, while the dissociation limit for the process

$$CO_2 + e^- \rightarrow CO\ (a\ ^3\Pi) + O\ (^3P) + e^- \qquad (5)$$

is 11.5 eV. This discrepancy can be resolved if the initial process leading to CO ($a^3\Pi$) is

$$CO_2 + e^- \rightarrow CO\ (a\ ^3\Pi) + O^-. \qquad (6)$$

No long-lived excited molecules of CO_2 were observed in these experiments.

D. Nitrous Oxide

An excited fragment from N_2O which is kinetically energetic and nonpolar was observed by Freund and Klemperer[3] at a threshold energy of 8.7 eV. In Fig. 5 is shown an experimental time-of-flight curve for this fragment together with three calculated curves. Curve A, from Eq. 4, shows good agreement. The measured threshold is 10.5 ± 0.3 eV and the mean kinetic energy is 0.20 ± 0.03 eV, giving an estimated dissociation limit of 9.95 eV (assuming the fragment is N_2^*). Two known repulsive combinations of N_2 and O giving rise to N_2^* in this region of energy are $N_2\ (B'\ ^3\Sigma_u^-) + O\ (^3P)$ (dissociation limit 9.87 eV), and $N_2\ (a\ ^1\Pi_g) + O\ (^3P)$ (dissociation limit 10.26 eV).

Footnotes and References

†Condensed from J. Chem. Phys. (to be published March 1, 1968).

*Present address: The Culham Laboratory, Abingdon, Berkshire, England.

1. J. Olmsted, A. S. Newton, and K. Street, J. Chem. Phys. 42 2321 (1965).
2. W. Lichten, J. Chem. Phys. 26, 306 (1957); Phys. Rev. 120, 469 (1960).
3. R. S. Freund and W. Klemperer. J. Chem. Phys. 47, 2897 (1867).
4. R. Clampitt and A. S. Newton, in Nuclear Chemistry Annual Report, 1967, UCRL-17989, Jan. 1968, p 172-9.
5. P. Chantry and G. J. Schultz, Phys. Rev. Letters 12, 49 (1964).
6. R. Clampitt and W. J. Dunning, J. Sci. Instr. 44, 336 (1967).
7. H. E. Stanton and J. E. Monahan, J. Chem. Phys. 41, 3694 (1964).
8. The detector collects all H_2^* molecules but only ≈ 0.02% of the total photons emitted assuming an isotropic distribution of photon emission.
9. S. P. Khare, Phys. Rev. 157, 107 (1967).
10. J. T. Dowell and T. E. Sharp, J. Chem. Phys. 47, 5068 (1967).
11. W. Lichten, Phys. Rev. 120, 848 (1960).
12. Experiments performed by R. Clampitt at the Culham Laboratory, AERE, Abingdon, Berkshire, England.
13. M. Leventhal, R. T. Robiscoe, and K. R. Lea, Phys. Rev. 158, 49 (1967).

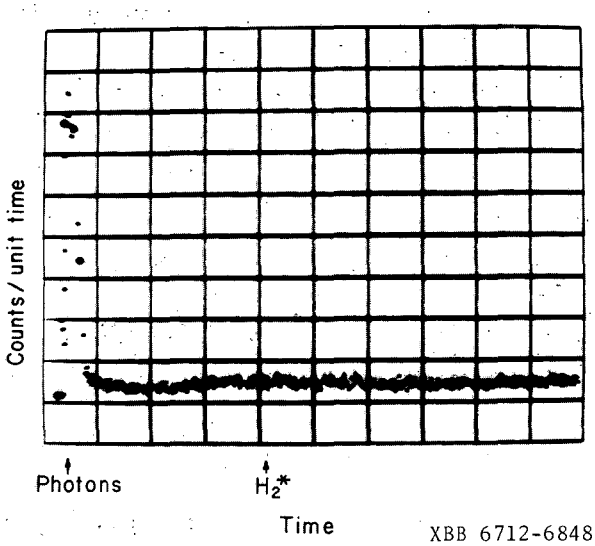

Fig. 1. Experimental time-of-flight distribution of photons and metastable molecules from H_2. Signal from H_2^* is barely visible with photon signal on scale.

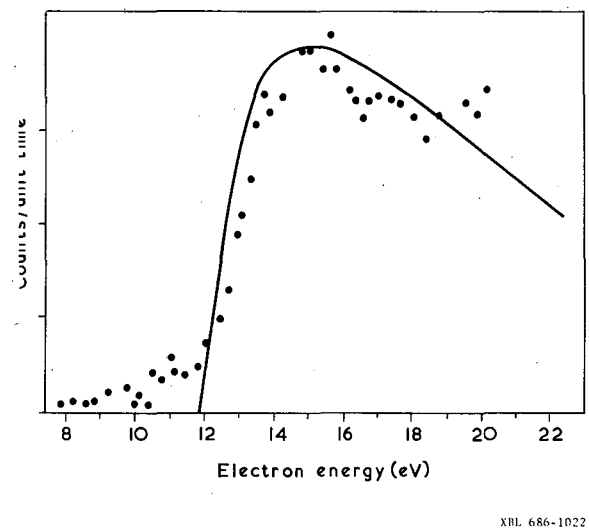

Fig. 2. Excitation functions for photon production from H_2. Points are experimental. Theoretical curve (full line) is for excitation to the $a\ ^3\Sigma_g^+$ state; the curves are normalized at 15 eV.

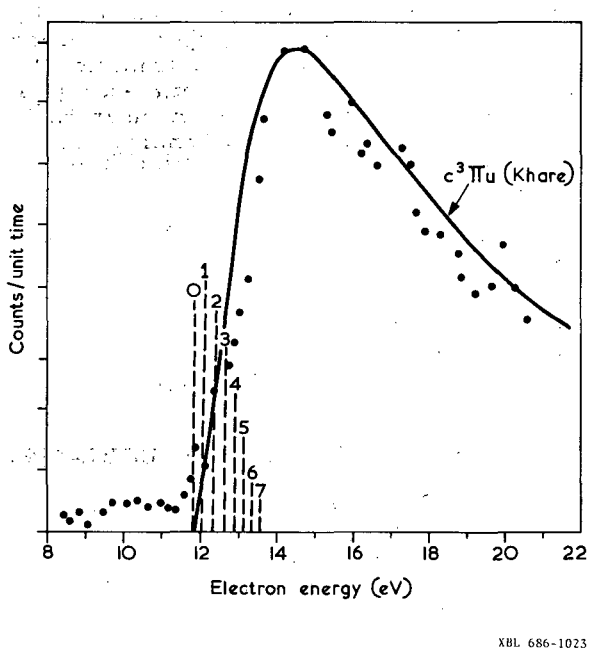

Fig. 3. Excitation functions for $c\ ^3\Pi_u$ state of H_2: theoretical curve (KHARE, Ref. 9) is shown as a full line. Line intensities at vibrational levels 0-7 are experimental inelastic electron scattering data from Ref. 10.

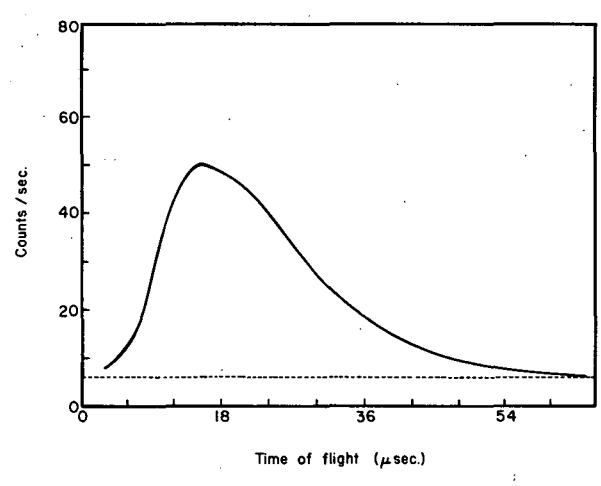

Fig. 4. Time-of-flight distribution of the low-energy group of H(2S) atoms produced in the dissociative excitation of H_2 by electron impact; —— observed distribution; ----- background counting rate of system. Electron energy 37.6 eV; current 10 μA.

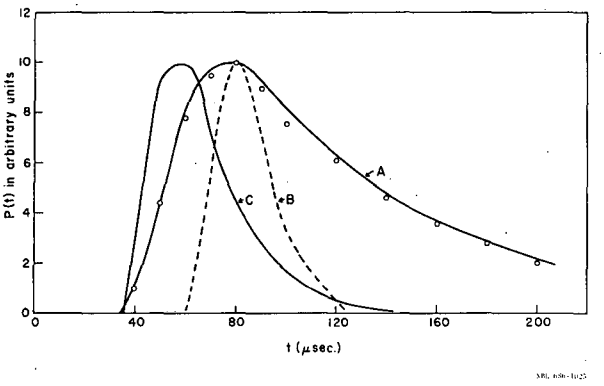

Fig. 5. Experimental P(t) distribution of electronically excited neutral fragments formed with initial kinetic energy from N_2O (open circles) and theoretical distributions. Curve A: calculated from Eq. (3), with t_0 = 115 μsec. Curve B: calculated from Eq. (3), with t_0 = 85 μsec. Curve C: calculated from Eq. (4) [transformed to a P(t) distribution and incorporating the factor $\exp(-t/\tau)$], with t_0 = 115 μsec, and $\tau = 2\times10^{-5}$ sec.

HYPERFINE INTERACTIONS

SPATIAL ASYMMETRY OF INTERNAL BREMSSTRAHLUNG PHOTONS FROM POLARIZED ^{119}Sb †

W. D. Brewer* and D. A. Shirley

Nuclear decays arising from the weak interaction, i. e. $\beta^{\pm}$ decays and electron capture, are accompanied by a weak continuous γ-ray spectrum known as inner bremsstrahlung (IB).[1] Since the discovery of parity violation by weak interactions in 1957, it has been clear that the IB, although it is a photon spectrum, should show parity-violating effects; e. g., the photons from unpolarized source nuclei should be circularly polarized, while those from polarized source nuclei should have an asymmetric spatial distribution.[2] A diagram for the process in the electron-capture case is shown in Fig. 1. Calculations by several authors have given quantitative descriptions of the effects to be expected from various decays.[3]

Observation of these parity-violating effects, however, is made difficult by the extremely small intensity of the IB spectrum and by the presence of interfering γ rays and external bremsstrahlung (EB) in $\beta^{\pm}$ decays. Measurements of circular polarization have been done in several cases of IB accompanying $\beta^{\pm}$ decays, and show agreement with theory.[4] However, no experimental confirmation has previously been done for the electron-capture case.

In this work the angular distribution of IB from polarized nuclei was observed for the first time. The decay of 38-hr ^{119}Sb by electron capture was chosen as a representative case and one in which a minimum of interference from normal γ rays or EB was present. The decay scheme is shown in Fig. 2. The IB spectrum from this decay has been measured by other workers.[5]

In order to produce nuclear polarization, the low-temperature thermal equilibrium method was employed. The ^{119}Sb activity, prepared by the reaction sequence $\mathrm{Sn}(\alpha, \mathrm{xn})^{119}\mathrm{Te} \xrightarrow{\mathrm{Ec}} {}^{119}\mathrm{Sb}$ and carefully purified from radioactive contaminants, was melted into iron samples and the Sb-Fe ingots were flattened to produce thin-foil (0.005-in.) sources. When a small polarizing field (H_0 = 2200 Oe) was applied to the foil, the Sb nuclei experienced a hyperfine field of 230 kOe.[6] The foil was at the same time cooled by contact with an adiabatically demagnetized paramagnetic salt in an apparatus similar to one described by Westenbarger and Shirley.[7] The combination of low temperature ($\approx 0.050°$K) and large magnetic field interacting with the Sb magnetic moment was sufficient to produce considerable nuclear polarization. IB photons from the ^{119}Sb were detected by two 3×3-in. NaI(Tl) counters placed at 0 and 180 deg with respect to the polarizing field H_0. The temperature of the source was determined by a combination of internal ^{60}Co γ-ray thermometry and magnetic susceptibility measurements on the cooling salt. The results for IB photons in the energy range 125 to 500 keV are shown in Fig. 3. The solid curves are the best fit to the theoretical correlation for IB photons accompanying s electron capture:

$$W(\theta) = 1 + AQ_1P(T) \cdot \cos(\theta).$$

Here W is the normalized counting rate, θ is the angle between the polarization axis and the detector, A is a theoretical coefficient which depends on the decay scheme, Q_1 is a correction for the finite solid angle subtended by the detectors, and P is the degree of nuclear polarization, a known function of the temperature T. The value of A obtained from Fig. 3 is $+0.506 \pm 0.026$. The theoretical value[3b,c] is + 1.0. To resolve this apparent disagreement, values of W(0) at a particular temperature were plotted against photon energy in Fig. 4. This reveals an energy dependance in W, although in principle the asymmetry for IB from an electron-capture decay is independent of photon energy (since the decay energy is shared only by a neutrino and a photon, both massless particles). The decrease in W(0) at low energies is attributable to three factors: increasing intensity of the p-capture IB intensity at low energies (for p-capture IB, $W \equiv 1$); experimental inaccuracies at low energies owing to scattering of IB photons in the apparatus; and relativistic and Coulomb corrections to the theory which remove the energy independence of W. The upper dotted line in Fig. 4 is the theoretical value of W(0) corrected for p-capture intensity; the lower dotted curve contains an estimated scattering correction also. As can be seen in Fig. 4,

the data still lie below the theoretical curve except at highest energies, where all corrections are expected to be negligible. Using the W values from photons of energy ≥400 keV gives

$$A = +1.001 \pm 0.093, \qquad \text{in agreement with theory.}$$

Footnotes and References

†Condensed from Phys. Rev. Letters 20, 885 (1968).

*NSF Graduate Fellow, 1967-68.

1. P. Morrison and L. I. Schiff, Phys. Rev. 58, 24 (1940); J. K. Knipp and G. E. Uhlenbeck, Physica 3, 425 (1936); F. Bloch, Phys. Rev. 50, 472 (1936).
2. T. D. Lee and C. N. Yang, Phys. Rev. 105, 1671 (1957).
3. (a) R. E. Cutkosky, Phys. Rev. 107, 3301 (1957); (b) Y. Koh, O. Miyatake, and Y. Watanabe, Nucl. Phys. 32, 246 (1962); (c) S. F. Timashev and V. A. Kaminskii, Soviet Phys.-JETP 38, 284 (1960).
4. H. Schopper and S. Galster, Nucl. Phys. 6, 125 (1958); G. Hartwig and H. Schopper, Z. Physik 152, 314 (1958); S. Galster and H. Schopper, Phys. Rev. Letters 4, 295 (1960).
5. J. L. Olsen, L. G. Mann, and M. Lindner, Phys. Rev. 106, 985 (1957).
6. M. Kontani and J. Itoh, J. Phys. Soc. Japan 22, 345 (1967); J. A. Barclay, W. D. Brewer, E. Matthias, and D. A. Shirley, Hyperfine Interactions and Nuclear Radiations, Matthias and Shirley, Eds. (North-Holland, Amsterdam, 1968), p. 902.
7. G. A. Westenberger and D. A. Shirley, Phys. Rev. 138, A161 (1965).

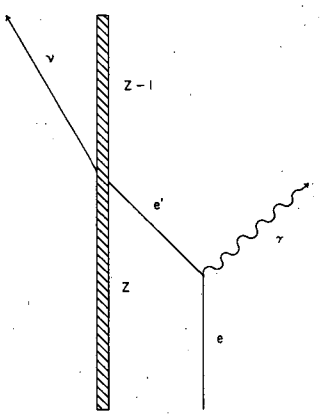

Fig. 1. Diagram of IB process in electron capture.

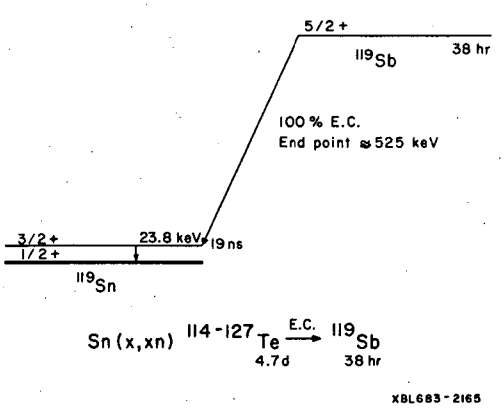

Fig. 2. Decay scheme of ^{119}Sb.

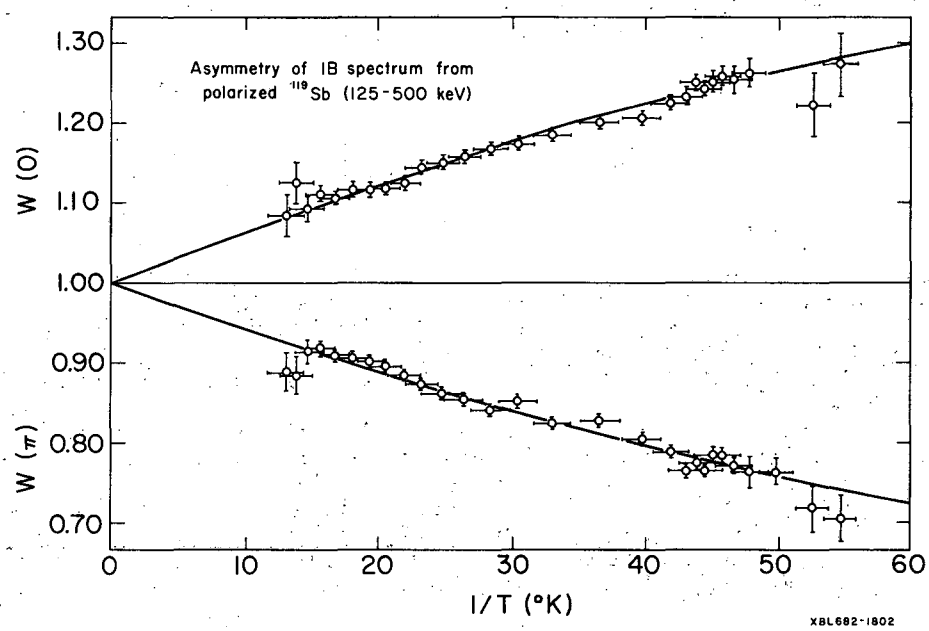

Fig. 3. Experimental asymmetry values at two values of angle θ as a function of temperature (averages of 14 runs with 3 different sources).

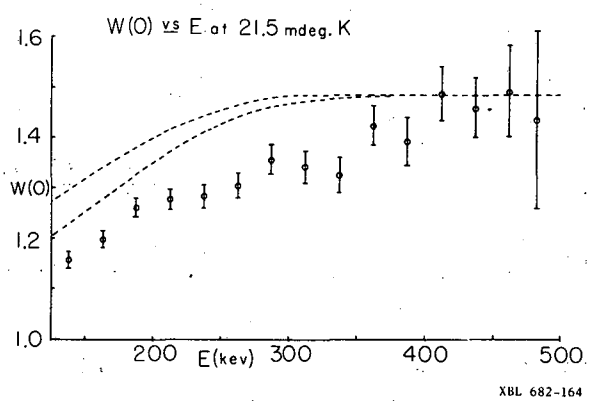

Fig. 4. Asymmetries W(0) at one temperature as a function of photon energy E.

MAGNETIC RESONANCE IN ORIENTED ^{125}Sb †

J. A. Barclay, W. D. Brewer, E. Matthias, and D. A. Shirley

In 1953 Bloembergen and Temmer[1] unsuccessfully attempted to detect NMR by observing the resonant destruction of γ-ray anisotropy of nuclei cooled to about 0.01°K. However, in 1966, Matthias and Holliday[2] succeeded using ^{60}Co nuclei in a Fe lattice. The NMR/ON (nuclear magnetic resonance of oriented nuclei) method was further elaborated by Templeton and Shirley[3] by using a frequency-modulated rf field. This paper reports the application of this method to ^{125}Sb in Fe and illustrates its versatility and accuracy.

The angular dependence of γ rays emitted from oriented nuclei can be described by

$$W(0, T_s) = \sum_{k \text{ even}} B_k(T_s)\, U_k F_k P_k(\cos\theta), \tag{1}$$

where U_k and F_k are coefficients characteristic of the nuclear decay and $P_k(\cos\theta)$ are the even Legendre polynomials. B_k describes the degree of orientation, and is related to the spin temperature according to the relation

$$B_k = \sqrt{2I+1} \sum_M (-1)^{I-M} (IIM\text{-}M\,|\,k\,0)\, \frac{\exp(-E_M/kT_s)}{\sum_M \exp(-E_M/kT_s)}\,. \tag{2}$$

In recent years ^{125}Sb has been the subject of several nuclear polarization experiments. The purpose was in all cases to determine the magnetic moment of ^{125}Sb by using the values of the internal fields at Sb nuclei in ferromagnetic hosts obtained by other methods. Hess et al.[5] reported a nuclear moment of 3.55 ± 0.3 nm, assuming an internal field of 200 kG for ^{125}Sb in Fe. However, these authors used NaI(Tl) detectors and were observing a superposition of several γ rays rather than a single transition. To avoid this difficulty Stone et al.[6] polarized ^{125}Sb in Fe and observed the anisotropy of the 462-keV γ rays only, well resolved with Ge(Li) detectors. Their result, 2.72 ± 0.15 nm, agreed well with expected systematics. These measurements have been continued by the Oxford group,[7] and the latest result is reported to be 2.55 ± 0.10 nm.

The method of nuclear orientation, NMR/ON, offers a considerably higher degree of accuracy. As pointed out earlier,[2] this accuracy allows one to observe the shift of the resonance as a function of the external polarizing field, H_0. Provided that the resonance is observed in domains, this functional dependence is linear, the slope giving the g factor directly and the $H_0 = 0$ intercept yielding the hyperfine field times the g factor.

In addition, NMR/ON can be employed in a very elegant manner to determine the nuclear spin-lattice relaxation time, T_1.[3] If T_L is the lattice temperature and T_s the nuclear spin temperature, thermal equilibrium, $T_L \equiv T_s$, leads to ordinary static nuclear orientation when T_L is sufficiently small.

Under the influence of an rf field at resonant frequency $\nu_R = g \cdot (\vec{H}_{int} + \vec{H}_0)\, \mu_n/h$, transitions between the Zeeman levels are induced and the Boltzman distribution is disturbed. If the rf field is switched off resonance, the nuclear spins relax back to the lattice equilibrium temperature with a characteristic time T_1(NMR/ON).

If we assume T_s is again defined by the Boltzman factor but $T_s \neq T_L$, the rate at which T_s and T_L equilibrate is <u>approximately</u> characterized by T_1, and described by the relation[3]

$$\frac{d}{dt}\left(\frac{1}{T_s}\right) = -\frac{1}{T_1}\left(\frac{1}{T_s} - \frac{1}{T_L}\right). \tag{3}$$

However, because NMR/ON uses the anisotropy instead of the magnetization (as in normal NMR) to measure T_1, T_1(NMR/ON) is not equal to T_1(NMR) except under special conditions.

Templeton[8] and Gabriel[9] have solved the problem relating the two T_1's. The nuclear spin relaxation curve is a sum of exponentials with amplitudes depending on the initial conditions of the spin system and decay constants depending on the lattice temperature,

$$\Delta W(\theta = 0, t) = \sum_{k=2,4} \sum_{k'}^{2I} \beta_{kk'} \exp(-\lambda_{k'} t) . \qquad (4)$$

The frequency sweep in Fig. 1 was slow compared with the relaxation time T_1, leading to symmetrical resonance curves. Still, in order to eliminate any possible frequency shift in sweep direction, the two curves of Fig. 1 were added together to give the center frequency of the resonance. The added data, shown in Fig. 2, yield $\nu_R = 132.15 \pm 0.10$ MHz for $H_0 = 787$ G.

In Fig. 3 the observed resonance frequency for various H_0 is shown. The linear behavior is described by the relation $\nu_R = (\mu_N/h)\, g\,(H_{hf} \pm H_0)$. The slope of the line thus gives the g factor, and with the known g factor the $H_0 = 0$ intercept yields H_{hf}. It is important to notice that the sign of the g factor cannot be obtained (for symmetry reasons) from this type of measurement. The sign of the hyperfine field, however, determines the sign of the slope. From Fig. 3 it is clear that the hyperfine field of ^{125}Sb in Fe is positive, as measured previously by Samoilov.[10] From a least-squares fit we obtain $g(\mu_N/h) = 0.570 \pm 0.014$ (MHz kG^{-1}) and $g(\mu_N/h)$ $H_{int} = 131.711 \pm 0.032$ (MHz). From this the g factor of ^{125}Sb is found to be $|g| = 0.748 \pm 0.018$. With spin 7/2, the magnetic moment is $|\mu| = 2.62 \pm 0.06$ nm, in excellent agreement with the latest value reported by Stone.[7] We note that this agreement is possible only if the spin is 7/2, and this constitutes a spin determination for ^{125}Sb. This result is a basic consequence[2] of the fact that the two methods, NMR and nuclear orientation, measure gH and μH, respectively.

The internal field value is $H_{int} = +231 \pm 6$ kG, slightly larger than the field reported by Samoilov,[10] but in excellent agreement with NMR results of Kontani and Itoh,[11] who found +230 kG.

Finally, the spin-lattice relaxation time for 125 Sb in iron was measured as described elsewhere,[3] and a least-squares fit was made to $W(0, t) \approx A + B \exp(-t/T_1)$, which is the first-order solution of Eqs. (1) through (3). We found $T_1 = 145 \pm 20$ sec at 0.015°K, or $T_1T = 2.2$ sec °K. This large value indicates that neither the orbital relaxation mechanism[12] nor additional relaxation due to localized moments[2] is present. The positive hyperfine on Sb in Fe is thought to arise from the s band, which is consistent with this large T_1T. The data are being refitted, with the sum of exponentials being used in order to obtain a better value for T_1.

Footnote and References

†Condensed from UCRL-17716.

1. N. Bloembergen and G. T. Temmer, Phys. Rev. 89, 883 (1953).
2. E. Matthias and R. J. Holliday, Phys. Rev. Letters 17, 897 (1966).
3. J. E. Templeton and D. A. Shirley, Phys. Rev. Letters 18, 240 (1967).
4. R. J. Blin-Stoyle and M. A. Grace, in Handbuch der Physik, Ed. H. Gelger and K. Scheel (Verlag von Julius Springer, Berlin, 1957), Vol. 42, p. 555.
5. J. Hess, W. Weyhmann, B. Greenebaum, and F. M. Pipkin, Bull. Am. Phys. Soc. 9, 562 (1964).
6. N. J. Stone, R. B. Frankel, J. J. Huntzicker, and D. A. Shirley, Nuclear Chemistry Division Annual Report, 1964, UCRL-11828, p. 58.
7. N. J. Stone (Clarendon Laboratory, Oxford University), private communication.
8. J. E. Templeton (Lawrence Radiation Laboratory), private communication.
9. H. Gabriel (Lawrence Radiation Laboratory), private communication.
10. B. N. Samoilov et al., in Proceedings of the IX International Conference on Low Temperature Physics, Columbus, Ohio, 1964.
11. M. Kontani and I. Itoh, J. Phys. Soc. Japan 22, 345 (1967).
12. T. Moriya, J. Phys. Soc. Japan 19, 681 (1964).

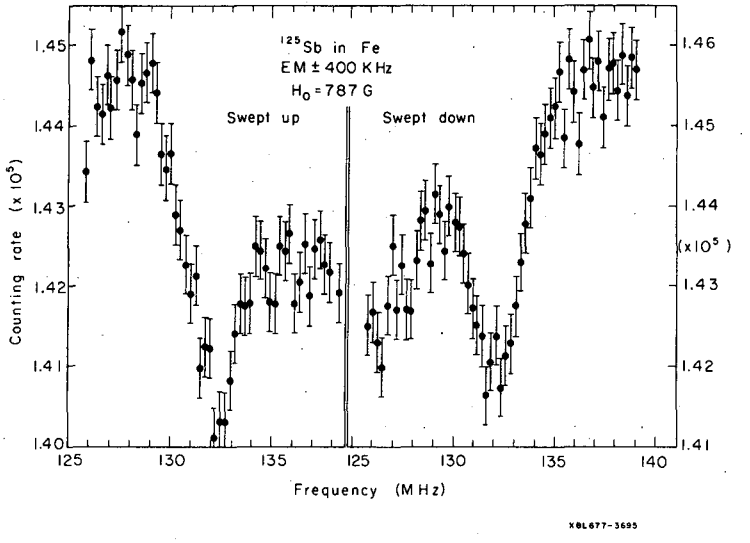

Fig. 1. Nuclear orientation NMR for ^{125}Sb in Fe. The data represent W(0°) for the combined 426-to-462-keV gamma group, which shows a positive net anisotropy. The frequency was swept in opposite directions in the left and right part of the figure, causing the opposite slopes in the warm-up curve.

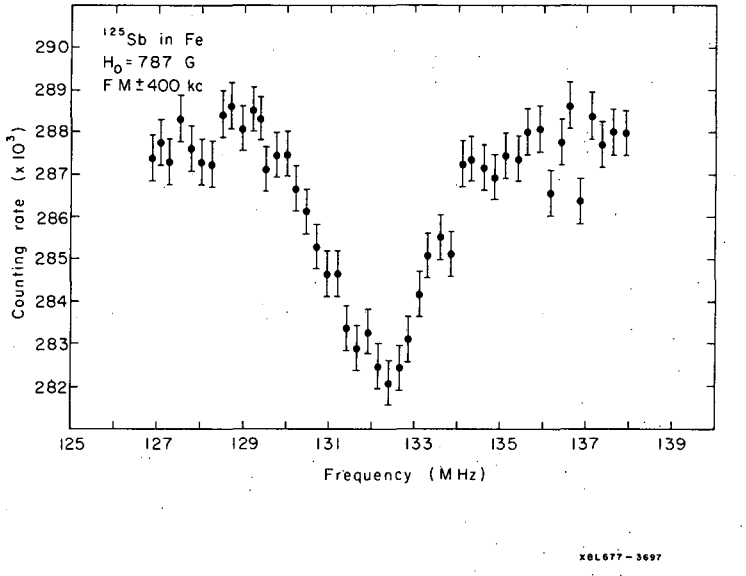

Fig. 2. Resonance for ^{125}Sb in Fe. The data points represent the sum of the frequency scans shown in Fig. 1. The center of the resonance appears at ν_R = 132.15 ± 0.10 MHz.

Fig. 3. Shift of the resonance frequency with external polarizing field. The linear behavior proves that domain resonances were observed. These data determine unambiguously g, H_{hf}, and the sign of H_{hf}.

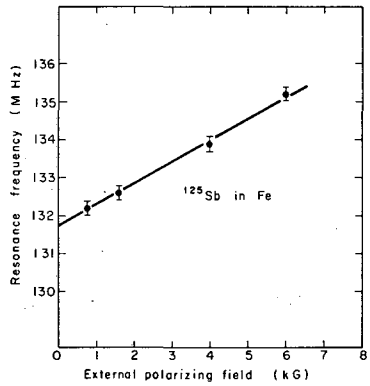

XBL677-3696

LOW-TEMPERATURE DEPARTURES FROM THE KORRINGA APPROXIMATION†

W. D. Brewer,* D. A. Shirley, and J. E. Templeton

Nuclear spin-lattice relaxation in metals often occurs via the magnetic hyperfine interaction, represented by an operator of the form $A\tilde{I}\cdot\tilde{S}$, where $\tilde{I}$ is the nuclear spin operator and $\tilde{S}$ the electronic (e.g., conduction electron) angular momentum operator.[1] In this case, the relaxation rate may be determined by the availability of electrons and electron vacancies of the appropriate energy separation γH, since for each downward nuclear transition of energy $-\gamma H$ there must be an upward electronic transition of energy $+\gamma H$, and vice versa. The availability of conduction electrons is given by the Fermi distribution function N(E), Fig. 1. The slope of the Fermi function near the Fermi energy E_F is dependent on the lattice temperature T; at low T ($kT \leq \gamma H$) it is quite sharp, whereas at high T ($kT \gg \gamma H$) it is broadened.

For a given nuclear transition during the relaxation process in which the nucleus changes in energy by $\pm\gamma H$, the probability of fulfilling the energy-conservation condition above is given by $\{N(E)[1-N(E\pm\gamma H)]\}$, i.e. the probability of finding an electron in a state of energy E times the probability of finding a vacant state at energy $E \pm \gamma H$. This quantity, integrated over energies E, is shown as the shaded regions of Fig. 1.

At high temperatures (right side of Fig. 1) both upward and downward transitions are possible and occur with approximately equal rates (as expected from microscopic reversibility, which gives $\frac{(\text{downward nuclear rate})}{(\text{upward nuclear rate})} = \exp(\gamma H/kT)$. Furthermore, the two rates are simply proportional to the width of the Fermi function, i.e., to kT. In this case the overall relaxation rate W is proportional to T and the relaxation time T_1 is proportional to inverse temperature, or $T_1 T = \text{const}$. The latter relation is known as the Korringa approximation. From Fig. 1 we see that the Korringa approximation should not hold at low temperatures, since the upward and downward rates become unequal and no longer simply proportional to T; in fact, the upward nuclear rate (corresponding to S_-) vanishes altogether in the extreme low-temperature limit. See left side of Fig. 1. The upward and downward nuclear transition rates may be likened to emission rates of radiation by atoms: at low temperatures only downward nuclear transitions are allowed, since there are no empty electronic states below the Fermi energy to allow a downward electron jump. This basic downward nuclear transition rate corresponds to spontaneous emission. As the temperature is raised, corresponding to the introduction of an external radiation source, "stimulated emission" and "absorption" begin to dominate, and at high temperatures the upward and downward rates are equal, corresponding to a system in equilibrium with a strong radiation source. The analogy is illustrated schematically in the lower part of Fig. 1.

Using the recently developed nuclear magnetic resonance of oriented nuclei (NMR/ON) technique,[2-4] we measured the spin lattice relaxation times for dilute solutions of radioactive ^{60}Co in Fe. This technique allows us to observe relaxation in the mdeg K range, which has previously been inaccessible for such measurements.

The experimentally observed quantity T_1' (defined below) deviates from the usual Korringa-type temperature dependence and becomes essentially constant below 14 mdeg K. This observation supports the model described above for nuclear spin relaxation via the conduction band.

This work uses essentially the same NMR/ON technique previously described[4] to obtain relaxation curves. T_1' is calculated from these by a least-squares fit of the deviation from equilibrium of the axial γ-ray intensity to the function

$$\Delta I(t) = \Delta I(0)[\,1 + a_1 t + a_2 \exp(-t/T_1')]\,.$$

The measured values of T_1' are shown in Fig. 2.

We note that the low-temperature inequality of W_+ and W_- mentioned above results in a relaxation which is no longer a simple exponential but only approximately so, and produces a relatively abrupt change of the effective (simple exponential) relaxation time to a constant value at very low temperatures.[5] It should be stressed that the sudden change to constant T_1' shown in Fig. 2 is a combined result of the inequality of S_+ and S_- and of the change in their temperature dependences. From Fig. 2 it may be seen that the temperature dependence of S_+ is by no means sufficient to account alone for this abrupt change, and furthermore $\gamma H = kT$ for ^{60}Co: Fe at T = 0.008° K, whereas the abrupt change occurs at T = 0.014° K.

The authors thank Mr. F. Bacon for his assistance in performing the experiments.

Footnotes and References

†Condensed from Phys. Letters 27A, 81 (1968).
*NSF Graduate Fellow, 1967-68.

1. T. Moriya, J. Phys. Soc. Japan 19, 681 (1964).
2. N. Bloembergen and G. T. Temmer, Phys. Rev. 89, 883 (1953).
3. E. Matthias and R. J. Holliday, Phys. Rev. Letters 17, 897 (1966).
4. J. E. Templeton, D. Phil. Thesis, Oxford University, 1967; J. E. Templeton and D. A. Shirley, Phys. Rev. Letters 18, 240 (1967).
5. J. A. Cameron, I. A. Campbell, J. P. Compton, and R. A. G. Lines, Phys. Letters 10, 24 (1964).

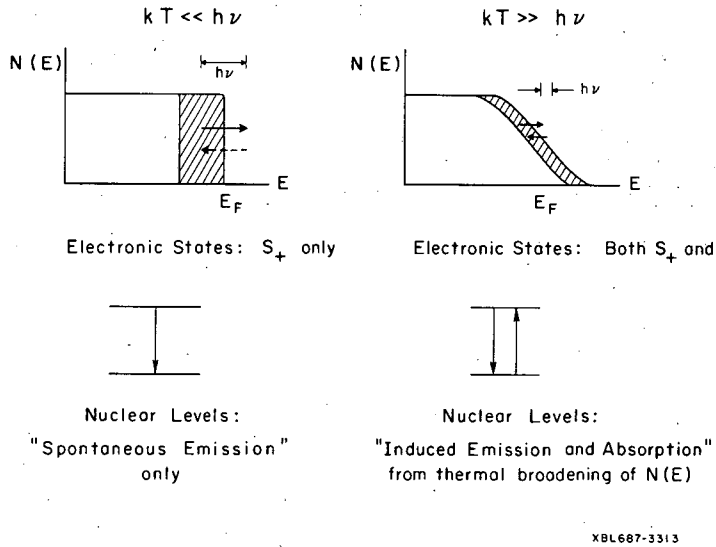

Fig. 1. Upper: Fermi functions N(E) for conduction electrons at low and high temperatures; hν = nuclear transition energy. Lower: Nuclear transitions permitted by the nuclear-electronic energy conservation condition during relaxation processes.

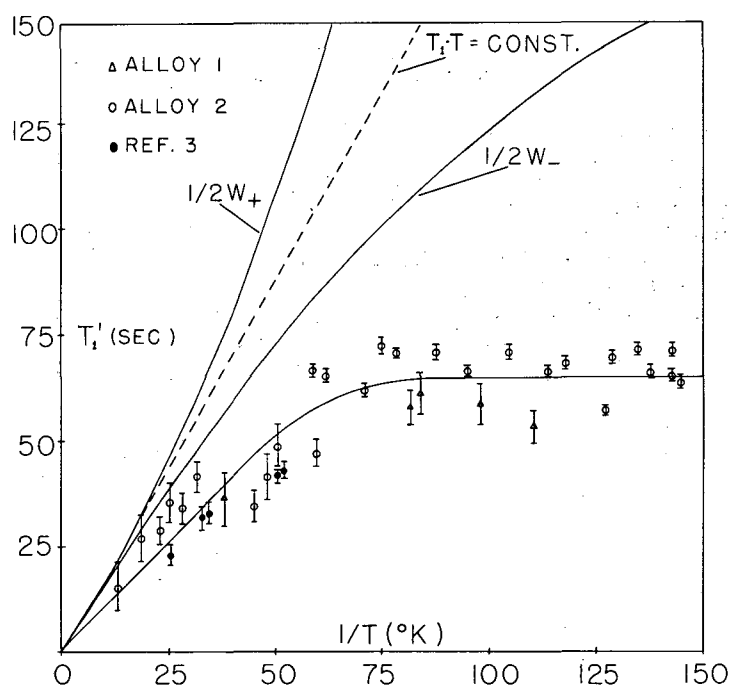

Fig. 2. Observed relaxation times T_1' versus 1/T. The errors shown are one standard deviation in the fit to an exponential decay; temperature errors are approximately the diameters of plotted circles. Scatter in points is primarily a result of variations in initial conditions (rf power, $\Delta I(0)$, frequency modulation of rf). The solid curve through data points represents the results of preliminary calculations. W_R is the reduced downward nuclear transition probability (proportional to S_+), which becomes constant at low T. The dashed line is the Korringa approximation.

NUCLEAR ORIENTATION OF ^{241}Am, ^{253}Es, AND ^{255}Fm IN NEODYMIUM ETHYLSULFATE

A. J. Soinski, N. J. Stone,* and D. A. Shirley

In order to study alpha decay and extend nuclear orientation studies of the lanthanides performed in this Laboratory, the actinides ^{241}Am, ^{253}Es, and ^{255}Fm, all in the 3+ valence state, were oriented in single crystals of neodymium ethylsulfate (NES) at low temperatures by means of the large, anisotropic hyperfine interactions that exist in these actinide ions.

In the lanthanides and actinides the spin-orbit interaction is stronger than the crystal field (CF) interaction, which is in turn stronger than the hyperfine interaction. A crystal field of lower than cubic symmetry will partially or completely remove the $(2J+1)$-fold degeneracy of the free ion, giving a series of CF levels which are in turn split by the hyperfine interaction. For the cases of interest the ground CF level is a doublet which has an effective spin of 1/2. The hyperfine interaction is described by a spin Hamiltonian

$$\mathcal{H} = AI_zS_z + 1/2\ B(I_+S_- + I_-S_+) + P[I_z^2 - 1/3\ I(I+1)], \tag{1}$$

where A and B are magnetic hyperfine interaction parameters and P is the electric hyperfine interaction parameter or quadrupole coupling constant.

Actinide ions are chemically analogous to the corresponding lanthanides, and the two series of elements are expected to have similar CF levels and hyperfine interaction parameters. This point is illustrated in Table I, which includes, in part, results reported here.

For the actinides it is most convenient to determine the degree of nuclear orientation by measuring the α-particle angular distribution because the subsequent γ rays, if present at all, are usually of low energy. In addition, the large recoil energy of the alpha-emitting nucleus can displace the ion from its lattice site, thereby "washing out" the γ-ray angular distribution. The angular distribution for α particles is given by

$$W(\theta) = 1 + \sum_{L,L'} \frac{a_L a_{L'}}{|a_L|^2}\, \phi_{LL'}\, [A_2B_2P_2(\cos\theta) + A_4B_4P_4(\cos\theta)], \tag{2}$$

where a_L is the relative intensity of the alpha wave of angular momentum L populating a given level of the favored band of the daughter (the total intensity to the unfavored bands is small and has no bearing on the analysis), and $\phi_{LL'} = \pm 1$ is the relative phase of the Lth and L'th waves. The A's arise in angular momentum theory and can be calculated exactly. The B's are orientation parameters giving the relative populations of the nuclear magnetic substates of the parent nucleus. They contain all the temperature and solid-state physics information and also permit the derivation of the hyperfine interaction parameters. The P's are Legendre polynomials for which θ is measured with respect to the crystalline c axis.

The relative intensities and phases for the alpha waves were predicted by Poggenburg,[6] using Mang's shell-model theory of alpha decay. With these predictions the angular distribution functions become

$$W(\theta) = 1 + 0.788\ B_2P_2(\cos\theta) + 0.100\ B_4P_4(\cos\theta) \text{ for } ^{241}\text{Am}, \tag{3a}$$

$$W(\theta) = 1 + 0.589\ B_2P_2(\cos\theta) - 0.0265\ B_4P_4(\cos\theta) \text{ for } ^{253}\text{Es}, \tag{3b}$$

$$W(\theta) = 1 + 0.658\ B_2P_2(\cos\theta) + 0.0003\ B_4P_4(\cos\theta) \text{ for } ^{255}\text{Fm}. \tag{3c}$$

Mang and Rasmussen[7] had predicted that the S, D, and G (L = 0, 2, and 4) alpha waves would be in phase for nuclei having a mass number of less than 244 and that the S and G waves would be out of phase otherwise.

^{253}Es has been previously oriented in NES by both Navarro[4] and Frankel.[8] Navarro determined the $|A|/k = 0.40(4)$ °K, but since he had limited data at $\theta = 90$ deg he could not determine

the relative phase of the S and G waves. Frankel found that these waves were cut of phase--which we confirmed--but his saturation anisotropy (the value of the angular distribution function if all nuclei are in one magnetic substate) at 0 deg, $W(0)_{satn}$, was 7% smaller than Navarro's value. The study presented here was undertaken to clarify this discrepancy.

Our experimental results are shown in Fig. 1. We found that $W(0)_{satn} = 1.88(3)$, which is 18% larger than Navarro's value. The dashed curve in Fig. 1 is the theoretical angular distribution given in Eq. (3b). The fit to the data is poor. The solid curve was obtained by modifying the relative intensities of the alpha waves to the ground and first excited states of ^{249}Bk; the S wave was decreased by 5%, the D wave was increased by 17.5%, and the G and I (L = 6) waves were increased by 200%. Poggenburg's calculations apparently put too much intensity in the S wave at the expense of the other waves.

This work raised more questions than it answered, because we obtained a substantially larger anisotropy than either Frankel or Navarro. Their sources may have been too thick, causing excessive scattering, or else a large number of the ^{253}Es nuclei in their crystals may not have been at lattice sites and were therefore emitting isotropically.

The angular distribution for ^{241}Am (see Fig. 2) is approximately linear in 1/T, which is characteristic for electric-hyperfine-structure alignment. The solid line in Fig. 2 is a plot of Eq. (3b) with $P/k = -0.0042(12)\,^{\circ}K$. The poorness of the fit of this curve to the experimental data indicates that Poggenburg's calculations do not accurately predict the L-wave intensities in this case also, but no attempt was made to improve the fit by altering the intensities. The S and D waves are in phase; we could not determine the relative phase of the S and G waves.

The electric field gradient (EFG) at the ^{241}Am nucleus--which interacts with the nuclear quadrupole moment, Q, to give alignment--arises from both the crystal lattice charges and the 5f electrons. Therefore the quadrupole coupling constant, P, can be written as a sum of a lattice contribution and a 5f-electron contribution, where

$$P_{lattice} = -3Q(1-\gamma_\infty)\, A_2^0/I(2I-1)$$

and

$$P_{5f} = 6e^2Q\, A_2^0 \langle r^2\rangle_{5f}(1-\sigma_2)\, \langle r^{-3}\rangle_{5f}(1-R_Q)\,|\langle 20||\alpha||00\rangle|^2/I(2I-1)(E_{^7F_2} - E_{^7F_0}).$$

Here γ_∞ is the Sternheimer antishielding factor, which is estimated[9] to be -125 for Am^{3+}. The Sternheimer factor arises because the quadrupolar part of the potential arising from the lattice charges distorts the closed electronic shells, thereby enhancing the EFG produced by the lattice charges. A_2^0 is a sum over lattice charges, which is usually determined experimentally from optical spectroscopy. From the optical data on Am^{3+} in $LaCl_3$,[10] we estimate that $V_2^0 = A_2^0 \langle r^2\rangle_{5f}(1-\sigma_2) = 185\ cm^{-1}$. A nonrelativistic calculation of the expectation value of r^2 for the 5f electrons of Am^{3+}, $\langle r^2\rangle_{5f} = 1.885\ a_0^2$, gives $A_2^0(1-\sigma_2) = 3.51\times10^{18}\ cm^{-1}/cm^2$. The shielding factor σ_2 accounts for the fact that the 5f electrons are shielded from the lattice charges by the 5d and 6s outer electron shells. The other symbols are explained by Blok and Shirley.[12]

P_{5f} is estimated to be less than 4×10^{-5}, which is smaller than the experimental uncertainty in P and was therefore neglected. Then $(1-\gamma_\infty)\,A_2^0 = -PI(2I-1)/3Q$ or $(1-\gamma_\infty)/(1-\sigma_2) = 430$, which may be in error by 50% because of inaccuracies in V_2^0, $\langle r^2\rangle_{5f}$, and Q.

For the ^{255}Fm angular distribution, the coefficient of the P_4 term is predicted to be small and therefore the relative phases of the S and G waves cannot be determined. The solid line in Fig. 3 is the function $1 - W(0\ deg) = 0.309\ B_2$ with $|B|/k = 0.040(10)\,^{\circ}K$. The positive coefficient before B_2 implies that the S and D waves are in phase.

Footnote and References

*Permanent address: Clarendon Laboratory, Oxford University, Oxford, England.

1. J. Blok and D. A. Shirley, Phys. Rev. 143, 911 (1966).
2. This work, in preparation.
3. J. M. Baker and B. Bleaney, Proc. Phys. Soc. (London) A68, 1090 (1955).

4. Q. O. Navarro, J. O. Rasmussen, and D. A. Shirley, Phys. Letters 2, 353 (1962).
5. G. S. Bogle, H. F. Duffus, and H. E. D. Scovill, Proc. Phys. Soc. (London) A65, 760 (1952).
6. John K. Poggenburg, Jr., Theoretical Alpha Decay Rates of Deformed Nuclei (Ph. D. Thesis), UCRL-16187, Aug. 1965.
7. H. J. Mang and J. O. Rasmussen, Kgl. Danske Videnskab. Selskab Mat.-Fys. Skr. 2, No. 3 (1962).
8. Richard B. Frankel, Nuclear Studies Using Semiconductor Detectors, (Ph. D. Thesis), UCRL-11871, Jan. 1965).
9. R. M. Sternheimer, Phys. Rev. 159, 266 (1967).
10. John B. Gruber, J. Chem. Phys. 35, 2186 (1961).
11. Allen C. Larson, private communication, 1967.
12. Johan Blok and D. A. Shirley, Phys. Rev. 143, 278 (1966).

Table I. Hyperfine interaction parameters for ions in an ethylsulfate crystalline lattice.

Ion	Electronic groundstate		A(cm^{-1})	B(cm^{-1})	P(cm^{-1})	Reference
Eu^{3+}	$4f^6$	$^7F_0$			$-4.17(28)\times10^{-4}$	1
Am^{3+}	$5f^6$	$^7F_0$			$-2.22(10)\times10^{-3}$	2
Ho^{3+}	$4f^{10}$	$^5I_8$	0.334(1)	0.020(4)	0.0003(3)	3
Es^{3+}	$5f^{10}$	$^5I_8$	±0.28(3)			4
Er^{3+}	$4f^{11}$	$^4I_{15/2}$	0.0052(1)	0.0314(1)	0.0030(3)	5
Fm^{3+}	$5f^{11}$	$^4I_{15/2}$		0.028(7)		2

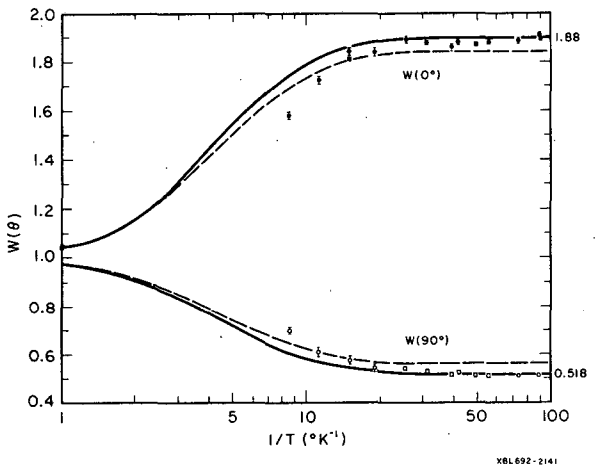

Fig. 1. Angular distribution for ^{253}Es in NES. The dashed curve was obtained by using theoretical intensities for the alpha partial waves as given by Poggenburg. The solid curve is also theoretical but with modified intensities to give an improved fit to the experimental points. The points for low values of 1/T vary from the theoretical curves because of radioactive heating of the NES crystal.

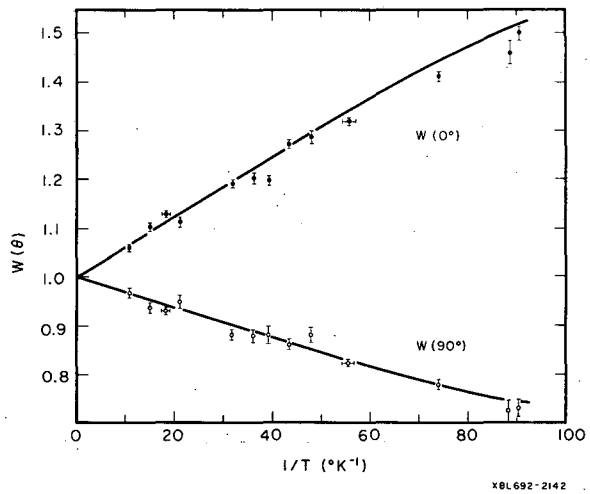

Fig. 2. Angular distribution for ^{241}Am in NES. The solid curve was obtained by using Mang's alpha decay theory and a value for P/k of -0.042 °K.

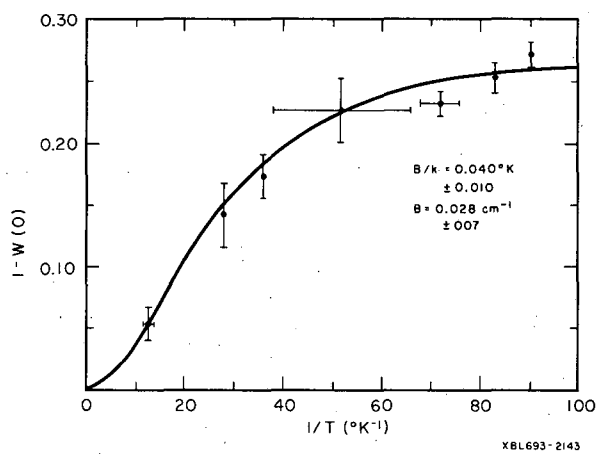

Fig. 3. Angular distribution at 0 deg with respect to the crystalline c axis for ^{255}Fm in NES. The curve drawn is for B/k = 0.04 °K.

NUCLEAR ORIENTATION STUDIES IN THE REGION 140 < A < 150 †

D. A. Shirley, P. H. Barrett, * J. Blok, ‡ and Morton Kaplan††

Nuclear orientation techniques were used to study the angular distribution of γ rays following the decays of ^{145}Sm and ^{147}Nd in the ethyl-sulfate and double nitrate lattices. [1] The magnetic moment of the spin-7/2 ground state of ^{145}Sm was determined as $|\mu| = 0.92 \pm 0.06$ mm. Two interesting features of this work (a) completion of a survey of low-lying states of odd-A nuclei in the A = 140 to 150 region, and (b) correlation of the attenuation coefficients following the decay of oriented nuclei.

Auxiliary measurements of γ-ray and electron spectra revealed that the excited state of ^{143}Nd at 742 keV must have 3/2 character (Fig. 1), and established that the 198-keV 3/2- state in ^{147}Sm is populated in the decay of ^{147}Pm (Fig. 2). With this information we can make some observations on these and neighboring odd-A nuclei.

Nuclear structure in the A = 140 to 150 region is not well understood as yet, partly because it is not well characterized experimentally and partly because neither the simplest spherical shell-model approaches nor the spheroidal nucleus model are applicable. The nuclei near beta stability in this region have Z ≈ 58 to 62, well removed from major shell closure and presumably susceptible to deformation. With N ≈ 83 to 87 the neutron configurations of these nuclei are too close to the shell closure at N = 82 to permit permanent deformation, which starts at N = 88 to 90. The softness of the proton configuration is manifest in low-lying collective states of phonon-plus-quasi-particle character. The effect on the level patterns in N = 83, 85, and 87 nuclei is dramatically illustrated in Fig. 3, where we have plotted the lowest-lying levels of 3/2-, 5/2-, 7/2-character for 11 nuclei, for those cases in which the assignments are certain or probable. In each case the levels shown are in fact the lowest 1, 2, or 3 levels known.

Nine of the 11 nuclei in Fig. 3 have ground-state spins of 7/2, presumably associated with the $f_{7/2}$ neutron state. For ^{143}Ce and ^{147}Nd, however, the ground-state assignments are 3/2- and 5/2- respectively. States with these assignments appear regularly in the N = 85 and 87 nuclei, and the first excited states of the N = 83 nuclei all seem to have 3/2- character. It is interesting, therefore, to inquire into the nature of these states.

For the N = 83 nuclei the 3/2- state may be largely a $p_{3/2}$ quasi-particle state. In the N = 85 and N = 87 cases both this state and the 5/2- state have moved down so far as to require a different mechanism, such as quasi-particle–phonon coupling. This explanation is supported by the fact that a neutron number of 3 (outside the N = 72 shell) makes neutron participation in phonon structure possible. Kisslinger and Sorensen studied[2] nuclear structure in this region, using a quasi-particle-plus-phonon approach, and they found low-lying states in the N = 85 and N = 87 nuclei of 7/2-, 5/2-, and 3/2- character, the latter two having strong phonon admixtures. In fact, the single basis vector with the largest amplitude coefficient in a quasi-particle-plus-phonon representation is, for the 5/2- state, composed of an $h_{9/2}$ quasi particle plus a phonon, and, for the 3/2- state, an $f_{7/2}$ quasi particle plus a phonon. Although these calculations did not predict the order of the energy levels correctly, they do provide a qualitative basis for interpreting the 3/2- and 5/2- states.

When the nuclear orientation in an intermediate state is perturbed by an extranuclear field, the angular distribution is given by

$$W(\theta) = 1 + B_2 U_2 G_2 F_2 P_2(\cos\theta) + \cdots,$$

where G_2 is a reorientation coefficient describing the effect of the perturbation. Results of this and other studies are given in Table I.

The experimental information regarding reorientation following the decay of oriented nuclei is sparse, but consistent. The picture that is emerging may tentatively be summarized as follows:

(a) In ferromagnetic metals and for closed-shell ions in dielectrics, reorientation times are very long, of the order of seconds at 10^{-2} °K. However, no experimental results are available for the latter case with electron-capture decay.

(b) For states with $T_{1/2}$ = 1 nsec or less there is no evidence for reorientation even in paramagnetic ions in dielectrics.

(c) For states with $T_{1/2}$ > 1 nsec, G_2 may or may not be significantly less than unity. Both

lifetime (as in the ^{155}Gd states) and environment (NES vs CMN for ^{145}Pm, ^{147}Pm, and ^{175}Lu) appear to affect G_2.

(d) As yet there is no demonstrated qualitative difference between the β^- and EC cases.

In summary, the experimental situation is fairly well characterized now, and more theoretical work on this problem seems justified. Time-dependent processes in the nanosecond region are strongly, but indirectly, suggested by (b) and (c) above. There is still no conclusive evidence that G_2 can be reduced below the static hard-core value, and time-differential measurements of $G_2(t)$ are highly desirable.

Footnotes and References

†Condensed from Phys. Rev. (to be published).

*Present address: General Electric Company, Schenectady, New York.

‡Permanent address: Department of Physics, University of California, Santa Barbara, California.

††Present address: Department of Chemistry, Yale University, New Haven, Connecticut.

1. Detailed reports are given in Morton Kaplan, J. Blok, and D. A. Shirley, Magnetic Moment of ^{145}Sm and Attenuation Following the Decay of Oriented Sm, UCRL-18035, Jan. 1968; Paul H. Barrett and D. A. Shirley, Nuclear Orientation Studies on ^{147}Nd and Interpretation of Some Neutron States for A = 140 to 150, UCRL-18036, Jan. 1968.

2. L. S. Kisslinger and R. A. Sorenson, Rev. Mod. Phys. 35, 853 (1963).

Table I. Summary of reorientation results for oriented nuclei.

	Daughter	Lattice	E_γ	T (°K)	Decay	Electron config. of patent	$T_{1/2}$ (nsec)	G_2
^{177}Lu	^{177}Hf	NES	many	0.011	β^-	$4f^{14}$	10^9	≈ 1
^{57}Co	^{57}Fe	Fe	14.4	0.05	EC	---	100	≈ 1
^{57}Co	^{57}Fe	Fe	136.4	0.02	EC	---	8.9	≈ 1
^{57}Co	^{57}Fe	CMN	136.4	0.007	EC	$3d^7$	8.9	0.81(10)
^{57}Co	^{57}Fe	FS[a]	136.4	0.02	EC	$3d^7$	8.9	0.32(2)
^{155}Eu	^{155}Gd	NES	86.5	0.011	β^-	$4f^6$	6.7	0.26(8)
^{155}Eu	^{155}Gd	NES	105.3	0.011	β^-	$4f^6$	1.0	0.80(9)
^{145}Sm	^{145}Pm	NES	61	0.011	EC	$4f^5$	2.6	B[b]
^{145}Sm	^{145}Pm	CMN	61	0.003	EC	$4f^5$	2.6	0.44(10)B
^{175}Yb	^{175}Lu	NES	396	0.02	β^-	$4f^{13}$	3.3	C
^{175}Yb	^{175}Lu	CMN	396	0.003	β^-	$4f^{13}$	3.3	$< \frac{C}{6}$[b]
^{147}Nd	^{147}Pm	NES	91	0.011	β^-	$4f^3$	2.5	0.89(11)
^{147}Nd	^{147}Pm	CMN	91	0.002	β^-	$4f^3$	2.5	0.42(12)
^{141}Ce	^{141}Pr	CMN	142	0.007	β^-	$4f^1$	1.9	1.08(8)

[a]Dilute nickel fluorosilicate.

[b]Only ratios of G_2(CMN)/G_2(NES) obtained.

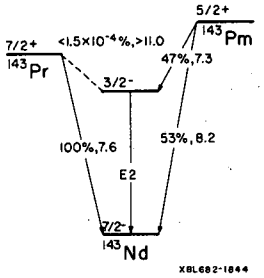

Fig. 1. Decay of ^{143}Pr and ^{143}Pm to ^{143}Nd. Excited-state energy is 742 keV.

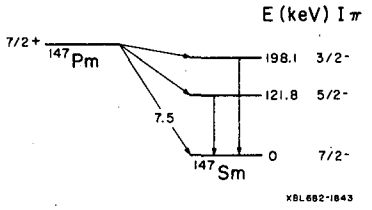

Fig. 2. Decay of ^{147}Pm.

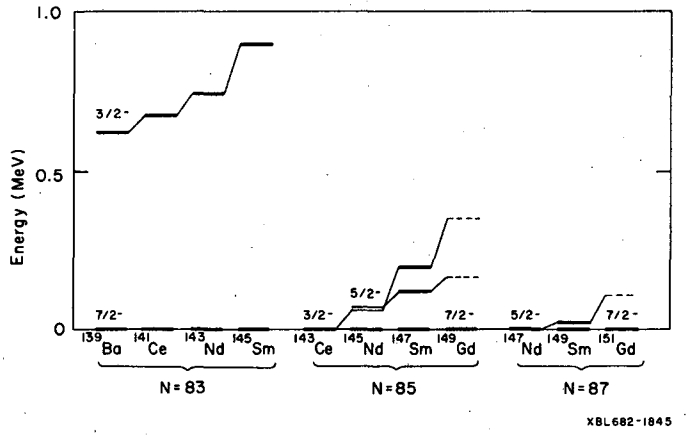

Fig. 3. Observed 3/2-, 5/2-, and 7/2- neutron levels for nuclei with N = 83, 85, and 87.

TEMPERATURE-DEPENDENT MAGNETIC HYPERFINE INTERACTION OF RHODIUM NUCLEI IN PARAMAGNETIC NICKEL

S. S. Rosenblum and D. A. Shirley

The time-differential perturbed angular correlation technique (TDPAC) has lately become a very powerful tool for investigating the microscopic behavior of extremely dilute impurities in ferromagnetic metals. The temperature region around the Curie point is of particular interest, and ^{100}Rh in nickel provides a good case for TDPAC in this region. The decay scheme of the parent ^{100}Pd, prepared by a (p, 4n) reaction on natural rhodium powder, is shown in Fig. 1. The level studied is the 2+ level at 74.8 keV via the 84-74.8-keV cascades. The g factor of this level has been accurately measured[1] [g = 2.151(4)]. In addition to the fact that the g factor is large and accurately known, the long lifetime of this level makes it a particularly attractive case for TDPAC studies in the critical region where magnetic hyperfine interactions are expected to be small.

Also, based on previous work on the system of ^{99}Ru in nickel and on hyperfine field systematics,[2] we expected that there would be some manifestations of "local moment" behavior, as was seen in ruthenium. Evidence for the existence of local moments is given below.

In Fig. 2, some typical data are presented showing the temperature dependence of the TDPAC spectrum in a constant applied field of 810 gauss. The data have been adjusted to remove the decay of the intermediate state. It is clear that the frequency of oscillation and the damping constant increase with decreasing temperature in this region.

In Fig. 3, the temperature dependence of the Larmor frequency of all the data is presented. The ordinate is $\beta = H_{eff}/H_{ext} = 1+K$, where K is the paramagnetic Knight shift described in Ref. 2. The solid curve is calculated from the macroscopic magnetization data of Weiss and Forrer on pure nickel,[3] assuming that the hyperfine field is proportional to the lattice magnetization. The fact that the data lie very close to this curve, rather than near $\beta = 1.0$, is strong evidence that the hyperfine field is produced by the conduction electrons rather than a local moment.

In Fig. 4 is shown the behavior of the TDPAC spectrum as a function of applied magnetic field at a constant temperature, $T = 365 \pm 0.5°C$. Aside from the expected result that the Larmor frequency increases with increasing field, we also see that the damping constant increases.

This damping might arise from either a static or a time-dependent hyperfine interaction. The static interactions causing this might result from inequivalent magnetic sites, anistropic magnetic interaction, or quadrupole interaction. We were able to eliminate the latter two possibilities by carrying out experiment on nickel single crystals in which no detectable difference was seen between different crystallographic directions.

To test the remaining supposition that a time-dependent interaction is present we performed a decoupling experiment, one in which a magnetic field is applied parallel to the direction of emission of one of the radiations.[4] If the interaction is static and decoupled, the anisotropy is restored, whereas if it is time-dependent, the anisotropy disappears. As can be seen from Fig. 5, the anisotropy disappears. The temperature and field dependence of the relaxation rate can be accounted for by assuming that they are due to exchange narrowing. A model based on this idea has recently been proposed by Silbernagel, Jaccarino, Pincus, and Wernick in which they described the nuclear relaxation of aluminun nuclei in XAl_2 compounds (X = rare earth) above the Curie point, assuming only pair correlations.[5]

With several modifications, this model leads to a relaxation rate $\lambda = 3/T_1 = 3/T_2$ proportional to σ^2, the induced lattice magnetization.

Figure 6 is a plot of λ vs σ^2 with temperature and applied field as implicit parameters. The linear behavior is quite good in spite of the large errors in the data.

References

1. E. Matthias and D. A. Shirley, Nucl. Instr. Methods 45, 309 (1966).
2. D. A. Shirley, S. S. Rosenblum, and E. Matthias, Phys. Rev. 170, 363 (1968).
3. P. Weiss and R. Forrer, Ann. Phys. (Paris) 15, 153 (1926).
4. R. M. Steffen and Hans Frauenfelder, The Influence of Extranuclear Fields on Angular Correlation, in Perturbed Angular Correlations, E. Karlsson, E. Matthias, and K. Siegbahn, Eds. (North Holland Publishing Co., Amsterdam, 1964), Chapter 1, p. 11.
5. B. G. Silbernagel, V. Jaccarino, P. Pincus, and J. H. Wernick, Phys. Rev. Letters 20, 1091 (1968).

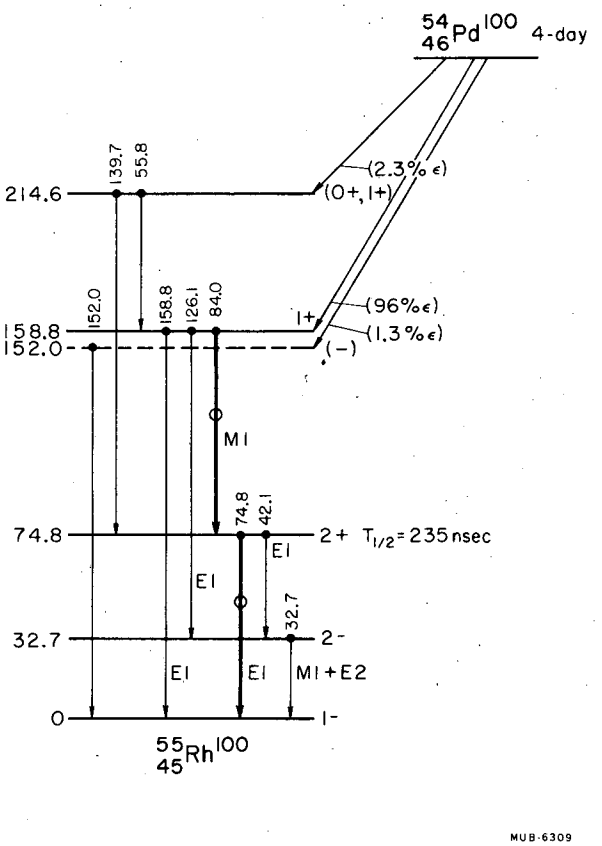

Fig. 1. Decay scheme of ^{100}Pd → ^{100}Rh.

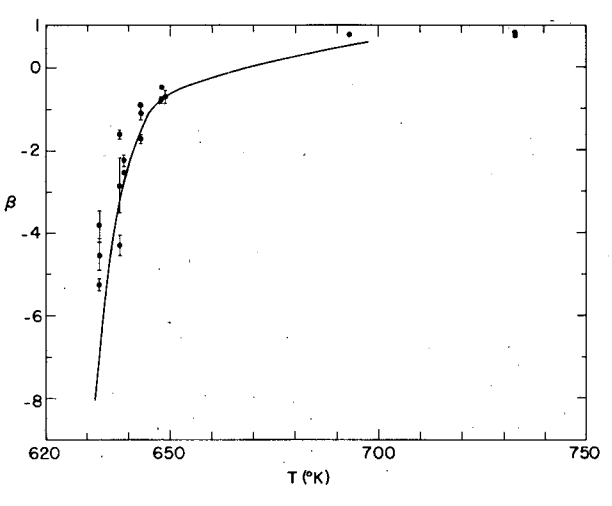

Fig. 3. Temperature dependence of β.

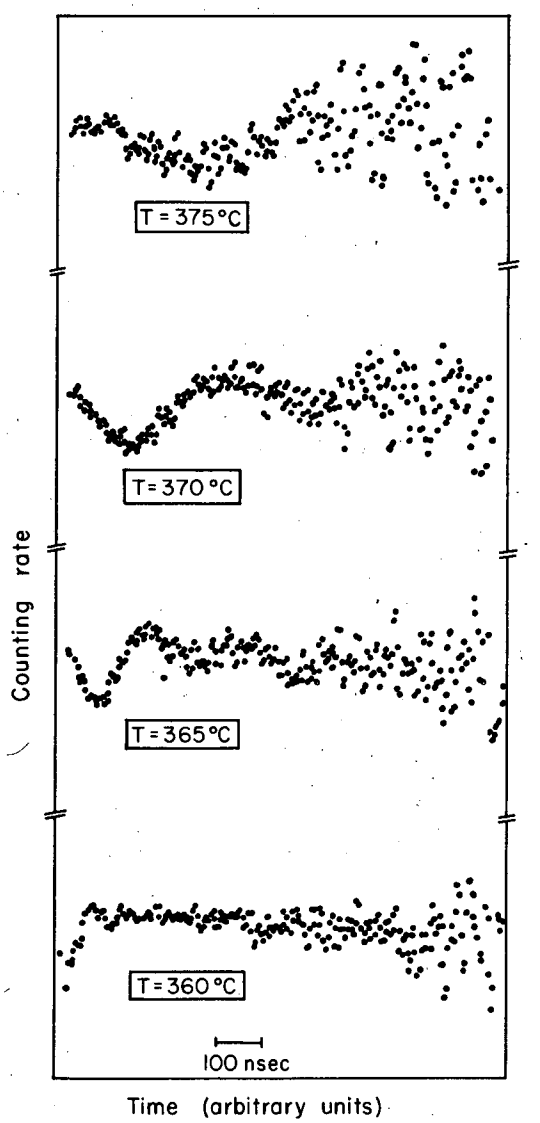

Fig. 2. Temperature dependence of the Larmor frequency in an applied field, H_0 = 810 gauss, θ = 180 deg.

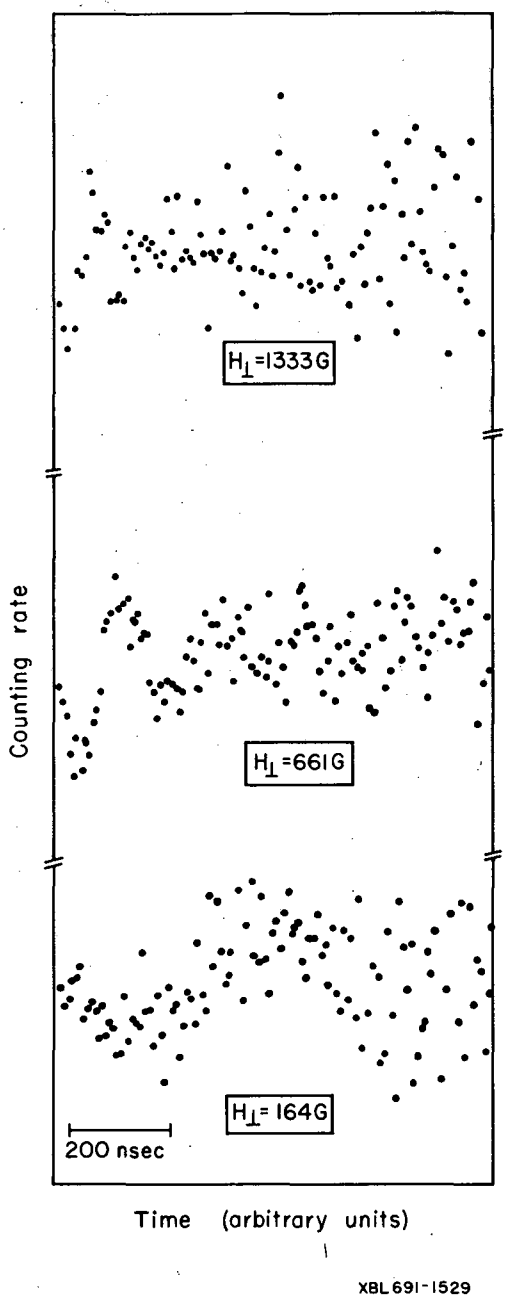

Fig. 4. Magnetic field dependence of the Larmor frequency at T = 365° C, θ = 135 deg.

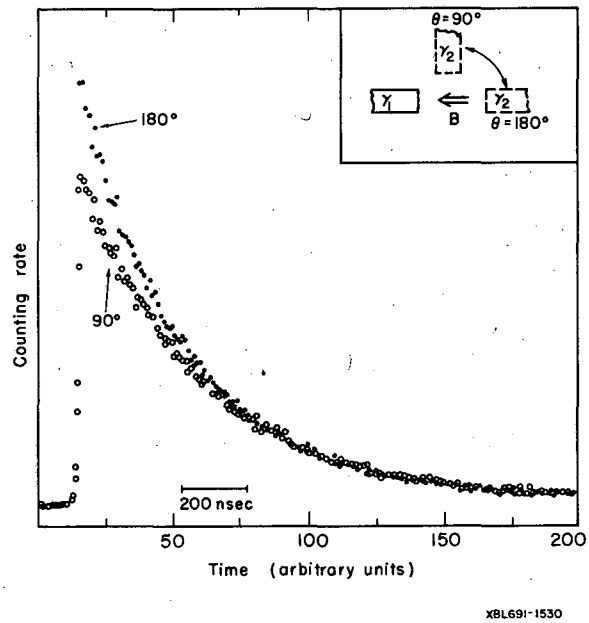

Fig. 5. Decoupling experiment showing time-dependent destruction of the anisotropy. The inset shown the experiment geometry.

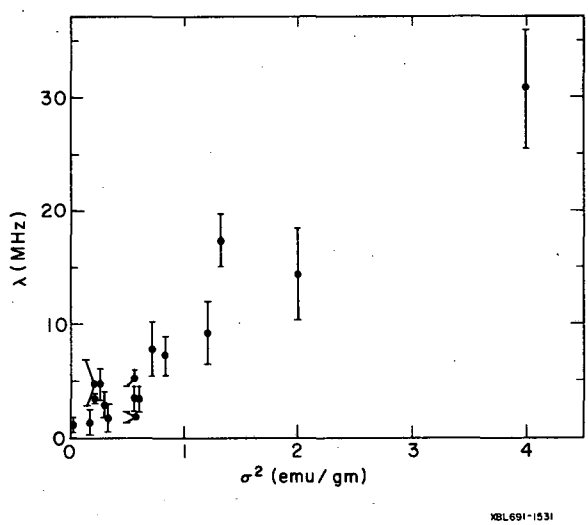

Fig. 6. Relaxation rate $\lambda = 3/T_1 = 3/T_2$ as a function of σ^2, showing a linear dependence as predicted by the exchange-narrowing model.

LOCALIZED MOMENTS ON RHODIUM IN Rh-Pd ALLOYS

G. N. Rao, E. Matthias, and D. A. Shirley

The formation of localized moments on impurity atoms in various metal alloys is well known for solute atoms of the 3d transition group.[1] Much less experimental evidence is presently available about localized states on 4d atoms in dilute alloy systems. To study this question we choose the Rh-Pd alloy system. The macroscopic properties of this system--susceptibility, resistivity, and specific heat--have been thoroughly studied. The anomalous variation of the susceptibility of Rh-Pd alloys with temperature as well as with rhodium concentration has been of particular interest.[2-4]

Perturbed angular correlation (PAC) techniques provide an excellent tool to sense microscopically the magnetism associated with the impurity atom. The rotation of the angular correlation pattern in an effective magnetic field $\vec{H}_{eff} = \vec{H}_{ext}(1 + K)$ gives the Knight shift,

$$K = \frac{\Delta H}{H_{ext}} = \frac{8\pi}{3} \langle |\psi(0)|^2 \rangle_{E_f} \chi_e .$$

Unlike the Mössbauer effect, the PAC technique is observable at any temperature and is therefore well suited for studying the temperature dependence of Knight shifts. To study very dilute Rh-Pd alloys we used the angular correlation of the 85-to-75-keV cascade in ^{100}Rh,[5] populated in the decay of 4-day ^{100}Pd. The intermediate state of this cascade has a half-life of $T_{1/2} = 235$ nsec and a g factor of $g = +2.151$.

The magnetic hyperfine interaction in the 75-keV level was measured through the periodic intensity modulation of the coincidence time spectrum. Properly prepared start and stop pulses, corresponding to γ_1 and γ_2, respectively, were fed into an "Eldorado 793" time-interval counter which measured the delay between these pulses to 1 nsec accuracy. This digitized time information was stored on magnetic tape and later processed to yield the time spectrum. Both Fourier analysis and autocorrelation techniques were used to extract the frequency of the Larmor precession from the data.[6] A typical result of the Fourier analysis is shown in Fig. 1, where the sine, cosine, and absolute transforms are given by the respective expressions

$$A(\nu) = \int I(\theta_0, t) \sin(2\pi\nu t)\, dt,$$

$$B(\nu) = \int I(\theta_0, t) \cos(2\pi\nu t)\, dt,$$

$$F(\nu) = \sqrt{A^2(\nu) + B^2(\nu)}.$$

Here, the time-dependent intensity is given by

$$I(\theta_0, t) = I_0\, e^{-t/\tau}\{1 + A_2(1)\, A_2(2)\, P_2[\cos(\theta_0 \pm \omega_L t)]\} + C,$$

with $\omega_L = g H \frac{\mu_N}{\hbar}$.

By using the autocorrelation function it is possible to improve the signal-to-noise ratio by more than an order of magnitude over the simple Fourier transform. In this technique the Fourier integral

$$G(\nu) = \int_0^{T_{max}} \frac{C(T)}{C(0)} \cos(2\pi\nu T) dT$$

contains the autocorrelation function

$$\frac{C(T)}{C(0)} = \frac{\text{ave}[W(t) - \bar{W}][W(t+T) - \bar{W}]}{\text{ave}[W(T) - \bar{W}][W(T) - \bar{W}]},$$

where T is the time lag at which the data are correlated. Typical autocorrelation spectra are shown in Fig. 2.

Using this technique, we measured the Knight shift of ^{100}Rh in extremely dilute Rh-Pd alloys as a function of temperature. The results are listed in Table I and plotted in Fig. 3. The insert in Fig. 3 shows the Knight shift and the susceptibility for the pure Pd host matrix according to Ref. 7. Two effects can be noticed: (a) there is a striking difference, between host and impurity, of the low-temperature behavior of the Knight shift and the susceptibility; and (b) the proportionality between K and χ, observed in the host, does not hold for the impurity.

The impurity susceptibility was calculated from the susceptibility data of Manuel and St. Quinton and V. E. Vogt et al.[8] by extrapolating their data to extremely small Rh concentrations. By use of these extrapolated values for χ_{alloy}, the impurity susceptibility can be obtained from the relation

$$\chi_i = \lim_{C_i \to 0} \frac{\chi_{\text{alloy}} - C_{Pd}\chi_{Pd}}{C_i},$$

where C_i and C_{Pd} are the number of rhodium and palladium atoms per gram. In Fig. 4 the impurity susceptibility is plotted versus $(T+T_K)^{-1}$, assuming that χ_i is described by a Curie-Weiss type relation[1] $\chi_i = \mu_e^2/3k(T+T_K)$, where T_K is a constant: it is expected to be the Kondo temperature at which a bound state is formed between the local moment on the Rh and the conduction electrons of the host. A fit of the data yields $T_K \approx 72.4°K$. Due to the uncertainty in the impurity susceptibility, this value should be considered as only approximate. There remains no doubt, however, that a bound state between the localized moment at the rhodium atom and the conduction electrons is formed in this alloy.

Because the Knight shift arises via spin polarization, its temperature-dependent part will be affected by the formation of a Kondo state. On the other hand, knowing the impurity susceptibility, one can deduce the hyperfine field arising from the d electrons, $H_{hf}^{(d)}$, from a measurement of the Knight shift as a function of temperature. Therefore, the formation of a bound state of the localized moment should influence the core-polarization hyperfine field.

The Knight shift as a function of temperature can be written in the form[9] $K(T) = \alpha_s \chi_p^s + \alpha_d \chi_p^d(T) + K_{vv} + \delta K_{dia}$, where χ_p^s and χ_p^d are the Pauli spin susceptibilities due to the s and d electrons, while K_{vv} and δK_{dia} are the Van Vleck and diamagnetic contributions to the total shift. The partial derivative of the Knight shift with respect to the impurity susceptibility, with temperature as an implicit parameter, yields[9] $dK(T)/d\chi_p^d(T) = \alpha_d = 0.895 \times 10^{-4} H_{hf}^{(d)}$. A plot of K(T) versus $\chi_i(T)$ is shown in Fig. 5. The data show a striking break about the χ_i value corresponding to 300°K (compare Fig. 3), not quite consistent with the T_K found from Fig. 4. Still, the break is attributed to the occurrence of two vastly different core-d hyperfine fields below and above the Kondo temperature. Above T_K the localized moment is undisturbed and the nuclei feel the full amount of $H_{hf}^{(d)}$. A fit of the data gives the value $H_{hf}^{(d)} = -663$ kG spin, which agrees well with calculated fields[10] of -749 kG/spin and -726 kG/spin for $Pd^{2+}(4d)^8$ and $Pd^{3+}(4d)^7$, respectively. The experimental value of Seitchik et al.[7] of -689 ± 20 kG/spin for palladium nuclei in Pd metal also compares favorably with our result.

Below the Kondo temperature, however, the core-d hyperfine field is drastically lowered due to the coupling of the localized moment to the surrounding conduction electrons. Judging from the three points at 4.2°K, 77°K, and 195°K, the hyperfine field is only $H_{hf}^{d} = -35$ kG. Thus, in a bound state, only a small fraction of the total electron polarization arising from the rhodium solute is still concentrated on that atom. The main fraction of the polarization must be distributed over those conduction electrons that are coupled to the bound state. Since the spatial dimensions of the bound state extend over many neighbors, the polarization of the matrix due to the impurity rhodium alone is comparatively long-range.

The present data show the considerable importance of microscopic methods in connection with collective effects in solids, which enable us to test hyperfine fields and thus spin distributions at specific atomic sites. The present investigation is to be continued.

References

1. For a recent comprehensive review on "Localized Magnetic Impurity States in Metals" see M. D. Daybell and W. A. Steyert, Rev. Mod. Phys. 40, 380 (1968).
2. F. E. Hoare and J. C. Matthews, Proc. Roy. Soc. (London) A212, 137 (1952); D. Budworth, F. E. Hoare, and J. Preston, ibid. A257, 250 (1960).
3. A. B. Lidiard, Proc. Roy. Soc. (London) A227, 161 (1954).
4. J. A. Seitchik, V. Jaccarino, and J. H. Wernick, Phys. Rev. 138, A148 (1965).
5. E. Matthias, D. A. Shirley, J. S. Evans, and R. A. Naumann, Phys. Rev. 140, B264 (1965).
6. E. Matthias and D. A. Shirley, Nucl. Instr. Methods 45, 309 (1966).
7. J. A. Seitchik, A. C. Gossard, and V. Jaccarino, Phys. Rev. 136, A1119 (1964).
8. A. J. Manuel and J. M. P. St. Quinton, Proc. Roy. Soc. A273, 412 (1963); V. E. Vogt, E. Oehler, and W. Treutmann, Ann. Phys. 18, 168 (1966).
9. A. M. Clogston, V. Jaccarino, and Y. Yafet, Phys. Rev. 134, A650 (1964).
10. A. J. Freeman in Hyperfine Structure and Nuclear Radiations, Ed. by E. Matthias and D. A. Shirley (North-Holland Publishing Co., Amsterdam, 1968), p. 427.

Table I. Knight shift data for dilute Rh-Pd alloys obtained at various temperatures. The values given represent weighted averages over several individual runs.

T (°K)	g(1 + K)	- K
4.2	1.835(7)	0.147(3)
77	1.914(7)	0.120(4)
195	2.006(6)	0.067(3)
300	2.014(2)	0.064(2)
503	2.070(4)	0.038(3)
803	2.132(5)	0.009(3)
1053	2.121(7)	0.014(4)

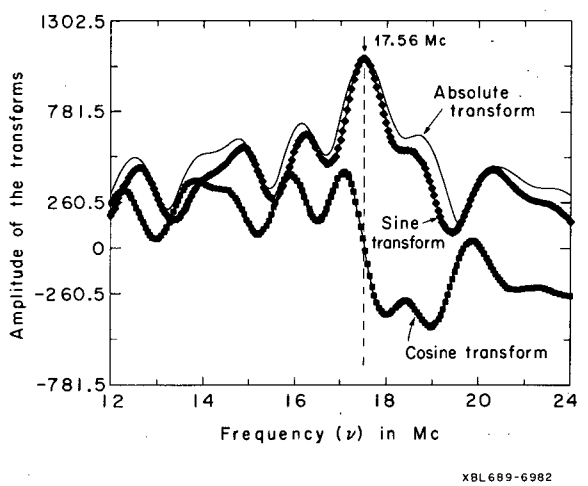

Fig. 1. Fourier analysis of the time spectrum for a Rh-Pd alloy at 77°K. The applied magnetic field was 5.922 kG.

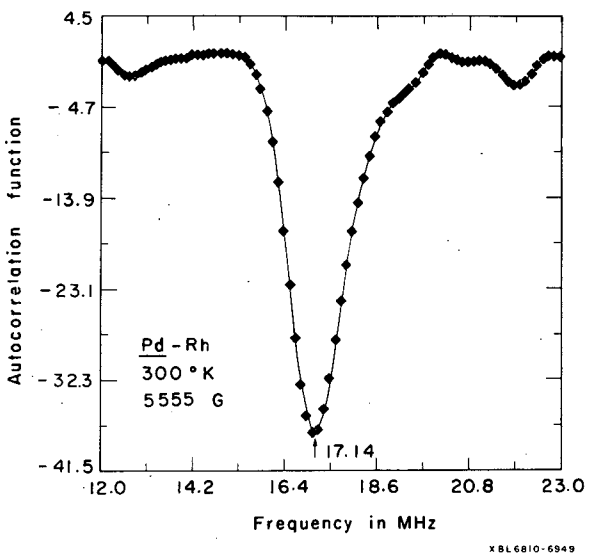

Fig 2. Autocorrelation spectrum obtained with a Rh-Pd alloy at 300°K in an external magnetic field of 5.555 kG.

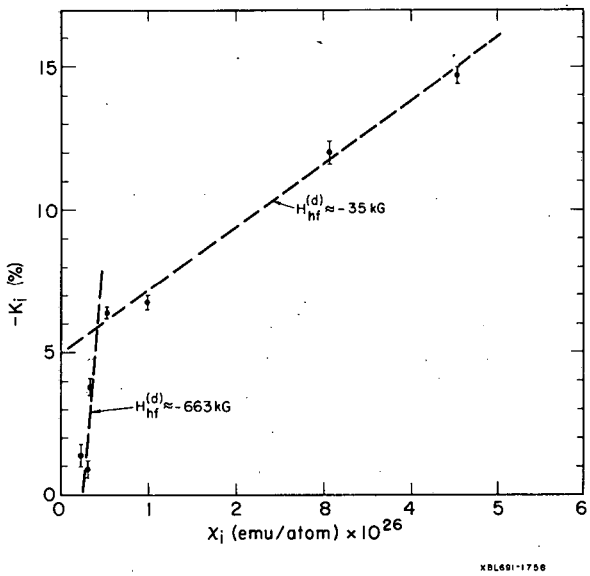

Fig. 3. Plot of Knight shift (Table I) and impurity susceptibility (calculated from data of Ref. 8) for dilute Rh-Pd versus temperature. The temperature dependence of both quantities for pure Pd is shown in the insert.

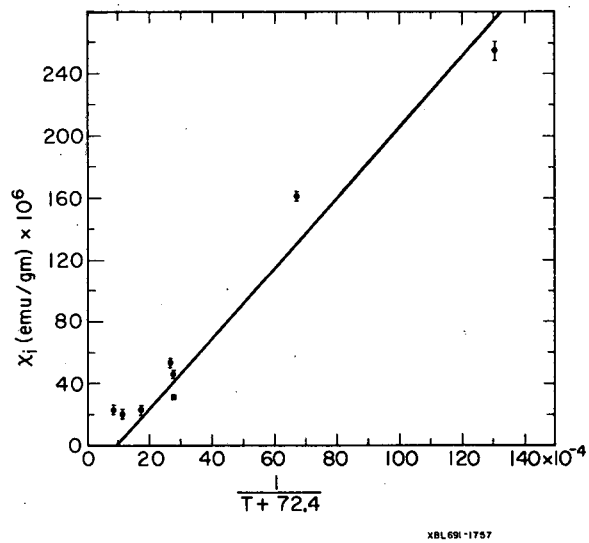

Fig. 4. Impurity susceptibility versus $(T + T_K)^{-1}$, indicating the formation of a Kondo state at about 72°K.

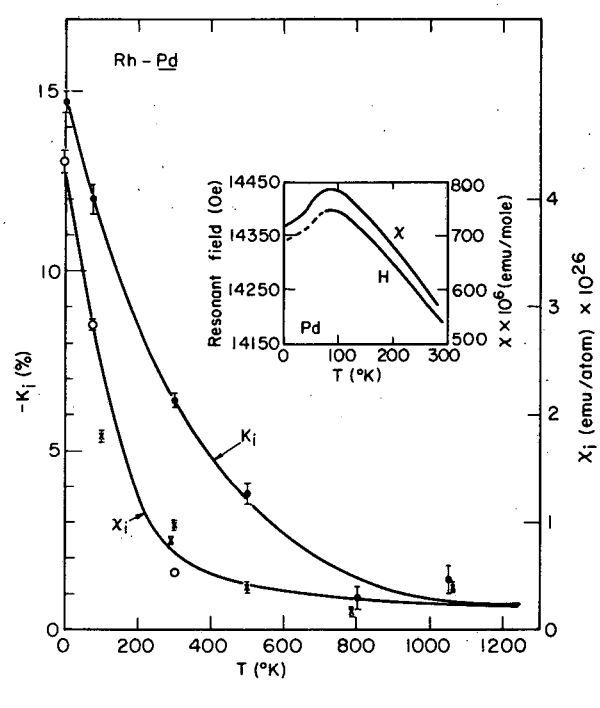

Fig. 5. Knight shift plotted versus impurity susceptibility. The slopes are proportional to the core-d hyperfine fields and indicate different fields above and below the Kondo temperature.

MÖSSBAUER RESONANCE STUDY OF GOLD COMPOUNDS

M. O. Faltens and D. A. Shirley

Mössbauer resonance experiments were performed on several diamagnetic gold compounds. These compounds belong to one of two groups of gold compounds: the linear gold(I) compounds, which have sp hybridization; or the square planar gold(III) compounds, which have dsp^2 hybridization. These experiments were performed at 4.2°K with a gold-in-platinum source and absorbers of gold compounds. From the Mössbauer spectra of the gold(I) and gold(III) compounds, direct relationships were established between the isomer shift (IS) and the quadrupole splitting (QS) values in each oxidation state. They were explained in terms of the hybridization of the bonds and of the number of bonding electrons on gold. The equations of the best straight lines for gold(I) and gold(III) compounds, determined by the least-squares method, are

$$\mathrm{IS[Au(I)]} = 0.782\ (eqQ/2) - 0.474\ \mathrm{cm/sec}, \tag{1}$$

$$\mathrm{IS[Au(III)]} = 0.542\ (eqQ/2) + 0.016\ \mathrm{cm/sec}, \tag{2}$$

where QS equals $\frac{1}{2}\,|eqQ|$.

The isomer shift for ^{197}Au compounds is

$$IS = 5.39\times10^{-24}\ \delta R/R \left[\sum_a \psi(0)^2 - \sum_s \psi(0)^2\right], \tag{3}$$

where $\delta R/R$ is the nuclear factor and the quantity in square brackets is the difference between the nuclear electron densities of the absorber and the source, respectively. $\delta R/R$ is a positive quantity[1] whose magnitude was determined to be 3.1×10^{-4} in this work.[2] Equation (3) implies that the absorbers with the larger number of 6s valence electrons will have the more positive IS values.

The quadrupole splitting for ^{197}Au, with $I_g = 3/2+$ and $I_e = 1/2+$, is

$$QS = \tfrac{1}{2}\,|eq_{zz}Q| \times (1 + \eta^2/3)^{1/2}, \tag{4}$$

where Q is $+0.60\times10^{-24}$ cm^2 and η^2 is zero for the axially symmetric gold(I) and gold(III) compounds. The molecular electric field gradients, q_{zz}, for the gold(I) and gold(III) compounds are given the following expressions, which neglect the small lattice field gradients:[3]

$$q_{zz}\,[\mathrm{Au(I),\ molecule}] = 2\alpha_I^2\, q_{610}, \quad \text{for } 0 \le \alpha_I^2 \le 1 \tag{5}$$

$$q_{zz}\,[\mathrm{Au(III),molecule}] = -2q_{522} + 2\alpha_{III}^2(q_{522} + 2q_{611}), \quad \text{for } 0 \le \alpha_{III}^2 \le 1, \tag{6}$$

where α is defined in the molecule-orbital expression for gold-ligand bonds as

$$\psi_{AuL} = \alpha\psi_{Au} + \beta\psi_L \tag{7}$$

and overlap is neglected in normalization: i.e., we take $\alpha^2 + \beta^2 = 1$. Equation (5) means that for gold(I) the magnitude of q_{zz} (Au(I)), and thus eqQ/2, increases as the gold(+1) ion ($\alpha^2 = 0$) gets a larger number of 6p electrons ($\alpha^2 > 0$). For gold(III), the q_{zz}[Au(III)] values go from a negative quantity to a positive one as gold(+3) ion ($\alpha^2 = 0$) gains 5d and 6p bonding electrons. The first quantity on the right in Eq. (6) represents the field gradient of the $5d^8$ spin-paired nonbonding electrons of gold.

The relationships of Eqs. (1) and (2) can therefore be explained in terms of the number of bonding electrons on gold. Given q_{522} and q_{610} of Eqs. (5) and (6), the values of α^2, the number of bonding electrons N, and the charge on gold X can be determined from

$$N = 2\alpha^2, \tag{8}$$

$$X[\mathrm{Au(I)}] = 1 - 4\alpha_I^2, \tag{9}$$

$$X'[\mathrm{Au(III)} = 3 - 8\alpha_{III}^2. \tag{10}$$

From free-atom Dirac-Fock wave functions calculated by Mann,[4] q_{522} was determined to be 26.86×10^{15} esu/cm^3. Unfortunately, the q_{610} value was much more difficult to determine, and was also found to be a very sensitive function of charge. From the free-atom wave function, we estimated q_{610} to be about -25×10^{15} esu/cm^3. However, by first considering $\delta R/R$ a constant in Eq. (3) and applying Eqs. (4), (5), and (6) to Eqs. (1) and (2) for $\alpha^2 = 0$ and $\alpha^2 = 1/2$, we arrived at a larger value of q_{610} equal to -44×10^{15} esu/cm^3. The first value, -25×10^{15} esu/cm^3, closely approximates that value for the 6p electron of mercury.[5] However, -44×10^{15} esu/cm^3 gives an internally more consistent set of results (e.g., $\delta R/R$ and X values).

From electronegativity considerations, we expect the charge on gold to be positive for the chlorides, bromides and iodides. This means that according to our model, q_{610} must be larger in magnitude. For gold(I) compounds, q_{610} of -44×10^{15} esu/cm^3 results in positive charges on gold in AuCl, AuBr, and AuI. For gold(III), however, a value of q_{610} equal to about -50×10^{15} esu/cm^3 is required for the gold atom in gold(III) halide compounds to be positively charged. This is approximately a 12% difference between the minimum required values for $|q_{610}|$. Since q_{610} values for gold(I(and gold(III) need not be the same value and indeed are probably not identical, this difference may not be unreasonable.

The results of this work are summarized in Figs. 1 and 2 and Table I. The IS vs QS values of the gold compounds are given in the figures along with the $\Delta\psi(0)^2$ values at the top and q_{zz} values to the right of the figures; $\Delta\psi(0)^2$ was calculated from Eq. (3), where $\delta R/R$ was taken to be 3.1×10^{-4}, and q_{zz} was determined from Eq. (4), with η^2 equal to zero. The values of α^2 and charges X for gold are listed in Table II for q_{610} values of -25×10^{15}, -35×10^{15}, -40×10^{15}, -44×10^{15}, and -50×10^{15} esu/cm^3. The results shown in Figs. 1 and 2 suggest that the hybridizations of the compounds remain essentially constant and that the changes in the isomer shift and quadrupole splittings are due to the differences in the ionic character of the various compounds.

References

1. D. O. Patterson, L. D. Roberts, J. O. Thomson, and R. P. Levey, Oak Ridge National Laboratory Report, ORNL-TM-1685, 1967.
2. D. A. Shirley estimated $\delta R/R$ to be (+) 3×10^{-4}, Rev. Mod. Phys. 36, 339 (1964).
3. Estimates of the lattice field gradients and the development of Eqs. (5) and (6) are given in Marjorie O. Faltens, Mössbauer Resonance Studies of Gold Compounds (Thesis), UCRL-18706, Feb. 1969.
4. J. B. Mann, (Los Alamos Scientific Laboratory), private communication.
5. H. G. Dehmelt, H. G. Robinson, and Walter Gordy, Phys. Rev. 93, 480 (1954).

Table I. Observed and derived parameters for several gold compounds.

Compounds	Isomer shift (cm/sec)	$\Delta\psi(0)^2 \times 10^{25}$ Relativistic	Quadrupole splitting (cm/sec)	$q_{zz} \times 10^{15}$ (esu/cm^3)
AuF_3	-0.107(0.001)	-6.611_5	0.274(0.002)	(-)7.860
$[AuF_4]^-$	-0.069(0.002)	-4.263_5	0.182(0.002)	(-)5.221
AuCl	-0.142(0.001)	-8.774	0.465(0.001)	13.339
$[AuCl_4]^-$	0.044(0.006)	2.718_7	0.127(0.008)	3.643
$AuCl_3$	0.057(0.009)	3.521	0.075(0.008)	2.151
AuBr	-0.147(0.001)	-9.083	0.432(0.004)	12.134
$[AuBr_4]^-$	0.067(0.002)	4.115	0.113(0.002)	3.241_5
$AuBr_3$*	0.079(0.007)	4.881	0.127(0.002)	3.643
AuI	-0.132(0.003)	-8.156	0.398(0.001)	-11.417
$Cs_2Au^IAu^{III}Cl_6$*	I-0.143(0.028)	---	0.410(0.065)	---
	III-0.059(0.022)	---	0.133(0.018)	---
AuCN	0.166(0.017)	10.257	0.809(0.003)	-23.207
$KAu(CN)_2$	0.325(0.008)	20.081_6	1.021(0.006)	-29.288
$KAu(CN)_4$	0.421(0.012)	26.013	0.699(0.005)	20.052
$KAu(CN)_2Cl_2$	0.256(0.002)	15.818	0.526(0.002)	~12.69
$KAu(CN)_2Br_2$	0.272(0.007)	16.807	0.546(0.001)	~13.53
$KAu(CN)_2I_2$	0.278(0.006)	17.177	0.587(0.003)	~13.85
$[AuS_4C_4(CN)_4]^-$	0.326(0.007)	20.143	0.197(0.006)	5.651
Au_2O_3	0.094(0.001)	5.808	0.168(0.004)	4.819
$Na_3Au(S_2O_3)_2$	0.072(0.029)	4.448_8	0.708(0.004)	-20.310

*Result of only one run.

The assumed sign changes for q_{zz} are given parenthetically.

Table II. Bonding results for gold compounds (in units of 10^{15} esu/cm^3).

Compound	q_{zz}	$q_{610} = -25$		$q_{610} = -35$		$q_{610} = -40$		$q_{610} = -44$		$q_{610} = -50$	
		α^2	X	α^2	X	α^2	X	α^2	X	α^2	X
Gold(I)											
AuCl	-13.339	0.27	-0.07	0.19	0.24	0.17	0.33	0.15	0.41	0.13	0.47
AuBr	-12.134	0.24	0.03	0.17	0.31	0.15	0.39	0.135	0.46	0.12	0.51
AuI	-11.417	0.23	0.09	0.16	0.35	0.14	0.43	0.126	0.49	0.11	0.54
$[Au(S_2O_3)_2]^{-3}$	-20.310	0.41	-0.62	0.29	-0.16	0.25	-0.02	0.23	0.10	0.20	0.19
AuCN	-23.207	0.46	-0.86	0.33	-0.32	0.29	-0.16	0.26	-0.03	0.23	0.07
$KAu(CN)_2$	-29.288	0.59	-1.34	0.42	-0.67	0.37	-0.46	0.33	-0.30	0.29	-0.17
Gold (III)											
AuF_3	(-)7.860	0.44	-0.54	0.37	0.04	0.34	0.26	0.32	0.41	0.29	+0.61
$[AuF_4]^-$	(-)5.221	0.47	-0.74	0.39	0.14	0.36	0.10	0.34	0.26	0.32	0.48
$KAuCl_4$	3.643	0.55	-1.42	0.46	-0.70	0.43	-0.43	0.40	-0.24	0.37	0.01
$AuCl_3$	2.151	0.54	-1.31	0.45	-0.61	0.42	-0.34	0.39	-0.15	0.36	0.09
$KAuBr_4$	3.242	0.55	-1.39	0.46	-0.88	0.43	-0.41	0.40	-0.21	0.37	0.04
$AuBr_3$ (?)	3.643	0.55	-1.42	0.46	-0.70	0.43	-0.43	0.40	-0.24	0.37	0.01
$KAu(CN)_4$	20.052	0.71	-2.69	0.60	-1.77	0.55	-1.41	0.52	-1.16	0.48	-0.84
$KAu(CN)_2Cl_2$	~12.69	0.64	-2.12	0.54	-1.29	0.50	-0.97	0.47	-0.75	0.43	-0.46
$KAu(CN)_2Br_2$	~13.53	0.65	-2.19	0.54	-1.35	0.50	-1.02	0.47	-0.80	0.44	-0.50
$KAu(CN)_2I_2$	~13.85	0.65	-2.21	0.55	-1.37	0.51	-1.04	0.48	-0.81	0.44	-0.52
$[AuS_4C_4(CN)_4]^-$	5.651	0.57	-1.58	0.48	-0.84	0.44	-0.55	0.42	-0.35	0.39	-0.09
Au_2O_3	4.819	0.56	-1.52	0.47	-0.78	0.44	-0.50	0.41	-0.30	0.38	-0.05

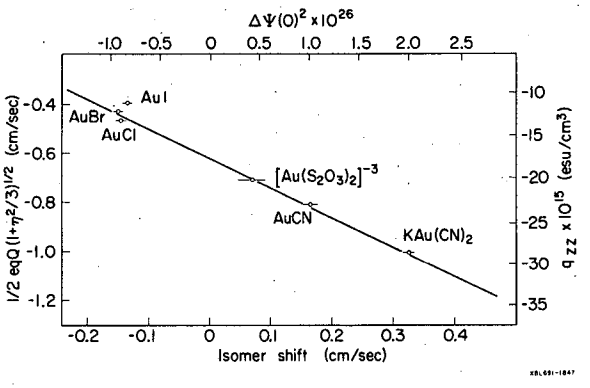

Fig. 1. The linear relationship of isomer shift and 1/2(eqQ) for gold(I) compounds.

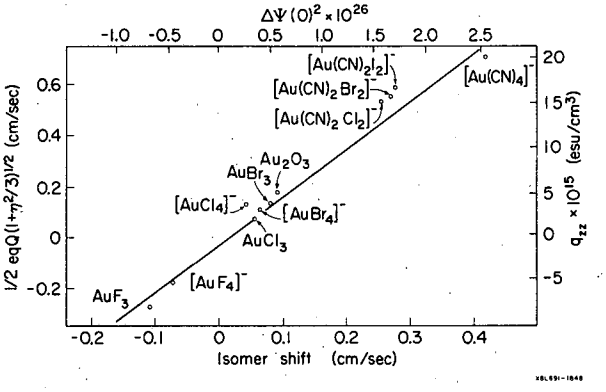

Fig. 2. The linear relationship of isomer shift and 1/2(eqQ) for gold (III) compounds.

THEORY OF THE INFLUENCE OF THE ENVIRONMENT ON THE ANGULAR DISTRIBUTION OF NUCLEAR RADIATION†

Helmut Gabriel*

Fano's expansion of operators into an orthonormal set of multipole operators[1] is also a powerful tool for treating relaxation phenomena in perturbed angular correlations (PAC) or in experiments with oriented nuclei. We choose the PAC case to outline our approach, which is a combination of the Liouville representation of quantum mechanics, Zwanzig's projection operator technique[2] (used for elimination of the unobserved variables of the environment), and Fano's multipole representation. The general expression for the directional correlation function for a perturbed nuclear double cascade can be written in terms of the density matrices $\rho(\underline{k}_1, 0)$, describing the nucleus immediately after the emission of the first radiation in the direction $\underline{k}_1$ ($\underline{k}_2$) at time t = 0(t), and $\rho(\underline{k}_2)$ for the second radiation, and an evolution superoperator $\hat{\Omega}(t)$ describing the entire interaction of the nucleus in the intermediate state with the surroundings. The correlation function is written as

$$W(\underline{k}_1, \underline{k}_2; t) = \mathrm{Tr}\{\rho(\underline{k}_2)\,\hat{\Omega}(t)\,\rho(\underline{k}_1, 0)\} = [\rho(\underline{k}_2|\hat{\Omega}(t)|\rho(\underline{k}_1, 0)]\,. \qquad (1)$$

In the right-hand side of (1) we have interpreted the density operators as supervectors in Liouville space. The definition of the scalar product $(A \mid B) = \mathrm{Tr}(A^+B)$ of two supervectors $|A)$ and $|B)$ has been used. We immediately obtain the common expression for the correlation if we express the supervectors of (1) in terms of an appropriate orthonormal basis $\{|U_q^{(k)})\}$, which in our case is constructed from the normalized spherical tensor operators $U_q^{(k)}$.[1] The dimension $(2I+1)^2$ of the Liouville space spanned by the supervectors $|U_q^{(k)})$ depends on the nuclear spin I of the intermediate state. The decomposition of the Liouville unit operator $\hat{1}$--i.e., the closure relation--reads $\sum_{kq} |U_q^{(k)})(U_q^{(k)}| = \hat{1}$. The meaning of the scalar products $(U_q^{(k)} \mid \rho(\underline{k}_2)$ and $[\rho(\underline{k}_1, 0)U_{q'}^{(k')}]$ arising from breaking up the matrix element in (1) is clear from the unperturbed case $\hat{\Omega}(t) = \hat{1}$, and comparison with standard angular correlation theory. The matrix elements of $\hat{\Omega}(t)$(which is a particular superoperator, since it transforms a super-vector $|\rho(\underline{k}_1, 0))$ into another at a later time t) are related to the usual perturbation factors. We have set $G_{kk'}^{qq'}(t) \equiv [U_q^{(k)}|\hat{\Omega}(t)|U_{q'}^{(k')}]$. The evolution superoperator $\hat{\Omega}(t)$ obeys the non-Markoffian integro-differential equation

$$\frac{d\hat{\Omega}(t)}{dt} = -i\hat{\mathcal{H}}'\,\hat{\Omega}(t) - \int_0^t \hat{M}(\tau)\,\hat{\Omega}(t-\tau)\,dt \qquad (2)$$

subject to the initial condition $\hat{\Omega}(t=0) = \hat{1}$. In (2) $\hat{\mathcal{H}}'$ is the Liouville operator for the static interactions of the nuclei with external or internal fields and $\hat{M}(t)$ is a relaxation operator describing the dynamic part of the nuclei with the surroundings. It has recently been used in a treatment of Mössbauer relaxation phenomena.[3] It is difficult to solve Eq. (2) in general. Easier to handle is an approximate Markoffian equation of motion, which can be deduced from (2) when the electronic correlation time, τ_c, is small compared with the nuclear lifetime, τ_N. The correlation time, τ_c, characterizes the time behavior of the relaxation operator, which has been defined in terms of a nuclear operator part of the nuclei mutually interacting with their surroundings and of electronic correlation functions containing the properties of the bath. In special situations it is possible to express the perturbation factors in terms of the usual longitudinal and transverse relaxation times T_1 and T_2 known from nuclear relaxation theory. As an illustrative example we mention the high-temperature solution for an axially symmetric system without static quadrupole interaction and a purely magnetic relaxation mechanism. The damping parameters entering the exponentials of the $G_{kk'}^{qq'}(t)$ are then given by

$$\lambda_{kq} = k(k+1)/2T_1 + q^2(1/T_2 - 1/T_1). \tag{3}$$

Applied to a case with $k_{max} = 2$ and a static magnetic field perpendicular to the detector plane with two collinear (perpendicular) counters, it finally gives get

$$W_{\perp}[\pi(\pi/2); t] = \exp(-t/\tau_N)[1 + (A_{22}/4)\exp -3t/T_1] \times \{1 \pm 3 \exp[-4t\,(1/T_2 - 1/T_1)] \cos 2\omega_L t\}. \tag{4}$$

The decoupling geometry yields

$$W_{\parallel}(\pi/2; t) = \exp(-t/\tau_N)[1 - (A_{22}/2)\exp(-3t/T_1)]. \tag{5}$$

Here A_{22} is the correlation factor of the unperturbed correlation and ω_L the Larmor frequency. A combination of measurements like those leading to Eqs. (4) and (5) should under favorable conditions lead to a simultaneous determination of T_1 and T_2 from PAC.

Footnotes and References

†Condensed from UCRL-18496, Sept. 1968.

*On leave from Institut für Theoretische Physik A, Technische Universität, Braunschweig, Germany.

1. U. Fano, Phys. Rev. 90, 577 (1953).
2. R. Zwanzig, Physica 30, 1109 (1964).
3. H. Gabriel, Phys. Status Solidi 23, 195 (1967); H. Gabriel, J. Bosse, and K. Rander, ibid. 27, 301 (1968).

PHOTOELECTRON SPECTROSCOPY

TRANSITION METAL STUDIES USING x-RAY PHOTOELECTRON SPECTROSCOPY†

C. S. Fadley and D. A. Shirley

High-resolution analysis of x-ray-produced photoelectron spectra has generally been used to detect chemical effects on core electron binding energies.[1,2] This technique has now been extended to studies of the valence electrons in solids and gaseous molecules.[3] In particular, we have studied both the core and valence electronic levels in the metals Fe, Co, Ni, Cu, and Pt. From these studies information concerning the valence-band density of states, as well as chemical and magnetic effects on core electrons, has been deduced.

The experimental aspects of x-ray photoelectron spectroscopy (XPS) have been reviewed in detail previously.[1,2] Mg Kα x rays (1253.6 eV) were used to excite electrons into continuum states, and they were magnetically analyzed for kinetic energy in the Berkeley iron-free spectrometer. The total instrumental line width including x-ray width was ≈ 1.0 eV. Since the photoelectrons originate primarily from sites near the surface,[1,2] the samples were cleaned continuously by heating them in a 10^{-2}-torr hydrogen atmosphere. The surface cleanliness was monitored by observing the oxygen 1s photoelectron line as indicated in Fig. 1. At the lower temperatures the iron 3p line is double because oxide formation chemically shifts the core levels in atoms near the surface. At higher temperatures the intensity of the oxygen "line" (oxide + H_2O + O_2 + CO_2) decreases and the iron 3p line narrows to a width characteristic of iron metal. Structure is resolvable even in the oxygen 1s line, the right peak probably being due to the more weakly bound adsorbed gases.

An XPS spectrum for Cu taken near the Fermi level (highest occupied level) is shown in Fig. 2. The uncorrected result is directly from the experimental data. The tail on the left side is due to inelastic electron scattering, and the peak on the right side is due to the Mg $K\alpha_{3,4}$ satellite x-ray lines. The corrected spectrum has been obtained by operating on the uncorrected data with an inverted response function $R^{-1}(E)$, where $R(E)$ was obtained empirically from the experimental distribution for the naturally sharper 3p core levels in the same sample. Any point in a corrected spectrum should thus be proportional to the number of occupied electronic states at the corresponding binding energy multiplied by an average photoelectric cross section characteristic of that energy. Previous photoelectron studies using ultraviolet radiation for excitation indicate that the cross section can be assumed constant.[4] Thus a corrected spectrum gives a good approximation to the valence band density of states $[N(E)]$ of the solid, appropriately broadened by our experimental line width. The intense peak in Fig. 2, for example, represents the 3d band of copper metal.

In Fig. 3 we present corrected Fermi level spectra for the five metals investigated. For Fe, Ni, and Cu we also present theoretical predictions of densities of states.[5-7] The qualitative agreement is good and, in particular for Fe, Co, and Ni, we predict a dominant peak in the density of states near the Fermi level. This result contradicts some early studies made with ultraviolet photoelectron spectroscopy (UPS), where the dominant peak was at 5 eV below the Fermi level for Fe,[8] Co,[9] and Ni.[10] Recent UPS work under better surface conditions indicates basic agreement with our results,[11-13] although UPS-derived densities of states would appear to be less reliable as one goes further below the Fermi level, due to enhanced surface or scattering effects or both. Despite somewhat lower resolution than UPS, XPS thus has given quite reliable information on the density of states of a metal over the entire valence band. The XPS results in Fig. 3 are also in good qualitative agreement with densities of states derived from soft x-ray spectroscopy[14] and ion-neutralization spectroscopy,[15] although both these techniques are in several respects less direct than XPS.

The results of free-atom Hartree-Fock calculations predict that the partially filled d shell of the transition metals will give rise to exchange-induced splittings of core levels.[16] This splitting gives rise to a doublet with 10 eV separation for the 3p level of atomic iron,[17] although simple

considerations indicate that this should be reduced by a factor of approximately 1/2 for metallic iron. Figure 2 indicates no splitting greater than 1 eV for metallic iron, and similar results were found for Co. Electron-electron correlation and detailed solid-state effects may be responsible for this decrease relative to the free-atom predictions but no simple explanation is adequate. Studies now under way will look for such splittings in gaseous metals, for which the solid-state effects do not exist.

Footnotes and References

†Condensed from Phys. Rev. Letters 21, 980 (1968).

1 K. Siegbahn et al., ESCA, Atomic, Molecular, and Solid State Structure Studies by Means of Electron Spectroscopy (Almqvist and Wiksells AB, Stockholm, 1967).
2. C. S. Fadley, S. B. M. Hagström, M. P. Klein, and D. A. Shirley, J. Chem. Phys. 48, 3779 (1968).
3. K. Hamrin et al., Chem. Phys. Letters 1, 613 (1968).
4. C. N. Berglund and W. E. Spicer, Phys. Rev. 136, A1044 (1964).
5. J. F. Cornwell, D. M. Hum, and K. G. Wong, Phys. Letters 26A, 365 (1968).
6. L. Hodges, H. F. Ehrenreich, and N. D. Lang, Phys. Rev. 153, 574 (1966).
7. J. C. Phillips (Bell Laboratories) and F. M. Mueller (Argonne National Laboratory), private communication.
8. A. J. Blodgett, Jr., and W. E. Spicer, Phys. Rev. 158, 514 (1967).
9. A. Y.-C. Yu and W. E. Spicer, Phys. Rev. 167, 674 (1968).
10. A. J. Blodgett, Jr., and W. E. Spicer, Phys. Rev. 146, 390 (1966).
11. R. C. Vehse and E. T. Arahawn, Bull. Am. Phys. Soc. 13, 936 (1968).
12. D. E. Eastman and W. F. Kroilikowski, Phys. Rev. Letters 21, 623 (1968).
13. D. E. Eastman, paper presented at Fourteenth Annual Conference on Magnetism and Magnetic Materials, New York, New York, 1968.
14. J. R. Cuthill, A. J. McAlister, M. L. Williams, and R. E. Watson, Phys. Rev. 164, 1006 (1967).
15. N. D. Hagstrum and G. E. Becker, Phys. Rev. 159, 572 (1967).
16. R. E. Watson and A. J. Freeman, in Hyperfine Interactions, A. J. Freeman and R. B. Frankel, editors (Academic Press, Inc., New York, 1967), p. 59 ff.
17. P. S. Bagus and B. Liu, Phys. Rev. 148, 79 (1966).

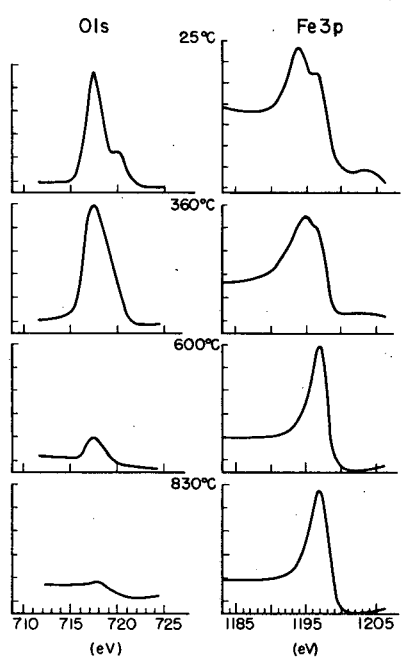

Fig. 1. Effect of hydrogen and increased temperature on the oxygen 1s and iron 3p photoelectron lines. The abscissa is electron kinetic energy. The ordinate scale for all O1s spectra is the same.

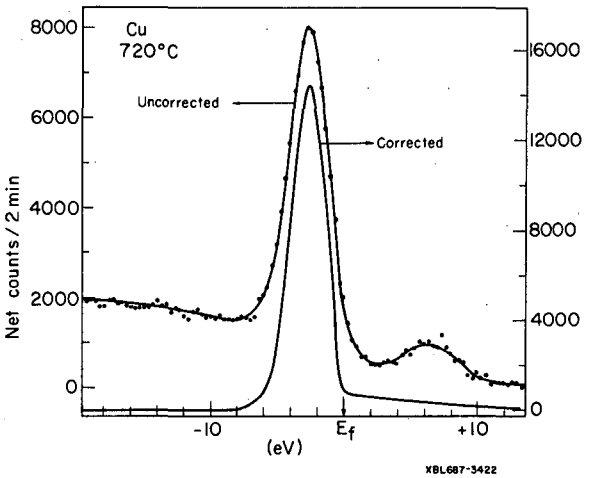

Fig. 2. Correction of a Cu XPS spectrum for the effects of scattering and satellite x-ray lines. A constant background of 4900 counts/2 min was subtracted from both spectra to give the net counts.

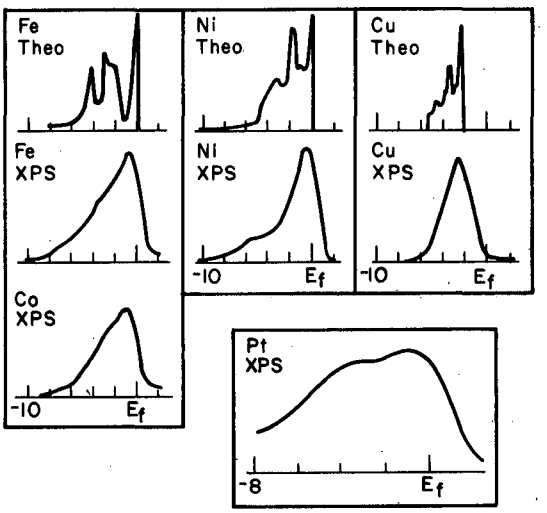

Fig. 3. XPS results for the densities of states of various metals. Comparison is also made to theoretical densities of states for Fe (Ref. 5), Ni (Ref. 6), and Cu (Ref. 7).

SPECTROSCOPY OF INNER ATOMIC LEVELS: ELECTRIC-FIELD SPLITTING OF CORE $p_{3/2}$ LEVELS IN HEAVY ATOMS†

T. Novakov and J. M. Hollander

Until recently, only limited study has been made of the chemical aspects of inner, or core, atomic levels. This has been due in part to a scarcity of experimental tools for probing these levels in detail. The recent development of the photoelectron spectroscopic technique[1,2] makes it possible to investigate the inner levels with high resolution. In this work, Mg K x rays (1254 eV) were used as the excitation source, and a 50-cm iron-free magnetic spectrometer was used to record the photoelectron spectra.

Splittings of the outer (optical) levels induced by external fields and by crystal fields have long been known, but little is known about such splittings of core levels. We describe here some experiments by which splittings of inner $p_{3/2}$ levels of heavy-element atoms have been observed.

The atomic level energy E_b (or electron binding energy) is related by energy conservation to the kinetic energy of an emitted atomic electron by $E_b = E_{exc} - E_{kin} - \phi$, where E_{exc} is the x-ray energy and E_{kin} is the kinetic energy of the emitted electron; ϕ is a small correction for the work function of the spectrometer material.

We have studied the photoelectron spectra from metallic sources of tantalum, platinum, gold, thorium, uranium, and plutonium, as well as from some compounds of thorium and uranium. Figure 1 shows some portions of the spectra produced from targets of U metal, Th metal, and UO_3, irradiated with Mg Kα radiation. In these spectra, photolines from $N_{VI}(4f_{5/2})$, $N_{VII}(4f_{7/2})$, $O_{III}(5p_{3/2})$, $O_{IV}(5d_{3/2})$, and $O_V(5d_{5/2})$ levels are shown. The $O_I(5s_{1/2})$ and $O_{II}(5p_{1/2})$ lines are apparently only very weakly excited and were not clearly observed in our spectra.

It was found that all these lines have a normal shape except the O_{III}, which shows a composite structure. The shape of the O_{III} line varies with the particular compound examined, but in all cases a splitting was seen. The magnitude of the splitting is evidently chemistry-dependent.

For uranium the sources used were the metal, UO_2, UO_3, uranyl nitrate, and uranyl acetate; of these, the largest splitting (10 eV) was found with the uranyl acetate, the smallest (3 eV) with UO_2. With plutonium metal, the separation between the main components appeared to be about 16 eV. The observed level splittings appear to be unique to the $p_{3/2}$ levels, and were not seen in the $p_{1/2}$ levels or in d or f levels.

In contrast to the results with thorium, uranium, and plutonium, the targets of tantalum, platinum, and gold metals produced no evidence for complexity in the O_{III} line or in any other line.

These results, which we interpret as evidence for level splitting, are believed to be distinct from the chemical shift effect that is well known in photoelectron spectroscopy.[1,2] The latter, which arises from small changes in the binding energies of electrons in different chemical environments, affects all core levels by about the same amount.

Although a mechanism to account for these observations has not been established, it is probable that the splitting of the core $p_{3/2}$ levels is caused by an effective electric field gradient in the interior of the atom. The origin of this field gradient may be related to the factors responsible for the field gradient at the nucleus (Sternheimer effects). On the other hand, a more direct effect arising from chemical bonding may be responsible for the field at the 5p shell. If, for example, the symmetries of the 6p or other outer orbitals in the actinides are altered because of their participation in chemical bonding, a gradient might be felt at the 5p levels that is large enough to split the $m = \pm 1/2$ and $m = \pm 3/2$ substates of the $5p_{3/2}$ level by the amount observed.

Similar observations have been made earlier by the authors from studies of internal conversion spectra of radioactive sources.[3-5] In some of those experiments, high external electric fields were employed.

Footnotes and References

†Condensed from Phys. Rev. Letters 21 [16], 1133 (1968).

1. K. Siegbahn, C. Nordling, A. Fahlman, R. Nordberg, K. Hamrin, J. Hedman, G. Johansson, T. Bergmark, S.-E. Karlsson, I. Lindgren, and B. Lindberg, ESCA, Atomic, Molecular, and Solid State Structure Studied by Means of Electron Spectroscopy (Almqvist and Wiksells Publishing Co., Stockholm, 1967).

2. C. S. Fadley, S. B. M. Hagström, J. M. Hollander, M. P. Klein, and D. A. Shirley, Science 157, 3796 (1967); C. S. Fadley, S. B. M. Hagström, M. P. Klein, and D. A. Shirley, J. Chem. Phys. 48, 3779 (1968).

3. T. Novakov, R. Stepić, and P. Janićijević, unpublished results.

4. T. Novakov and J. M. Hollander, Phys. Letters 13, 301 (1964).

5. T. Novakov and P. Janićijević, Z. Physik 205, 359 (1967).

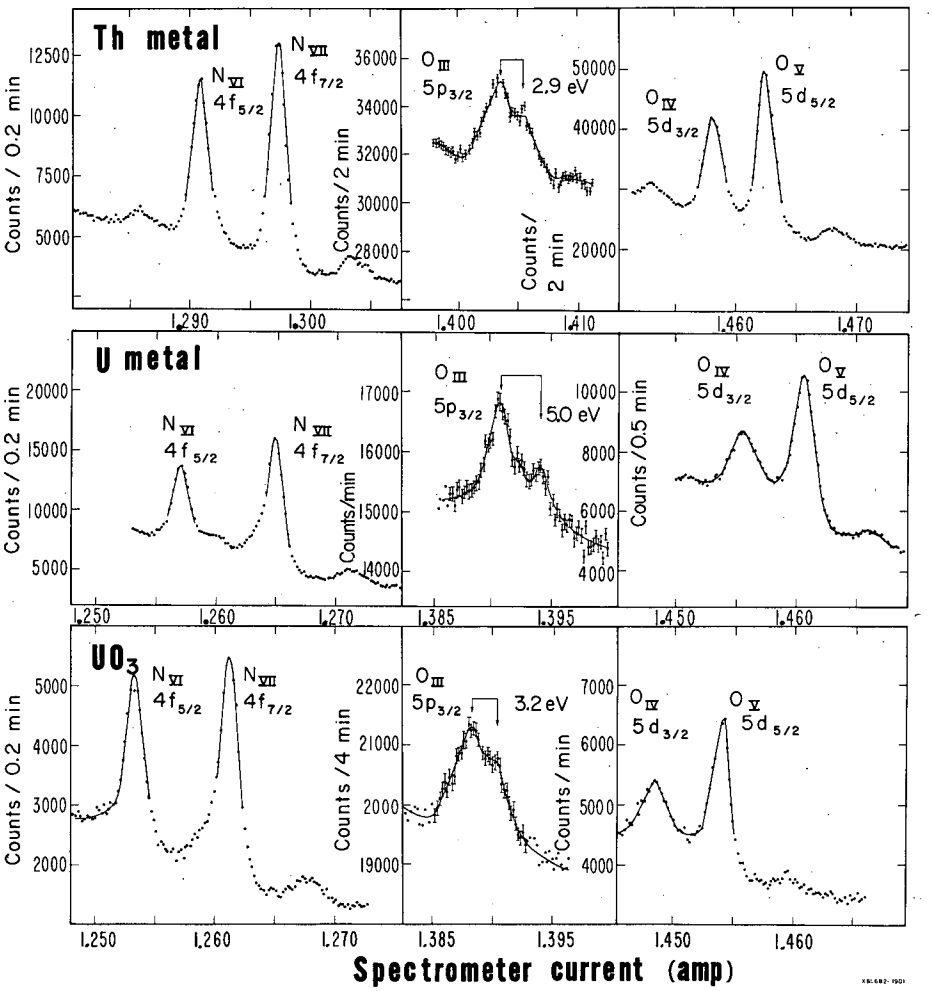

Fig. 1. Portions of the photoelectron spectra from targets of thorium metal, uranium metal, and UO_3 irradiated with Mg Kα radiation. N_{VI}, N_{VII}, O_{III}, O_{IV}, and O_V photo lines are shown. These data were recorded with the Berkeley iron-free spectrometer.

PHOTOELECTRON SPECTROSCOPY OF NITROGEN COMPOUNDS†

D. N. Hendrickson,* J. M. Hollander, and W. L. Jolly*

Recent developments in photoelectron spectroscopy have made possible the measurement of chemical shifts in inner-electron binding energies.[1] Binding energies for 1s electrons have been correlated with formal oxidation state in nitrogen compounds by Nordberg et al.[1,2] We have extended the group of nitrogen compounds for which nitrogen 1s binding energies have been measured, and have shown that these binding energies are linearly related to nitrogen atomic charges calculated from (CNDO) molecular orbital eigenfunctions.[3]

The binding energy (the difference in energy between the Fermi level and the 1s atomic level for the solid) is given by the relation $E_b = E_{h\nu} - E_{kin} - \phi_{sp}$, where $E_{h\nu}$ is the incident photon energy, E_{kin} is the kinetic energy of the photoelectron as it enters the spectrometer chamber, and ϕ_{sp} is the work function of the spectrometer material. We have used magnesium Kα x rays (1254 eV) and a 50-cm iron-free magnetic spectrometer for these measurements. The work

function of the spectrometer was determined to be 4.0 eV by using several of the compounds studied by Siegbahn et al.[1] as calibration standards.

The data for a group of nitrogen compounds for which CNDO charges were calculated are given in Table I, and the correlation is shown in Fig. 1. Two different lines were found in this correlation--one characteristic of anions, and the other characteristic of neutral molecules and possibly cations (although insufficient data are available to show definitely that the cation points fall on the same line as the neutral molecule points). The observance of separate lines for anions and neutral species can be rationalized by the fact that anions in an ionic crystal lattice experience a greater positive lattice potential than neutral molecules in a molecular lattice. It may be that the separate lines are an artifact of the CNDO method for calculating atomic charges.

Nitrogen atomic charges, calculated from extended Hückel molecular orbital[4] (EHMO) eigenfunctions for the series of nitrogen compounds considered in the CNDO correlation plus several sulfur- or phosphorus-containing nitrogen compounds, were also found to correlate with the measured nitrogen 1s binding energies. However, only one line seems to be indicated by this correlation.

Nitrogen 1s binding energies have also been measured for about 20 other nitrogen compounds, including many transition metal complexes. The spectrum of sodium oxyhyponitrite, $Na_2N_2O_3$, showed two peaks. Consideration of the two measured nitrogen 1s binding energies, plus CNDO and EHMO atomic charge calculations for various geometries of the oxyhyponitrite ion, indicates that the structure of the anion is

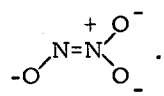

Footnotes and References

†Condensed from J. Chem. Phys. 49, 3315 (1968).

*Inorganic Materials Research Division.

1. K. Siegbahn et al., ESCA, Atomic, Molecular, and Solid State Structure Studied by Means of Electron Spectroscopy (Almqvist and Wiksells AB, Stockholm, 1967).

2. R. Nordberg et al., Nature 214, 481 (1967); R. Nordberg et al., Arkiv Kemi 28, 257 (1968).

3. J. A. Pople, D. P. Santry, and G. A. Segal, J. Chem. Phys. 43, 5130 (1965).

4. R. Hoffmann, J. Chem. Phys. 39, 1397 (1963).

Table I. Nitrogen 1s binding energies and calculated CNDO charges.

Compound number	Compound	Binding energy (eV)	Calculated nitrogen atom charge
1	$NaNO_3$	407.4	+0.429
2	$NaNO_2$	404.1	+0.100
3	$Na_2[ONNO_2]$	403.9	+0.140
3	$Na_2[ONNO_2]$	400.9	-0.195
4	$Na[NNN]$	403.7	+0.096
4	$Na[NNN]$	399.3	-0.548
5	$Na_2N_2O_2$	401.3	-0.256
6	KCN	399.0	-0.518
7	KOCN	398.3	-0.550
8	p-$HOC_6H_4NO_2$	405.3[a]	+0.353
9	$C_6H_5NO_2$	405.1[a]	+0.347
10	n-$C_5H_{11}ONO$	403.7[a]	+0.288[b]
11	$N_2H_6SO_4$	402.5	+0.094
12	$(CH_3)_3NO$	402.2[a]	+0.079
13	NH_4NO_3	402.3	+0.039
14	$(CH_3)_4NB_3H_8$	402.2	+0.185
15	NH_3OHCl	402.1	+0.219
16	$(CONH_2)_2$	400.0	-0.133
17	$(NH_2)_2CNCN$	399.2 (broad)	-0.17 to -0.31[c]
18	C_6H_5CN	398.4[a]	-0.226
19	C_5H_5N	398.0[a]	-0.166

[a]Data of Siegbahn et al. [1]
[b]Charge calculated for CH_3ONO, the structure of which is known.
[c]The four structurally different nitrogen atoms of this molecule bear different calculated charges.

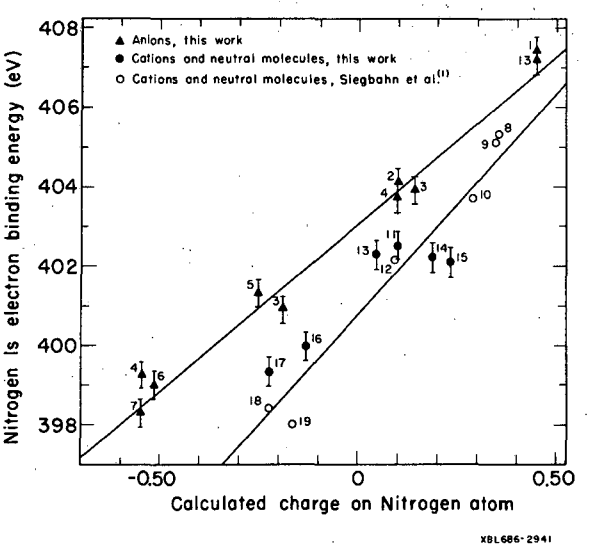

Fig. 1. Plot of nitrogen 1s binding energies vs CNDO-calculated charges on nitrogen atoms.

PHOTOELECTRON SPECTROSCOPY OF PHOSPHORUS COMPOUNDS

D. N. Hendrickson, J. M. Hollander, W. L. Jolly,† and M. L. Pelavin

Phosphorus 2p (and some 2s) binding energies have been measured for about 50 phosphorus compounds by the photoelectron spectroscopic method (see preceding report). EHMO-calculated phosphorus charges have been found to correlate poorly with the phosphorus 2p binding energies for 25 compounds. Phosphorus atomic charges calculated by Pauling's method[1] with charge-independent atom electronegativities gave a similar correlation. A marked improvement in the later correlation was obtained by using the self-consistent Pauling method in which the atom

electronegativities are charge-dependent. A similar improvement would be expected in the EHMO case if the calculation were made self-consistent with charge-dependent valence orbital ionization potentials.[2]

Footnotes and References

[†]Inorganic Materials Research Division.

1. L. Pauling, The Nature of the Chemical Bond, 3rd ed. (Cornell University Press, Ithaca, N. Y., 1960), p 97.

2. H. Basch, A. Viste, and H. B. Gray, Theoret. Chim. Acta (Berlin) 3, 458 (1965).

III. Physical, Inorganic, and Analytical Chemistry

X-RAY CRYSTALLOGRAPHY

CRYSTAL STRUCTURES AND LATTICE PARAMETERS OF EINSTEINIUM TRICHLORIDE AND EINSTEINIUM OXYCHLORIDE†

D. K. Fujita, B. B. Cunningham, and T. C. Parsons

The first preparations and structure determinations of compounds of ^{253}Es are discussed in this report. Although the radioactive decay of ^{253}Es is accompanied by the release of enormous amounts of energy (3500 kilocalories per mole per minute), satisfactory x-ray diffraction patterns were obtained under conditions favoring rapid annealing of lattice damage and resynthesis of the compounds.

About 3 μg of ^{253}Es, purified by ion exchange, were used in these studies. Because of rapid self-contamination of ^{253}Es by its decay product ^{249}Bk (3.3% per day), repurification was necessary at frequent intervals.

Approximately 0.25 to 0.50 μg of the purified material was absorbed in a single 0.18-mm cube of highly purified porous charcoal. Conversion of the charcoal to CO_2 by heating at 600°C in oxygen for 10 min left a solid residue of white einsteinium oxide.

Einsteinium trichloride was obtained by heating the oxide in anhydrous HCl gas at 500°C for 20 min. Einsteinium oxychloride was prepared by heating the oxide at 500°C for 20 min in a mixture of HCl(g) and H_2O(g). Several samples of both EsOCl and $EsCl_3$ were prepared having ^{249}Bk contents ranging from 4% to 21%.

The diffraction equipment used has been described previously.[1] Modifications included a 57.3-mm-diameter Phillips-Norelco Precision Powder Camera containing a platinum–10% rhodium heating coil and a 0.3-mil nickel radiation shield for heating the sample, as shown in Fig. 1. Sample temperature was established to within ± 10°C by correlating heater coil current with the melting points of standard substances inclosed in x-ray capillaries.

Diffraction lines were obtained only when the einsteinium samples were heated to 400 to 430°C. At an ambient temperature of ≈450°C no diffraction lines for $EsCl_3$ were observed; at this higher temperature $EsCl_3$ was believed to be in the molten state.

Einsteinium oxychloride exhibits the PbFCl-type tetragonal structure at ≈430°C, with $a = 3.97 \pm 0.01$ Å and $c = 6.75 \pm 0.02$ Å.

At 425°C $EsCl_3$ was found to exhibit the UCl_3-type hexagonal structure, with $a = 7.47 \pm 0.01$ Å and $c = 4.10 \pm 0.02$ Å. These high-temperature lattice parameters were corrected to 20°C by using the thermal expansion data available for $PuCl_3$ and $AmCl_3$.[2] The room-temperature values were then corrected for the known ^{249}Bk content of the $EsCl_3$ samples in accordance with Vegard's Law.[3] The averages of these corrected lattice parameters are $a = 7.40 \pm 0.02$ Å and $c = 4.07 \pm 0.02$ Å, where the error limits represent the 95% confidence intervals for variations in lattice parameters between different preparations.

A reasonable agreement of the $EsCl_3$ results with trends in the a and c parameters for other actinide trichlorides can be seen in Fig. 2.

It is possible that some of the techniques described in this report will be useful in future determinations of the physical and chemical properties of actinide elements beyond einsteinium.

Footnotes and References

†Condensed from UCRL-18612, Nov. 1968; submitted to Inorg. Nucl. Chem. Letters.

1. J. C. Copeland, Preparation and Crystallographic Analysis of Californium Sesquioxide

and Californium Oxychloride (M. S. Thesis), UCRL-17718, Aug. 1967.
2. J. Fuger, J. Inorg. Nucl. Chem. 28, 3066 (1966).
3. A. F. Wells, Structural Inorganic Chemistry, Chapter XXVII (Oxford University Press, London, 1962), p 971-1028.

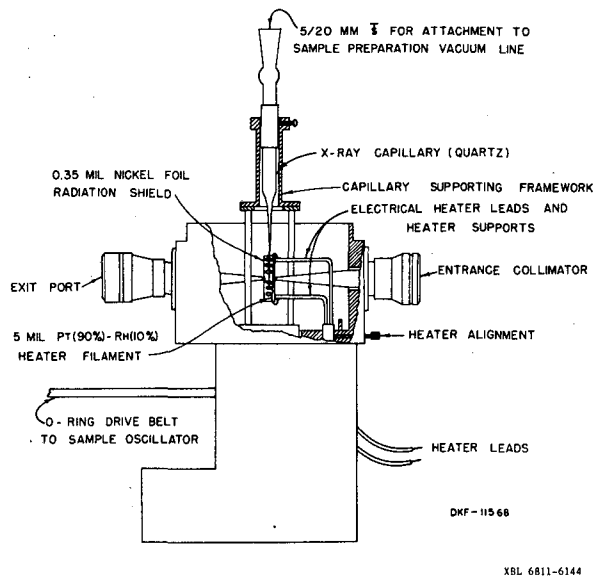

Fig. 1. Modified x-ray camera.

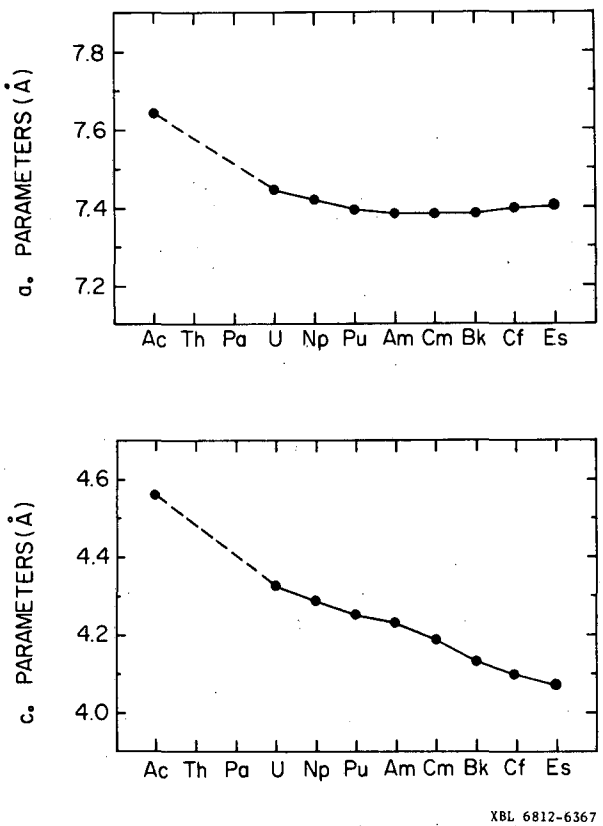

Fig. 2. Lattice parameters of the UCl_3-type hexagonal actinide trichlorides.

CRYSTAL STRUCTURE OF $[Xe_2F_3]^+[AsF_6]^-$

Neil Bartlett,* F. O. Sladky,* B. G. De Boer,† and Allan Zalkin

Xenon difluoride interacts with arsenic pentafluoride to form the 2:1 XeF_2-AsF_5 adduct. The compound is a pale yellow-green solid, mp 99–100°. A single-crystal x-ray structure determination has revealed a molecular geometry consistent with an ionic formulation $[Xe_2F_3]^+[AsF_6]^-$.

Suitable small crystals were obtained by sublimation under nitrogen (at ≈ 1 atm) in sealed quartz x-ray capillaries, using the focused beam of a microscope lamp to heat the source material. A tablet measuring < 0.1 mm in any dimension was used for the intensity data. Crystals of F_9AsXe_2 are monoclinic, with unit cell dimensions a = 15.443, b = 8.678, c = 20.888 Å, β = 90.13 deg, V = 2799 Å^3. The space group is I2/a, and there are 12 formula units in the unit cell. Three-dimensional data were manually collected by using Mo-Kα radiation, a quarter-circle goniostat, and a scintillation counter; 1182 nonzero independent reflections were obtained. Two xenon and one arsenic atoms were located with a three-dimensional Patterson map, and the remaining atomic positions from subsequent electron density maps. Full matrix least-squares refinement led to a final conventional R value of 0.066.

The geometric arrangement is best represented by $Xe_2F_3^+$ and AsF_6^- ions. There are two crystallographically nonequivalent representatives of each ion in the structure, but the structure analysis has not revealed any significant differences between the two representatives. The molecular arrangement is represented in Fig. 1. The AsF_6^- species are approximately octahedral, the 6 As-F distances being in the range 1.62 ± 0.04 to 1.70 ± 0.04 Å and the cis F-As-F bond angles in the range 84 ± 2 deg to 97 ± 2 deg. The average of nine As-F distances is 1.67 Å, and is identical to the value obtained by Bartlett and Beaton[1] for As-F in the salt $IF_6^+AsF_6^-$.

The cation is of particular interest since it contains a bridging fluorine atom. The V-shaped $[F\text{-}Xe\text{-}F\text{-}Xe\text{-}F]^+$ cation is planar to within the accuracy of the structure determination, and symmetrical about the bridging fluorine atom. The cation can be represented as two linear XeF_2 molecules[2] sharing a common fluorine atom, as is shown in Fig. 2. The cation is pseudo-isoelectronic with the symmetrical, planar V-shaped I_5^- ion, in which the terminal I-I distances are significantly shorter, 2.81 versus 3.17 Å. The V angle in I_5^-, however, is 95 deg versus 150 deg in $Xe_2Fe_3^+$.

The atomic parameters for $Xe_2F_3^+AsF_6^-$ are shown in Table I.

Footnotes and References

*Present address: Frick Chemical Laboratory, Princeton University, N. J. 08540.

†Present address: Massachusetts Institute of Technology, Cambridge, Mass. 02139.

1. Neil Bartlett and S. P. Beaton, to be published in Chem. Commun.

2. H. A. Levy and P. A. Agron, in Noble-Gas Compounds, H. H. Hyman, Ed. (University of Chicago Press, Chicago and London, 1963), p 221-225.

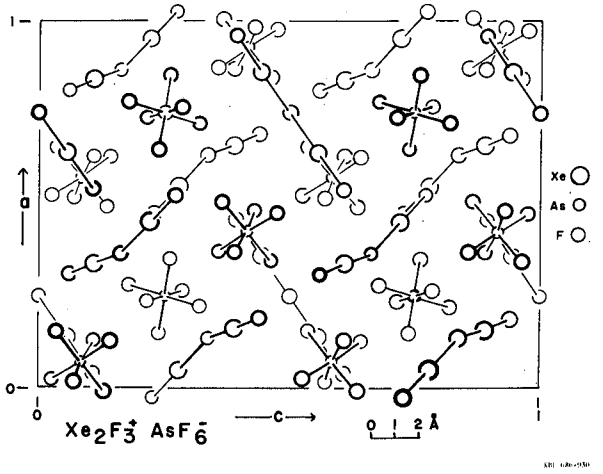

Fig. 1. Molecular packing of $Xe_2F_3^+AsF_6^-$.

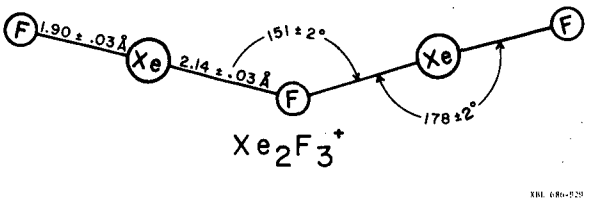

Fig. 2. Dimensions of $Xe_2F_3^+$ ion.

Table I. Atomic parameters in $Xe_2F_3 \cdot AsF_6$.[a, b]

Atom	x	y	z	B(A^2)[c]
Xe(1)	0.1397(2)	0.2975(3)	0.5563(1)	4.1(2)
Xe(2)	-0.0485(2)	0.0458(3)	0.2216(1)	4.0(2)
Xe(3)	0.8394(2)	0.3864	0.1101(1)	4.4(2)
As(1)	0.4271(3)	0.7649(4)	0.4153(2)	3.9(2)
As(2)	0.2500(0)	0.2500(0)	0.2500(0)	3.8(2)
F(1)	0.041(2)	0.249(3)	0.607(1)	6.4(5)
F(2)	0.2500(0)	0.358(4)	0.5000(0)	6.6(7)
F(3)	0.025(2)	-0.078(3)	0.271(1)	5.6(5)
F(4)	0.865(2)	0.185(3)	0.163(2)	7.5(6)
F(5)	0.810(2)	0.563(3)	0.060(2)	8.0(6)
F(6)	0.345(3)	0.702(4)	0.463(2)	11.8(9)
F(7)	0.483(3)	0.602(4)	0.429(2)	12.3(10)
F(8)	0.507(3)	0.821(4)	0.365(2)	11.2(9)
F(9)	0.369(3)	0.919(5)	0.391(2)	12.9(10)
F(10)	0.476(3)	0.849(5)	0.474(2)	13.3(11)
F(11)	0.372(3)	0.673(5)	0.358(2)	13.9(11)
F(12)	0.149(3)	0.213(5)	0.238(2)	13.0(10)
F(13)	0.221(3)	0.325(5)	0.320(2)	14.0(11)
F(14)	0.236(3)	0.418(5)	0.215(2)	16.0(13)

[a] Standard deviations are indicated in parenthesis and apply to the least significant figure.
[b] The I2/a positions are x, y, z and $\frac{1}{2}+x$, -y, z plus the I centering and a center of symmetry.
[c] Isotropic thermal parameters.

CRYSTAL AND MOLECULAR STRUCTURE OF PHOSPHORUS TRIFLUORIDE-TRIS(DIFLUOROBORYL)BORANE, $B_4F_6PF_3$[†]

Barry G. De Boer,[*] Allan Zalkin, and David H. Templeton

Introduction

Timms has recently reported[1] the synthesis of a number of novel boron fluoride compounds by reactions of the high temperature species, boron monofluoride, on cold surfaces. Cocondensation of BF and PF_3 produces $B_4F_6PF_3$, a pyrophoric and water-sensitive substance which readily sublimes (mp 55°, bp 74°) to form well-developed, colorless crystals which are stable at room temperature. The present x-ray diffraction investigation was undertaken to verify the proposed structure

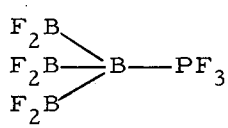

and to determine the bond distances and angles in this molecule.

Samples of the compound, sealed into thin-walled glass capillaries, were provided by Professor Timms. Crystals formed quite readily as the compound was sublimed back and forth in the capillaries under the very mild heating provided by a beam of light from a low-voltage lamp. The crystal obtained had the shape of a cylinder ≈ 0.14 mm long and ≈ 0.15 mm in diameter. A data set of 703 intensities, including 100 recorded as zero, was manually measured by using Cu Kα radiation, a scintillation counter, and a quarter-circle Eulerian cradle. Four formula units of $(BF_2)_3BPF_3$ are contained in the orthorhombic unit cell, space group Pnma, with a = 13.893 ± 0.005 Å, b = 10.578 ± 0.005 Å, and c = 6.075 ± 0.005 Å. The calculated density is 1.82 g/cm^3. No direct measurement of the density was attempted because of the highly reactive nature of the compound. Six atoms are on the mirror plane in the fourfold special position and four atoms are in the general set of positions. The trial structure was determined by the application of the statistical method.[2] A Fourier synthesis using the derived phases gave the ten largest peaks, six of them in the mirror plane, which formed the expected molecule.

The $B_4F_6PF_3$ molecule is shown in Fig. 1. The duplicate atom labels are caused by the crystallographic mirror plane which bisects the molecule and contains F1(P), P, B(1), B(2), F1(2), and F2(2). The atoms F2(P), P, B(1), and B(3) all lie in another plane to within the accuracy of this determination; F1(3) and F2(3) deviate from it by only a small rotation (≈ 3 deg) of the BF_2 group about the B-B bond. This second plane makes an angle of 120 ± 1 deg with the mirror plane so that the molecule has approximately 3m (C_{3v}) point symmetry, only one mirror of which is required by the crystal symmetry. The fluorines on phosphorous atoms are in a staggered configuration with respect to the BF_2 groups on B(1), and the angles at B(1) are tetrahedral to within the experimental accuracy. The up-and-down orientation of the BF_2 groups was unexpected because the F-F distances between different groups would be greater if the BF_2 groups were in a propeller-like configuration. The observation that each fluorine has at least two intermolecular F-F contacts shorter than any intramolecular one (except between two fluorines bonded to the same atom) shows that the fluorine contacts within the molecule are not short enough to control the configuration. The BF_2 orientations are evidently governed by the meshing together of fluorine atoms on adjacent molecules (see Fig. 2). The existence of intermolecular F-F contacts shorter than the intramolecular ones also indicates that the B-P distance is not controlled by F-F interactions. This, and the fact that the B-P distance found here is not significantly different from that found for H_3BPF_3,[1] indicates that BF_2 will not only formally replace hydrogen, but is quite similar to hydrogen in its electronic effects on the rest of the molecule.

Footnotes and References

†Condensed from Inorg. Chem. (to be published, March 1969).
*Present address: Massachusetts Institute of Technology, Cambridge, Mass. 02139.
1. P. L. Timms, J. Am. Chem. Soc. 89, 1629 (1967).
2. J. Karle and I. L. Karle, Acta Cryst. 21, 849 (1966).

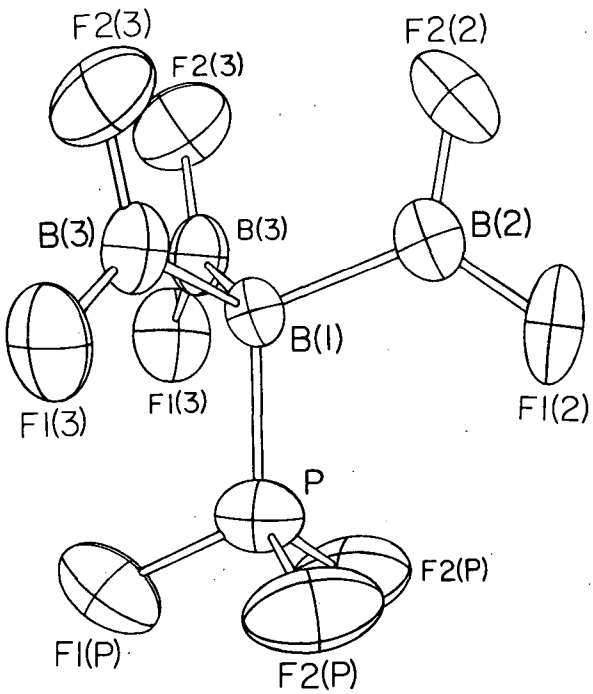

Fig. 1. The $B_4F_6PF_3$ molecule. The molecule is bisected by a crystallographic mirror plane which contains F1(P), P, B(1), B(2), F1(2), and F2(2). The thermal ellipsoids have been reduced to 30% probability contours for the sake of clarity.

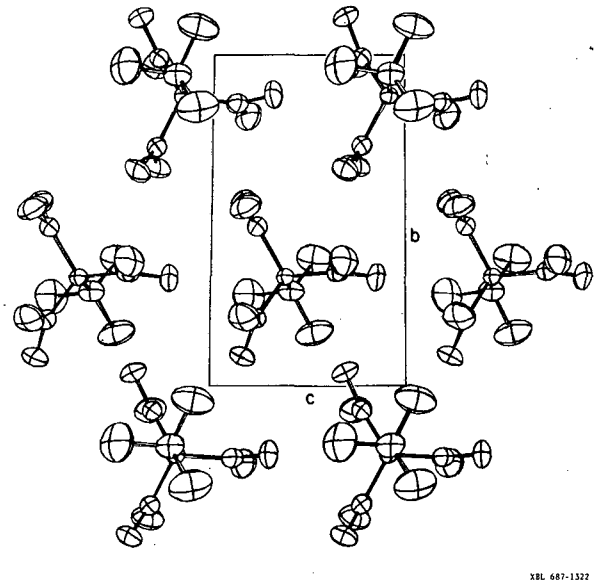

Fig. 2. Molecular packing in $B_4F_6PF_3$. This is one layer, approximately a/2 thick, seen in perspective. The other layers are related to the one shown by the a glide perpendicular to c.

CRYSTAL STRUCTURE OF A BROMINATED CARBORANE–METAL SANDWICH COMPOUND, $N(CH_3)_4[(B_9C_2H_8Br_3)_2Co]$ †

Barry G. De Boer, * Allan Zalkin, and David H. Templeton

Hawthorne and co-workers[1-6] have recently synthesized a number of π-dicarbollyl metal compounds analogous to the π-cyclopentadienyl "sandwich" compounds. They found[6,7] that one of these substances, $Co(B_9C_2H_{11})_2^{-1}$, could be electrophilically brominated by treatment with neat bromine or bromine in glacial acetic acid to give $Co(B_9C_2H_8Br_3)_2^{-1}$. This determination of the crystal structure of the tetramethylammonium salt of the product ion once again establishes the bis-dicarbollyl metal structure as two icosahedra with the metal atom as their common vertex. This work was undertaken in order to ascertain the positions of bromine substitution upon these icosahedra. It was found that the bromines are bonded to three borons in each icosahedron which form a triangular face, one corner of which is adjacent to the cobalt atom. The other two corners of the brominated face are as far as possible from the two carbon atoms, which are adjacent to each other and to the cobalt.

Intensity data were collected from two orange-brown crystals approximately 0.1 mm square and 0.05 mm thick. In all, 3002 independent intensities were scanned, θ to 2θ, with an automatic G.E. diffractometer using Cu Kα x rays, a scintillation counter, and a quarter-circle Eulerian cradle.

The monoclinic unit cell, space group $P2_1/c$, a = 19.893 ± 0.010 Å, b = 19.487 ± 0.010 Å, c = 15.058 ± 0.010 Å, β = 93.15 ± 0.05 deg, contains eight formula units of $N(CH_3)_4[Co(B_9C_2H_8Br_3)_2]$. The calculated density of 1.967 g/cm^3 agrees with the value (1.98 ± 0.01 g/cm^3) found by flotation in a mixture of bromoform and ethylene dichloride.

The bromine positions were obtained from a Fourier, whose phases were determined by the application of statistical-symbolic addition procedures.[8,9] A difference Fourier phased by the bromine atoms showed all 54 of the nonhydrogen light atoms. The bromines were refined with anisotropic thermal parameters, and the carbons and borons isotropic. Hydrogen atoms were not included. The final R value was 0.087.

Figure 1 illustrates the structure of the $Co(B_9C_2H_{11}Br_3)_2^{-1}$ anion. The top and bottom halves of the anion are related by a crystallographic inversion center located at the cobalt. The same atomic arrangement was found for all four crystallographically unrelated anions. The anions are also all the same shape, within the accuracy of this determination. The average B-B, B-C, C-C, B-Br, and Br-Br distances are in agreement with those found[10-15] for similar compounds. The packing of the approximately dumbbell-shaped anions and the tetramethylammoniums is very similar to that of KHF_2,[16] as indicated in Fig. 2. The higher symmetry (tetragonal, I4/mcm) of the KHF_2 structure[16] is broken down to its $P2_1/c$ subgroup (on the doubled cell) by the anion's lack of cylindrical symmetry and the up and down (in z) distribution of the bromine substituents. If we consider only the arrangement of plus and minus charges, this is approximately a CsCl-type structure.

Footnotes and References

†Condensed from Inorg. Chem. 7, 2288 (1968).

*Present address: Massachusetts Institute of Technology, Cambridge, Mass. 02139.

1. M. F. Hawthorne, D. C. Young, and P. A. Wegner, J. Am. Chem. Soc. 87, 1818 (1965).
2. M. F. Hawthorne and T. D. Andrews, ibid. 87, 2496 (1965).
3. M. F. Hawthorne and R. L. Pilling, ibid. 87, 3987 (1965).
4. M. F. Hawthorne and T. D. Andrews, Chem. Commun. 443 (1965).
5. L. F. Warren, Jr., and M. F. Hawthorne, J. Am. Chem. Soc. 89, 407 (1967).
6. M. F. Hawthorne et al., ibid. 90, 879 (1968).
7. M. F. Hawthorne, private communication.
8. J. Karle and I. L. Karle, Acta Cryst. 21, 849 (1966).
9. R. E. Long, (Ph. D. Thesis), University of California, Los Angeles, 1965.
10. A. Zalkin, D. H. Templeton, and T. E. Hopkins, J. Am. Chem. Soc. 87, 3988 (1965).
11. A. Zalkin, D. H. Templeton, and T. E. Hopkins, Inorg. Chem. 5, 1189 (1966).
12. A. Zalkin, D. H. Templeton, and T. E. Hopkins, ibid. 6, 1911 (1967).
13. H. Beall and W. N. Lipscomb, ibid. 6, 874 (1967), and references therein.
14. J. A. Potenza and W. N. Lipscomb, ibid. 5, 1471, 1478, 1483 (1966), and references therein.
15. J. A. Potenza and W. N. Lipscomb, ibid. 3, 1673 (1964).
16. R. W. G. Wyckoff, Crystal Structures, vol. 2 (Interscience Publishers, New York, 1964), p 277 ff.

Fig. 1. $(B_9C_2H_8Br_3)_2Co^-$ (hydrogens omitted).

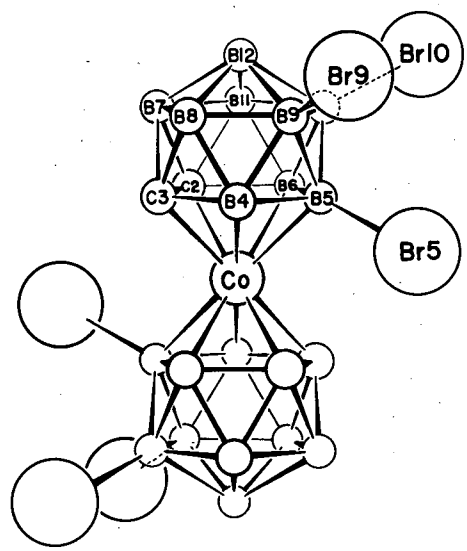

XBL 6711-6069

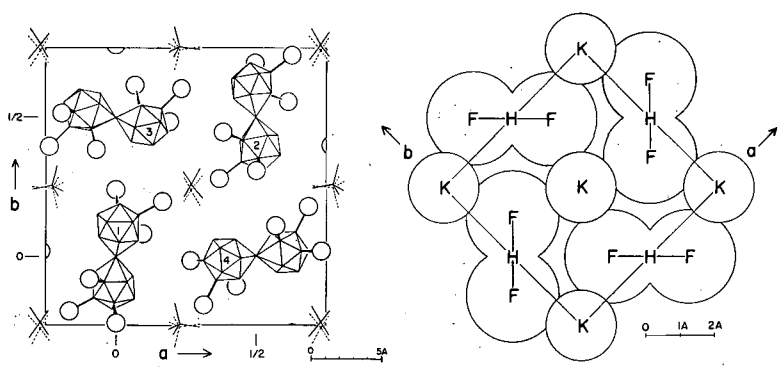

XBL 6711-6068

Fig. 2. The crystal structure of $N(CH_3)_4[(B_9C_2H_8Br_3)_2Co]$ compared with that of KHF_2. In both drawings, the cations are at $z = \pm 1/4$ and the anions at $z = 0$. The anions at $z = 1/2$ (not shown) are related to those shown by the c-glide, which runs horizontally across the center of each drawing.

CRYSTAL STRUCTURE OF $[Ni_2Cl_3(C_7H_6N_2)_8]\cdot Cl\cdot 4(CH_3)_2CO$ †

Michael G. B. Drew, * David H. Templeton, and Allan Zalkin

During studies[1,2] of the nickel(II) complexes with benzimidazole (I),

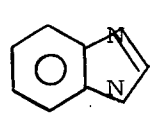

(I)

three compounds--colored blue, green, and olive green--of the general formula Ni(benzimidazole)$_4$Cl$_2$·(acetone)$_2$ were prepared. Those three compounds had differing magnetic properties, with magnetic moments of 3.15, 3.06, and 2.35 B. M. at room temperature and Weiss constants of -8°, -77°, and -400° respectively. The green compound held to Curie-Weiss behavior over the range 200-300°K: in the range 100-200°K deviation from the law is small, but on reaching 100°K, the susceptibility values show a sudden drop and the initially crystalline solid is found to be reduced to an amorphous powder without loss of acetone. In order to form a reference point for consideration of these compounds, the crystal structure of the green complex has been determined by three-dimensional x-ray analysis.

The cell dimensions are a = 12.551(6), b = 16.517(7), c = 17.794(7) Å, β = 106.72(5) deg. The observed density (by flotation) is 1.35 g/cm^3. The calculated density for two formula units is 1.354 g/cm^3. The extinction rules are characteristic of space group $P2_1/c$. The diffraction data were obtained from a crystal of approximate dimensions 0.4 × 0.3 × 0.3 mm. The crystal was sealed inside a glass capillary. Diffraction intensities were measured with a General Electric XRD-5 apparatus equipped with a quarter-circle Eulerian cradle, a scintillation counter, and pulse-height discriminator using Mo Kα radiation. The stationary-crystal, stationary-counter method was used to manually measure 3284 reflections, of which 792 were recorded as zero.

A three-dimensional Patterson function was calculated from which the Ni-Ni vectors were identified. Subsequent three-dimensional Fouriers revealed the positions of 46 of the 48 independent atoms. The positions of the two methyl groups of one of the acetone molecules are disordered and were each handled as two half atoms. These half atoms were refined successfully. The nickel and chlorine atoms were refined anisotropically and light atoms isotropically. The final R value from the 2492 observed data was 0.095.

The unit cell contains two cations with general formula $[Ni_2Cl_3(C_7H_6N_2)_8]^+$, two chloride ions, Cl^-, and eight acetone molecules. The acetone molecules occupy general positions, while the free chloride ion, Cl(3), and the central chlorine atom, Cl(2), are one center of symmetry. In the cation, the angle subtended at the nickel by the terminal and bridging chlorine atoms Cl(1) and Cl(2) is 179.3(1), thus the five "heavy" atoms are nearly collinear; see Fig. 1. The nickel-to-chlorine distances are appreciably different [Ni-Cl(1) is 2.424(4) and Ni-Cl(2) is 2.941(2) Å]. The Ni-Cl(1) distance is similar to that observed in octahedral Ni(II)-Cl bonds. For example, in $NiCl_2$, where each nickel occupies an octahedral site, the Ni-Cl distances are 2.426 Å,[3] while in Ni(pyridine)$_4$Cl$_2$, Ni-Cl distances of 2.387 Å are found.[4] These distances are greater than the value of 2.27 Å found in the tetrahedral $NiCl_4^{--}$ ion.[5]

Figure 2 shows the arrangement of the four independent benzimidazole groups around one nickel atom. The figure is a projection of half the cation down the Cl(2)-Ni vector, with the chlorine atoms Cl(1) and Cl(2) omitted for clarity. The cation comes close to fourfold (4/m) symmetry. The average N(1)-Ni-N(1) angle, for adjacent nitrogen atoms, is 89.6 deg. The four Ni-N(1) bonds are bent towards the bridging rather than the terminal chlorine, the average N(1)-Ni-Cl(1) angle being 94.2 deg. The benzimidazole groups are approximately planar, and they are tilted such that the benzene rings are closer to the terminal chlorine Cl(1) than the bridging chlorine Cl(2). The average bond distance C-C in the six-membered rings is 1.41 Å with a maximum deviation of 0.05 Å. The two internal angles at C(5) and C(8) are shorter than the remaining four angles in the six-membered ring. It is possible for the hydrogens attached to the N(3) atoms in the benzimidazole groups to participate in hydrogen bonding with the chlorine atoms. The configuration of the Cl(3) ion and N(3a), N(3b), as shown in Fig. 1, strongly suggest hydrogen bonding. Each Cl(3) ion, situated on a center of symmetry, is surrounded by four nitrogen atoms in an approximately square planar configuration. The N-Cl distances are 3.13 and 3.10 Å, which are within the range of hydrogen bonding of this type.[6]

The thermal parameters, bond distances, and evidence for disorder found for the acetone molecules show that for both acetone molecules the positions are not well defined. As can be seen from the packing diagram, the acetone molecules fill the gaps between the cations in an approximately symmetrical way.

Footnotes and References

†Condensed from Inorg. Chem. 7, 2618 (1968).

*Department of Chemistry, University of Whiteknights Park, Reading, Berkshire, England.

1. M. J. Weeks (Ph. D. Thesis), University of London (1966).
2. D. M. L. Goodgame, M. Goodgame, and M. J. Weeks, J. Chem. Soc. (A) 1125 (1967).

3. A. Ferrari, A. Braibanti, and G. Bigliardi, Acta Cryst. 16, 847 (1963).
4. M. A. Porai-Koshits, Tr. Inst. Kristallogr. Akad. Nauk. SSSR 10, 117 (1954).
5. P. Pauling, Inorg. Chem. 5, 1498 (1966).
6. G. C. Pimentel and A. L. McClellan, The Hydrogen Bond (W. H. Freeman and Co., 1960), p 290.

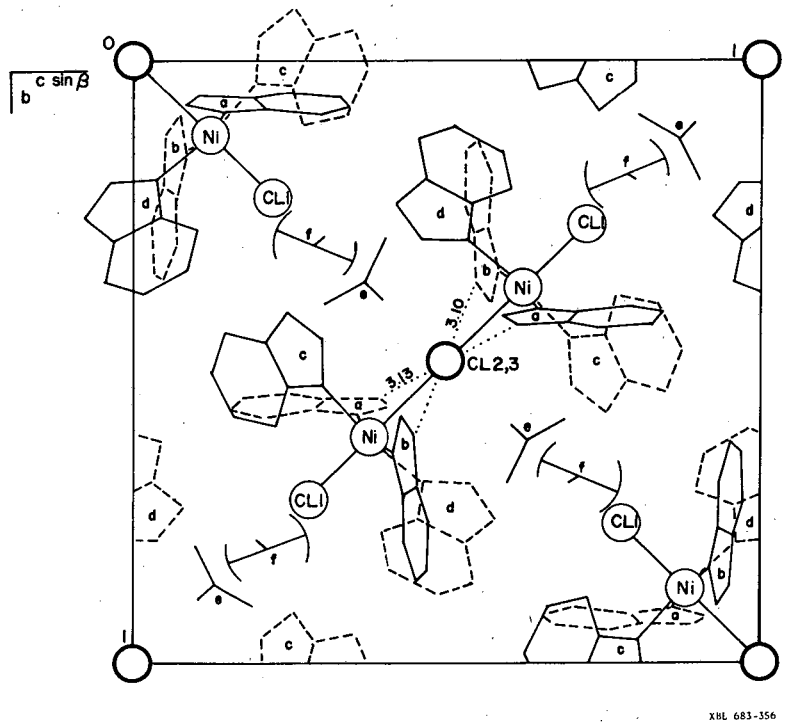

XBL 683-356

Fig. 1. The a projection of the unit cell.

Fig. 2. The environment of a single nickel atom. The terminal and bridging chlorines are above and below the nickel atom in this projection.

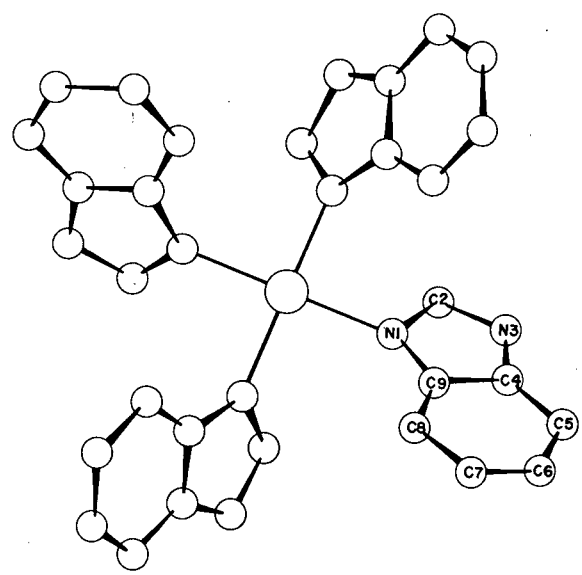

XBL 683-355

CRYSTAL AND MOLECULAR STRUCTURE OF HEXAAQUOALUMINUM HEXACHLORORUTHENATE TETRAHYDRATE†

Ted E. Hopkins,* Allan Zalkin, David H. Templeton, and Martyn G. Adamson‡

The aqueous ruthenium species are being studied in this Laboratory by R. E. Connick and others, and this research has provided a number of interesting ruthenium salts. We have investigated the structures of several of these compounds to help in the correlation of the optical spectra of the solutions with the environment of the ruthenium ion. Structures involving the aquotetrachloro and aquo-pentachloro ruthenium species are reported elsewhere.[1]

The light red plates of $Al(H_2O)_6RuCl_6 \cdot 4H_2O$ which crystallized out of a concentrated HCl solution were washed with a minimum volume of ice-cold ethanol followed by ether, and then dried by suction. The crystals are stable in air at room temperature. A single crystal in the form of a triangular plate 0.17 mm on an edge and 0.07 mm thick was used for the intensity measurements by the stationary-crystal stationary-counter technique; 1503 independent reflections were measured manually using Mo Kα x rays, a quarter-circle goniometer, and a scintillation counter.

The primitive cell contains two formula units of $Al(H_2O)_6RuCl_6 \cdot 4H_2O$ in the space group $P2_1/n$. It is monoclinic with dimensions $a = 10.492 \pm 0.005$ Å, $b = 11.415 \pm 0.005$ Å, $c = 7.069 \pm 0.005$ Å, and $\beta = 92.69 \pm 0.02$ deg. The calculated density is 2.045 g/cm^3.

The cell contents and space group require Ru and Al to be at centers of symmetry. Trial coordinates for the chlorines and the five water molecules coordinated to aluminum were derived from the Patterson and difference Fourier functions. With all atoms anisotropic, and hydrogens included isotropically but not refined, the structure refined to an R value of 0.049.

Figure 1 shows a clinographic projection of the unit cell. In the figure, the chlorine atoms are labeled "Cl1, 2, 3" and the water molecules are labeled "W1 to W5." The structure consists of nearly regular $Al(H_2O)_6$ and $RuCl_6$ octahedra, tied together with hydrogen bonds to each other or to the interstitial water molecules. Of the ten independent hydrogen atoms, four are in bonds of type O–H···O, three in bonds of type O–H···Cl, and three are not in simple hydrogen bonds. Figure 2 is a view down the a axis, and shows the relative orientation of the two octahedra.

The Ru–Cl distances are slightly larger, by about 0.02 Å, than the distances that were found for the tetra and penta chlorides involving Ru(III).[2] The octahedron of water molecules around the aluminum is less symmetrical than the octahedron found by Okaya et al. in monomethylammonium aluminum sulfate alum.[3] In that compound, the aluminum is at a site of point symmetry $\bar{3}$, and there is less than 0.01 Å spread in the O–O distances. They found an average O–O distance of 2.669 Å, compared to our 2.65 Å, and reported an Al–O distance of 1.886 Å compared to 1.87 Å in the compound we have studied.

Footnotes and References

†Condensed from article to be submitted to Inorg. Chem.

*Present address: Stanford University, Palo Alto, California.

‡Rothman Research Fellow, c/o Department of Physics and Inorganic Chemistry, University of Adelaide, Adelaide, South Australia.

1. T. E. Hopkins, A. Zalkin, D. H. Templeton, and M. G. Adamson, J. Inorg. Chem. 5, 1427, 1431 (1966).

2. T. S. Khodashova, Zh. Struckt. Khim. 1, 333 (1960).

3. Y. Okaya, M. S. Ahmed, R. Pepinsky, and V. Vand, Z. Krist. 109, 367 (1957).

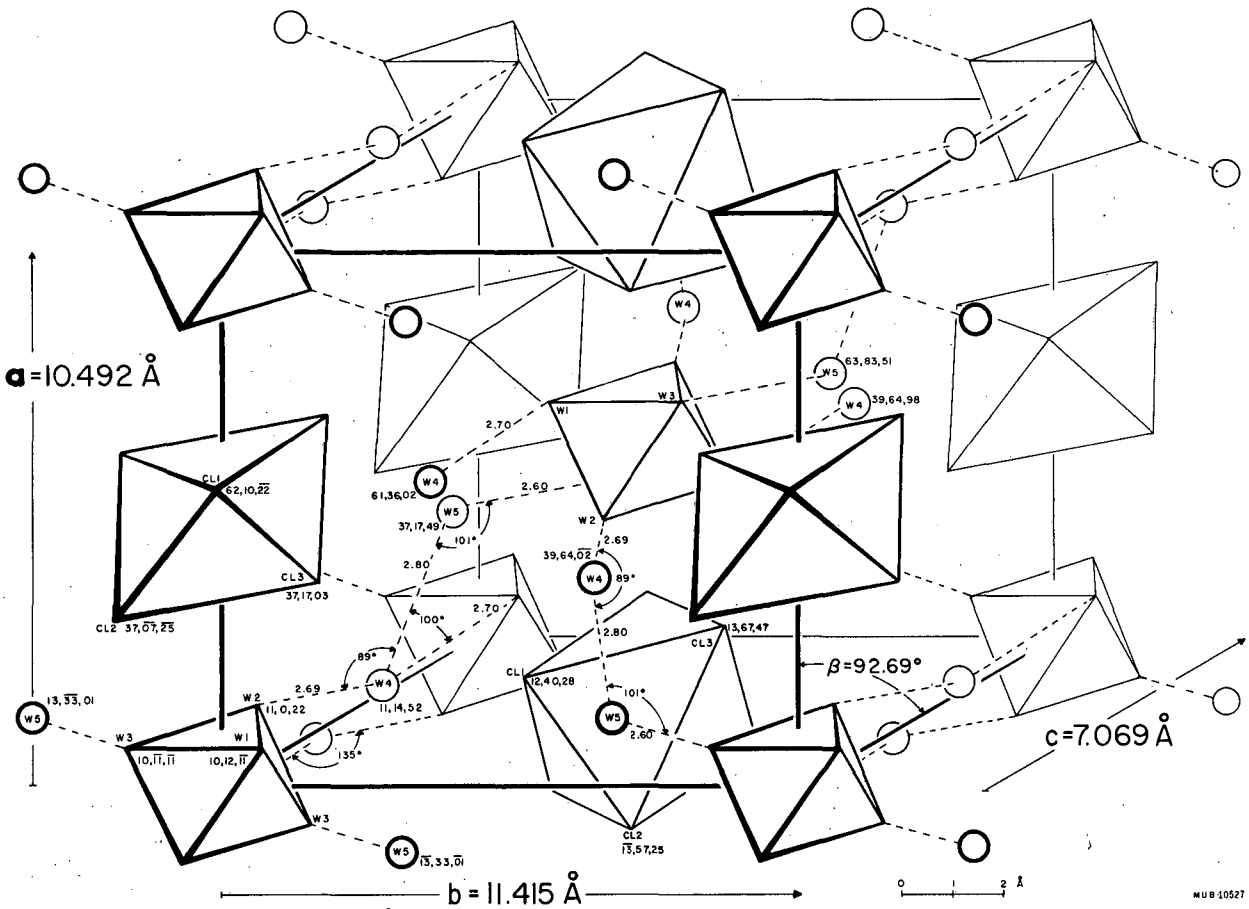

Fig. 1. Unit cell of $Al(H_2O)_6RuCl_6 \cdot 4H_2O$.

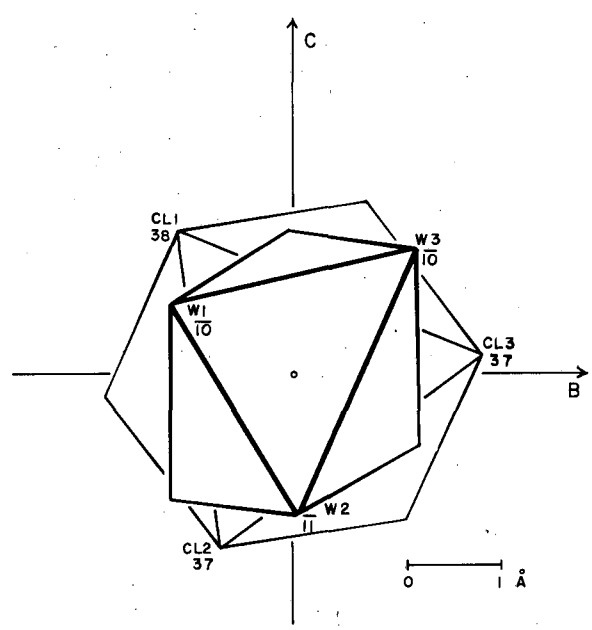

Fig. 2. Projection down the a axis for $Al(H_2O)_6RuCl_6 \cdot 4H_2O$.

CRYSTAL AND MOLECULAR STRUCTURE OF TETRA-n-BUTYLAMMONIUM TRIBROMO(QUINOLINE)NICKELATE(II), $[(n\text{-}C_4H_9)_4N][Ni(C_9H_7N)Br_3]$ †

William DeW. Horrocks, Jr.,* David H. Templeton, and Allan Zalkin

Reliable evidence concerning the existence of nickel(II) complexes with tetrahedral or pseudotetrahedral coordination has been available only within the last decade.[1] These complexes fall into several stoichiometric classes: NiX_4^{2-}, $NiLX_3^-$, NiI_2X_2, and $Ni(L\text{-}L)_2$, where X is a halogen, L a neutral ligand such as an amine, phosphine, or phosphine oxide, and L-L represents a mononegative bidentate chelate such as N-alkylsalicylaldimato with a very bulky N-substituent. Complexes of this type are of interest for several reasons. First, they represent examples of axially distorted ligand fields of approximate C_{3v} symmetry. The present structural determination is a prelude to a series of detailed oriented single-crystal magnetic resonance, bulk magnetic anisotropy, and polarized light studies of molecules in the isomorphous[2] series $[Bu_4N^+][M(quinoline)Br_3^-]$, where M=Fe(II), Co(II), Ni(II), and Zn(II).

Crystals of tetra-n-butylammonium tribromo(quinoline)nickelate(II), $[(n\text{-}C_4H_9)_4N][Ni(C_9H_7N)Br_3]$, were prepared according to the method of Forster[2] by mixing stoichiometric quantities of anhydrous nickel bromide dissolved in a minimum of n-butanol with tetra-n-butylammonium bromide and quinoline dissolved in a minimum quantity of ethanol. A crystal of approximate dimensions $0.23 \times 0.20 \times 0.18$ mm was chosen for intensity measurements. A primitive unit cell was chosen and the cell dimensions were determined by a least-squares treatment of 51 carefully centered reflections. The cell dimensions are $a = 12.282 \pm 0.002$ Å, $b = 10.291 \pm 0.002$ Å, $c = 12.726 \pm 0.002$ Å, $\alpha = 101.02 \pm 0.01$ deg, $\beta = 99.51 \pm 0.01$ deg, $\gamma = 106.55 \pm 0.01$ deg. The density measured by flotation in a carbon tetrachloride-methylcyclohexane mixture is 1.51 ± 0.01 g/cm^3, which compares favorably with the calculated density of 1.512. With two formula units per unit cell space group $P\bar{1}$ was suggested; this choice of $P\bar{1}$ was confirmed by the subsequent refinement of the structure. All atoms occupy general positions and no molecular symmetry conditions are imposed by crystallographic symmetry. The intensity data were recorded on an automated G.E. XRD-5 diffractometer by use of nickel-filtered copper radiation. Of the 5830 independent reflections measured, 5388 were observed as nonzero. Based on the space group $P\bar{1}$, a Patterson synthesis located the three bromines and the nickel. A Fourier synthesis based on these positions disclosed the remaining 27 nonhydrogen atoms. All 31 heavy atoms were then refined anisotropically, yielding R = 0.077. A difference Fourier computed at this point disclosed all 41 hydrogen atoms. These were refined, with the heavy atoms kept fixed, and then the heavy atoms were refined, with the hydrogens held fixed by the full matrix least-squares method. A final R = 0.061 was obtained.

The crystal consists of a lattice of discrete tetra-n-butylammonium cations and tribromo(quinoline)nickelate(II) anions. A stereo pair showing an anion and cation as they are juxtaposed in the unit cell (which is comprised of two such units related by a center of symmetry) is provided in Fig. 1. Each cation is surrounded by four anions. The cation butyl chains are for the most part fully extended (Fig. 1), which produces a structure with heavy interleaving of anion and cation features. A projection of the anion viewed down the crystal a axis is shown in Fig. 2. The nickel is surrounded in a roughly tetrahedral fashion by the three bromines and the quinoline nitrogen. The three Ni–Br distances must be considered identical to within the accuracy of the determination, with an average value of 2.375 Å. As expected for tetrahedral coordination, this distance is less than that predicted (≈ 2.50 Å) on the basis of covalent radii for Ni–Br distances in octahedral nickel complexes.

As expected the quinoline molecule is quite accurately planar, with none of the atoms deviating from the least-squares plane through all ten atoms by more than 0.011 Å. An interesting facet of the coordination is that the nickel atom lies 0.158 Å from the quinoline plane so that the Ni–N–Q bond makes an angle of 4.5 deg with this plane. This can be seen in Fig. 3. Similar deviations have been found in the coordination of other heterocycles to metals.[3] The bond angles internal to quinoline are normal. Of fourteen of these all but one are within 2 deg of 120 deg; the exception is 123 deg.

The configuration of the tetra-n-butylammonium ion in this structure is illustrated in Fig. 1. Three of the butyl chains adopt the trans conformation but the fourth (Bu3) adopts a gauche conformation. A similar configuration was found[4] for Bu_4N^+ in $[Bu_4N^+]_2[Co(MNT)_2^{2-}]$, where MNT = maleonitrile dithiolate; however, in two other structures[5,6] containing this cation all the

butyl groups adopt the trans configuration. The energy differences involved are not great, and packing considerations for the crystal structure as a whole undoubtedly dictate the conformation adopted in any instance.

Footnotes and References

†Inorg. Chem. 7, 2303 (1968).
*Princeton University.

1. For a discussion see F. A. Cotton and G. Wilkinson, Advanced Inorganic Chemistry, second ed. (Interscience Publishers, Inc., New York, 1966), p. 883 ff.
2. D. Forster, private communication.
3. E. B. Fleischer, C. K. Miller, and L. E. Webb, J. Chem. Soc. 86, 2342 (1964), and references therein.
4. J. D. Forrester, A. Zalkin, and D. H. Templeton, Inorg. Chem. 3, 1500 (1964).
5. J. D. Forrester, A. Zalkin, and D. H. Templeton, Inorg. Chem. 3, 1507 (1964).
6. B. Granoff (Ph. D. Thesis), Princeton University, 1966.

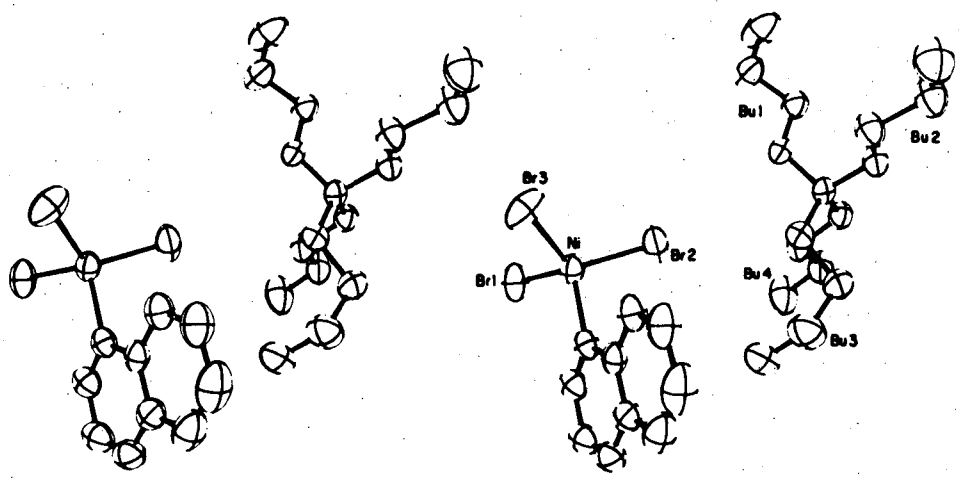

XBL 691-155

Fig. 1. Stereoscopic pair showing anion and cation as they are juxtaposed in the unit cell.

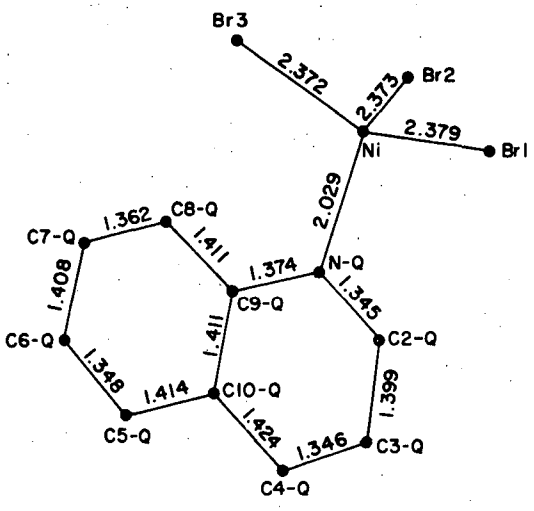

XBL 691-156

Fig. 2. Anion geometry viewed down crystal a axis showing bond distances.

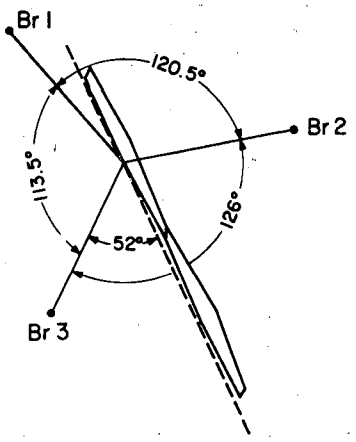

XBL 691-157

Fig. 3. Projection of the anion on the plane normal to the Ni–N bond. The angles quoted refer to the projection and not the actual bond angles.

CRYSTAL AND MOLECULAR STRUCTURE OF TETRAPHENYLARSONIUM TRIIODO(TRIPHENYLPHOSPHINE)NICKELATE(II), $[(C_6H_5)_4As][Ni(C_6H_5)_3PI_3]$ †

Ronald P. Taylor,* David H. Templeton, Allan Zalkin, and William DeW. Horrocks, Jr.*

Not long ago it was discovered[1, 2] that large proton chemical shifts occur for diamagnetic cations in the presence of certain paramagnetic anions as a result of a dipolar nucleus–unpaired electron interaction between ions in an ion pair. The phenomenon was first observed[1] in chloroform solutions of the tetra-n-butylammonium salts of the pseudotetrahedral anions $M(C_6H_5)_3PI_3^-$, M = Co, Ni. Such dipolar shifts (resonance frequency displacements from their diamagnetic positions) generally occur when one of the ions in the ion pair exhibits significant magnetic anisotropy and there is a preferred relative orientation of the partners. In principle at least, it should be possible to obtain information about the geometry of ion pairing in solution from the observed dipolar shifts. The first such attempt was by LaMar, who estimated[2] a 3.8-Å (Co–N) separation between the counter ions of $[(n\text{-}C_4H_9)_4N][Co(C_6H_5)_3PI_3]$ in chloroform solution. The model used involved no preferred rotational orientation of the cation as it approached the anion along the latter's C_3 axis on the side opposite the bulky triphenylphosphine ligand. The use of the above "spherical" model for the tetra-n-butylammonium ion has been criticized.[3] A model based on rigidly extended butyl chains gives a more reasonable estimate[3] of this interionic distance (6 Å). In a recent attempt[4] to remedy the uncertainties arising from the nonrigidity of the butyl chains, a proton magnetic resonance (pmr) study of the tetraphenylarsonium salt of $Co(C_6H_5)_3PI_3^-$ was undertaken. Again a model based on approach by the cation along the C_3 axis of the anion was employed, and an interionic distance in solution of ≈9.0 Å was obtained from the two independent dipolar shift ratios. Although ion association in solution and solid-state structure are not strictly comparable, it was nevertheless of interest to determine the mode and closeness of counter ion approach of a tetraphenylarsonium salt of a $M(C_6H_5)_3PI_3^-$ ion in the solid state.

Dark red plate-like monoclinic crystals of tetraphenylarsonium triiodo(triphenylphosphine)-nickelate(II), $[(C_6H_5)_4As][Ni(C_6H_5)_3PI_3]$ were prepared as described elsewhere.[4] Systematic absences imply space groups Ic or I2/c. The density measured by flotation in methylene iodide–carbon tetrachloride was 1.73 ± 0.02 g/cm^3, which compares favorably with the calculated density of 1.745. With eight molecules per unit cell the space group I2/c, with an eightfold general position, was chosen, and this choice was confirmed by the subsequent successful refinement of the

structure. A crystal of approximate dimensions $0.18 \times 0.13 \times 0.05$ mm was chosen for intensity measurements. The unit cell dimensions are a = 33.971 ± 0.004 Å, b = 14.992 ± 0.002 Å, c = 16.253 ± 0.004 Å, and β = 92.06 ± 0.05 deg. The intensities of 2548 independent reflections were measured by using zirconium-filtered molybdenum radiation out to 2θ = 35 deg by 10-sec peak counts with a 4-deg takeoff angle; 268 of the reflections were recorded as zero. A three-dimensional Patterson synthesis located the nickel, arsenic, and three iodine atoms. A Fourier phased on the heavy atoms disclosed the phosphorus and all 42 carbon atoms. The six atoms heavier than carbon were allowed anisotropic temperature factors, and the structure was refined to a final R value of 0.082. The hydrogen atoms were not located.

The structures of seven phenyl groups were determined in the course of this work. The average C–C bond distance is 1.408 Å, in good agreement with the accepted value for aromatic C–C bonds. The individual values range from 1.326 to 1.514 Å, but the scatter from the mean value is that expected on the basis of the standard deviations. The phenyl rings are quite accurately planar. The 42 C–C–C bond angles are, with six exceptions, within ± 5 deg of the expected 120-deg angle.

The anion and the atom labeling scheme are illustrated in Fig. 1. The pseudotetrahedral structure expected on the basis of spectral and magnetic studies[5] is substantiated. The bond angles at the nickel atom are all quite near the tetrahedral angle (109.5 deg), with the I–Ni–I angles averaging slightly greater than this angle and the I–Ni–P angles averaging slightly less than this angle. This behavior is presumably due to the fact that I–I steric repulsion is greater than that for I–P. The stereo view of the anion viewed down the Ni–P bond axis (Fig. 2) shows the anion to have nearly C_{3v} symmetry (excluding the phenyl rings). It is seen that the iodine atoms are rotationally staggered with respect to the phenyl groups. Furthermore, the phenyl groups are "pitched" and can be described quantitatively by the angle made by the least-squares plane through the phenyl group with the plane of the nickel, phosphorus, and phenyl carbon atom to which the phosphorus atom is bonded. In terms of this definition the "pitches" are as follows: phenyl(25-30), 52.9 deg; phenyl(31-36), 50.6 deg; phenyl(37-42), 34.5 deg. The Ni–P distance of 2.28 Å is in perfect agreement with that found[6] in another pseudotetrahedral nickel(II) complex, $Ni[(C_6H_5)_3P]_2Cl_2$. The Ni–I distances agree quite well among themselves and average 2.55 Å. As expected for tetrahedral coordination, this distance is less than that predicted (≈2.67 Å) on the basis of covalent radii for a Ni–I distance in an octahedral nickel(II) complex. Provided one takes the tetrahedral covalent radii for the halogens--Cl, 0.99 Å; Br, 1.11 Å; I, 1.28 Å--this Ni–I distance is in excellent agreement with that predicted (2.56 Å) from the Ni–Cl distance (2.27 Å) in $NiCl_4^{2-}$ (Ref. 7) and $Ni[(C_6H_5)_3P]_2Cl_2$ (Ref. 6) when the difference in the Cl and I radii is taken into account. An exactly similar situation occurred for Ni(quinoline)Br_3^-.

The structure of the tetraphenylarsonium ion and the carbon atom labeling scheme are shown in the stereo view provided by Fig. 3. The phenyl groups are disposed in an almost perfect tetrahedral fashion about the arsenic atom. The six C–As–C angles average 109.5 deg, and no deviation from the tetrahedral angle of more than 2.3 deg is observed. The average As–C bond length of 1.91 Å observed here is in excellent agreement with values found in two recent crystal structure determinations involving the tetraphenylarsonium ion: 1.90 Å (Ref. 9), 1.91 Å (Ref. 10). When the phenyl rings are considered, the cation possesses no overall symmetry. The phenyl rings apparently are free to achieve that rotational orientation with respect to their As–C bond axes which produces the most favorable crystal packing energy. This was found to be the case in the two other recently determined structures[9, 10] despite the fact that the tetraphenylarsonium ion exhibited some crystallographically imposed symmetry in some earlier x-ray determinations.[11]

The stereo view provided by Fig. 4 illustrates the juxtaposition of the four nearest-neighbor cations with respect to an anion when viewed down the latter's "C_3" axis on the side away from the triphenylphosphine. It is immediately evident that no cation lies directly along this axis. Cations A and B, which are nearest the viewer, occupy positions about equally displaced on either side of the "C_3" axis. The Ni–As distances of 6.64 and 7.33 Å represent the closest anion-cation approach in the crystal.

The present results indicate that some caution must be exercised when interpreting solution-state pmr results in terms of quantitative interionic distance estimates. The assumption that the sole mode of counter ion approach is along the "C_3" axis of the anion is particularly questionable, but a reevaluation of the solution-state data in terms of alternative modes of approach would not be fruitful in view of the additional unknown parameters involved.

Footnotes and References

†Condensed from Inorg. Chem. 7, 2629 (1968).
*Princeton University.

1. G. N. LaMar, J. Chem. Phys. 41, 2992 (1964).
2. G. N. LaMar, ibid. 43, 235 (1965).
3. D. W. Larsen, Inorg. Chem. 5, 1109 (1966).
4. G. N. LaMar, R. H. Fischer, and W. D. Horrocks, Jr., Inorg. Chem. 6, 1798 (1967).
5. F. A. Cotton, O. D. Faut, and D. M. L. Goodgame, J. Am. Chem. Soc. 83, 344 (1961).
6. G. Garton, D. E. Henn, H. M. Powell, and L. M. Venanzi, J. Chem. Soc. 3625 (1963).
7. P. Pauling, Inorg. Chem. 5, 1948 (1966).
8. W. D. Horrocks, Jr., D. H. Templeton, and A. Zalkin, Inorg. Chem. 7, 2303 (1968).
9. F. A. Cotton and S. J. Lippard, Inorg. Chem. 5, 416 (1966).
10. T. E. Hopkins, A. Zalkin, D. H. Templeton, and M. G. Adamson, ibid. 5, 1427 (1966).
11. R. C. L. Mooney, J. Am. Chem. Soc. 62, 2955 (1940); R. C. L. Mooney-Slater, Acta Cryst. 12, 187 (1959); B. Zaslow and R. E. Rundle, J. Phys. Chem. 61, 490 (1957).

Fig. 1. The triiodo(triphenylphosphine)-nickelate(II) anion.

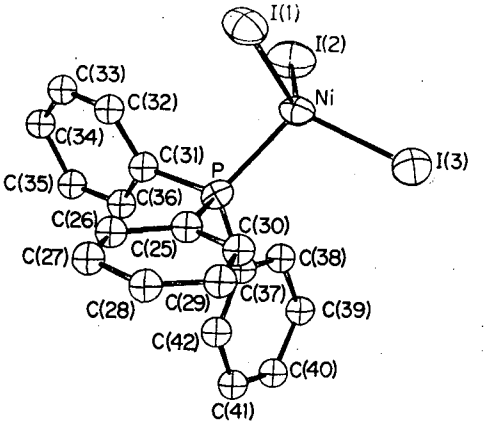

XBL 691-158

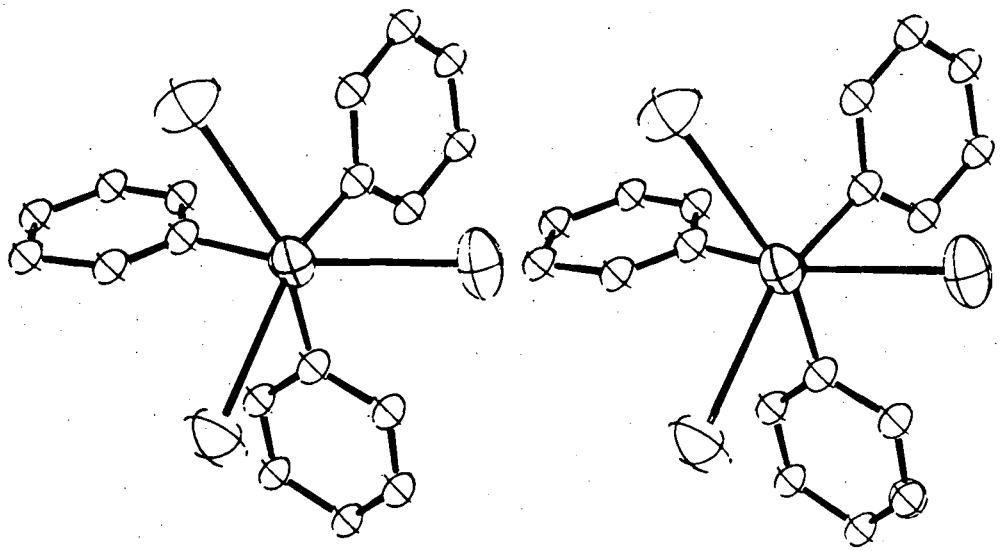

XBL 691-159

Fig. 2. Stereo pair showing the anion viewed down the nickel-phosphorous bond ("C_3" axis).

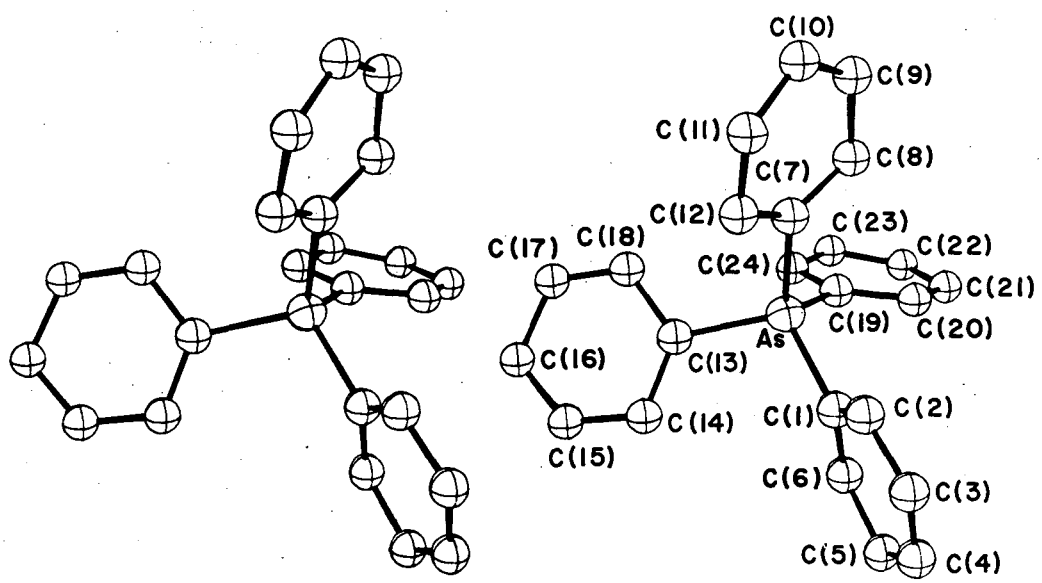

XBL 691-160

Fig. 3. Stereo pair showing the tetraphenylarsonium ion.

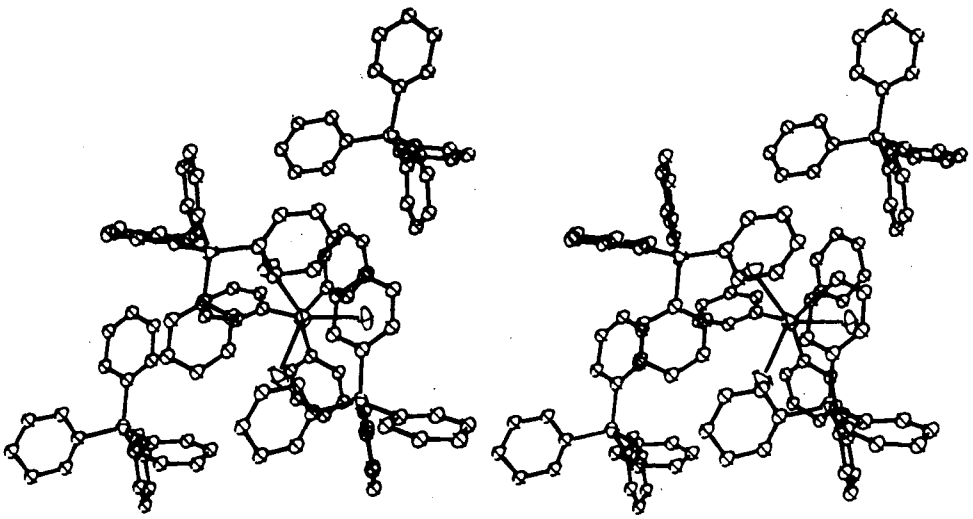

XBL 691-161

Fig. 4. Stereo pair showing an anion and the four nearest-neighbor cations as they are juxtaposed in the unit cell viewed down the "C_3" axis of the anion.

CRYSTAL STRUCTURE OF TRIMETHYL PLATINUM HYDROXIDE†

Thomas G. Spiro,* David H. Templeton, and Allan Zalkin

In 1947 Rundle and Sturdivant[1] published the structure of "tetramethyl platinum." They found that the platinum occurs in tetrahedra, 3.44 Å to an edge. The methyl carbons could not be located with their limited set of film data, but on chemical and symmetry grounds a structure was assigned which included hexavalent carbon atoms, each bonded to three platinum atoms and three hydrogen atoms. Cowan, Krieghoff, and Donnay[2] have now shown that the crystals used by Rundle and Sturdivant were in fact trimethyl platinum hydroxide. The study reported here confirms this structure in the crystals, and provides molecular parameters for the oxygens and carbons as well as the platinums.

Trimethylplatinum(IV) hydroxide was prepared by the method of Pope and Peachey.[3] The cell dimension and intensities were measured at 23°C with a quarter-circle goniostat equipped with a scintillation counter, using Mo Kα radiation. Our value for the cell edge, $a = 10.165 \pm 0.005$ Å, is in agreement with that of Rundle and Sturdivant,[1] 10.165 Å, whereas that of Cowan et al.,[2] 10.179 ± 0.002 Å, is slightly higher. The experimental density,[1,2] 3.2 g/cm^3, indicates eight molecules of $(CH_3)_3PtOH$ per unit cell (d_{calc} = 3.23 g/cm^3). The space group is $I\bar{4}3m$. A total of 1083 intensities was measured with 2θ values up to 60 deg. The reflections were divided equally between the hkl and $\bar{h}kl$ octants (which are equivalent in the Laue group but not in $1\bar{4}3m$). Because of the high symmetry there were only 169 nonequivalent reflections in each octant, so that the data set was overdetermined by a factor of three. The structure was refined by least-squares methods, and the residual R was decreased to 0.059. The final parameters (standard deviations given in parentheses) are, for Pt: $x = y = z = 0.6193(0.0006)$, $B_{11} = B_{22} = B_{33} = 2.62(0.02)$, $B_{12} = B_{13} = B_{23} = -0.28(0.02)$; for O: $x = y = z = 0.903(0.001)$, $B = 2.6(0.4)$; for C: $x = y = 0.624(0.002)$, $z = 0.819(0.002)$, $B = 4.4(0.4)$. Preliminary low-temperature x-ray results of M. R. Truter[4] are consistent with these coordinates.

The structure of the tetrameric unit in $(CH_3)_3PtOH$ is shown in Fig. 1. It is substantially the same as that proposed by Rundle and Sturdivant[1] for "tetramethyl platinum." The interatomic distances and angles are given in Table I. The platinum is in near-octahedral coordination, although the O–Pt–O angles are significantly lower than 90 deg. The Pt–C and Pt–O distances

are in good agreement with those reported by Truter et al.[5,6] for other compounds containing trimethyl platinum groups bridged by oxygen atoms. The Pt–Pt distances in these dimeric species, 3.38 Å (Ref. 5) and 3.41 Å (Ref. 6), are nearly the same as that found here, 3.43 Å. The internuclear distance in metallic platinum is significantly shorter, 2.77 Å (Ref. 7).

Footnotes and References

†Inorg. Chem. 7, 2165 (1968).
*Princeton University.

1. R. E. Rundle and J. H. Sturdivant, J. Am. Chem. Soc. 69, 1561 (1947).
2. D. O. Cowan, N. G. Krieghoff, and G. Donnay, Acta Cryst. B24, 287 (1968).
3. W. J. Pope and S. S. Peachey, J. Chem. Soc. 95, 571 (1909).
4. M. R. Truter (University of London), private communication.
5. J. E. Lydon and M. R. Truter, J. Chem. Soc. 1965, 6899.
6. M. R. Truter and R. C. Watling, J. Chem. Soc. (A) 1967, 1955.
7. Interatomic Distances, Chem. Soc. (London) Special Publication No. 11, p M100.

Table I. Interatomic distances and angles in $[(CH_3)_3PtOH]_4$.[a]

	Distance (Å)	Angle	(deg)
Pt–C	2.04(2)	O–Pt–O	77.6(2)
Pt–O	2.22(1)	C–Pt–C	87(1)
Pt–Pt	3.430(2)	Pt–O–Pt	101.2(2)

[a]Standard deviations in parentheses refer to the least significant digits.

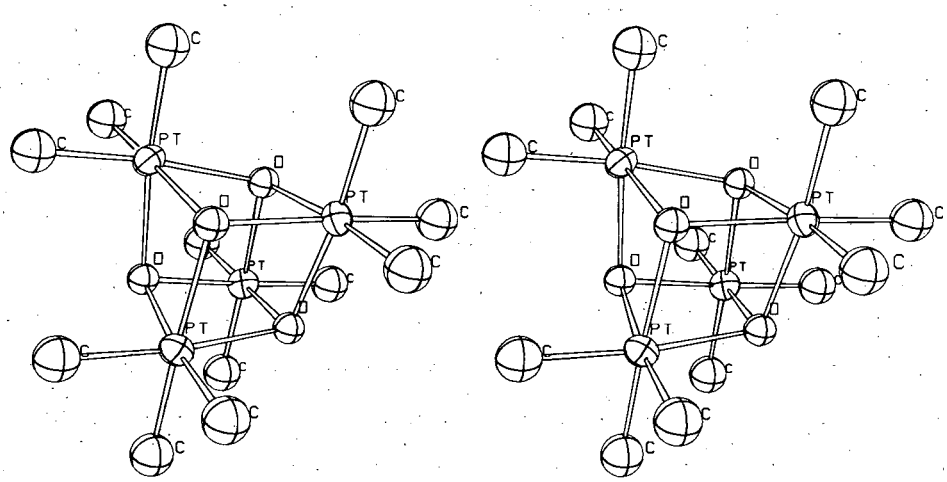

XBL 681-14

Fig. 1. Stereoscopic view of the tetrameric unit in $(CH_3)_3PtOH$.

CRYSTAL STRUCTURE OF A HEXANUCLEAR BASIC LEAD(II) PERCHLORATE HYDRATE, $Pb_6O(OH)_6(ClO_4)_4 \cdot H_2O$†

Thomas G. Spiro,* David H. Templeton, and Allan Zalkin

Recently Maroni and Spiro[1] investigated the vibrational spectra of a series of hydroxy- and alkoxy-bridged polyhedra of Bi(III), Pb(II), and Tl(I). The most significant result was the finding of a set of low-frequency Raman bands attributable almost entirely to the motions of the metal atoms. The high intensity of these bands was taken as evidence for some degree of metal-metal bonding, and the simplicity of their pattern suggested that they might be useful in structural characterization of polynuclear species. Of particular interest in this connection were the species present in perchlorate solutions of lead(II) containing 1.33 moles of hydroxide per mole of lead. Potentiometric[2] and ultracentrifuge[3] data were consistent with an equilibrium between $Pb_3(OH)_4^{2+}$ and $Pb_6(OH)_8^{4+}$. Crystals of composition $Pb_3(OH)_4(ClO_4)_2$ were described in 1930 by Willard and Kassner.[4] The Raman spectrum[1b] of these crystals showed three strong low-frequency bands similar to those exhibited[1a] by octahedral $Bi_6(OH)_{12}^{6+}$. Since in the concentrated solutions from which the crystals were obtained $Pb_6(OH)_8^{4+}$ was presumably predominant, it was inferred that these crystals also contained this complex, and its structure was predicted to be octahedral.[1b] A normal coordinate analysis[1b] showed that an octahedral structure was capable of predicting all the observed Raman and infrared bands of the crystals. The crystal structure results are consistent with the chemical analysis by Willard and Kassner,[4] but indicate that the crystals should be formulated as $Pb_6O(OH)_6(ClO_4)_4 \cdot H_2O$ and that the Raman prediction of structure is incorrect. Discrete hexanuclear complexes are indeed found, but the lead atoms are arranged at the corners of three face-sharing tetrahedra rather than at the corners of an octahedron.

Crystals of composition $Pb_3(OH)_4(ClO_4)_2$ were prepared by the method of Willard and Kassner.[4] For the measurements, a crystal was ground and etched with water to a sphere of diameter 0.13 mm and glued to a glass fiber. Each reflection was measured with the stationary-crystal stationary-counter technique, using Mo Kα x rays and a scintillation counter. The crystals are orthorhombic, space group Pbca. The cell dimensions are $a = 10.814 \pm 0.005$, $b = 16.706 \pm 0.006$, and $c = 26.273 \pm 0.008$ Å ($t = 23$ deg). For eight formula units $Pb_6O(OH)_6(ClO_4)_4 \cdot H_2O$ per cell the calculated density is 4.973 g/cm^3. The density measured with pycnometer and carbon tetrachloride at 24° is 5.07 ± 0.03 g/cm^3. Part of the discrepancy may be the result of contamination of the pycnometer sample, for example with lead carbonate ($d = 6.6$ g/cm^3). The structure was solved by use of the symbolic addition procedure[5] to determine the phases. It was refined by least-squares methods to $R = 0.055$.

Apart from the perchlorate ions, the asymmetric unit contains eight oxygen atoms of three distinct types. These atoms possess eight hydrogen atoms according to the chemical stoichiometry. On the basis of the structure we assign these as an oxide ion, O(1), a water molecule, O(8), and six hydroxide ions. The lead atoms occur in discrete clusters of six, with seven oxygen atoms intimately bound to each cluster, as shown in Fig. 1. We formulate this cluster as $Pb_6O(OH)_6^{4+}$. These lead atoms are arranged at the corners of three face-sharing tetrahedra, as seen in Fig. 2. The structure of this cluster is related to that[6] of $Pb_4(OH)_4^{4+}$, in which the lead atoms form a single tetrahedron, and to that[7] of Sn_2OSO_4, in which an isolated Sn_8 unit has four tin atoms at the corners of a central tetrahedron all four faces of which are covered by the remaining tin atoms.

The oxide ion is near the center of the central tetrahedron, at an average distance 2.29 Å from its lead neighbors. The oxygen atoms in tetragonal PbO have similar tetrahedral coordination, with lead neighbors at 2.30 Å.[8] Thus the central tetrahedron of the cluster can be considered as a fragment of the PbO structure. Each of the six hydroxide ions is adjacent to three lead atoms on an external face of a noncentral tetrahedron, and all such faces are covered in this way. This topology gives the three lead atoms in each face of every tetrahedron one, and only one, oxygen neighbor in common. The oxide ion fills this role for four faces, while each hydroxide ion is involved with only one face. The water molecule is only loosely bonded to this complex, at a distance 2.74 Å from Pb(6) on one corner. It is remote from any other lead atoms. The lead cluster conforms only approximately to the symmetry mm2 (C_{2v}) which is permitted by its topology, but the lead positions are very close to symmetry 2 (C_2). The hydroxide ions are expected to have their protons directed outward from the cluster, and they tend to form hydrogen bonds to the surrounding perchlorate ions. Each hydroxide ion has one or two perchlorate-oxygen neighbors at distances between 2.94 and 3.15 Å to which it could form weak hydrogen bonds. The perchlorate ions are not significantly coordinated, the closest distance from a lead to a perchlorate

oxygen being 2.9 Å. This is in accord with the Raman and infrared spectra,[9] which show bands characteristic of unbound ClO_4^-.

Footnotes and References

†Condensed from UCRL-18570, submitted to Inorgan. Chem.

*Princeton University.

1. V. A. Maroni and T. G. Spiro, Inorg. Chem. (a) 7, 183 (1968); (b) 7, 188 (1968); (c) 7, 193 (1968).
2. A. Olin, Acta Chem. Scand. 14, 126, 814, 1999 (1960); Svensk Kem. Tidskr. 73, 482 (1961).
3. O. E. Esval and J. S. Johnson, J. Phys. Chem. 69, 959 (1965).
4. H. H. Willard and J. L. Kassner, J. Am. Chem. Soc. 52, 2395 (1930).
5. I. L. Karle and J. Karle, Acta Cryst. 16, 969 (1963).
6. O. E. Esval (Thesis), University of North Carolina, 1963.
7. G. Wernfors, Acta Chem. Scand. 15, 1007 (1961).
8. W. T. Moore and L. Pauling, J. Am. Chem. Soc. 63, 1392 (1941).
9. V. A. Maroni and T. G. Spiro, J. Am. Chem. Soc. 89, 45 (1967).

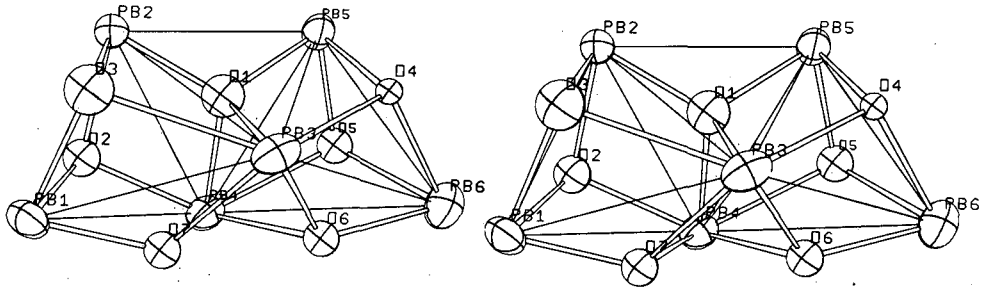

XBL 681-13

Fig. 1. Stereoscopic view of the $Pb_6O(H)_6^{4+}$ complex. The stick bonds connect oxygen and lead atoms; the lines define the lead polyhedra.

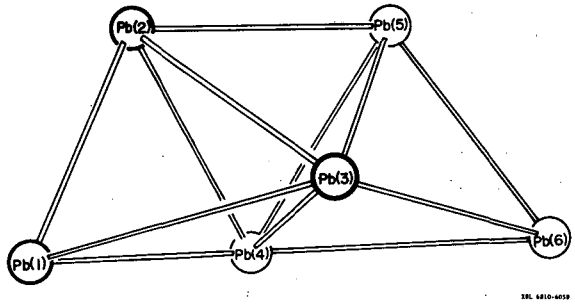

Fig. 2. The three face-sharing tetrahedra of Pb atoms in the $Pb_6O(OH)_6^{4+}$ cluster.

PHYSICAL AND INORGANIC CHEMISTRY

SEARCH FOR ELEMENT 110

S. G. Thompson, R. C. Gatti, L. G. Moretto,† H. R. Bowman, and M. C. Michel

From the calculations of Nilsson and Tsang (pages 148, 150) the isotope $^{294}110$ was estimated to have a half-life of $\approx 10^8$ years for alpha decay. This isotope is also estimated to be β stable and have a spontaneous-fission half-life of 10^{11} years. On this basis a search for element 110 in nature was undertaken.

The first question was where to search for such an isotope. Figure 1 shows that chemically element 110 falls naturally in the platinum group. The next question is how similar to platinum should it be. Some attempts have been made by Waber, Cromer, and Liberman[1] at Los Alamos to calculate the total energies of several configurations of the elements in the range of atomic numbers 104 to 128, using a SCF Dirac-Slater method in which finite nuclear size effects are taken into account. It turned out that elements 104 to 118 should have chemical properties similar to their homologs hafnium to radon. The only exception is element 110, nominally a homolog of platinum. The ground state for platinum is $5d^9 6s$, whereas 110 has a calculated ground state of $6d^8 7s^2$. Therefore we assumed that ekaplatinum might also resemble osmium, iridium, or gold. We attempted to find a natural platinum ore which contained all of these elements. Finally some platinum placer metal ore from Northern California was obtained. The composition is indicated in Table I.

The following tests were performed on the platinum ore:

(a) Low-background neutron counting was carried out on 12 ounces of the platinum ore. The level was 1.35±0.05 neutron counts/min. Within the statistical errors this was exactly the same as background (1.40±0.05 counts/m), and therefore the half-life must be $< 2 \times 10^8$ years or $> \approx 10^{15}$ years. One should note here that the alpha decay of $^{294}110$ is expected to be followed by spontaneous fission decay somewhere in the chain. In this case several neutrons would accompany each fission.

(b) Low-background counting of γ rays was carried out by using a NaI detector as shown in Fig. 2, and also with large Ge detectors. The observed spectrum can be reproduced exactly by 34 ppm of thorium and 3.3 ppm of uranium impurities in 134 g of lead.

(c) Direct spontaneous fission counting of a large area (90 cm^2) of the platinum in three low-background fission ionization counters was performed. The limit set here is < 1 fission count per 3 weeks.

The last test was the most sensitive of its kind. What this means is illustrated in Fig. 3. The significance is that the ekaplatinum half-life cannot be in the range between $\approx 2 \times 10^8$ years and $\approx 10^{15}$ years, if it is assumed that the isotope was formed in reasonable abundance in the beginning. From discussions with Seeger,[2] abundance is largely an open question.

Then we proceeded on the assumption that $^{294}110$ was present but with a half-life longer than $\approx 10^{15}$ years. The following experiments were carried out:

(1) X-ray fluorescence analysis. This method finally gave an upper limit of one part in $\approx 10^3$. In this case one needs to know what energies to assume for the x rays. The energies and relative intensities of characteristic x rays for element 110 are indicated in Tables II and III, based on the calculations by Tucker et al.[3] at Oak Ridge. The K electron binding energy for element 110 is calculated to be $\approx$ 200 keV.

(2) Isotopic analysis. A direct mass spectrometric examination of the vapor emitted from a heated filament was made. The vapor was ionized by slow electrons and analyzed in a 30-cm radius 60 deg deflection single-direction focusing spectrometer. Detection of the analyzed beam was by integration of the output of a 16-stage electron multiplier capable of detecting single ions. The sample temperature was raised in $\approx$ 100°C steps from well below the melting point of platinum until the filament burned out (total time $\approx$ 36 hours). The spectrum of masses from 275 to 330 was scanned at each temperature and the intensity of the ions of the major elements was determined at each temperature. At burnout the primary beams were osmium and iridium. The

limits on the presence in platinum ore (on the basis of mass spectroscopy) of elements in the region of $Z \approx 110$, $A \approx 275$-330 relative to the various elements in the sample are given in Table IV. No limit can be set if the vapor pressure of element 110 is much less than that of osmium. The relative vapor pressures that might be expected are indicated by Table V.

(3) Activation analysis. Activation analysis, an extremely sensitive method, was used as the next step. To illustrate the basis of this approach let us consider Fig. 4, taken from Nilsson and Tsang.[4] In this case we attempt to produce a product which falls outside the region of maximum stability. One should be able to produce products having half-lives not too different from those corresponding to the time of the bombardment and the period of counting. We used two different methods of activation:

(a) Bombardments with heavy ions at energies approximately 10 MeV over the Coulomb barrier and bombardments at maximum energy (10 MeV/nucleon). The ions ^{11}B, ^{12}C, ^{16}O, and neon were used. In 16 hours of bombardments with good beams we did not observe any spontaneous fission events.

(b) Bombardments with protons. The targets were then bombarded with >1-μA beams of protons of energies 13, 15, 17, 19, 30, 45, and 55 MeV. Periods of bombardments ranged from 10 min to 2 hr. No spontaneous fission events were observed when the targets were immediately placed in fission ionization counters. At the lower energies, 13 to 19 MeV, the prompt fissions produced in the target were observed directly with mica detectors. The number of prompt fission events observed corresponded closely with that expected from the thorium and uranium impurities known to be present.

As a result of the limits established in the activation experiments a limit of < 1 part per 10^{10} relative to platinum was established.

The only other commonly available ion not used in the bombardments was ^4He. This was not used on the grounds that it might have produced ekamercury, which should be quite volatile and would escape from the targets.

The conclusion is that ekaplatinum, if it exists at all in nature, must be present in extremely small abundance or that the half-life is less than 10^8 years. However, it may still be possible to detect fission products produced by this element as a result of spontaneous fission decay which occurred long ago. One possibility is to search for unusual isotopic composition in our platinum ore. Attempts are also being made to obtain some platinum ore which is much older than our material, which is of the order 5×10^7 years. There is some hope of obtaining material from South Africa, which comes from formations having an age of the order 2×10^9 years.

Acknowledgments

We are very grateful to Elio Giusti, who has helped us in getting the platinum ore and with all geological aspects of our problem.

Footnote and References

†Present address: Laboratorio di Radiochimica, Università di Pavia, Pavia, Italy.

1. J. T. Waber, D. T. Cromer, and D. Liberman, SCF Dirac-Slater Calculations of the Trans-Lawrencium Elements, Los Alamos Scientific Laboratory preprint.

2. P. Seeger (Los Alamos Scientific Laboratory) private communication.

3. T. C. Tucker, L. D. Roberts, C. W. Nestor, Jr., T. A. Carlson, and F. B. Malik, Calculation of the Electron Binding Energies and X-Ray Energies for the Superheavy Elements 114, 126, and 140 Using Relativistic SCF Atomic Wave Functions, Oak Ridge National Laboratory preprint.

4. S. G. Nilsson, S. G. Thompson, and C. F. Tsang, Stability of Superheavy Nuclei and Their Possible Occurrence in Nature, Phys. Letters (to be published); S. G. Nilsson, Lecture Notes: Nuclear Structure, Fission, and Superheavy Elements, UCRL-18355, Sept. 1968; S. G. Nilsson, J. R. Nix, A. Sobiczewski, Z. Szymanski, S. Wycech, C. Gustafson, and P. Möller, On the Spontaneous Fission of Nuclei with Z Near 114 and N Near 184, Nucl. Phys. A115, 545 (1968).

Table I. Composition of Northern California placer metal platinum ore.

Element	Percent
Platinum	73.9
Osmium	6.5
Iridium	7.05
Rhodium	2.00
Palladium	0.8
Ruthenium	0.5
Gold	0.2
Additional common elements	9.05

Table II. Relative intensities of K x rays.

Z	α_2/α_1	β_1'/α_1	β_2'/α_1
106	0.583	0.420	0.194
107	0.584	0.423	0.199
108	0.586	0.426	0.203
109	0.587	0.429	0.207
110	0.588	0.432	0.212
111	0.590	0.434	0.216
112	0.591	0.437	0.220
113	0.592	0.440	0.224
114	0.594	0.443	0.228

Table III. K x ray energies.

Z	$K\alpha_2$ $K\text{-}L_{II}$	$K\alpha_1$ $K\text{-}L_{III}$	$K\beta_1$ M_{II}	$K\beta_1'$ $K\beta_3$ M_{III}	$K\beta_5$ M_{IV}	$K\beta_2'$ $K\beta_2$ $K\text{-}N_{II}$	$K\beta_4$ N_{III}
106	134.2	142.2	157.8	159.8	160.42	163.8	164.4
107	137.3	145.7	161.6	163.6	164.28	167.8	168.3
108	140.8	149.65	165.8	168.0	168.61	172.2	172.8
109	143.8	153.15	169.5	171.8	172.45	176.1	176.7
110	147.4	157.1	173.7	176.1	176.8	180.5	181.1
111	150.50	160.8	177.6	180.1	180.8	184.6	185.3
112	154.2	165.0	182.1	184.8	185.3	189.3	190.0
113	158.0	169.4	186.8	189.6	190.3	194.2	195.0
114	160.9	172.8	190.40	193.4	194.1	198.0	198.9

Table IV. Limits on natural abundance of isotopes of elements $Z \approx 110$ ($275 \leq A \leq 330$).

For heavy element with vapor pressure similar to:	Abundance limit
Au	125 parts per million
Pd	1.4
Rh	1.2
Pt	0.3
Ru	0.2
Ir	0.5
Os	8.3

Table V. Melting and boiling points of periodic-table groups containing elements with Z = 107 to 112.

Element	Melting point (°C)	Boiling point (°C)
Zinc	419	907
Cadmium	321	765
Mercury	-39	357
112	—	—
Copper	1083	2595
Silver	961	2212
Gold	1063	2966
111	—	—
Nickel	1455	2730
Palladium	1549	2200
Platinum	1773	4300
110	—	—
Cobalt	1495	2900
Rhodium	1966	3700
Iridium	2410	4527
109	—	—
Iron	1535	3000
Ruthenium	2250	4150
Osmium	3000	5000
108	—	—
Manganese	1244	2097
Technetium	2200	—
Rhenium	3167	5900
107	—	—

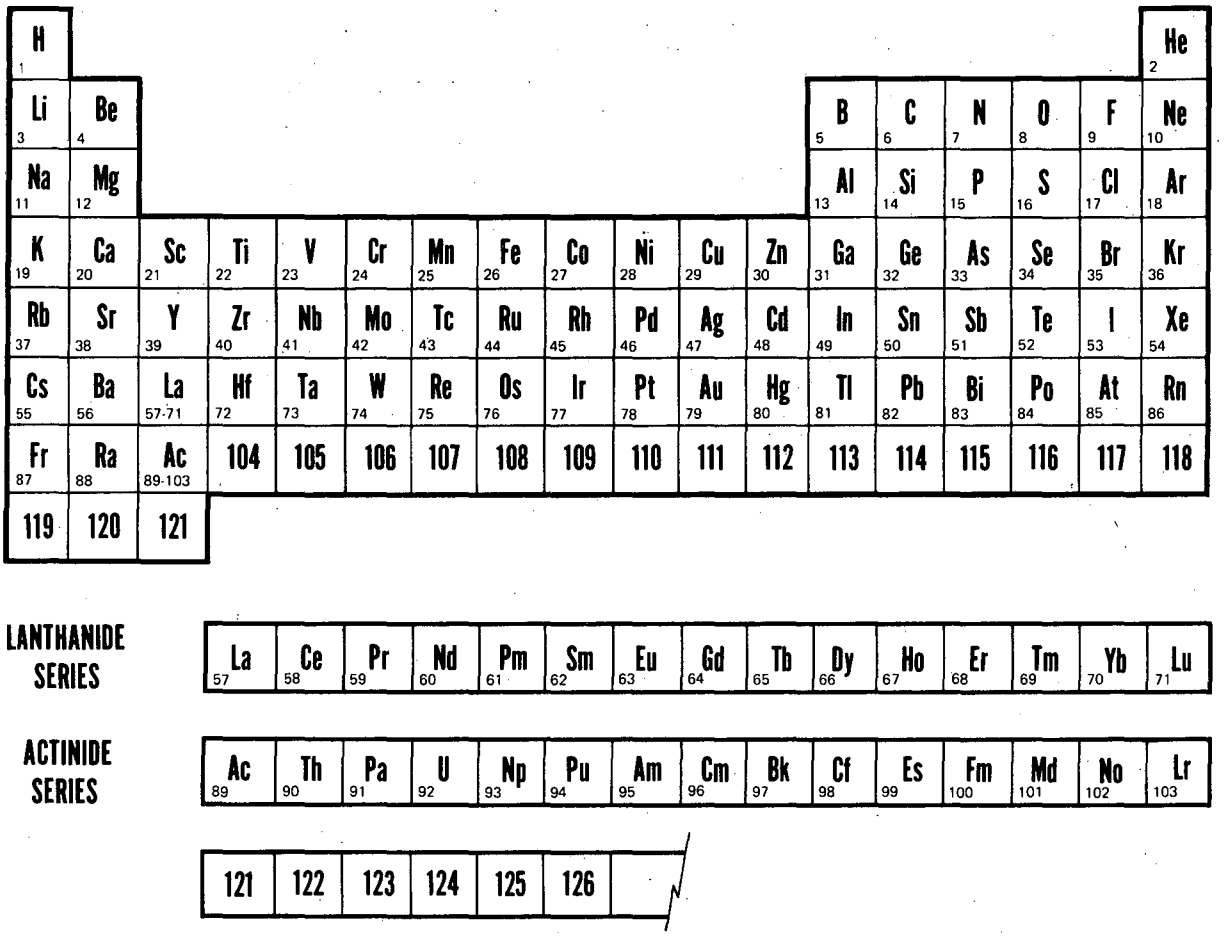

XBL-693-344

Fig. 1. Periodic table, showing predicted locations of new elements.

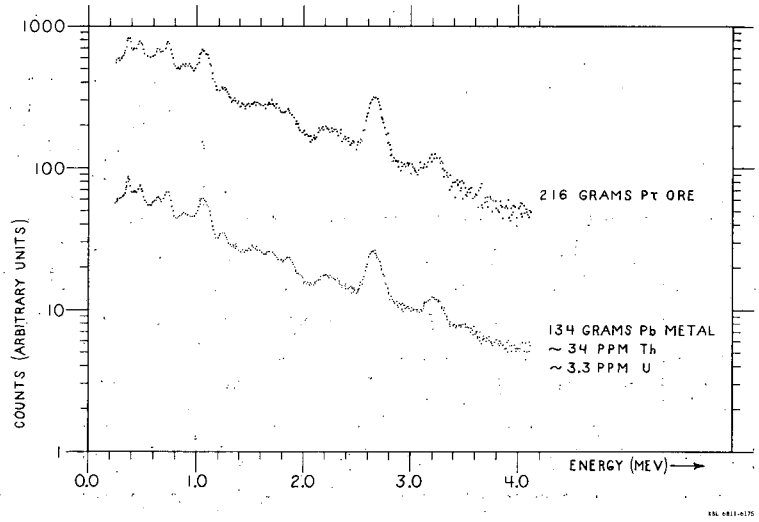

Fig. 2. Low background γ-ray spectrum of platinum ore taken with NaI detector in upper part of figure. Lower part of figure shows spectrum taken with NaI on 134 grams of lead metal containing 34 ppm of thorium and 3.3 ppm of uranium. The lower spectrum is shifted down by a factor of ten to facilitate comparison.

Fig. 3. Relationship between counting rate and half-life on the basis of different assumptions regarding initial composition.

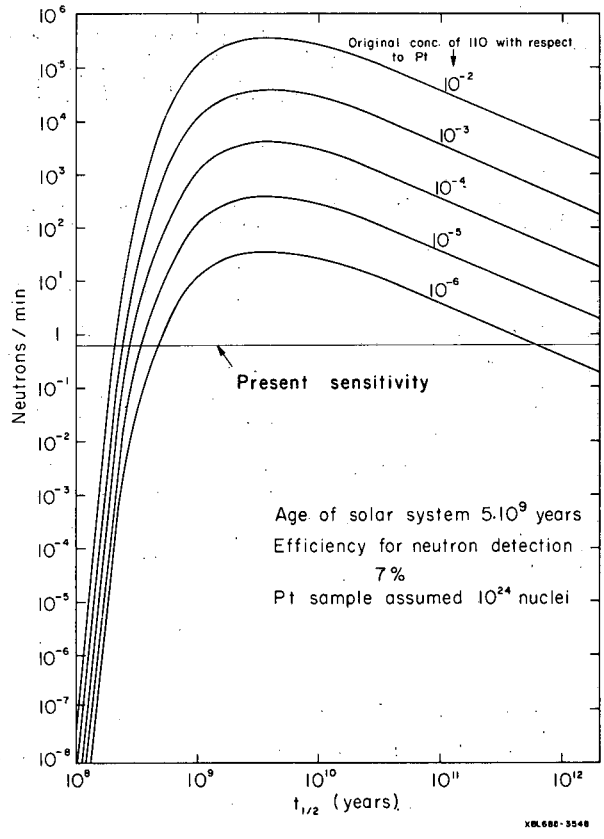

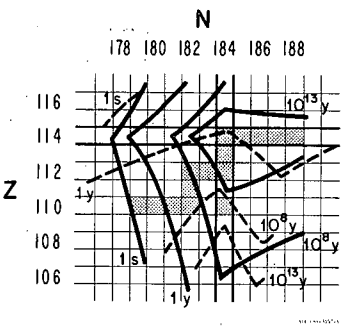

Fig. 4. Half-life contours calculated by Nilsson and Tsang for various possible superheavy nuclei. Dashed lines represent α decay; solid lines refer to spontaneous fission half-life.

SEARCH FOR ELEMENT 114

S. G. Thompson, W. J. Swiatecki,† R. C. Gatti, H. R. Bowman, L. G. Moretto,* R. C. Jared, and R. M. Latimer

The Nuclear Chemistry Annual Report for 1967 described experiments carried out in an attempt to produce and observe isotopes of element 114. The calculations by Nilsson and Tsang have given predicted properties and half-lives for isotopes in the region of elements near Z = 114. Atomic number 114 is a magic number and neutron number 184 is also magic.

Since the 1967 annual report the detection system was redesigned to improve the sensitivity for detection of spontaneous fission of nuclei of atomic number 114. A schematic drawing of the apparatus is given in Fig. 1. The background of fission tracks coming from impurities from the recoil catcher has been reduced by using very pure silicon as the catcher material. A further reduction of the background was accomplished by covering the mica detectors with aluminum foils of $\approx$ 2.18 mg/cm^2 thickness. The energies, in the backward direction, of fission fragments coming from the prompt fission of compound nuclei having a large momentum in the forward direction is considerably reduced. In the case of uranium impurities the improvement resulting from the 2.18 mg/cm^2 aluminum mica covers is of the order of a factor of 10. For lighter elements the ratio is larger.

As a result of these improvements the limits on the cross sections for production of isotopes of element 114 have been lowered considerably. The upper limits on the cross sections for the products of the following reactions are given in Table I for the reaction

$$^{248}_{96}\mathrm{Cm} + ^{40}_{18}\mathrm{Ar} \rightarrow ^{288-x}114 + x\mathrm{n}.$$

The ^{40}Ar energy ranged from 213 MeV (Coulomb barrier) to 250 MeV. The limits are relevant only for the isotopes with half-lives between nanoseconds and years, depending on the cross section. The transit time of the recoil nucleus to the catcher is of the order of nanoseconds and the duration of a shift at the Hilac is of the order of a day.

The negative results are consistent with the calculations by Nilsson and Tsang, who predict that the half-lives of the expected products would be much less than a nanosecond. If products with a larger neutron excess could be produced by using combinations of targets and projectiles with larger neutron excess, the chances of producing and detecting isotopes of atomic number 114 would be considerably improved.

Footnotes

†Theoretical Physics Group, Lawrence Radiation Laboratory, Berkeley.

*Present address: Laboratorio di Radiochimica, Università di Pavia, Pavia, Italy.

Table I. Upper limits for cross sections for reaction $_{96}^{248}Cm + _{18}^{40}Ar \rightarrow {}^{284}114 + 4n$.

E_{lab} (MeV)	Cross section with Al cover (cm^2)
218	$3.3 \pm 2.4 \times 10^{-32}$
227	$1.1 \pm 1.1 \times 10^{-32}$
231	$4.3 \pm 2.5 \times 10^{-32}$
237	$1.5 \pm 1.5 \times 10^{-32}$
242	$2.1 \pm 2.1 \times 10^{-32}$

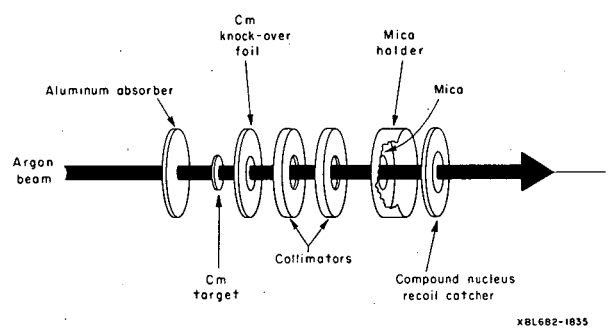

Fig. 1. Schematic diagram of experimental apparatus.

AMALGAMATION BEHAVIOR OF HEAVY ELEMENTS. THE TRACER CHEMISTRY OF DIVALENT MENDELEVIUM†

Jaromír Malý*

The extraction of mendelevium into sodium amalgam from sodium acetate solutions results in about a tenfold enrichment relative to the lighter actinides (Pu, Am, Cm, Bk).

Separation of Md from the heavier actinides may be accomplished also by electrolysis in acetate or citrate-acetate solution on an electrode of mercury amalgamated with sodium. The sequence of electrodeposition of actinides in acetate-citrate solution is Md > Fm > Es > Cf.

These separation methods probably depend on the formation of stable Md^{2+}. The potential of the $Md^{3+} + e \rightarrow Md^{2+}$ couple was estimated by a series of reductions, using $YbCl_2$, Zn, $EuCl_2$, $CrCl_2$, VCl_2, and $TiCl_3$, all in 2 M HCl. All except $TiCl_3$ appear to reduce Md^{3+} to Md^{2+}, which can then be coprecipitated with $EuSO_4$ or $BaSO_4$; Md in the precipitate is thereby enriched 10 to 30 times relative to the daughter isotope ^{256}Fm in solution.

A previous communication[1] reported preliminary results concerning the possible separation of Md from higher actinides by extraction into sodium amalgam from sodium acetate solutions, or by an electrolytic one-step separation of Md and Fm from Es. This and a subsequent publication[2] reported the first experimental evidence of the Md^{2+} state, an oxidation state which now appears to exist for other heavy actinides as well. This paper presents a more detailed study of Md^{2+}.

Experimental Procedure

Isotopes of Md, Fm, and Es Produced by Irradiation

^{256}Md, produced by irradiation with ≈ 46-MeV He ions of an einsteinium target, consisting of ≈ 5 μg ^{253}Es mounted on 4 $\mu g/cm^2$ Be foil, was used for the work reported here. The Es target contained ≈ 1% of ^{254}Es and ^{255}Es, the latter being in equilibrium with ^{255}Fm.

Irradiation for ≈ 30 min with a beam current of 50 to 100 $\mu A/cm^2$ (10 to 20 μA through the target) yielded approximately 10^5 atoms of ^{256}Md (and also some ^{251}Fm, ^{252}Fm, ^{253}Fm, ^{254}Fm, ^{255}Fm, and ^{256}Fm isotopes) which were collected on a Be catcher foil, along with about 10^5 to 10^7 α d/m of ^{253}Es, knocked out from the target. The catcher foil was dissolved in 6 M HCl, containing ≈ 500 μg La^{3+}. This solution was treated with an excess of KOH to form $La(OH)_3$, which coprecipitated Md, Fm, and Es. The $La(OH)_3$ precipitate, washed with 6 M KOH and water, was usually dissolved in 200 λ of 2 M HCl, to form a "stock Md" solution.

The isotopes ^{252}Md, ^{253}Md, and ^{254}Md, which also were produced during irradiation by (He,xn) reactions, could not be detected. They are short-lived and decayed by K capture to their Fm isotopes. A few 7.34-MeV α particles were observed in the α spectrum due to ^{255}Md ($T_{1/2}$ = 30 min). However, this isotope was observed mainly after K capture as ^{255}Fm.

Radioactive Tracers

The tracer isotopes ^{238}U (in the U^{4+} state), ^{237}Np (as Np^{4+}), ^{239}Pu (Pu^{4+}), ^{241}Am, ^{244}Cm, ^{249}Bk, ^{252}Cf, ^{253}Es, ^{152}Eu, and ^{154}Eu (all 3+) were used in ≈ 0.5 M HCl solution.

^{252}Fm, ^{255}Fm, and ^{254}Fm were used for measurement of the yield of Fm in chemical operations. The yield of ^{252}Fm was corrected for the growth of ^{255}Fm from ^{255}Es (measured 40 days after bombardment and compared with the original ^{255}Es present in the target) and for growth from ^{255}Md (determined from the amount of ^{255}Md as measured by its 7.34-MeV α energy and 30-min half-life). A known amount of the "stock Md" solution was used for the chemical separation procedures (extraction, electrolysis, reduction, and coprecipitation), and at the end of a particular procedure a part of each separate fraction was electroplated and then counted by α-pulse analysis as described in Refs. 1 and 3. The amount of ^{256}Fm activity was determined for each fraction, either by measuring the decay curve for spontaneous fission (SF) along with its α spectrum, or by utilizing a separate α chamber and a surface barrier Si-Au detector employing a discriminator for SF counts. At the same time SF and α decay curves were measured for a known amount of the stock solution in order to calculate the yield of separated isotopes in each fraction.

Chemicals

Sodium amalgam was prepared by dissolving freshly cut sodium metal in hot mercury.

Calculation of Md Yield

A. Yield from decay curves

The growth and decay curve of the SF activity is described by

$$Fm(t) = Fm_0 \exp(-\lambda_{Fm}t) + R_{Md}Md_0 \left[\exp(-\lambda_{Fm}t)-\exp(-\lambda_{Md}t)\right], \quad (1)$$

where $R_{Md} = \lambda_{Md}/(\lambda_{Md}-\lambda_{Fm}) = 1.73$.

The time t is measured from the end of bombardment, when Fm and Md are Fm_0 and Md_0 respectively. Because $\lambda_{Md} > \lambda_{Fm}$, for large values of t the curve becomes a fermium decay

curve described by

$$Fm(t) \approx [\ (Fm_0 + R_{Md}Md_0)\ \exp(-\lambda_{Fm}t)] \qquad (2)$$

The yield of Md was calculated from the difference between the growth curve for Fm described by Eq. (1) and the decay curve (Eq. 2), extrapolated to the time of separation. For this difference,

$$\Delta\ Fm(t_{sep}) = Fm(t_{sep}) - [\ (Fm_0 + R_{Md}Md_0)\ \exp(-\lambda_{Fm}t_{sep})] = R_{Md}Md_0\ \exp(-\lambda_{Fm}t_{sep}); \qquad (3)$$

$\Delta\ Fm(t_{sep})$ represents the difference between total fermium after decay of Md, and fermium before Md decay. Hence the difference may be used to calculate the yield of Md.

B. Calculation of yield from the ratio SF of ^{256}Fm: α activity of ^{253}Es

In the case of electrolysis, when the SF activity was too low to give a good growth curve, the activity ratio $SF/\alpha^{253}Es$ was followed for 3 to 6 hours, after a wait of more than 15 hours (t long $= t_L$) after the end of the bombardment for essentially all ^{256}Md present at t_{sep}, to decay to ^{256}Fm. From this ratio of $SF/\alpha^{253}Es$ in the original solution and in the separated fraction and with the aid of ^{253}Es yield, the yield of SF in the fraction [% $SF(t_L)$] was calculated. For calculation of the yield of Md separated at t_{sep}, we used the formula

$$\%\ SF(t_L) = \%\ ^{256}Fm(t_{sep})\ \frac{A}{A+1} + \%\ ^{256}Md(t_{sep})\ \frac{1}{A+1}\ , \qquad (4)$$

where $\frac{1}{A} = R_{Md}Md(t_{sep})/Fm(t_{sep})$,

and for $\%\ ^{256}Fm(t_{sep})$ we used the yield $\%\ ^{255}Fm(t_{sep})$, measured in a given fraction and in the unseparated mixture. The value of the factor A is read from a standard decay curve for the unseparated mixture, at t_{sep}.

In the above equations, $R_{Md}Md_0\ \exp(-\lambda_{Fm}t)$ is equal to that part of the SF activity of ^{256}Fm contributed by the decay of ^{256}Md at t_{sep}, whereas $^{256}Fm(t_{sep})$ in (4) represents that part coming from Fm present in the fraction at t_{sep}. The $1/A$ is the ratio of SF activity from Fm produced by mendelevium decay to Fm produced directly; $A/(A+1)$ is the fraction of SF activity from Fm produced directly. Multiplication by 100 gives the % of total SF activity originating from this source.

Measurement of α activity from ^{253}Es permitted a check on the yield of total α's and consequently of total SF's through the chemical procedure.

Extraction Procedure

The extraction experiments usually were carried out from a mixture of 20 λ of the "stock Md" solution in 0.15 M HCl, 25 λ of tracers in 1 M HCl, 9 λ of 1 M HCl containing 120 μg of Sm^{3+} and 150 μg each of Eu^{3+} and Yb^{3+}, 150 λ of 7 M sodium acetate, 5 λ of 8 M ammonium acetate, and selected amounts of HCl, as shown in Table I.

The extractions were performed in a 3-ml cone using 250 λ of sodium amalgam, containing $\approx$ 3.5 milliequivalents Na/ml. The actinide elements were back-extracted from part of the amalgam with 6 M HCl, the extract neutralized by NH_4OH, and then electroplated on a Pt disk. Details of the extraction procedure are described in Ref. 3.

The remaining portion of the amalgam, after being washed with H_2O, was decomposed by ice-cold concentrated HCl; NaCl crystals together with $EuCl_2$ were centrifuged out, washed with concentrated HCl, and dissolved in 1 ml of H_2O, and, after neutralization with NH_4OH, an aliquot was electroplated on a platinum plate.

The combined HCl supernatants were diluted to 2 ml. A known fraction of this solution was neutralized and electroplated as before.

Electrolytic Procedure

The compositions of the solutions used in electrolysis were similar to those used for amalgam extractions: in the first experiment, 150 λ "stock Md" in 1 M HCl (containing $\approx$ 200

μg La^{3+}), 600 λ of 7 M sodium acetate, 20 λ of 8 M ammonium acetate, and 100 λ of 0.5 M HCl, and in the second 200 λ of "stock Md" in 3 M HCl, 25 λ of 0.5 M sodium citrate, 300 λ of 7 M sodium acetate, and 50 λ of 0.5 M HCl. In the first experiment 110 λ of tracer solution in 0.5 M HCl, containing ≈ 1 mg ^{238}U, was also present.

The electrolyses were performed in the open air, using 900 λ and 300 λ of pure mercury in the first and second experiments, respectively. The anode consisted of a platinum spiral, held at the surface of the electrolyte. The Md-rich fraction from electrolysis was subsequently used for experiments on the reduction of Md^{3+} to Md^{2+}.

The electrolyses were carried out for 35 min, with periodic interruption at 5-min intervals for sampling the mercury phase. Following any 5-min period of electrolysis, the current was stopped, and after 1 min of mixing of both phases, 5 λ of mercury was withdrawn by pipeting. This sample was washed three times with water, transferred to a platinum disc, the mercury driven off by heating, and the residue counted for Md and Es as in the extraction experiments.

Reduction Procedure

The Md "stock" solution was reduced by adding 4 to 5 mg of $YbCl_2$ or $EuCl_2$, or else with amalgamated zinc in the presence of ≈ 5 mg $EuCl_3$. In other experiments solutions of Cr^{2+}, V^{2+}, and Ti^{3+} were prepared by reduction with amalgamated zinc. In a typical experiment, the reducing solution was prepared by adding a 0.1 M solution of the oxidized species in 2 M HCl to ≈ 0.5 g of amalgamated zinc (20 mesh) contained in a 1-ml cone. The solution was heated and repeatedly mixed by pipeting for 5 min. The concentration of HCl after reduction to Cr^{2+}, V^{2+}, or Ti^{3+} was about 1 M, because of the Zn dissolution during reduction. One ml of this freshly prepared reducing solution was added to a 2-ml cone containing 50 λ of "stock Md," ≈ 6 mg Eu^{3+}, and 300 μg of Ba^{2+} in 100 λ of 0.5 M HCl. After 1 to 2 min of reduction, $BaSO_4$ was precipitated by the addition of 25 μl of 40% H_2SO_4. After centrifuging, the precipitate was washed with water, transferred to a platinum counting plate, dried, and counted. A sample of the stock solution was counted at the same time.

In reductions with $YbCl_2$, $EuCl_2$, and amalgamated Zn, only 400 λ of solution was used, which was 0.1 M in Eu, and pure $EuSO_4$ was precipitated in place of $BaSO_4$.

Results and Discussion

Extraction Behavior of Md and Evidence of $MdCl_2$

The results of the extraction of the tracer mixture and "stock Md" solution are shown in Table I. The results in parts A and B of the table are equivalent to the addition of 52 λ and 276 λ of 1 M HCl, respectively, shown in graph 3 in Ref. 4. Table I shows a high extraction yield for Cf^{3+}, Es^{3+}, Fm^{3+}, and Md^{3+}, whereas Cm^{3+}, Am^{3+}, Pu^{4+}, and Np^{4+} are extracted with low yield, especially when only 15 λ of 1 M HCl is present. This same method successfully separates Eu from Sm, the former showing preferential retention in the solid chloride precipitate.[5-8] The SF activities separated in the $EuCl_2$ and $SmCl_3$ fractions respectively are shown in Fig. 1. It is evident from the figure that Md appears only in the $EuCl_2$ fraction (growth of SF activity), and is practically not present in the supernatant ($SmCl_3$ fraction). The distribution of tracers shown in Table I indicates that other actinides are largely aasent from the $EuCl_2$ fraction, but are found instead in the $SmCl_3$ fraction. It appears that after decomposition of the amalgam, Md was present as $MdCl_2$, which is carried by $EuCl_2$, and that Md^{2+} must be relatively stable in HCl solution, whereas the other actinides are oxidized in conc. HCl by H^+ ions very rapidly to the 3^+ state.

Electrolytic Behavior of Md, Fm, and Es

Because of time limitations, it was possible to perform only two electrolytic runs. In the first run (with ≈ 1 mg U^{4+} present) a current density of 5 mA/cm^2 was used. The separation of ^{253}Es, ^{255}Fm, SF activity, and ^{256}Md is shown in Fig. 2. The yield of ^{256}Md was calculated according to procedure B under "Calculation of Md Yield." The second experiment was done with a current density of 10 mA/cm^2 in the absence of uranium. These results are shown in Fig. 3. Figure 2 shows a yield ratio of Es:Fm:Md = 0.8% :4% :90% , after 35 min of electrolysis; in the second experiment the best relative yields are Es:Fm:Md = 1.2% :13% :52% , after 5 min of electrolysis. In the first experiment the yield of Md and Fm in mercury was increasing during the

first 150 mA minutes of charge passed; in the second experiment (10 mA/cm^2 curr. dens.) a drop of the yield of Md in mercury was observed, between 200 and 350 mA minutes of charge passed. It is possible that this effect might be caused by a more alkaline solution near the cathode after prolonged electrolysis, leading to re-solution of Md from the cathode. However, more work is necessary to sufficiently prove this effect and to find its explanation. In the first electrolysis much better separation of ^{255}Fm from ^{256}Md was found (with a factor ≈ 20), whereas in the second the separation was only a factor ≈ 4. This observation probably cannot be explained solely by the lower current density. The reason probably lies in the effect of citrate ion in the second electrolysis and the higher pH.

For comparison with other data reported in the literature, we recalculated the data of Fig. 2 to obtain the "amount left in solution," shown in Fig. 4. After finishing the second electrolysis we replaced the mercury phase by 300 λ of fresh Hg and proceeded in the electrolysis of ^{253}Es and ^{255}Fm with 30 mA/cm^2 current density, with results shown in Fig. 5. Both Figs. 4 and 5 show, in agreement with the literature,[9,10] an approximately linear relation between these quantities. One can read from these curves the "periods of amalgamation" introduced by Boussières et al.[9] The results are ≈ 100 mA min for Md, from Fig. 4 and ≈ 300 mA min for Fm and ≈ 800 mA min for Es, from Fig. 5. The curves for ^{256}Md in Fig. 4 and ^{255}Fm in Fig. 5 show deviations from a straight line (dropping faster when more charge is passed, as observed by Onstott in rare earth electrolyses[11]).

Potential of the Md^{3+} - Md^{2+} Couple

Although a correlation between the amount of extraction into sodium amalgam and the formation of a chemically stable +2 state has been established for the 4f elements,[5,12] a similar correlation has not been demonstrated for the 5f series.

The expected analogy between Tm and Md led Seaborg[13] in 1949 to predict that Md might have a +2 state.

Accordingly, we sought direct evidence for a dipositive state of mendelevium, and have attempted to establish rough limits for the potential of the $Md^{3+} + e = Md^{2+}$ couple. To this end, various reducing agents were added to the "stock Md" solution, and $BaSO_4$ or $EuSO_4$ was precipitated from the mixture. The distribution of ^{253}Es, ^{256}Fm, and ^{256}Md activities between the precipitate and supernatant was then determined.

Typical decay curves of the original solution and the $EuSO_4$ or $BaSO_4$ fractions are shown in Fig. 6 (for reduction by amalgamated zinc--in the presence of Eu^{2+}), Fig. 7 (reduction with Cr^{2+}), Fig. 8 (reduction with V^{2+}), and Fig. 9 (attempt at reduction with Ti^{3+}). The curves in Figs. 6, 7, and 8 show good evidence of growth of SF activity from ^{256}Md separated in the $EuSO_4$ or $BaSO_4$ fractions. For Ti^{3+} only slight growth of ^{256}Fm was observed relative to the original solution, which indicated incomplete reduction of Md^{3+} to Md^{2+} by Ti^{3+}.

The reduction data are collected in Table II. The enrichment factor of Md in the $EuSO_4$ or $BaSO_4$ fraction [defined as the ratio

$$\frac{\dfrac{R_{Md}^{Md(t_{sep})}}{Fm(t_{sep})}\ \text{ppt fraction}}{\dfrac{R_{Md}^{Md(t_{sep})}}{Fm(t_{sep})}\ \text{original solution}]}$$

in all reduction runs with Zn, Eu^{2+}, Cr^{2+}, and V^{2+} was between 10 and 90, as shown. The yield of Md^{2+} coprecipitated with $BaSO_4$ was from 50 to 100%, but with $EuSO_4$ the yield was only ≈ 5 to 10% when the $EuSO_4$ yield was also 5 to 10%. The reduction with $YbCl_2$ gave the same result as with $EuCl_2$, with an enrichment factor ≈ 20. These results show that Md^{3+} was reduced to Md^{2+} by Yb^{2+}, Zn, Eu^{2+}, Cr^{2+}, and V^{2+}, but with Ti^{3+} the reduction was low. Since partial reduction occurred with Ti^{3+} [E^0 = - 0.09 V (Ref. 14) in 1 M HCl] the $Md^{3+} + e \rightarrow Md^{2+}$ reduction potential apparently is about -0.1 V.

Conclusion

The results presented in Table I indicate that Md is extracted by sodium amalgam somewhat more readily than is einsteinium, and on comparison with results presented previously,[1] it appears that Md is extracted more readily than californium. This suggests that Md^{2+} is more stable than Cf^{2+} or Es^{2+}. Additional data in Table I show that, in the separation of $EuCl_2$ from $SmCl_2$, if these amalgams are treated with ice cold concentrated HCl all the Md is carried by the solid $EuCl_2$ fraction. This suggests the existence of a solid, slightly soluble $MdCl_2$ (in conc HCl), isostructural with $EuCl_2$.

Figures 2 and 3 demonstrate a very substantial separation of Md from Es and Fm by electrolysis. The maximum separation observed was 0.8% Es:4% Fm:90% Md by electrodeposition in mercury during the first electrolysis (Fig. 2).

The maximum ratio of spontaneous fission activity due to ^{256}Fm to α activity of ^{253}Es and ^{255}Fm was reached after passage of $\approx$ 9 C of electric charge. The enrichment of ^{256}Fm in the mercury phase by a factor $\approx$ 30 is due to preferential electrodeposition of ^{256}Md on the cathode while Es and Fm remain mostly in solution. This result is similar to the well-known electrolytic separation of Eu and Sm from other rare earths on a lithium-amalgamated cathode.[11,15,16] The observed large separation of Es from Md by electrolysis suggests that a substantial difference exists in the potentials of their 3+-2+ couples. To prove this difference, the reduction experiments summarized in Table II were carried out. These data indicate that Md^{3+} can be reduced to Md^{2+} and then precipitated with $EuSO_4$ or $BaSO_4$, usually with an enrichment factor > 10 (in comparison with Es) with any of the following reducing agents: $YbCl_2$, Zn (Jones' Reductor in the presence of Eu^{3+}), Eu^{2+}, Cr^{2+}, or V^{2+} in 2 M HCl solution.

It follows that the reduction potential for the Es^{3+} - Es^{2+} couple must be more negative than for the Md^{3+} - Md^{2+} couple by $\approx$ 1 V or more. The oxidation potential of $Md^{3+} \rightarrow Md^{2+}$ couple is close to the oxidation potential of $Ti^{3+} \rightarrow Ti^{4+}$ in 1 M HCl, about -0.1 V.

The results suggest that the +2 state of mendelevium is more stable than the dispositive state of ytterbium, and even of europium. The substantially greater ease of reduction of Md than of Es affords a basis for a rapid and efficient separation of the elements as shown by the reduction experiments. The Md^{3+} can be separately reduced, for instance by zinc, using a Jones' Reductor, to Md^{2+}, while Es and Fm remain in the 3+ state.

Footnotes and References

†Condensed from paper submitted to J. Inorg. Nucl. Chem.

*Permanent address: The Nuclear Research Institute of Czechoslovak Academy of Sciences, Řež u Prahy, Czechoslovakia.

1. J. Malý and B. B. Cunningham, Inorg. Nucl. Chem. Letters 3, 445 (1967).
2. E. K. Hulet, R. W. Lougheed, J. D. Brady, R. E. Stone, and M. S. Coops, Science 158, 486 (1967).
3. J. Malý, Inorg. Nucl. Chem. Letters 3, 373 (1967).
4. Jaromír Malý, Lawrence Radiation Laboratory Report UCRL-17987, December 1967.
5. J. K. Marsh, J. Chem. Soc. 398 (1942).
6. J. K. Marsh, J. Chem. Soc. 523 (1942).
7. J. K. Marsh, J. Chem. Soc. 8 (1943).
8. J. K. Marsh, J. Chem. Soc. 531 (1943).
9. F. David and G. Bouissières, Bull. Soc. Chim. France, 1001 (1965).
10. F. David and G. Bouissières, Inorg. Nucl. Chem. Letters, in press.
11. E. I. Onstott, J. Am. Chem. Soc. 78, 2070 (1956).
12. W. Noddack and A. Brukl, Angew. Chem. 50, 20, 302 (1937).
13. G. T. Seaborg, J. J. Katz, and W. M. Manning, The Transuranium Elements, Part II, National Nuclear Energy Series, Vol. 14B, McGraw-Hill Book Company, Inc., New York, 1949), Paper 21.1.
14. J. J. Lingane, Electroanalytical Chemistry, Second Edition (Interscience Publishers, Inc., New York, 1964).
15. E. I. Onstott, J. Am. Chem. Soc., 81, 4451 (1959).
16. J. K. Marsh, Syn. 5, 22 (1957).

Table I. Sodium amalgam extraction of actinides and separation with $EuCl_2$ - $SmCl_3$ by conc. HCl.

Element	^{237}Np	^{239}Pu	^{241}Am	^{246}Cm	^{252}Cf	^{253}Es	^{255}Fm	^{256}Md
A. 15 λ 1 M HCl added before extraction:								
% extracted into sodium amalgam	4.0	5.3	5.65	6.8	58.1	89	≈100	≈ 95
% in $EuCl_{2(s)}$	0.33	0.37	0.25	0.15	1.5	1.4	3.1	≈ 85
% in Sm^{3+} fraction	3.6	4.9	5.9	6.6	56.6	87.5	97	≈ 10
B. 75 λ 1 M HCl added before extraction:								
% extracted into sodium amalgam	18.2	19.3	20.6	12.0	96.2	≈100	≈100	≈100
% in $EuCl_{2(s)}$	1.0	0.95	4.7	0.65	5.6	2.6	4.4	97
% in Sm^{3+} fraction	17.2	18.3	15.9	11.3	90.5	97.4	95.6	3

Table II. Results of reduction of Md.

Reducing ion	Precipitate	Reduction potential (volts)	Corresponding reaction	Experiment No.	$\frac{R_{Md}Md(t_{sep})}{Fm(t_{sep})}$ of input	$\frac{R_{Md}Md(t_{sep})}{Fm(t_{sep})}$ of reduction	Enriching factor in precipitate
$Zn + Eu^{3+}$ (Jones' Reductor)	$EuSO_4$	-0.763	$Zn^{2+} + 2e \rightarrow Zn$	1	0.6	19.0	31.7
				2	0.22	4.0	18.2
				3	1.00	90.0	90.0
Eu^{2+}	$EuSO_4$	-0.43	$Eu^{3+} + e \rightarrow Eu^{2+}$	1	0.21	5.25	25.0
				2	0.25	5.0	20.0
				3	2.00	35.0	17.5
Cr^{2+}	$BaSO_4$	-0.41	$Cr^{3+} + e \rightarrow Cr^{2+}$	1	0.15	1.54	10.3
				2	0.086	3.0	34.8
V^{2+}	$BaSO_4$	-0.255	$V^{3+} + e \rightarrow V^{2+}$	1	0.107	2.0	18.6
				2	0.67	9.0	13.4
				3	0.28	5.7	20.4
Ti^{3+}	$BaSO_4$	-0.09	$TiOCl^+ + 2H^+ + 3Cl^- + e \rightarrow TlCl_4 + H_2O$	1	0.26	0.8	3.1
				2	0.24	1.15	4.8

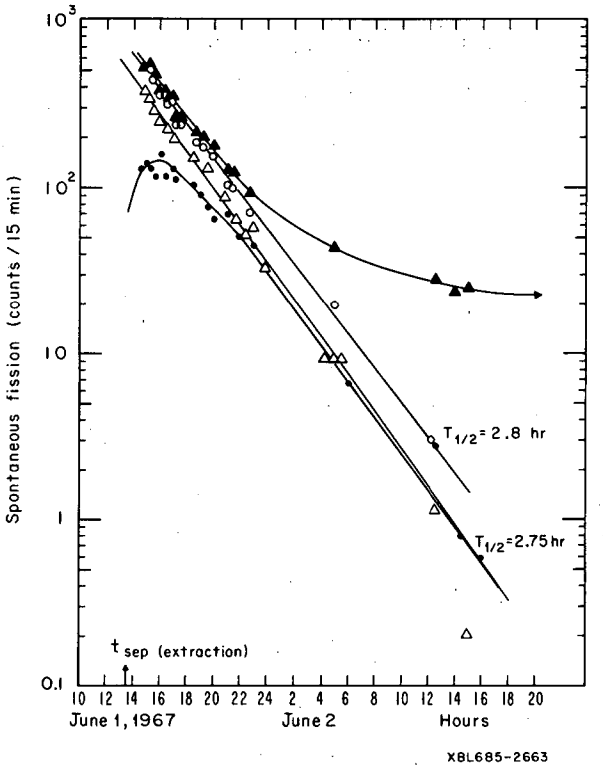

Fig. 1. Spontaneous fission activity present in the $EuCl_2$ fraction (precipitate) and the $SmCl_3$ fraction (supernatant). The SF data for the $EuCl_2$ fraction are represented by ●●●; the data for the $SmCl_3$ fraction by ▲▲▲, the $SmCl_3$ data corrected for background by ooo. A small amount of the "stock Md" solution is represented by ΔΔΔ.

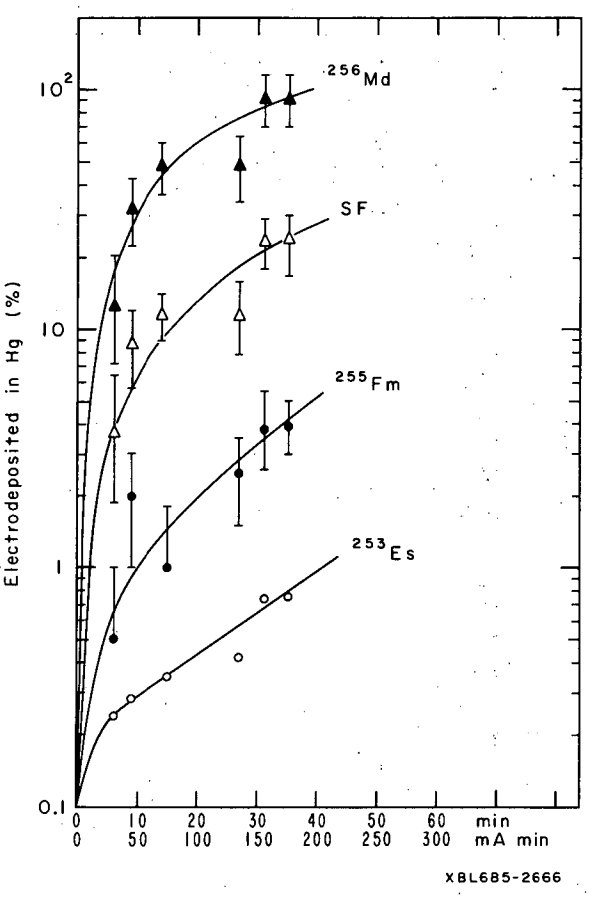

Fig. 2. Percentage of actinide tracers electrodeposited in mercury as a function of time and passed charge. Current density used in this experiment was 5 mA/cm^2.

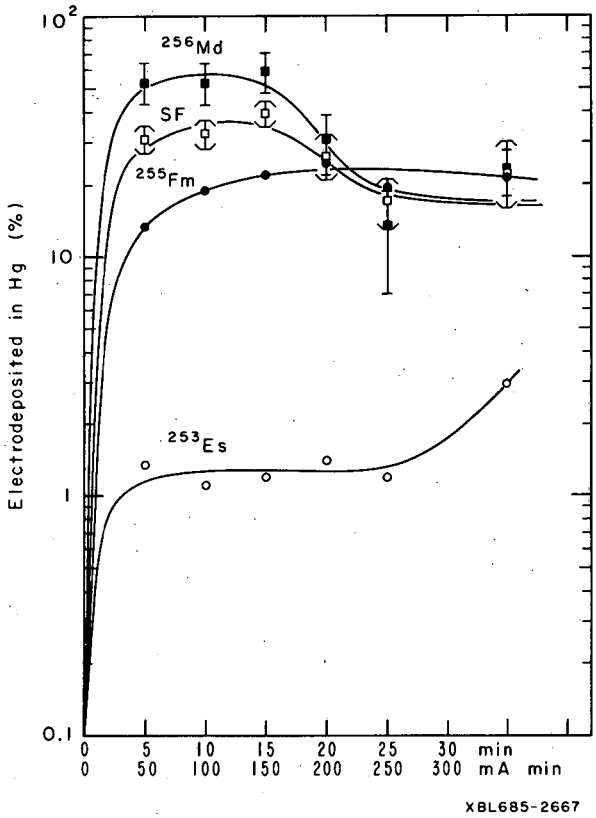

Fig. 3. Percentage of actinide tracers electrodeposited in mercury as a function of time and passed charge. Current density used in this experiment was 10 mA/cm^2.

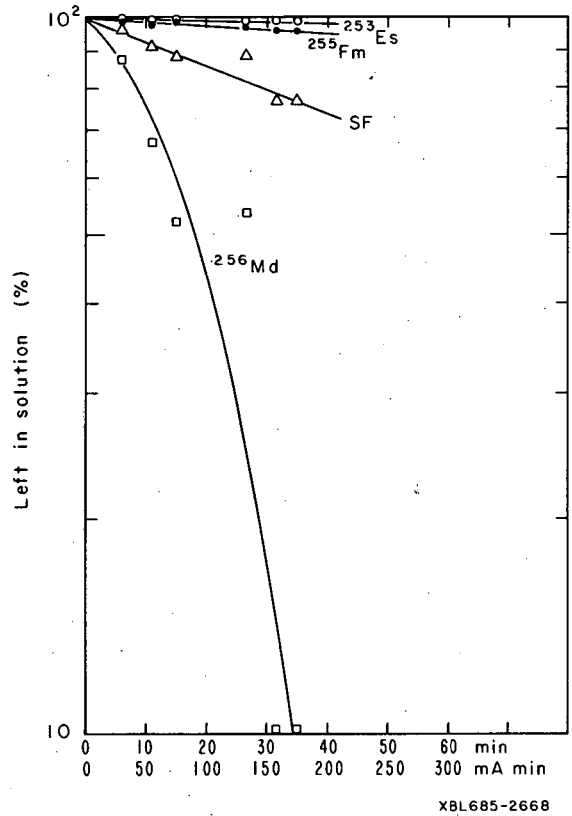

Fig. 4. Percentage of actinide tracers left in solution as a function of time and passed charge (5 mA/cm^2).

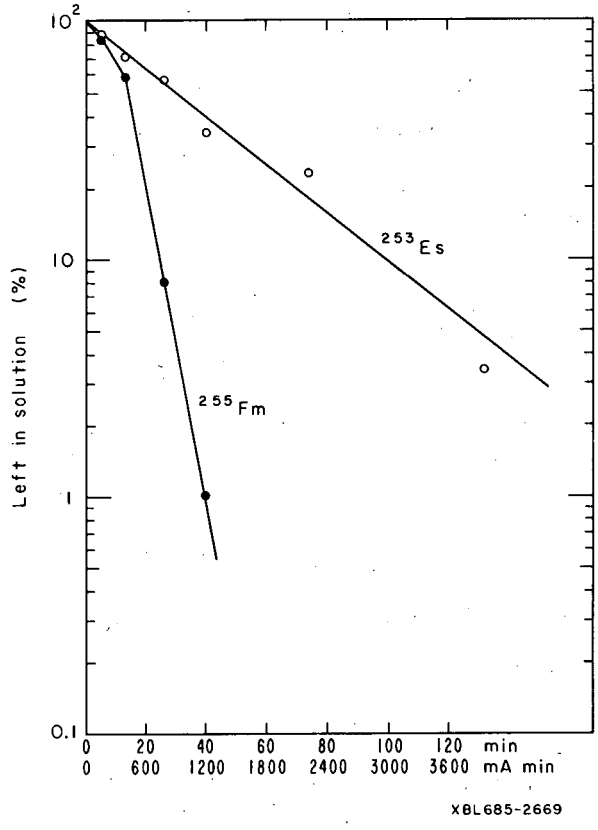

Fig. 5. Percentage of actinide tracers left in solution as a function of time and passed charge. Current density used in this experiment was 30 mA/cm^2.

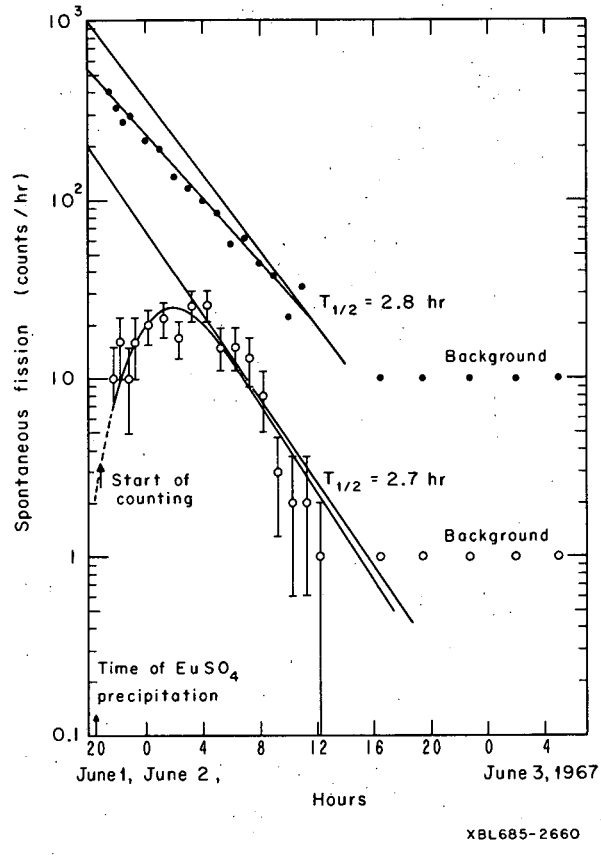

Fig. 6. Decay curves for the original solution and the $EuSO_4$ fraction, o. The reducing agent used was amalgamated zinc.

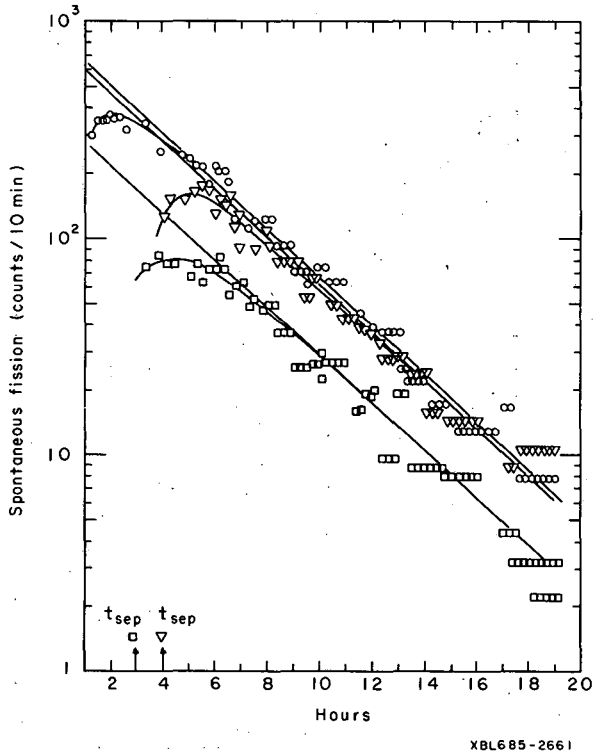

Fig. 7. Decay curves for the original solution, o, and the $BaSO_4$ fraction, ▽ , □ . The reducing agent used was Cr^{2+}.

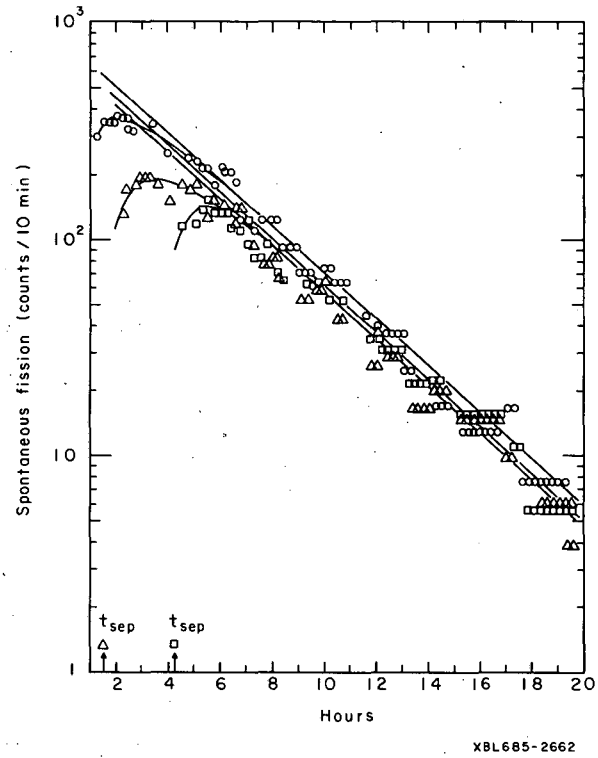

Fig. 8. Decay curves for the original solution, o, and the $BaSO_4$ fraction, △ , □ . The reducing agent used was V^{2+}.

Fig. 9. Decay curves for the original solution, △, and the $BaSO_4$ fraction, o. The reducing agent used was Ti^{3+}.

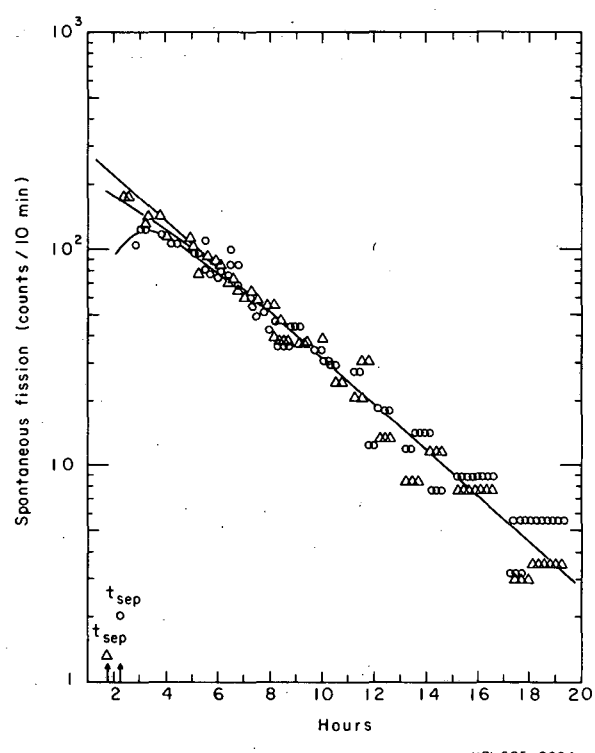

NOBELIUM: TRACER CHEMISTRY OF THE DIVALENT AND TRIVALENT IONS†

Jaromír Malý,* Torbjørn Sikkeland,‡
Robert Silva, and Albert Ghiorso

Three-minute ^{255}No was produced by irradiation of a plutonium target, 0.8 mg/cm^2 thick and supported by a 25.4-μ Be foil, with ^{16}O ions from the Berkeley Hilac. The isotopic composition of the target was (atom %) ^{244}Pu, 74.21; ^{242}Pu, 25.32; ^{241}Pu, 0.094; ^{240}Pu, 0.312; ^{239}Pu, 0.064; and ^{238}Pu, 0.002. The beam current was 2 to 4 μA over an area of 0.2 cm^2. The nobelium atoms recoiling from the target were stopped in helium and transferred to a platinum catcher foil by gas jet.[1,2] The ^{255}No was identified by its alpha-decay energy. The maximum yield was obtained at an oxygen-ion energy of approximately 97 MeV, as expected for the reaction ^{244}Pu (^{16}O, 5n)^{255}No.

The first evidence of unexpected behavior for No was found during cathodic-electrodeposition experiments using standard procedures;[3] the No atoms were washed from the catcher foil with a saturated NH_4Cl plating solution containing tracer quantities of the radioactive elements to be compared with the No. The pH during plating is very high near the cathode, and tracers are deposited in approximately inverse proportion to the solubilities of their hydroxides; Table I shows the percentages of tracers and nobelium that were plated,[4] together with the number of ^{255}No alpha decays observed per number of decays expected. The latter was computed for each experiment from the average number of countable atoms by allowing for decay during the chemical operations. The fact that No is plated with a low yield suggests hydroxide solubility similar to that of Ra rather than the other actinides.

Our attempts to elute No from a heated (80 °C) Dowex-50 X 12 column of ion-exchange resin with ammonium alpha-hydroxyisobutyrate in the predicted pre-einsteinium elution position[5] were unsuccessful. The elution was carried out in two fractions: five column volumes of dilute elutriant (0.3 M, pH 4.0), followed by an equal volume of concentrated elutriant (1.9 M, pH 4.8). The results (Table I) clearly show that No does not elute before Es.

An elution position for No relative to tracer quantities of Y, Sr, Ba, and Ra was obtained for a heated (80 °C) column, 0.2 cm in diameter by 2 cm long, with the concentrated elution solution. The composite result for 13 experiments appears in Fig. 1. Under these conditions nobelium does not exhibit the slightest resemblance to the +3 actinides. In similar tracer experiments, Es, Cm, Am, and Ac were eluted in the Y position, which is promptly after the first free column volume; the same was true for Th, Pa, Pb, and Ce.

For study of the coprecipitation behavior of nobelium fluoride we used the residue-adsorption technique.[6] A drop of 0.1 M HCl containing the tracers with which No was to be compared, plus about 5 μg of each of the various charge-state carriers Ba, La, and Zr, was used to dissolve the No atoms from the catcher foil. Two drops of 40% HF was added for conversion to the fluorides, and the solution was taken to dryness. The plate was then washed with H_2O, and both residue plate (LaF_3 fraction) and H_2O washes (BaF_2 fraction) were analyzed. The results (Table I) suggest that the solubility of nobelium fluoride is more like that of BaF_2 than of LaF_3.

Assuming that the nobelium was exhibiting a +2 valence under the above conditions, we attempted to oxidize the No^{2+} to No^{3+}, which should form a less soluble fluoride. The procedure was the same as that just described except that the oxidant ceric nitrate was substituted for the Zr. After oxidation with Ce^{4+} the distribution was in favor of the LaF_3 phase (Table I).

Yttrium-90 can be separated from ^{90}Sr at room temperature by elution from a $SrSO_4$ column with H_2SO_4.[7] Generally the more soluble sulfates are eluted before the less soluble ones. We used a similar column for study of the behavior of nobelium sulfate; in each experiment the No, tracer activities with which No was to be compared, and about 5 μg each of Zr and La were converted to the sulfate form on the platinum catcher foil and transferred to the column in the elutriant, 6 M H_2SO_4. The mass of Zr and La added was the same as the mass of Ce^{4+} and Ce^{3+} used in later oxidation experiments, in order to duplicate the mass effects on the column. The elution from a column 0.2 cm in diameter by 1 cm long was carried out in two fractions; the results (Table I) show No to be more strongly adsorbed on the column than are Es and Am.

Similar experiments under oxidizing conditions used Ce^{4+} (Table I); the No was eluted with

Es and before Am. This apparent change in solubility of nobelium sulfate is consistent with a change in valence state from +2 to +3.

These tracer experiments show that the divalent ion is the most stable species for nobelium in aqueous solution; thus the element exhibits chemical behavior substantially different from those of the other actinides. This finding appears to confirm Seaborg's prediction[8] in 1949 of a possible stable +2 state for element 102, due to the special stability of the $5f^{14}$ electronic configuration.

We thank B. B. Cunningham for suggestions, T. Bowman for help in preparation of the Pu target, and the Hilac crew. One of us (J. M.) thanks the International Atomic Energy Agency, Vienna, for a research grant.

Footnotes and References

†Condensed from Science 160, 1114 (1968).

*Present address: Paris, France.

‡Present address: Norsk Hydro's Institute for Cancer Research, Oslo, Norway.

1. A. Ghiorso, T. Sikkeland, and M. J. Nurmia, Phys. Rev. Letters 18, 11 401 (1967).
2. A. Ghiorso and T. Sikkeland, Phys. Today 20, 25 (1967).
3. G. R. Choppin, Experimental Nuclear Chemistry (Prentice-Hall, Englewood Cliffs, New Jersey, 1961).
4. In this and subsequent experiments the probable error is less than 10% of the tracer percentages.
5. G. T. Seaborg, in The Transuranium Elements (Yale University Press, New Haven, Connecticut, 1958).
6. H. W. Kirby, J. Inorg. Nucl. Chem. 25, 483 (1965); 27, 1700 (1965).
7. H. Hamoguchi, N. Onuma, T. Watanabe, and R. Kuroda, Nature 211, 1295 (1965).
8. G. T. Seaborg, J. J. Katz, and W. M. Manning, in The Transuranium Elements, National Nuclear Energy Series, Vol. 14B (McGraw-Hill, New York, 1949), part 4, paper 21.1.

Table I. Summary of results of experiments with electrodeposition cation-exchange columns, and coprecipitation.

Fraction drops (No.)	Oxidizer	Percentages in fractions ^{253}Es	^{243}Am	^{223}Ra	^{255}No	Counts of No (obs/pred)
		Electrodeposition				
Electrodeposited	None	43	48	4	4±2	2/76
		Cation-exchange column				
0.3 M butyrate	None	43	6	< 0.1	2±1	1/113
1.9 M butyrate	None	0	59	< .1	65±12	52/80
		Fluoride coprecipitation				
LaF_3	None		60	15	7±3	6/98
BaF_2	None		11	37	56±10	48/87
LaF_3	Ce^{4+}		34	18	48±8	63/134
BaF_2	Ce^{4+}		17	33	31±6	35/117
		Strontium sulfate column				
1-10	None	38	10	<1	2±1	1/122
11-22	None	5	36	<1	13±4	9/75
1-10	Ce^{4+}	47	3	<1	58±10	54/94
11-22	Ce^{4+}	3	28	<1	5±3	3/74

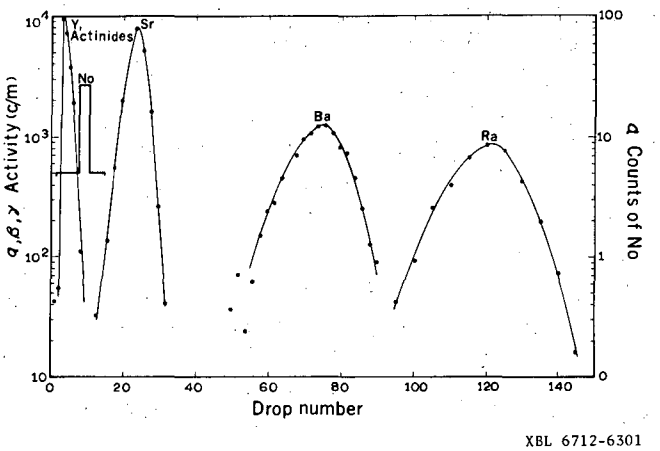

Fig. 1. Elution of nobelium from a heated (80 °C) Dowex-50 X 12 cation-exchange column with 1.9 M ammonium α-hydroxisobutyrate (pH 4.8).

DETERMINATION OF THE No(II) — No(III) POTENTIAL FROM TRACER EXPERIMENTS†

R. J. Silva,* T. Sikkeland,‡ M. Nurmia, A. Ghiorso, and E. K. Hulet††

Only very recently has an isotope of element 102, ^{255}No (Refs. 1-3), of sufficiently long half-life (3 min) become available in sufficient quantity (50 to 100 atoms per experiment) so that information about its tracer chemical behavior could be obtained from average behavior observed during repetitive series of experiments.[4] Ion exchange and coprecipitation studies showed nobelium to behave in aqueous solution like a divalent alkaline earth element rather than a trivalent rare earth element as expected. However, after oxidation with ceric ions, nobelium appeared to behave like a trivalent actinide. The experiments described in this work were conducted in order to estimate the value of the oxidation potential of the No(II)–No(III) couple in aqueous solution.

The ^{255}No was produced by irradiation of a 0.8-mg/cm^2 thick ^{244}Pu target with 97-MeV ^{16}O ions from the Berkeley Hilac. The details of the experimental procedures and system have been described in Ref. 4. The ^{255}No was identified from the emission of 8.1-MeV α particles and from its 3-min half-life.

The distinction between No(II) and No(III) was made on a few-atoms-at-a-time basis by multiple solvent extractions with di(2-ethylhexyl) orthophosphoric acid (HDEHP), using the column elution technique of extraction chromatography.[5] In this method, the aqueous phase is passed through an inert Kel-F powder bed on which the extractant HDEHP has been adsorbed; the HDEHP behaves much like a liquid cation exchanger in that its ionizable hydrogen atoms can be replaced by other positive ions. In ≈ 0.1 M acid, mono- and divalent metal ions are poorly adsorbed by the extractant,[6] and pass through the column in a few column volumes, whereas tri- and tetravalent ions are strongly adsorbed in the extractant and are not eluted from the column.

In our experiments, the nobelium recoil atoms were dissolved from a platinum catcher foil with ≈ 1 column volume (3 drops) of a dilute acid solution containing an oxidizing agent and tracer quantities of ^{252}Cf(III) and ^{244}Cm(III). Tracer ^{213}Ra(II), produced by the (^{16}O, αxn) reactions from lead impurity in the target, was useful for comparison with the behavior of divalent nobelium. The tracers were used also as a check on proper column operation and chemical yield. After dissolution and oxidation by heating at 80 to 100 °C for ≈ 1 min, the solution was passed through a column bed 2 mm in diameter by 2 cm long. In the case of the oxidants HIO_3 and CrO_3, the solution was evaporated to near dryness to obtain a high acid concentration found necessary for oxidation of the Tl. The solution was then diluted to ≈ 0.1 M in the oxidant with 0.1 M HNO_3 before transfer to the column. The 3+ ions were recovered by elution with 2 to 3 column volumes of 3 M HNO_3. The 0.1 M and 3 M HNO_3 fractions were collected on platinum disks and evaporated

to dryness, and the number of α particles with energies between 5.4 and 9 MeV were measured with a gridded ionization chamber. The average time necessary for the chemical procedures was ≈ 5 min.

Table I shows the analysis of the tracers in the extracted phase for each set of oxidizing conditions together with the standard potentials of the oxidants. Also shown for comparison are the results of identical experiments performed with ^{204}Tl and ^{144}Ce which were carried out during or immediately following the nobelium experiments.

The data for No, Tl, and Ce are also shown in Fig. 1.

So far as extraction indicates oxidation from the 2+ to 3+ valence state, the results show nobelium to be oxidized appreciably by solutions of periodate, bromate, and peroxysulfate-silver, but only slightly, if at all, by dichromate, iodate, and nitrate. The comparison made in Table I of the percent oxidation of Ce(III) and Tl(I) under identical conditions suggests that the standard oxidation potential of the No(II)—No(III) couple in aqueous solution lies between that of the Tl(I)–Tl(III) and Ce(III)–Ce(IV) couples. Our best estimate for the potential of the half-reaction, No(II) = No(III) + e^-, is $E^0 \approx -1.4$ to -1.5 volts.

The plutonium used in these experiments was produced and made available through the National Transplutonium Program. We acknowledge the excellent machine operation and support of the Hilac operations staff.

Footnotes and References

†Condensed from paper to be submitted to J. Inorg. Nucl. Chemistry.

*Present address: Special Training Division, Oak Ridge Associated Universities, Oak Ridge, Tennessee 37830.

‡Present address: Norsk Hydro's Institute for Cancer Research, Oslo, Norway.

††Lawrence Radiation Laboratory, Livermore.

1. V. A. Druin, G. N. Alkapjev, A. G. Denier, Yu. V. Lobanov, B. V. Fefilov, G. N. Flerov, and L. P. Cheluokov, At. Energ. (USSR) 22, 127 (1967).
2. A. Ghiorso, T. Sikkeland, and M. J. Nurmia, Phys. Rev. Letters 18, 11, 401 (1967).
3. G. N. Flerov, S. M. Polikanov, V. L. Micheev, V. J. Iljuschenko, V. F. Kuschinruk, M. V. Miller, A. M. Sukhov, and V. A. Schegolev, Yadern. Fiz. 5, 1186 (1967).
4. J. Malý, T. Sikkeland, R. J. Silva, and A. Ghiorso, Science 160, 1114 (1968).
5. D. F. Peppard, E. P. Horwitz, and G. W. Maxon, in Rare Earth Research, J. F. Nachman and C. E. Lundin, Eds. (Gordon and Breach, New York, 1962), p. 15.
6. E. K. Hulet, J. Inorg. Nucl. Chem. 4, 334 (1957).

Table I. Analysis of tracers in extracted phase

Conditions for oxidation	Standard potential of oxidant (volts)	Extracted by HDEHP column (%)						Total number of No events observed
		Cf	Cm	Ra	Tl	Ce	No	
≈ 0.1 M HNO_3	-0.94	> 91	92	1	4	1	7±3	72
≈ 0.1 M HIO_3 [a]	-1.20	> 87	93	2	58	---	6±3	59
≈ 0.1 M CrO_3 [a]	-1.33	> 94	89	1	63	---	22±8	50
≈ 0.1 M $HBrO_3$	-1.52	> 96	71	4	99	5	56±10	68
≈ 0.25 M H_5IO_6	-1.6	> 90	88	2	97	28	86±12	73
≈ 0.1 M $(NH_4)_2S_2O_8$ + 0.1 M HNO_3 [b]	-2.01	> 89	77	2	92	79	69±10	72

a. Evaporated to near dryness.
b. + Trace Ag.

Fig. 1. Distribution ratio of No, Tl, and Ce between HDEHP and 0.1 M acid vs standard potential of the oxidant used.

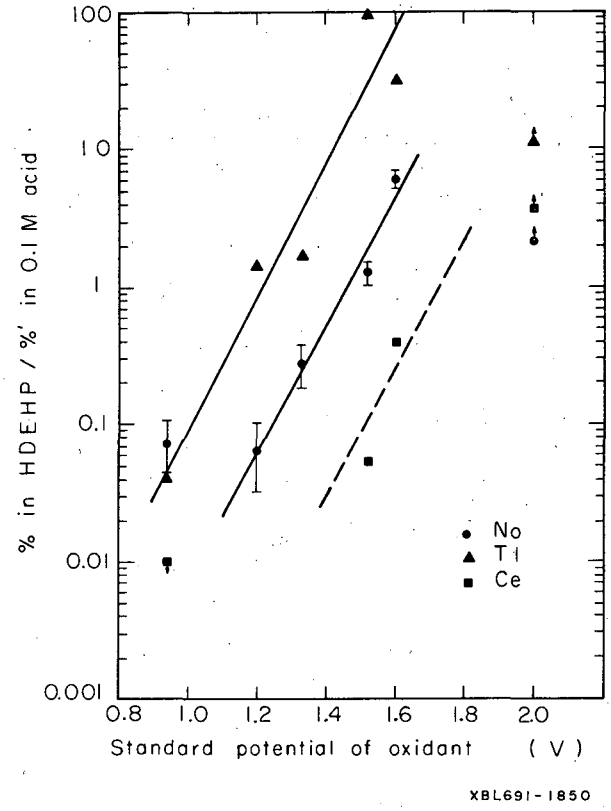

TRACER CHEMISTRY OF LAWRENCIUM†

Robert Silva,* Matti Nurmia, Torbjørn Sikkeland,‡ and Albert Ghiorso

The recent discovery of ^{256}Lr, with half-life of 35 sec and alpha energy of 8.3 to 8.6 MeV, has made it possible to carry out tracer chemical experiments to determine the oxidation state of element 103 in aqueous solution. Approximately 1000 atoms of ^{256}Lr were produced for study in nearly 150 individual experiments by the irradiation of a ^{249}Cf target with ^{11}B ions from the Berkeley Hilac.

A very fast solvent-extraction procedure using 100 λ of 0.2 M TTA in methyl isobutyl ketone as the organic phase and 100 λ of acetic acid and sodium acetate buffer solution as the aqueous phase was designed to distinguish between the 2+, 3+, and 4+ oxidation states. The distribution of actinides between the phases takes place very rapidly, and nearly complete extraction can be obtained in only 10 sec. The entire procedure, from beam off to counting, required only from 45 to 60 sec.

Figure 1 shows the percent extracted from the aqueous phase into the organic phase as a function of the pH of the aqueous phase for a number of transuranium and alkaline earth elements (solid lines) and for element 103 (points with error bars).

Similar experiments were also carried out with tracer quantities of a number of lanthanide elements, and, by analogy with the lanthanide behavior, one would expect Lr(III) to extract at about the same pH as Cf(III) and Fm(III). The data shown in Fig. 1 indicate that the most stable species for lawrencium in aqueous solution is 3+, as expected for the last member of the actinide series.

Footnotes

†Summary of UCRL-18713, Jan. 1969.

*Present address: Special Training Division, Oak Ridge Associated Universities, Oak Ridge, Tennessee 37830.

‡Present address: Norsk Hydro's Institute for Cancer Research, Oslo, Norway.

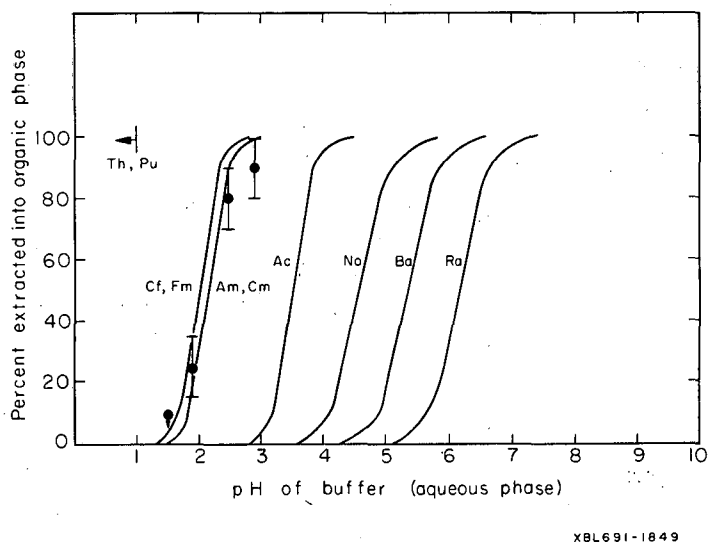

Fig. 1. TTA extraction behavior of Lr (points) compared with that of some other actinides and alkaline earths.

PREPARATION AND CRYSTAL STRUCTURES OF DICESIUM BERKELIUM HEXACHLORIDE AND DICESIUM SODIUM BERKELIUM HEXACHLORIDE†

L. R. Morss and J. Fuger*

Cerium and berkelium(III) and (IV) have similar redox potentials in aqueous solution, and their crystal chemistries are also similar. Although Ce^{4+} oxidizes Cl^- in aqueous solution, and although no simple tetrachloride of cerium exists, solutions of Ce^{4+} in concentrated aqueous HCl are remarkably stable and intensely red, presumably due to the presence of the complex ion $CeCl_6^{2-}$. Further, addition of large monovalent ions such as Cs^+ or $N(CH_3)_4^+$ to such solutions results in the precipitation of complex compounds.

Being familiar with the preparation of Cs_2CeCl_6, we planned to synthesize and characterize the corresponding Bk compound. As a preliminary to the proposed synthesis, techniques were developed to prepare Cs_2CeCl_6, starting with 1 μg of Ce. X-Ray powder patterns of the Ce precipitate showed it to be Cs_2CeCl_6.

^{249}Bk was available for preliminary experiments, with about 20% of its decay daughter, ^{249}Cf, present. Further experiments were carried out using Bk recently purified by alpha-hydroxyisobutyric acid cation-exchange columns and cation "clean-up" columns. Bk solutions were prepared in 2 M H_2SO_4 in a concentration of 1 μg/μl.

Cs_2BkCl_6 was prepared using 1, 5, and 40 μg of Bk. $NaBrO_3$ was added to the Bk solution

and the solution heated to boiling to oxidize the Bk; green-yellow $Bk(OH)_4$ was then precipitated with aqueous NH_3. About 20% excess of CsCl in concentrated HCl was added with cooling to the centrifuged hydroxide. The red-orange precipitate of Cs_2BkCl_6 was then centrifuged and washed with glacial acetic acid and diethyl ether.

An identical experiment performed under nonoxidizing conditions gave a precipitate whose powder pattern was similar to $Cs_2NaAmCl_6$.[1] Subsequent experiments, including one with excess hydroxylamine present as reducing agent, precipitated $Bk(OH)_3$ and then $Cs_2NaBkCl_6$ by adding slight excesses of CsCl and NaCl. With hydroxylamine present, both the hydroxide and chlorocompound were white; without hydroxylamine, the hydroxide was pale green and the chlorocompound yellow, presumably due to air oxidation of the hydroxide.

X-Ray powder patterns were generally taken by mounting the capillary-tip reaction microcone itself as an x-ray capillary. Cs_2BkCl_6 is not isomorphous with Cs_2CeCl_6 (which is trigonal),[2] but is hexagonal, space group $P6_3mc$. Lattice parameters are $a = 7.451 \pm 6$, $c = 12.097 \pm 9$ Å. The structure is similar to that of Cs_2CeCl_6, doubling the c axis with alternate layers rotated 180 deg about sixfold screw axes. Figure 1 is a projection of the unit cell upon the $a\ b$ plane. $Cs_2NaBkCl_6$ is isostructural with $Cs_2NaAmCl_6$: space group Fm3m, $a = 10.805 \pm 3$ Å.

The 40-μg preparations of $Cs_2Bk\ Cl_6$ were used for chemical analyses. Samples were weighed in quartz buckets on a quartz fiber torsion balance to ± 0.02 μg, then were titrated potentiometrically for Bk(IV) with standard Fe^{2+} and for Cl^- with standard Ag^+. They were then assayed for total Bk by counting the alpha growth of ^{249}Cf ($t_{1/2}$ = 345 years).[3] Anal. Calcd for Cs_2BkCl_6: Bk, 34.2; Cl, 29.24. Found: total Bk, 31.6; Bk(IV), 29.9; Cl, 27.8. The analytical results indicate the presence of about 7 wt % of CsCl, but clearly prove that the Bk was present in the tetravalent state. These experiments have demonstrated that aqueous Bk(IV) chlorocomplex ions such as $BkCl_6^{2-}$ are at least as stable thermodynamically (toward dissociation or reduction) as the corresponding Ce(IV) ions.

Footnotes and References

†Condensed from Inorganic Chemistry to be published.

*Permanent address: Laboratory of Nuclear Chemistry, University of Liège, Liège, Belgium.

1. K. W. Bagnall, J. B. Laidler, and M. A. A. Stewart, J. Chem. Soc. Sect. A, 133 (1968).
2. T. Kaatz and M. Marcovich, Acta Cryst. 21, 1011 (1966).
3. J. Milsted, E. P. Horwitz, A. M. Friedman, and D. N. Metta, J. Inorg. Nucl. Chem., in press.

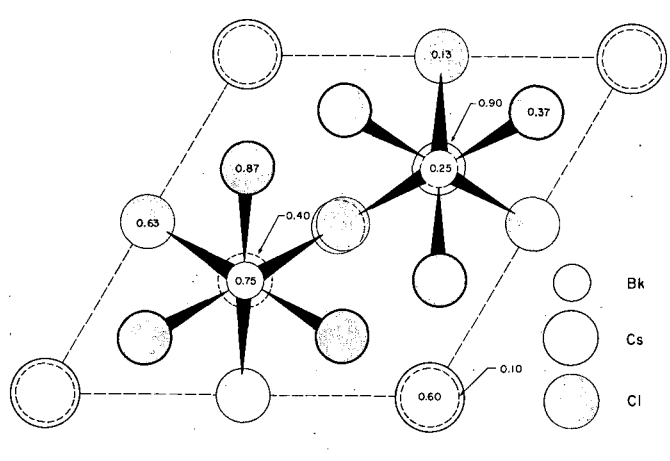

Fig. 1. Projection of unit cell of Cs_2BkCl_6 upon $a\ b$ plane.

PREPARATION AND CRYSTAL STRUCTURES OF SOME CUBIC CHLOROCOMPLEX COMPOUNDS OF TRIVALENT METALS

L. R. Morss, N. Edelstein, and M. Siegal†

Many compounds of the general composition $L_xM_yX_{3x}$ are known to exist in crystal structures of high symmetry.[1] In general, the ions L and X are of similar radius and form close-packed "planes," with smaller ions X filling some of the octahedral holes between "planes." Some examples of such compounds are shown in Table I.

The recent preparation of $Cs_2NaAmCl_6$[2] and $Cs_2NaBkCl_6$[3] encouraged us to synthesize similar compounds for other large trivalent cations. Since these ions are in sites of cubic symmetry (surrounded by an octahedron of Cl^- nearest neighbors with Na^+ at the corners of a cube such that the M^{3+}-Na^+ distance is about $\sqrt{3}$ that of the M^{3+}-Cl^-), these compounds might be valuable as matrices for the study of trivalent ions in cubic sites. We began with the lanthanide element of smallest ionic radius, hoping that the complex $LuCl_6^{3-}$ might exist in appreciable enough concentration in concentrated aqueous HCl to precipitate out the compound $Cs_2NaLuCl_6$. This compound was indeed formed (with some NaCl, which also is quite insoluble in concentrated HCl). We found that this compound, as well as the corresponding one for other lanthanides, could be prepared by evaporating a solution of the metal ions in aqueous HCl to dryness. (For La and Ce, the dried material had to be melted and resolidified to yield identifiable powder patterns.) These compounds for all lanthanide elements appeared to be air-stable for at least several hours, even as finely divided powders. Most of these compounds melt in air without decomposition.

Isomorphous compounds have been prepared with several other trivalent ions replacing the lanthanide ion; the smallest trivalent ion with which we have succeeded is Cr^{3+} and the largest is La^{3+}. (No recognizable compound was precipitated with Pu^{3+}, but an anhydrous synthesis will be attempted.) $Cs_2NaBiCl_6$ can be recrystallized from dilute HCl by cooling or evaporation; crystals of this compound larger than 1 mm on a side have been prepared. These crystals are octahedra, and as expected for the cubic system are optically isotropic. Their index of refraction is greater than 1.74.

All compounds synthesized to date and identified by x-ray powder diffraction have been listed in Table II. All are face-centered cubic; observed intensities agree with those calculated for space group Fm3m, with atomic positions as follows: 4 M^{3+} (a), 4 Na (b), 8 Cs (c), 24 Cl (e). There are four formula units per unit cell.

The cubic lattice parameters have been plotted vs ionic radii of M^{3+} in Fig. 1. These radii[4] are those derived for sixfold coordination in oxides. The observed change of lattice parameter with crystal radius is remarkably linear ($\Delta a/\Delta r = 1.52$). If a hard-sphere model, such as the unit-cell face of Fig. 2, were correct, the lattice parameter would be

$$a = 4r_{Cl^-} + 2r_{Na^+} + 2r_{M^{3+}}$$

$$da/dr_{M^{3+}} = 2.$$

For this model, the lattice parameter would cease to change when the radius of M^{3+} became so small that chloride-chloride contact was reached (at $r_{M^{3+}} = 0.72$ Å). This does not occur, since observed lattice parameters are about 3% smaller than those calculated by summing ionic radii, and because $\Delta a/\Delta r_{M^{3+}} \neq 2$, the hard-sphere model is quite inadequate.

Footnotes and References

†Undergraduate Summer Visitor, 1968.

1. A. F. Wells, Structural Inorganic Chemistry (Oxford, London, 1962), p. 374 ff.
2. K. W. Bagnall, J. B. Laidler, and M. A. A. Stewart, J. Chem. Soc. Sect. A, 133 (1968).
3. L. R. Morss and J. Fuger, preceding paper.
4. R. D. Shannon and C. T. Prewitt, Acta Cryst. (in press).

Table I. Some examples of compounds of general composition $L_xM_yX_{3x}$.

Compound	M	Crystal system	a	c	Stacking
Cs_2PtCl_6	Pt	Cubic	10.192		ABCABC
Cs_2PuCl_6	Pu	Trigonal	7.44	6.04	ABAB
Cs_2BkCl_6	Bk	Hexagonal	7.451	12.097	ABACABAC
$Cs_2NaBkCl_6$	Na, Bk	Cubic	10.805		ABCABC
$(NH_4)_3AlF_6$	Al 1/3 of NH_4	Cubic	8.92		ABCABC
K_2NaAlF_6	Na, Al	Cubic	8.093		ABCABC
$Cs_3Tl_2Cl_9$	Tl	Hexagonal	12.8	18.3	ABAB
$RbCaF_3$	Ca	Cubic	4.452		ABCABC

Table II. Compounds synthesized to date and identified by x-ray powder diffraction.

Compound	Trivalent metal ionic radius[a]	Lattice parameter
$Cs_2NaCrCl_6$	0.615	10.28
$Cs_2NaFeCl_6$	0.645	10.33
$Cs_2NaTlCl_6$	0.67	10.40
$Cs_2NaScCl_6$	0.73	10.49
$Cs_2NaTlCl_6$	0.88	10.62
$Cs_2NaLuCl_6$	0.848	10.65
Cs_2NaYCl_6	0.892	10.73
$Cs_2NaGdCl_6$	0.938	10.79
$Cs_2NaBkCl_6$	0.96	10.805
$Cs_2NaEuCl_6$	0.950	10.81
$Cs_2NaBiCl_6$	1.02	10.84
$Cs_2NaAmCl_6$	1.01	10.86
$Cs_2NaNdCl_6$	0.995	10.89
$Cs_2NaPrCl_6$	1.013	10.91
$Cs_2NaCeCl_6$	1.034	10.95
$Cs_2NaLaCl_6$	1.061	10.99

[a]From Ref. 4.

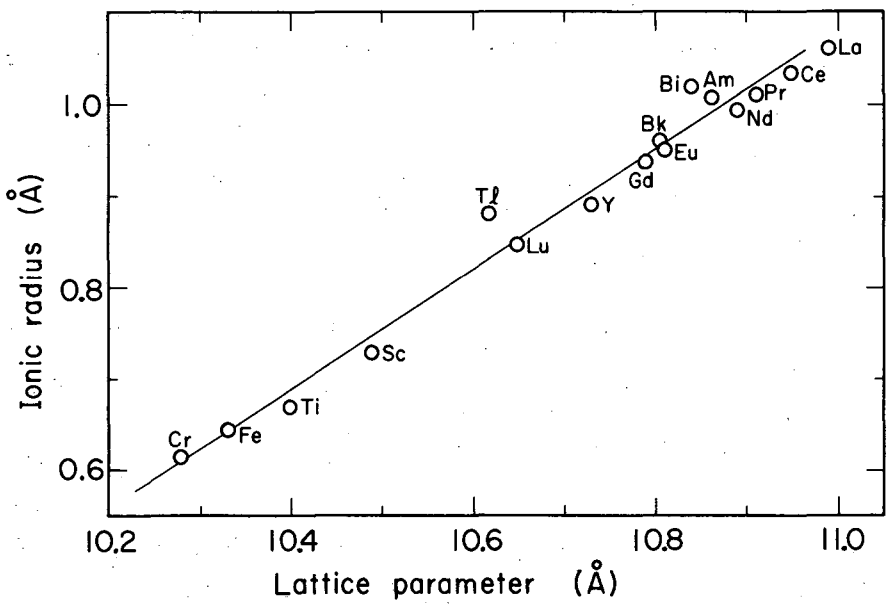

XBL693-2205

Fig. 1. Change of lattice parameter of Cs_2NaMCl_6 with M^{3+} ionic radius.

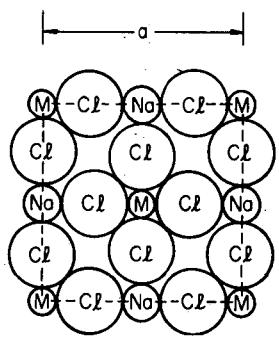

XBL693-2206

Fig. 2. Side of unit cell of $Cs_2NaM^3Cl_6$.

OXIDATION STATES OF U IN CaF_2

R. McLaughlin, N. Edelstein, U. Abed, and E. Huffman

When CaF_2 crystals are grown containing small amounts of U, crystals of many different colors are obtained. Brown, green, yellow, and red of various shades have all been reported.[1,2] Work described in this paper was undertaken in an effort to determine the oxidation states of the U ion responsible for the many different properties of these crystals. There are three general areas which would be expected to provide the explanation: the valence of the U ion, the charge compensation about the U ion, and solid solution formation (i.e., the U is incorporated into the crystal as UO_2).

As the color changes suggest, the spectral differences between different crystals is large. It has been demonstrated that effects of changing the charge compensation (site symmetry) have a small effect on the spectral characteristics when rare earths are incorporated into CaF_2.[3] No evidence of solid solution formation in this type of system was found in the literature, so the valence of the U ion seems the most likely explanation. There are still many possibilities, however, since U is known to exist in every valence state from 6+ to 3+; recently 2+ has also been suggested.[2]

The valence of U in these crystals is unknown, since a valence change occurs while the CaF_2:U melt is at a high temperature in the crystal-growing crucible. It has been reported,[1] for example, that if U is added as the metal, U^{4+} is found in the crystal, whereas if it is added as the tetravalent ion UF_4, it is found as the trivalent ion in the crystal. An attempt was made to avoid changing the valence of the U ion by performing the following experiment.

An acid solution of uranyl ion was reduced to U^{4+} by passing through a Pb reductor.[4] $CaCl_2$ was dissolved in the solution so that the U concentration was $\approx$ 5% of the Ca ion. Excess HF was added which coprecipitated the U and Ca as fluorides. It was felt that in this way there would be no question about the valence of the U ion that was incorporated into the CaF_2 lattice. After washing and drying a mull was made of the precipitate, and the absorption spectrum obtained is shown in Fig. 1.

The similarity between the spectrum of U^{4+} in CaF_2 and the green crystal of Ref. 2 is very apparent. In every case, where one material shows a group of absorption features, a corresponding group is shown by the other material. The spectrum of U^{4+} is known to be very sensitive to the crystal field that surrounds the ion.[5] The fact that there is not exact agreement between the two spectra could be explained by the presence of water molecules trapped at the next nearest neighbor site around the U^{4+} ions. An attempt to further dehydrate the material resulted in the formation of UO_2.

In order to further verify our assignment of the spectrum of the green crystal to U^{4+}, a chemical analysis was done on the reducing power of the U ion in the crystal, and also the total U content was determined. From these measurements the U valence state was ascertained. This was accomplished by dissolving a green CaF_2:U crystal in a solution which contained an excess of oxidizing agent known to take U to the 6+ state. If the amount of U in the sample was known and the amount of oxidizing agent that reacted was determined, then the initial valence of the U ion would be determined. In actual practice a $HClO_4$ solution containing Ce^{4+} as the oxidizing agent and an Fe^{3+} catalysis was used. The reducing power of the crystal was determined by back-titrating with Fe^{2+}, using Ferrion indicator.

Separate portions of the sample were used to determine total U content. The total sample was ground to a powder before any determination was made to insure that the U content would be homogeneous. The total U content of two portions of the sample was determined by neutron-activation analysis. A spectrophotometric method[6] was also used to determine total U of two other portions of the sample. All these results are summarized in Table I. The near agreement of values in column 3 with the value 2 makes it almost certain that the U ion was in the 4+ valence state before the crystal was put into solution.

There seems little need to question the valence of U in the red crystals. Much work has been done with these crystals and all of it has been consistent with the assumption the U is in the 3+ state. It is planned to apply this same approach to yellow and brown crystals in the future.

It is a pleasure to acknowledge the help of Helen Michel and Frank Asaro, who performed the neutron-activation analysis. Discussions with John G. Conway and Burris Cunningham were invaluable. The crystals were generously supplied by W. A. Hargreaves of Optovac Inc.

References

1. S. D. McLaughlan, Phys. Rev. 150, 118 (1966).
2. W. A. Hargreaves, Phys. Rev. 156, 331 (1967).
3. J. Markovsky, J. Chem. Phys. 46, 390 (1967).
4. W. D. Cooke, F. Hazel, and W. M. McNabb, Anal. Chem. 22, 654 (1950).
5. I. Richman, P. Kisliuk, and E. Y. Wong, Phys. Rev. 155, 262 (1967).
6. F. D. Sherif and A. M. Awad, Anal. Chim. Acta 26, 235 (1962).

Table I

Equivalents of Ce^{4+} consumed[a] (meg/mg CaF_2:U)	Total U content (%)	Valence change to produce U^{6+} (0.805% used as U content value)
6.57×10^{-5}	0.82[b]	1.94
6.92×10^{-5}	0.79[b]	2.05
6.88×10^{-5}	0.80[c]	2.03
7.18×10^{-5}	0.81[c]	2.12
7.31×10^{-5}	av 0.805±0.01	2.16

a. Five separate determinations.
b. By activation analysis.
c. By spectrophotometric method.

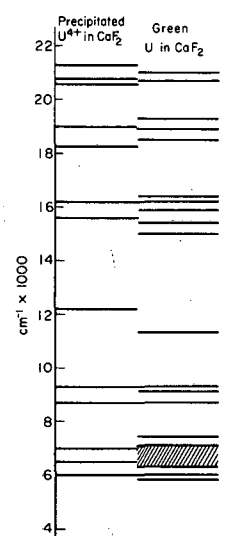

Fig. 1. The spectrum of coprecipitated U^{4+} in CaF_2 compared with the spectrum of a green CaF_2:U crystal.

EXTRACTION OF $HReO_4$ BY TRIOCTYL PHOSPHINE OXIDE IN NITROBENZENE AND IN 1,2-DICHLOROETHANE

J. J. Bucher, T. J. Conocchioli, and R. M. Diamond

Strong organic bases such as the alkyl amines dissolved in a relatively inert diluent can react with solutions of strong aqueous acid by extracting the proton away from the water to form a one-to-one complex, the ammonium ion,

$$R_3N(org)+H_3O^+ + X^- = R_3NH^+ \cdots X^-(org)+H_2O \qquad (1)$$

where the species $R3NH^+ \cdots X^-$ may be dissociated, associated to ion pairs, or aggregated to still higher associations, depending upon the nature of the anion and of the diluent. With large anions, such as ClO_4^- or ReO_4^-, and diluents of relatively high dielectric constant, such as nitrobenzene, the ammonium salt is usually dissociated and essentially anhydrous.

Weaker organic bases, such as tributyl phosphate (TBP), cannot take the proton away from the water molecule, and so must extract the hydronium ion, H_3O^+. Depending upon the anion and diluent, three, two, or one TBP molecules may be needed to satisfy the solvation requirements of the hydronium ion and additional water may be co-extracted. Again, depending upon the conditions, a dissociated or associated species may result,

$$nTBP(org)+H_3O^+ + X^- + xH_2O = nTBP \cdot xH_2O\text{-}H_3O^+ \cdots X^-(org). \qquad (2)$$

The alkyl phosphine oxides are intermediate in basicity between the two previously considered classes of extractants, and therefore might be expected to show an intermediate behavior. It is of interest to see, for example, if trioctyl phosphine oxide (TOPO) extracts a proton or a hydronium ion, and if the latter whether it is further hydrated, and how many extractant molecules are necessary to provide solvation for the cation. The use of a large monovalent anion such as ClO_4^- or ReO_4^- (the latter is particularly advantageous, as it has a convenient tracer, ^{186}Re) minimizes the cation-anion interactions and leads in high-dielectric-constant media such as nitrobenzene and dichloroethane to dissociated species. The extraction may then be expressed as

$$H^+ + X^- + xH_2O + nTOPO(org) = H^+ \cdot nTOPO \cdot xH_2O(org) + X^-(org), \qquad (3)$$

with the corresponding equilibrium constant for the dissociated species

$$K_n^d = [H^+ \cdot nTOPO \cdot xH_2O]_o [X^-]_o y_\pm^2 / (TOPO)_o^n (H_2O)^x (HX). \qquad (4)$$

Here [ ] denotes concentration, ( ) signifies activity, $y_\pm$ is a mean molar activity coefficient, and the subscript o means an organic-phase quantity.

However, before examining $HReO_4$ extraction by TOPO, it is necessary to establish the extent and nature of the extraction of water by TOPO. The organic-phase water concentration $[H_2O]_o$, corrected for extraction by the diluent, is plotted against the initial TOPO concentration in Fig. 1. The slope of 1.0 for each system in such a log-log plot indicates that one TOPO molecule is involved in each water complex, and the stoichiometry suggests a ratio of water to TOPO of 1:1 for TOPO in 1,2-dichloroethane and of 1.3:1 for TOPO in nitrobenzene. Thus the amount of free uncomplexed TOPO is very small. Consequently, when in later discussions the concentrations of TOPO, [TOPO], are considered they will actually denote hydrated extractant molecules.

From log-log plots (not shown) of organic-phase acid concentration vs the aqueous $HReO_4$ activity at constant TOPO concentrations, it was determined that the extracting species in both diluents was indeed a pair of dissociated ions. Similarly, from log-log plots of organic acid vs equilibrium TOPO concentration at fixed aqueous $HReO_4$ activities it was determined that the number of TOPO molecules involved in the extraction complex was two in both diluents. A compact presentation of the data is seen in Fig. 2, where the square root of the numerator in Eq. (3) is shown vs the square root of the denominator in a log-log plot (the square roots were taken so as to halve the number of decades necessary). Activity coefficients in the organic phase were calculated on the Mayer-Poirier theory, and aqueous activity coefficients were taken to be the same as those of $HClO_4$ solutions of the same concentration. The organic-phase acid concentrations went from 10^{-7} to 0.24 M, and TOPO concentrations varied from 10^{-4} to 1 M. The excellent fits to straight lines of unit slope indicate that over this range of conditions (up to 30-40%

loading of the initial TOPO concentration), the two systems can be described by a single organic-phase species which is dissociated and involves two TOPO molecules. The values of K_2^d for $HReO_4$ in nitrobenzene and in 1,2-dichloroethane are 1.2×10^3 and 9.6, respectively.

Figure 3 shows, for 0.3 M TOPO in nitrobenzene and in 1,2-dichloroethane, the amount of water less diluent water co-extracted by the organic-phase acid complex as the acid concentration increases. In both diluent systems the total amount of water decreases as $[H^+]_o$ increases. When the amount of water extracted by the remaining free TOPO is substracted, curves 3 and 4 suggest that essentially no excess water co-extracts with the acid complex in either diluent; the complex is anhydrous. This means that the TOPO molecules in these two diluents are sufficiently basic to pull the proton away from water and extract it alone. But TOPO is not so basic towards the proton as the trialkylamines, and so two TOPO molecules are needed where one amine suffices. Since it is most unlikely that the TOPO's bond to the ReO_4^-, the extracted species consists of the pair of dissociated ions,

$$R_3PO\text{---}H^+\text{---}OPR_3 \quad \text{and} \quad ReO_4^- ,$$

and we do not know yet whether the cation is symmetrical or not.

The fact that the protonic cation in these diluents is both anhydrous and dissociated from the anion leads to an interesting possibility. If a dissociated 2TOPO species is also found with other strong acids, it seems reasonable to assume the same anhydrous cation (it may be possible to prove this by NMR). But then any water co-extracting must be bound to the anion; values for the hydration of anions under these conditions can be determined relatively unambiguously.

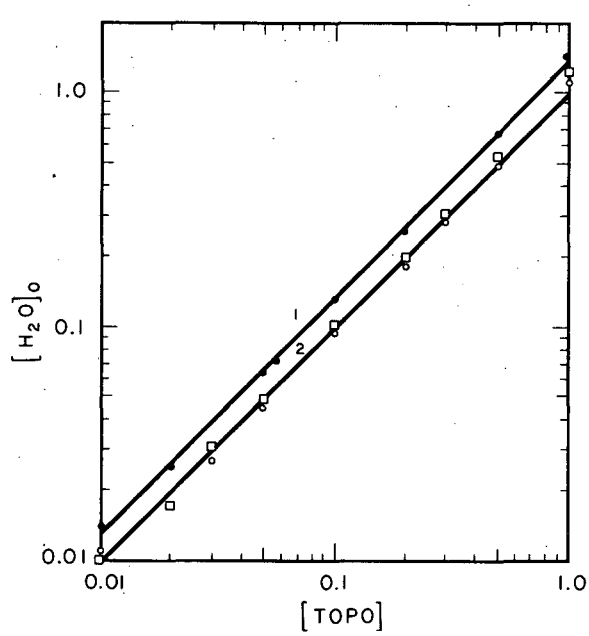

Fig. 1. Variation of water content of organic phase with TOPO concentration in nitrobenzene and 1,2-dichloroethane. ($[H_2O]_o$ = total H_2O minus H_2O dissolved by diluent.) Line 1, ●, is for TOPO-nitrobenzene system. Line 2, O, □ , is for TOPO-1,2-dichloroethane system. O, denotes results using Karl Fischer titrations; □ , denotes results using tritiated water as a tracer. Lines are drawn with unit slope.

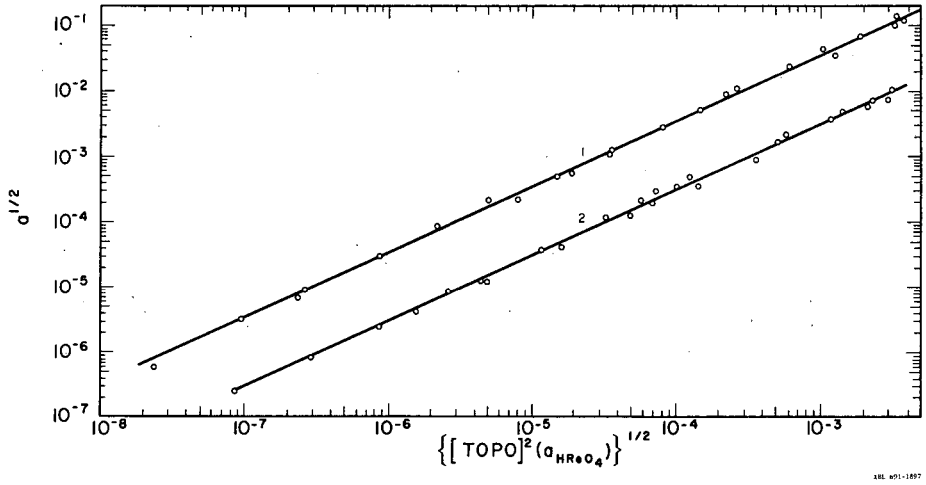

Fig. 2. Variation of organic-phase acid activity vs the product $\{[TOPO]^2_{(o)}(HReO_4)\}^{1/2}$. Line 1 is for the TOPO-nitrobenzene system. Line 2 is for the TOPO-1,2-dichloroethane systems. Lines are drawn with unit slope.

Fig. 3. Water content vs $HClO_4$ concentration in the organic phase (as the aqueous $HClO_4$ concentration increases) for total TOPO concentration of 0.3 M in nitrobenzene and 1,2-dichloroethane. Lines 1 and 2 are the total organic-phase water less diluent water respectively for nitrobenzene and 1,2-dichloroethane. Lines 3 and 4 are the total organic-phase water less both the solvent water and the water bound to TOPO for 1,2-dichloroethane and nitrobenzene respectively.

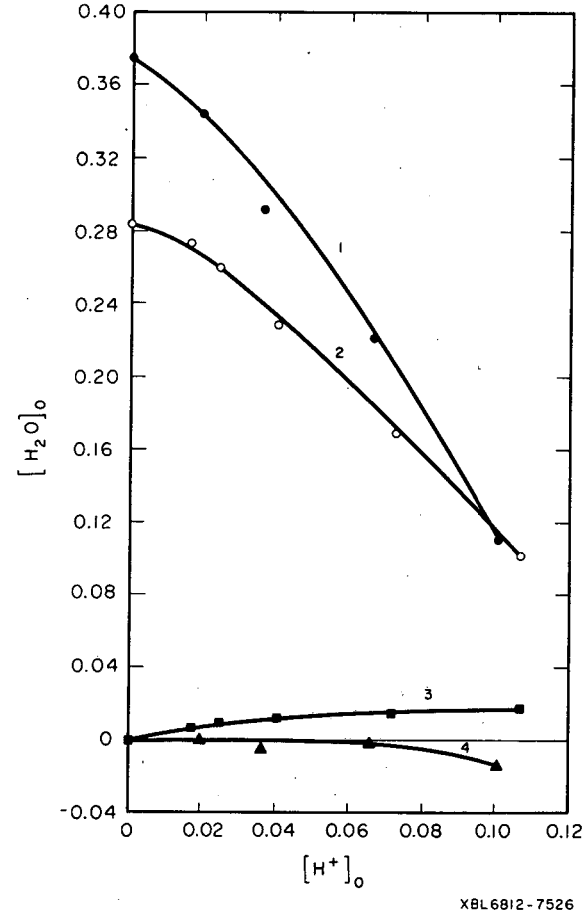

XBL6812-7526

EXTRACTION OF HBr AND HCl BY DILUTE SOLUTIONS OF TRIOCTYL PHOSPHINE OXIDE IN NITROBENZENE AND IN 1,2-DICHLOROETHANE AND HYDRATION OF Br^- AND Cl^- IN THESE DILUENTS

J. J. Bucher, E. R. Held,† J. A. Labinger,††
B. A. Sudbury,† and R. M. Diamond

In the first part of this study of inorganic acid extractions by tri-n-octyl phosphine oxide (TOPO), it was shown that $HReO_4$ is extracted into dilute TOPO solutions in nitrobenzene and 1,2-dichloroethane as a dissociated, anhydrous species and the cationic species is $2TOPO\cdot H^+$. It was suggested if the same extraction pattern held for HBr and HCl as for $HReO_4$, information concerning anion (Br^-, Cl^-) hydration, in other than aqueous media, could be obtained.

The extraction of HBr and HCl into nitrobenzene and 1,2-dichloroethane, if similar to the $HReO_4$ system, can be expressed

$$2TOPO(org)+H^+ +X^- + xH_2O = 2TOPO\cdot H^+(org) + X^-\cdot xH_2O(org). \quad (1)$$

The corresponding equilibrium constant is

$$K_2^d = \left[2TOPO\cdot H^+\right]_o \left[X^-\cdot xH_2O\right]_o y_\pm^2 / (TOPO)_o^n (H_2O)^x (HX) . \quad (2)$$

From log-log plots (not shown) of organic-phase acid concentration $[H^+]_o$, vs the aqueous acid activity at constant TOPO concentration, it was determined that the extracting species for HBr-nitrobenzene and 1,2-dichloroethane systems and for HCl-1,2-dichloroethane was indeed a pair of dissociated ions. Similarly, from log-log plots of organic-phase acid vs equilibrium TOPO concentration at fixed aqueous acid activities, it was determined that the number of TOPO molecules involved in the extraction complex was two for each of the HBr, HCl-TOPO-diluent systems studied, the same as in the $HReO_4$-TOPO-diluent systems.

These data are summarized in Fig. 1, which is a log-log plot of the square root of the numerator of Eq. (2) vs the square root of the denominator. (The square roots are taken to halve the number of decades necessary for the plot.) The good agreement found between the experimental points and the lines drawn with unit slope for each system indicate the validity of Eq. (2). The values of K_2^d are 0.1 for HBr-nitrobenzene, 4.2×10^{-3} for HBr-1,2-dichloroethane, and 2.0×10^{-4} for HCl-1,2-dichloroethane. The range of TOPO concentrations covered is from 0.00001 to 1.0 M, and the range of $[H^+]_o$ was up to 0.2 M. Data for HCl-nitrobenzene-TOPO were not obtained because of the limited solubility of the HCl acid complex in this diluent.

Since the extracted acid species observed with HCl-TOPO in dichloroethane and with HBr-TOPO in nitrobenzene and in dichloroethane are dissociated $2TOPO\cdot$ acid species, just as found previously for $HReO_4$, it seems to us reasonable to suppose that the same anhydrous cation is involved as with $HReO_4$. Consequently any excess water found to co-extract with the acid complex can be attributed to anion hydration.

Figures 2 and 3 show the amount of excess water corrected for that extracted by the diluent and by uncomplexed TOPO, co-extracted by HBr-diluents and HCl-1,2-dichloroethane respectively. The slope of the line drawn through the combined diluent data for HBr gives a ratio of 1.9 H_2O molecules per acid complex. The initial slope of the curve for the HCl data is about 4, but tails off to less than 3. It is unfortunate that the necessary aqueous acid concentrations needed to load the organic phase sufficiently to get meaningful results are high enough that the activity of water has changed appreciably from unity. To what extent the water activity affects the suggested chloride ion hydration is not clear. Another problem with HCl is that at these aqueous acid concentrations the bichloride ion, HCl_2^-, starts to form and extracts much more readily than Cl^-; the larger anion should be less highly hydrated, and also requires only half as many TOPO molecules per mole of HCl, e.g., $2TOPOH^+$ and HCl_2^-.

These last two effects tend to compensate each other in correcting the excess water curve in Fig. 3, but the first effect dominates, and so the appearance of the bichloride anion makes the water curve fall off more rapidly than if it were Cl^- alone. For this reason and because the water activity remains closer to unity, more weight is given the data at low organic-phase acid concentrations in spite of the larger errors inherent in obtaining the results as a difference between

more equal numbers. We feel that our results indicate that a free bromide ion in nitrobenzene and 1,2-dichloroethane has two waters of hydration and that a chloride ion probably has four.

Footnotes

†Undergraduate summer visitor, 1968.

††Undergraduate summer visitor, 1967.

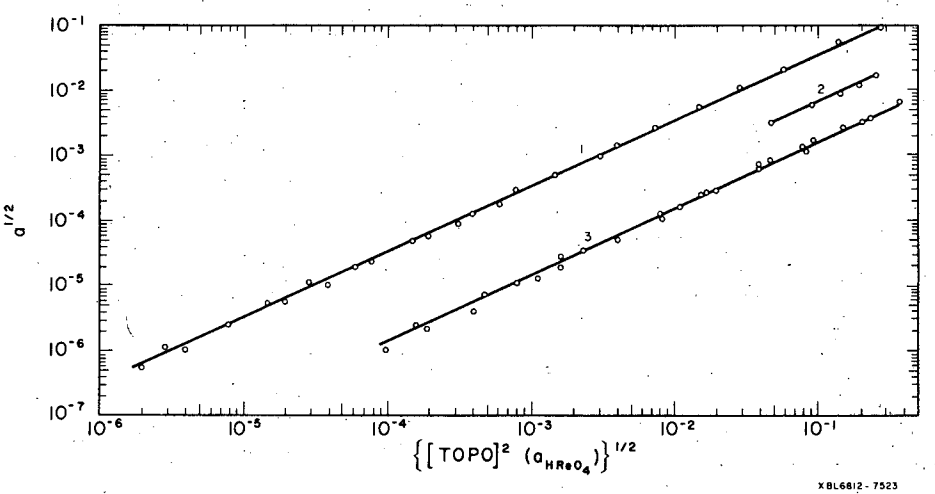

Fig. 1. Variation of organic-phase acid activity vs the product $\{[TOPO]_o^2 (HReO_4)\}^{1/2}$. Line 1 is for the TOPO-HBr-nitrobenzene system; line 2 is for TOPO-HBr-1,2-dichloroethane system; line 3 is for TOPO-HCl-1,2-dichloroethane system. All lines are drawn with unit slope.

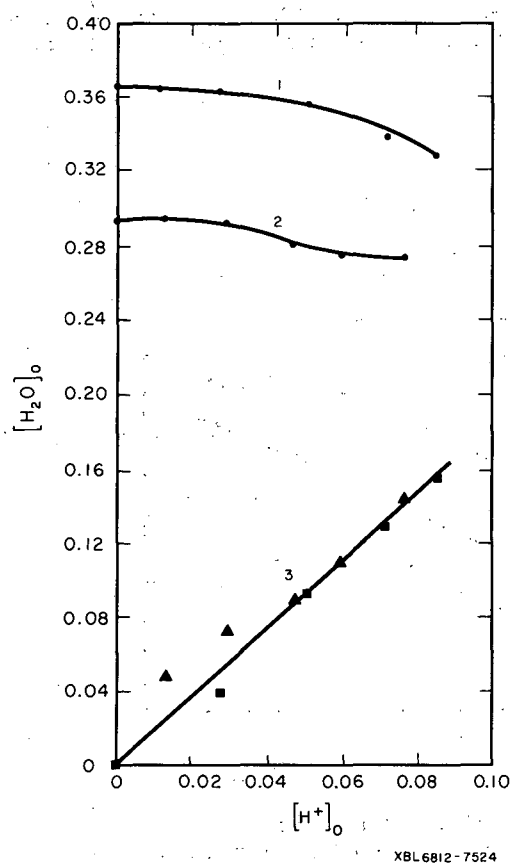

Fig. 2. Water content vs HBr concentration in the organic phase (as the aqueous HBr concentration increases) for total TOPO concentration of 0.3 M in nitrobenzene and 1,2-dichloroethane. Lines 1 and 2 are the total organic-phase water content less diluent water for nitrobenzene and 1,2-dichloroethane, respectively. Line 3 is the total organic-phase water less both the solvent water and the water bound to TOPO; ■ , nitrobenzene, ▲ , 1,2-dichloroethane.

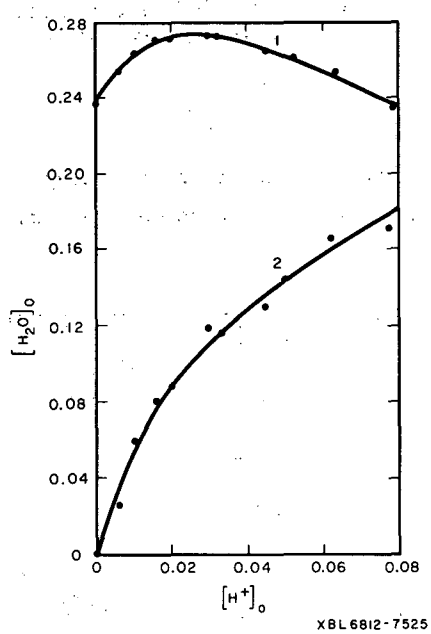

Fig. 3. Water centent vs HCl concentration in the organic phase (as the aqueous HCl concentration increases) for total TOPO concentration of 0.25 M in 1,2-dichloroethane. Line 1 is the total organic-phase water less diluent water; line 2 is the total organic-phase water less both diluent water and that bound to TOPO.

RADIATION CHEMISTRY OF THE α-AMINO ACIDS: γ RADIOLYSIS OF SOLID CYSTEINE†

Donald B. Peterson,* John Holian, and Warren M. Garrison

Radiolysis of the simpler α-amino acids such as glycine and alanine leads to deamination as a major chemical consequence both in aqueous solution[1] and in the solid state.[2] And there is accumulating evidence that the intermediate processes of deamination in the solid state are closely analogous to those that occur in aqueous solution. For example, in aqueous solution the ionization step[3]

$$H_2O \longrightarrow H^+, OH, e^-_{aq} \tag{1}$$

is followed by[4]

$$e^-_{aq} + NH_3^+CH(R)COO^- \longrightarrow NH_3 + \dot{C}H(R)COO^-, \tag{2}$$

$$OH + NH_3^+CH(R)COO^- \longrightarrow H_2O + NH_3^+\dot{C}(R)COO^-, \tag{3}$$

where e^-_{aq} represents the hydrated electron. The experimental evidence is that e^-_{aq} adds initially to the C=O linkage of the carboxyl group and that dissociation of the reduced intermediate then ensues.[4b, c] Subsequent interactions of $\dot{C}H(R)COO^-$ and $NH_3^+\dot{C}(R)COO^-$ yield keto acid and fatty acid as the major organic products.[1c, d]

The identification of reaction 2 prompted the suggestion[4a] that dissociative electron capture is also involved in the formation of ammonia as a major product in the radiolysis of the α-amino acids in the solid state. Ionic processes in these irradiated polar solids would then be represented by

$$NH_3^+CH(R)COO^- \longrightarrow NH_3^+\dot{C}(R)COO^- + H^+ + e^-, \tag{4}$$

$$e^- + NH_3^+CH(R)COO^- \longrightarrow NH_3 + \dot{C}H(R)COO^-, \tag{5}$$

where reactions 4 and 5 are the stoichiometric equivalents of reactions 1 through 3.

It has since been established elsewhere[5] that glyoxylic and acetic acids are indeed formed as major products in the γ radiolysis of solid glycine, with $G(NH_3)$ = G(glyoxylic acid) + G(acetic acid) = 5.

In this work we examine the role of the SH function as a competing locus of reaction in the γ radiolysis of cysteine[6] in the solid state. Data on a number of related compounds are also included. Although there have been numerous studies of the paramagnetic-resonance properties of irradiated cysteine,[7] the detailed radiation chemistry of this system has not been elucidated.

G values for the various products formed in the γ radiolysis of solid polycrystalline L-cysteine at 30°C are summarized in Table I. Dose-yield plots for all products are linear up to doses in the range 10^{21} eV/g; typical plots are shown in Fig. 1. Yields of hydrogen, hydrogen sulfide, and ammonia from a number of related sulfur-containing compounds are given in Table II.

We find that the radiation chemistry of solid cysteine may be interpreted in terms of the radiation-induced steps[6]

$$RSH \longrightarrow \dot{R}S + H^+ + e^-, \tag{6}$$

$$RSH \longrightarrow \dot{R}S + H, \tag{7}$$

followed by

$$H + RSH \begin{cases} \rightarrow H_2 + \dot{R}S & (8) \\ \rightarrow H_2S + NH_3^+\dot{C}H(CH_2)COO^- \quad \text{(Ref. 8)}, & (8a) \end{cases}$$

$$e^- + RSH \longrightarrow NH_3 + \dot{C}H(CH_2SH)COO^-, \quad (9)$$

$$e^- + RSH \begin{cases} \rightarrow H_2 + NH_2CH(CH_2\dot{S})COO^- & (10) \\ \rightarrow H_2S + NH_2CH(\dot{C}H_2)COO^-, & (10a) \end{cases}$$

and by the radical-removal steps

$$RSH + \dot{C}H(CH_2SH)COO^- \longrightarrow \dot{R}S + CH_2(CH_2SH)COO^-, \quad (11)$$

$$RSH + NH_2CH(\dot{C}H_2)COO^- \longrightarrow \dot{R}S + NH_2CH(CH_3)COO^-, \quad (12)$$

$$2\dot{R}S \longrightarrow RSSR \text{ (Cystine)}. \quad (13)$$

That e^- in the dissociative capture reaction 12 adds initially to the carboxyl C=O linkage of cysteine (as in the reaction of e^- with solid glycine) is supported by the results obtained with cystamine $NH_3^+CH_2CH_2SH$ (Table II). We find that cystamine which does not contain the carboxyl group as a trapping center for e^- does not form ammonia in any appreciable yield; $G(NH_3) \leq 0.1$.

The SH group of cysteine represents a competing trapping center for e^-.[9] Recent studies in other systems[10-12] indicate that simple dissociative capture reactions of the type

$$RSH + e^- \longrightarrow R + HS^-, \quad (14)$$

$$RSH + e^- \longrightarrow RS^- + H \quad (15)$$

become exothermic[13] only if solvation energies in a polar medium can be utilized in the overall energetics.[14] Whether or not such factors are involved in the reactions of e^- in a polar solid such as cysteine we cannot say.

However, simple dissociative attachment of e^- need not necessarily be involved in steps 10, 10a. An alternate explanation is that e^- is captured by the sulfhydryl group to give RSH^- and that chemistry then ensues as a consequence of proton transfer from an adjacent NH_3^+ group. Some evidence for such concerted action is to be found in the fact that $G(H_2) + G(H_2S)$ from N-acetylcysteine, $CH_3CONHCH(CH_2SH)COOH$, is markedly lower than the corresponding value for cysteine as shown in Table II.

Footnotes and References

†Condensation of UCRL-18532; submitted to J. Phys. Chem.

*Present address: Department of Chemistry, University of San Diego, San Diego, California.

1. (a) W. M. Dale, J. V. Davies, and C. W. Gilbert, Biochem J. 45, 93 (1949); (b) G. Stein and J. Weiss, J. Chem. Soc. 3256 (1949); (c) C. R. Maxwell, D. C. Peterson, and N. E. Sharpless, Radiation Res. 1, 530 (1954); (d) B. M. Weeks and W. M. Garrison, Radiation Res. 9, 291 (1958).

2. (a) W. M. Dale, J. V. Davies, and C. W. Gilbert, Ref. 1a; (b) B. Rajewski and K. Dose, Z. Naturforsch. 12B, 384 (1957); (c) G. Meshitsuka, K. Shindo, A. Minegishi, H. Suguro, and Y. Shinozaki, Bull. Chem. Soc. Japan 37, 928 (1964); (d) A. Minegishi, Y. Shinozaki, and G. Meshitsuka, Bull. Chem. Soc. Japan 40, 1271 (1967); (e) W. C. Gottschall, Jr., and B. M. Tolbert, J. Phys. Chem. 72, 922 (1968).

3. For a recent review of the radiation chemistry of water, see M. S. Matheson, Advan. Chem. Ser. 50, 45 (1965).

4. (a) W. M. Garrison, Actions of Ionizing Radiations on Nitrogen Compounds in Aqueous Media, UCRL-10827, May 1963; Radiation Res. Suppl. 4, 1964; (b) B. M. Weeks, S. A. Cole, and W. M. Garrison, J. Phys. Chem. 69, 4131 (1965); (c) R. L. S. Willix and W. M. Garrison, J. Phys. Chem. 69, 1579 (1965), Radiation Res. 32, 452 (1967).

5. (a) G. Meshitsuka, private discussion, Sept. 1963; (b) G. Meshitsuka, Y. Shinozaki, A. Minegishi, K. Shindo, and H. Suguro, Annual Report Tokyo Metropolitan Isotope Center 2 (1963). See also Refs. 2c, d.

6. For purposes of simplicity we use the symbol RSH to represent the cysteine zwitterion, $NH_3^+CH(CH_2SH)COO^-$.

7. For example, see (a) W. Gordy, W. B. Ard, and H. Shields, Proc. Natl. Acad. Sci. U.S. 41, 983 (1955); (b) T. Hendriksen, J. Chem. Phys. 37, 2189 (1962); (c) M. K. Pulatov and O. A. Azizova, Biofizika 9, 33 (1964).

8. G. Navon and G. Stein, Israel J. Chem. 2, 151 (1964).

9. The radical RSH^- has been identified in γ-irradiated cysteine at 77°K (Ref. 7c).

10. G. Lunde and R. R. Hentz, J. Phys. Chem. 71, 863 (1967).

11. J. J. J. Myron and R. H. Johnson, J. Phys. Chem. 70, 2951 (1966).

12. (a) D. El Samahy, H. L. White, and C. N. Trumbore, J. Am. Chem. Soc. 86, 3175 (1964); (b) D. A. Armstrong and V. G. Wilkening, Can. J. Chem. 42, 2631 (1964).

13. (a) T. L. Cotrell, The Strengths of Chemical Bonds (Butterworths, London, 1954); (b) D. A. Ansdell and F. M. Page, Trans. Faraday Soc. 58, 1084 (1962). Reaction 15 represents a major process in the photolysis of cysteine in the solid state as recently shown by H. C. Box, H. G. Freund, and E. E. Budzinzki, J. Phys. Chem. 45, 809 (1966).

14. For a discussion of the effects of solvation energy on reactions of the type $RX^- \longrightarrow R + X^-$ see: J. A. Ward and W. H. Hamill, J. Am. Chem. Soc. 87, 1853 (1965).

Table I. Product yields in the γ radiolysis of solid L-cysteine.

Product	G
Hydrogen	3.1 ± 0.1
Hydrogen sulfide	1.5 ± 0.1
Ammonia	1.8 ± 0.1
Cystine	5.0 ± 0.5
"NH_2-free" fraction	1.0 ± 0.1
Pyruvic acid	≤ 0.1
Total carbonyl	≤ 0.1

Table II. Comparative product yields in the γ radiolysis of cysteine and related compounds in the solid state.

	G		
	H_2	H_2S	NH_3
Cysteine $NH_3^+CH(CH_2SH)COO^-$	3.1	1.5	1.8
Cystamine $(NH_3^+CHCH_2SH)Cl^-$	5.6	1.2	<0.1
N-acetyl cysteine $CH_3CONHCH(CH_2SH)COOH$	0.5	0.9	<0.1
S-methyl cysteine $NH_3^+CH(CH_2SCH_3)COO^-$	≈0.2	—[a]	5.1
Glycine $NH_3^+CH_2COO^-$	≈0.2		5.2
Alanine $NH_3^+CH(CH_3)COO^-$	≈0.2		5.4

a. H_2S was not expected, nor was it observed as a product from S-methyl cysteine; other measurements with S-methyl cysteine gave $G(CH_4) \approx 0.5$; $G(CH_3SH) \leq 0.1$. These results indicate that e^- is not captured via dissociative attachment at the sulfur locus; the observed H_2 and NH_3 yields suggest that the "glycine" mechanism is of major importance in the radiolysis of S-methyl cysteine.

Fig. 1. Production of hydrogen (●), ammonia (●), and hydrogen sulfide (○), from solid cysteine as a function of γ-ray dosage.

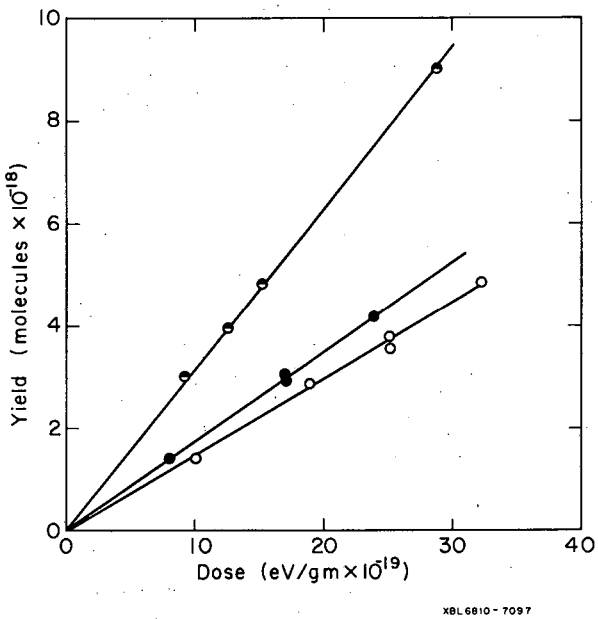

ON THE RADIATION-INDUCED REDUCTION OF AMIDE AND PEPTIDE FUNCTIONS IN AQUO-ORGANIC SYSTEMS†

John Holian and Warren M. Garrison

In the γ radiolysis of neutral, oxygen-free solutions of peptides such as N-acetylglycine and N-acetylalanine, the labile products of the radiation-induced step[1, 2]

$$H_2O \longrightarrow H_2O_2, H_2, OH, H, H^+, e^-_{aq} \quad (1)$$

are removed through reactions of the type[3, 4]

$$e^-_{aq} + RCONHR + H_2O \longrightarrow \dot{R}C(OH)NHR + OH^-, \quad (2)$$

$$OH + RCONHR \longrightarrow R' + H_2O, \quad (3)$$

$$H + RCONHR \longrightarrow R' + H_2. \quad (4)$$

In subsequent chemistry, the radical combination reactions which lead to net reductive cleavage of the amide linkage,

$$2\dot{R}C(OH)NHR \longrightarrow (RCO)_2 + 2NH_2R, \quad (5)$$

$$2\dot{R}C(OH)NHR \longrightarrow RCHO + NH_2R + RCONHR, \quad (6)$$

$$\dot{R}C(OH)NHR + R' \longrightarrow R(R')CO + NH_2R, \quad (7)$$

occur in relatively low yield. We find, for example, that the combined yield of carbonyl products $(RCO)_2$, RCHO, R(R')CO in neutral solutions of N-acetylglycine and N-acetylalanine corresponds to $G(>CO) \leq 0.2$.[3b] The indirect evidence is that a reconstitution reaction with the stoichiometry

$$\dot{R}C(OH)NHR + R' \longrightarrow 2RCONHR \quad (8)$$

represents an important path for removal of the radical species derived from $RCONHCH(R)COO^-$ through reactions 2 through 4.

We have investigated the analogs of reactions 2 through 8 in oxygen-free solutions of acetamide and of N-ethylacetamide under γ radiolysis. And, because of the relative simplicity of the chemistry of the aqueous acetamide system, we have been able on the basis of stoichiometric considerations to wholly substantiate the validity of the proposed reaction scheme given in Eqs. 1 through 8.

To establish the locus of OH attack on acetamide and to eliminate any contribution of the back-reaction 8, we make use of the fact that dissolved N_2O and H^+ convert e^-_{aq} to OH and H respectively, via

$$N_2O + e^-_{aq} + H_2O \longrightarrow N_2 + OH + OH^- \quad \text{and} \tag{9}$$

$$e^-_{aq} + H^+ \longrightarrow H. \tag{10}$$

The data of Table I, columns 1 and 2, show that both the OH and H radicals react preferentially at the methyl group of acetamide to yield the radicals $\dot{C}H_2CONH_2$, which subsequentially dimerize to give G(succinamide): = 2.6 ≈ $[G_{OH} + G_{e^-_{aq}} + G_H]/2$.[2] The yield of carbonyl products is essentially zero in solutions containing the electron scavengers H^+ and N_2O.

In the absence of these added scavengers we find, as shown in Table I, column 3, that succinamide is produced in quite low yield, G(succinamide) ≈ 0.3. The combined yield of carbonyl products is also low, with G(>CO) < 0.2. Detailed analytical probes of this relatively simple system have failed to reveal any other organic products in significant yield.

Since we know from the rate data[3,5] that both e^-_{aq} and OH are quantitatively scavenged by acetamide in 0.25 M solution at pH 7, we are led to conclude that radical termination in this system occurs almost exclusively through the reconstitution reaction 8.

Direct substantiating evidence for the occurrence of such reactions in neutral solutions of amides and peptides has been obtained. We find that certain labile organic compounds--notably the thiols, RSH--are effective at low concentrations in blocking the back-reaction 8 by virtue of the H-atom transfer reaction

$$\dot{R}C(OH)NHR + RSH \longrightarrow RCH(OH)NHR + \dot{R}S, \tag{11}$$

which leads in turn to the cleavage of the amide (peptide) linkage,

$$RCH(OH)NHR \longrightarrow RCHO + NH_2R. \tag{12}$$

As indicated in Table II, acetaldehyde appears as the major product, with $G(CH_3CHO) \approx 2.5$, in solutions of acetamide and N-ethylacetamide containing the thiol, cysteine.

Of interest from both the chemical and biological standpoint is the present finding that RSH at low concentrations induces a very striking enhancement in the radiolytic lability of the amide (peptide) linkage.

Footnotes and References

†Condensation of UCRL-18428; J. Phys. Chem. (to be published).

1. (a) A. O. Allen, Radiation Res. Suppl. 4, 54 (1964); (b) E. J. Hart and R. L. Platzman, Mech. Radiobiology 1, 93 (1961); (c) C. S. Hochanadel and R. Casey, Radiation Res. 25, 198 (1965).

2. Recent measurements (Ref. 1c) of the 100-eV yields for reaction 1 give $G_{OH} = 2.59$, $G_{e^-} = 2.58$, $G_H = 0.55$, $G_{H_2} = 0.45$, $G_{H_2O_2} = 0.72$.

3. (a) R. L. Willix and W. M. Garrison, Radiation Res. 32, 452 (1967); (b) M. A. J. Rodgers, H. A. Sokol, and W. M. Garrison, J. Am. Chem. Soc. 90, 795 (1968); (c) W. M. Garrison, Current Topics in Radiation Research, Vol. IV, 1968; (d) H. L. Atkins, W. Bennett-Corniea, and W. M. Garrison, J. Phys. Chem. 71, 772 (1967).

4. (a) For purposes of simplicity, we use the general formulation, RCONHR, to represent both the primary amide and the monosubstituted primary amide (peptide); (b) In the radiolysis of N-acetylglycine and N-acetylalanine, OH attack and H attack occur at C-H linkage of the main chain, i.e., R' = RCONHC(R)COOH (Ref. 3c).

5. For a recent compilation of rate data see M. Anbar and P. Neta, Intern. J. Appl. Radiation Isotopes 17, 493 (1967).

Table I. Product yields in the γ radiolysis of oxygen-free solutions of acetamide.[a]

Product	G value		
	pH 7 (+.02 M N_2O)	pH 1	pH 7
Succinamide	2.6		0.3
Acetaldehyde	<0.05	<0.05	0.1
Other carbonyls[b]	<0.05	<0.05	≈0.03
Hydrogen	c	3.8	0.9

a. 0.25 M
b. Acetone plus biacetyl
c. Not measured

Table II. Effect of cysteine (RSH) on the γ-ray-induced reduction of acetamide and N-ethylacetamide in oxygen-free solution.

Amide solution (M pH7)[a]	(RSH), M	$G(CH_3CHO)$
acetamide	none	≈0.1
acetamide	4×10^{-4}	2.4[b]
N-ethylacetamide	none	<0.05
N-ethylacetamide	4×10^{-4}	2.8[c]

a. Since the rate constant for reaction of cysteine with e^-_{aq} corresponds to $k = 2 \times 10^{10}$ $M^{-1}sec^{-1}$ (Ref. 5) it was necessary in this series of experiments to increase the amide concentration to 1 M to insure the preferential scavenging of e^-_{aq} by RCONHCHR. Concentrations of RSH much below 4×10^{-4} M are experimentally impracticable because of excessive depletion of the mercaptan during radiolysis.
b. This yield is dose-dependent, and the value 2.4 represents the extrapolated yield at zero dose.
c. At dosages below 2.5×10^{18} eV/g.

IONIZATION AND EXCITATION IN PEPTIDE RADIOLYSIS†

Warren M. Garrison, Michael E. Jayko, Michael A. J. Rodgers, Harvey A. Sokol, and Winifred Bennett-Corniea

A major chemical effect of γ rays on simple peptides such as the N-acylamino acids under oxygen-free conditions, both in the solid state and in concentrated aqueous solution, leads to formation of labile amide-like compounds which are readily degraded on mild hydrolysis to yield ammonia as a characteristic product. Several classes of nitrogen-deficient products are formed concomitantly with the ammonia. Earlier communications have discussed certain limited aspects of the radiolytic lability of simple peptides in the solid state and in concentrated solutions.[1-3] The radiation chemistry of these systems is more complex than that involved in the radiolysis of simple peptides in dilute oxygen-free aqueous solution, under which conditions main-chain degradation is of minor importance.[4] In this paper we report detailed experimental evidence and specific formulations for a number of degradation modes that have been found to be induced directly through ionization and excitation of peptides in the polycrystalline state and in the glassy state.

The 100-eV yield for the radiolytic degradation of the peptide bond, as measured in terms of $G(NH_3)$ after mild hydrolysis, has been determined for a variety of aliphatic, aromatic, and sulfur-containing amino acids in the N-acetyl form. These data are summarized in Table I. In the aliphatic series, we note that the length of the side chain has relatively little effect on the yield of main-chain degradation. The effect of the aromatic groups of acetyl phenylalanine and of acetyl tyrosine is to quench in part the yields of those reactions that lead to formation of amide ammonia. The sulfur moiety of methionine, on the other hand, appears to be relatively ineffective in quenching such reactions.

We have completed a detailed study of the reaction products formed in the γ radiolysis of simple peptide derivatives of alanine, viz., poly-DL-alanine and acetyl-DL-alanine polycrystalline. These data are summarized in Table II. We find that the major organic products, in the order of decreasing yield, are propionic acid, acetaldehyde, pyruvic acid, and lactic acid. The labile ammonia from acetylalanine, G = 3.4, is derived primarily from acetamide, G = 2.8, plus

a small amount of free ammonia, G = 0.6. From these studies of the concomitant products it is clear that the observed $G(NH_3)$ values represent the combined yield of a number of different modes of degradation of the peptide chain.

The initial radiation-induced step in solid peptides may be represented in terms of the ionization

$$RCONHCHR_2 \longrightarrow (RCONHCHR_2)^+ + e^-. \qquad (1)$$

It is of interest, therefore, to consider the effects of added electron scavengers on the yield of main-chain rupture. Fortunately, for this purpose we have been able to prepare N-acetylalanine in the form of a clear glassy solid at room temperature. The glass has the composition $CH_3CONHCH(CH_3)COONa \cdot 2H_2O$, and gives product yields that are essentially the same as those obtained with the polycrystalline solid, e.g., $G(NH_3) \approx 3.4$, G(propionic) = 1.6, G(acetaldehyde) = 0.8. Chloracetate ion, which has been shown to be an effective electron scavenger,

$$e^- + RCl \longrightarrow R + Cl^-, \qquad (2)$$

in other polar glasses,[5] is soluble (as the sodium salt) in acetylalanine glass. We find that $G(Cl^-)$ increases with chloracetate concentration in the concentration range 1 to 10 mole %, as shown in Fig. 1; the reciprocal-yield plot of Fig. 2 gives a limiting value of $G(Cl^-) \approx 3$, which value provides a measure of the yield for ion-pair production via reaction 1 in this system. At the same time there is but a small effect of added chloracetate ion on $G(NH_3)$, even under the condition in which $G(Cl^-)$ is maximal. The evidence is, then, that charge recombination, i.e.

$$(RCONHCHR_2)^+ + e^- \longrightarrow \text{products}, \qquad (3)$$

is not of major importance in the radiolytic degradation of the peptide N-C linkage.

From these and other data obtained on the effects of various classes of added scavengers we conclude that the γ-ray-induced cleavage of the N-C linkage to yield fatty acid involves excitation of the peptide bond by low-energy electrons via

$$e^- + RCONHCHR_2 \longrightarrow (RCONHCHR_2)^* + e^-. \qquad (4)$$

A theoretical treatment of this mode of excitation for the general case has been given by Platzman.[6] We envisage the chemistry of the excited (triplet) state in these solid systems to be of the form

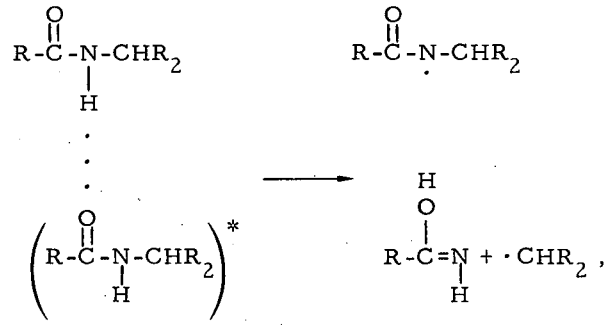

(5)

where $RCONCHR_2$ rearranges instantaneously to give the long-lived radical $RCONHCR_2$.[7] Since the radical products of reaction (5) are formed at a distance, the effects of caging will be minimal. The overall energy requirement for reaction (5) is essentially that required for dissociation of the aliphatic N-C bond, i.e., ≈3 eV.[8]

If solid acetylalanine is irradiated at the temperature of liquid nitrogen, then the propionic acid is almost wholly quenched from $G(\text{propionic})_{290°K} = 1.6$ to $G(\text{propionic})_{77°K} \leq 0.1$. The ammonia yield shows a corresponding drop from $G(NH_3)_{290°K} = 3.4$ to $G(NH_3)_{77°K} = 1.3$. We interpret this as evidence that an energy of activation is involved in reaction (5). The yields of carbonyl products, on the other hand, are unchanged at the lower temperature, with $G(\text{carbonyl})_{77°K} = G(NH_3)_{77°K} = 1.3$. We suggest that the carbonyl products arise from positive ion precursors

$$RCONHCHR_2 \longrightarrow (RCONHCHR)^+ + R + e^-, \quad (6)$$

$$RCONHCHR_2 \longrightarrow (RCONHCR_2)^+ + H + e^-, \quad (7)$$

which species undergo proton stripping in the polar solid, e.g.,

$$(RCONCHR_2)^+ \longrightarrow RCON{=}CR_2 + H^+, \quad (8)$$

to yield dehydropeptide products which are labile[9] and readily hydrolyze to yield amide plus carbonyl products respectively,

$$RCON{=}CR_2 + H_2O \longrightarrow RCONH_2 + R_2CO, \quad (9)$$

$$RCON{=}CHR + H_2O \longrightarrow RCONH_2 + RCHO. \quad (10)$$

Acetyl α-aminobutyric acid yields α-ketobutyric acid and propionaldehyde in accord with the above formulation.

Footnotes and References

†Condensation of Advan. Chem. Series 81, 384 (1968).

1. W. M. Garrison, M. E. Jayko, B. M. Weeks, H. A. Sokol, and W. Bennett-Corniea, J. Phys. Chem. 71, 1546 (1967).
2. W. M. Garrison, Radiation Res. Suppl. 4, 148 (1964).
3. M. A. J. Rogers and W. M. Garrison, J. Phys. Chem. 72, 758 (1968).
4. B. M. Weeks and W. M. Garrison, Radiation Res. 9, 291 (1958).
5. P. B. Ayscough, R. G. Collins, and F. S. Dainton, Nature 205, 965 (1965).
6. R. L. Platzman, Radiation Res. 2, 1 (1955).
7. N. C. Box, H. G. Freund, and K. Lilga, Free Radicals in Biological Systems, M. Blois et al., Ed. (Academic Press, New York, N. Y., 1961).
8. T. L. Cottrell, The Strengths of Chemical Bonds (Butterworths Scientific Publications, London, 1954.
9. J. P. Greenstein and M. Winitz, Chemistry of Amino Acids (John Wiley and Sons, Inc., New York, N. Y., 1961).

Table I. γ-Ray-induced degradation of solid N-acetylamino acids, $CH_3CONHCH(R)COOH$.

N-acetyl derivative[a]	(R)	$G(NH_3)$[b]
glycine	-H	2.68
alanine	$-CH_3$	3.4
α-aminobutyric acid	$-CH_2CH_3$	2.7
leucine	$-CH_2CH(CH_3)_2$	3.2
glutamic acid	$-CH_2CH_2COOH$	2.3
phenylalanine	$-CH_2(C_6H_5)$	0.8
tyrosine	$-CH_2(C_6H_4OH)$	1.6
methionine	$-CH_2CH_2SCH_3$	2.3

a. N-acetyl-DL-amino acids were used with the exception of N-acetyl-L-glutamic acid.
b. After hydrolysis.

Table II. Product yields in the γ radiolysis of N-acetyl-DL-alanine and poly-DL-alanine.

	G	
Product	N-acetyl-alanine	Poly-alanine
ammonia (total)	3.4	3.6
amide	2.8	3.1
free	0.6	0.5
propionic acid	1.4	1.8
pyruvic acid	0.4	$\approx$1
acetaldehyde	0.8	$\approx$0.4
lactic acid	$\leq$0.2	--
acrylic acid	trace	--
hydrogen	0.40	0.45

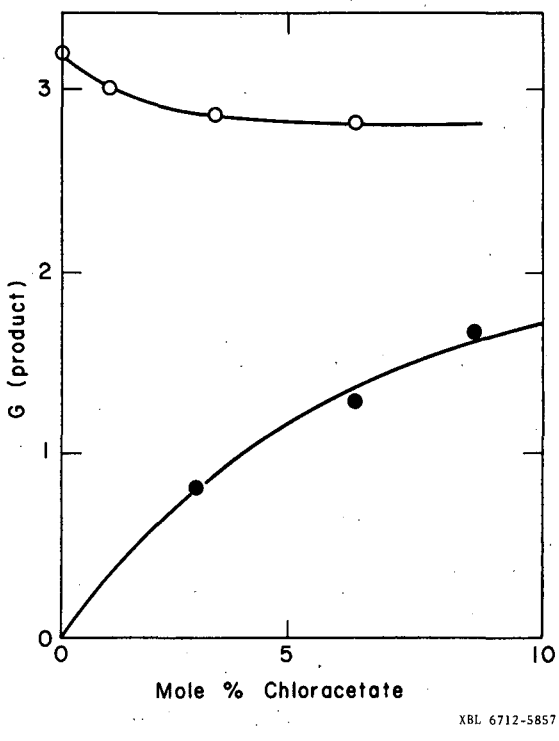

Fig. 1. Ammonia (O) and chloride-ion (●) yields as a function of chloracetate concentration in acetylalanine glass, RCONHCH(R)COONa · $2H_2O$.

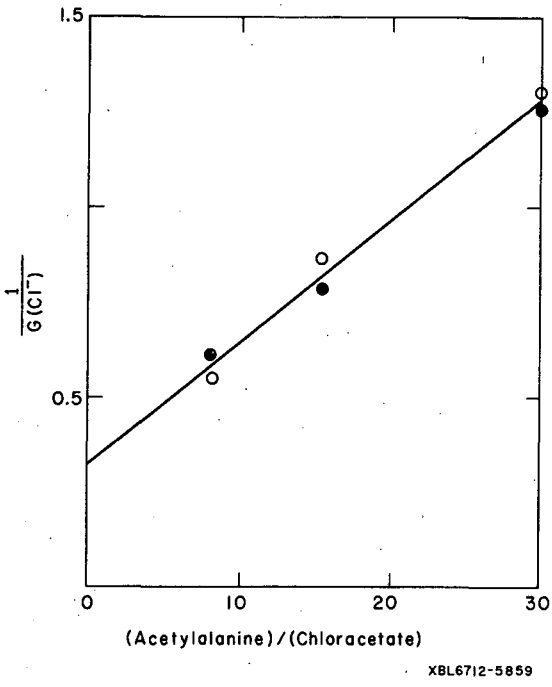

Fig. 2. Reciprocal chloride-ion yield as a function of (acetylalanine)/(chloracetate) concentration ratio in the systems RCONHCH(R)COONa · $2H_2O$, (O); RCONHCH(R)COONa · $8H_2O$, (●).

CHEMICAL ENGINEERING

LIQUID MIXING IN RECTANGULAR VESSELS

Thomas D. Coughlen† and Theodore Vermeulen

The power-speed relations of mixers are a guide to the optimum choice of agitation conditions, in many blending and contacting systems. Rectangular tanks are sometimes used instead of cylindrical vessels, and have not been examined systematically. In this study, power requirements have been investigated for liquid agitation in a closed rectangular tank having variable cross section, using both four-bladed flat paddles and flat-bladed turbines with a varying number of blades.[1]

In tanks 10 in. high and 10 in. long, widths of 10.0 and 7.5 in. were investigated with a centered impeller, and a width of 8.75 in. with an off-center impeller. Data obtained with four-blade flat paddles of varying width and length showed moderately good agreement on a plot of modified power number against impeller Reynolds member (Fig. 1) and are all seen to lie between those for unbaffled and for fully baffled cylindrical tanks.

Less effect of tank shape was found with four-blade turbine impellers of similar dimensions, all these giving power numbers about one-third less than those for paddle impellers in the square tank. The effect of number of blades on a turbine impeller was also investigated. For a turbine with 5-in. tip-to-tip diameter, and with 1.25-in.-square blades set perpendicular to a 3.25-in.-diameter disk, the number of blades giving maximum power input at a given speed varied from 10 at an impeller Reynolds number of 10^5 to 14 at a Reynolds number of 2000. The modified power number varied from 12 at the former to 24 at the latter condition. Similar relations are believed to apply in cylindrical tanks, and the effect of number of blades should therefore be studied further.

In measurements on air-water mixtures involving 2.5 to 15 vol-% air, four-blade flat paddle impellers gave greater percentage reductions in power requirement for the cross sections exhibiting the higher air-free power inputs.

Footnotes and References

†Present address: Humble Oil and Refining Co., Baytown, Texas.

1. T. D. Coughlen and T. Vermeulen, Power Requirements for Liquid Agitation in Rectangular Vessels, UCRL-16289, Aug. 1968.

2. J. H. Rushton, E. W. Costich, and H. J. Everett, Chem. Eng. Progr. 46, 395 and 467 (1950).

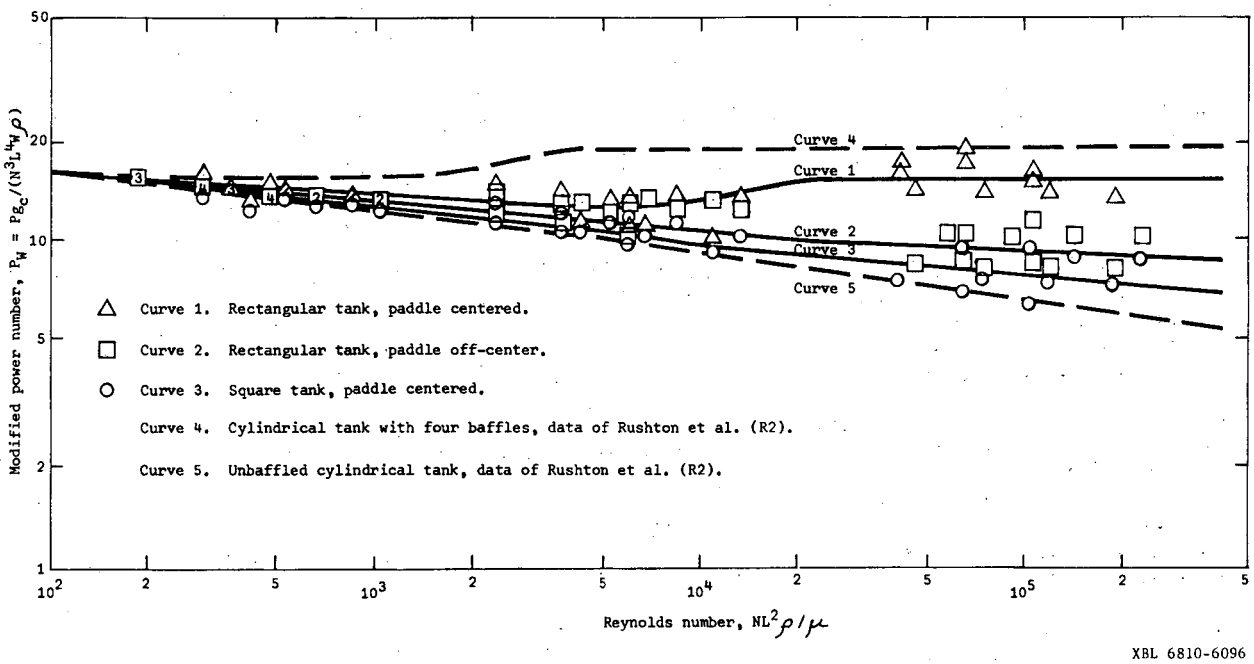

Fig. 1. Modified power number vs Reynolds number for flat paddles in different tank geometries.

OSCILLATING-JET MEASUREMENT OF DYNAMIC LIQUID-LIQUID INTERFACIAL TENSION

Sugihiko Tada and Theodore Vermeulen

The oscillating-jet technique has been used previously for measuring the surface tension between a gas and a liquid. Here it is extended to the measurement of the interfacial tension between two immiscible liquids. This work was undertaken to establish a hydrodynamical theory for the oscillating jet, so as to allow this technique to be used to indicate interfacial concentrations in liquid-liquid systems undergoing mass transfer. The mathematical theory by Bohr for the gas-liquid case has been extended to the liquid-liquid case to give an exact but implicit analytical solution.[1] In the study presented here,[2] corrections have been made to the previous result, and a simple correction multiplier f to the Rayleigh-Bohr formula has been developed to give an explicit representation of the exact solution:

$$\frac{c^2 a\rho c}{\sigma} = \left\{ \frac{I_2'(ba)}{I_2(ba)} \cdot \frac{3+b^2a^2}{ba} \right\} \cdot \left[1 + \frac{37}{24} \left(\frac{r_{max}-r_{min}}{r_{max}+r_{min}} \right)^2 \right]^{-1} \cdot f,$$

where f has been found to be

$$f = \left[1 + 1.44 \left(\frac{2ca\rho_i}{\mu_i} \right)^{-.050} (ba)^{-.141} \left(\frac{\mu_e}{\mu_i} \right)^{.029} \left(\frac{\rho_e}{\rho_i} \right)^{.897} \right]^{-1},$$

with c the effective plug-flow velocity; a the mean jet radius; r_{max} and r_{min} the elliptical major and minor half-axes; b the wave number ($2\pi/\lambda$, with λ the wavelength); μ viscosity; ρ density; and subscripts i and e designating the interior and exterior fluids.

Experimental data were taken on immiscible liquid pairs whose interfacial tension ranges from 6 to 42 dynes/cm, and were analyzed by the theory developed. A further correlation is

needed to estimate c from the local interface velocity and average interior-jet velocity. Figure 1 shows the agreement obtained for the experimental measurements that have been made to date.

As an essential step in this study, a calculational method has been developed to predict the velocity profile of a circular liquid jet in a stationary surrounding liquid. Figure 2 is an example of such profiles, for a benzene jet into water, at various downstream distances z measured as ratios to the orifice radius. The resulting values of jet radius and interfacial velocity have been used to correlate the effective plug-flow velocity which is required as an input for the oscillating-jet theory.

In order to improve the stability of the oscillating jet, and also to approach closer to theoretical flow conditions, the use of a flowing external phase at a velocity near the average velocity of the oscillating jet is proposed. A calculational method to predict the velocity profile for such a case is given as an extension of the method used for a stationary surrounding liquid. Figure 3 shows a typical initial profile, along with one calculated at a considerable distance downstream.

References

1. A. E. Vandegrift, P. N. Tenney, and T. Vermeulen, Liquid-Liquid Interfacial-Tension Measurement with an Oscillating Jet, UCRL-10717, March 1963.
2. S. Tada, A. E. Vandegrift, and T. Vermeulen, Oscillating-Jet Measurement of Dynamic Liquid-Liquid Interfacial Tension, UCRL-18629, Dec. 1968.

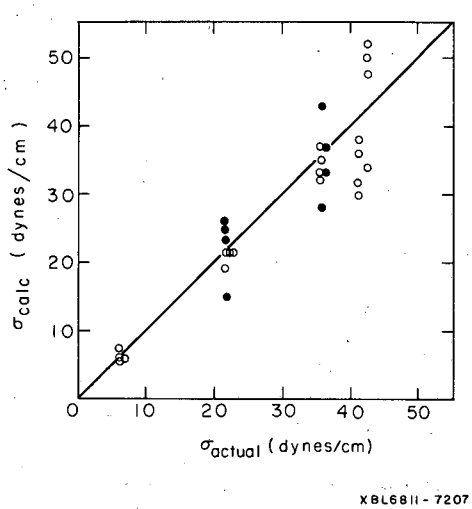

Fig. 1. Calculated interfacial-tension values obtained from oscillating-jet wavelengths, compared with values by tensiometer.

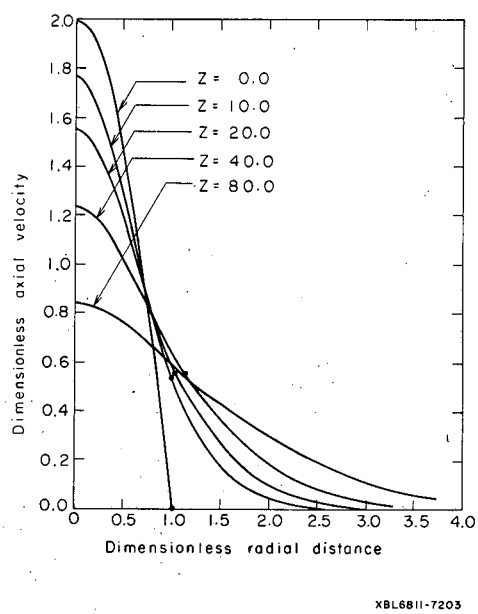

Fig. 2. Profiles of relative axial velocity as functions of radial distance, at several axial distances downstream from injection nozzle.

Fig. 3. Jet radius and radial variation of axial velocity, for laminar jet injected into flowing exterior liquid, at injection nozzle and at a downstream cross section.

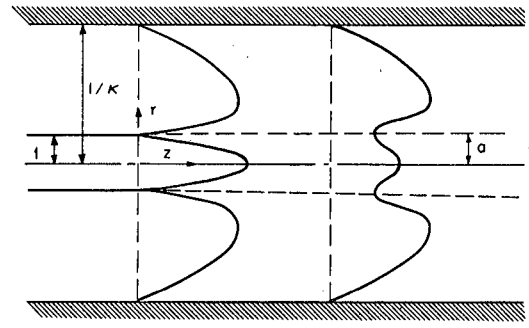

XBL6811-7228

DEVELOPMENT OF A JET-MIXED EXTRACTION COLUMN

Daniel R. Kahn and Theodore Vermeulen

A jet-mixed extraction column has been developed[1] which incorporates most advantages of existing column-type extractors, while eliminating the need for internal moving parts. The column was designed to provide high rates of mass transfer, with only normal or even decreased extents of unwanted longitudinal dispersion ("axial mixing").

The column utilizes uniformly spaced horizontal tubular jetting and intake rings at the inner and outer boundaries of an annular cross section. At each level, both rings are perforated so as to promote nearly straight-line radial flow between the jetting and intake rings. Externally these rings are connected by way of a small centrifugal circulating pump. The experimental column as set up for visual testing is shown in Fig. 1. The apparatus is part of a complete solvent-extraction unit which has been used in previous LRL studies.[2]

Semiquantitative tests of the column in single-phase and two-phase operation have been made to study the effects of number, size, and position of the ring ports, compartment height, jetting circulation rate, and longitudinal flow rates on the vortex patterns, the extent of longitudinal dispersion, the extent of interception (desired) of the discontinuous phase, and the extent of colloidal dispersion (undesired) of discontinuous phase.

Further experimentation, involving a complete mass-transfer analysis using two different solvent-solute systems, and a larger number of jet-mixed stages, is needed to complete the performance evaluation of this new design.

References

1. Daniel R. Kahn and Theodore Vermeulen, Development of a Jet-Mixed Extraction Column, UCRL-18679, Feb. 1969.

2. Joon S. Moon, Alphonse Hennico, and Theodore Vermeulen, Longitudinal Dispersion in Packed Extraction Columns With and Without Pulsation, UCRL-10928, Oct. 1963.

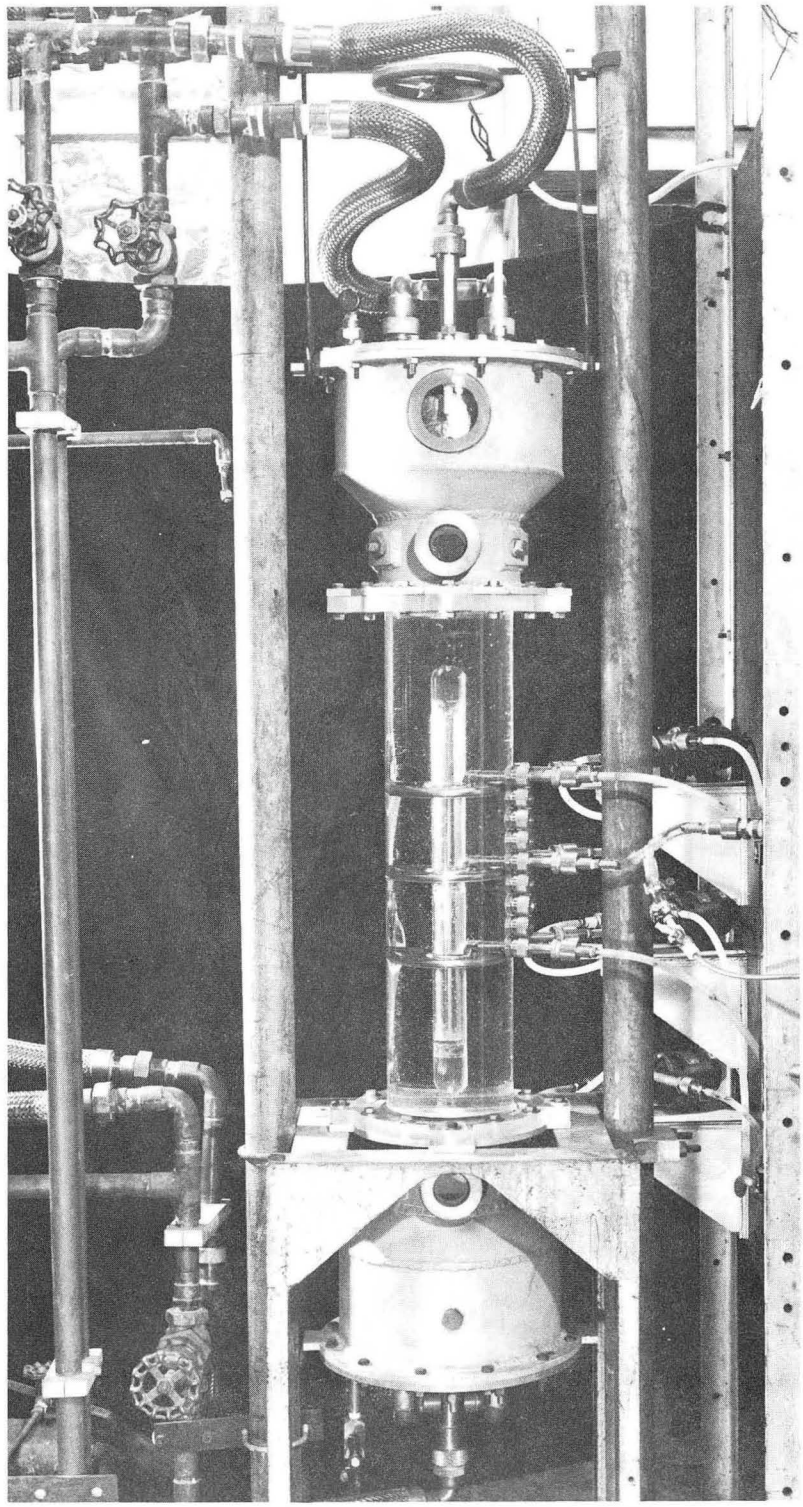

XBB 6812-7660

Fig. 1. Test unit for jet-mixed extraction device.

IMPROVED METHODS FOR CONTACTING FLUID PHASES IN SEPARATION PROCESSES

Edward J. Palkot, Jr., and C. Judson King

This project has been concerned with the evaluation of various novel gas-liquid contacting devices for absorption separation processes of practical importance. Attention has been focused upon situations in which a highly nonlinear equilibrium curve is encountered, leading to the requirement of relatively few equilibrium stages for any realistic degree of separation. Two chemical systems of this sort are currently being examined--the absorption of carbon dioxide into catalyzed potassium carbonate solutions and the adiabatic absorption of hydrogen chloride (or hydrogen fluoride) into water. Both these systems are of interest in connection with nuclear processing.

When a highly nonlinear equilibrium relationship is encountered along with the need for relatively few stages, cocurrent flow contacting devices can become attractive. A cocurrent flow contactor is not limited in throughput by flooding, which occurs in countercurrent and crosscurrent contactors. Consequently, cocurrent contactors can receive a very high throughput, which often results in a very high mass transfer efficiency in a relatively small equipment volume. Nearly all of the carbon dioxide–carbonate absorbers now in practical use involve countercurrent plate or packed columns. The plate efficiencies are very low, with the result that 25 or 30 stages are required for a separation that requires only one or two equilibrium stages. Hence it appears that there can be considerable incentive for using cocurrent flow devices for that system.

The following devices are being evaluated as cocurrent flow absorbers for the systems indicated above:

(a) rapid, cocurrent flow in a packed bed,
(b) slug-annular flow in an open pipe,
(c) froth flow in an open pipe,
(d) spray contacting.

The evaluation of froth flow makes use of the results obtained by Heuss, King, and Wilke[1, 2] (see also Chemistry Annual Report, 1964). The evaluation of the other systems makes use of other fundamental data available in the literature.

The carbon dioxide–carbonate system is rate-limited by a pseudo-first-order chemical reaction. As a result the gas-liquid interfacial area is an important design parameter. The interfacial area for high-velocity cocurrent flow through packing is not well known, and this generates uncertainty regarding the utility of the packed column. The froth flow system for carbon dioxide absorption requires a substantial liquid recycle, but compensates for this by providing very small bubbles, which give a large interfacial area. Froth flow is attractive for this application, and it appears that a countercurrent arrangement of two moderate lengths of pipe with cocurrent froth flow inside the pipes can replace a 25- or 30-plate column, with the pipe diameter being an order of magnitude less than that of the plate column. Two stages of slug-annular flow contacting are also attractive.

Although spray columns are ordinarily favored for low ratios of liquid to gas flow, they can be used for the carbon dioxide–carbonate system because of the large interfacial area they provide. A countercurrent arrangement of three internally cocurrent spray columns, each about 15 feet high, can replace the 25- to 30-plate column, but the system volume will not be reduced. Hence the spray tower does not seem to be so useful as the other cocurrent contacting methods.

References

1. J. M. Heuss, C. J. King, and C. R. Wilke, Mass Transfer in Cocurrent Gas-Liquid Flow, UCRL-11570, Aug. 1964.
2. J. M. Heuss, C. J. King, and C. R. Wilke, Gas-Liquid Mass Transfer in Cocurrent Froth Flow, A. I. Ch. E. J. 11, 866 (1965).

GROWTH OF STREPTOCOCCUS FAECALUS IN DENSE CULTURE[†]

L. D. Sortland[*] and C. R. Wilke

A fermentation system was designed and constructed to study the growth characteristics of microorganisms at low and high cell concentrations. The technique used to develop high cell densities utilized a rotating microfiltration unit to permit the removal of cell-free product from the fermenter. Figure 1 is a schematic diagram of the system. The fermenter volume and the filter were contained in a single unit composed of a series of concentric cyclinders. The annuli served as the fermenter volume; the second outermost cylinder supported a microfiltration membrane. Feed to the system was pumped at constant rates and the internal pressure built up to a value which would effect the required filtration rate. The system was operated batchwise and continuously, with and without filtration.

The anaerobic growth characteristics of Streptococcus faecalus were determined at 37°C and pH 7.0 for batch, continuous, and continuous-with-filtration modes of operation. Filtration rates in excess of a liter per hour (2.2 ml/cm^2-hr) were maintained for several days with cell concentrations up to 20% packed cell volume. The maximum cell density obtained was 40% packed cell volume, a factor of 45 larger than could be obtained in the usual batch culture. Excellent filtration efficiency was achieved; the concentration of cell in the filtrate was six orders of magnitude smaller than in the fermenter.

The filtration-fermenter combination has a larger productivity per unit volume than a continuous stirred tank fermenter when both are operated at the same specific growth rate. The advantage of the filtration-fermenter over the continuous stirred tank increases with decreasing specific growth rate and with increasing filtration rate. Very large increases in productivity are possible at low specific growth rates. The application of high-density fermentation to industrial processes will depend largely on the cost of filtration membranes, which are expensive at present. The presence of a cell-free effluent is advantageous when product recovery systems require the separation of cells from the fermentation broth. The filtration equipment is more complex than a stirred tank, but the added cost is offset by the smaller size required for the same throughput.

In batch culture, glucose was converted almost stoichiometrically to lactic acid. When an excess of glucose was present, disassociation of the rate of glucose consumption from the growth rate occurred as the culture entered stationary phase. In continuous culture with glucose limitation, the fraction of glucose going to lactate decreased with the dilution rate. The consumption of glucose for cell maintenance was negligible. Results in terms of substrate conversion, yields, viability, etc., from steady-state high-density experiments were similar to those obtained from low-density continuous culture.

The transient high-density experiments showed that the yield of cells per mole of glucose changed quite abruptly as a run progressed. Complex interactions between the cell and its environment were probably responsible. No consistent correlation between these yield changes and cell density was evident. The changes in cell yield were usually accompanied by alteration in the lactate yield constant, but no correlation could be developed.

The transient technique of operating the filtration-fermenter and the plotting methods employed for the data obtained appear useful for the rapid determination of changes in metabolic pathways which affect cell and product yield constants.

More detailed description of the experiments and tabulations of data are available.[1]

Footnotes and References

[†]Condensed from a paper submitted to Third International Fermentation Symposium, Rutgers University, September 2-6, 1968, New Brunswick, N. J.

[*]Present address: Bellcomm Inc., Washington, D. C.

1. L. D. Sortland and C. R. Wilke, Kinetics of a Dense Culture Fermentation, UCRL-18340, June 1968.

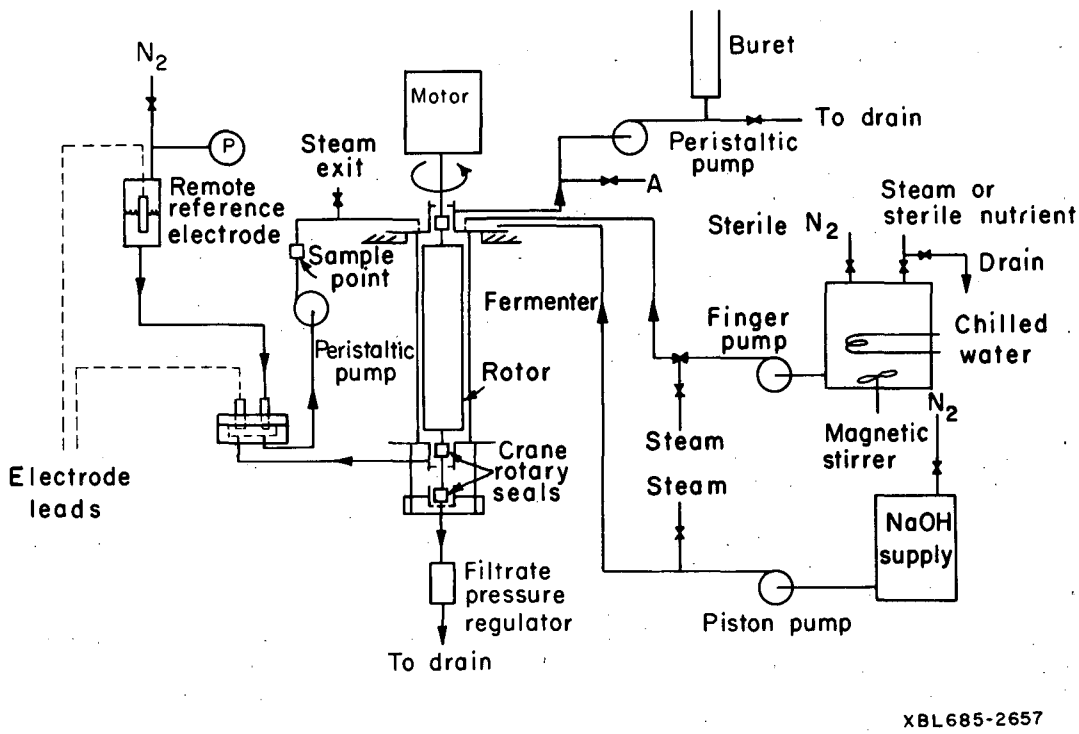

Fig. 1. A schematic diagram of the fermentation system.

IV. Instrumentation and Systems Development

ELECTRONIC INSTRUMENTATION AND SEMICONDUCTOR DEVICES

HYPERCRYOGENIC DETECTOR—FET UNIT—CORE OF HIGH-RESOLUTION SPECTROMETER†

Emanuel Elad* and Michiyuki Nakamura

A hypercryogenic high-resolution x-ray and γ-ray spectrometer consists of a lithium-drifted germanium detector and a germanium junction field-effect transistor (JFET) preamplifier.[1] The preamplifier uses two germanium JFET's cooled to liquid helium temperatures. Pulse generator resolution of the preamplifier for zero external capacitance is 0.28 keV FWHM (Ge), with a slope of 0.018 keV/pF.

Radiation detectors require thick depletion layers, which are realized by lithium compensation, forming p-i-n structures. In these devices only the leakage current generation components in the bulk and surface are significant. The generation current in the bulk space charge layer can be shown to be mostly dependent on the density of thermally generated carriers and the lifetime of the carriers. The density of thermally generated carriers is decreased strongly with decreasing temperature, which reduces bulk generation current. Unfortunately, there is little information on carrier lifetime (or capture cross sections) at cryogenic temperatures. There is evidence of increased trapping of carriers at liquid helium temperatures. This reduces the effective lifetime, as the probability of detrapping at these temperatures is very small. Therefore the increased trapping causes deterioration of resolution but does not increase bulk generation current.

The surface component of leakage current is mostly dependent on the density of thermally generated carriers and the surface recombination velocity. The density of thermally generated carriers exhibits the same temperature effects for surface leakage currents as for the bulk-generation currents. The main difference for the surface component of leakage current is the indirect temperature dependence on the concentration of generation-recombination centers. Because liquid helium cooling acts in effect as a cryopump, the vacuum of the cryostat is improved considerably, and the probability of adsorption of polar molecules on the detector surface is reduced.

The total leakage current should be reduced significantly by reducing the temperature from 77°K to 10 to 20°K.

The capacitance of germanium detectors is only weakly temperature-dependent, but is reduced with decreasing temperature. The parasitic resistance effects in germanium detectors are reduced with decreasing temperature.

Summarizing, we can say that the noise sources of the detector, both shot and thermal, are reduced and the signal-to-noise ratio improved as its temperature is lowered below 77°K. Higher bias voltage can be applied to the detector and this has the advantage of improving charge-collection statistics and reducing the capacitance of the detector, but has the disadvantage of higher microphonics.

The spectrometer was tested with three different germanium detectors from different ingots and with different histories. All three detectors were tested for temperature dependence of their resolution and behavior. Longer differentiation and integration pulse-shaping time constants were used at the lower temperatures. Improved resolutions were obtained, on the order of 0.4 keV for low-energy x rays and 0.68 keV for the γ rays of ^{57}Co. On one detector the bias applied at 12°K was 1500 V, whereas at 77°K it withstood only 600 V. Increased trapping effects were noticeable at the lower temperatures.

Footnotes and Reference

†Condensed from IEEE Trans. on NS-15 3, 477-485 (June 1968), 11th Scintillation and Semiconductor Symposium, Washington D. C., February 28-March 1, 1968.

*Present address: Nuclear Diodes, Inc., Prairie View, Illinois.

1. E. Elad and M. Nakamura, IEEE NS-15 1, 283 (1968).

DEVELOPMENT OF A GERMANIUM COUNTER SYSTEM FOR CHARGED-PARTICLE NUCLEAR SPECTROSCOPY†

E. A. McClatchie, M. S. Zisman, A. D. Bacher, C. Glashausser, R. H. Pehl, E. Rivet, and F. S. Goulding*

In recent months an intensive effort has been made to put into operation a Ge counter system for use in charged-particle nuclear spectroscopy. The higher density and atomic number of germanium make it superior to silicon for detecting high energy particles from nuclear reactions.

Figure 1 is a schematic diagram of the germanium counter holder installed in the 36-inch scattering chamber at the 88-inch cyclotron. The scattering chamber has been modified to allow liquid nitrogen to be pumped through a copper cold bar which runs around its circumference. A counter holder has been designed which is clamped to the cold bar by means of a stainless steel bellows, which is expanded against it by compressed air. The counter holder is also attached to a movable hub inside the chamber, and can be rotated to any angle by evacuating the bellows to unclamp the counter holder, rotating the hub, and then repressurizing the bellows. Under equilibrium conditions, the temperature of the counter when clamped is about -150° C.

The counter is operated as a windowless system. During an experiment the counter and the scattering chamber share a common vacuum (typically about 5×10^{-6} mm Hg) provided by a molecular sieve pump in the counter-holder unit and the diffusion pump on the chamber itself. The counter holder has a motor-driven vacuum valve which can isolate the counter from the chamber vacuum while the molecular sieve pump maintains a low internal pressure. Figures 2 and 3 are photographs of the counter holder.

Tests using the 42-MeV proton beam from the 88-inch cyclotron gave an optimum resolution (FWHM) of about 20 keV at 1.5 kV bias for scattering off a 70-$\mu g/cm^2$ Au target at a lab angle of 12 deg. The energy spread in the beam itself was 10 keV and the electronic noise was 8 keV. The peak-to-background ratio 1 MeV down from the elastic peak was about 5000:1. During a later experiment with a different detector, in which the resolution had degraded to 55 keV (because of radiation damage), a peak-to-background ratio of 19 000:1 was observed looking directly at the beam particles in the absence of collimators (see Fig. 4). The ratio of integrated counts in the background to counts in the peak was 3% (see Fig. 5), which can be accounted for by nuclear reactions in the germanium crystal.[1] These measurements were obtained by using 0.6- to 0.9-cm-thick lithium-drifted germanium detectors. It was found that the observed resolution depends on detector bias up to about 1.5 kV but improves very little between 1.5 and 2.5 kV.

We are also planning to use the Ge counter in conjunction with a Si ΔE counter for particle identification.

Reference

1. M. Q. Makino, C. N. Waddell, and R. M. Eisberg, Nucl. Instr. Methods 60, 109 (1968).

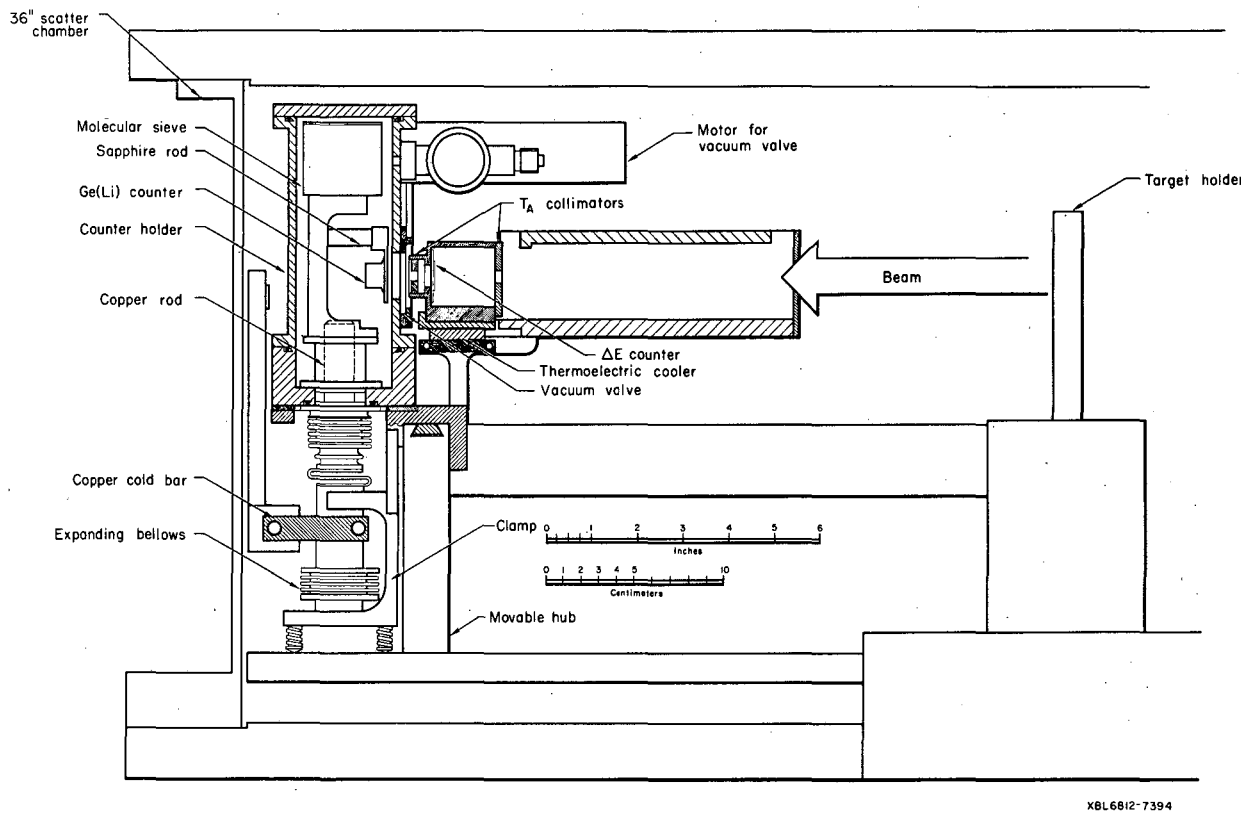

Fig. 1. Schematic diagram of the germanium counter holder.

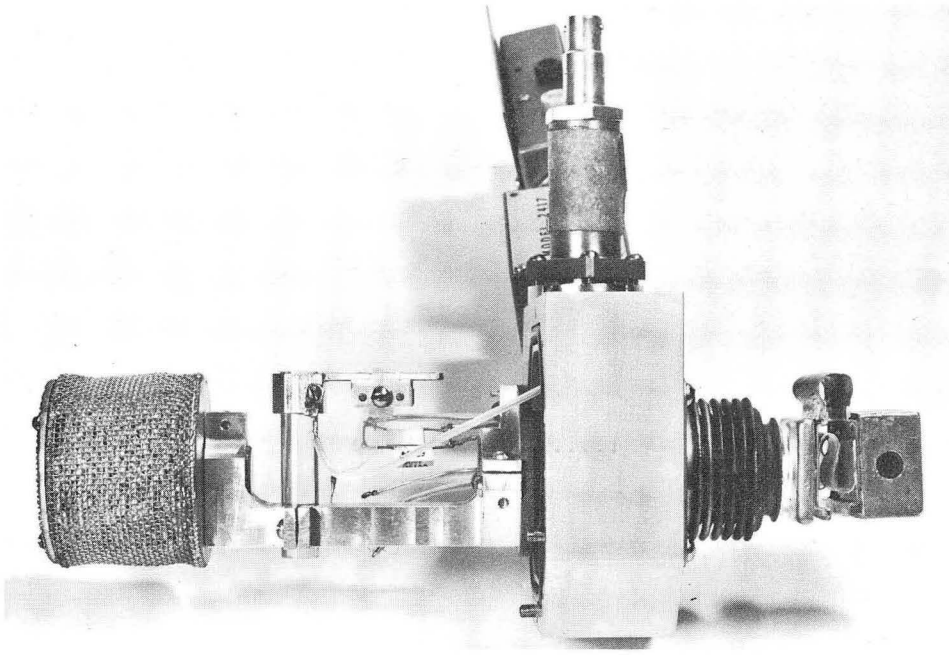

XBB 6812-7636

Fig. 2. Counter holder, showing molecular sieve pump and internal first stage of the FET preamplifier.

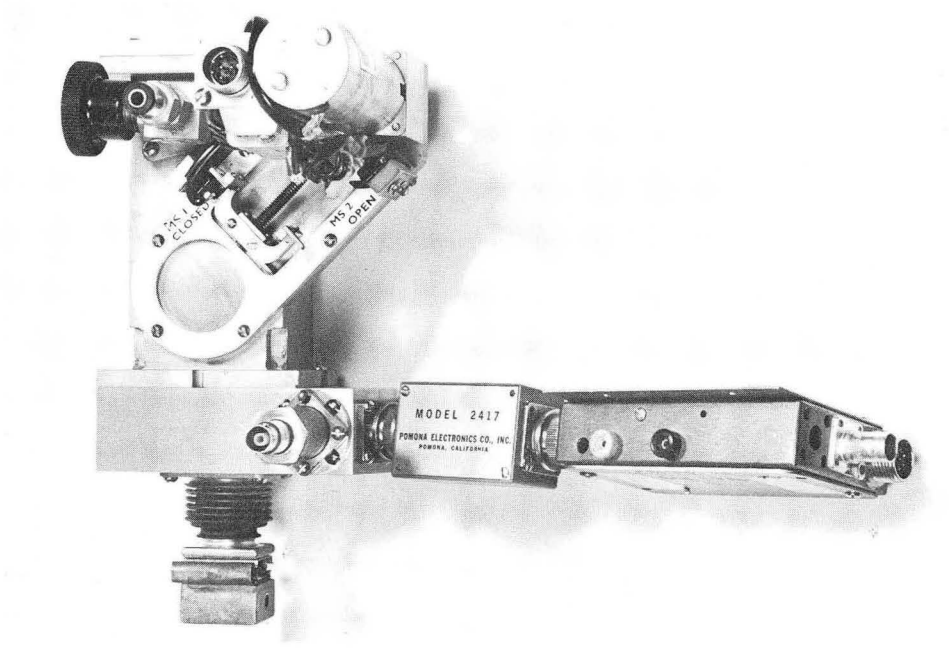

XBB 6812-7634

Fig. 3. Counter holder, showing motor-driven vacuum valve and external part of the preamplifier.

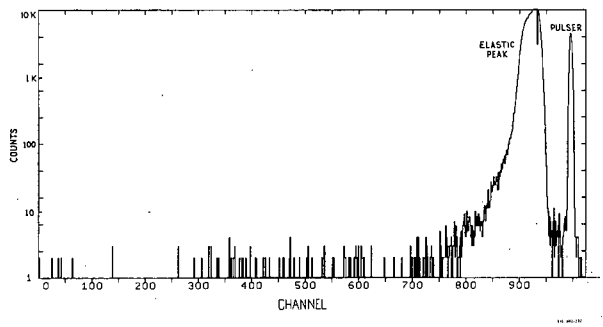

Fig. 4. Spectrum with counter in 42-MeV proton beam, 3 keV per channel.

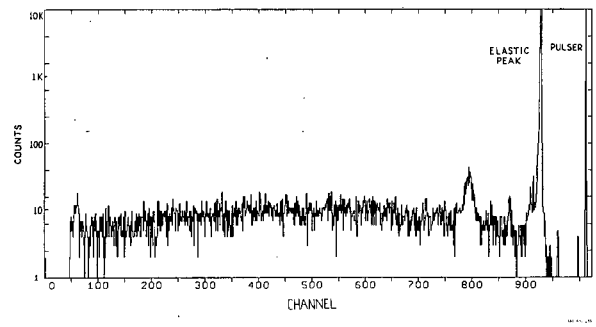

Fig. 5. Spectrum with counter in 42-MeV proton beam, 45.5 keV per channel.

GERMANIUM DETECTOR SYSTEM DEVELOPMENT

R. H. Pehl, F. S. Goulding, W. L. Hansen, E. Rivet, J. T. Walton, D. F. Malone, R. C. Cordi, R. C. Davis, and G. I. Saucedo

Progress in the development of germanium detectors continues to be largely determined by the quality of germanium crystals that can be obtained. Nearly all the new detectors produced this year were made from crystals pulled in our laboratory. The best of these detectors are approximately equal to the very best that we have made from Hoboken material.

The quality of detectors that can be made from different crystals varies decidedly, and there is a definite tendency for the detector quality to become worse as the crystal diameter becomes larger. In fact, we have not succeeded in making a high-quality detector (< 2.4-keV resolution at ^{60}Co) from crystals of greater than 4.0 cm diam.

During the calendar year 1968, 43 detector systems were put into service. Better high-capacity field-effect transistors enabled us to improve the resolution on most of the spectrometer systems produced. For example, we have obtained a resolution of 1.3 keV for the 122-keV ^{57}Co γ ray with a 35-cm^3 true coaxial detector having a capacitance of about 30 pF. With an 11-cm^3 planar detector a resolution of 1.8 keV for the 1173-keV ^{60}Co γ ray was obtained.

METHOD FOR COPPER-STAINING GERMANIUM CRYSTALS†

Ernest J. Rivet

Techniques capable of showing junctions and impurity inhomogeneities in semiconductor crystals constitute an important tool in device fabrication and development. Copper staining by white-light illumination of a sample immersed in a Cu^{++} solution has been used as a tool to decorate Si crystals.[1,2] However, to our knowledge, the decoration of Ge devices could be accomplished only through various adaptations of techniques based upon preferential chemical etching and electrolytic plating.[3] This report describes how to provide excellent decoration of Ge crystals by

copper staining.

The key conditions for proper decoration of Ge crystals by copper staining are:
(a) Low solution temperature ≈ 3° C.
(b) Illumination of the sample by infrared light.
(c) Careful positioning of the light source relative to the germanium sample so as to minimize the absorption of the infrared light.

The staining solution used in this work contained 20 g $CuSO_4$ $5H_2O$ and 1 cm^3 48% HF per liter of solution.[4] Ten fold variation in $CuSO_4$ and HF concentration showed no significant effect on the quality of the stain.

The solution must be kept at a temperature near the freezing point to obtain clear stains. As the temperature is increased to > 10° C the stains on the p-i-n junctions of a device become fuzzy; at room temperature a lack of contrast, especially between the p-i regions, makes the stain unusable. A brief investigation with solutions containing methanol and ethylene glycol indicated that stains cannot be obtained at temperatures lower than ≈ -10° C.

The use of light is essential in copper staining since the method is based on a photovoltaic effect causing more electrons to accumulate on n-type material, and therefore preferential plating of the Cu^{++} ions.[3] By comparison, the i region, on which more electrons accumulate than on the p region but less than on the n region, is plated accordingly. Most distinct region separation has been obtained with the use of an infrared lamp. Since infrared radiation is absorbed by the Cu^{++} solution, the sample is irradiated through the glass bottom of the dish and therefore through the sample rather than through the top of the solution.

A diagram of the apparatus utilized is presented in Fig. 1. The surface to be stained is carefully lapped and dried with a jet of dry nitrogen. The sample is then immersed in the solution, kept at ≈ 3° C by an ethylene glycol cooling coil. After a 30-sec delay the infrared light is turned on for a period of 2 to 4 minutes, depending upon the size of the sample. A liquid-nitrogen-cooled collimator allows longer exposure if desired without causing a serious temperature rise of the staining bath. During the staining exposure a 0.3-liter/min flow of Ar is bubbled into the bath to provide a stirring action, without which the presence of heat currents rising from the faces of the device cause severe distortion of the stain. A piece of copper pipe located in the bath promotes a circular motion of the solution.

Figure 2 shows a stain on a typical Li-drifted germanium crystal. The sharpness of the boundaries illustrates the usefulness of the method as a tool to investigate the shape and depth of the p-i-n regions. The method is sufficiently sensitive to show nonuniformities in germanium crystals prior to Li drifting.

The best detectors from the point of view of good resolution and low trapping have been made from materials exhibiting very uniform copper deposition when stained prior to lithium drifting. Therefore, as with our previous observation, when copper staining was used on silicon, the technique can be used to weed out poor-quality crystals without requiring the elaborate process of lithium drifting. The better crystals must still be graded by testing detectors, however.

Footnote and References

†Condensed from Nucl. Instr. Methods (to be published).

1. P. J. Whoriskey, J. Appl. Phys. 29, 867 (1958).
2. P. A. Iles and P. J. Coppen, J. Appl. Phys. 29, 1514 (1958).
3. P. J. Holmes, The Electrochemistry of Semiconductors (Academic Press, London and New York, 1962), Chapters 6, 7, and 8.
4. R. P. Lothrop and H. E. Smith, Lithium-Drifted Silicon Radiation Detector Production Process, UCRL-16190, June 1965.

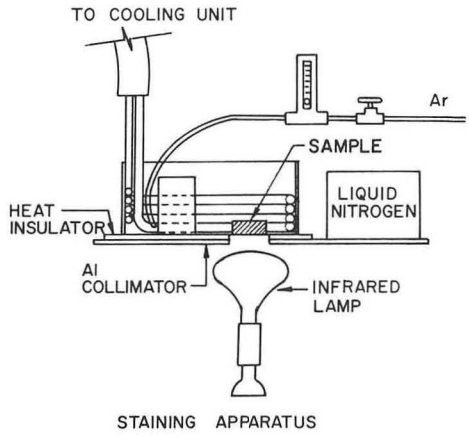

Fig. 1. Cutaway view of the staining apparatus.

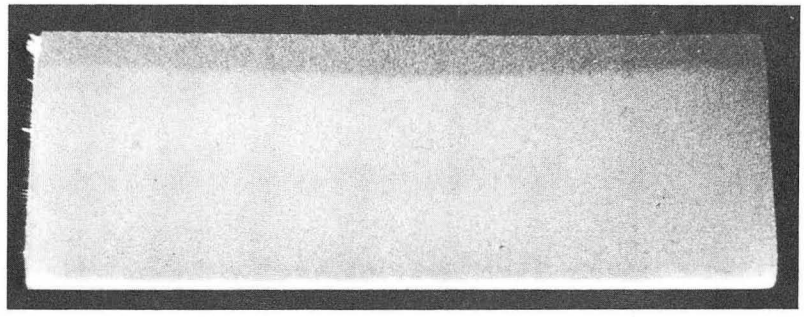

XBB 688-4906

Fig. 2. Stain of a Ge(Li) device. Heavy plating on the n material causes this region to appear as a white section at the bottom of the picture; the dark area at the top and the thick gray section in the middle correspond to the p and i regions respectively.

COMPUTER CONTROL SYSTEM FOR THE FIELD-FREE SPECTROMETER

Ron Zane, R. L. LaPierre, and Joseph E. Katz

Early in 1968, a system utilizing a Digital Equipment Corporation PDP 8 computer was assembled to collect data and control the operation of the Field-Free Spectrometer. The system hardware is interconnected as shown in Fig. 1.

An experimenter can, via the teletype, enter the initial spectrometer current, the current increment, the number of increments, the increment rate, and the number of scans. The real-time clock module provides the time base for the system. The spectrometer magnet current is set, by means of the output register, to the value determined by the system program. Magnet current is controlled to an accuracy of $1:10^6$. The setting of the relays in the magnet current supply is monitored by the shunt relay monitor. Computer-controlled scalers totalize the counts detected during each current increment. The interlock control provides a program interrupt whenever any one of 12 external sensors indicates a fault condition. The software system determines which sense line caused the interrupt and then either issues a warning for nonfatal faults or

terminates the experiment and preserves the "good" data for fatal faults. This system has been running a series of experiments, without the need of operator intervention, on an around-the-clock schedule with a high degree of reliability.

The software system program was written by Derik V. Armstrong of the Mathematics and Computing Group. Presently the system software produces, on the CRT, an on-line histogram display of the data. High-quality permanent graphic output is available by incorporating the CalComp 565 plotter in the system program. It is not possible at the present time, because of computer memory limitations, to provide both CRT and CalComp displays simultaneously.

It is intended to write a system program that will incorporate the high-speed paper tape reader and punch to perform these several functions. The system will first acquire the data from a series of scans and then perform a limited amount of analysis and produce permanent high-quality CalComp plots.

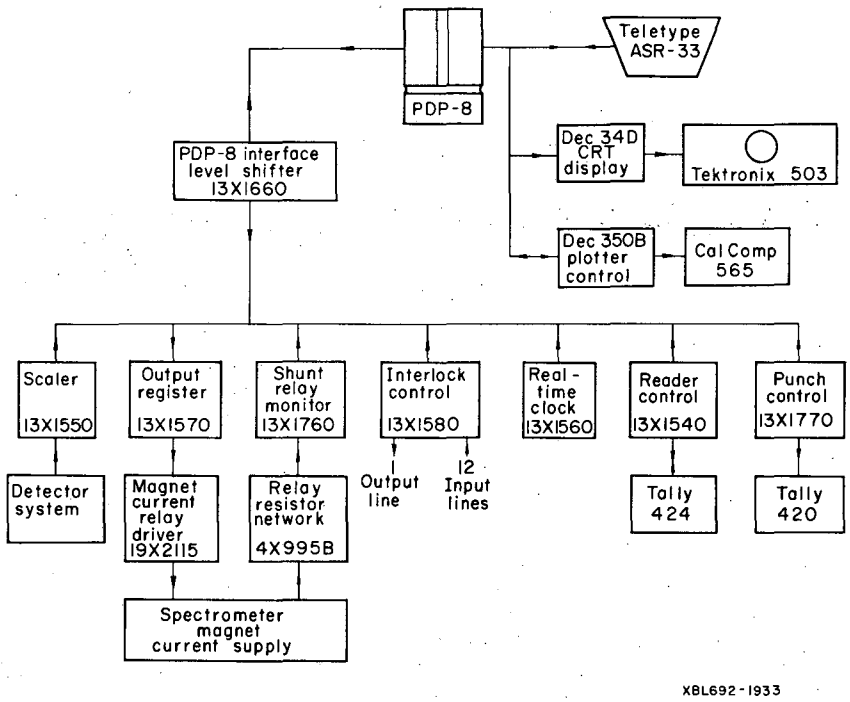

Fig. 1. Field-free spectrometer computer control and data-acquisition system.

CONTROL UNIT FOR LINKING PULSE-HEIGHT ANALYZERS TO A PDP-9 COMPUTER

Richard L. LaPierre

We are in the process of building a unit that will link the various pulse-height analyzers at this installation to a PDP-9 computer. The transfer of data will be under computer control, and will occur via programmed data transfer.

One of the design objectives is to allow the memories of suitable pulse-height analyzers to function as fast random-access bulk-storage devices for the PDP-9 computer. We have a Nuclear Data 160 analyzer with a 4K 18-bit memory which will be used in this manner.

The design of the control unit allows the following modes of operation for the transfer of data between the computer and the memory of the analyzer:

(a) "Read" into the computer, commencing at location X in the analyzer, the contents of m successive locations.

(b) "Write" into the analyzer, commencing at location X, m successive words.

(c) "Add-1" to the contents of location X in the analyzer.

Due to the differences in the various analyzers, it was decided to have one central control station which would serve as the link between the computer and all the analyzers. The design philosophy is such that this unit will also serve as the link for a commercial memory system when one is added to the PDP-9 system. At each analyzer station will be an auxiliary unit which serves as the interface between the specific analyzer and the central control station.

The auxiliary unit offers an inexpensive solution to the problem of changing the analyzer's system configuration without the accompanying change of numerous cables. The auxiliary unit becomes a part of the analyzer system and the analyzer operates in normal local control. A standard cable connection to the central control station permits the option of computer control of the system.

SPECIAL-PURPOSE COMPUTER FOR LINKING PULSE-HEIGHT ANALYZERS WITH A DIGITAL INCREMENTAL PLOTTER

Richard L. LaPierre and Michiyuki Nakamura

We have designed a fixed-wire computer which features the advantages of a computer-digital plotter for displaying the information stored in an analyzer. The special-purpose computer is portable and has its own digital plotter, which eliminates the inconvenience and time delay normally encountered when work is submitted to a computer center.

The instrument contains the electronics to allow it to be interfaced with either binary-coded-decimal or binary-type analyzers. The plotted output can be on linear or semilog paper. Logarithms of the input data are computed in base 2 and converted to base 10, for y-axis control in semilog plots. The logarithms are generated by a method reported in the literature,[1,2] and the organization of our machine readily lends itself to an expansion of the error-reduction technique suggested by Combet et al.[2]

A machine language program was written for the CDC 6600 computer which duplicates the operations performed by our system. The errors introduced in generating the logarithms are shown in Fig. 1. The accuracy of the logarithm generator is sufficient to produce an overall positional accuracy of ±1 step of the incremental plotter.

The length of time to plot a graph is determined primarily by the pen cycle time of the plotter; however, it is also dependent on the complexity of the spectrum and the number of channels (data points) per inch. A typical plot time for a SCIPP 1600-channel analyzer is 3.5 minutes for a six-cycle log graph with 20 channels per inch.

The operation of the system is fully automatic once the zero reference of the plotter has been established. Graphs are then produced whenever the analyzer enters the parallel readout mode, and a paper-advance feature provides suitable separation of the plots. During the last year, the system has been in nearly continuous around-the-clock operation. In a recent series of runs in which spectra from various specimens were taken on the SCIPP 1600, the entire series was completed in 16 hours for 25 spectra of 0.5-hour data-collecting periods. The spectrum from each individual run was analyzed immediately following each run and during the data collecting of the following run.

The technique of generating logarithms can be readily used by computers with small memories in which use of subroutines may not be desirable.

References

1. J. Mitchell, Computer Multiplication and Division Using Binary Logarithms, IRE Trans. Electron. Computers EC-11, 512-517 (1962).
2. M. Combet, H. Van Zonneveld, and L. Verbeck, Computation of the Base Two Logarithm of Binary Numbers, IEEE Trans. Electron. Computers, EC-14, 863-867 (1965).

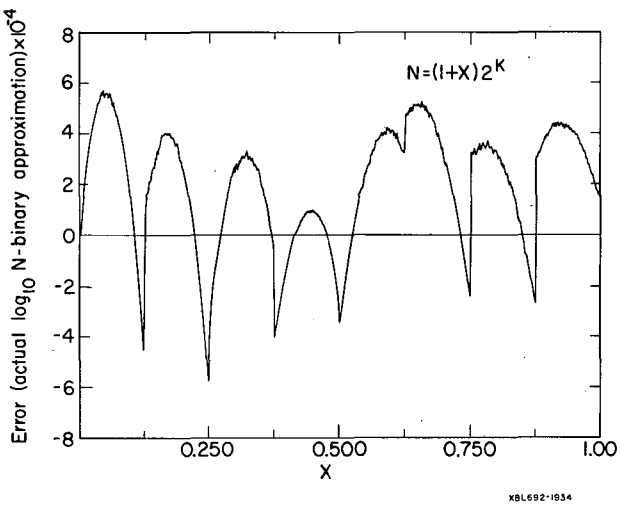

Fig. 1. Errors introduced by the logarithm generator.

ON-LINE PDP-9 COMPUTER FOR FISSION RESEARCH

Craig A. Denison, James B. Hunter, Richard C. Jared,* Richard L. LaPierre, Michiyuki Nakamura, and Elizabeth Quigg

A Digital Equipment Corporation PDP-9 computer was installed and put into operation this past year. The PDP-9 is being used on-line for data acquisition of fission experiments and off-line for data analysis, sorting, and calculations. More complex computations and analysis are done at the main computer center with the Control Data Corporation 6600 computer.

The PDP-9 system, when originally installed, consisted of 8K 18-bit word memory, extended arithmetic element, CalComp plotter and control, and oscilloscope display and control. Later, we added Dectapes, additional 8K memory, automatic priority interrupt, and a large-screen CRT display. We built our own controllers for an IBM compatible magnetic tape transport and a 130 track, movable head disk (manufactured by Data Disk). Presently under construction is a device synchronizer for a Data Link[1, 2] which will allow the PDP-9 to communicate directly with the CDC 6600 computer. Interfaces and controls were built for ADC's, stretchers, digital gain stabilizers, and pulse-height analyzers.

The programming for the PDP-9 is built around the advanced software package supplied by DEC. Several small utility programs have been written, such as CalComp plotting, pulse-height analysis, CRT display, maintenance, and test routines. A program for a multidimensional experiment has been written for on-line data acquisition with these features: (a) digital gain stabilization, (b) sorting and display for any of up to eight "singles" spectra, (c) dumping of all data on magnetic tape for later analysis on the CDC 6600, and (d) off-line analysis of data. We feel that the recent addition of the automatic priority interrupt and the additional 8K of memory will ease some of the programming obstacles and problems encountered in the past.

Footnote and References

*Presently on educational leave with an AEC scholarship.

1. S. W. Andreae, A Computer Data Link for High Energy Physics Experiments, UCRL-17918, Nov. 1967.

2. R. W. Lafore, Error Checking and Other Aspects of Data-Link Organization, UCRL-17934, Nov. 1967.

PULSE-HEIGHT COMPENSATION SYSTEM FOR Ge(Li) TIMING†

J. M. Jaklevic, F. M. Bernthal, J. O. Radeloff, and D. A. Landis

Due to the variation in the rise time of the pulses produced by Ge(Li) γ-ray detectors, it has become common practice to employ a leading-edge discriminator to extract the timing information from the detector pulse.[1-3] This method has the advantage over crossover or fractional amplitude pickoff timing of a smaller variation of trigger time with rise-time variations, but suffers the disadvantage of introducing a dependence of trigger time upon the energy of the pulse. Although this energy dependence is of little consequence in measurements involving coincidences between narrow energy regions of the Ge(Li) spectrum, it can produce a significant broadening in the time-resolution curve in the more frequently encountered cases in which one is interested in the full energy spectrum of γ rays. We describe here a Ge(Li) fast-timing system which employs a relatively simple method of compensating for the energy dependence of the timing signal.

Operation of the pulse-height compensation system can best be explained with reference to Fig. 1. The upper curve is a plot of centroid position of a time-to-amplitude converter (TAC) output as a function of energy for a 13-mm depletion depth planar Ge(Li) detector. The data were obtained by using a three-parameter incremental tape data storage program on the PDP-7 computer.[4] The source was ^{60}Co and the "START" signal was provided by a NaI scintillation detector. The "error" bars are used to indicate the full width at half maximum (FWHM) of the time distribution. Analysis of the dependence of centroid position on energy shows that the time shift can be approximated by a function proportional to log E, where E is the energy of the signal. Therefore by mixing a signal proportional to log E with the time output one can essentially compensate for this energy dependence. The lower curve in Fig. 1 is a plot of centroid positions taken under conditions identical to those for the upper curve, except that the compensation signal has been mixed with the TAC output. The compensated signal exhibits only a slight energy dependence over the range shown. This could be improved by more careful adjustment of the logarithmic amplifier gain, and perhaps by generating a more complex function than the simple logarithmic one used here.

Figure 2 is a plot of the ^{22}Na time distribution obtained with the NaI detector and the 10-mm planar Ge(Li) detector. The plots represent uncompensated and compensated data respectively. As indicated in the figure, the broader distributions are data for all energies above threshold ($\approx$ 20 keV); the narrower peaks include only events with energy greater than 100 keV. The broadening of the distribution in the former case is caused by the poor time resolution obtained at very low energies and by incomplete pulse-height compensation due to the inadequacy of the log E approximation at lower energies. In general, the effect of the low energy pulses on the time distribution is a very slight broadening at FWHM and a 10 to 20% broadening in the full width at tenth maximum [FW(0.1)M].

The compensation system has been applied to several different types and sizes of detectors. In general there is approximately a factor of 2 improvement in both FWHM and FW(0.1)M. Since the FW(0.1)M is a more realistic measure of the coincidence resolving time possible in a given configuration, one can conclude from these measurements that if one uses pulse-height compensation, resolving times of 2τ = 29 nsec and 2τ = 60 nsec possible for planar-planar and coax-coax configurations respectively. Although this improvement is not so great as that which should be obtainable by using other techniques,[5-7] we feel that the simplicity of the method makes it attractive for a large number of applications.

Footnote and References

†Condensed from Nucl. Instr. Methods, (to be published).

1. R. L. Graham, I. K. McKenzie, and G. T Ewan, IEEE Trans. Nucl. Sci. 13[1], 72 (1966).
2. G. T. Ewan, R. L. Graham, and I. K. McKenzie, IEEE Trans. Nucl. Sci. 13[3], 297 (1966).
3. J. Pigneret, J. J. Samueli, and H. Sarazin, IEEE Trans. Nucl. Sci. 13[3], 306 (1966).
4. L. B. Robinson and J. D. Meng, Multiparameter Data System, privately circulated report, June 1967.
5. J. P. Fouan and J. P. Passerieux, Nucl. Instr. Methods 62, 327 (1968).
6. S. Gorni, G. Hochner, E. Nadav, and H. Zmora, Nucl. Instr. Methods 53, 349 (1967).
7. B. T. A. McKee, Nucl. Instr. Methods 62, 333 (1968).

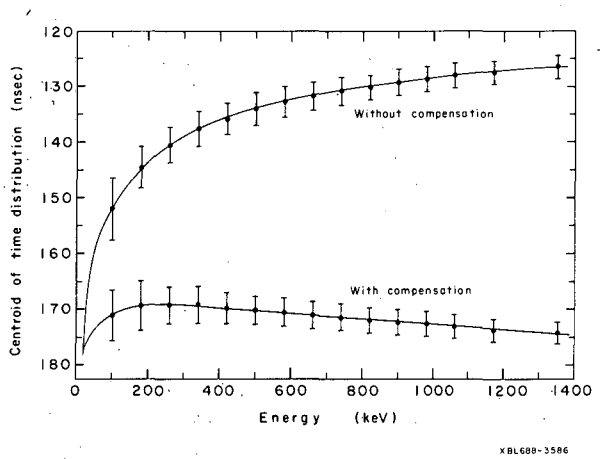

Fig. 1. Plot of centroid position as a function of energy for a 13-mm depletion depth planar Ge(Li) detector. The "error" bars are used to indicate the FWHM of the time distribution. The upper curve is without compensation; the lower curve shows the effect of mixing the log E compensation signal with the TAC output.

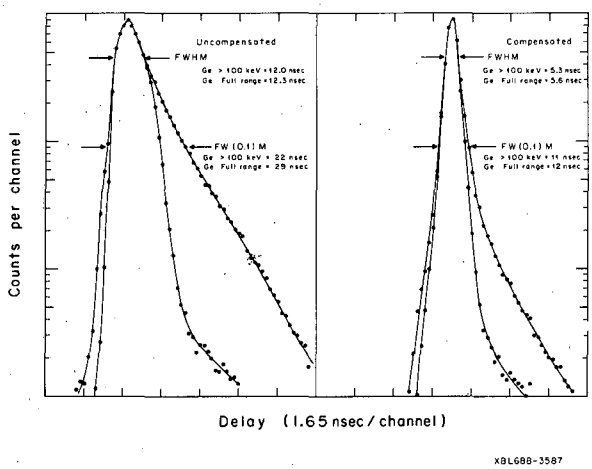

Fig. 2. Timing curves obtained with a 10-mm depletion depth planar Ge(Li) detector in coincidence with a NaI scintillation spectrometer, showing the effect of pulse-height compensation on the time distribution. Curves are shown for both the full-energy spectrum (all events above approximately 20 keV) and the spectrum of events with energies greater than 100 keV. The "STOP" signal was supplied by the Ge(Li) detector.

GENERAL INSTRUMENTATION AND DEVELOPMENT

WAIST-TO-WAIST TRANSPORT IN THIN-LENS OPTICS[†]

A. U. Luccio

A simple graphical method has been developed that would enable one to calculate very quickly the transport of a charged beam through an optical system of many elements, in the thin-lens approximation. The method can be used to deal with accelerating (immersion) lenses as well, and it is hence useful as an aid in designing ion guns.

The basic system of equations used is

$$v = \gamma\phi\,[u(u-\phi)+1]/[(u-\phi)^2+1], \tag{1}$$

$$\mu^2 = X_2/\gamma X_1 = \phi^2/[(u-\phi)^2+1], \tag{2}$$

where $u = z_{01}/X_1$, $v = z_{02}/X_1$, $\phi = f/X_1$, and the following definitions apply:
γ = acceleration factor,
z_{01}, z_{02} = distances from the lens to the source and image waist,
X_1, X_2 = characteristic lengths of waists,
μ = linear magnification,
f = focal length.

A first family of curves (Figs. 1 and 2), with parameter ϕ, represents the function v/γ vs u from Eq. (1), and allows one to calculate z_{02}, given z_{01}, X_1, and f.

A second family, μ^2 vs u (Fig. 3), from Eq. (2), allows one to calculate the linear magnification and X_2.

Putting $X_1 = X_2$, one proceeds with the calculation for the next lens.

Footnote

[†]Condensed from UCRL-18217.

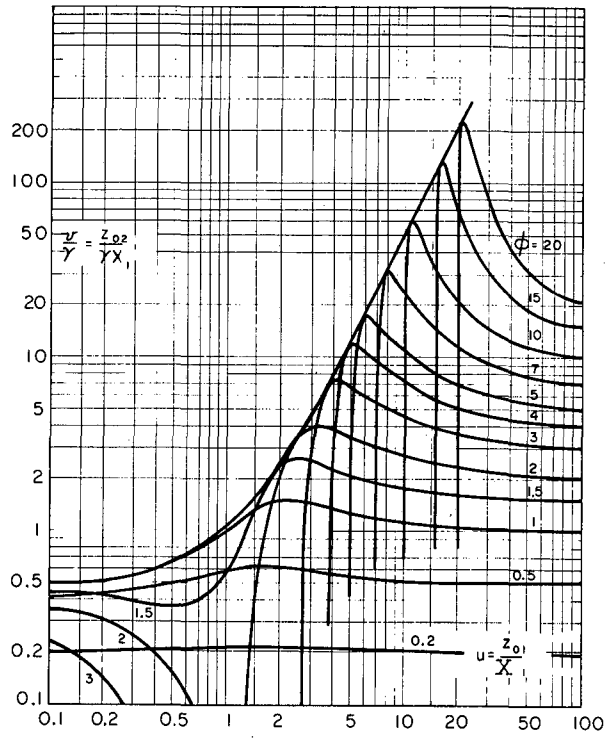

Fig. 1. The function $v(u, \phi)/\gamma$. Positive values.

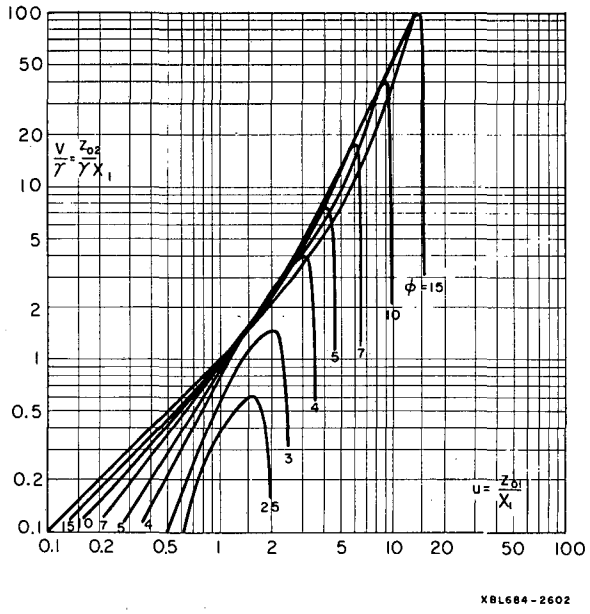

Fig. 2. The function $v(u, \phi)/\gamma$. Negative values. $\phi > 2$.

Fig. 3. The function $\mu^2(u, \phi)$, magnification.

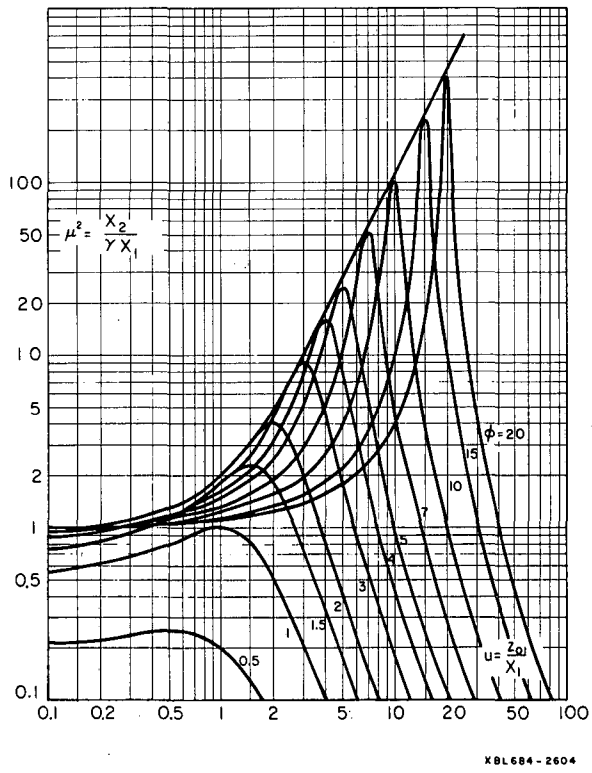

88-INCH CYCLOTRON DEVELOPMENT

D. J. Clark, J. Ernst, A. U. Luccio, and F. Resmini

In 1968 the improvements to the cyclotron and beam-handling system included the installation of another 10-inch oil diffusion pump on the dee tank, the installation for testing of another center-region defining slit called the "3/4-turn collimator," the installation and successful testing[1] of the two 110-deg analyzing magnets in the new Cave 4 area, and the operational use of a fast vacuum valve.[2]

Beam Development

Beam development work at the 88-inch cyclotron has been mainly devoted to some special items in connection with new experimental needs or the installation of the analyzing-magnet system. Work on the development of single-turn extraction, reported in 1967, has been temporarily abandoned because of the problems deriving from the high dee-voltage ripple. The consequent smearing out of the turn structure prevents single-turn operation except for very low energy beams. This work might then be successfully reconsidered only when the ripple is reduced to no more than 0.1% (peak to peak) rather than the present typical values of 0.6% to 0.8%.

In connection with a series of experiments requiring the use of time-of-flight techniques,[3] a few runs have been devoted to the production of narrow-phase-width beams. The goal was to produce beams of width in the range of 1 to 2 nsec FWHM, with a reasonable extracted intensity, around 1 μA, initially for 95-MeV alphas and 55-MeV protons. For these particles and energies the corresponding phase widths are of the order of 6 to 8 deg. The technique used was to properly clip the internal beam, usually distributed over a 30- to 40-deg phase interval, by means of a slit placed 1/2 turn after the ion source called the "half-turn collimator," which has been described elsewhere.[4] The internal phase probe, whose signal is fed to a sampling scope, is used to monitor the internal beam width and to check the phase history as a function of radius.

A typical phase probe picture for 95-MeV alphas is shown in Fig. 1. The horizontal scale is 4 deg/cm, which, at the operating frequency of 10.8 MHz, corresponds to 1.3 nsec/cm. The beam is seen to have a FWHM of about 2 nsec. The half-turn collimator gap is 1.5 mm. In these conditions we would extract up to 1.50 μA. Similar results were obtained with 55-MeV protons. Figure 2 shows a time-of-flight spectrum recorded under the experimental conditions reached for this last beam: the FWHM is about 1.5 nsec, the intensity of the extracted beam 2 μA.

No attempt has been made so far to further reduce the time width of the beam by means of the other collimators available, namely the 3/4-turn collimator and the defining slits. The limit of 6 to 8 deg has to be considered as the minimum obtainable with only the use of the half-turn collimator, in the sense that a further reduction in its gap width merely reduces the transmitted beam intensity, without appreciable effects on the phase width. This behavior is clearly understandable as due to the presence of radial oscillations whose amplitude is of the same order of magnitude as the difference in radius corresponding to different phases.

Transmission tests through the analyzing magnets[1] were carried out with two beams, namely 50-MeV alphas and 45-MeV protons. The purpose was to measure the transmission efficiency for two rather different beams (different in terms of the machine operating conditions) and look at the millisecond time structure of the analyzed beams. These last measurements were desired because one expects the dee-voltage ripple to produce important effects.

The slit widths of the analyzing magnets were chosen so as to give an energy resolution $\Delta E/E = 0.02\%$. The beam optics were tuned so that the radial emittance of the analyzed beam is of the order of 4 mm-mrad. The measurements of the time structure were performed by intercepting the beam with a copper plate, amplifying the signal with a direct coupled amplifier, and feeding it to an oscilloscope.

The transmission efficiencies to the target ranged between 0.5% and 0.7% of the whole extracted cyclotron beam for 45-MeV p and 50-MeV α. The beam currents on target were about 0.5 μA for a well tuned beam. Under these conditions a typical time structure of the analyzed beam is shown in Fig. 3, the horizontal scale being 2 msec/cm. One can clearly locate periodicities at 60 Hz resulting from the presence of the dee-voltage ripple.

The almost complete absence of beam for long periods of time, pointing out a very low macroscopic duty cycle, indicate dramatically the need for better dee-voltage regulation. Also one could reasonably guess that considerably higher transmission efficiencies could be obtained if the cause of the low duty cycle were suppressed. Present programs call for installing a better regulated dee voltage supply early in 1969, and at that time these measurements will be repeated.

Deflector Development

In October the old deflector developed some leaks and had to come out for repair. It was decided to use the new Mk II deflector as a spare. It had been used successfully on several previous tests[4] with the positive regenerator electrode turned on for higher-energy beams, and turned off for some low and medium energies. Since the regenerator caused some voltage-holding problems, and did not significantly improve the energy resolution or extraction efficiency, we decided to remove the regenerator and operate the deflector as a conventional electrostatic channel. Optimum electrode positions for stable operation were found for beams throughout the cyclotron operating range, including 55-MeV protons and 120-MeV α particles. Deflected beam powers of 1 to 2 kW were obtained--approximately as much as with the old deflector.

For the setup of beam transport lines it is very important to know the size and position of the radial and vertical cyclotron external beam virtual beam source as a function of particle, energy, magnetic field, and deflector settings. In order to study the properties of the present (or an improved) electrostatic deflector a FORTRAN program FLECT (based on CYCLONE) was developed for the integration of particle paths through the fringe field of a cyclotron.

Calculations were done for medium and high magnetic fields corresponding to 65- and 130-MeV α particles. The motions of particles contained in a phase ellipse of 30 mm-mrad were traced through the deflector. The virtual source properties derived are in good agreement with measurements for the present deflector. A calculation for a radially focusing second electrode with quadrupole shape showed that it is possible to increase the transmission of the deflector by producing a more parallel beam leaving the cyclotron, rather than the present very divergent beam without a radially focusing device. Changing radial position, gap, and voltage of the quadrupole electrode would allow variation of the position and size of the virtual source over a wide range, adjusting the transmission efficiency and the dispersion of the cyclotron to experimental conditions.

Proposed High-Transmission Beam of Variable Energy Resolution to Cave 4

The present beam optics for Cave 4 (UCID-3094) satisfy the original requirement of high energy resolution. It now appears desirable to also obtain solutions with high transmission efficiency, especially for experiments with polarized beams in which the intensity is low. The requirements for good beam optics may be summarized as

(a) variable energy resolution over a wide range,
(b) full transmission of analyzed beam to target,
(c) nondispersive, variable-size focus on target.

Beam optics calculations were performed with the program BEAM.

The transport elements of a system with variable energy spread are shown in Fig. 4. The elements different from the present system are an additional quadrupole doublet between the two 110-deg magnets, together with an alternative analyzing slit II. Also the doublet in front of the scattering chamber has been replaced by a quadrupole triplet to provide variable beam size on target.

Horizontal and vertical beam envelopes for one special triplet setting are plotted in Fig. 5. The second doublet provides a parallel beam entry to the analyzing magnet with a focus at the new analyzing slit II. The best energy resolution at this point is 0.11%. For smaller radial size of the virtual source, even higher resolution may be obtained.

In order to get a sharp, nondispersive focus at the target the dispersion due to the analyzing magnet has to be compensated by the following 110-deg magnet. The requirements for that purpose are

(a) Parallel beam out of second 110-deg magnet achieved by an intermediate horizontal focus at point III, which is symmetric to slit II with respect to slit I.

(b) Parallel beam after the cleanup magnet nondispersive if the beam size at the intermediate focus III is the same as at slit II (-1 magnification).

These conditions can be fulfilled by the settings of the quadrupole doublet Q3. The vertical focusing is done by providing a focus at the position of the analyzing slit I. For the vertical focusing through the doublet Q3 the calculation (Fig. 5) shows that the beam is well below the critical limit inside the second 110-deg magnet.

Axial Injection

The construction and installation of the new axial injection transport line[6] was completed during 1968. This line contains three sets of 3-in.-aperture electric quadrupole triplet lenses. For beam monitoring there are scanning wires, quartz plates with TV viewing, and Faraday cups (Fig. 6). This system replaces the old line of quadrupole doublets.[7] The duoplasmatron test source, constructed previously, was tested on the bench and then installed with the new bending magnet on the axial injection line. A new 8-inch diameter plug for the upper magnet yoke, with removable sections, was installed. The sections allow median plane balancing, and a 1-in. hole lets the beam travel to the median plane. Small concrete shielding blocks were stacked on top of the magnet yoke, and in the hole in the vault roof, to reduce the cyclotron neutron flux in the axial injection area.

The effect of the magnet-yoke magnetic field on the particles injected axially into the cyclotron has been studied.[8] The behavior of the beam has been computed, with the measured magnetic field, by numerical integration of the equations of motion. The "hole lens" shapes the beam, bringing it to periodic focusing near the center of the cyclotron. By choosing properly the injection energy and the focal power of the last element of the axial injection system, a waist can be set at the cyclotron center. Two operation modes appear possible: mode I, $3\lambda/2$ (Fig. 7) and mode II, λ (Fig. 8).

Studies were done on increasing the cyclotron time acceptance of axially injected beam by bunching the dc beam into 20- to 40-deg wide rf pulses synchronized with the dee frequency. One possible design for such a buncher[9] would be a drift tube with a sawtooth voltage on it (Fig. 9). For source-limited beams, the increase in intensity made possible by a buncher is a factor ranging from 5 to 20, depending on buncher wave shape, cyclotron phase acceptance, and beam energy spread (Fig. 10). Some study of the production of the sawtooth wave shape on a drift tube or on a single-gap ferrite-loaded cavity shows that large power is required at frequencies up to 16 MHz, voltages of 2 to 3 kV, and a 10% reset time. This power could be produced, but we are now investigating the alternative of using drift tubes with harmonic sine wave voltages.

References

1. E. A. McClatchie, R. L. Hintz, F. B. Selph, W. S. Flood, B. G. Harvey, and F. Resmini, Beam Analyzing System for a Variable-Energy Cyclotron, Bull. Am. Phys. Soc. 13 [11], 1443 (Abstract).
2. A. Hartwig, Fast Acting Valves, UCID-3211.
3. Joseph Cerny (Lawrence Radiation Laboratory), private communication.
4. D. J. Clark, P. Frazier, A. Luccio, P. Morris, and F. Resmini, 88-Inch Cyclotron Development, in Nuclear Chemistry Annual Report, 1967, UCRL-17989, Jan. 1968, p 292.
5. J. Ernst, Mech. Engr. Note M4116, Lawrence Radiation Laboratory–Berkeley.
6. F. Resmini, Optics of the Axial Injection Line for the 88-Inch Cyclotron, UCRL-18442, Sept. 1968.
7. R. Burger, D. J. Clark, E. Close, and H. Kim, Machine Development at the Berkeley 88-Inch Cyclotron, IEEE Trans. Nucl. Sci. 13 [4], 364 (1966).
8. A. U. Luccio, Axial Injection Studies on the 88-Inch Cyclotron: "Hole Lens," UCRL-18016, Jan. 1968.
9. F. Resmini and D. J. Clark, A Proposed Sawtooth Buncher for the 88-Inch Cyclotron Axial Injection System, UCRL-18125, March 1968.

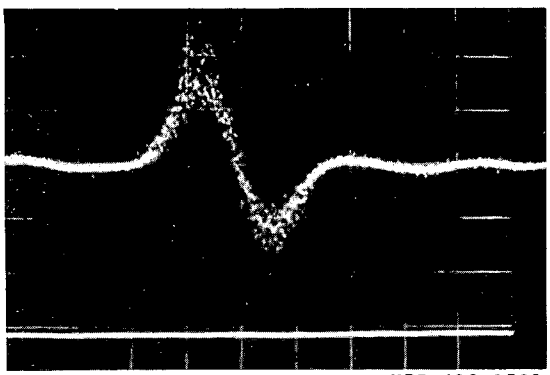

XBB 692-1382

Fig. 1. Beam pulse on internal phase probe of 95-MeV α particles. Horizontal scale: 4 deg/cm.

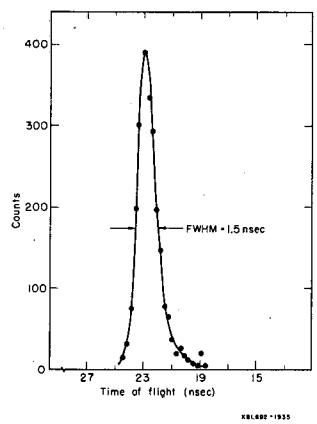

Fig. 2. Time-of-flight spectrum for 10-MeV α particles from ^{28}Si (p, α) ^{25}Al.

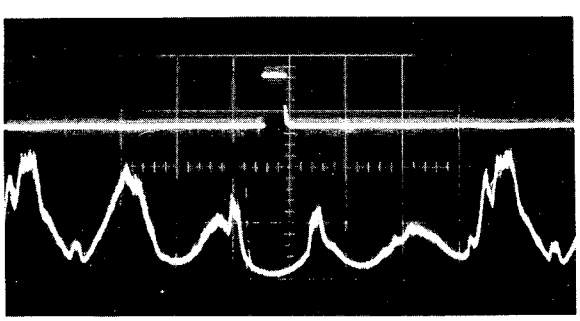

XBB 692-1381

Fig. 3. Time structure of analyzed external beam. Energy spread is about 0.02%. Time scale is 2 msec/cm. Bottom line is zero beam.

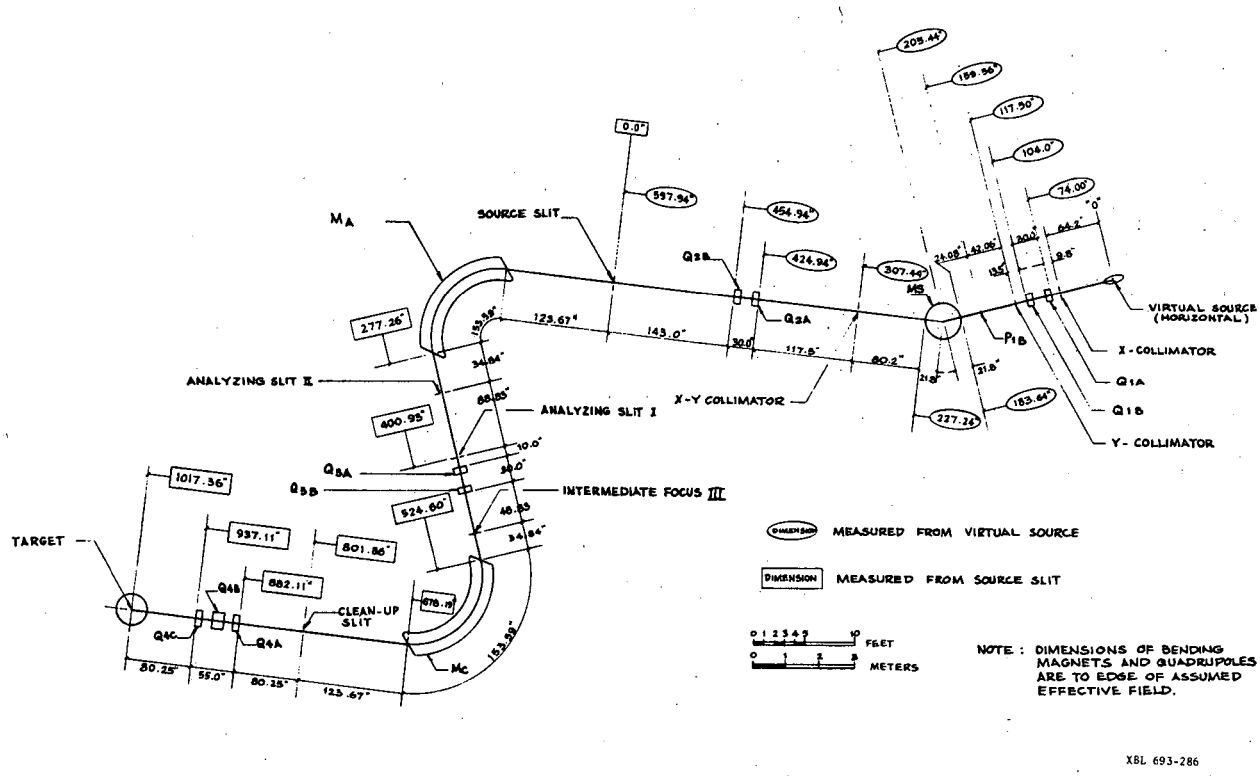

Fig. 4. 88-Inch cyclotron beam-analysis system for high transmission.

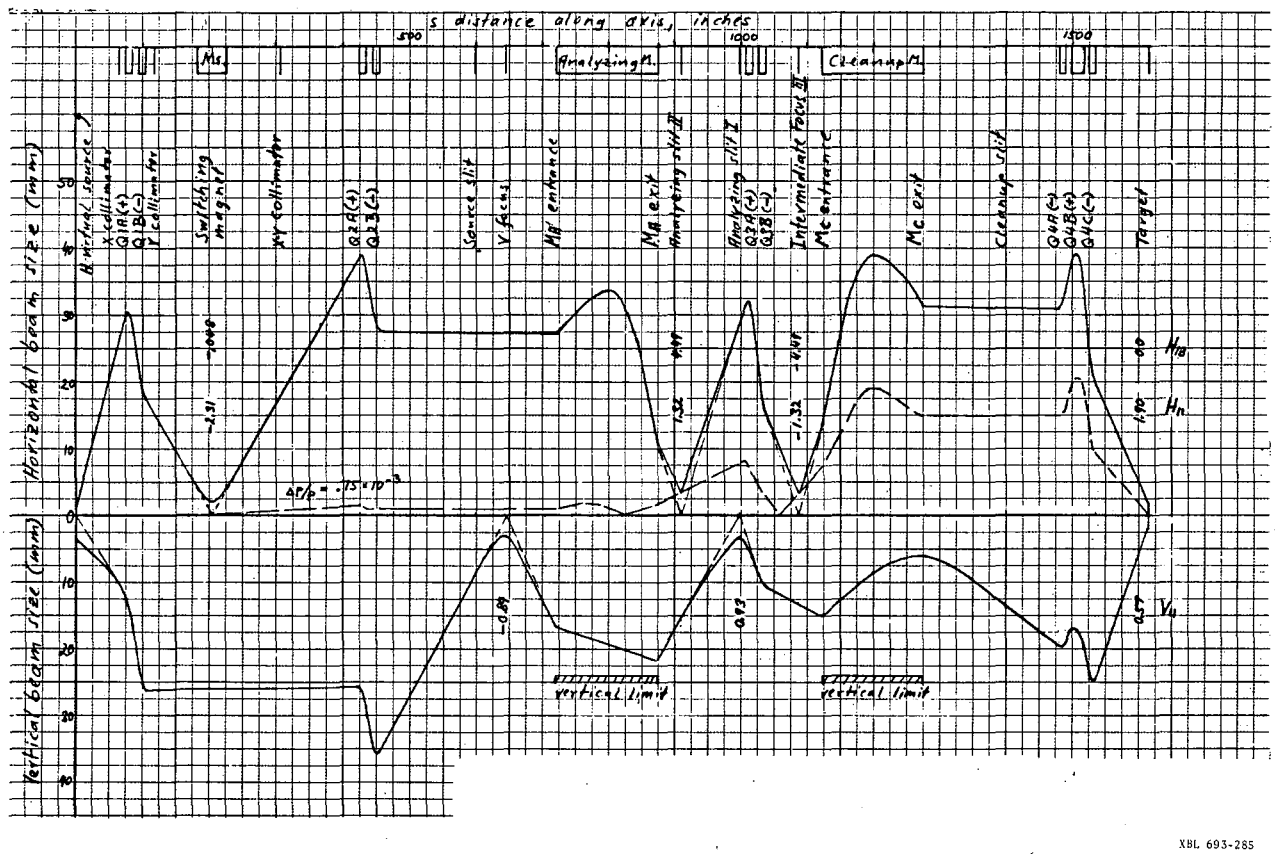

XBL 693-285

Fig. 5. Beam optics for high transmission and variable energy resolution: Solution III (quadrupoles +-, +-, +-, -+-) with new elements added.

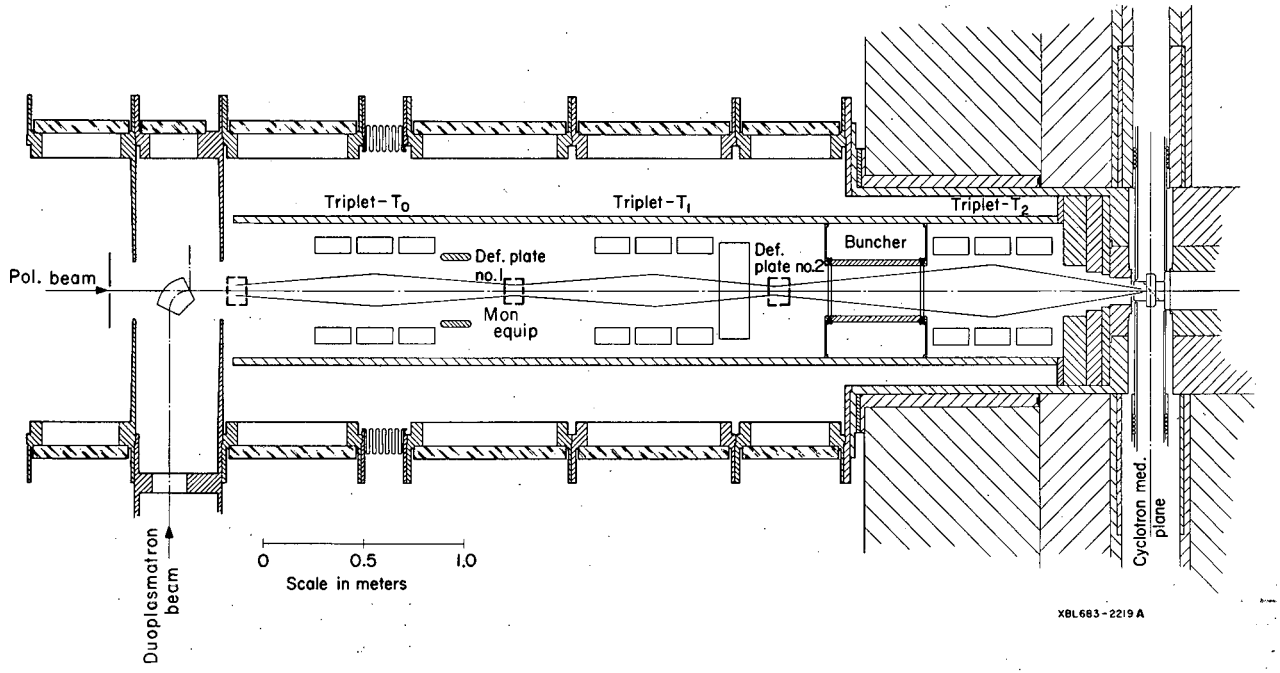

Fig. 6. New axial injection transport line installed in 1968, except for buncher.

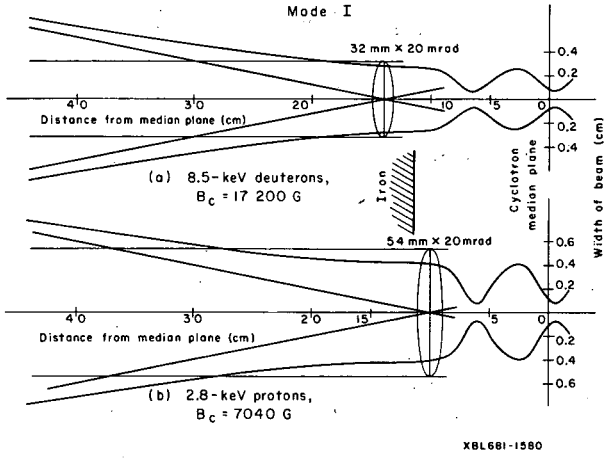

Fig. 7. Beam profiles through the magnet yoke for Mode I, 3/2 λ.

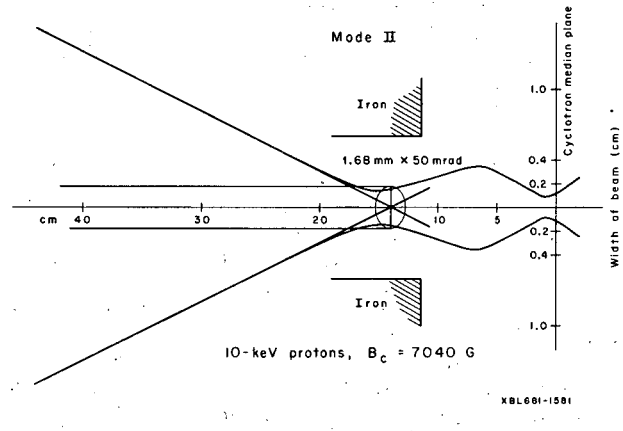

Fig. 8. Beam profile for Mode II, λ.

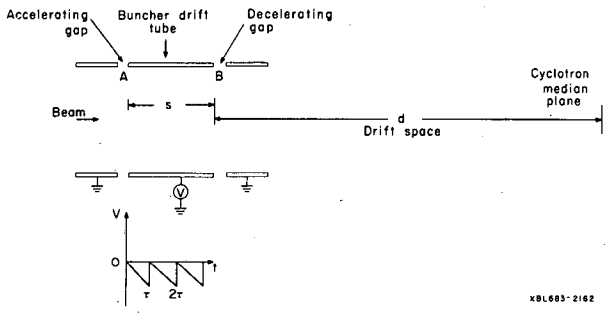

Fig. 9. Proposed drift tube buncher driven by a sawtooth voltage wave. Beam is velocity-modulated by gaps A and B to give space bunching at cyclotron median plane.

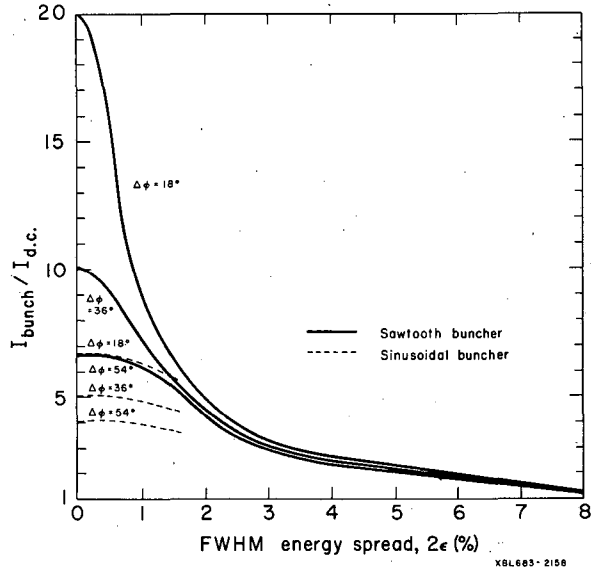

Fig. 10. Ratio of bunched to unbunched beam intensity for sawtooth and sine-wave bunchers as a function of cyclotron phase acceptance $\Delta\phi$, and beam energy spread.

POLARIZED ION SOURCE FOR THE 88-INCH CYCLOTRON

A. U. Luccio and D. J. Clark

The assembly of the polarized ion beam for the 88-inch cyclotron has been almost completed and tests have been carried out.

The general layout of the source has been previously described (Fig. 1). Its main components are (i) a dissociating unit to produce atomic hydrogen and deuterium, (ii) a differential vacuum system to produce a high-intensity, well collimated atomic beam, (iii) a magnetic sextupole to split the beam into its hfs states, (iv) a set of adiabatic rf transitions, (v) an ionizer to produce ions from the atomic beam.

(i) The dissociator, consisting of a "hairpin" discharge tube powered by a 2-kW 20-MHz rf supply, has been successfully tested, for gas flow up to 200 atm cm^3/sec. Work is in progress to improve the matching between the rf supply and the discharge, which would allow increasing the atomic ion intensity from the dissociator.

(ii) The engineering and operation of the vacuum system have been very satisfactory. Typical operating conditions under heavy beam load are 2×10^{-2} torr, 10^{-4} torr and 10^{-6} torr in the first, second, and third sections of the vacuum housing.

(iii) The magnetic sextupole (Fig. 2) has been installed and tested. Measurements of the magnetic field, performed by means of rotating coils at various distances along its axis, have shown that a field in excess of 10 000 gauss at the pole tips can be achieved with a current of 150 A. The reading of the coil current has been recorded continuously and analyzed into its harmonic components. The field appears almost perfectly that of a sextupole, with less than 5% of 4-, 12-, and 18-pole components.

(iv) The nonuniform field magnet and the rf oscillator for the 7-MHz adiabatic field transition have been built and installed. The unit has been tested under vacuum, but, of course, only the actual acceleration of polarized protons and a scattering experiment will allow us to test its efficiency.

(v) The ionizer, purchased from the ORTEC Company, has been tested on the bench with background gases. The power supply unit has been partially rebuilt to meet our special requirements,

as far as ion energy and optical quality of the ion beam are concerned. The unit is now being installed.

The whole atomic beam system has been tested. Molybdenum oxide pictures of the beam (Fig. 3) with the sextupole "off" and "on" have been taken at a distance of 40 cm from the sextupole end. The beam appears well collimated, with a cross section of about 1 cm^2. The distribution of the atomic density across the beam has been computed, and the experimental results agree satisfactorily with the calculated values. By means of a compression gauge and the focusing action of the sextupole on the atoms of hydrogen, the intensity of the beam and the dissociation yield have been estimated as 10^{17} atoms/sec/cm^2 and 70% respectively.

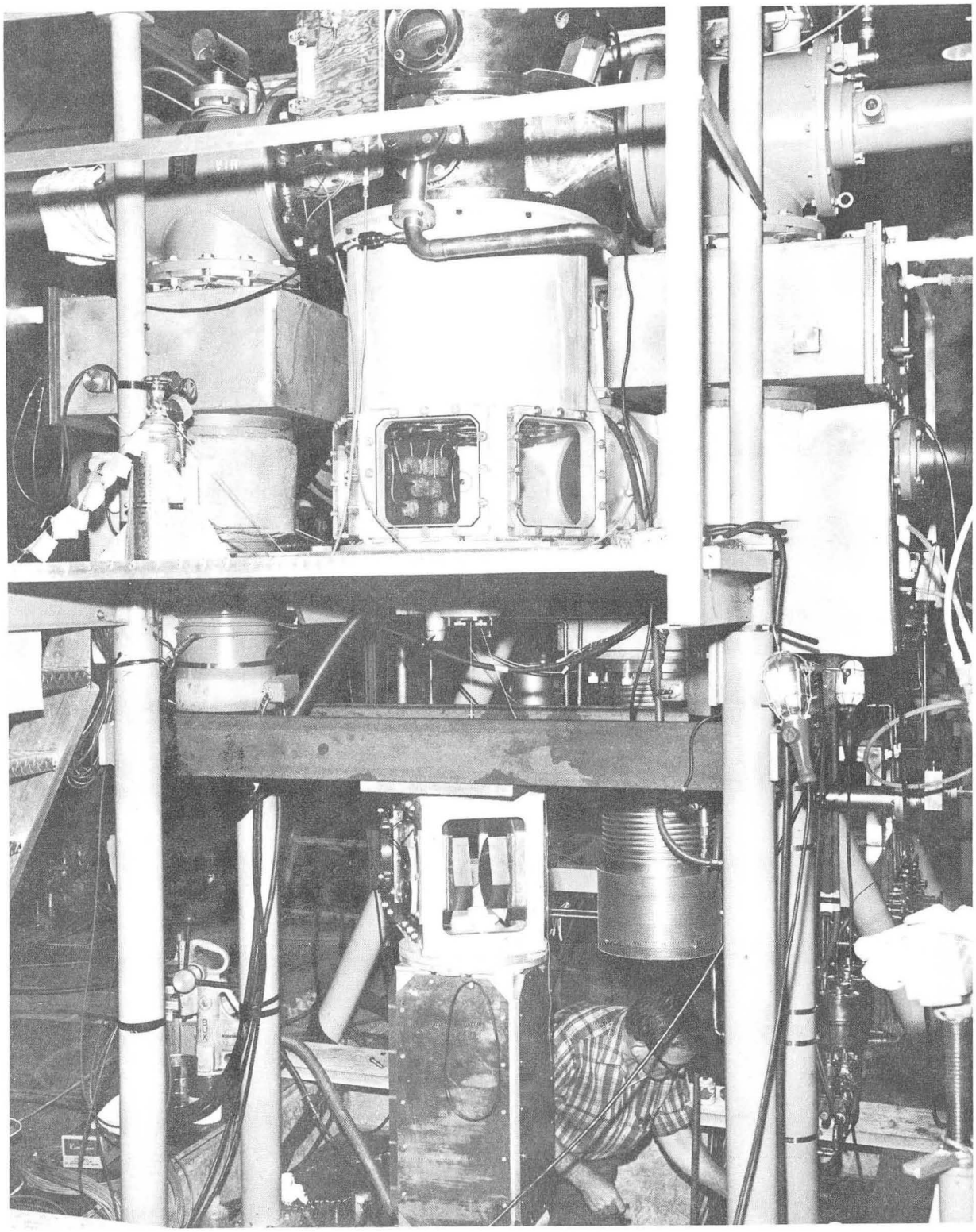

XBB 689-5468

Fig. 1. Polarized ion source--general assembly.

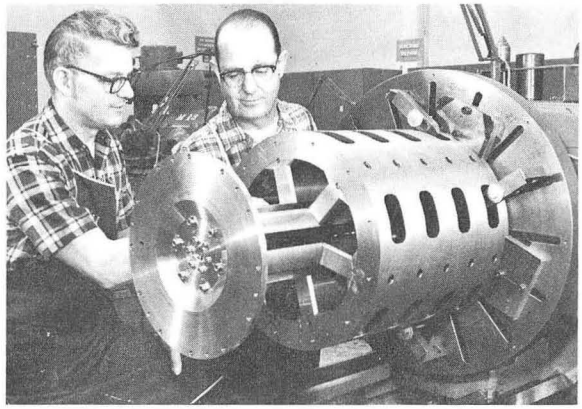

XBB 682-791

Fig. 2. Magnetic sextupole with removable pole tips.

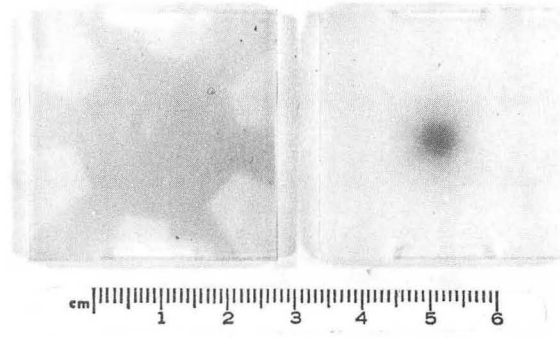

CBB 689-5823

Fig. 3. Molybdenum oxide picture of the hydrogen beam. Left: sextupole "off"; right: "on."

NEW BEAM-ANALYSIS SYSTEM INSTALLED AT THE 88-INCH CYCLOTRON

B. G. Harvey, E. A. McClatchie, F. G. Resmini
W. S. Flood, R. E. Hintz, and F. B. Selph

The Berkeley 88-inch cyclotron produces intense beams of protons (10 to 55 MeV), deuterons (10 to 65 MeV), ^{3}He (20 to 150 MeV), and ^{4}He (23 to 130 MeV) with small emittance and a typical energy resolution of 0.3% FWHM. For several years the best energy resolution obtained in a counter experiment had been 0.09%, limited by the resolution of the best analyzed beam of 0.08%. Since there seemed to be no inherent barrier to obtaining resolutions of better than 0.05% with solid-state counters, [1] a new beam-preparation system having a resolution of 0.02% was designed. Of equal importance was the removal of "tails" (due to slit-scattered particles) in the primary beam.

The analyzing system consists of two identical uniform field magnets (Fig. 1). The beam from the cyclotron is brought to a horizontal focus at the entrance slit. This slit, of width 0.5 mm, defines a source for the first magnet. An energy-dispersed image of the slit is formed at the analyzing slit, which is at the radial focus of Magnet 1. The analyzing slit, gap 0.5 mm, is used to energy-analyze the beam and to provide a source for Magnet 2. At the radial focus of the second magnet an image of the analyzing slit is formed. Slit-scattered particles have lower energy, and therefore a third slit (the clean-up slit) can be used to remove them. The clean-up slit is normally set at a gap of 2 to 5 mm to avoid further scattering the beam.

Magnet Parameters

A flat-field edge-focusing magnet design was used, with equal entrance and exit edges. This is shown diagrammatically in Fig. 2. For this magnet the necessary description parameters are α, the turn angle; β, the edge angle; ρ, the magnetic radius; ℓ_{sx}, ℓ_{fx}, the radial and vertical focal distances; and X_f, the analyzing-slit width. To get good resolution, X_f must be made small and ρ large. To achieve a compact design it is desirable to have α large, while β is determined by the need for adequate vertical focusing. We decided to operate symmetrically with the following parameters: $\ell_{sx} = \ell_{fx} = \ell_{fy} = 3.14$ m, $\ell_{sy} = 2.11$ m, $\alpha = 110$ deg, $\beta = 38$ deg, $X_f = 0.5$ mm, $\rho = 2.03$ m.

The radial magnification m_x is thus -1. These parameters give a first-order resolution $P_1 = 5.6 \times 10^{-5}$, i.e., P_1 is the momentum spread that will just be transmitted by object and image slit widths of 0.5 mm.

The maximum field needed (to deflect 130-MeV α particles) is 8.15 kG, which is comfortably below the region of iron saturation effects. We used internal high-current-density coils in the magnet to keep down the overall size. The coils have 36 turns of 0.5-in.-square copper with 0.25-in.-diam holes for water cooling. A current of 1000 A is required to produce the maximum field. A cross section of the iron, coil, and vacuum tank is shown in Fig. 3. An existing 130-kW silicon-controlled rectifier power supply was utilized and provided with a series transistor pass element designed to provide a long-term field stability of 1 part in 10^5. Both magnets are operated in series; individual control is provided by shunt transistor timmers permitting up to 2.2 A to be diverted around each magnet. This individual control provides adequate compensation for minor differences in the magnets and for alignment errors.

The entrance and exit poles of the magnets were chamfered and field clamps were used in such a way as to minimize the change in effective field length with magnet excitation and to make the fringing field as uniform as possible parallel to the magnet edge. A diagram of the field clamp is shown in Fig. 4.

Magnet aberrations were studied with a computer program which integrates the equations of motion. The procedure is fully described in Ref. 2. The desired field shape turned out to have an r^2 dependence, where r is a radial coordinate extending from the magnet center axis, i.e., the field should have a shape $B(r) = B_0 - B_2r^2$, where B_0 is the central field. Magnetic field measurements were made only in the median plane of the magnets, using coils and a precision integrator. The central region (24 in. from each pole edge) was studied with a point-measuring coil that could be moved azimuthally at a given radius or radially at a given azimuth. The ends of each magnet were studied separately with long coils which extended from 16 in. outside to 24 in. inside the magnet, and were constrained to move parallel to the pole edge.

Measurements were made at three field values, approximately 2, 5, and 8 kG. Shims were designed to correct for the field sag found and to introduce the required field shaping.

The aberration calculations indicated that residual aberrations could increase the first-order resolution by a factor of 1.4, still leaving the resolution $\Delta P/P$ less than 1.0×10^{-4}.

Energy Resolution Measurements

The energy resolution obtained from the first magnet can be rapidly measured with the second magnet. The clean-up slit is closed to 0.5 mm and the field of the second magnet is adjusted to give maximum beam in the Faraday cup. The beam is then swept across the clean-up slit by raising and lowering the field to values that give beam intensities of half the maximum. Then, to first order,

$$\left(\frac{\Delta E}{E}\right)_{\text{FWHM}} = \frac{2\Delta B}{B} = \frac{2\Delta I}{I}.$$

After correction for finite slit widths[2] the typical values of $\Delta E/E$ found lie in the range 0.015 to 0.02%.

A further energy resolution test was made by measuring the well-known[3] T = 3/2 resonance in ^{13}N, which can be observed in ^{12}C + p elastic scattering at 14.233 MeV proton lab energy. Protons scattered at 165 deg lab from a 15-$\mu g/cm^2$ natural carbon target were detected in two Si(Li) counters. The resonance curve is shown in Fig. 5. The energy resolution is obviously of the order of 2 keV; from some unpublished work of Temmer[4] we estimate $\Delta E/E \approx 1.5$ keV $\approx 0.011\%$.

The calculated $\Delta E/E$ is 0.011 to 0.015% depending on the vertical size of the beam in the analyzing magnet, and so we feel the performance has in practice achieved the design value.

Conclusion

In initial operating experience, the system has proved to be quick to set up and convenient to use. Up to 600 nA of 50-MeV α particles have been obtained at the highest resolution levels, representing about 1% of the total extracted cyclotron beam. More beam is of course available by relaxing the resolution requirements. If the source and image slits of the analyzing magnet are opened to 1 mm, the beam intensity increases fourfold with only a twofold loss of resolution.

By opening all slits wide and using somewhat different beam optics to give a radial focus midway between the entrance slit and the analyzing magnet, a dispersionless solution has been obtained, with roughly 50% of the total cyclotron beam transmitted by the magnets. This mode of operation will be useful for experiments with polarized protons, where intensity conservation is crucial.

The new beam-analysis system has proven to be a valuable addition to the experimental facilities of the 88-inch cyclotron.

References

1. F. S. Goulding, D. A. Landis, and R. H. Pehl, The Energy-Resolution Capabilities of Semiconductor Detectors for Particles in the 10- to 100-MeV Range, UCRL-17556, May 1967.
2. R. E. Hintz, F. B. Selph, W. S. Flood, B. G. Harvey, F. G. Resmini, and E. A. McClatchie, Beam-Analyzing System for a Variable-Energy Cyclotron, UCRL-18383, Aug. 1968.
3. J. B. Marion, Rev. Mod. Phys. 38, 660 (1966).
4. G. M. Temmer (Rutgers University), private communication.

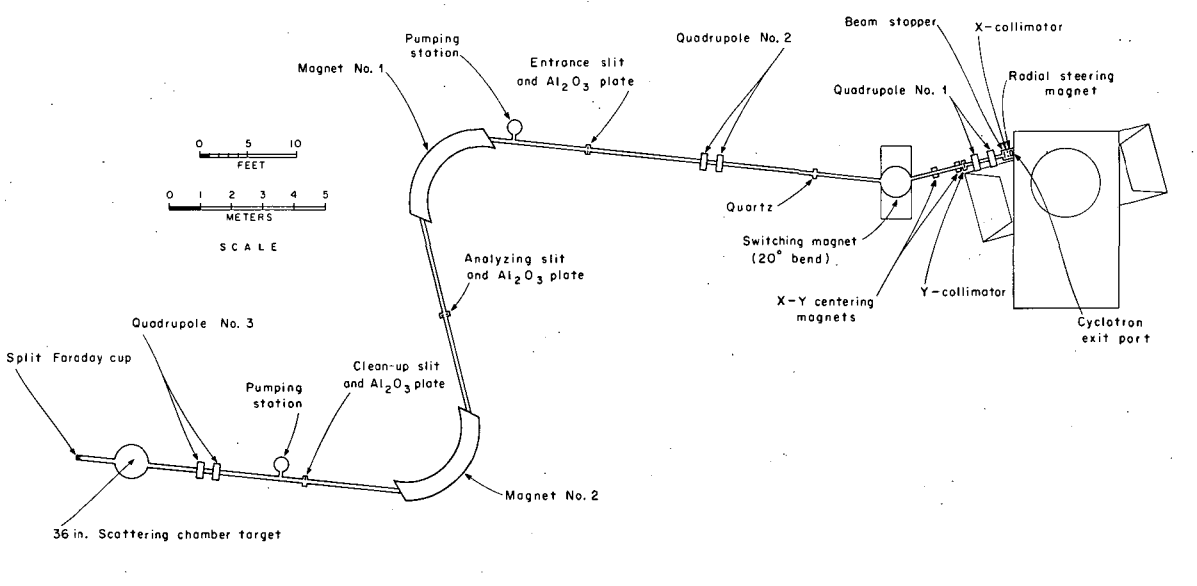

Fig. 1. Beam-transport system for analyzing magnets. Quartz or Al_2O_3 plates are observed with television cameras for beam focusing.

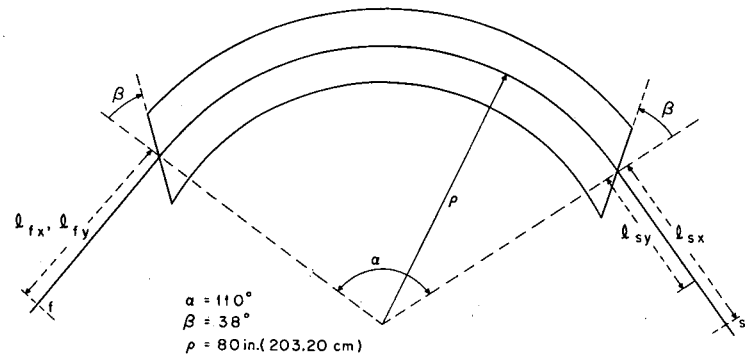

XBL687-3270

Fig. 2. Plan view of 110-deg magnet.

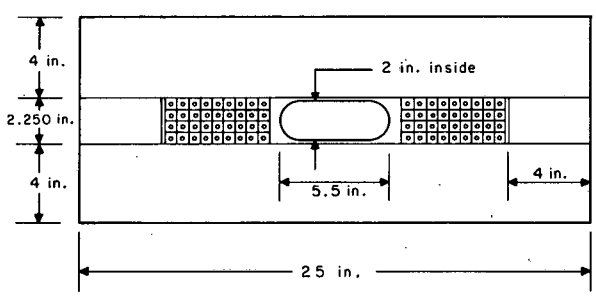

XBL687-3266

Fig. 3. Cross section of iron, coil, and vacuum tank.

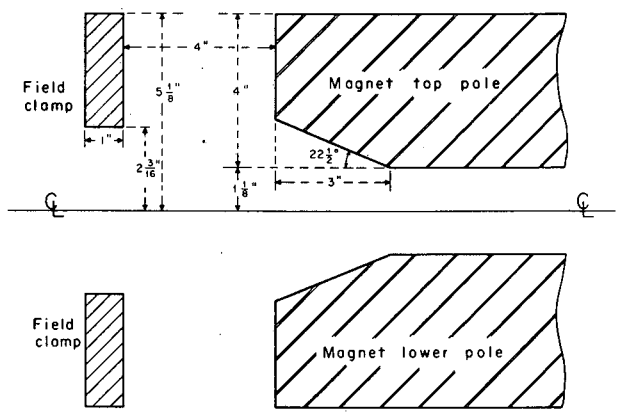

XBL687-3271

Fig. 4. Cross section of edge of magnet, showing field clamp and beveled pole edge.

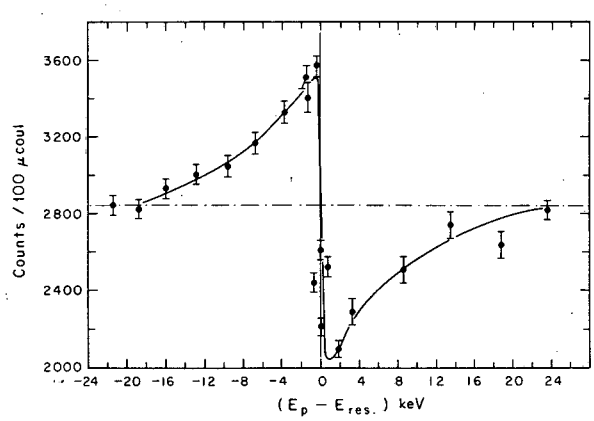

XBL687-3260

Fig. 5. $^{12}C(p, p)\,^{12}C$ resonance at 14.233 MeV (lab).

CASCADE ISOTOPE SEPARATOR

M. C. Michel and F. L. Reynolds

During the last year the first stage of a projected two-stage electromagnetic isotope separator has been successfully operated and tested. This instrument was designed and constructed for the Nuclear Chemistry Division with assistance from many support groups of the Laboratory. It is meant to be a general-purpose separator as well as an improvement in some respects upon the existing instruments in use elsewhere. A complete description will be published elsewhere, but a short summary of the present status and future capabilities is given here as a progress report.

As seen in Fig. 1 the basic design of the first stage is a 90-deg-deflection single-direction-focusing magnetic analyzer with vertical refocusing accomplished by an electrostatic cylindrical lens. It is similar in design to the so-called Scandinavian or low-intensity research separators used extensively in Western Europe in the 1950's, but with improvements suggested by the almost two decades of experience accumulated by others. With a radius of deflection of 60 in. the dispersion is adequate ($\approx$ 6 mm/mass number at mass 250) without a shaped field, and the size simplifies many design and vacuum problems which would offset the advantage of a smaller machine. Particularly, decontamination by the electrolytic process chosen would be more difficult with a smaller instrument.

Several design criteria were involved in the construction of this separator, which have not, to our knowledge, all been achieved in one design before. Some of these are listed below.

(a) The separator should be capable of separating samples containing reasonably large levels of radioactivity with no unusual health or technical hazards.

(b) Separation factors (determining isotope purity) should be optimized and not limited by any known and easily controllable features of the instrument.

(c) Decontamination from radioactivity deposited internally must be relatively easily accomplished with minimum hazard and down-time.

(d) The separator vacuum system should be compatible with possible future use in solid-state research, especially with respect to the ability to keep surfaces free of the grosser forms of contamination by hydrocarbons.

(e) The separator should have the ability to run samples with decay lifetimes comparable to the delivery time of targets from the local accelerators.

(f) The separator should be easily operable by one person and be as free from maintenance problems as possible.

We believe that most of these aims have been met although much evaluation remains to be done. The present machine has a strongly differentially pumped metal-gasketed vacuum system consisting of a mercury-diffusion-pumped system on the source chamber with base pressure $\approx 1\times10^{-8}$ torr, an effective speed at the source of 250 ℓ/sec for noncondensable gases, and considerably higher speed for gases condensable at liquid nitrogen temperatures. The beam is extracted from this vacuum through a small hole after traveling less than 2 cm, and the rest of the path is in a system pumped by two 500-ℓ/sec triode sputter-ion pumps having a base pressure of 1 to 2×10^{-9} torr. More than a hundredfold pressure difference can be maintained between these two regions, so that for >95% of the beam path pressures greater than 1×10^{-7} torr should not occur except in unusual cases. Typical pressures in operation have been 2 to 5×10^{-8} torr, with beams of several microamperes being collected. Since residual gas scattering is one important source of isotope contamination, these pressures represent an improvement in potential separation factor attainable with this system.

Beam intensities usually are limited not by ion source output, but rather by space-charge defocusing in the electrostatic lenses. Even so, beams of 10 μA are quite well focused, and intensities up to 100 μA and even beyond are usable at reduced separation factor. This does limit the amounts collected in a reasonable time to quantities below 1 mg for most elements, although in special cases larger amounts might be processed. For research uses of radioactive isotopes this is more than adequate for most samples. The beam may be focused to a variety of shapes at the collector, the narrowest dimension being a line 0.5 to 0.7 mm in width and of height (determined by the cylindrical lens potential) from several centimeters to $\approx$ 1.5 mm. Thus a round spot of $\approx$ 1.5 mm diameter is a typical minimum size, increasing at the higher current densities.

Transmission by the ion optical system after initial extraction is $\geq$95%, so that total efficiencies of collection are determined primarily by ion source efficiencies or--perhaps more realistically--extraction efficiencies in the case of small-aperture plasma-type sources. These efficiencies depend on the type of source and the element being separated, but a typical collection

efficiency might be 5% of the charge material for many elements, including many of the rare earths and actinides. Recent work here and elsewhere indicates that for a few elements efficiencies considerably higher are attainable, and of course for some elements (such as the platinum group metals) a much lower yield is the rule.

Decontamination is accomplished by dismantling the entire vacuum enclosure, using plastic film bagging and seal-off techniques where necessary, followed by conversion of each subsection of the vacuum tank into a container for liquid electrolyte by the use of appropriate plastic flanges and other fittings. Insertion of a copper cathode into this solution and electrolytic dissolution of a very thin layer of the stainless steel wall (leaving an electropolished surface) in a controlled atmosphere area allows removal and disposal of most radioactive elements in solution. Cleaning and reassembly, which is simplified by the construction of various sections on individual wheeled support carts, completes the decontamination. This technique has been tested on other contaminated systems and a test run has been made on each section of the finished machine during the assembly process.

Quick operating probes (see page 372) of two different designs allow easy and quick introduction of samples into the ion source and removal of collected samples from the collector region.

Facilities for deceleration of the beam at the collector to very low energies is built in so that nuclear spectroscopy sources of low self-absorption can be made by avoiding the penetration of the full-energy (30- to 100-keV) particles into the substrate.

Preliminary testing and modifications have been completed and radioactive isotope separations are now planned as the next step. This will be followed by completion of the second stage after sufficient operating experience is accumulated to assure that the second-stage design will achieve maximum improvement in isotopic purity. Figure 2 shows an overall view of the first stage viewed from the collector region.

Expected uses of the separator are

(a) separation of single radioactive isotope samples to be used as sources in nuclear spectroscopy research.
(b) separation of radioactive isotopes for identification or nuclear reaction studies, or both,
(c) preparation of thin monoisotopic accelerator targets (either stable or radioactive), especially for the Hilac,
(d) solid-state studies, including the preparation of Mössbauer sources and doping of semiconductors,
(e) as a mass spectrometer of very high resolution and adjacent-mass sensitivity,
(f) as a possible chemical purification technique for preparing ultrapure materials as accelerator targets or for solid-state work.

Although many people have contributed effort toward the construction and testing of the separator, we are especially indebted to C. E. Miner, R. M. Reimers, and R. H. Escobales for mechanical design, to G. G. Young and J. F. Wiltens for technical support, and to F. Vogelsberg and D. E. McClure for electronic design.

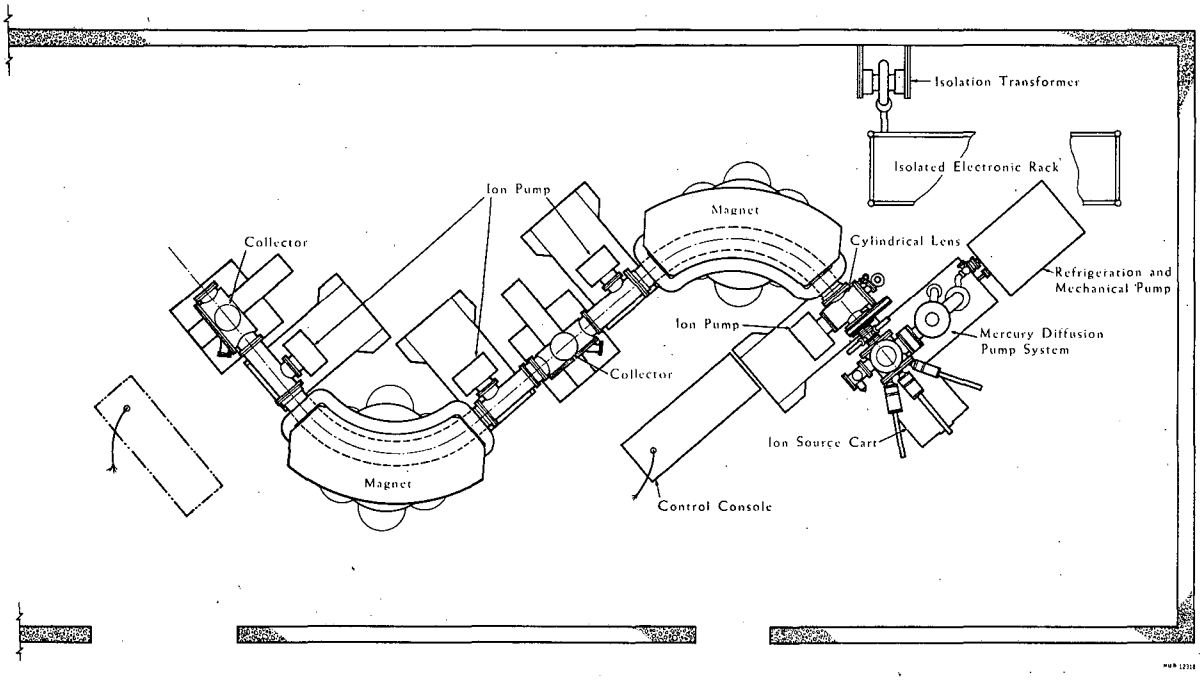

Fig. 1. Overall layout of cascade isotope separator.

CBB 688-5038

Fig. 2. View of cascade isotope separator from first-stage collector area.

PARTICLE IDENTIFICATION OF THE ELEMENTS UP TO ARGON PRODUCED BY THE INTERACTION OF 5-GeV PROTONS WITH URANIUM

A. M. Poskanzer, E. K. Hyde, and G. W. Butler

The study of fragments produced by the interaction of high-energy protons with uranium in the external proton beam of the Bevatron has continued. Identification of isotopes is based on the measurement of their energy losses in solid-state detectors. Energy spectra and angular distributions are being measured for isotopes from hydrogen to carbon. Above carbon it is necessary to use a very thin transmission detector to measure the energy spectra to low energies, and then it becomes difficult to separate isotopes. However, by just separating elements we have been able to go as heavy as argon, as is shown in Fig. 1. The cutoff above argon is electronic, and there is probably no reason that we could not observe heavier elements. The energy spectra and angular distributions will be used to study the mechanism of the production of these fragments in the high energy interaction.

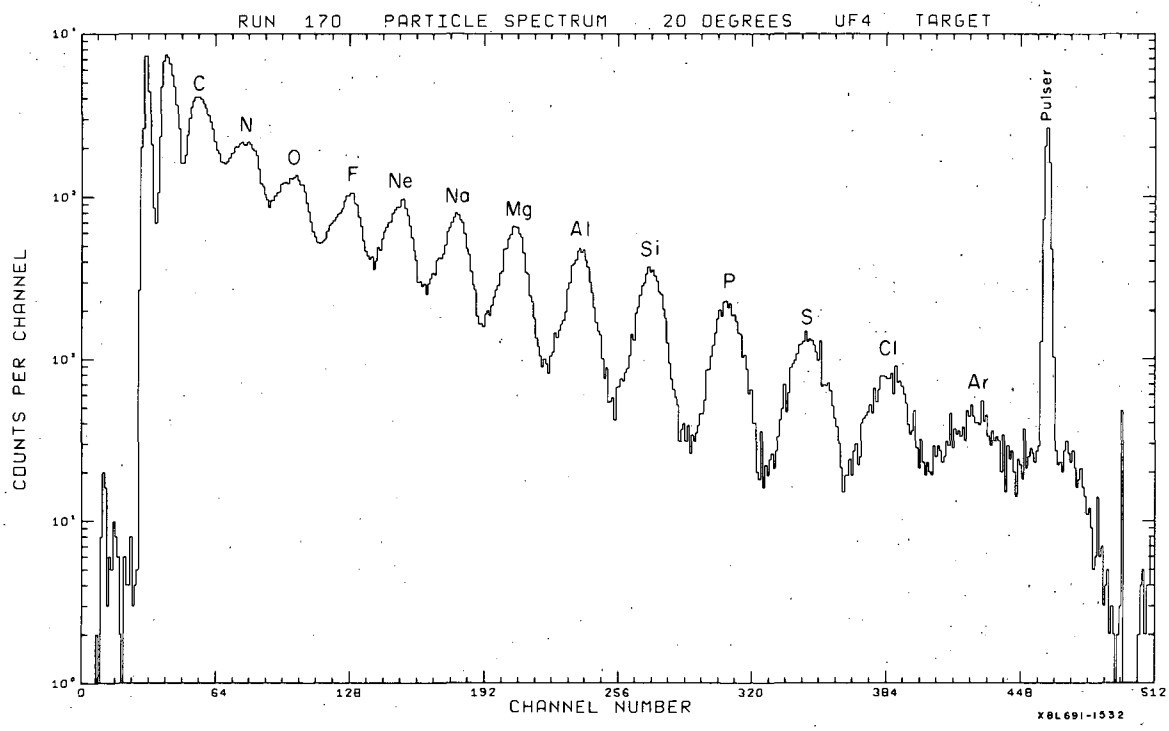

Fig. 1. A particle spectrum obtained from the 5.5-GeV proton bombardment of a UF_4 target 0.7 mg/cm^2 thick. The telescope consisted of a 20-μ ΔE detector, a 100-μ E detector, and an E reject detector. The power law was adjusted to optimize the separation in the region of Si. The peaks represent the relative yields of the elements which penetrate the 20-μ ΔE detector and deposit at least 20 MeV in the E detector.

SLIT SCATTERING EFFECTS WITH 50-MeV α PARTICLES AND 20-MeV PROTONS†

F. Resmini, A. D. Bacher, D. J. Clark, E. A. McClatchie, and R. de Swiniarski

The continuum background arising from particles scattered by slits in front of detectors is of importance in high resolution nuclear spectroscopy experiments and may set a lower limit on the observable cross sections. The purpose of this experiment was therefore to measure the scattering arising from slits of different materials and properties and compare the results with existing theories. Measurements were taken with beams of 20-MeV protons and 50-MeV α particles.

Figure 1 sketches the experimental setup. Beams from the Berkeley 88-inch cyclotron were energy-analyzed to 0.02% FWHM and focused at the center of the scattering chamber, where a silicon counter, 12 mm in diameter, was placed. The various slits, of 2 mm width and 10 mm height, could then be positioned successively in front of the detector. This technique allows spectra to be taken, in the same beam conditions, with and without slits, and therefore one has a clear measurement of the slit-scattering effect alone. The beam spot, as seen on aluminum oxide, is approximately 6 mm wide and 1 mm high. For an emittance of 10 mm-mrad that means an essentially parallel beam. The uniformity of illumination of the slits was checked by sweeping the beam by ± 1 mm across a 0.005-inch slit and measuring the transmitted intensity, which remained constant within ± 5%. The measurements were taken with a beam intensity between 1000 and 1500 particles per second. Some slit profiles are shown in the bottom of Fig. 1. The thickness of the slits was stopping thickness + 15%, materials being brass, tantalum, and aluminum. Straight-edge slits were tried with a high degree of polishing of the surface and no polishing (i. e., only fine machine finishing).

Figure 2 shows two spectra obtained with 20-MeV protons. The scale covers a range of approximately 2 MeV below the peak. The effect of slit scattering can be easily appreciated. From these spectra, subtracting the contributions due to reactions in the detector, one can evaluate the peak-to-valley ratios, defined as the ratio between the counts/channel on the peak, referred to a given FWHM, and the counts/channel in the background. The best results obtained, 1 MeV below the peak, are 4 to 5×10^5:1 for 50-MeV α particles and 8×10^4:1 for 20-MeV protons (referred, respectively, to 30 keV and 20 keV FWHM) with brass straight-edge polished slits. Other profiles give poorer results.

Some of our experimental results, namely those for straight-edge slits, can be directly compared with the Courant theory, [1] which is particularly simple for the case of a parallel beam, such as the one we used. In Fig. 3 the percentage of particles scattered with energy losses between 0 and ΔE is plotted as a function of $\Delta E/E_{inc}$. The agreement with the theory is very good up to a $\Delta E/E_{inc} \approx 50\%$, the theoretical results being somewhat lesser (by 25% in some cases) only at higher energy losses. This partial discrepancy is, however, expected because of the simple assumption, in the theory, of constant scattering cross section. The size of the points is a measure of the statistical errors alone.

In conclusion, the measurements presented here prove the applicability of the Courant theory to the treatment of slit scattering for straight-edge slits and parallel beams. Because the theory also provides the mathematical method for treating the problem of nonparallel beams, which one would encounter in an actual experiment, we believe that, on the basis of these results, the slit-scattering background can be estimated for any particle, energy, and beam divergence.

Footnote and Reference

†Presented as a contributed paper to the APS Fall Meeting, Miami Beach, 1968: Bull. Am. Phys. Soc. Series II 13 [11], (1968).

1. E. D. Courant, Multiple Scattering Corrections for Collimating Slits, Rev. Sci. Instr. 22, 1003 (1951).

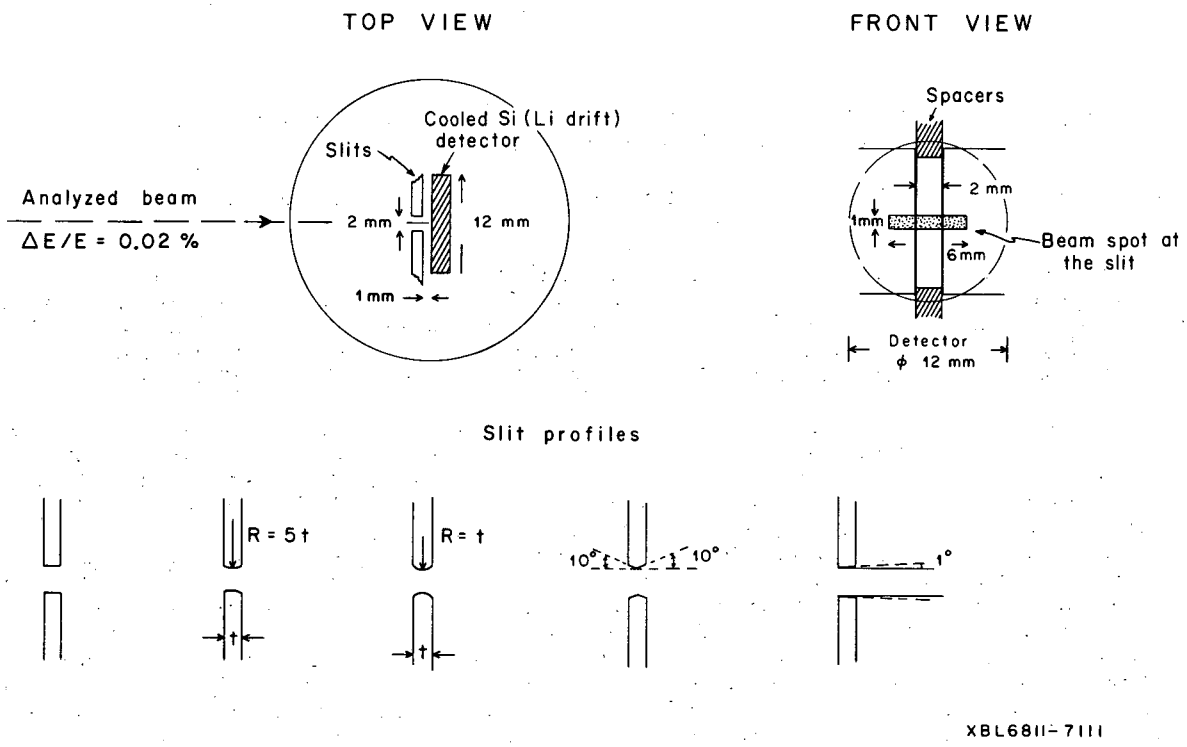

Fig. 1. Experimental setup.

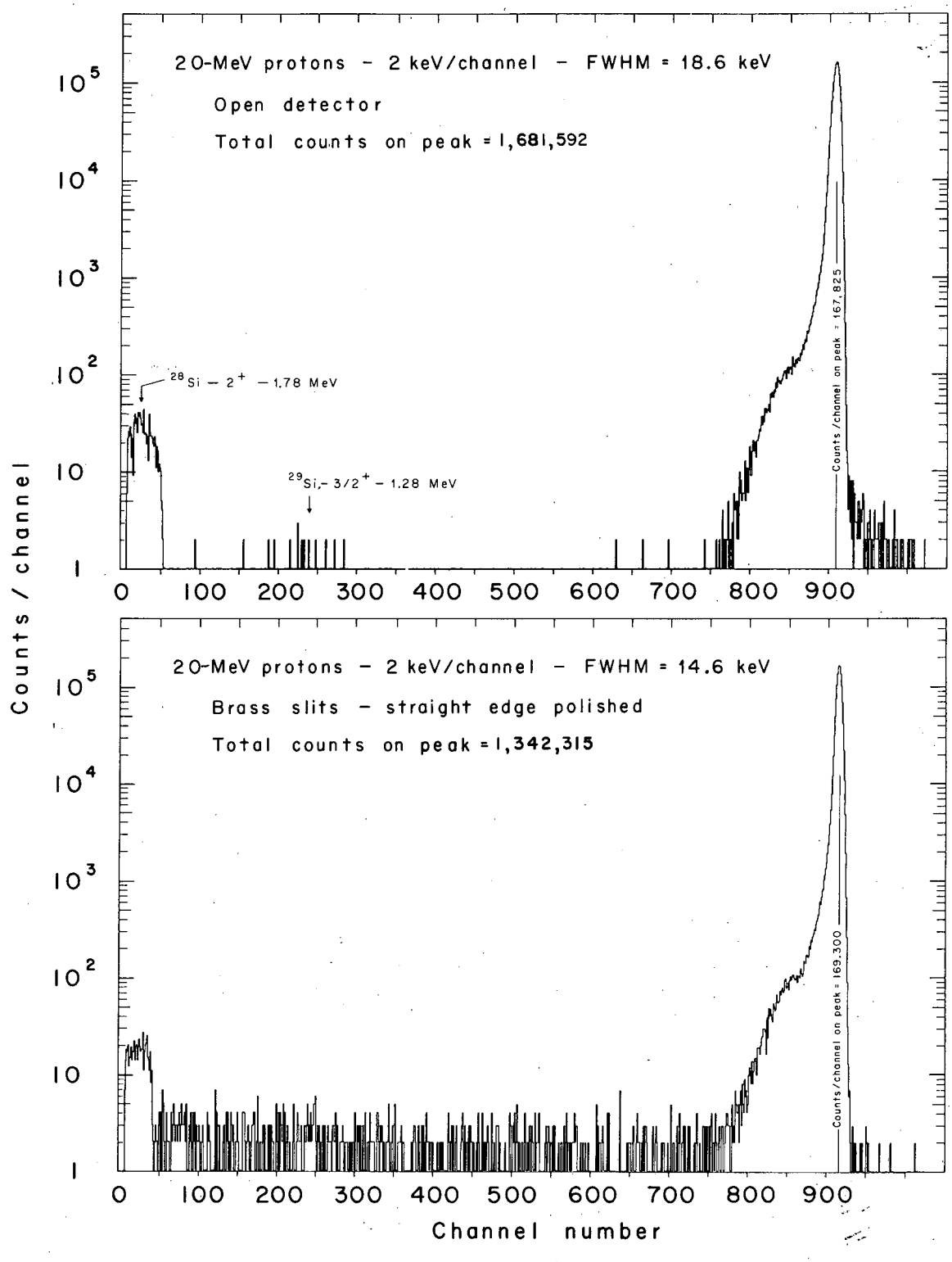

Fig. 2. Spectra of 20-MeV proton, without slit (top) and with a straight-edge polished brass slit (bottom).

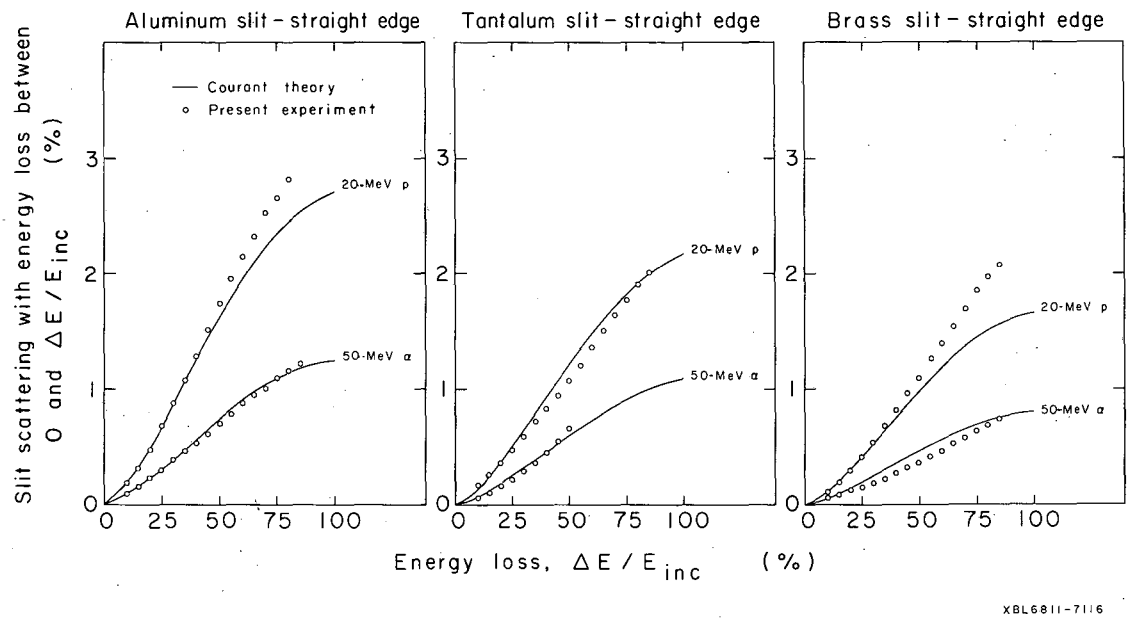

Fig. 3. Comparison between these experimental results and the Courant theory predictions.

RADIOISOTOPE SOURCE-TARGET ASSEMBLY FOR x-RAY SPECTROMETRY†

Robert D. Giauque

Radioisotope source-target assemblies have been constructed to be used in conjunction with high-resolution semiconductor detectors for nondispersive x-ray fluorescence analysis. As shown in Fig. 1, the radioisotope source has annular geometry, as does the primary target. A radioisotope source is used to excite the K x rays of a selected target material, and these in turn excite x rays from the specimen. In order to obtain high sensitivity in analysis, primary targets are chosen whose characteristic K x-ray energies are not too far above the absorption edges of the elements to be determined. Similarly the radioisotope source should have photons not too much higher in energy than the absorption edge of the target.

Some of the radioisotopes that can be used as sources are ^{241}Am, ^{109}Cd, ^{125}I, and ^{57}Co. Table I lists the half-lives of these radioisotopes, their useful radiations, and the intensities of these radiations per disintegration. The primary targets are either cut from pure metal sheets or made from plastic castings of the metal powders, metal oxides, or appropriate compounds.

Rhodes[1] reports the use of a radioisotope source-target assembly to correct for several of the major problems of x-ray fluorescence analysis, matrix enhancement, and absorption effects. High analytical sensitivity is obtained by using a target which has its characteristic Kα x-ray energy just above the absorption edge of the element to be determined. Matrix enhancement is usually eliminated by this procedure, and matrix absorption is compensated by normalizing to the backscatter peak of the target's Kα x rays.

This source-target assembly in Fig. 1 has been used to analyze glass and ceramic archaeological artifacts when the destruction of these artifacts was not permitted. A detailed description of the equipment used along with a multichannel pulse-height analyzer has been given elsewhere.[2] When present in low concentrations (1% or less), several elements with comparable x-ray energies may often be determined with the same target. Detection limits of 100 ppm and less for many elements can usually be obtained. Typically, analysis of a specimen for more than a dozen elements (Mn and higher atomic number elements) can be accomplished in less than 1 hour.

Figure 2 shows a Mosley plot of a glass specimen containing 1.0% Cu, 0.15% Co, 0.8% Fe, and 0.9% Mn excited with As K x rays excited from an As_2O_3 target by an ^{241}Am source and detected with a lithium-drifted silicon detector. It will be noted that the peaks from manganese, iron, and cobalt are not resolved. With the data still in the memory of the pulse-height analyzer, the specimen is replaced by a piece of iron and the analyzer is run in the "subtract mode" until the iron x-ray peak, as seen in the oscilloscope screen, is reduced to the background level, as shown in Fig. 3. The accuracies of many of these analyses were often good only to 10%. An accuracy of around 1% should be obtainable for many analyses in which the compositions of the samples do not vary over a wide range, when particular care is taken in the sample preparation, and when sufficient care is taken in standardization.

Footnote and References

†Condensed from Anal. Chem. 40, 2075 (1968).

1. J. R. Rhodes, Analyst 91, 693 (1966).
2. H. R. Bowman, E. K. Hyde, S. G. Thompson, and R. C. Jared, Science 151, 562 (1966).

Table I. Radioisotopes for source-target assemblies.

Radioisotope	Half-life	Useful radiations		Intensity per disintegration
		Energy (keV)	Radiation	
Americium-241	458 years	13.9	Np Lα x rays	0.14
		17.8	Np Lβ x rays	0.18
		20.8	Np Lγ x rays	0.05
		26.4	γ ray	0.03
		59.6	γ ray	0.36
Cadmium-109	453 days	22.1	Ag Kα x rays	0.7
		25.0	Ag Kβ x rays	0.15
		87.7	γ ray	0.03
Iodine-125	60 days	27.4	Te Kα x rays	1.1
		31.0	Te Kβ x rays	0.2
		35.5	γ ray	0.07
Cobalt-57	270 days	14.4	γ ray	0.09
		122.0	γ ray	0.87
		136.3	γ ray	0.11

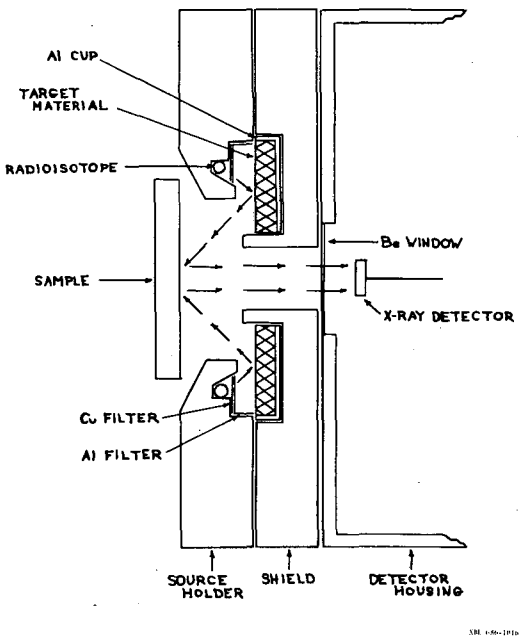

Fig. 1. Source-target assembly.

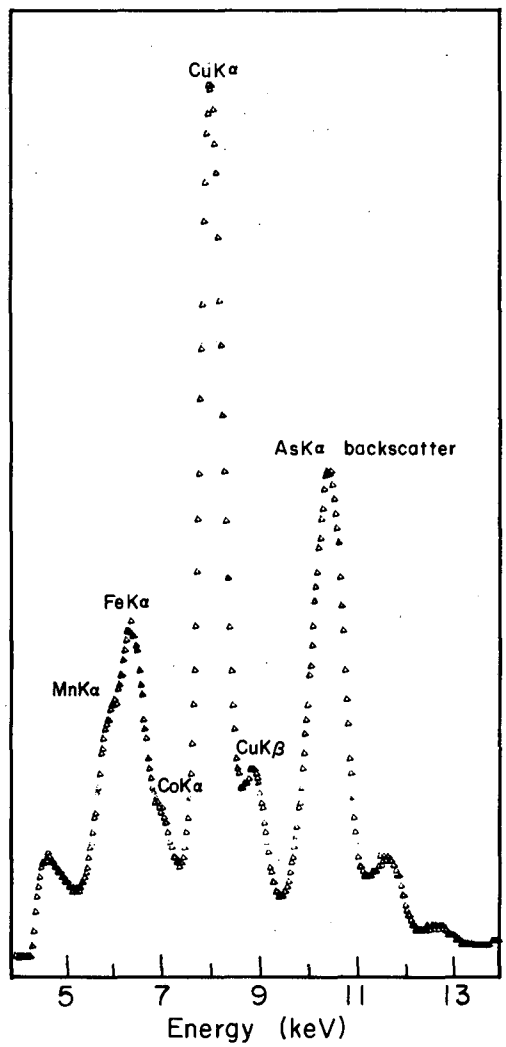

XBL686-2943

Fig. 2. Spectrum from a specimen of glass containing 1.0% Cu, 0.15% Co, 0.8% Fe, and 0.9% Mn excited with As K x-rays and detected with a lithium-drifted silicon detector.

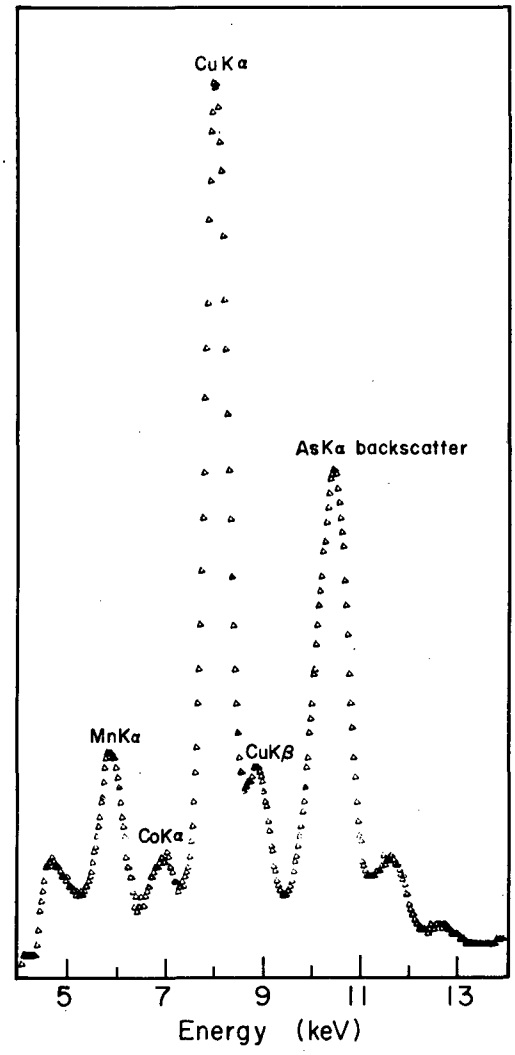

Fig. 3. Spectrum from Fig. 2 with the iron peak subtracted out by exciting a pure piece of iron metal with the analyzer in the "subtract mode."

UNIQUELY DETERMINED METASTABLE IONS BY ION ACCELERATOR DECOUPLING

C. W. Koch

The CEC 21-110B high-resolution mass spectrometer (Mattauch-Herzog geometry) has a drift region between the electrostatic and magnetic sectors sufficiently short that metastable ion transitions cannot be readily exploited for structure determinations. Recently Shannon et al. [1] have reported on a technique particularly suited to the much longer drift region between the ion-source object slit and the electrostatic analyzer. This technique involves decoupling the ion accelerator from the electric sector. By this procedure after a peak of interest has been located magnetically in the usual manner, the ion accelerator voltage is scanned. As the voltage is increased, the normal peak disappears, and at the voltage

$$V_1 = \frac{(\text{mass of precursor})}{(\text{mass of daughter})} \times V_0$$

the precursor ion from the metastable transition appears. Consequently, the precursor is uniquely determined at the same time as normal ions are removed from the spectrum because they have too much energy to pass through the electrostatic sector.

We have recently modified our instrument to permit decoupling of the ion accelerator. Preliminary studies are in good agreement with those observed by Shannon et al.,[1] providing about a 50-fold increase in sensitivity above that obtained conventionally. The modification consists primarily of a 10-turn potentiometer for adjusting accelerating voltages over a range from 2 to 10 kV (independent of the sector voltages); they are read from a four-place digital voltmeter. To utilize the range between 2 and 10 kV requires changing the output range switch at appropriate intervals in order to maintain regulation of the circuit. Careful selection of the region of linearity for each range switch setting is necessary at present in order to give correct voltage readings. Figure 1 is a plot of voltage change vs potentiometer reading with the output range switch set progressively at 2, 4, 6, and 8 kV. The arrows indicate roughly the initial ion accelerator voltage when the daughter ion has been found before the ion accelerator is decoupled. So long as voltage measurements are made in those ranges where $\Delta V/\Delta Pot$ is linear with changing accelerator voltage, a reproducibility of $\pm 0.1\%$ in mass measurement is obtained. In those regions where $\Delta V/\Delta Pot$ deviates from these slopes the voltage reading is incorrect.

To compare the sensitivity of our present design with that reported by Shannon and co-workers we repeated that portion of their studies of n-hexane between the masses 52 and 143 (56 metastables). We were able to confirm all those metastable transitions which they classified as weak, medium, strong, or very strong at source pressures of approximately 1×10^{-6} torr and ion currents ranging from 1 to 4×10^{-12} A. Those metastables which were classified as very weak we could, in general, detect, but not measure with reliability under the above conditions.

To test the method utilizing the direct introduction probe we investigated in some detail the metastable transitions for the compound 1, 2, 2a, 3-tetrahydrocyclobuta[b]quinoxaline, which has the structure

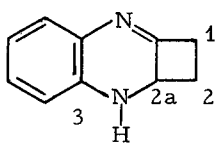

MW = 158

Its normal low-resolution spectrum on the CEC-21-110B at an ion current of 2×10^{-5} A/torr showed only two metastable peaks of sufficient relative abundance to be detected, one at m/e = 156.0 and the other at 110.3, corresponding to the transitions

$$158^+ \longrightarrow 157^+ + H,$$
$$158^+ \longrightarrow 132^+ + C_2H_2.$$

The decoupling technique identified the precursor ions corresponding to the fragmentation pathways shown in Fig. 2. The conditions were approximately those used for the low-resolution scan except that the resolution of the instrument was fixed at 2500 when the instrument was in the normal mode. Usually the resolution for the precursor ion was about one-half that for the daughter ion. All masses calculated from the voltage measurements were within ± 0.2 mass unit. Relative abundances above 5% obtained from the low-resolution spectrum are listed. The compositions were established by high-resolution mass measurement, and the abbreviations beneath the arrows represent the approximate intensities of the metastable transition ions.

The precursors for the transitions

$$158^+ \longrightarrow 156^+ + H_2,$$
$$64^+ \longrightarrow 63^+ + H,$$
$$63^+ \longrightarrow 62^+ + H$$

could be readily distinguished from their daughter ions and the voltages were easily measured. For the transition

$$158^+ \longrightarrow 157^+ + H$$

the 158^+ precursor could just be resolved and measured in the 8-kV range ($\Delta V \approx 50$ V and resolution 2500). With the output range switch set at 4 kV ($\Delta V \approx 25$ V) the precursor ion was not

separated from the daughter at 2500 resolution. With increased resolving power the two peaks could be separated, but the relative abundance of the precursor ion was reduced to very nearly a minimal measurable value. At present we consider 1 part in 150 about the limit of our resolving power.

Distinguishing the alternate pathways represented by the transitions

$$130^{+} \xrightarrow{-HCN} 103^{+} \xrightarrow{-C_2H_3} 76^{+}$$
$$130^{+} \xrightarrow{-C_2H_3} 103^{+} \xrightarrow{-HCN} 76^{+}$$

is an impossibility at present, since the difference in masses of C_2H_3 and HCN is about 13 milli-mass units. We have not yet explored relative-abundance differences of metastable transitions of isomers, but McLafferty and Bryce[2] have shown the utility of this technique for distinguishing the five hexane isomers.

As a consequence of the success of our very crude instrumental modifications for obtaining pure metastable spectra, we plan to further improve the instrumental design and to automate the measurements in order to reduce sample size and operator time.

References

1. T. W. Shannon, T. E. Mead, C. G. Warner, and F. W. McLafferty, Anal. Chem. 39, 1748 (1967).
2. F. W. McLafferty and T. A. Bryce, Chem. Commun. 1215 (1967).

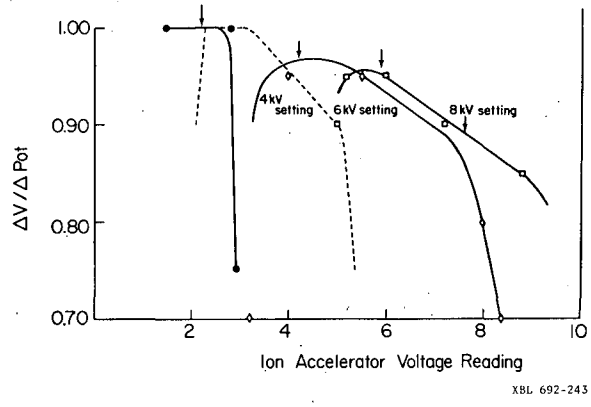

Fig. 1. Plot of the ratio δV/d Pot reading for the CEC 21-110B when the output range switch is altered from 2 kV to 8 kV.

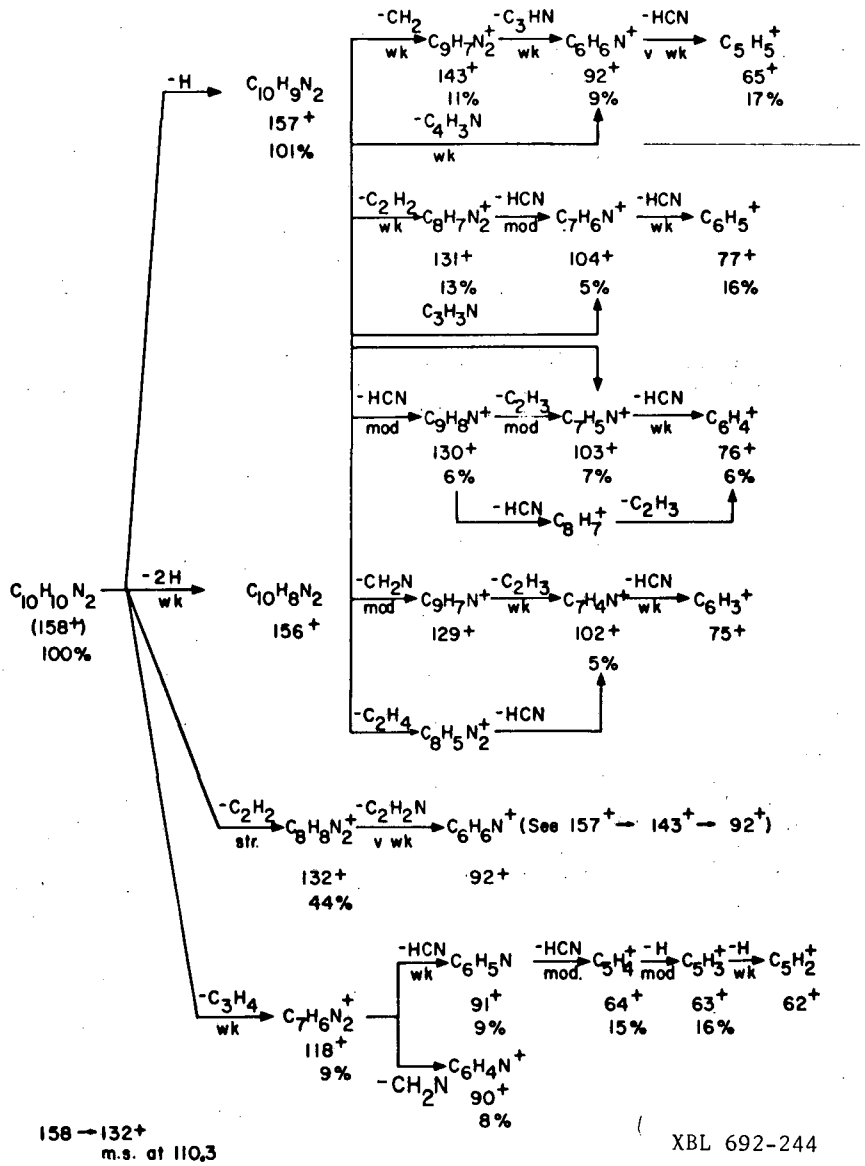

Fig. 2. Fragmentation pathway established by decoupling procedure for 1, 2, 2a, 3-tetrahydrocyclobuta(b)quinoxaline.

DIFFERENTIALLY PUMPED VACUUM PROBE USING CRYOGENIC AND ION PUMPING

R. H. Escobales, C. E. Miner, R. M. Reimers, and M. C. Michel

As part of the design of the cascade isotope separator, it was desirable to achieve minimum base pressure of the main vacuum tank with low pumping speed because of the relatively high cost per speed unit for ion pumps. It was also necessary to be able to retrieve samples from the vacuum rapidly for the study of short-lived radioactive samples. The first requirement could easily be met with a low-outgassing low-speed system, giving a long pumpdown time but good base pressure. This effectively blocks the use of conventional sample vacuum locks because of the outgassing of the soft seals common in these designs. Therefore a vacuum probe system similar to

those in use for many years on mass spectrometers at both sites of the Laboratory was designed. This in turn was based on a design by Stevens.[1]

As shown in Fig. 1 this is a cylinder making a very tight fit in the differentially pumped housing, allowing insertion or removal of a sample-carrying probe by displacing a similar cylinder to a similar device on the opposite side. Figure 1 shows three positions of the probe (not complete in all details).

(a) Operating position: Both differentially pumped (at CP1, CP2, and IP2) housings are closed by either the blank cylinder (at left) or the actual collector probe on the right (the blank system is always in vacuum and never is removed).

(b) Partial extraction: The left blank cylinder has been moved by a screw mechanism (operating through an O-ring seal in vacuum space pumped by CP1) to cover the probe. Closure of the left housing is now by the longer blank cylinder, and the shorter cylinder, attached to it by a slightly articulated joint, is about to push the probe out of the right housing. The articulated joint avoids the need for accurate alignment of the two housings, a difficult task and a defect in the original designs (fit of the cylinder and housing is of the order of 0.0005 in. to reduce leakage).

(c) Probe extracted: Probe has been pushed out by continued advance of the screw drive forcing the two blank cylinders to occupy both housings. Note that at no time is a significant leak present between any two differential pumping ports or to the outside.

Reversing the removal procedure allows insertion of the probe, which is attached to the short blank cylinder by a simple bayonet joint and pulled in by reversal of the screw mechanism. (Pumpout through radial ports occurs as the probe passes the pumping annuli.) When the probe has reached the limit of travel the bayonet can be disengaged by slight rotation of the probe and the covering blank cylinder retracted as in a, Fig. 1.

The effectiveness of the articulated joint was shown by adequate operation within a few minutes of initial assembly, whereas previous designs required many days of effort to achieve alignment of the two pump housings, and equal times in case of reassembly.

Since the main separator vacuum was ion-pumped, it was felt desirable to replace the mechanical pump-diffusion pump combination in use on the previous probes with cryogenic and ion pumps. The mass spectrometer probes had avoided all possibility of organic contaminants in the main vacuum by allowing a permanent leak to the pumping port CP1 from atmosphere instead of using the auxiliary O-ring seal in the design of Stevens.[1] To avoid unnessarily frequent regeneration of the cryogenic pumps, this feature, slightly modified to avoid contact of this secondary seal with any part that reaches the main vacuum, was restored as shown in the inset detail in Fig. 1. Thus the maximum leak to CP1 is present only during transfer of a probe in or out. At either extreme a tight secondary seal is made either by the probe or by a removable plug when the probe is out. Thus the two cryogenic pumps are loaded only during a probe transfer, and almost a year of use has required no regeneration of either cryogenic pump. The two spaces at IP2 are pumped by an 8-ℓ/sec and an 11-ℓ/sec sputter-ion pump respectively, normally operating at $\approx 1\times10^{-7}$ torr.

The main vacuum has a base pressure of 1 to 2×10^{-9} torr, and removal of the probe raises this by less than a factor of two for a very short time. Insertion of a probe from atmosphere does disturb the system, and the rise in pressure depends on the exposure of the probe to contaminants. In general pressures do not rise above 1×10^{-7} torr and the return to pressures below 5×10^{-8} torr (which is satisfactory for operation) can be achieved in less than 30 minutes. Return to base pressure requires several hours.

Figure 2 shows a view of the collector with the system installed and the probe in operating position. Figure 3 shows the probe itself removed from the system.

Reference

1. C. M. Stevens, A Vacuum Lock for Routine Solid Analyses with a Mass Spectrometer, ANL-4816, Dec. 1951.

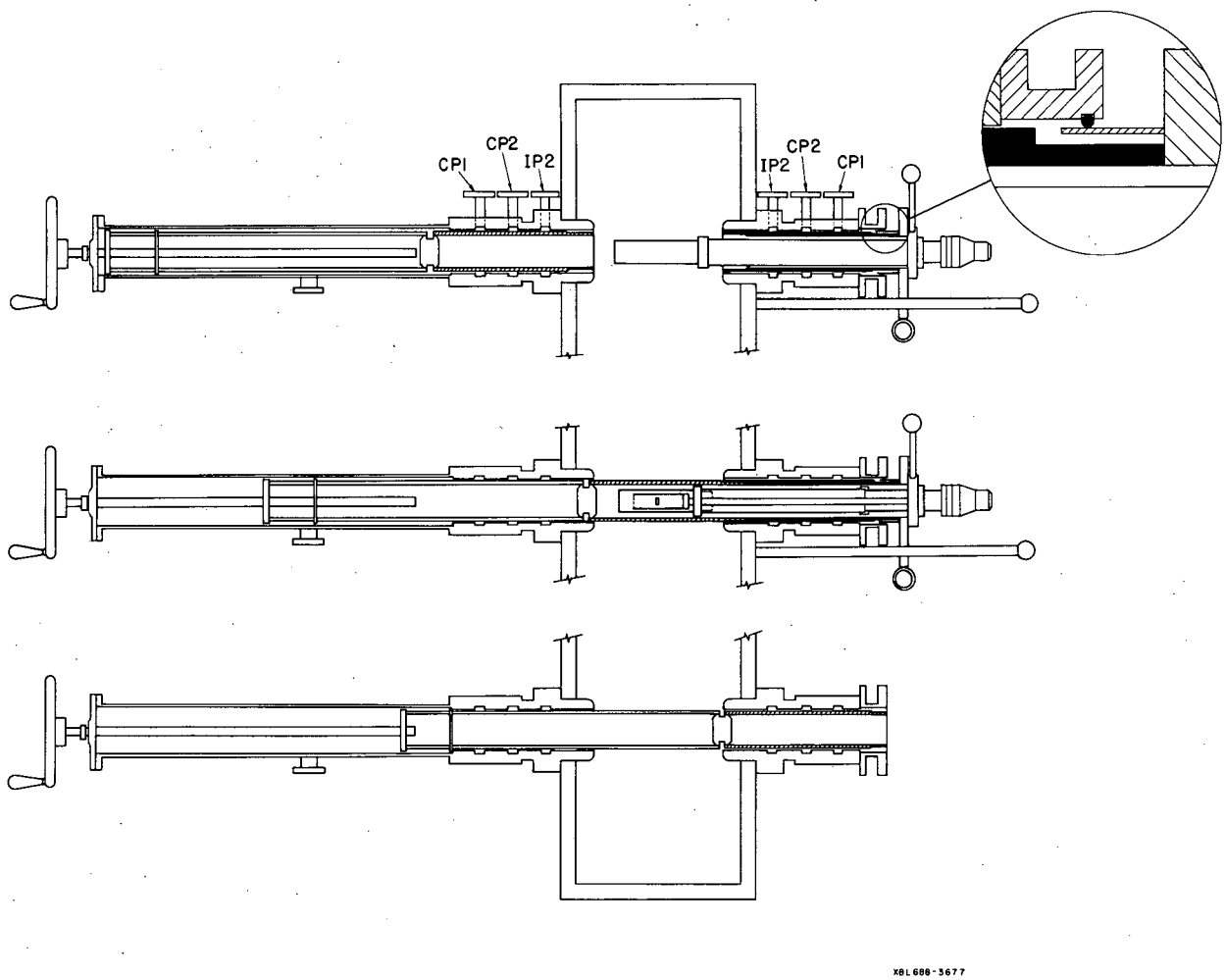

Fig. 1. Simplified schematic drawing of vacuum probe system.

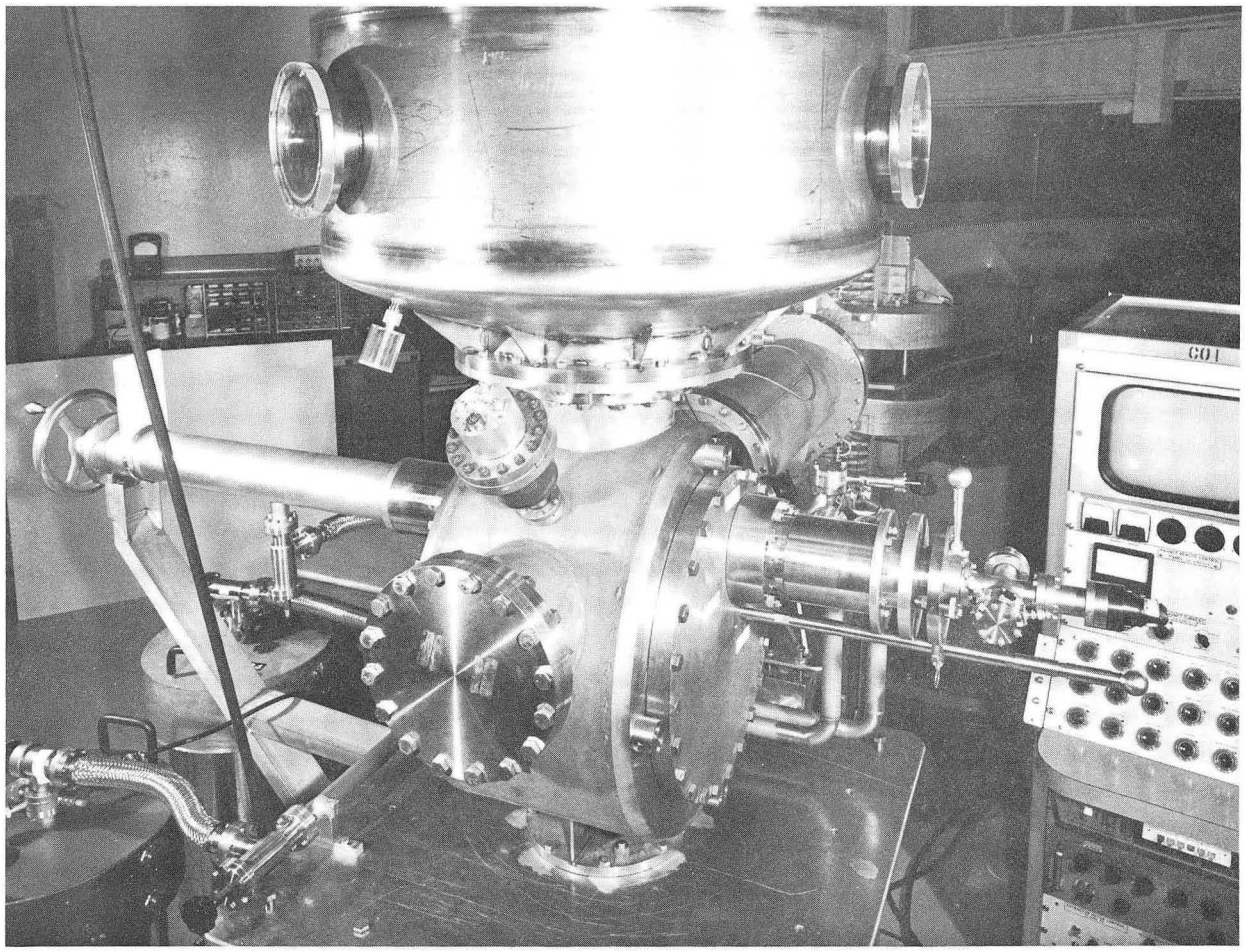

XBB 688-5128

Fig. 2. View of cascade isotope separator, showing vacuum probe.

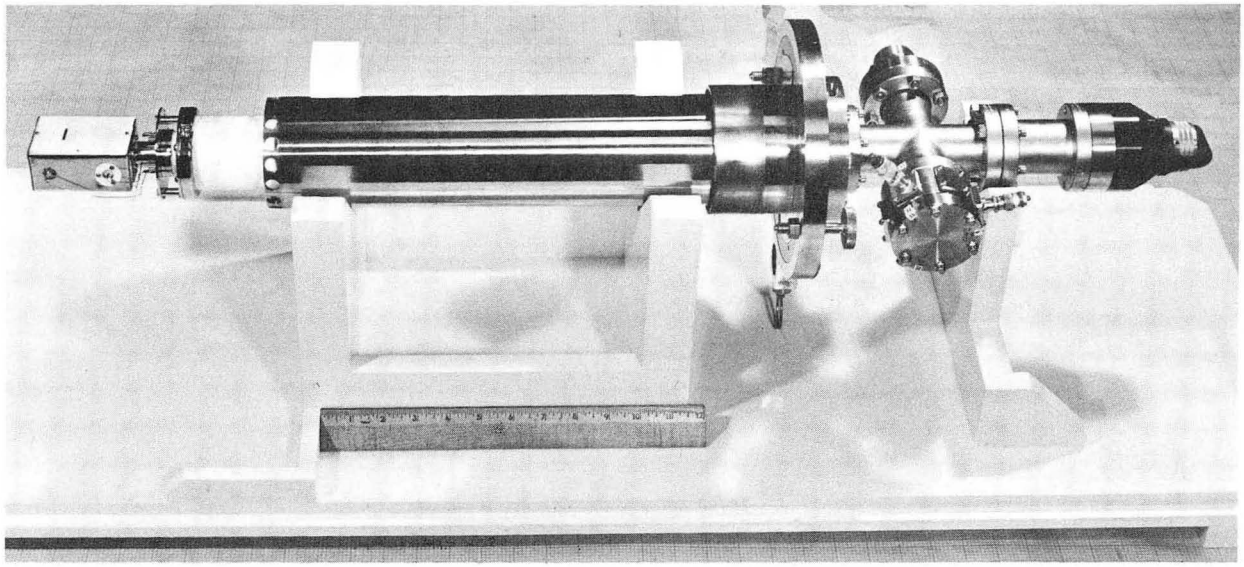

XBB 688-5124

Fig. 3. Collector probe for cascade isotope separator.

SIMPLE METHOD FOR DETERMINING WAIST-TO-WAIST TRANSFER PROPERTIES OF QUADRUPOLE DOUBLETS AND TRIPLETS†

F. Resmini*

The method reported here is based on a proper combination of transfer matrix tabulation and graphical plotting, and has proved quite successful in solving exactly any waist-to-waist (WW) transfer problem associated with quadrupole doublets or triplets. The major advantage stems from the fact that it eliminates the need for fairly close guesses of the lens strengths and visualizes at once all possible solutions for any given geometry.

A beam traveling along the z axis is represented in a general way by referring to the phase spaces associated with the (x, z) radial and (y, z) vertical planes. The (x, x') and (y, y') variables, i.e., position and divergence, describe the beam behavior in phase space, the units being usually mm and mrad. The beam has a waist, at some position along the z axis, at which it is represented by upright ellipses in both phase spaces, and along a drift length the waist position is thus the place where the beam has its minimum size. The ellipses can be represented, at any waist, through their characteristic length X, defined as $X_r = x_0/x'_0$ and $X_v = y_0/y'_0$ for the radial and vertical planes respectively, the subscripts (0) referring to the semiaxes of the ellipses. When WW transfer is obtained, the shape of the image ellipse will be different from that of the source and characterized by a different X'_r or X'_v. The matching ratio ρ is then defined by $X'_{r,v} = \rho_{r,v} X_{r,v}$, and is related to the usual linear magnification by $\rho_{r,v} = M^2_{r,v}$. In order to have WW transfer with matching ratio ρ, for a beam with a given X_{in}, it must be possible to reduce the 2-by-2 transfer matrix to the form[1]

$$\begin{vmatrix} \rho^{1/2}\cos\phi & X_{in}\rho^{1/2}\sin\phi \\ -(X_{in}\rho^{1/2})^{-1}\sin\phi & \rho^{-1/2}\cos\phi \end{vmatrix} \qquad (1)$$

where ϕ is an arbitrary phase angle used in describing the image ellipse.

Referring to Fig. 1, we consider the following problem: given the upstream and downstream distances U and D (which in the most general case could be different for the radial and vertical planes) and given $X_{r,\,in}$ and $X_{v,\,in}$, the characteristic lengths of the initial ellipses, find the strengths of the quadrupoles which allow WW transfer between U and D, together with the radial and vertical magnifications.

If we deal with a triplet in which the outer quadrupoles are equally excited, as in Fig. 1, or a doublet, then the problem is one with two free parameters, i.e., the gradients of the quadrupoles, and can be treated conveniently by the present method.

We write symbolically the transfer matrices of Fig. 1 as

$$T_r = \begin{vmatrix} \alpha_{11} & \alpha_{12} \\ \alpha_{21} & \alpha_{22} \end{vmatrix}, \qquad T_v = \begin{vmatrix} \beta_{11} & \beta_{12} \\ \beta_{21} & \beta_{22} \end{vmatrix},$$

with self-explanatory notation. It can be shown that the following equations must be satisfied in order to have WW transfer in both planes:

$$\frac{\alpha_{12}\,\alpha_{22}}{\alpha_{21}\,\alpha_{11}} = -X^2_{r,\,in}, \tag{2}$$

$$\frac{\beta_{12}\,\beta_{22}}{\beta_{21}\,\beta_{11}} = -X^2_{v,\,in}, \tag{3}$$

where the element α_{ij} and β_{ij} are only functions, for a given geometry, of the strengths K_1 and K_2 of the quadrupoles.

The solutions (K_1, K_2) of the equations above correspond to WW transfer in both planes for the given beam. Once they are found, the magnifications are also determined.

The best way to solve this system is to tabulate and plot the ratios of the matrix elements as functions of K_1, for different values of K_2.

In the (K_1, X^2) plane any beam of characteristic length X_{in} is then simply represented by a line parallel to the K_1 axis and with ordinate $-X^2_{in}$. The intersections of this line with the plotted curves mentioned above provide pairs of values (K_1, K_2) and thus in a K_1, K_2 plane generate a curve which corresponds to radial (vertical) WW transfer. The intersections in the (K_1, K_2) diagram of the curves for the radial and vertical matrices give, finally, the required quadrupole gradients for the simultaneous WW transfer.

As an example, for U = D = 50 cm, Figs. 2 and 3 present the ratios (2) and (3) tabulated as functions of $(K_1L)^2$, for different values of $(K_2L)^2$. The units are so chosen that the beam size and divergence are expressed in mm and mrad and the quoted X^2's are consistent with this choice.

Only the negative half plane of each plot, corresponding to negative $(-X^2_{in})$, is of physical significance and is shown here. Points on the $X^2 = 0.0$ axis correspond to WW transfer for a point source. In the "radial" plot, Fig. 2, for every K_2L there is only one curve which lies in the negative half plane. In the "vertical" plot instead, Fig. 3, the curves for each K_2L split into two branches, each of which allows WW transfer in the sense of Eq. (3). Thus, for any $(-X^2_{in})$ value we have, in the (K_1L, K_2L) diagram, one line for the radial matrix and two for the vertical, like those shown in Fig. 4 for $X^2_{in} = 1$. The two points of intersection represent the only solutions to the desired WW transfer. Point O gives a magnification of unity in both planes, an obvious case for this geometry. Also the point O' yields a magnification of unity in the radial plane and in the vertical.

The same pattern is observed for any other symmetric upstream-downstream triplet geometry for which WW transfer is possible.

It is to be noted that once graphs like Figs. 2 and 3 are constructed they immediately give the solutions for any X_{in}. In terms of the quadrupole gradients, these solutions, of course, are different for different values of X_{in}.

Footnotes and References

†Condensed from Nucl. Instr. Methods (to be published).
*On leave of absence from University of Milan, Italy.

1. A. P. Banford, The Transport of Charged Particle Beams (E. and F. N. Spon, London, 1966) and references therein.

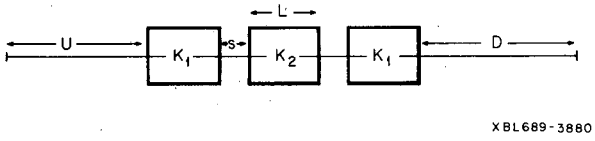

Fig. 1. Schematic triplet geometry.

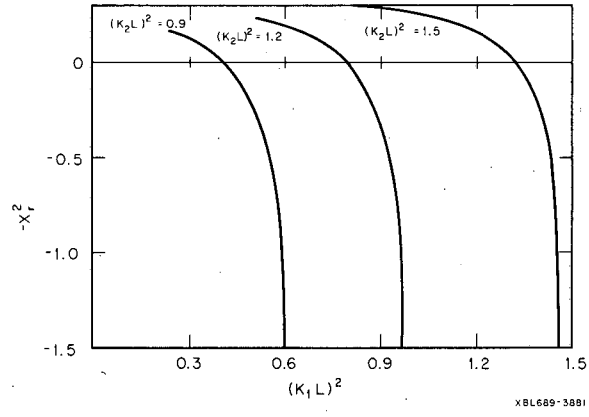

Fig. 2. Plots of the ratio (2) for the radial transfer matrix, in the case U = D = 50 cm.

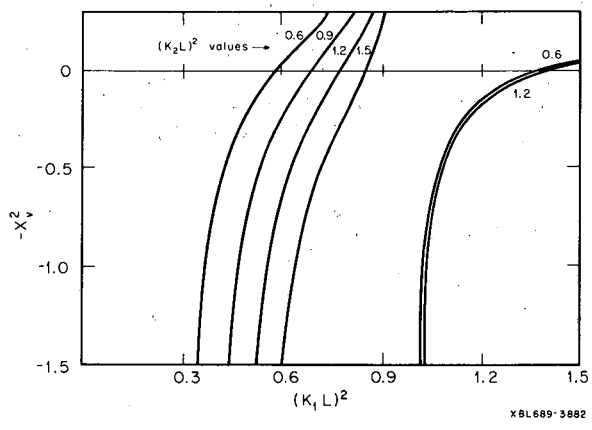

Fig. 3. Plots of the ratio (3) for the vertical transfer matrix, in the case U = D = 50 cm.

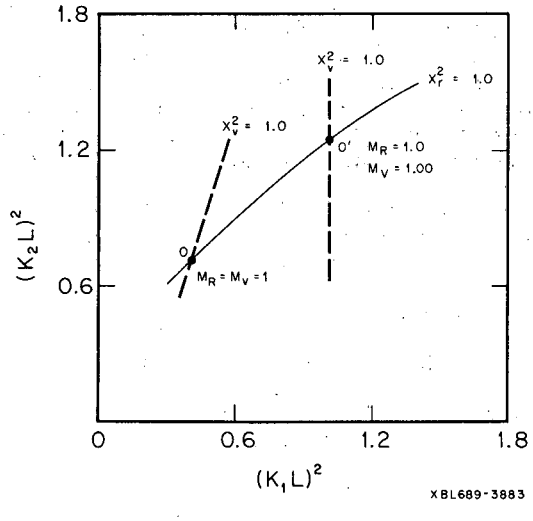

Fig. 4. Solutions for waist-to-waist transfer in the case U = D = 50 cm for a beam characterized by $X^2_{in} = 1$.

ROTATING VACUUM SEAL AND ANODE

Herman P. Robinson

Electron Spectroscopy for Chemical Analysis (ESCA),[1] as developed by Professor Kai Siegbahn and co-workers at the University of Uppsala, uses a high-intensity low-energy x-ray beam. This requires the use of a high-speed water-cooled anode rotating in a vacuum.

Figure 1 shows a cross section of the bearing, vacuum seal, and anode developed for this purpose. The anode consists of a copper structure about 3 in. in diameter mounted on the end of a hollow stainless steel shaft. The hollow shaft was made by boring lengthwise a stainless steel rod and inserting a smaller stainless steel tube to provide for water flow to and from the target. The face of the anode is coated with a layer of aluminum, since Al Kα x rays are desired. Cooling water is conducted through the hollow shaft to the target. The electron beam impinges on the face of the target in a spot about 1×3 mm. An electron beam power of 6 kW requires a speed of 5000 rpm or more to prevent local melting of the aluminum. The present design has been run at 2000 rpm only.

Three sleeve bearings made of Rulon A (or LD), a loaded Teflon, provide shaft support and separate incoming and outgoing water. The water also lubricates the bearings. Slight leakage of water past the bearings is necessary, and this leakage is drained away at the two ends of the bearing assembly. Two other bearing materials were tried, but were not so satisfactory as Rulon. Lignum vitae, which is sometimes used in bearings that are submerged in water, was satisfactory except that if the bearings dried out, shrinkage and cracking occurred. The shrinkage of about 2% was not completely reversible.

Nylon was also tried, but slight local heating caused a flow of material which interfered with the lubrication of the bearing, further aggravating the difficulty. Bronze was considered but not tried because of the short time available for testing before the unit was dismantled and shipped to Uppsala, where the work will be continued.

A very critical element in the design is the vacuum seal. Materials sliding in a high vacuum exhibit a much higher coefficient of friction than they do in air, and as a consequence the wear rate is much higher. Rulon has been used by others for a vacuum seal and was chosen for the present design. The vacuum seal consists of a copper collar faced with stainless steel, running in contact with Rulon. Provision was made for differential pumping to reduce leakage. The higher-pressure side of the Rulon vacuum seal disk is pumped with a mechanical pump to reduce air leakage across the rotating seal.

The seal has been run for several hours at 2000 rpm with moderate wear of the Rulon seal. At 5000 rpm the wear rate is excessive. There is another material called Meldin which is a polyimide plastic, much harder than Rulon, which should withstand higher speeds under vacuum. No time was available to try this material.

Professor Siegbahn and Sven-Erik Karlsson, both from Uppsala, were active in the development of this device.

Reference

1. Kai Siegbahn et al., ESCA (Almqvist & Wiksells Boktryckeri Ab, Uppsala, 1967).

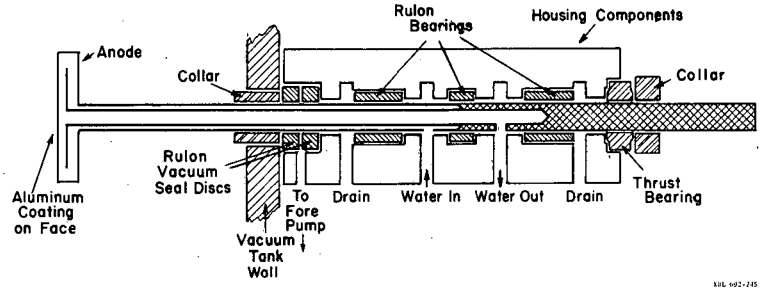

Fig. 1. A cross-section view of the bearing, vacuum seal, and anode for use in the Electron Spectroscopy for Chemical Analysis apparatus.

V. Thesis Abstracts

On the following pages the abstracts of theses issued in 1968 are given as they appeared in the original documents.

AN INVESTIGATION OF THE (^{3}He, t) AND (^{3}He, ^{3}He') REACTIONS ON 1p SHELL NUCLEI

Gordon Charles Ball
(Ph. D. Thesis)

(From UCRL-18263)

The (^{3}He, t) and (^{3}He, ^{3}He') reactions on ^{9}Be, ^{12}C, ^{13}C, ^{14}C [(^{3}He, t) reaction only], ^{14}N, and ^{15}N have been investigated at ^{3}He energies of 39.9, 49.8, 39.6, 44.8, 44.6, and 39.8 MeV, respectively. Angular distributions were obtained for all prominent states up to excitations of 20 MeV. A microscopic analysis of these data has been carried out using a local two-body interaction with an arbitrary spin-isospin exchange mixture. Spectroscopic factors were calculated using intermediate-coupling wave functions for p shell states while simple j-j configurations were assumed for the levels which were populated by promoting a p nucleon to the s-d shell. A Yukawa interaction with a range of $\alpha^{-1} = 1.2$ F was found to give the best results. The strength of the effective nucleon-nucleon interaction required to fit these data is in good agreement with recent (p, p'), (p, n), and (^{3}He, t) calculations on light nuclei. In particular, dominant L = 0 transitions observed in the (^{3}He, t) reaction gave values for the isospin $V_{ST} = V_{01}$ and spin-isospin V_{11} dependent terms (converted to an effective nucleon-nucleon interaction at $\alpha^{-1} = 1.0$ F) of 20.6 and 16.5 MeV, respectively, while the strengths required to fit (^{3}He, t) L = 2,3 transitions were generally enhanced. For inelastic transitions, the average strengths obtained for V_{00}, assuming a Serber exchange mixture, varied from 47.2 to 67.3 MeV depending upon the L transfer involved. A comparison of the (^{3}He, t) and (^{3}He, ^{3}He') reactions populating analog final states (where $T_f = T_i + 1$) is also presented. In general, these transitions were weakly populated; however, it was possible to observe the lowest T = 3/2 levels in the mirror nuclei ^{9}B - ^{9}Be and ^{13}N - ^{13}C and several T = 1 levels in ^{12}N - ^{12}C.

THE CRYSTAL AND MOLECULAR STRUCTURES OF THREE BORON COMPOUNDS

Barry Goodwin DeBoer
(Ph. D. Thesis)

(From UCRL-18391)

The crystal and molecular structures of three boron-containing compounds have been determined by x-ray diffraction studies of single crystal specimens. They are: the rubidium salt of an octadecahydroeicosaborate(2-) photoisomer, $Rb_2B_{20}H_{18}$; the tetramethylammonium salt of a brominated carborane-metal "sandwich" ion, $N(CH_3)_4[(B_9C_2H_8Br_3)_3Co]$; and tris-difluoroboraborane—phosphorous trifluoride, $B_4F_6PF_3$.

Crystals of $Rb_2B_{20}H_{18}$ are orthorhombic, space group $Pn2_1a$, with $a = 12.344 \pm 0.007$ A, $b = 19.014 \pm 0.010$ A, $c = 7.260 \pm 0.005$ A, and contain four formula units per unit cell. The calculated density is 1.58 g/cc (by flotation, 1.57 g/cc). The structure was determined by Patterson and Fourier techniques and refined by a full-matrix least-squares procedure to a conventional R of 0.127 for 1175 scintillation-counter data (0.073 for the 935 non-zero data). The non-centric

nature of the space group was demonstrated by the measurement of anomalous dispersion effects. The anion consists of two capped-square-antiprismatic B_{10} polyhedra joined by a pair of hydrogen bridges, one between each pair of equatorial four-rings, such that the result has an approximate $2/\underline{m}$ ($\underline{C_{2h}}$) point symmetry. A list of thirteen possible isomers covering reasonable choices of bridge positions is presented together with their point symmetries.

Crystals of $N(CH_3)_4[(B_9C_2H_8Br_3)_2Co]$ are monoclinic, space group $P2_1/c$, with $\underline{a} = 19.893 \pm 0.010$ A, $\underline{b} = 19.487 \pm 0.010$ A, $\underline{c} = 15.058 \pm 0.010$ A, $\beta = 93.15^\circ \pm 0.05^\circ$, and contain eight formula units and four crystallographically independent anions per unit cell. The calculated density is 1.967 g/cc, in agreement with the measured value of 1.98 ± 0.01 g/cc. The structure was solved by statistical methods and refined by a least-squares procedure to a conventional $\underline{R}$ of 8.7% on 3002 data collected by counter methods. All four independent anions have the same shape to within the accuracy of this determination. The anion, the product of a bromination during which the bis-dicarbollyl cobalt "sandwich" is believed to remain intact, consists of two substituted icosahedra with the cobalt as their common vertex. In each icosahedron, the carbons are adjacent to each other and to the cobalt, while the three borons bonded to bromine form the corners of a triangular face. Two corners of this face are as far as possible from the carbons, and the third is adjacent to the cobalt. These bromination sites are consistent with a charge distribution in the reactant which is analogous to that in $\underline{o}$-$B_{10}C_2H_{12}$, but modified slightly by the presence of the Co(III).

Crystals of $B_4F_6PF_3$ are orthorhombic, space group Pnma, with $\underline{a} = 13.893 \pm 0.005$ A, $\underline{b} = 10.578 \pm 0.005$ A, $\underline{c} = 6.075 \pm 0.005$ A, and contain four formula units per unit cell. The calculated density is 1.82 g/cc. The structure was solved by statistical methods and refined by full-matrix least-squares to a conventional $\underline{R}$ of 9.3% for 703 data collected by counter methods (6.7% for the 603 non-zero data). The molecule consists of a central boron atom, tetrahedrally bonded to three BF_2 groups and the PF_3 group in such a way that the molecule has approximately 3m (C_{3v}) point symmetry, one mirror of which is required by the crystal symmetry. Distances found (uncorrected for thermal motion) are: B-F, 1.305 A; B-B, 1.68 A; B-P, 1.825 A; and P-F, 1.51 A (all ± 0.015 A).

AN ABSOLUTE TEMPERATURE SCALE FOR CERIUM MAGNESIUM NITRATE BELOW 0.002° K

James John Huntzicker
(Ph. D. Thesis)

(From UCRL-18476)

The absolute temperature scale for single crystal cerium magnesium nitrate (CMN) has been extended to $S/R = 0.002$ by adiabatic demagnetization from values of H/T up to 68 kOe/°K. The temperature dependence of the highly anisotropic angular distribution of the 255 keV γ-ray from oriented ^{137m}Ce in the CMN provided the thermometric parameter. The nuclear orientation results were interpreted with the spin Hamiltonian $\mathcal{H} = g_{\perp}\beta H_x S_x + B(S_x I_x + S_y I_y)$ where H_x (a calculated dipolar field) = 60.67 Oe and $B/k = 0.00820 \pm 0.00042$°K. The hyperfine structure constant B was determined by normalizing the nuclear orientation results to the calorimetric results of Hudson and Kaeser in the entropy range $0.063 \leq (\ln 2 - S/R) \leq 0.164$. Analytic relations between temperature and entropy are presented for the entropy range $0.002 \leq S/R \leq 0.640$. The lowest temperature measured was 0.00135 ± 0.00008°K. The present results are in reasonable agreement with both the earlier nuclear orientation results of Frankel, Shirley, and Stone, and with the calorimetric results of Hudson and Kaeser. These results and the results of Hudson and Kaeser are compared in detail. The effect of recent high-field magnetization measurements on the CMN temperature scale are discussed.

The ^{137m}Ce γ-ray thermometer was also used to investigate the thermal behavior of cerium zinc nitrate (CZN). The preliminary nuclear orientation results indicate a high degree of similarity between CZN and CMN.

PAIRING IN NUCLEI

Oliver Davis Johns
(Ph. D. Thesis)

(From UCRL-18614)

Parts I and II of this thesis deal with the general problem of adapting the quasi-particle approximation to give satisfactory results in nuclear systems. Part I shows that the projection of correct particle number from the number non-conserving quasi-particle ground state vector can give excellent agreement with exact ground states, when the quasi-particle ground state is first modified by an exponential four, eight, etc., quasi-particle operator.

The similarity of this ground state exponential form to that predicted by the quasi-boson method leads to Part II, which considers the generalized problem of computing both ground and excited seniority zero 0+ states of nuclei. The results of Part II demonstrate that excellent overlap of boson and exact 0+ states is obtained if the following revisions are made in the quasi-boson method:

1) The zero energy boson used to help define the boson ground state should be a certain linear sum of the spurion and its conjugate, and not the spurion alone.

2) The first excited state for moderate to weak pairing potential strength is a two boson state consisting of one zero energy boson and one non-zero energy boson.

3) The striking failure of the method at subshell closures can be circumvented by slightly altering the average particle number.

Part III of the thesis illustrates the method of exact, number conserving diagonalization of the many body Hamiltonian matrix. This method, which is practical only for non-deformed nuclear systems, is conceptually simpler than the quasi-particle method in which much effort must go into the isolation and correction of approximation produced inaccuracies.

THE (α, d) REACTION ON LIGHT AND MEDIUM MASS NUCLIDES

Chi Chang Lu
(Ph. D. Thesis)

(From UCRL-18470)

The (α, d) reactions on targets of ^{13}C, ^{14}C, ^{15}N, and ^{20}Ne were studied using alpha particle beams of 40.1, 46.0, 45.4, and 44.5 MeV, respectively. Angular distributions were obtained. States with $(1d_{5/2})^2_{5+,\,0}$ configuration were located and possible spin assignments were suggested. These states are: ^{15}N 13.03 MeV (11/2-), 11.95 MeV (9/2-); ^{16}N 5.75 MeV (5+); ^{17}O 7.74 MeV (11/2-), 9.14 MeV (9/2-); ^{22}Na 1.528 MeV 5+.

Separated isotopes of ^{52}Cr, $^{54,56}Fe$, ^{59}Co, $^{58,60,62}Ni$, ^{63}Cu, and $^{64,66,68}Zn$ were used as targets to study the (α, d) reaction with a 50 MeV alpha particle beam. States with a probable configuration of $(1g_{9/2})^2_{9+,\,0}$ were located. These states are ^{54}Mn 9.47 MeV, ^{56}Co 8.92 MeV, ^{58}Co 6.79 MeV, ^{60}Cu 5.99 MeV, ^{62}Cu 4.75 MeV, ^{64}Cu 4.57 MeV, ^{66}Ga 2.99 MeV, ^{68}Ga 2.88 MeV, ^{70}Ga 2.88 MeV.

The residual interaction energies between the proton and neutron in the configurations $(1d_{5/2})^2_{5+,\,0}$ and $(1f_{7/2})^2_{7+,\,0}$, and $(1g_{9/2})^2_{9+,\,0}$ were extracted from the excitation energies determined in the present work and previous work on $(1d_{5/2})^2_{5+,\,0}$ and $(1f_{7/2})^2_{7+,\,0}$ states. For $T_z \neq 0$ nuclides, an "interaction model" method was proposed to extract the residual interaction energy. The mean values of the residual interaction energies are about -3.9, -3.0, -2.2 MeV respectively for the three mentioned configurations. There is a slight decrease of residual interaction energy with increasing A. These results are reproduced excellently by conventional shell model calculations.

The results of (α, t) reactions studied simultaneously with the (α, d) reactions are also briefly reported.

ENERGY LEVEL CALCULATIONS FOR SINGLY IONIZED HAFNIUM

Rolf Mehlhorn
(Ph. D. Thesis)

(From UCRL-18040)

The parametric theory of atomic structure, developed by Giulio Racah, was used to derive formulas for matrix elements, including those of configuration interaction not hitherto available in the literature. These formulas were incorporated into a series of computer codes for calculating matrix elements, energy levels, g-values, and intensities. The programs were designed to deal with the commonly occurring configurations ℓ^n, $\ell^{n-1}\ell'$, and $\ell^{n-2}\ell'\ell''$.

With the aid of these programs an analysis of HfII was conducted. The odd parity levels could be described with a mean error of 143 cm^{-1} for 56 energies, corresponding to about 0.5% of the configuration width. However, many calculated g-values did not agree with the observations. Therefore a new least squares fit, utilizing both the g-values and energy levels was developed. With this fit the mean error for the g-values was reduced from 0.100 to 0.023, but the error in energies rose to 453 cm^{-1} for 62 energies.

To investigate the eigenvector errors, intensities were calculated. With the eigenvectors of the energy calculation no reasonable agreement was found between the calculated and observed intensities. The theoretical intensities were considerably improved by assuming a crude model for configuration interaction. An admixture of excited configurations into the known eigenvectors, depending linearly on the energy of the known level, was postulated. In the final result the mean error for 300 observed transitions was about 50%, due in part to large experimental errors.

Although the experimental intensities are certainly in need of improvement, much of the error must be ascribed to the theoretical eigenvectors. It is felt that significant corrections to these would result from an improved energy calculation, taking into consideration relativistic corrections, such as the spin-other-orbit interaction, and the effective operators of configuration interaction. These refinements are recommended for future work.

RADIO-FREQUENCY STARK SPECTRA OF NaCl, NaBr, AND BaS BY THE MOLECULAR BEAM ELECTRIC RESONANCE METHOD

Carlos A. Melendres
(Ph. D. Thesis)

(From UCRL-18344)

The strong-field radio-frequency Stark spectra of $Na^{23}Cl^{35}$, $Na^{23}Cl^{37}$, $Na^{23}Br^{79}$ and $Na^{23}Br^{81}$ have been observed by the molecular beam electric resonance method of molecular spectroscopy. Analysis of spectral lines obtained by observing transitions of the type $J = 1$, $m_J = \pm 1 \rightarrow J = 1$, $m_J = 0$ at strong electric fields yielded molecular dipole moments and nuclear hyperfine interaction constants for the different vibrational states of the molecules.

A beam of BaS was successfully obtained. The Stark line corresponding to $J = 1$, $m_J = 0 \rightarrow J = 1$, $m_J = \pm 1$ transition was observed at moderately weak fields from which was obtained the ratio μ^2/B for the three lowest vibrational states.

A mass spectrometric study of the composition of indium monohalide beams was undertaken. Dimers and atomic species were observed in addition to the more preponderant diatomic molecules.

THE EXCITATION OF UNNATURAL-PARITY STATES IN ^{24}Mg ^{20}Ne AND ^{16}O BY INELASTIC α SCATTERING

Mary Reed
(Ph. D. Thesis)

(From UCRL-18414)

The excitation of unnatural-parity states ($\pi \neq (-)^J$) in even-even nuclei has been studied by inelastic α scattering over the energy range of 33 to 120 MeV. Data are reported for the low-lying states in three nuclei—^{24}Mg, ^{20}Ne, and ^{16}O.

The excitation of unnatural-parity states is forbidden in simple, one-step, direct reaction theories by spin and parity considerations. Since these states are excited with moderately large cross sections, the study of them sheds light on more complicated reaction mechanisms.

When the angular distributions for these reactions at the various energies are compared with each other, consistent results are obtained for the natural-parity states and for the 2- state in ^{16}O. However, for the 2- state in ^{20}Ne and the 3+ state in ^{24}Mg, unusual angular distributions are obtained which bear no resemblence to the theories.

Calculations of compound nucleus and multiple excitation cross sections are made using Hauser-Feshbach and coupled-channel computer codes. The multiple excitation cross sections produced in this way give fairly good agreement with the experimental data, even reproducing the unusual appearance of the 3+ angular distributions. Thus the excitation of the unnatural parity state in ^{24}Mg is determined to be mainly a multiple-step process.

THE MOLECULAR-BEAM ELECTRIC-RESONANCE SPECTRA OF THE LITHIUM HYDRIDES

Elaine Rothstein
(Ph. D. Thesis)

(From UCRL-17948)

Radio-frequency spectra have been observed in the first rotational state of Li^7H, Li^7D, Li^6H, and Li^6D by the molecular-beam electric-resonance method. Analysis of the spectra has made possible the determination of accurate dipole moments and nuclear-hyperfine interaction constants.

The experimental values are compared to the available quantum mechanical calculations. The polarizable ion model is also compared to the experiment.

KINETICS OF A DENSE CULTURE FERMENTATION

Lyman Dale Sortland
(Ph. D. Thesis)

(From UCRL-18340)

A fermentation system was designed and constructed to study the growth characteristics of micro-organisms at low and high cell concentrations. The technique used to develop high cell densities utilized a rotating micro-filtration unit to permit the removal of cell-free product from the fermenter. The fermenter volume and the filter were contained in a single unit composed of a series of concentric cylinders. The annuli served as the fermenter volume while the second outermost cylinder supported a micro-filtration membrane. Feed to the system was pumped at

constant rates and the internal pressure built up to a value which would effect the required filtration rate. The system was operated batchwise and continuously with and without filtration.

The anaerobic growth characteristics of Streptococcus faecalus were determined at 37° C and pH 7.0 for batch, continuous and continuous with filtration modes of operation. Cell concentrations 45 times more concentrated than could be produced in batch culture were obtained using the filtration technique.

DIPOLE MOMENTS OF ALKALI HALIDES BY THE ELECTRIC DEFLECTION METHOD

Troy Lee Story, Jr.
(Ph. D. Thesis)

(From UCRL-18484)

The radio-frequency Stark spectra and the microwave spectra of $^{6}Li^{35}Cl$ and $^{6}Li^{37}Cl$ are investigated by the molecular-beam electric-resonance method of spectroscopy. Observations of transitions of the type $(J, M_J) \rightarrow (J, M_J \pm 1)$ and $(J+1, M_J) \rightarrow (J, M_J)$ have allowed a determination of dipole moments, rotational constants, and chlorine quadrupole and spin-rotation interaction constants for several vibrational states of these molecules.

A method of determining dipole moments by deflecting a beam of velocity selected molecules with an electric field is presented. Dipole moments of KI, RbBr, RbI, CsBr, and CsI have been determined by this method. Deflection analysis of CsOH and LaF_3 are carried out, and implications concerning the geometrical configurations of these molecules are given. The design and construction of the velocity selector which was used in the deflection experiments is presented.

HYPERFINE STRUCTURE OF Dy^{165} AND SPIN OF Er^{163}

Sanford Stein
(Ph. D. Thesis)

(From UCRL-17969)

The atomic beam magnetic resonance flop-in method was used to measure the hyperfine structure of Dy^{165} and the spin of Er^{163}.

The result for the $_{66}Dy^{165}_{99}$ ground state is $a = \pm 89.8(7)$ MHz, $b = \mp 1520(30)$ MHz where a and b are the magnetic dipole and electric quadrupole hyperfine interaction constants. The spin was previously measured to be $I = 7/2$. From these values one can calculate the nuclear magnetic dipole moment μ_I and the nuclear electric quadrupole moment Q which are $\mu_I(\text{uncorr}) = \mp 0.50(4)$ nm, $Q(\text{uncorr}) = \pm 2.8(3)$ barns.

These values are in good agreement with that predicted by the strong deformation collective model.

The spin of the ground state of $_{68}Er^{163}_{95}$ is $I = 5/2$ which agrees with the Nilsson state assignment.

The theory underlying the atomic beam method, a description of the technique and equipment used, and a comparison with appropriate theoretical calculations are presented.

ATOMIC BEAM MEASUREMENT OF THE ISOTOPE SHIFTS IN ^{127}Cs, ^{129}Cs, ^{133}Cs, ^{134}Cs, ^{134m}Cs, AND ^{137}Cs

Edmond Chen-ching Wang
(Ph. D. Thesis)

(From UCRL-18434)

A new atomic-beam technique has been employed to measure the isotope shifts of five radioactive cesium isotopes relative to the stable isotope ^{133}Cs. The shifts (in 10^{-3} cm^{-1}) in the D_1 line are found to be

Isotope:	^{127}Cs	^{129}Cs	^{134}Cs	^{134m}Cs	^{137}Cs
IS:	+5.9(1.5)	+2.8(1.5)	+1.8(1.0)	-2.2(1.2)	-6.0(1.5)

Here a positive sign means that the wave number of the D_1 line for the indicated isotope is greater than that for ^{133}Cs.

The normal volume shift is calculated to be 10.7×10^{-3} cm^{-1} for the addition of one neutron. There is evidence that points to the cancellation of the normal volume effect by the deformation effect as a possible explanation of the smallness of the observed shifts.

VI. 1968 Publications

PAPERS PUBLISHED AND UCRL REPORTS ISSUED, 1968

ABECASIS, S. B. (See Bosch, H. E., Nucl. Phys. A108, 209 (1968))

ABED, U.
Determination of valence states of iron in glass and of uranium in calcium fluoride single crystals
UCRL-18655, December 1968
Anal. Chem.

ALEXANDER, J. M. (See Croft, P. D., Phys. Rev. 165, 1380 (1968))

ASARO, F. (See Perlman, I., UCRL-18212 Abstract)

ASCUITTO, R. J. (See Glendenning, N. K., UCRL-18529)

BACHER, A. D., and T. A. Tombrello
Reaction mechanism studies in $^{3}He(^{3}He, 2p)^{4}He$
UCRL-18071 Abstract, February 1968
Bull. Am. Phys. Soc. 13, 564 (1968)

BACHER, A. D., T. A. Tombrello, E. A. McClatchie, and F. Resmini
^{3}He-^{3}He Elastic scattering from 18 to 80 MeV
UCRL-18606 Abstract, November 1968
Meeting of the American Physical Society, Miami Beach, Florida, 25-27 November 1968

BACHER, A. D. (See de Swiniarski, R., UCRL-18527 Abstract)

BACHER, A. D. (See Resmini F., UCRL-18478 Abstract)

BAKER, B., III (See Pigford, R. L., UCRL-18483)

BALDESCHWIELER, J. D. (See Leipert, T. K., UCRL-18511)

BALL, G. C.
An investigation of the $(^{3}He, t)$ and $(^{3}He, ^{3}He')$ reactions on 1p shell nuclei
UCRL-18263, May 1968
Ph. D. Thesis

BALL, G. C., and J. Cerny
A microscopic analysis of the $(^{3}He, t)$ and $(^{3}He, ^{3}He')$ reactions on 1p shell nuclei
UCRL-18277, June 1968
Phys. Rev.

BALL, G. C. (See Cerny, J., UCRL-18074 Abstract)

BARRETT, P. H., and D. A. Shirley
Nuclear orientation studies on Nd^{147} and interpretation of neutron states for A = 140 - 150
UCRL-18036, November 1968
Phys. Rev.

BARTLETT, N., F. O. Sladky, B. G. DeBoer, and A. Zalkin
The crystal structure of $[Xe_2F_3][AsF_6]$
UCRL-18314 Abstract, June 1968
Meeting of the American Crystallographic Association, Buffalo, New York, 12-16 August 1968

BAR-TOUV, J., A. Goswami, A. Goodman, and G. Struble
Generalized pairing in light nuclei. I. Solutions of HFB equations in N = Z even-even nuclei
UCRL-18363, July 1968
Phys. Rev.

BECK, A. (See Turner, D. J., UCRL-17879)

BERNTHAL, F. M. (See Jaklevic, J. M., UCRL-18389)

BICHSEL, H., and C. Tschalaer
A range energy table for heavy particles in silicon
UCRL-17663 Rev 1, July 1968

BLOK, J. (See Kaplan, M., UCRL-18035)

BLUM, D. E. (See Pigford, R. L., UCRL-18483)

BOSCH, H. E., A. J. Haverfield, E. Szichman, and S. M. Abecasis
High-resolution studies in the decay of ^{133}Ba with semiconductor counters
Nucl. Phys. A108, 209 (1968)

BOWMAN, H. R., M. Croissiaux, R. C. Gatti, J. H. Heisenberg, R. Hofstadter, R. C. Jared, G. Kilian, L. M. Middleman, L. G. Moretto, S. G. Thompson, and M. R. Yearian
Electron induced fission in ^{238}U, ^{209}Bi, and ^{181}Ta
Suppl. J. Phys. Soc. Japan 24, 545 (1968)

BOWMAN, H. R., R. D. Giauque, and I. Perlman
Rapid x-ray fluorescence analysis of archaeological materials
UCRL-17968, December 1967
Applications of Science to Medieval Archaeology, International Conference at the University of California, Los Angeles, California, 26-28 October 1967

BREWER, W. D., and D. A. Shirley
Parity nonconservation by inner bremsstrahlung from polarized ^{119}Sb
UCRL-18087, February 1968
Phys. Rev. Letters 20, 885 (1968)

BREWER, W. D., D. A. Shirley, and J. E. Templeton
Low-temperature departures from the Korringa approximation
UCRL-18120, March 1968
Phys. Letters 27A, 81 (1968)

BRUNNADER, H., J. C. Hardy, and J. Cerny
Carbon-10 and mass measurements for light nuclei
UCRL-18272, June 1968
Phys. Rev. 174, 1247 (1968)

BRUNNADER, H. (See Hardy, J. C., UCRL-18075 Abstract)

BUCHER, J. J., and R. M. Diamond
Extraction of $HClO_4$ and $HReO_4$ by dilute solutions of tributyl phosphate in CCl_4, isooctane, and 1,2-dichloroethane
UCRL-17972, April 1968
J. Phys. Chem.

BUCHER, J. J., and R. M. Diamond
Extraction of $HClO_4$ and $HReO_4$ by dilute solutions of tributyl phosphate in benzene 1,3,5-triethylbenzene and $CHCl_3$
UCRL-17973, June 1968
J. Phys. Chem.

BURGER, R. (See Clark, D., UCRL-18608 Abstract)

BUSS, D. R., and T. Vermeulen
Optical isomer separation: Quest for a new biochemical technology
Ind. Eng. Chem. 60, 12 (1968)

BUTLER, G. W. (See Poskanzer, A. M., UCRL-18207)

CARNEIRO, A. (See Clark, D., UCRL-18608 Abstract)

CERNY, J., and G. C. Ball
(^{3}He, t) and (^{3}He, ^{3}He') reactions in the 1p shell
UCRL-18074 Abstract, February 1968
Bull. Am. Phys. Soc. 13, 632 (1968)

CERNY, J.
High-isospin nuclei and multiplets in the light elements
UCRL-18106, February 1968
"Annual Review of Nuclear Science," Vol. 18 (Annual Reviews, Inc., Palo Alto, California, 1968) p. 27

CERNY, J. (See Ball, G. C., UCRL-18277)

CERNY, J. (See Brunnader, H., UCRL-18272)

CERNY, J. (See Cosper, S. W., UCRL-18366)

CERNY, J. (See Hardy, J. C., UCRL-18075 Abstract)

CERNY, J. (See McGrath, R. L., UCRL-18335)

CERNY, J. (See Poskanzer, A. M., UCRL-18207)

CLAMPITT, R., and A. S. Newton
Metastable species produced by electron excitation of N_2, H_2, N_2O, and CO_2
UCRL-18032 Rev, September 1968
J. Chem. Phys.

CLAMPITT, R., and A. S. Newton
Surface effects in the ejection of electrons by electronically excited molecules
UCRL-18239, May 1968
Surface Science 12, 92 (1968)

CLARK, D., R. Burger, A. Carneiro, D. Elo, P. Frazier, A. Luccio, D. Morris, M. Renkas, and F. Resmini
Design and construction of the axial injection system for the 88-inch cyclotron
UCRL-18608 Abstract, November 1968
1969 Particle Accelerator Conference, Washington, D. C., 5-7 March 1969

CLARK, D. J. (See Luccio, A., UCRL-18607 Abstract)

CLARK, D. J. (See Resmini, F., UCRL-18125)

CLARK, D. J. (See Resmini, F., UCRL-18478 Abstract)

CLARK, D. J. (See Resmini, F., UCRL-18596 Abstract)

CLARK, M. W., and C. J. King
Evaporation rates of volatile liquids in a laminar flow system. Part I: Pure liquids
UCRL-17655, November 1967
American Institute of Chemical Engineers—Instituto de Ingenieros Quimicos de Puerto Rico, 2nd Joint Meeting, Tampa, Florida, 19-22 May 1968

CLARK, M. W., and C. J. King
Evaporation rates of volatile liquids in a laminar flow system. Part II: Liquid mixtures
UCRL-17656, November 1967
American Institute of Chemical Engineers—Instituto de Ingenieros Quimicos de Puerto Rico, 2nd Joint Meeting, Tampa, Florida, 19-22 May 1968

COLE, F. T., and R. M. Main
The OMNITRON: A medium-energy synchrotron for the acceleration of light and heavy ions
UCRL-17869, September 1967
Sixth International Conference on High-Energy Accelerators, Cambridge, Massachusetts, 11-15 September 1967

CONZETT, H. E., and R. J. Slobodrian
Elastic α-α scattering and the $^{7}Li(p, \alpha)\alpha$ reaction
UCRL-18479 Abstract, September 1968
Meeting of the American Physical Society, Miami Beach, Florida, 25-27 November 1968

CONZETT, H. E. (See Slobodrian, R. J., UCRL-18148)

CONZETT, H. E. (See Slobodrian, R. J., UCRL-18221)

COPELAND, J. C., and B. B. Cunningham
Crystallography of the compounds of californium. II. Crystal structure and lattice parameters of californium oxychloride and californium sesquioxide
UCRL-18304, June 1968
J. Inorg. Nucl. Chem.

COSPER, S. W., R. L. McGrath, J. Cerny, C. C. Maples, G. W. Goth, and D. G. Fleming
Observation of the lowest p-shell $T = 3/2$ states of ^{11}B and ^{11}C
UCRL-18366, July 1968
Phys. Rev.

COUGHLEN, T. D., and T. Vermeulen
Power requirements for liquid agitation in rectangular vessels
UCRL-16289, August 1968
From M. S. Thesis by Coughlen

CROFT, P. D., and K. Street, Jr.
Range-energy studies of Po and At recoils in Al and Al_2O_3
Phys. Rev. 165, 1375 (1968)

CROFT, P. D., J. M. Alexander, and K. Street, Jr.
Recoil studies of nuclear reactions of ^{209}Bi and ^{208}Pb with ^{16}O
Phys. Rev. 165, 1380 (1968)

CROISSIAUX, M. (See Bowman, H. R., Suppl. J. Phys. Soc. Japan 24, 545 (1968))

CUNNINGHAM, B. B.
Recent research on actinide element chemistry at Lawrence Radiation Laboratory, Berkeley
UCRL-18054 Abstract, January 1968
Meeting of the American Chemical Society, San Francisco, 31 March - 5 April 1968

CUNNINGHAM, B. B.
Use of ion exchange substances in research on the transcurium actinides
UCRL-18659 Abstract, December 1968
Meeting of the American Chemical Society, 14-18 April 1969

CUNNINGHAM, B. B.
Compounds of the actinides
Preparative Inorganic Reactions, Vol. 3, ed. by William L. Jolly (Interscience Publishers, New York, 1966) p. 79

CUNNINGHAM, B. B. (See Copeland, J. C., UCRL-18304)

CUNNINGHAM, B. B. (See Fujita, D. K., UCRL-18612 Rev)

CUNNINGHAM, B. B. (See Peterson, J. R., UCRL-18052 Abstract)

DeBOER, B., A. Zalkin, and D. H. Templeton
The crystal structure of a brominated carborane - metal sandwich compound - $N(CH_3)_4[(B_9C_2H_8Br_3)_2Co]$
UCRL-18163, April 1968
Inorg. Chem.

DeBOER, B. G.
The crystal and molecular structures of three boron compounds
UCRL-18391, August 1968
Ph. D. Thesis

DeBOER, B. G. (See Bartlett, N., UCRL-18314 Abstract)

deBOER, J. (See Ward, D., UCRL-18079 Abstract)

deSWINIARSKI, R., A. D. Bacher, J. Ernst, A. Luccio, F. Resmini, R. Slobodrian, and B. Tivol
Elastic scattering of polarized protons on ^{40}Ca at 20 MeV
UCRL-18527 Abstract, October 1968
Meeting of the American Physical Society, San Diego, California, 18-20 December 1968

deSWINIARSKI, R. (See Resmini, F., UCRL-18478 Abstract)

deSWINIARSKI, R. (See Sherif, R., UCRL-18569)

DIAMOND, R. M., A. Poskanzer, F. S. Stephens, W. J. Swiatecki, and D. Ward
Potential energy effects in heavy-ion transfer reactions
UCRL-18013, January 1968
Phys. Rev. Letters 20, 802 (1968)

DIAMOND, R. M. (See Bucher, J. J., UCRL-17972)

DIAMOND, R. M. (See Bucher, J. J., UCRL-17973)

DIAMOND, R. M. (See Stephens, F. S., UCRL-17976)

DIAMOND, R. M. (See Stephens, F. S., UCRL-18358)

DIAMOND, R. M. (See Turner, D. J., UCRL-17879)

DIAMOND, R. M. (See Turner, D. J., UCRL-17997)

DIAMOND, R. M. (See Turner, D. J., UCRL-18024)

DIAMOND, R. M. (See Ward, D., UCRL-17945)

DIAMOND, R. M. (See Ward, D., UCRL-18085 Abstract)

ELO, D. (See Clark, D., UCRL-18608 Abstract)

ELO, D. (See Luccio, A., UCRL-18607 Abstract)

ERNST, J. (See deSwiniarski, R., UCRL-18527 Abstract)

EWAN, G. T. (See Yamazaki, T., UCRL-18058)

EWAN, G. T. (See Yamazaki, T., UCRL-18175)

FADLEY, C. S., and D. A. Shirley
X-ray photoelectron spectroscopic study of iron, cobalt, nickel, copper, and platinum
UCRL-18375, August 1968
Phys. Rev. Letters 21, 980 (1968)

FADLEY, C. S., and D. A. Shirley
X-ray photoelectron spectroscopy on magnetic metals
UCRL-18418 Abstract, August 1968
14th Conference on Magnetism and Magnetic Materials, New York, 18-21 November 1968

FADLEY, C. S., G. L. Geoffroy, S. B. M. Hagström, and J. M. Hollander
Direct voltage calibration of an electron spectrometer
UCRL-18571, October 1968
Nucl. Instr. Methods

FLEMING, D. G. (See Cosper, S. W., UCRL-18366)

FLOOD, W. S. (See Hintz, R. E., UCRL-18383)

FLOOD, W. S. (See McClatchie, E. A., UCRL-18477 Abstract)

FRAENKEL, Z.
Emission of long-range alpha particles in the spontaneous fission of Cf^{252}
Phys. Rev. 156, 1283 (1967)

FRANKEL, R. B., J. J. Huntzicker, D. A. Shirley, and N. J. Stone
Magnetic hyperfine structure in ^{125}Te
UCRL-18064, February 1968
Phys. Letters 26A, 452 (1968)

FRANKEL, R. B. (See Stone, N. J., UCRL-18000)

FRAZIER, P. (See Clark, D., UCRL-18608 Abstract)

FRAZIER, P. (See Luccio, A., UCRL-18607 Abstract)

FUGER, J. (See Morss, L. R., UCRL-18456)

FUJITA, D. K., B. B. Cunningham, and T. C. Parsons
Crystal structures and lattice parameters of einsteinium trichloride and einsteinium oxychloride
UCRL-18612 Rev, December 1968
Inorg. Nucl. Chem. Letters

GABRIEL, H.
Theory of the environment's influence on the angular distribution of nuclear radiation
UCRL-18496 Rev, November 1968
Phys. Rev.

GABRIELLI, I., B. G. Harvey, D. L. Hendrie, J. Mahoney, J. R. Meriwether, and J. Valentin
Scattering of alpha particles by ^{55}Mn
UCRL-18488, September 1968
Nuovo Cimento

GAVIN, B.
A sputtering type penning discharge for metallic ions
UCRL-18082, March 1968
Nucl. Instr. Methods

GARRISON, W. M. (See Holian, J., UCRL-18428)

GARRISON, W. M. (See Holian, J., UCRL-18449)

GARRISON, W. M. (See Peterson, D. B., UCRL-18198 Abstract)

GARRISON, W. M. (See Peterson, D. B., UCRL-18532)

GATTI, R. C. (See Bowman, H. R., Suppl. J. Phys. Soc. Japan 24, 545 (1968))

GATTI, R. C. (See Moretto, L. G., UCRL-18390)

GATTI, R. C. (See Moretto, L. G., UCRL-18535)

GEOFFROY, G. L. (See Fadley, C. S., UCRL-18571)

GHIORSO, A.
Recent transuranium element research at Berkeley
UCRL-17907, October 1967
Centenary Symposium in Warsaw, 17-20 October 1967

GHIORSO, A.
Research with the Berkeley HILAC
UCRL-18633 Abstract, December 1968
Meeting of the American Chemical Society, Minneapolis, Minnesota, 14-18 April 1969

GHIORSO, A. (See Maly, J., UCRL-17995)

GHIORSO, A. (See Maly, J., UCRL-17996)

GHIORSO, A. (See Sikkeland, T., UCRL-18011)

GIAUQUE, R. D.
A radioisotope source—target assembly for x-ray spectrometry
UCRL-18292 Rev, August 1968
Anal. Chem. 40, 2075 (1968)

GIAUQUE, R. D. (See Bowman, H. R., UCRL-17968)

GILBERT, A.
Shell effects in nuclear level densities
UCRL-18095, June 1968
Annals of Physics

GLASHAUSSER, C., and J. Thirion
Polarization phenomena in nuclear reactions
UCRL-17920, November 1967
Advances in Nuclear Physics, Vol. 2, ed. by M. Baranger and E. Vogt (Plenum Publishing Corp, New York, 1968)

GLASHAUSSER, C., B. G. Harvey, D. L. Hendrie, J. Mahoney, E. A. McClatchie, and J. Saudinos
Excitation of single neutron hole states in Pb^{207} by inelastic proton scattering at 20.2 MeV
UCRL-18376, July 1968
Phys. Rev. Letters 21, 918 (1968)

GLENDENNING, N. K.
Coupled channel treatment of inelastic scattering based on microscopic nuclear descriptions
UCRL-18104, February 1968
Nucl. Phys. A117, 49 (1968)

GLENDENNING, N. K.
Two nucleon transfer reactions
UCRL-18225, May 1968

GLENDENNING, N. K.
Tables of structure amplitudes for (p, t) reactions
UCRL-18268, June 1968

GLENDENNING, N. K.
Tables of structure amplitudes for (p, He^3) reactions
UCRL-18269, August 1968

GLENDENNING, N. K.
Tables of structure amplitudes for (α, d) reactions
UCRL-18270, June 1968

GLENDENNING, N. K., and R. J. Asciutto
Inelastic processes in particle transfer reactions
UCRL-18529, October 1968
Phys. Rev.

GLENDENNING, N. K. (See Mangelson, N. F., UCRL-17977)

GLENDENNING, N. K. (See Mangelson, N. F., UCRL-18047)

GOODMAN, A. (See Bar-Touv, J., UCRL-18363)

GOSWAMI, A. (See Bar-Touv, J., UCRL-18363)

GOTH, G. W. (See Cosper, S. W., UCRL-18366)

GOULDING, F. S. (See Poskanzer, A. M., UCRL-18207)

GUSTAFSON, C. (See Nilsson, S. G., UCRL-18068)

HAGSTRÖM, S. B. M. (See Fadley, C. S., UCRL-18571)

HALBACH, K.
Application of conformal mapping to evaluation and design of magnets containing iron with nonlinear B(H) characteristics
UCRL-18173, February 1968
Nucl. Instr. Methods 64, 279 (1968)

HALBACH, K.
Calculation of the stray field of magnets with POISSON
UCRL-18379, July 1968
Nucl. Instr. Methods

HALBACH, K. (See Main, R. M., UCRL-18240)

HALBACH, K. (See Yourd, R., UCRL-18378)

HARDGROVE, G. L., L. K. Templeton, and D. H. Templeton
Crystal and molecular structures of three dihalobenzocyclobutenes
UCRL-8803, June 1959
J. Phys. Chem. 72, 668 (1968)

HARDY, J. C., H. Brunnader, and J. Cerny
Isobaric multiplets in the $d_{5/2}$ shell
UCRL-18075 Abstract, February 1968
Bull. Am. Phys. Soc. 13, 561 (1968)

HARDY, J. C. (See Brunnader, H., UCRL-18272)

HARDY, J. C. (See McGrath, R. L., UCRL-18335)

HARVEY, B. G. (See Gabrielli, I., UCRL-18488)

HARVEY, B. G. (See Glashausser, C., UCRL-18376)

HARVEY, B. G. (See Hintz, R. E., UCRL-18383)

HARVEY, B. G. (See Lu, C. C., UCRL-18157)

HARVEY, B. G. (See Mangelson, N. F., UCRL-17977)

HARVEY, B. G. (See Mangelson, N. F., UCRL-18047)

HARVEY, B. G. (See McClatchie, E. A., UCRL-18477 Abstract)

HAVERFIELD, A. J. (See Bosch, H. E., Nucl. Phys. A108, 209 (1968))

HEBERT, A. J., and K. Street, Jr.
Nuclear quadrupole ratio of bromine isotopes in molecular LiBr
UCRL-18353 Rev, August 1968
Phys. Rev.

HEBERT, A. J. (See Melendres, C. A., UCRL-17916)

HEISENBERG, J. H. (See Bowman, H. R., Suppl. J. Phys. Soc. Japan 24, 545 (1968))

HEISENBERG, J. H. (See Moretto, L. G., UCRL-18535)

HENDRICKSON, D. N. (See Hollander, J. M., UCRL-18298)

HENDRIE, D. L. (See Gabrielli, I., UCRL-18488)

HENDRIE, D. L. (See Glashausser, C., UCRL-18376)

HINTZ, R. E., F. B. Selph, W. S. Flood, B. G. Harvey, F. G. Resmini, and E. A. McClatchie
Beam analyzing systems for a variable energy cyclotron
UCRL-18383, August 1968
Nucl. Instr. Methods

HINTZ, R. E. (See McClatchie, E. A., UCRL-18477 Abstract)

HOLIAN, J., and W. M. Garrison
On the radiation-induced reduction of amide and peptide functions in aquo-organic systems
UCRL-18428, August 1968
J. Phys. Chem.

HOLIAN, J., and W. M. Garrison
Reconstitution ("repair") mechanisms in the radiolysis of aqueous biochemical systems: inhibitive effects of thiols
UCRL-18449, November 1968
Radiation Effects

HOLIAN, J. (See Peterson, D. B., UCRL-18198 Abstract)

HOLIAN, J. (See Peterson, D. B., UCRL-18532)

HOLLANDER, J. M., D. N. Hendrickson, and W. L. Jolly
Nitrogen 1s electron binding energies correlation with CNDO charges
UCRL-18298, June 1968
J. Chem. Phys. 49, 3315 (1968)

HOLLANDER, J. M. (See Fadley, C. S., UCRL-18571)

HOLLANDER, J. M. (See Jaklevic, J. M., UCRL-18389)

HOLLANDER, J. M. (See Lederer, C. M., UCRL-18530)

HOLLANDER, J. M. (See Novakov, T., UCRL-18086 Rev)

HORROCKS, W. DeW., Jr., D. H. Templeton, and A. Zalkin
The crystal and molecular structure of tetra-n-butylammonium tribromo(quinoline) nickelate(II), $[(n\text{-}C_4H_9)_4N][Ni(C_9H_7N)Br_3]$
Inorg. Chem. 7, 2303 (1968)

HOFSTADTER, R. (See Bowman, H. R., Suppl. J. Phys. Soc. Japan 24, 545 (1968))

HOFSTADTER, R. (See Moretto, L. G., UCRL-18535)

HOLTZ, M. D. (See Stephens, F. S., UCRL-17976)

HUIZENGA, J. R. (See Moretto, L. G., UCRL-18390)

HUNTZICKER, J. J., and D. A. Shirley
A temperature scale by nuclear orientation for cerium magnesium nitrate below 0.002°K
UCRL-18006 Abstract, December 1967
Bull. Am. Phys. Soc. 13, 490 (1968)

HUNTZICKER, J. J.
An absolute temperature scale for cerium magnesium nitrate below 0.002°K
UCRL-18476, September 1968
Ph. D. Thesis

HUNTZICKER, J. J. (See Frankel, R. B., UCRL-18064)

HYDE, E. K. (See Poskanzer, A. M., UCRL-18207)

HYDE, E. K. (See Treytl, W., UCRL-17529)

HYDE, E. K. (See Valli, K., UCRL-18098)

JAKLEVIC, J. M., F. M. Bernthal, J. O. Radeloff, D. Landis, and J. M. Hollander
A pulse-height compensation system for Ge(Li) timing
UCRL-18389, August 1968
Nucl. Instr. Methods

JARED, R. C. (See Bowman, H. R., Suppl. J. Phys. Soc. Japan 24, 545 (1968))

JOHNS, O. D.
Pairing in nuclei
UCRL-18614, November 1968
Ph. D. Thesis

JOLLY, W. L. (See Hollander, J. M., UCRL-18298)

KAPLAN, M., J. Blok, and D. A. Shirley
Magnetic moment of Sm^{145} and attenuation following the decay of oriented Sm^{145}
UCRL-18035, January 1968
Phys. Rev.

KARLSSON, E. (See Soinski, A. J., UCRL-17970)

KELLY, W. H. (See Stephens, F. S., UCRL-18358)

KELLY, W. H. (See Ward, D., UCRL-18079 Abstract)

KENNEDY, P. (See Main, R. M., UCRL-18240)

KIEFER, R. L., and K. Street, Jr.
Isomer ratio of Ce^{137m} to Ce^{137g} produced in several charged-particle reactions
UCRL-11049, October 1963
Phys. Rev. 173, 1020 (1968)

KING, C. J. (See Clark, M. W., UCRL-17655)

KING, C. J. (See Clark, M. W., UCRL-17656)

KILIAN, G. (See Bowman, H. R., Suppl. J. Phys. Soc. Japan 24, 545 (1968))

KOLODY, D. (See Main, R. M., UCRL-18240)

LAMB, J. F., D. M. Lee, and S. S. Markowitz
^{3}He-induced nuclear reactions with fluorine, oxygen, silicon, and germanium for chemical activation analysis
UCRL-18053 Abstract, January 1968
Meeting of the American Chemical Society, San Francisco, March 31 - April 5, 1968

LANDIS, D. (See Jaklevic, J. M., UCRL-18389)

LANDIS, D. (See Poskanzer, A. M., UCRL-18207)

LEDERER, C. M., J. M. Hollander, and L. M. Meissner
A computer-based system for the nuclear data compilation "Table of Isotopes"
UCRL-18530, October 1968

LEE, D. M. (See Lamb, J. F., UCRL-18053 Abstract)

LEIPERT, T. K., J. D. Baldeschwieler, and D. A. Shirley
The application of gamma-ray angular correlations to the study of biological macromolecules in solution
UCRL-18511, October 1968
Nature

LU, C. C., M. S. Zisman, and B. G. Harvey
Proton-neutron two-particle excited states of $(1g_{9/2})^2_{9+}$ configuration
UCRL-18157, April 1968
Phys. Letters 27B, 217 (1968)

LU, C. C.
The (α, d) reaction on light and medium mass nuclides
UCRL-18470, August 1968
Ph. D. Thesis

LUCCIO, A.
Axial injection studies on the 88" cyclotron: (hole-lens)
UCRL-18016, January 1968

LUCCIO, A.
Waist-to-waist transfer in thin lens optics
UCRL-18217, April 1968

LUCCIO, A., D. J. Clark, D. Elo, P. Frazier, D. Morris, and M. Renkas
A polarized ion source for the Berkeley 88" cyclotron
UCRL-18607 Abstract, November 1968
1969 Particle Accelerator Conference, Washington, D. C., 5-7 March 1969

LUCCIO, A. (See Clark, D., UCRL-18608 Abstract)

LUCCIO, A. (See deSwiniarski, R., UCRL-18527 Abstract

MAHONEY, J. (See Gabrielli, I., UCRL-18488)

MAHONEY, J. (See Glashausser, C., UCRL-18376)

MAIN, R. M., K. Halbach, P. Kennedy, R. Yourd, A. Watanabe, and D. Kolody
High gradient magnetic drift tube quadrupoles
UCRL-18240, May 1968
1968 Linear Accelerator Conference, Brookhaven National Laboratory, New York, 20-24 May 1968

MAIN, R. M. (See Cole, F. T., UCRL-17869)

MALY, J.
The amalgamation behavior of heavy elements 3. Extraction of radium, lead, and the actinides by sodium amalgam from acetate solutions
UCRL-17987, December 1967
J. Inorg. Nucl. Chem.

MALY, J.
The amalgamation behavior of heavy elements 4. The tracer chemistry of divalent mendelevium
UCRL-18046, January 1968
J. Inorg. Nucl. Chem.

MALY, J., T. Sikkeland, R. Silva, and A. Ghiorso
Nobelium: tracer chemistry of the divalent and trivalent ions
UCRL-17995, February 1968
Science 160, 1114 (1968)

MALY, J., T. Sikkeland, R. Silva, and A. Ghiorso
Tracer chemistry studies of nobelium
UCRL-17996, December 1967

MANGELSON, N. F., B. G. Harvey, and N. K. Glendenning
Spectroscopy of ^{14}N by use of the $^{12}C(^{3}He, p)^{14}N$ reaction
UCRL-17977, December 1967
Nucl. Phys. A117, 161 (1968)

MANGELSON, N. F., B. G. Harvey, and N. K. Glendenning
Study of ^{18}F by use of $(^{3}He, p)$ and (α, d) reactions
UCRL-18047, May 1968
Nucl. Phys.

MARKOWITZ, S. S. (See Lamb, J. F., UCRL-18053 Abstract)

MARRUS, R., E. Wang, and J. Yellin
Atomic beam measurement of isotope shifts in the D_1 line of Cs^{127}, Cs^{129}, Cs^{133}, Cs^{134m}, Cs^{134}, and Cs^{137}
UCRL-18349, July 1968
Phys. Rev.

MARRUS, R., and J. Yellin
Electric polarizabilities of the 4^2p level of potassium
UCRL-18354, July 1968
Phys. Rev.

MARRUS, R. (See Yellin, J., UCRL-18601 Abstract)

MAPLES, C. C. (See Cosper, S. W., UCRL-18366)

MATTHIAS, E. (See Rao, G. N., UCRL-18020 Abstract)

MATTHIAS, E. (See Yamazaki, T., UCRL-18153)

McCLATCHIE, E. A., R. E. Hintz, F. B. Selph, W. S. Flood, B. G. Harvey, and F. Resmini
Beam analyzing system for a variable energy cyclotron
UCRL-18477 Abstract, September 1968
Meeting of the American Physical Society, Miami Beach, Florida, 25-27 November 1968

McCLATCHIE, E. A. (See Bacher, A. D., UCRL-18606 Abstract)

McCLATCHIE, E. A. (See Glashausser, C., UCRL-18376)

McCLATCHIE, E. A. (See Hintz, R. E., UCRL-18383)

McCLATCHIE, E. A. (See Resmini, F., UCRL-18478 Abstract)

McGRATH, R. L., J. C. Hardy, and J. Cerny
The location and isospin-forbidden alpha decay of the lowest T = 2 state in ^{28}Si
UCRL-18335, July 1968
Phys. Letters 27B, 443 (1968)

McGRATH, R. L. (See Cosper, S. W., UCRL-18366)

McHUGH, J. A., and M. C. Michel
Fission-fragment mass and charge distribution for the moderately excited U^{236} compound nucleus
UCRL-10673, February 1963
Phys. Rev. 172, 1160 (1968)

MEHLHORN, R.
Energy level calculations for singly ionized hafnium
UCRL-18040, January 1968
Ph. D. Thesis

MEISSNER, L. M. (See Lederer, C. M., UCRL-18530)

MELDNER, H.
Realistic nuclear single-particle Hamiltonians and the proton shell 114
UCRL-17801, October 1968
Phys. Rev.

MELENDRES, C. A., A. J. Hebert, and K. Street, Jr.
The molecular-beam electric resonance spectra of NaCl and NaBr
UCRL-17916, November 1968

MELENDRES, C.
Radio-frequency Stark spectra of NaCl, NaBr, and BaS by the molecular beam electric resonance method
UCRL-18344, June 1968
Ph. D. Thesis

MERIWETHER, J. R. (See Gabrielli, I., UCRL-18488)

MICHEL, M. C. (See McHugh, J. A., UCRL-10673)

MIDDLEMAN, L. M. (See Bowman, H. R., Suppl. J. Phys. Soc. Japan 24, 545 (1968))

MIDDLEMAN, L. M. (See Moretto, L. G., UCRL-18535)

MILLERON, N., R. Wolgast, and J. M. Nitschke
Measurement of OMNITRON cryopumping and outgassing by 10^{-16} torr pulse counting mass filter
UCRL-17845, April 1968
Fourth International Vacuum Congress, The University of Manchester, Institute of Science and Technology, London, S. W. I., England, 17-19 April 1968

MILLERON, N.
Evaluating ultra vacuum pumping and outgassing by counting ions or measuring ion currents
UCRL-18213, May 1968
First Combined Symposium, Delaware Valley Section and Greater New York Chapter—Thin Film Division, Princeton, New Jersey, May 16, 1968

MÖLLER, P. (See Nilsson, S. G., UCRL-18068)

MORETTO, L. G., R. C. Gatti, S. G. Thompson, J. R. Huizenga, and J. O. Rasmussen
Pairing effects at the fission saddle point of ^{210}Po and ^{211}Po
UCRL-18390, August 1968
Phys. Rev.

MORETTO, L. G., R. C. Gatti, S. G. Thompson, J. T. Routti, J. H. Heisenberg, L. M. Middleman, M. R. Yearian, and R. Hofstadter
Electron and bremsstrahlung-induced fission of heavy and medium-heavy nuclei
UCRL-18535, October 1968
Phys. Rev.

MORETTO, L. G. (See Bowman, H. R., Suppl. J. Phys. Soc. Japan 24, 545 (1968))

MORRIS, D. (See Luccio, A., UCRL-18607 Abstract)

MORRIS, D. (See Clark, D., UCRL-18608 Abstract)

MORSS, L. R., and J. Fuger
Preparation and crystal structures of dicesium berkelium hexachloride and dicesium sodium berkelium hexachloride
UCRL-18456, October 1968
Inorg. Chem.

NEIMAN, M., and D. Ward
Energy levels in ^{154}Dy
UCRL-17963, December 1967
Nucl. Phys. A115, 529 (1968)

NEWTON, A. S., and A. F. Sciamanna
Metastable peaks in the mass spectra of N_2 and NO
UCRL-18495 Rev, October 1968
J. Chem. Phys.

NEWTON, A. S. (See Clampitt, R., UCRL-18032 Rev)

NEWTON, A. S. (See Clampitt, R., UCRL-18239)

NEWTON, J. O. (See Stephens, F. S., UCRL-17976)

NEWTON, J. O. (See Stephens, F. S., UCRL-18358)

NILSSON, S. G., R. Nix, A. Sobiczewski, Z. Szymanski, S. Wycech, C. Gustafson, and P. Möller
On the spontaneous fission of nuclei with Z near to 114 and N near to 184
UCRL-18068, February 1968
Nucl. Phys. A115, 545 (1968)

NILSSON, S. G.
Nuclear structure, fission, and superheavy elements
UCRL-18355 Rev, September 1968
Institut d'Etudes Scientifiques de Cargese (Corsica), Summer Institute on Nuclear Physics, 2-28 September 1968

NILSSON, S. G., S. G. Thompson, and C. F. Tsang
Stability of superheavy nuclei and their possible occurrence in nature
UCRL-18531, November 1968
Phys. Letters

NITSCHKE, J. M.
On-line isotope separation at the HILAC
UCRL-18463, September 1968
Nucl. Instr. Methods

NITSCHKE, J. M. (See Milleron, N., UCRL-17845)

NIX, J. R.
Further studies in the liquid-drop theory of nuclear fission
UCRL-17958, July 1968
Nucl. Phys.

NIX, J. R. (See Nilsson, S. G., UCRL-18068)

NOVAKOV, T., and J. M. Hollander
Spectroscopy of inner atomic levels: electric-field splitting of core $p_{3/2}$ levels in heavy atoms
UCRL-18086 Rev, September 1968
Phys. Rev. Letters 21, 1133 (1968)

NURMIA, M. J. (See Sikkeland, T., UCRL-18011)

PALMER, K. J., and D. H. Templeton
Crystal and molecular structure of 1-bromotriptycene $BrC_{20}H_{13}$
Acta Cryst. B24, 1048 (1968)

PARSONS, T. C. (See Fujita, D. K., UCRL-18612 Rev)

PERLMAN, I., and F. Asaro
Trace element analysis of pottery by neutron activation
UCRL-18212 Abstract, April 1968
American Chemical Society, 4th Symposium on Archaeological Chemistry, Division of the History of Chemistry, Atlantic City, New Jersey, 8-13 September 1968

PERLMAN, I. (See Bowman, H. R., UCRL-17968)

PETERSON, D. B., J. Holian, and W. M. Garrison
Ionic processes in the radiolysis of cysteine and related compounds in the solid state
UCRL-18198 Abstract, April 1968

PETERSON, D. B., J. Holian, and W. M. Garrison
Radiation chemistry of the α-amino acids: γ-radiolysis of solid cysteine
UCRL-18532, October 1968
J. Phys. Chem.

PETERSON, J. R., and B. B. Cunningham
The crystal structures and lattice parameters of berkelium trifluoride
UCRL-18052 Abstract, November 1967
Meeting of the American Chemical Society, San Francisco, 31 March - 5 April 1968

PIGFORD, R. L., B. Baker III, and D. E. Blum
An equilibrium theory of the parametric pump
UCRL-18483, September 1968
Ind. Eng. Chem.

POSKANZER, A. M., G. W. Butler, E. K. Hyde, J. Cerny, D. A. Landis, and F. S. Goulding
Observation of the new isotope ^{17}C using a combined time-of-flight particle-identification technique
UCRL-18207, April 1968
Phys. Letters 27B, 414 (1968)

POSKANZER, A. (See Diamond, R. M., UCRL-18013)

PRUSSIN, S. G. (See Yamazaki, T., UCRL-18175)

RADELOFF, J. O. (See Jaklevic, J. M., UCRL-18389)

RAO, G. N., E. Matthias, and D. A. Shirley
Knight shift measurements in ^{100}Rh in Rh-Ag and Rh-Pd alloys
UCRL-18020 Abstract, January 1968
Bull. Am. Phys. Soc. 13, 409 (1968)

RASMUSSEN, J. O. (See Moretto, L. G., UCRL-18390)

RASMUSSEN, J. O. (See Wilhelmy, J. B., UCRL-18248 Abstract)

REED, M.
The excitation of unnatural-parity states in ^{24}Mg, ^{20}Ne, and ^{16}O by inelastic α scattering
UCRL-18414, August 1968
Ph. D. Thesis

RENKAS, M. (See Clark, D., UCRL-18608 Abstract)

RENKAS, M. (See Luccio, A., UCRL-18607 Abstract)

RESMINI, F. G., and D. J. Clark
Beam optics and space charge effects in the axial injection line for the 88" cyclotron
UCRL-18596, November 1968
1969 Particle Accelerator Conference, Washington, D. C., 5-7 March 1969

RESMINI, F., and D. J. Clark
A proposed sawtooth buncher for the 88-inch cyclotron axial injection system
UCRL-18125, March 1968

RESMINI, F.
Optics of the axial injection line for the 88-inch cyclotron
UCRL-18442, August 1968

RESMINI, F.
A simple method for determining waist to waist transfer properties of quadrupole doublets and triplets
UCRL-18448, September 1968
Nucl. Instr. Methods

RESMINI, F., A. D. Bacher, D. J. Clark, E. A. McClatchie, and R. deSwiniarski
Slit scattering effects with medium energy alpha particles
UCRL-18478 Abstract, September 1968
Meeting of the American Physical Society, Miami Beach, Florida, 25-27 November 1968

RESMINI, F. (See Bacher, A. D., UCRL-18606 Abstract)

RESMINI, F. (See Clark, D., UCRL-18608 Abstract)

RESMINI, F. (See deSwiniarski, R., UCRL-18527 Abstract)

RESMINI, F. (See Hintz, R. E., UCRL-18383)

RESMINI, F. (See McClatchie, E. A., UCRL-18477 Abstract)

RESMINI, F. (See Slobodrian, R. J., UCRL-18148)

REYNOLDS, F. L.
Surface ionization: an experimental study of strontium and lanthanum on tungsten
UCRL-18233, May 1968
Surface Science

ROTHSTEIN, E.
The molecular-beam electric-resonance spectra of the lithium hydrides
UCRL-17948, December 1967
Ph. D. Thesis

ROUTTI, J. T. (See Moretto, L. G., UCRL-18535)

ROUTTI, J. T. (See Wilhelmy, J. B., UCRL-18248 Abstract)

SAUDINOS, J. (See Glashausser, C., UCRL-18376)

SCIAMANNA, A. F. (See Newton, A. S., UCRL-18495 Rev)

SELPH, F. B. (See Hintz, R. E., UCRL-18383)

SELPH, F. B. (See McClatchie, E. A., UCRL-18477 Abstract)

SHERIF, R., and R. deSwiniarski
Thomas form of the spin-dependent optical potential and asymmetry of 20 MeV polarized ^{3}protons
UCRL-18569, October 1968
Phys. Letters

SHIELD, E. (See Slobodrian, R. J., UCRL-18221)

SHIRLEY, D. A.
Chemical tools from nuclear physics
UCRL-18196, April 1968
Science 161, 745 (1968)

SHIRLEY, D. A.
The detection of NMR by nuclear radiation
UCRL-18315 Rev, July 1968
XV^{e} Colloque A. M. P. E. R. E., Grenoble, France, 16-21 September 1968

SHIRLEY, D. A. (See Barrett, P. H., UCRL-18036)

SHIRLEY, D. A. (See Brewer, W. D., UCRL-18087)

SHIRLEY, D. A. (See Brewer, W. D., UCRL-18102)

SHIRLEY, D. A. (See Fadley, C. S., UCRL-18375)

SHIRLEY, D. A. (See Fadley, C. S., UCRL-18418 Abstract)

SHIRLEY, D. A. (See Frankel, R. B., UCRL-18064)

SHIRLEY, D. A. (See Huntzicker, J. J., UCRL-18006 Abstract)

SHIRLEY, D. A. (See Kaplan, M., UCRL-18035)

SHIRLEY, D. A. (See Leipert, T. K., UCRL-18511)

SHIRLEY, D. A. (See Rao, G. N., UCRL-18020 Abstract)

SHIRLEY, D. A. (See Soinski, A. J., UCRL-17970)

SHIRLEY, D. A. (See Stone, N. J., UCRL-18000)

SIKKELAND, T.
Synthesis of nuclei in the region of Z = 126 and N = 184
Arkiv Fysik, Band 36, no. 62, 539 (1967)

SIKKELAND, T., A. Ghiorso, and M. J. Nurmia
Analysis of excitation functions in Cm(C, xn)No reactions
UCRL-18011, December 1967
Phys. Rev. 172, 1232 (1968)

SIKKELAND, T.
Evidence for the production of compound nuclei with atomic number 110
UCRL-18177, June 1968
Phys. Letters 27B, 277 (1968)

SIKKELAND, T. (See Maly, J., UCRL-17995)

SIKKELAND, T. (See Maly, J., UCRL-17996)

SILVA, R. (See Maly, J., UCRL-17995)

SILVA, R. (See Maly, J., UCRL-17996)

SLADKY, F. O. (See Bartlett, N., UCRL-18314 Abstract)

SLOBODRIAN, R. J., H. E. Conzett, and F. G. Resmini
Neutron-neutron scattering length from a comparison of the $^{2}H(p, n)2p$ and $^{2}H(n, p)2n$ reactions
UCRL-18148, April 1968
Phys. Letters 27B, 405 (1968)

SLOBODRIAN, R. J., H. E. Conzett, E. Shield, and W. F. Tivol
Proton-proton elastic scattering between 6 and 10 MeV
UCRL-18221, May 1968
Phys. Rev. 174, 1122 (1968)

SLOBODRIAN, R. J.
S-wave shape independent scattering parameters of the proton-proton interaction
UCRL-18223, May 1968
Phys. Rev. Letters 21, 438 (1968)

SLOBODRIAN, R. J. (See Conzett, H. E., UCRL-18479 Abstract)

SLOBODRIAN, R. J. (See deSwiniarski, R., UCRL-18527 Abstract)

SOBICZEWSKI, A. (See Nilsson, S. G., UCRL-18068)

SOINSKI, A. J., E. Karlsson, and D. A. Shirley
Spins and attenuation coefficients of the 86.5- and 105.3-keV states in ^{155}Gd
UCRL-17970, December 1967
Phys. Letters 26B, 440 (1968)

SORTLAND, L. D.
Kinetics of a dense culture fermentation
UCRL-18340, July 1968
Ph. D. Thesis

SORTLAND, L. D., and C. R. Wilke
Growth of Streptococcus faecalus in dense culture
UCRL-18372, July 1968
3rd International Fermentation Symposium, Rutgers University, New Brunswick, N. J., 2-6 September 1968

SPIRO, T. G., D. H. Templeton, and A. Zalkin
The crystal structure of trimethylplatinum hydroxide
Inorg. Chem. 7, 2165 (1968)

SPIRO, T. G., D. H. Templeton, and A. Zalkin
The crystal structure of a hexanuclear basic lead(II) perchlorate hydrate: $Pb_6O(OH)_6(ClO_4)\cdot H_2O$
UCRL-18570, October 1968
Inorg. Chem.

STEIN, S.
Hyperfine structure of Dy^{165} and spin of Er^{163}
UCRL-17969, December 1967
Ph. D. Thesis

STEPHENS, F. S., M. D. Holtz, R. M. Diamond, and J. O. Newton
Coulomb excitation of ^{235}U
UCRL-17976, March 1968
Nucl. Phys. A115, 129 (1968)

STEPHENS, F. S., R. M. Diamond, W. H. Kelly, J. O. Newton, and D. Ward
Gamma ray deexcitation of compound-nucleus-reaction products
UCRL-18358, July 1968
Phys. Rev. Letters

STEPHENS, F. S. (See Diamond, R. M., UCRL-18013)

STEPHENS, F. S. (See Ward, D., UCRL-17945)

STEPHENS, F. S. (See Ward, D., UCRL-18079 Abstract)

STEPHENS, F. S. (See Ward, D., UCRL-18085 Abstract)

STONE, N. J., R. B. Frankel, and D. A. Shirley
Three-quasiparticle intruder state in Te^{125} and the magnetic moment of Sb^{125}
UCRL-18000, December 1967
Phys. Rev. 172, 1243 (1968)

STONE, N. J. (See Frankel, R. B., UCRL-18064)

STORY, T. L., Jr.
Dipole moments of alkali halides by the electric deflection method
UCRL-18484, September 1968
Ph. D. Thesis

STREET, K., Jr. (See Croft, P. D., Phys. Rev. 165, 1375 (1968))

STREET, K., Jr. (See Croft, P. D., Phys. Rev. 165, 1380 (1968))

STREET, K., Jr. (See Hebert, A. J., UCRL-18535 Rev)

STREET, K., Jr. (See Kiefer, R. L., UCRL-11049)

STREET, K., Jr. (See Melendres, C. A., UCRL-17916)

STRUBLE, G. (See Bar-Touv, J., UCRL-18363)

SWIATECKI, W. J. (See Diamond, R. M., UCRL-18013)

SZICHMAN, E. (See Bosch, H. E., Nucl. Phys. A108, 209 (1968))

SZYMANSKI, Z. (See Nilsson, S. G., UCRL-18068)

TEMPLETON, D. H. (See DeBoer, G., UCRL-18163)

TEMPLETON, D. H. (See Hardgrove, G. L., UCRL-8803)

TEMPLETON, D. H. (See Palmer, K. J., Acta Cryst. B24, 1048 (1968))

TEMPLETON, D. H. (See Spiro, T. G., Inorg. Chem. 7, 2165 (1968))

TEMPLETON, D. H. (See Spiro, T. G., UCRL-18570)

TEMPLETON, D. H. (See Vogt, L. H., Inorg. Chem. 6, 1725 (1967))

TEMPLETON, J. E. (See Brewer, W. D., UCRL-18102)

TEMPLETON, L. K. (See Hardgrove, G. L., UCRL-8803)

TEWARI, S. N.
Energy spectrum of ^{20}Ne using Hartree-Fock and Tamm-Dancoff wave functions
UCRL-18628, November 1968
Phys. Letters

THIRION, J. (See Glashausser, C., UCRL-17920)

THOMPSON, S. G. (See Bowman, H. R., Suppl. J. Phys. Soc. Japan 24, 545 (1968))

THOMPSON, S. G. (See Moretto, L. G., UCRL-18390)

THOMPSON, S. G. (See Moretto, L. G., UCRL-18535)

THOMPSON, S. G. (See Nilsson, S. G., UCRL-18531)

THOMPSON, S. G. (See Wilhelmy, J. B., UCRL-18248 Abstract)

TIVOL, B. (See deSwiniarski, R., UCRL-18527 Abstract)

TIVOL, W. F. (See Slobodrian, R. J., UCRL-18221)

TOMBRELLO, T. A. (See Bacher, A. D., UCRL-18071 Abstract)

TOMBRELLO, T. A. (See Bacher, A. D., UCRL-18606 Abstract)

TREYTL, W., E. K. Hyde, and T. Yamazaki
Levels of ^{208}Po from radioactive decay and nuclear reaction γ-ray spectroscopy
UCRL-17529, April 1968
Nucl. Phys. A117, 481 (1968)

TSANG, C. F. (See Nilsson, S. G., UCRL-18531)

TSCHALAER, C. (See Bichsel, H., UCRL-17663 Rev 1)

TURNER, D. J., and R. M. Diamond
The extraction of tetrabutylammonium nitrate and the solvation of the nitrate ion
UCRL-17997, January 1968
J. Phys. Chem.

TURNER, D. J., A. Beck, and R. M. Diamond
The extraction of tetraheptylammonium fluoride and the solvation of the fluoride ion
UCRL-17879, December 1967
J. Phys. Chem. 72, 2831 (1968)

TURNER, D. J., and R. M. Diamond
The extraction of perchloric acid by 1-decanol
UCRL-18024, January 1968
J. Phys. Chem. 72, 3504 (1968)

VALENTIN, J. (See Gabrielli, I., UCRL-18488)

VALLI, K., and E. K. Hyde
New isotopes of thorium studied with an improved helium-jet recoil transport apparatus
UCRL-18098, May 1968
Phys. Rev.

VERMEULEN, T. (See Buss, D. R., Ind. Eng. Chem. 60, 12 (1968))

VERMEULEN, T. (See Coughlen, T. D., UCRL-16289)

VOGT, L. H., Jr., A. Zalkin, and D. H. Templeton
The crystal and molecular structure of phthalocyanatopyridinemanganese(III)-μ-oxo-phthalocyanatopyridinemanganese(III) dipyridinate
Inorg. Chem. 6, 1725 (1967)

WANG, E. C.
Atomic beam measurement of the isotope shifts in ^{127}Cs, ^{129}Cs, ^{133}Cs, ^{134}Cs, ^{134m}Cs, and ^{137}Cs
UCRL-18434, September 1968
Ph. D. Thesis

WANG, E. (See Marrus, R., UCRL-18349)

WANG, E. (See Yellin, J., UCRL-18601 Abstract)

WARD, D., R. M. Diamond, and F. S. Stephens
Collective levels in light even cerium isotopes
UCRL-17945, May 1968
Nucl. Phys. A117, 309 (1968)

WARD, D., J. deBoer, W. H. Kelly, and F. S. Stephens
Measurement of nuclear centrifugal stretching from electromagnetic transition moments
UCRL-18079 Abstract, February 1968
Meeting of the American Physical Society, Washington, D. C., 22-25 April 1968

WARD, D., R. M. Diamond, and F. S. Stephens
In-beam spectroscopy of the light even-even ceriums
UCRL-18085 Abstract, February 1968
Meeting of the American Chemical Society, San Francisco, 31 March - 5 April 1968

WARD, D. (See Diamond, R. M., UCRL-18013)

WARD, D. (See Neiman, M., UCRL-17963)

WARD, D. (See Stephens, F. S., UCRL-18358)

WATANABE, A. (See Main, R. M., UCRL-18240)

WILHELMY, J. B., S. G. Thompson, J. O. Rasmussen, and J. T. Routti
Spectroscopic studies of short-lived fission products
UCRL-18248, May 1968
Meeting of the American Chemical Society, Atlantic City, New Jersey, 8-13 September 1968

WILKE, C. R. (See Sortland, L. D., UCRL-18372)

WOLGAST, R. (See Milleron, N., UCRL-17845)

WYCECH, S. (See Nilsson, S. G., UCRL-18068)

YAMAZAKI, T., and G. T. Ewan
Method of measuring nanosecond isomeric states produced in (particle, xn) reactions
UCRL-18058, January 1968
Nucl. Instr. Methods 62, 101 (1968)

YAMAZAKI, T., and E. Matthias
g-factor measurement of the 100 nsec 17/2- isomer of ^{209}Po following pulsed generation in (α, xn) reactions
UCRL-18153, March 1968
Phys. Rev. Letters

YAMAZAKI, T., G. T. Ewan, and S. G. Prussin
Level and isomer systematics in even Sn isotopes
UCRL-18175, April 1968
Phys. Rev. Letters 20, 1376 (1968)

YAMAZAKI, T. (See Treytl, W., UCRL-17529)

YEARIAN, M. R. (See Bowman, H. R., Suppl. J. Phys. Soc. Japan 24, 545 (1968))

YEARIAN, M. R. (See Moretto, L. G., UCRL-18535)

YELLIN, J., R. Marrus, and E. C. Wang
Atomic beam study of the ^{39}K, ^{42}K isotope shift
UCRL-18601 Abstract, November 1968
Meeting of the American Physical Society, New York, 3-6 February 1968

YELLIN, J. (See Marrus, R., UCRL-18349)

YELLIN, J. (See Marrus, R., UCRL-18354)

YOURD, R., and K. Halbach
Magnetic field computation for two-dimensional air coil system
UCRL-18378, July 1968

YOURD, R. (See Main, R. M., UCRL-18240)

ZALKIN, A.
Carborane sandwich compounds of transition elements
UCRL-18286 Abstract, June 1968
Meeting of the American Chemical Society, Atlantic City, New Jersey, 8-13 September 1968

ZALKIN, A. (See Spiro, T. G., Inorg. Chem. 7, 2165 (1968))

ZALKIN, A. (See Spiro, T. G., UCRL-18570)

ZALKIN, A. (See Bartlett, N., UCRL-18314 Abstract)

ZALKIN, A. (See DeBoer, B., UCRL-18163)

ZALKIN, A. (See Vogt, L. H., Inorg. Chem. 6, 1725 (1967))

ZAMICK, L.
Is Ni^{56} a good closed shell?
UCRL-18406, August 1968
Phys. Letters

ZAMICK, L.
Lectures on effective interactions, effective operators, and closed shell nuclei
UCRL-18445, August 1968

ZISMAN, M. S. (See Lu, C. C., UCRL-18157)

VII. Author Index

CONTRIBUTORS TO THIS REPORT

Abed, U., 305
Adamson, M. G., 265
Asaro, F., 1, 3
Ascuitto, R. J., 133

Bacher, A. D., 94, 104, 107, 332, 363
Ball, G. C., 65
Barclay, J. A., 221
Barrett, P. H., 231
Bartlett, N., 256
Bernthal, F. M., 22, 341
Blok, J., 231
Bowman, H. R., 168, 277, 283
Brewer, W. D., 218, 221, 224
Browne, E., 1
Brunnader, H., 69, 72
Bucher, J. J., 307, 310
Butler, G. W., 44, 362

Cerny, J. III, 44, 65, 69, 72, 77
Cheifetz, E., 168
Clampitt, R., 214
Clark, D. J., 100, 345, 352, 363
Conocchioli, T. J., 307
Conway, J. G., 193
Conzett, H. E., 87, 89, 94, 96, 100
Cordi, R. C., 335
Corniea, W. B., 318
Coughlen, T. D., 322
Cunningham, B. B., 198, 255

Darcey, W., 80, 84
Davies, W. G., 80, 84
Davis, R. C., 335
DeBoer, B. G., 256, 258, 260
Denison, C. A., 340
deSwiniarski, R., 107, 137, 363
Diamond, R. M., 47, 51, 54, 307, 310
Drew, M. G. B., 262
Duong, T. H., 189

Easley, W. C., 195
Edelstein, N. M., 195, 302, 305
Elad, E., 331
Ernst, J., 94, 107, 345
Escobales, R. H., 372
Eskola, K., 62, 63
Eskola, P. L., 62, 63

Fadley, C. S., 247
Faltens, M. O., 241
Flood, W. S., 355
Fuger, J., 300
Fujita, D., 198, 255

Gabriel, H., 245
Garrison, W. M., 313, 316, 318
Gatti, R. C., 143, 174, 178, 277, 283
Ghiorso, A., 61, 62, 63, 64, 295, 297, 299
Giauque, R. D., 366
Glashausser, C., 118, 121, 125, 128, 129, 137, 332
Glendenning, N. K., 113, 133, 135
Go, M. K., 29, 31, 32
Goulding, F., 44, 332, 335

Hansen, W. L., 335
Hardy, J. C., 69, 72, 77, 80, 84
Harris, J. A., 61, 62
Harvey, B. G., 109, 113, 118, 355
Hebert, A. J., 200, 201, 203
Heisenberg, J. H., 174
Held, E. R., 310
Hendrickson, D. N., 251, 253
Hendrie, D. L., 113, 118, 121, 125, 128, 129
Hintz, R. E., 355
Hofstadter, R., 174
Holian, J., 313, 316
Hollander, J. M., 9, 12, 15, 22, 249, 251, 253
Hopkins, T. E., 265
Horrocks, W. D., Jr., 267, 269
Huffman, E. H., 305
Huizenga, J. R., 178
Hunter, J. B., 340
Hyde, E. K., 39, 40, 42, 44, 362

Jaklevic, J. M., 12, 15, 18, 341
Jänecke, J., 72
Jared, R. C., 283, 340
Jayko, M. E., 318
Jolly, W. L., 251, 253

Kahn, D. R., 325
Kaplan, M., 231
Katz, J. E., 337
Kelly, W. H., 47, 51
King, C. J., 326

Koch, C. W., 369
Kumar, K., 153

Labinger, J. A., 310
Lamb, J. F., 34
Landis, D. A., 44, 341
LaPierre, R. L., 337, 338, 339, 340
Latimer, R. M., 283
Lederer, C. M., 3, 9, 12, 15, 18
Lee, D. M., 34
Lu, C. C., 109
Luccio, A. U., 107, 343, 345, 352

Mackintosh, R. S., 135
Mahoney, J., 118, 125, 128
Malone, D. F., 335
Maly, J., 284, 295
Markowitz, S. S., 29, 31, 32, 34
Marrus, R., 183, 189, 190
Matthias, E., 221, 237
McClatchie, E. A., 104, 118, 121, 125, 128, 332, 355, 363
McGrath, R. L., 77
McKee, J. S. C., 100
McLaughlin, R. D., 305
Mehlhorn, R. J., 194, 195
Meiner, H., 94
Meldner, H., 140
Melendres, C. A., 200
Meriwether, J. R., 128
Michel, M. C., 277, 359, 372
Middleman, L. M., 174
Miner, C. E., 372
Mollet, H. F., 195
Moretto, L. G., 143, 174, 178, 277, 283
Morss, L. R., 300, 302
Moss, J. M., 129

Nakamura, M., 331, 339, 340
Neiman, M., 59
Newton, A. S., 207, 214
Newton, J. O., 51
Nilsson, S. G., 148, 150
Novakov, T., 249
Nurmia, M. J., 61, 62, 63, 64, 297, 299

Palkot, E. J., 326
Parsons, T. C., 198, 255
Pehl, R. H., 332, 335
Pelavin, M. L., 253
Perlman, I., 3
Peterson, D. B., 313
Peterson, J. R., 198
Poskanzer, A. M., 44, 362
Prussin, S. G., 18

Quigg, E., 340

Radeloff, J. O., 341
Rao, G. N., 237
Rasmussen, J. O., 22, 170, 178
Reed, M. F., 113
Reimers, R. M., 372
Resmini, F. G., 94, 96, 104, 107, 345, 355, 363, 376
Reynolds, F. L., 204, 359
Rivet, E. J. M., 332, 335
Robinson, H. P., 379
Rodgers, M. A. J., 318
Rosenblum, S. S., 233
Routti, J. T., 143, 174

Saucedo, G. I., 335
Saudinos, J., 118
Sciamanna, A. F., 207
Selph, F. B., 355
Sherman, J., 128
Shield, E., 89
Shirley, D. A., 218, 221, 224, 227, 231, 233, 237, 241, 247
Siegal, M., 302
Sikkeland, T., 64, 295, 297, 299
Silva, R. J., 63, 295, 297, 299
Sladky, F. O., 256
Slobodrian, R. J., 87, 89, 94, 96, 100, 102, 107, 151
Soinski, A. J., 227
Sokol, H. A., 318
Sørensen, B. E., 153, 155, 159, 163
Sortland, L. D., 327
Spiro, T. G., 273, 275
Stephens, F. S., 47, 51, 54
Stone, N. J., 227
Story, T. L., Jr., 201
Street, K., Jr., 200, 201, 203
Sudbury, B. A., 310
Swiatecki, W. J., 283

Tada, S., 323
Taylor, R. P., 269
Templeton, D. H., 258, 260, 262, 265, 267, 269, 273, 275
Templeton, J. E., 224
Tewari, S. N., 165
Thirion, J., 129
Thompson, S. G., 143, 150, 168, 170, 174, 178 277, 283
Tivol, W. F., 89, 100, 107
Tombrello, T. A., 102, 104
Treytl, W. J., 42
Tsang, C. F., 148, 150

Valli, K., 39, 40
Vermeulen, T., 322, 323, 325

Walton, J. T., 335
Wang, E. C., 183
Ward, D., 47, 51, 54, 59
Wilhelmy, J., 170
Wilke, C. R., 327
Worden, E. F., 193

Yamazaki, T., 42
Yearian, M. R., 174
Yellin, J., 183, 189, 190

Zalkin, A., 256, 258, 260, 262, 265, 267, 269, 273, 275
Zane, R., 337
Zisman, M. S., 109, 332